Total synthesis of Reniochalistatin E and synthetic efforts towards Lagunamide C

by

Anthony James Fatino

B.S., University of Central Missouri, 2015

AN ABSTRACT OF A DISSERTATION

submitted in partial fulfillment of the requirements for the degree

DOCTOR OF PHILOSOPHY

Department of Chemistry
College of Arts and Sciences

KANSAS STATE UNIVERSITY
Manhattan, Kansas

2021

Abstract

Natural products (NPs) are compounds isolated from any living organisms and continue to be a rich source of medicines, especially chemotherapeutics. In order to develop new anticancer compounds, this work aimed to synthesize two NPs, reniochalistatin E and lagunamide C, shown below. Reniochalistatin E is a cyclic octapeptide with anticancer activity in a variety of cancer cell lines; including, myeloma (RPMI-8226: IC_{50} = 4.9 μM), gastric (MGC-803: IC_{50} = 9.7 μM), and cervical (HeLa: IC_{50} = 24.4 μM). To this end, the first total synthesis of reniochalistatin E has been completed in 15 steps with an overall 5% yield. Analog synthesis and biological testing identified the tryptophan amino acid (shown in red) as a site for drug conjugation. Future work will harness the synthetic route to generate a cysteine analog in order to conjugate the FDA approved chemotherapeutic, 6-thiopurine (6TP), though a disulfide linkage. Lagunamide C is a cyclic depsipeptide with potent cytotoxic activity in a number of cell lines including lymphoma (P388: IC_{50} = 24.4 nM), lung (A549: IC_{50} = 2.4 nM), colon (PC3: IC_{50} = 2.1 nM), and ovarian (SK-OV3: IC_{50} = 4.5 nM). This work highlights a module-based approach to access the diastereoselective polyketide fragment (shown in blue). Key stereogenic steps include an aldol reaction with an *N*-acetylated Crimmins auxiliary, an asymmetric cyclopropanation with tandem ring-opening, and an iridium catalyzed allylation. Future work will look to complete the first total synthesis of lagunamide C and identify the importance of each subunit of the NP through SAR and analog synthesis.

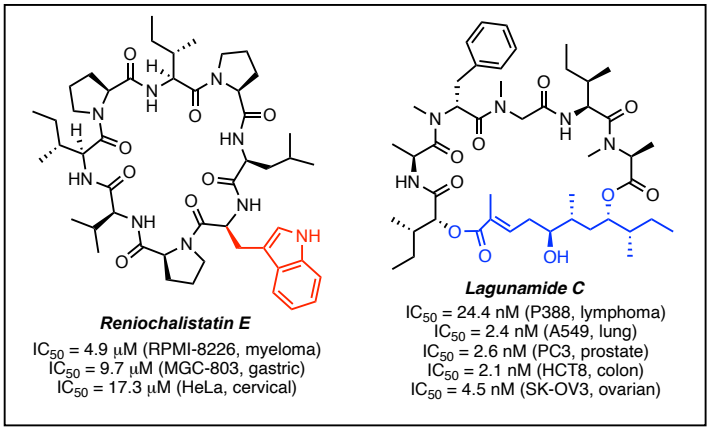

Total synthesis of Reniochalistatin E and synthetic efforts towards Lagunamide C

by

Anthony James Fatino

B.S., University of Central Missouri, 2015

A DISSERTATION

submitted in partial fulfillment of the requirements for the degree

DOCTOR OF PHILOSOPHY

Department of Chemistry
College of Arts and Sciences

KANSAS STATE UNIVERSITY
Manhattan, Kansas

2021

Approved by:

Major Professor
Ryan J. Rafferty

Copyright

Abstract

Natural products (NPs) are compounds isolated from any living organisms and continue to be a rich source of medicines, especially chemotherapeutics. In order to develop new anticancer compounds, this work aimed to synthesize two NPs, reniochalistatin E and lagunamide C, shown below. Reniochalistatin E is a cyclic octapeptide with anticancer activity in a variety of cancer cell lines; including, myeloma (RPMI-8226: IC_{50} = 4.9 μM), gastric (MGC-803: IC_{50} = 9.7 μM), and cervical (HeLa: IC_{50} = 24.4 μM). To this end, the first total synthesis of reniochalistatin E has been completed in 15 steps with an overall 5% yield. Analog synthesis and biological testing identified the tryptophan amino acid (shown in red) as a site for drug conjugation. Future work will harness the synthetic route to generate a cysteine analog in order to conjugate the FDA approved chemotherapeutic, 6-thiopurine (6TP), though a disulfide linkage. Lagunamide C is a cyclic depsipeptide with potent cytotoxic activity in a number of cell lines including lymphoma (P388: IC_{50} = 24.4 nM), lung (A549: IC_{50} = 2.4 nM), colon (PC3: IC_{50} = 2.1 nM), and ovarian (SK-OV3: IC_{50} = 4.5 nM). This work highlights a module-based approach to access the diastereoselective polyketide fragment (shown in blue). Key stereogenic steps include an aldol reaction with an *N*-acetylated Crimmins auxiliary, an asymmetric cyclopropanation with tandem ring-opening, and an iridium catalyzed allylation. Future work will look to complete the first total synthesis of lagunamide C and identify the importance of each subunit of the NP through SAR and analog synthesis.

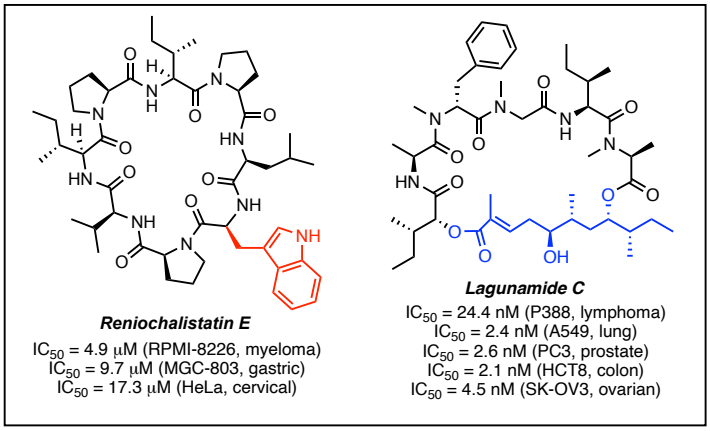

Table of Contents

List of Figures

List of Tables

List of Schemes

Acknowledgements

First, I would like to thank my Ph. D. advisor, Dr. Ryan Rafferty for his support and guidance. Your passion for teaching and dedication to your work has inspired me to always push myself to limits I didn't know were possible. This journey has not been easy, and I wish many things had gone differently, but I will continue to uphold the highest of expectations of myself because of you. Thank you for all your hard work and time, and most of all, thank you for never giving up on me.

I would like to acknowledge my committee members including; Dr. Duy Hua, Dr. Tendai Gadzikwa, Dr. Robert Delong, and Dr. Anna Zolkiewska (former member). Your comments and suggestions have guided me to think deeply about my work and led me to become a better scientist.

Next, I would like to thank my amazing wife, Mrs. Callie Ferguson. You have been a constant source of support for me over the past 5 years. Helping me to understand the importance of grace has allowed me to become the best version of myself. You are and always will be my light, and I am so excited to see where our journey leads us.

I would like to thank all of the current and former Rafferty lab members. The family we have built has not only supported me in difficult times, but also encouraged me to continue to grow and learn. I look forward to hearing all of the great things that come for each of you!

A special thank you to Kansas State University for the opportunity to peruse my education. In particular the chemistry department that supported and challenged me to achieve my highest potential. I am thankful for the guidance and feedback from all of my teachers and professors along this process, as well as the supporting faculty. A special thanks to the department head Dr. Dan Higgins, to the NMR technicians Dr. Leila Maurman, and Dr. Simon Sham; to the teaching advisors Mr. Michael Hinton, Dr. James Townsend, and Dr. Ahibijeet Sinha. Thank you to the

department faculty including Mr. Jim Hodgson, Mr. Ron Jackson, and Mr. Tobe Eggers, and Mr. Bart Bath, this facility would not run without each of you.

I would like to thank my undergraduate advisors Dr. Chen Zhou and Dr. Jay Steinkruger; who prepared me for graduate school and believed in me. Thank you to all the other teachers along the way who encouraged me to always ask hard questions.

I would like to thank my parents Mrs. Dawn Simko, Mr. Steven Simko, and Mr. Frank Fatino, for their endless support. Encouraging me to chase my dreams gave me the confidence to be who I am today. I love you all and I hope I can continue to make you proud.

To my brothers Mr. Joshua Simko, Mr. Shawn Simko, and Mr. Christopher Oden, thank you for your brotherhood. Your love and support have inspired me to lead the best I can, and I hope my journey encourages each of you to believe in your dreams and to pursue the greatest good you can.

Finally, I would like to thank God for the many opportunities. My faith has grown over these years and supported me in hard times. I am grateful for my journey and humbled by the experience I have gained. My faith has carried me far beyond my own expectations and I will continue to stive for greatness though Christ in my future endeavors.

Dedication

This work is dedicated to the late Ms. Diana Worland, my grandmother. She was an amazing friend and always encouraged me to strive for greatness.

Chapter 1: History of Medicinal Natural Products

1.1 Cancer, Treatments, and Chemotherapeutics

1.1.1 Cancer Types

Cancer is defined as unregulated cell growth leading to the development of tumors, which if untreated, can spread throughout the body in a process called metathesis. With 1.9 million new cases and nearly 10 million deaths in 2020, cancer remains the second leading cause of death in the United States (US) following only heart disease.[1] There are over 100 different types of cancers based on organ system including, but not limited to; eye & orbit, bones & joints, endocrine system, soft tissue (including heart), oral cavity and pharynx, skin (excluding basal & squamous), myeloma, brain and other nervous system, lymphoma, leukemia, urinary system, breast, genital system, respiratory system, and digestive system.[2] Shown in Table 1 are the new cases and deaths for a collection of cancer types in the US for 2020.[3] Each of these classes provide unique challenges with respect to diagnosis, treatment, and recovery; however, early identification is critical for remission regardless of the cancer type.

New Cancer Cases and Deaths by Class in the US for 2020				
Cancer Site	**# of New Cases**	**% of all Cases**	**# of Deaths**	**% of Total Deaths**
Breast	253,465	11%	42,617	7%
Lung	227,875	10%	138,225	23%
Prostate	209,512	9%	32,438	5%
Colon	101,809	4%	37,930	6%
Melanoma of skin	96,445	4%	7,201	1%
Bladder	80,617	4%	18,130	3%
Kidney	69,569	3%	14,589	2%
Leukemia	61,152	3%	23,753	4%
Pancreas	56,654	2%	47,683	8%
Thyroid	52,912	2%	2,161	0%
Liver	42,284	2%	31,078	5%
Stomach	26,259	1%	11,413	2%
Brain, central nervous system	24,538	1%	18,133	3%
Lip, oral cavity	24,470	1%	4,285	1%
Ovary	23,820	1%	14,359	2%
Oesophagus	18,309	1%	16,209	3%
Total	2,281,658		612,390	

Table 1: New cases of cancer and deaths in the US for 2020.

1.1.2 Cancer Stages and Survival

A cancer diagnosis is assigned a stage that indicates the severity and progression of the disease. The stage of the cancer is used to determine optimal treatment options and survival likelihood. Table 2 shows the 5-year survival rate for a collection of tumorous cancer types based on the location in the body which can be local, regional, or distant.[4] Local is an invasive growing cancer that is confined to the original organ.[2] Regional cancers are known to invade surrounding tissue and can also affect the nearby lymph nodes. Distant cancers have spread to remote parts of the body away from the primary tumor site either by direct extension or via metathesis. The stage of the cancer is determined by a variety of tests depending on the type and location; but include physical examination and tests such as mammography, X-rays, MRI, CT scan, PET scans, ultrasound, endoscopy, colonoscopy, blood tests, and biopsy. The general trend of the data in Table 2 identifies a significant decrease in survival rates based on more advanced stage of diagnosis. For

Table 2: 5-year survival rate for solid tumor cancers based on stage of diagnosis. (Taken from the American Cancer Society)

Five-year Relative Survival Rates (%) by Stage at Diagnosis, US, 2010-2016				
	All stages	**Local**	**Regional**	**Distant**
Breast (female)	90	99	86	28
Colon	63	91	72	14
Rectum	67	89	72	16
Esophagus	20	47	25	5
Kidney	75	93	70	13
Larynx	61	78	45	34
Liver	20	34	12	3
Lung & bronchus	21	59	32	6
Skin melanoma	93	99	66	27
Oral cavity & pharynx	66	85	67	40
Ovary	49	93	75	30
Pancreas	10	39	13	3
Prostate	98	>99	>99	30
Stomach	32	70	32	6
Testis	95	99	96	73
Thyroid	98	>99	98	55
Urinary bladder	77	69	37	6
Uterine cervix	66	92	58	17
Uterine corpus	81	95	69	17

example, the survival rate of breast cancer patient when diagnosed as local is 99%; however, if the cancer spreads to the regional or distant stage, the survival odds decrease significantly to 86% and 28%, respectively. Other cancer types have a similar result, as with the case of distant spread pancreatic cancer where only 3% of patents are expected to survive 5 years. This data stresses the need for improved detection methods, and the need for enhanced treatment options for advanced cancers. Regular diagnostic testing, such as the Papanicolaou test has been used for early identification of cervical cancer for the past 70 years and as a result there has been a 70% decrease in cervical cancer related deaths since 1950.[5] While early identification is ideal for enhanced treatment outcomes, many cancer types, such as blood cancers, present unique challenges for diagnosis and treatment.

Diagnosing blood cancer requires a comprehensive blood test to measure levels of individual cell types that comprise the blood; including plasma, red blood cells, white blood cells, and platelets.[6] To date, no simple diagnostic tests have been developed to identify irregularity in the blood and most blood cancers patients are unaware they have cancer until symptoms such as anemia, shortness of breath, fever, bone pain, and confusion. The disfunction of each of these types of cells type identifies the type of blood cancer including leukemia, lymphoma, and myeloma. Leukemia is the dysfunction of white blood cells and is the most common form of blood cancer in children under 15.[7] Lymphoma is a malfunction of the lymphatic system that affects the lymphocytes carried by white blood cells. Myeloma is the dysfunction of plasma which carries antibodies and nutrients thought the body. The relative survival rates for these cancer types from 1975 to 2016 is illustrated in Figure 1. While the remission rates for all blood cancer types has improved, myeloma remains the deadliest with only 54% of patients surviving longer than 5 years.[6]

This data shows a need for new treatment options to help reduce the mortality of blood-based cancers.

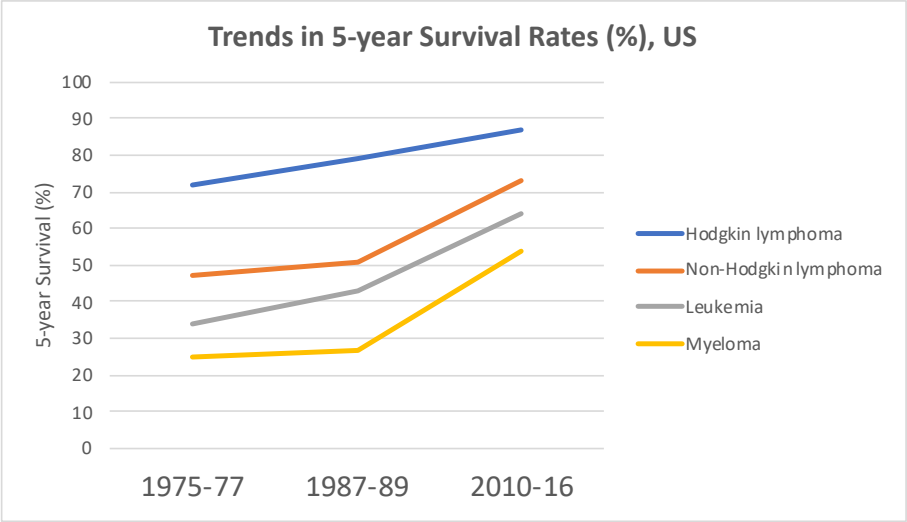

Trends in 5-year Survival Rates (%), US			
	1975-77	1987-89	2010-16
Hodgkin lymphoma	72	79	87
Non-Hodgkin lymphoma	47	51	73
Leukemia	34	43	64
Myeloma	25	27	54

Figure 1: Trends in 5-year survival rates for blood cancers based on stage of diagnosis.

1.1.3 Treatment options

Depending on the type of cancer, stage, and aggressiveness, treatment options are generally a combination of localized and systematic approaches. Localized cancer treatments include surgery, radiation, and cryotherapy by targeting an area of cancerous tissue. Surgical removal of the cancerous tissue was the predominant form of cancer treatment until the 1960's when remission rates plateaued at ~33%.[8] Unknown at the time, attempts to surgically remove the tumorous cells left behind small portions of the cancer, called micrometastases, leading to cancer recurrence. Together the inability to treat metathesized cancers, the invasive procedures, and the inability to treat non-tumorous cancer types such as blood cancers, continues to limit localized therapeutic options. To improve remission rates, systematic treatments were envisioned to be used in tandem

to treat the remaining cancer cells. Systematic treatments circulate the bloodstream acting on all cells and can include; immune therapy, hormone therapy, and chemotherapy. Chemotherapy has become the predominant form of treatment with approximately 650,000 of all cancer patients per year receiving chemotherapy in the US.

1.1.3.1 Chemotherapeutics

Of the numerous cancer treatment strategies, this work highlights the use of chemotherapeutic approaches, which are principally composed of small molecules. One example in the development of small molecule chemotherapeutics was designed by Gertrude B. Eliot and Dr. George H. Hitchings in 1950, who drew inspiration from the recently discovered structure of DNA. Their efforts were aimed at developing nucleic acid analogs for cancer treatment. To this end, they synthesized 6-mercatopurine (6TP, **1**) which is biosynthetically transformed into 6-thioguanine (**2**) and incorporates into DNA acting as a guanine mimic, as shown in Figure 2. Compound **2** is incorporated into DNA after ribosylation and phosphorylation and activates the natural DNA mismatch repair mechanisms to induce apoptosis. These sulfur analogs have shown success for treatment of hematological cancers and continues to be used for the treatment of acute lymphocytic leukemia (ALL).[8] Through their work in the construction of nucleotide analogs Eliot and Hitchings were awarded the Nobel Prize in Medicine in 1988. Rapid distribution and use of 6TP in the 1950's helped to spur the foundation of

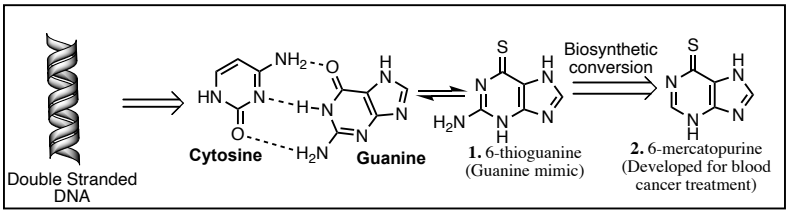

Figure 2: Chemotherapeutics 6-thioguanine (**1**), 6-mercatopurine (**2**) were based on nucleotide mimics.

chemotherapeutics. However, today's drug approval process has become extensive and lengthy due scrutinized regulations set forth by the US Food and Drug Administration (FDA).

1.1.4 FDA Drug Approval Process

The process of developing new therapeutics is both time and cost intensive, requiring on average 10 years and approximately $2.6 billion USD.[9] The strict drug regulations set forth by the FDA is a result of the 1962 drug crisis caused by thalidomide (**3**, Figure 3). Thalidomide was developed for treatment of morning sickness for pregnant woman and was originally sold as a racemic mixture; however, both enantiomers were not rigorously tested independently. Upon widespread European distribution, the drug was identified to cause sever birth defects impacting approximately 10,000 embryos with a 40% fatality rate.[10] Contrary to the European market where a majority of the cases occurred, the FDA's Dr. Frances Kelsey declined the drug approval for sale in the US. Dr. Kelsey's decision to refuse the approval of the drug not only saved many American lives but also inspired a wave of new regulations that scrutinize the FDA drug approval process. It was later discovered that the (*R*)-enantiomer was responsible for the therapeutic effects, while the (*S*)-enantiomer caused the toxic side-effects. The thalidomide crisis led to the current FDA regulation that requires full evaluation of drugs sold as racemates.

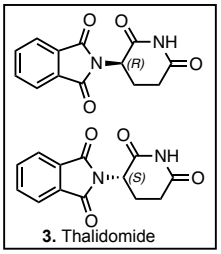

Figure 3: Structural isomers of thalidomide.

The FDA drug approval process is highly restrictive; on average one of 10,000 potential small molecule candidates acquires approval. The 4 stages of the drug approval process are depicted in Figure 4. The process starts with 5,000-10,000 lead compounds which are tested for biological activity. In this stage, the mechanism of action is identified in efforts to optimize the observed activity. Once a potential drug is identified, the pre-clinical investigation determines drug-like characteristics and bioavailability including traditional absorption, distribution, metabolism, excretion and transport (ADMET) evaluations. After the drugs characteristics are identified, clinical trials are undertaken to investigate the safety for human use. Each phase of clinical trials works with increasing populations of volunteer patients to identify drug safety and efficacy. Finally, the FDA reviews the data collected through the process and determines the approval status. The approval of the drug by the FDA does not end the agencies involvement. The FDA continuously monitors the status through post-market surveillance and if deemed necessary they can retract approval at any time.

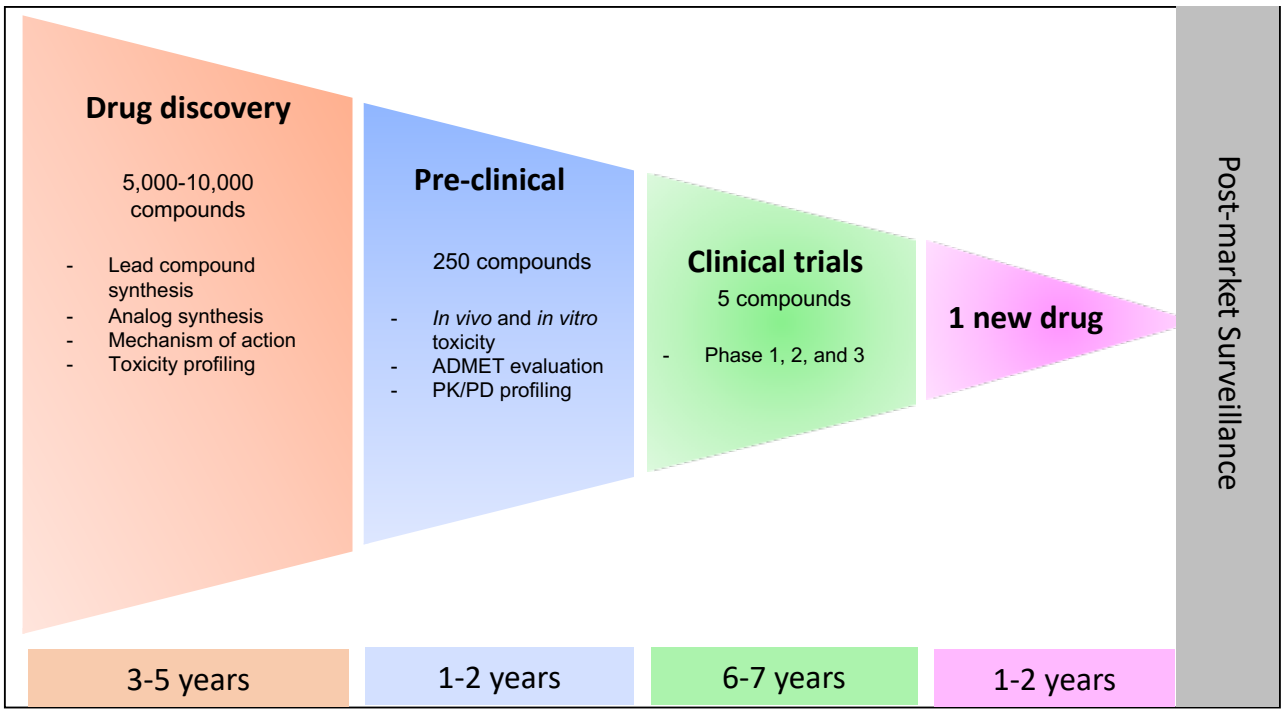

Figure 4: The drug discovery pipeline for new FDA approved compounds.

Rightfully, the process of developing new drugs for diseases, like cancer, is closely monitored and regulated. To develop a new cancer drug is time and costs intensive, so comparing the origin of the drug can help indicate which compounds are likely to be successful. Historically, a majority of the compounds that have led to FDA approved drugs are, or have been inspired by, naturally occurring compounds known as natural products (NPs). These naturally occurring compounds have dominated the field of small molecule therapies either as sole agents, hybrids, or as points of synthetic inspiration (vide infra).

1.2 Natural Products as Therapeutics

NPs are molecules isolated from any living organisms including aquatic and terrestrial species. A vast majority of all NPs are secondary metabolites, meaning their production is for non-essential functions such as cell signaling, defense, or mating. From 1946 to 2019, a majority of the drugs approved by the FDA have been based on NPs (Figure 5); including, unaltered NPs (N = 35), NP derivatives (ND = 65), synthetic drugs as NP mimics (S/NM = 38), synthetic drugs with a NP pharmacophore (S* = 22) and

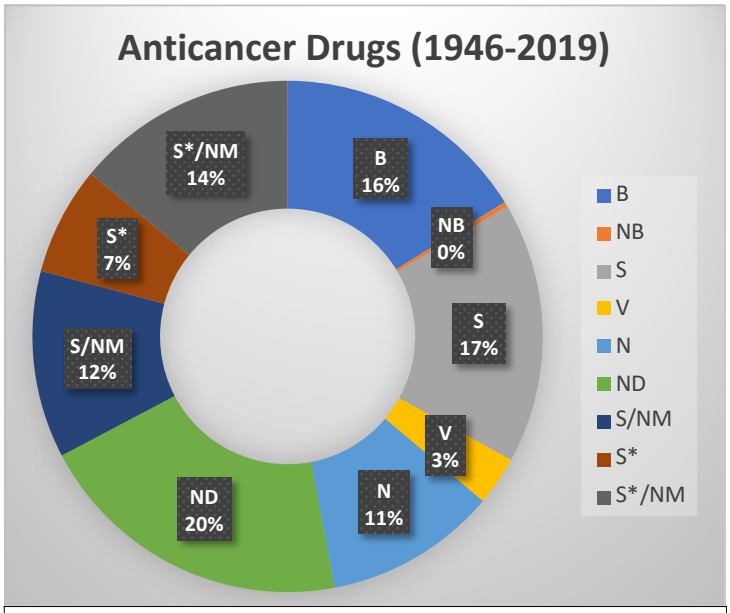

Type of Cancer Treatment	Abbreviation	# of FDA Approved
Biological Macromolecules	B	52
Botanical Drug	NB	1
Synthetic Drug	S	53
Vaccines	V	10
Unaltered Natural Products	N	35
Natural Product Derivatives	ND	65
Synthetic Natural Product Mimic	S/NM	38
Synthetic drugs (NP pharmacophore)	S*	22
Synthetic/ Natural product mimic	S*/NM	45
	Total	321
	Based on NPs	205
	% of NP Drugs	**64%**

Figure 5: Prevalence of natural products in FDA approved chemotherapeutics.

synthetic drugs acting as NP pharmacophore mimics (S*/NM = 45). Other FDA approved treatments include biological macromolecules, botanical drugs, synthetic drugs, vaccines, but combined have not yet surpassed the utility of NPs as medicines. Moreover, with respect to the development of cancer treatments, 40 of the 75 small molecule approved by the FDA from 1946 to 1980, were based on NPs and despite advances in high throughput screening and computer aided drug design, this has continued from 1981 to 2019, with 120 of the 185 cancer treatments deriving from NPs.[11]

The use of NPs in drug development continues to be critical. Illustrated in Figure 6 is a representative sample of NPs that have been approved, or are under investigation by the FDA, this list is not inclusive. Included in this list are anticancer compounds, including arglabin (**4**), masoprocol (**5**), vinblastine (**7**), pentostatin (**8**), doxorubicin (**10**). In addition, some NPs have immunosuppressive activity like myfortic acid (**6**), antibacterial activity as in the case of penicillin G (**11**), cognitive enhancing abilities; as with galantamine (**9**), and pain management compounds such as morphine (**12**). However, the use of NPs from isolation is limited by the finite amount present within the original organism. For example, the isolation of

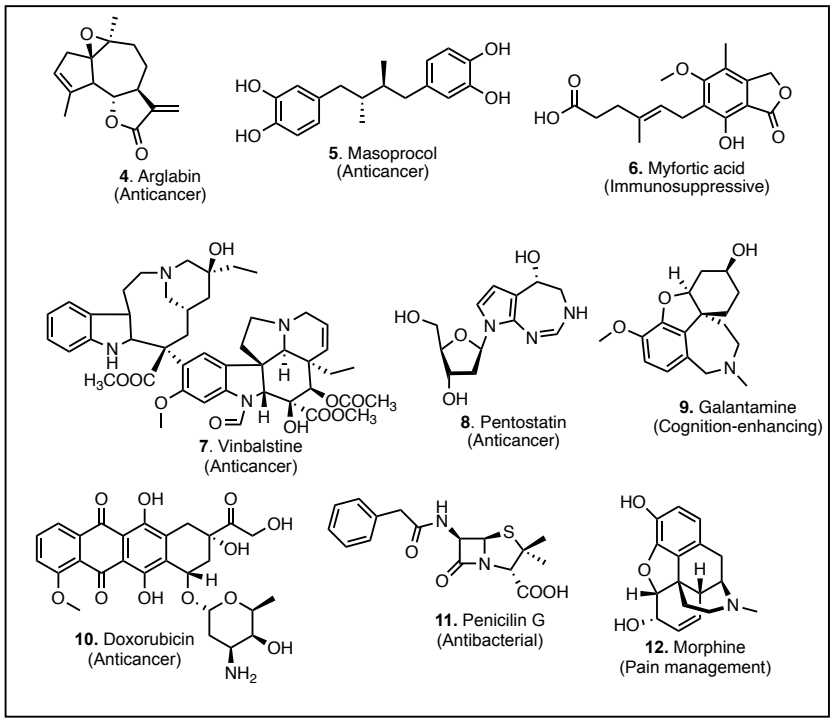

Figure 6: Examples of NPs approved or under investigation by the FDA.

vinblastine (**7**) requires 1 liter of cultured fungi from the leaves of *Catharanthus roseus* to produce 76 μg of the drug.[12] There are several ways of producing NPs including fermentation and extraction, semi-synthesis, and total synthesis.

1.2.1 Methods of Accessing NPs

There are three main methods for accessing NPs including extraction or fermentation, semi-synthesis, and total synthesis. Advances in NP biosynthetic pathways has enabled sustainable production of various drugs through fermentation and extraction. Penicillin G (**11**) remains the predominant method of treating bacterial infections with more 3 x 10^7 kg/year being produced through fermentation.[13] Production of pharmaceuticals from microorganisms has had an overwhelming contribution in the last 80 years, and with 99% of bacteria and 95% of fungi having never been cultivated in a labs, the potential of cultivated NPs is optimistic. However, low quantities of the NPs can be demanding to some organisms and can negatively impact their ecosystems. In these cases, a biosynthetic intermediate can be isolated, and a semi-synthetic route can be developed to access to the drug in large-scale. The semi-synthetic method has been particularly useful for the production of Paclitaxel (known as Taxol, **13**, Figure 7). Taxol was originally isolated from the bark of the pacific yew (*Taxus brevifolia)* and is a widely used

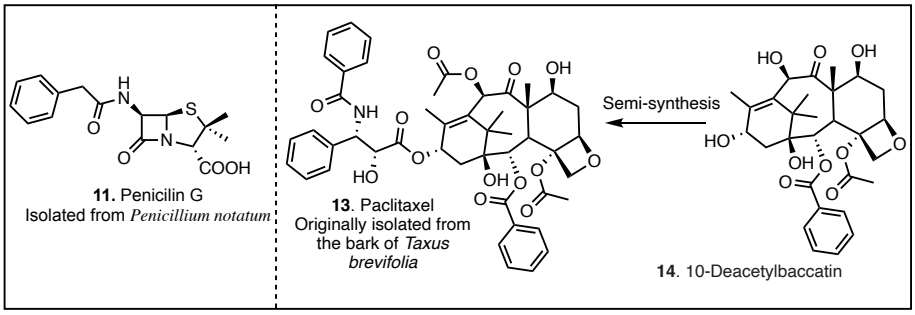

Figure 7: Natural products can be produced by fermentation like Penicillin G (**11**), from semi-synthesis such as Paclitaxel (**13**) arising from 10-deacetylbaccatin (**14**)

chemotherapeutic to treat breast, lung, and ovarian cancer; however, harvesting from the bark of the tree is fatal and provides limited quantities of the drug. Luckily, a biosynthetic intermediate, 10-Deacetylbaccatin (**14**), was discovered to be abundant in the pine needles allowing for non-toxic harvesting and a semi-synthetic route was developed to access **13** for commercial use. Accessing NPs through total synthesis continues to be a rich source of knowledge. In addition to allowing scalable access to the drug, total synthesis routes also expand our knowledge of the biosynthetic pathways used to produce the compound and leads to the development of new chemical reactions. Additionally, total synthesis can enable testing of synthetic intermediates to determine structure activity relationship (SAR) and can generate new analogs of the NP for further testing. Overall, total synthesis is a powerful tool to access NPs but can also serve as a technique to learn about the therapeutic mode of action.

1.3 Types of Natural Products

NP are grouped into classes based on their structural features. There are many types of NPs including, but not limited to, alkaloids, peptides, terpenes, and chalcones. The focus of this work is on peptide NPs, including both cyclic peptides and depsipeptides. Peptide-based NPs have diverse biological activities and have led to several FDA approved drugs. This work will highlight our synthetic efforts towards two molecules in the class and will look to harness the peptide core to develop novel drug delivery platforms.

1.3.1 Peptide Natural Products

Peptide-based NPs, both linear and macrocyclic, have continued to be a rich source of bioactive compounds. Peptide NPs currently occupy ~2% of the drug market; however, with more

than 600 compounds under investigation in the preclinical stage, this class is likely to have an increasing impact in future of drug development.[14] Currently there are 60-70 peptide drugs approved for the global market, including gramicidin S[15] (**15**) tyrocidine (**16**), kurahyne B[16] (**17**), and dolastatin15[17] (**18**) (Figure 8), and more than 100 other molecules are currently under clinical investigation.[18] Within the peptide family, proline-rich peptides show diverse biological activity including; antibacterial, antifungal, cytotoxic, immunosuppresive, anti-inflammatory, anti-HIV, and antiviral. Interestingly, the structural conformation of proline-rich cyclic peptides has been suggested to play a key role in the biological activity.[19]

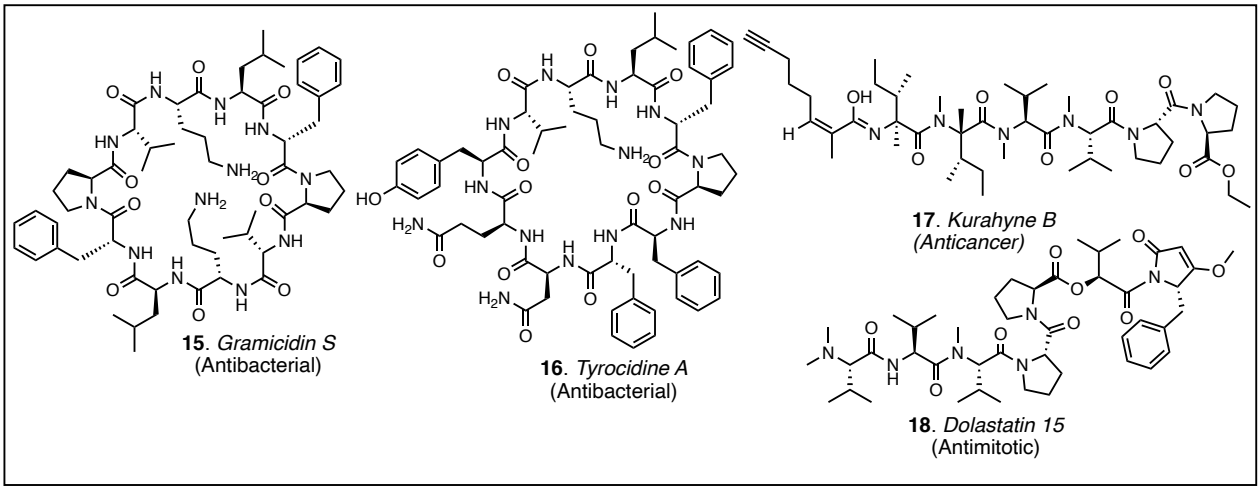

Figure 8: Chemical structure of FDA approved peptide natural products. Gramicidin S (**15**), Tyrocidine A (**16**), Kurahyne B (**17**), and Dolastatin 15 (**18**).

1.3.1.1 Proline-Rich Cyclic Peptides

Linear peptides with less than 10 amino acids are considered highly flexible; however, peptides with 10 to 20 amino acids can adopt secondary confirmations in the form of α-helices, and β-turns, and other conformations.[19] In some cases, cyclized peptides are restricted to a limited number of molecular configurations which is suggested to enable more specific interactions within cells.[20,21] Proline-rich cyclic peptides have been shown to possess diverse biological activities,[19] which is suggested to arise from the constrained geometries of the tertiary nitrogen of proline.[21]

These cyclic proline-rich peptides have prolonged half-lives in biological systems due to the limited confirmational flexibility. This is suggested to promote additonal resistance to enzymatic degradation via proteases, more specific interaction with protein targets, and are more membrane permeable than their linear counterparts. One recently discovered proline-rich peptide are the reniochalistatin family of NPs.

1.3.1.2 Reniochalistatin Family of Natural Products

The reniochalistatin family of NPs were isolated from *Reniochalina stalagmitis* by Lin and coworkers in 2014.[22] The isolation of the family was a result of a screening campaign in the South China Sea aimed to identify new bioactive peptides. All of the reniochalistatin family are proline rich, with reniochalistatins A-D (**19**-**22**) being heptapeptides and reniochalistatin E (**23**) an octapeptide (Figure 9). Reniochalistatin E was shown to possess modest cytotoxicity in multiple

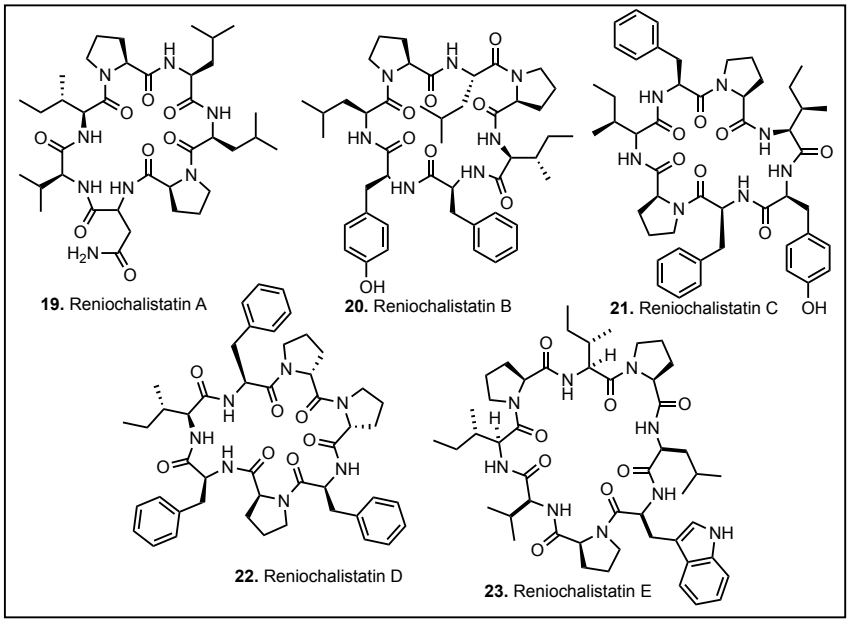

Figure 9: The reniochalistatin family of natural products: reniochalistatin A (**19**), reniochalistatin B (**20**), reniochalistatin C (**21**), reniochalistatin D (**22**), and reniochalistatin E (**23**).

cancer cell lines including myeloma (RPMI-8226, IC_{50} = 4.9 μM), gastric (MGC-803, IC_{50} = 9.7 μM), and cervical (HeLa, IC_{50} = 17.3 μM).

We speculate the modest cytotoxicity of reniochalistatin E is derivied from the enhanced cellular penetration associated with proline-rich cyclic peptides. In addition, we believe the cytotoxic activity in myeloma cells could be harnessed as a drug delievery vehicle. We hypothesize that conjugating reniochalistin E to potent theraputics could allow for enhanced penetration leading to new treatment strategies. To this end, we undertook the development of a total synthesis route to allow for additional biological evaluation and SAR investigations.

1.3.2 Depsipeptide Natural Products

Depsipeptides are defined as peptide containing NPs wherein one or more amide bonds are replaced by an ester(s) via a hydroxy acid moiety. Depsipeptides NPs have been shown to possess a variety of therapeutic properties, such as: anticancer, antifungal, antibacterial, cholesterol-lowering, antiparasitic, insecticidal, and immunosuppressive.[23,24] These types of NP have resulted in over 50 compounds investigated as potential drugs; however, only FK-228 has been approved by the FDA.[25]

The depsipeptide FK-228 (**24,** Figure 10), also known as Romidepsin, is a NP chemotherapeutic approved by the FDA in 2009 for the treatment of cutaneous T-cell lymphoma. Originally accessed

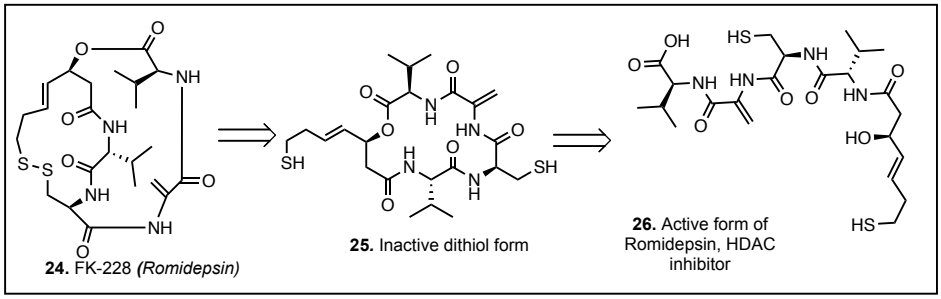

Figure 10: Activation of anticancer drug FK-228 (**24**) through reduction to the dithiol (**25**), and further activation through ester cleavage (**26**).

synthetically by Prof. Robert M. Williams at Colorado State University, **24** is used for the treatment of lymphoma through the inhibition of histone deacetylases (HDACs). HDACs are responsible for altering the histone coiling of DNA which affects protein expression. However, **24** is known to be inactive in the original form and must be activated to elicit a therapeutic effect. The activation starts with the reduction of the disulfide, producing a dithiol (**25**); however, the length of the carbon tether is too short to reach the zinc binding domain of the HDAC protein. Hydrolysis of the ester within **25** to the open chain form (**26**) allows the thiol to reach into the binding sight of HDAC and bind to the zinc center within. This biochemical transformation of romidepsin is an example of a prodrug (vide infra).

1.3.2.1 Prodrug Chemotherapeutics

Prodrugs are therapeutics that possess a labile bond allowing bioconversion *in vivo* to the medicinal active species. Prodrugs can occur naturally, as seen with FK-228, or can be designed to overcome pharmacokinetic limitations such as; poor solubility/absorption, rapid metabolism/excretion, or pharmacodynamic limitations such as side-effects, off-target toxicity, and poor efficiency. Aldoxorubicin (**27**, Figure 11) was designed with two functional moieties imparted to allow for cancer cell targeting through human serum albumin (HSA) conjugation. Efficient delivery of the doxorubicin (**29**) is acquired by the rapid uptake of HSA by cancer cells,

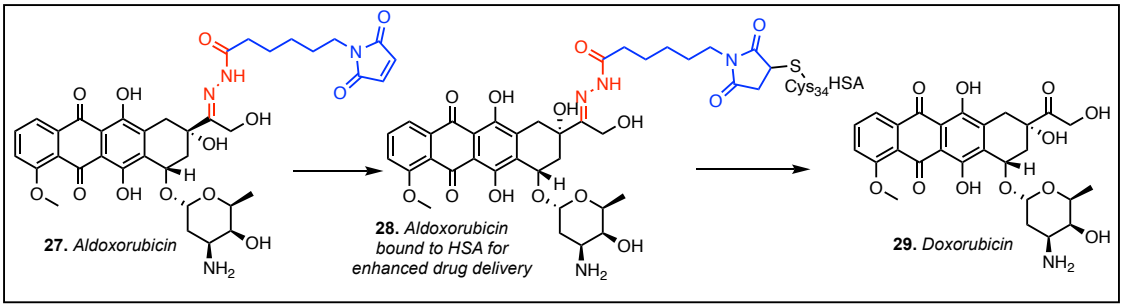

Figure 11: Aldoxorubicin (**27**) is bio converted to the active form, doxorubicin (**29**) through two steps. First human serum albumin (HSA) adds into the maleimide moiety (shown in blue), followed by acidic cleavage of the hydrazone linker (shown in red).

and cleavage of the hydrazone linker. The targeting of cancer cells via HSA is accomplished via covalent modification by the cysteine (C34) residue within HSA to the alkene moiety of the maleimide functional group (shown in blue on **27**). Circulation of HSA leads to accumulation of the drug-conjugate near the tumor site where the hydrazone linker (shown in red) is cleaved by the acidic microenvironment of the tumor releasing doxorubicin (**29**) near the cancer site. This prodrug allows for enhances efficiency and decreased toxic side-effects associated with **27** treatment alone.

While aldoxorubicin has shown success as a rationally designed prodrug, this strategy does not work in all cases. Altering the structure of a drug by adding prodrug moieties can affect the biological activity and render the molecule inactive. For this reason, it is important to understand the active portions of the drug, also known as the pharmacophore. To explore what portion of a new drug is active, SAR investigations are undertaken by synthesizing analogs and performing biological evaluation. In the synthetic works of FK-228, researchers identified that replacing the ester linkage with an amide prevented ring-opening and rendered the molecule inactive.[26] Analog synthesis and SAR can help to understand the active pharmacophore of the molecule and help to identify how the molecule elicits a therapeutic effect, such as a ring-opening in the case of FK-228. In the case of NPs, SAR investigations can be done during synthesis by performing biological testing on synthetic intermediates and structural analogs. This can illuminate key features of the molecule and provide evidence for the drugs mechanism of action. Naturally occurring prodrugs containing hydrolyzable bonds, such as esters, and disulfides are common in depsipeptide NPs.

1.3.2.2 Aurilide Natural Products

Another family of bioactive depsispetide NPs is the aurlide family. Aurilide (**30,** Figure 12) was first issolated in 1996 by Suenaga and coworkers from the Japanese sea hare *Dolabella Auricularia*.[27] Later, aurilide B (**31**) and aurilide C (**32**) were isolated by Gerwick and coworkers in 2006 from a sample of *Lyngbya majuscula* harvested in Papa New Guinea.[28] The aurilide family were identified to consist of two subunits namely, a hexapeptide containing two α-hydroxy acid residues linked to a stereospecific dihydroxy acid polyketide, highlighted in blue. The structure of the peptide differ by single amino acids changes, shown in red in Figure 12. Cytotoxic evaluation of the class revealed potent toxicity in a number of cancer cell lines including; HeLa cells (**30,** IC_{50} = 1.2 μg/mL), NCI-H460 human lung tumor cells (**31,** LC_{50} = 0.04 μM, **32,** LC_{50} = 0.13 μM) and neuro-2a mouse neuroblastoma cells (**31,** LC_{50} = 0.01μM, **32,** LC_{50} = 0.05μM). In addition, **31** was tested for activity in the NCI-60 cancer cell line panel showing a mean GI_{50} of less than 10 nM with potent activity in leukemia, renal, and prostate cancer cell lines.

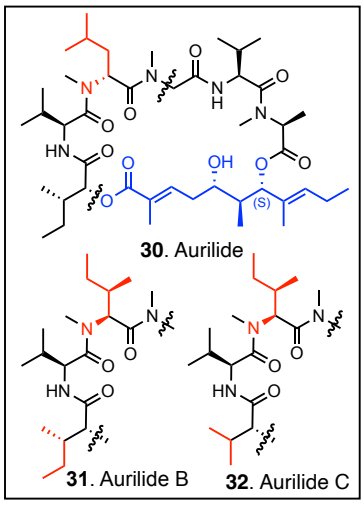

Figure 12: The Aurilide NP family: Aurilide (**30**), Aurilide B (**31**), Aurilide C (**32**).

1.3.2.3 Lagunamide Family of Depsipeptides: Isolation and Characterization

In 2010 Tan and coworkers isolated the lagunamide family of NPs, new bioactive secondary metabolites from a sample of cyanobacteria *Lyngbya majuscula* from a lagoon in Singapore. Through their efforts, they reported the strucutral elucidation and biological evaluation of lagunamide A (**33**) and lagunamide B (**34**), shown in Figure 13.[29] One year later, Tan and

coworkers reported the isolation of lagunamide C (**35**) from the same biological source.[30] The lagunamide family grew in 2019 when Luesch and coworkers isolated laguanmide D (**36**) from the same bacterium harvested near the Florida coast.[31] Compounds **33, 34,** and **36** are 26-membered macrocyclic depsipeptides differing only by an exocyclic carbon chain, shown as R in Figure 13. In contrast, **36** is the first 27-membered macrocycle of the class owing to the additional methylene carbon (C39) within the polyketide. Only 4.7 mg of **36** were obtained from the 169 grams (0.003% extraction yield) of the cyanobacterium. The stereochemistry of the polyketide was determined by adjacent proton coupling calculations ($^3J_{H,H}$) and 2D NOSEY correlations from which the following assignemnts were made: C37(*S*), C38(*S*), C40(*R*), and C41(*S*). However, the limited quantity of the NP prevented full confidence of the polyketide stereochemistry (vida infra). Biological testing of **36** revealed potent cytotoxicity in a number of cell lines including; murine leukemia (P388: IC_{50} = 24.4 nM,), lung carcinoma (A549: IC_{50} = 2.4 nM), prostate cancer (PC3: IC_{50} = 2.6 nM), ileocecal colorectal adenocarcinoma (HCT8, IC_{50} = 2.1 nM), and ovarian cancers (SK-OV3: IC_{50} = 4.5 nM). In addition, **36** was tested for antimalarial activity in *Plasmodium falciparum* with IC_{50} value of 0.29 μM, and showed weak anti-swarming acitivty against gram-negative bacterial growth when tested at 100 ppm against *Pseudomonas aeruginosa* (PA01). The potent cytotoxicity and diverse biological activity of the aurilide class has drawn interest from several research labs; resulting in the total synthesis of lagunamide A;[32–36] however, there have been no reports of synthetic efforts towards lagunamide B to date.

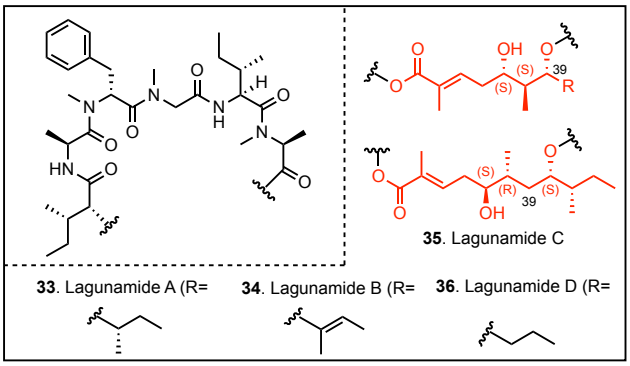

Figure 13: The lagunamide family: lagunamide A (**33**), lagunamide B (**34**), lagunamide D (**36**), and lagunamide C (**35**).

1.3.3 Research Motivations

With no previously reported total synthesis of either reniochalistatin E or lagunamide C, we set out to design a synthetic route to access each. Moreover, the anticancer activity and the limited understanding of these molecules drew our interest for acquiring a deeper understanding of their biological activity. We hypothesized these molecular frameworks could be used to develop new and potent drug delivery systems and as sole therapeutics agents. To this end, a conjugation strategy was envisioned to generate new prodrugs to repurpose currently approved chemotherapeutics. This work looks to use total synthesis as a tool to develop new and effective chemotherapeutics for the treatment of cancer.

Chapter 2- Previous Work Towards Peptide NPs and Biological Evaluation

2.1 Research Motivations and Chapter Outline

Reniochalistatin E and lagunamide C are peptide based NPs that have complex biological activity; however, no synthetic efforts have been made for further studies. The unique strcutral features of both molecules such as the proline rich cyclic peptide, or the stereoselective polyketide drew our interest to develop a total synthesis route to study their mechanism of toxicity. The previous works identifying the general cytotoxicity of the molecules encouraged the hypothesis that each has the ability to penetrate cancer cells to elicit a toxic effect. Moreover, devloping a total sysnthesis route would allow for exploration of these NPs as a new platforms for drug delievery systems. This chapter will focus on the general protocols for the formation of peptide based NPs and discuss the previous used routes to access the polyketide structure of the aurilide class of NPs. Finally, a comparison of the work will be done to rationalize each synthetic route and highlight the utility in developing a synthesis towards lagunamide C.

2.1.1 Review of Synthetic Means to Access Peptide Natural Products

Linear and cyclic peptides have gained interest in the synthetic community due to their complex interactions with cells leading to diverse biological activity.[37–39] To synthesize peptide NPs, there are two main techniques; solid phase peptide synthesis (SPSS) and solution phase peptide synthesis. SPSS uses resin-bound amino acids as starting blocks for peptide chain formation, this allows for solvent washes to remove unreacted starting material, unused coupling reagents, and by products. However, a drawback of SPSS is the use of strongly acidic reagents,

like TFA, which are needed to cleave the peptide from the resin and are known to cause epimerization in some cases. In contrast, solution phase peptide synthesis requires both aqueous workup and chrotomographic purification for each amino acid addition. While more time consuming, it allows for full characterization of the intermediates which can be tested for biological activity helping to identify potential SAR. Solution phase peptide synthesis employes an array of coupling reagents that assist in the formation of peptide bonds.

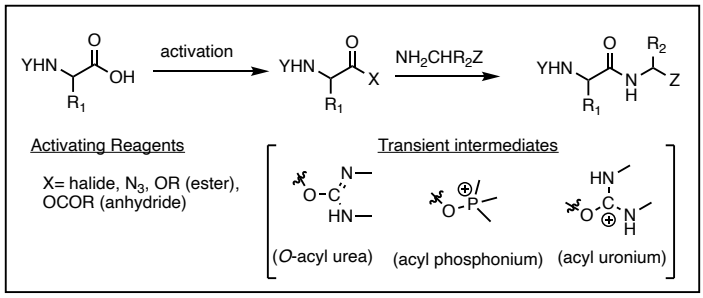

Scheme 1: General amide bond formation.

2.2 Peptide Coupling Reagents

Numerous methods allow for the formation of amide bonds through nucleophilic attack of an amine to an activated carboxylic acid, shown in Scheme 1. Activation the carbonyl carbon through electron withdrawing groups such as, but not limited to; acid halides, azides, esters, and anhydrides can be generated by activating reagents to favor aminolysis. In addition, there are coupling reagents that form transient intermediates including acyl urea, acyl phosponium, and acyl uronium that further activate the carboxylic acid and enhance the formation of new amide bonds. To be discussed and compared are the relevant

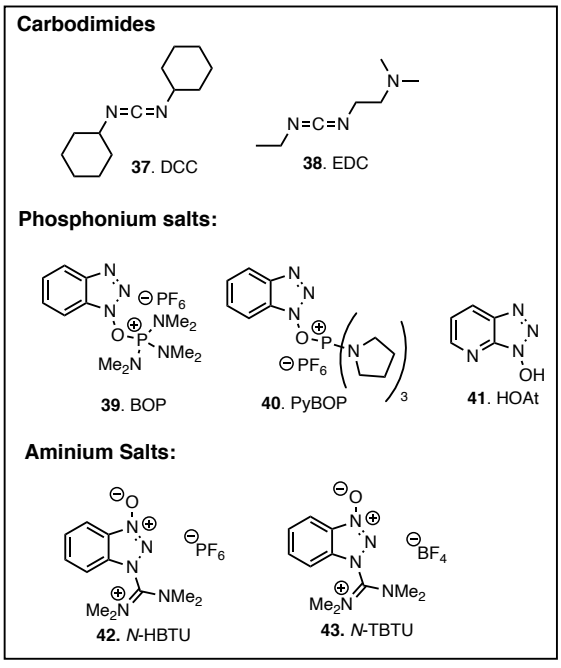

Figure 14: Standard peptide coupling reagents.

reagents to our synthetic efforts; including, carbodiimides, phosphonium salts, and aminium/uronium salts (shown in Figure 14). For a full list of peptide reagents there are several reviews.[39–41]

2.2.1 Carbodiimide Method

Carbodiimide methods employ reagents like DCC (**37,** dicyclohexylcarbodiimide), and EDC (**38**, 1-(3-dimethylaminopropyl)-3-ethylcarbodiimide) and are known as the traditional method for peptide coupling.[42] Mechanistically, the basic nitrogen in the carbodiimide structure is enough to deprotonate the carboxylic acid to form the *O*-acylisourea, as shown in Scheme 2; however, general reaction conditions include a base to assist in deprotonation. The activated *O*-acylisourea is highly reactive and aminolysis occurs rapidly. Carbodiiamide reagents can also facilitate by product formation in addition to standard urea displacement (Route I). Formation of the symetric anhydrides (Route II) can occur with the attack of a second moleclue of acid, but will enevitably be aminolyzed to the peptide product. Intramolecular attack by the nitrogen leads to formation of oxazolones (Route III), a lesser reactive intermediate, which limits the activation of the carbonyl carbon and increases steric bulk, therefore decreasing reactivity.[43] Nucleophilic attack upon this intermediate can be from either face and will lead to racemization of the product. Finally, rearrangement of the *O*-acylisourea to the *N*-acylurea (Route IV) is irreversible and

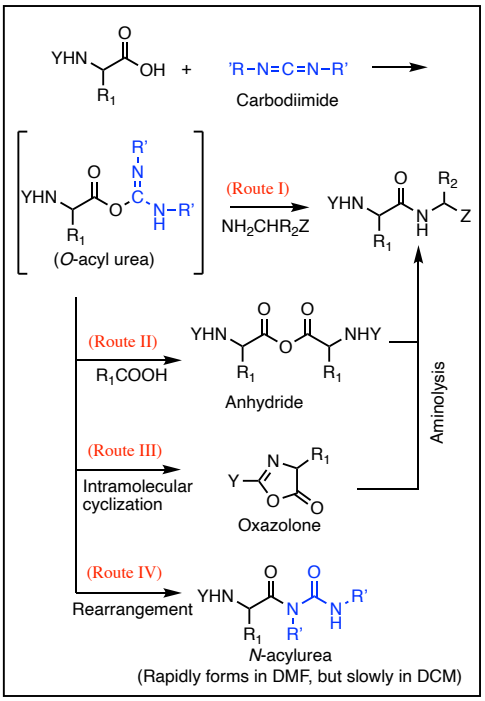

Scheme 2: Carbodiimide method of peptide formation.

prevents the formation of the desired peptide. Some solvents including dimethylformamide (DMF) favor *N*-acylurea formation leading to parcipitation and slows reaction progress; however, dichloromethane (DCM) has been shown to limit the formation of the *N*-acylurea and is the prefered solvent for carbodiimide reagents.[42] One disadvantage of the carbodiimide reagents are the incapatability with fluorenylmethyloxycarbonyl (Fmoc) protecting groups. An advantage of these reagents is the ease of purification via aqueous work up because the urea by product is aqueous soluble in acidic conditions. Moreover, reactions run with *N*-hydroxy compounds like 1-hydroxybenzotriazole (HOBt) or 1-hydroxy-7-azabenzotriazole (HOAt) can help to decrease by product formation and limit racemization.[43]

2.2.2 Phosphonium salts

Phosphonium salts such as BOP (**39**, (benzotriazol-1-yloxy)tris(dimethylamino)-phosphonium hexafluorophosphate), PyBOP (**40,** benzotriazol-1-yloxytripyrrolidinophosphonium hexafluorophosphate), and HOAt (**41**, 1-hydroxy-7-azabenzotriazole) are shown in Figure 14 (above). The mechanism of phosphonium salts starts with the deprotonation of the carboxylic acid followed by phosphonium addition. Mechanistically, there is debate over the activated species, but

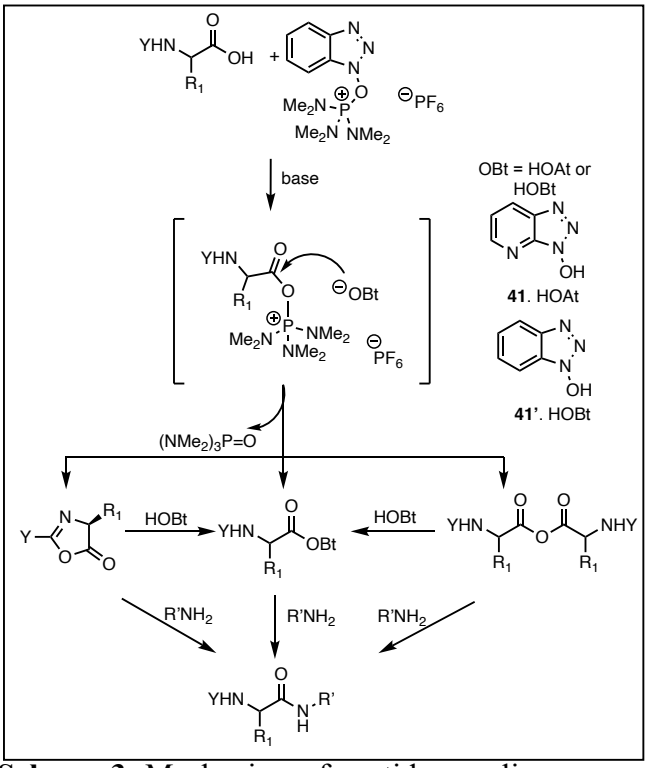

Scheme 3: Mechanism of peptide coupling through phosphonium salt.

the acyloxyphosphonium salt, shown in brackets in Scheme 3, is considered the key reactive intermediate. This activated species is then displaced by an N-hydroxy compound such as HOBt of HOAt further activating the carbonyl carbon and faciliatating amide bond formation. The acyloxyphosphonium salt can also undergo intramolecular cyclization to form the oxazolone, or attack from a second molecule of carboxylic acid to form an anhydride. In either case, either an N-hydroxy compound or amine attack will inevitably form the desired peptide. One advantage of the phosphonium salt is the lack of interaction with the amine which enables cyclization without excess reagent preventing coupling.

2.2.3 Aminium/Uronium salts

While phosphonium reagents contain a positivly charged phosphonium, the aminium/uronium salts contain a iminium ion, shown in Scheme 4. One equivelent of base forms the activated ester species leading to the *N*-acyl or *O*-acyl esters and favors amide bond formation at room temperature. Additional hydroxylamine derivatives allow for the displacement of the activating reagent and amide bond formation through nucleophilic amine attack. However, if the activation of the carboxylate is slow, the aminium/uronium salts can react with the amine functionality and terminate the peptide chain elongation. This limits the uronium salts applicability, as cyclization or fragment based

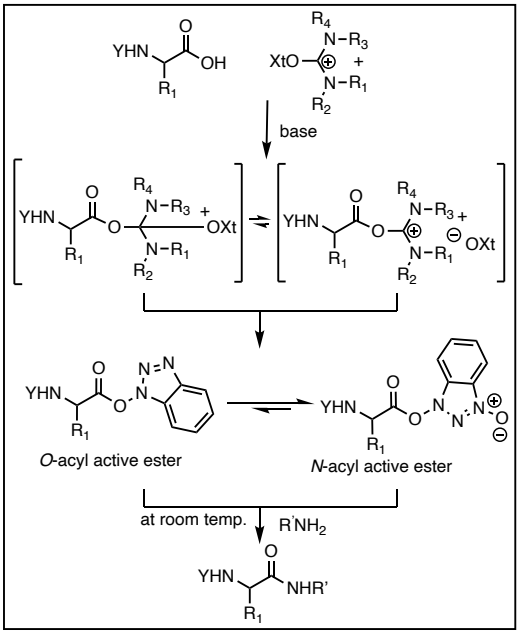

Scheme 4: Mechanism of aminium/uronium peptide coupling.

coupling reagents. This obstacle can as overcome with the use of selective protecting groups to mask the amine functionality.

2.2.3.1 Summary of Peptide Coupling Reagents

In the last 200 years peptide bond formation has evolved from Emil Fisher's original acid chloride formation to coupling reagents with high selectivity and broad substrate scope. While progress can still be made, peptide coupling reagents are a powerful tool for synthetizing new peptide-based NPs. The reactivity of the reagents discussed in this work are all viable options with distict advantages. For example, carbodiimide reagents when used in the proper solvent can allow for high yielding peptide bond formation and aqueous workup removes the urea by product of the reaction allowing for easier purification. Phosphonium salts are easy to use and do not react with the amine functionality making them highly usefull in cycilization conditions. Finally the aminium/uronium reagents are low cost and can be used on peptides with protecting groups enabling high yielding reactions. In summary, there are many reagents that can facilitate in peptide bond formation, and exploring each can allow for optimized yields to generate peptide NPs.

2.3 Previous Total Synthesis of Peptide Natural Products

Employing peptide coupling reagents has led to the total synthesis of several NPs including but not limited to; Zizyphine A (**44**), Seongsnamide B (**45**), Dendroamide A (**46**), Dehydrodidemnin B (**47**), and GE2270 A (**48**), shown in Figure 15. Each of these routes harnessed peptide coupling reagents to access the NP structure. With some expoloration of reaction optimization, peptide bond fomration has become a managable hurdel in the total synthesis of NPs. The favorable conditions of forming peptide bonds has been disclosed herein, and the reminder of this work will focus on efforts made towards the polyketide of depsipeptide NPs. Exploration of reaction conditions in the following sections are usefull to understand chemical reactivity, in addition to the peptide chemistry discussed, to achieve the total synthesis of lagunamide C.

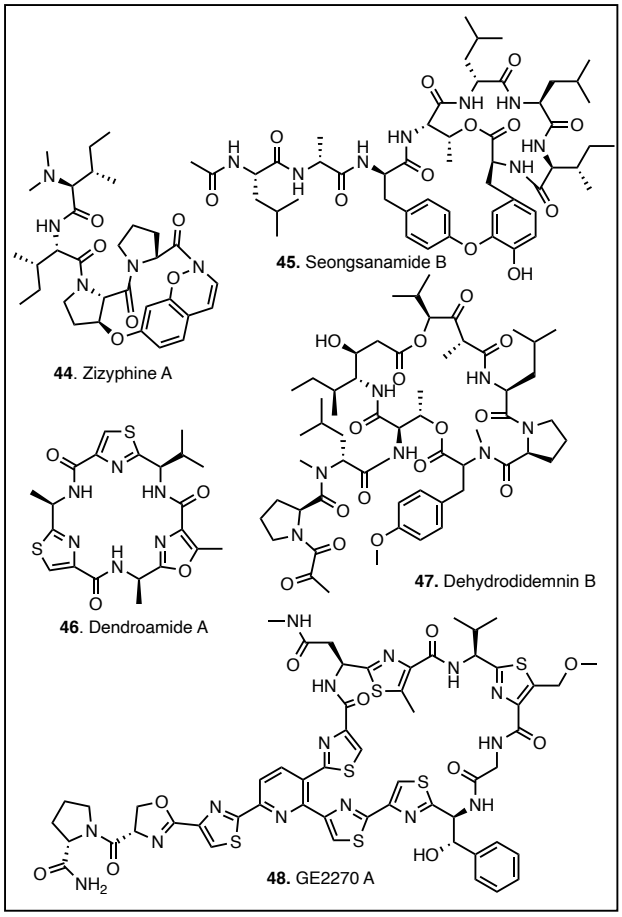

Figure 15: Peptide NPs accessed via peptide bond formation employing coupling reagents.

2.4 Synthesis of Cyclodepsipeptides

The depsipeptides discussed in this report are compounds of a polypeptide and polyketide components, which contains at least one ester in place of an amide bond. Biosynthetically, polyketides are synthesized via condensations of acetyl coenzyme A through malonyl coenzyme A, producing alternating carbonyl and methylene groups.[38] Synthetically, there are many strategies

for constructing polyketides; however this report will focus on the synthetic efforts made towards the Aurilide class of NPs. In addition, the biological activity and SAR findings of previous works will be discussed. This work will summarize the key synthetic steps in the stereoselective formation of the polyketides and will emphasize the critical need of a stereoselective approach towards lagunamide C by highlighting previously disclosed SAR investigations.

2.4.1 Aurilide Family of NPs

NPs are grouped into classes based on common structural features. One class of cyclodepsipeptides containing a polyketide and hexapeptide backbone are the aurilide family. The complete family of Aurilide NPs is shown in Figure 16. This class of NPs includes the aurilides (**30**-**33**), Odoamide (**49**), Kulokekahilide (**50**), palau'amide (**51**), and the lagunamides A-D (**33**-**36**) and have been shown to possess an array of biological activities including; antifungal, antibacterial, and anticancer. A key feature of this class is the 26-membered macrocyclic structure in all members except palau'amide, which is a 24-membered epimer, and lagunamide C (**35**) which has an added methylene (C37) in the polyketide making it the first 27-membered macrocycle of the family. The

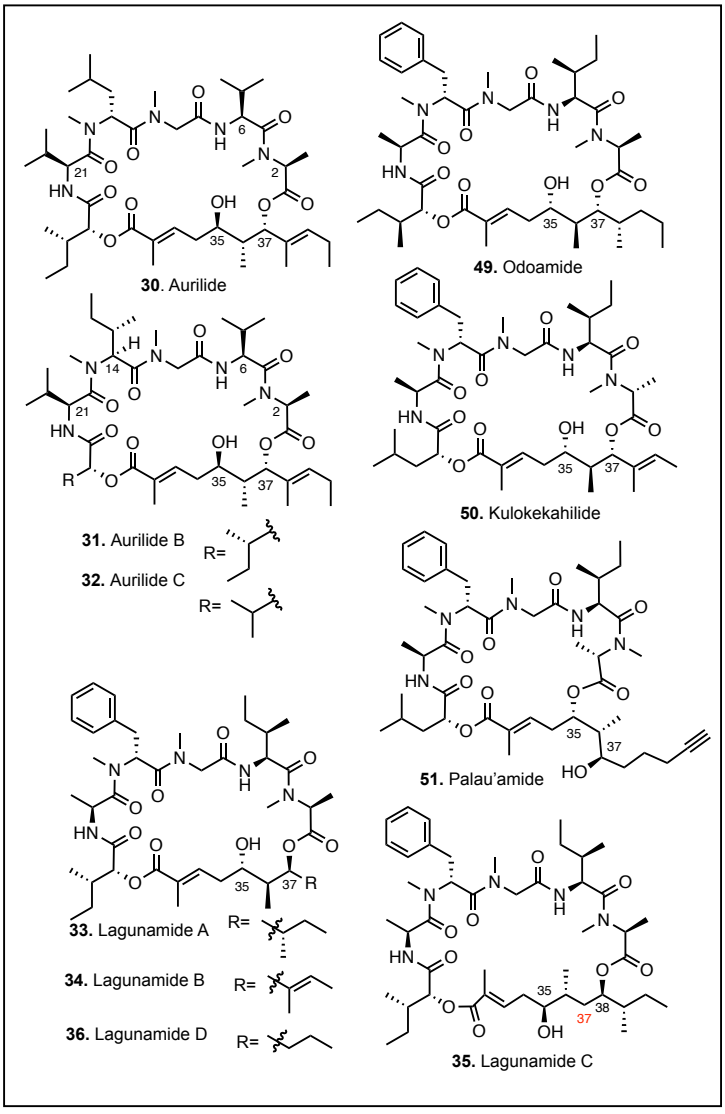

Figure 16: Aurilide class of NPs.

additional methylene requires a unique synthetic route to access the polyketide, but the previous works outlined herein, serve as a tool in developing a route to the first total synthesis of lagunamide C.

2.4.2 Synthesis of Aurilide Polyketide Fragment

Aurilide (**30**) was isolated in from the Japanese sea hare *D. Auricularia* in 1996 by Suenaga and coworkers.[27] To determine the absolute stereochemistry of the polyketide, **30** was reduced by $LiAlH_4$ and acylated using *p*-BrC_6H_4COCl to give **52**, shown in Scheme 5. However, they were unable to identify the absolute configuration of the 3 stereocenters in the polyketide fragment and proposed the structure **52**. To validate the stereochemistry, a synthetic route was designed to access

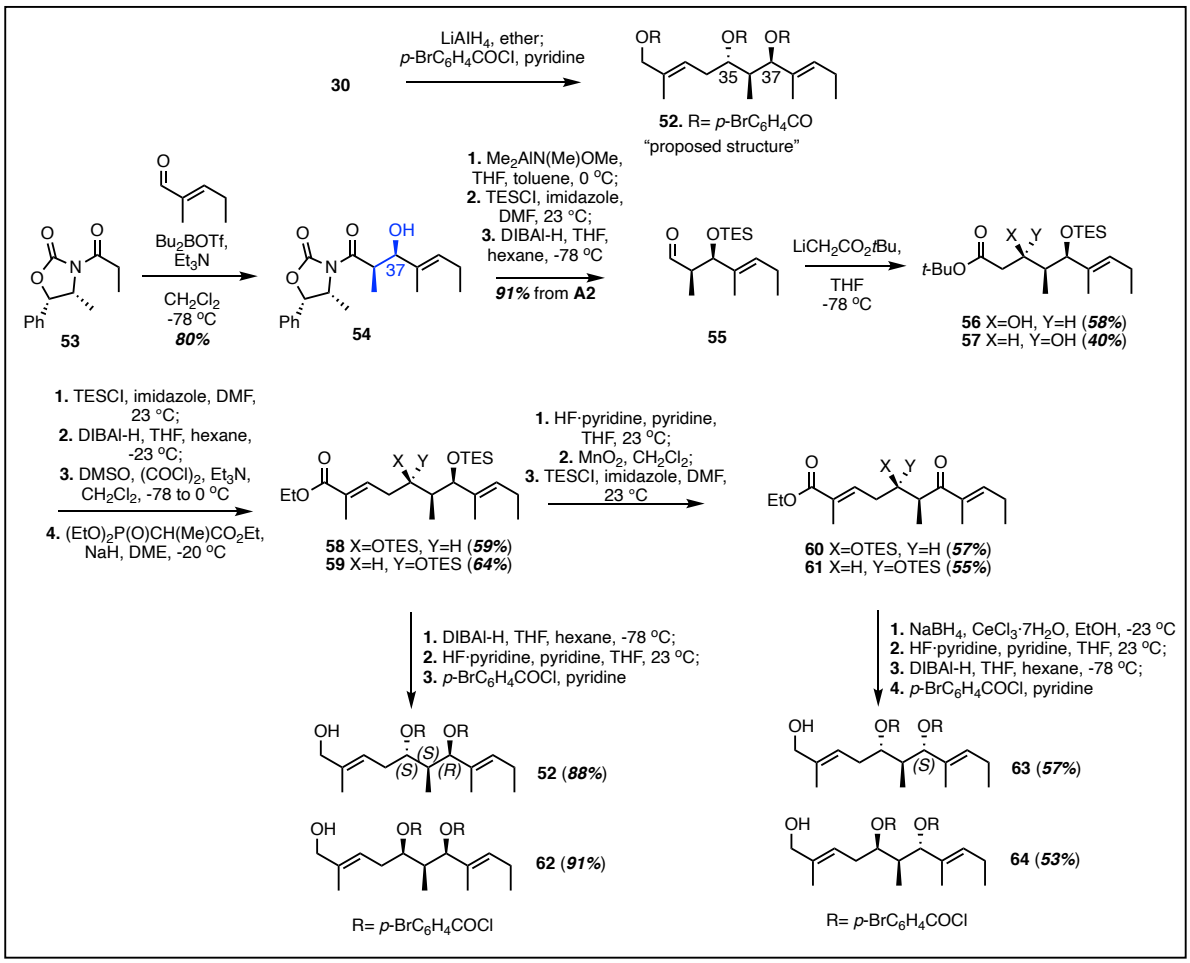

Scheme 5: Synthesis of the polyketide of Aurilide A by Suenaga and coworkers.

the four possible stereoisomers about C35 and C37 to be compared with the natural **52**. The synthesis, shown in Scheme 5, begins with a boron mediated aldol reaction with the *N*-propyl oxazolidinone (**53**) to give the Evan's *syn* product (**54**) in 80% yield. The Weinreb amide was generated followed by protection of the hydroxyl via triethylsilane (TES), and finally DIBAl-H reduction afforded aldehyde **55** in 91% over 3 steps. Nucleophilic attack by an organolithium containing the *t*Bu-ester provided both diastereomers about C35 to form **56** and **57** in 58% and 40% yield, respectively. The newly formed hydroxyl was protected with TES, followed by full reduction to the alcohol. Subsequent oxidation via Swern conditions provided an aldehyde which was subjected to Horner-Wadsworth-Emmons (HWE) olefination conditions to afford **58** and **59** in 59% and 64% yields, respectively. Each diastereomer was subjected to reduction under DIBAl-H conditions followed by a global deprotection of the TES groups and finally acylation to afford the **52** and **62** in 88% and 91% respectively. In order to access the C37(*S*) diastereomer, deprotection of **58** and **59** followed by MnO_2 oxidation afforded ketones **60** and **61** in 57% and 55% yield, respectively. The ketones were reduced to the 1,3-*syn*-diol and deprotected to afford the allylic alcohols **63** and **64** in 57% and 53% yield, respectively. This 9-step reaction sequence allowed for the synthesis of the 4 diastereomers (**52**, **62**, **63**, **64**) to be compared with **52** generated from **30**. The 4 diastereomers were analyzed by H^1 NMR and CD to assign the stereocenter polyketide as C35(*S*), C36(*S*), and C37(*S*).

In 1997 Mutou and coworkers used a similar route to achieve the enantioselective total synthesis of **30**.[44] Analogous to previous reports, a boron mediated enolate was generated from the

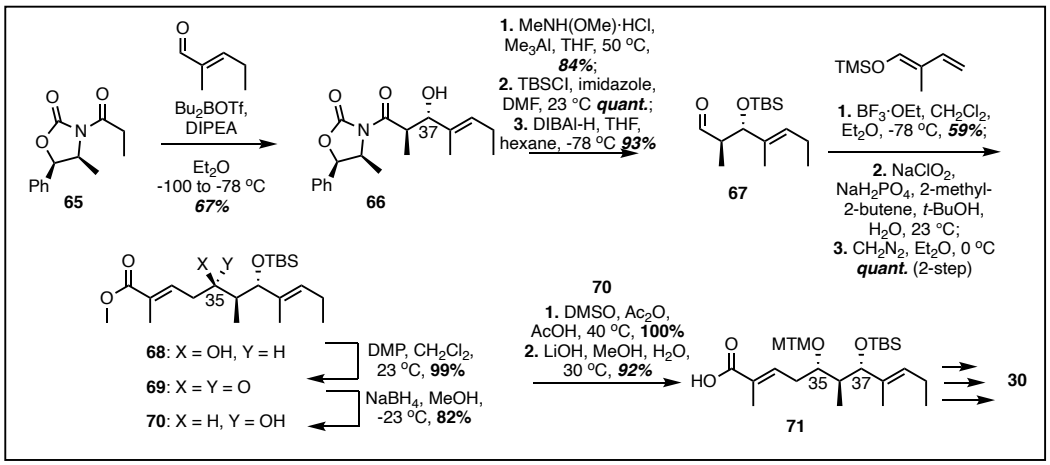

Scheme 7: Synthetic efforts towards the polyketide of Aurilide by Mutou and coworkers.

N-propyl oxazolidinone (**65**) providing the Evan's *anti* product (**66**) setting the C37(*S*) hydroxyl (Scheme 6). In an analogous approach to the previous report, Weinreb amide formation followed by protection via *tert*-butyldimethylsilyl chloride (TBSCl) and DIBAl-H reduction to afford the aldehyde **67** in 3 steps in 93% yield. Compound **67** was subjected to Mukaiyama aldol conditions with the TMS-enol ether (2-methyl-1-trimethylsiloxy-1,3-butadiene) (59% yield) and subsequent treatment with diazomethane afforded **68** in quantitative yields over 2 steps. However, these conditions afforded the C35(*R*) hydroxyl which was undesired. To overcome this, oxidation to the ketone via DMP produced **69** in 99% yield and was treated with $NaBH_4$ to afford the 1,3-*syn*-diol, successfully inverting the stereochemistry about C35 to the desired (*S*) configuration. The selectivity of this reaction can be understood by the 6-membered ring transitions state of the reaction, show in Scheme 7. Lithium coordination with the 1,3-diol forms a 6 membered ring which allows for facially selective reduction favoring the formation of the 1,3-*syn*-diol, **70**. Protection of the hydroxyl via methylthiomethyl

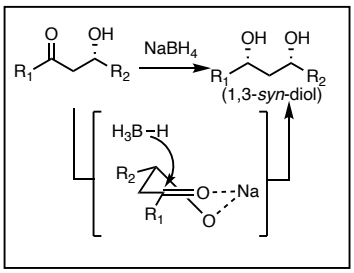

Scheme 6: Selectivity of 1,3-*syn*-diol formation.

ether (MTM), followed by saponification afforded the carboxylic acid **71** in 92% yield. From there, peptide couplings with the peptide portion allowed for the total synthesis of **30**.

In 2003, Takahashi and coworkers harnessed a similar route to access the polyketide fragment and explored the effects of peptide analogs.[45] A library of compounds based on the C37(*R*) diastereomer **52** was coupled to various pentapeptides described in Table 3.[46] The purity of each analog produced was determined by reverse-phase HPLC; however, the biological activity of these analogs has not been reported. To date, there have been no reported synthetic works towards **31**, or **32**, likely due to the high homology with **30**.

Table 3: Peptide analogs of Aurilide and observed purity.

	Sequence AA_4-AA_3-AA_2-AA_1	Purity (%)
1	D-Val-*N*-Me-L-Leu-Sar-D-Val	41
2	D-Val-*N*-Me-L-Leu-Sar-L-Val	26
3	D-Val-*N*-Me-D-Leu-Sar-D-Val	42
4	D-Val-*N*-Me-D-Leu-Sar-L-Val	31
5	L-Val-*N*-Me-L-Leu-Sar-D-Val	45
6	L-Val-*N*-Me-L-Leu-Sar-L-Val	42
7	L-Val-*N*-Me-D-Leu-Sar-D-Val	51
8	L-Val-*N*-Me-D-Leu-Sar-L-Val	57
9	D-Val-L-Leu-Gly-D-Val	25
10	D-Val-L-Leu-Gly-L-Val	47
11	D-Val-D-Leu-Gly-D-Val	36
12	D-Val-D-Leu-Gly-L-Val	42
13	L-Val-L-Leu-Gly-D-Val	36
14	L-Val-L-Leu-Gly-L-Val	58
15	L-Val-D-Leu-Gly-D-Val	48
16	L-Val-D-Leu-Gly-L-Val	45
17	L-Val-Sar-*N*-Me-D-Leu-L-Val	29
18	*N*-Me-D-Leu-Sar-L-Val-L-Val	27
19	*N*-Me-D-Leu-L-Val-Sar-L-Val	20
20	Sar-L-Val-*N*-Me-D-Leu-L-Val	22

2.5 Summary of Aurilide Polyketide Syntheses

In summary, the synthetic work towards aurilide has been an inspiration for the development of a route towards lagunamide C and are summarized in Figure 17. The key stereogenic steps in the 1997 Suenaga synthesis include a boron mediated Evan's aldol, a

nucleophilic addition via organolithium, and an HWE olefination to grant access to diastereomers of the polyketide in 18% over 9 steps. In 1997 Mutou achieved the total synthesis of **30** featuring key stereogenic steps such as; a boron mediated Evan's aldol reaction, TMS-enol ether addition, and a selective 1,3-*syn*-diol formation using $NaBH_4$. This route afforded the enantioselective synthesis of **30** with access to the polyketide subunit in 9-steps with an overall 25% yield. The Takahashi synthetic route featured analogous stereogenic steps to access the diastereoselective polyketide in 9-steps with an overall 26% yield. A library of compounds with various peptide moieties was described, but the biological activity was not reported.

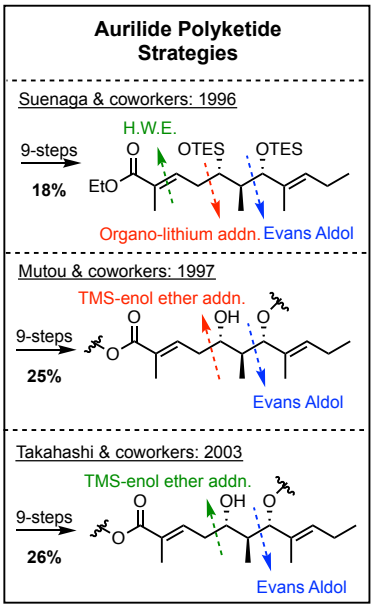

Figure 17: Summary of Aurilide polyketide strategies

The additional methylene within the polyketide (C37) of lagunamide C limits the above mention routes for the following reasons. Each of the above reaction sequences begin with an Evan's type aldol reaction with the *N*-acetyl variant of the chiral auxiliary. This aldol reaction sets both the C37 alcohol and the directly adjacent C36 methyl (shown in red, Figure 18). However, the additional methylene in lagunamide C requires the aldol reaction be with an *N*-propyl auxiliary, which have much lower enantioselectivity and reactivates (vida infra). Moreover, these routes previously described produce a mixture of diastereomers about

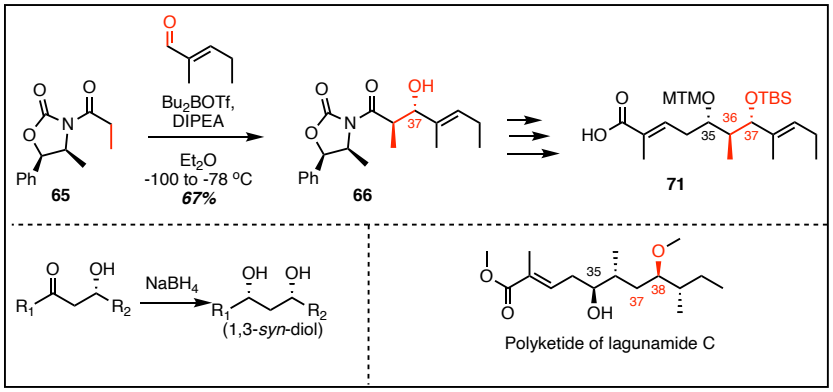

Figure 18: Highlights of the aurilide polyketide routes and the polyketide of lagunamide C

the C35 alcohol; or are dependent on a facially selective reduction that is observed in 1,3-*syn*-diol formation. In contrast, the polyketide of lagunamide C contains a 1,4-diol; meaning the controlled reduction induced by the 6-membered ring transition state is voided. However, the utility of these routes cannot be understated and was taken in high regard when developing the route towards lagunamide C.

2.6 Aurilide SAR Investigations

With synthetic access to aurilide via the routes discussed above, several groups aimed to identify the SAR of the molecule. In 2008 Suenaga and coworkers generated several analogs to be of **30** and examined the cytotoxicity in HeLa cells (Table 4).[47] Through their SAR investigations, they found that reduction of the alcohol at C35 (**72**) had little effect on the cytotoxicity (IC_{50} = 17 ng/mL) when compared to **30**. Further studies revealed that inversion of the valine from *L* to *D* (**73**) resulted in a loss of all cytotoxicity (IC_{50} = >4000 ng/mL). The addition of a Boc-protected amine via a carbon tether $(CH_2)_4$ at position C2 (**74**), C6 (**75**), or C20 (**76**) all significantly reduced cytotoxicity to IC_{50} = 20, 260, and 32 ng/mL, respectively. Taken together, these results indicate

Table 4: Analogs of **30** generated for SAR.

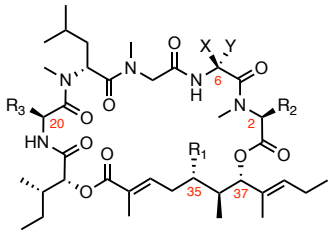

	R1	R2	R3	X	Y	IC50 (ng/mL)
30 Aurilide	OH	Me	*i* Pr	*i* Pr	H	2.4-11
72	H	Me	*i* Pr	*i* Pr	H	17
73	OH	Me	*i* Pr	*i* Pr	*i* Pr	>4000
74	OH	(CH2)4NHBoc	*i* Pr	*i* Pr	H	20
75	OH	Me	*i* Pr	(CH2)4NHBoc	H	260
76	OH	Me	(CH2)4NHBoc	*i* Pr	H	32

the importance of specific configuration of the amino acid residues in the peptide portion, and the need for further SAR investigations

2.7 Aurilide Mode of Action Investigations

In 2011, Sato and coworkers were able to isolate the protein target of **30** by using a polyproline linker at the C35 hydroxyl, as shown in Figure 19.[48] Identifying the C35 hydroxyl has limited effect on the biological activity from the work by Suenaga, the researchers attached a polyproline linker with a biotin moiety to identify the protein target of the NP. The analog was treated in cells and purified through gel electrophoresis showing a strong interaction with a 30-kDa protein band which was identified as prohibitin 1 (PHB1). Interestingly, the C6-epimer of **30** (**77**) was used to generate the linker molecule **79,** which showed a >1000-fold decreased interaction with PHB1. Several other biochemical and visualization experiments revealed **30** binds to prohibitin (PHB1) and disrupts mitochondrial fragmentation by effecting the optic atrophy 1 (OPA1) protein. The OPA1 protein has been previously reported to effect mitochondrial-mediated apoptosis[49,50], and

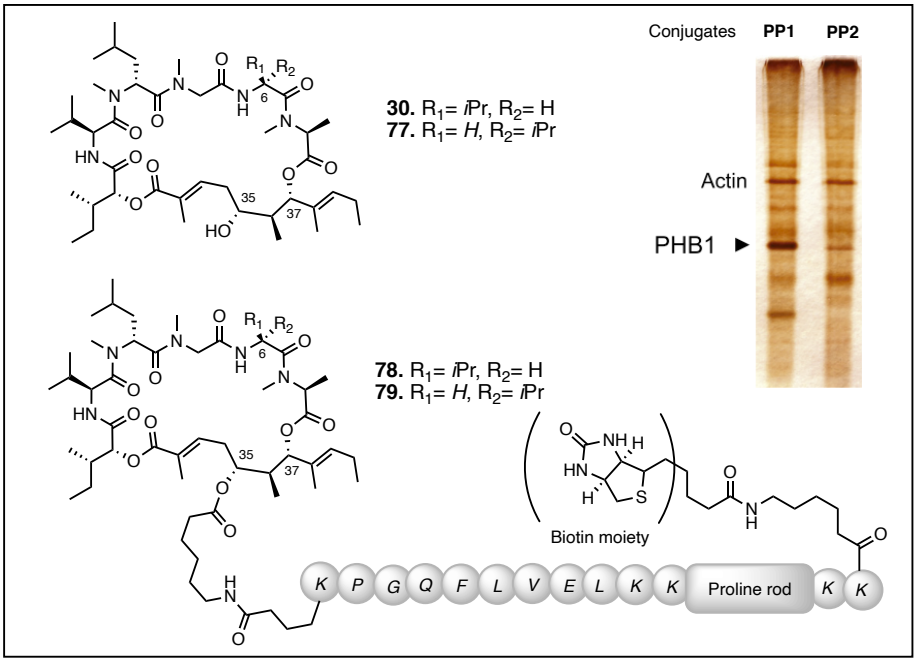

Figure 19: Sato and coworkers' investigation the mode of action of **30**.

for more information regarding the PHB1 and OPA1 proteins and their cellular interactions, please refer to the review by Scorrano and coworkers.[51]

In 2017, Takase and coworkers developed a barcoded genome-wide RNA interference (RNAi) library to determine the mode of action for **31**.[52] In conclusion, the gene expression of a Na+/K+ ATPase complex protein *(ATP1A1)* is downregulate upon treatment with **31**. However, there is no evidence of direct ATP1A1 inhibition, as there may be some other inhibition leading to decreased gene expression. In summary, how aurilide induces cell death is still unclear, but further studies will hopefully reveal its cellular interactions and mechanism of toxicity.

2.8 Synthesis and Stereochemical Determination of Kulokekahilide-2

Nakao and coworkers isolated kulokekahilide-2 (**50** in Figure 15) in 2004.[53] Their work on the structure elucidation revealed their newly isolated compound was composed of a heptapeptide and a polyketide similar to the architecture of **30**. To determine the correct structure of the NP, **50** was reduced to the polyketide and peptide fragments; however, there were still unable to identify the absolute stereochemistry of C35, C36, and C37 within the polyketide. In order to determine the stereochemistry about C35 and C37, a synthetic route was developed to access the 4 possible diastereomers shown in Scheme 8. The synthesis commenced with an Evan's aldol reaction between the *N*-propionyl oxazolidinone (**80)** and (*E*)-2-methylbut-2-enal (**81**). Equivalent control of the coordinating reagent Bu_2BOTf allowed for control of the C36 stereochemistry to afford the aldol products **82** and **83** in 94% and 60% yields, respectively. This reaction proceeds through a 6-membered ring transition state and is controlled by coordination to the oxazolidinone. More details regarding the transition state of the aldol reaction will be discussed in chapter 3. Analogously, oxazolidinone (**84)** was used in a similar fashion to afford the C37(*S)* compounds **85**

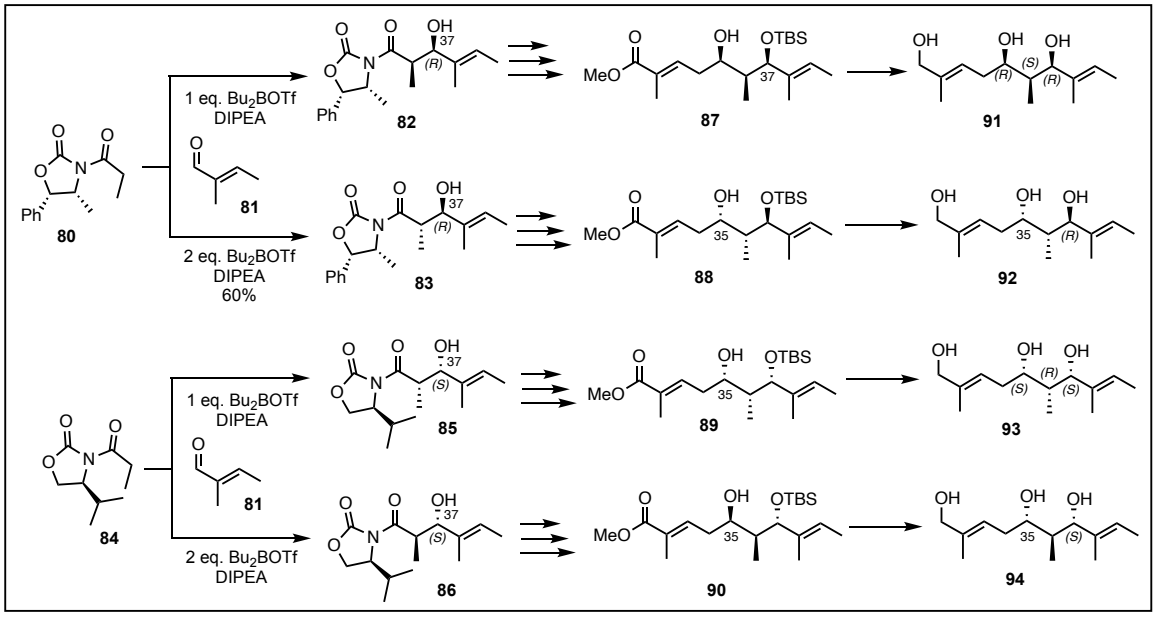

Scheme 8: Route used to access to the polyketide of **50** and possible C35 and C37 diastereomers.

and **86** in an unreported yield. Orthogonal chemistry to the work towards aurilide afforded the methyl ester compounds **87**-**90**. Silyl deprotection conditions afforded the triols **91**, **92**, **93**, and **94** to be used for NMR comparison to the polyketide derived from the NP. As a result, compound **94** correlated closely to the NP assigning the stereochemistry of the polyketide as C35(*S*), C36(*S*), and C37(*S*). However, limited supply of the NP also made identify the peptide portion difficult. Efforts towards the total synthesis in 2007 were reported, but were only able to identify possible structural misassignments of the NP.[54] Their follow up report in 2007 synthesized the possible confirmation of the peptide portion in question and identified the absolute stereochemistry as 21-*L*-Ala, 24-*D*-MePhe and the 43-*D*-Ala, as shown in Figure 16.[55]

In 2014, Han and coworkers published their synthetic efforts towards a ^{11}C-labeled polyketide of **50** that was envisioned for future applications as a positron emission tomography (PET) tracer.[56] Probes designed as PET tracers are radiolabeled with short-life positron-emitting nucleotides such as ^{11}C, ^{13}N, ^{15}O, or ^{18}F to name a few. This technique can be used as a non-invasive molecular imaging tool to investigate the *in vivo* biochemistry of the toxic compounds.

In this work, Han and coworkers envisioned a late stage Suzuki cross-coupling with a [^{11}C]methyl iodide source, as shown in Scheme 9. Referring to previous reports by Nakao and coworkers, methacrylaldehyde (**81**) was reacted with the Evan's oxazolidinone **84** in the presence of *n*Bu$_2$BOTf with DIPEA to afford **95** in 47% yield setting the C37(*S*) alcohol. Standard reactions afforded the TBS protected aldehyde **96** which was subjected to vinylogous Mukaiyama aldol reaction (VMAR) conditions with the TBS-enol ether (**97**) to provide compound **98** in 69% yield as a mixture of diastereomers. These diastereomers of the C35 alcohol were oxidized via a Pfitzner–Moffatt oxidation employing *N,N′*-dicyclohexylcarbodiimide (DCC) and was reduced under $NaBH_4$ conditions to afford the 1,3-*syn*-diol **99** selectively. Compound **99** was further elaborated onto the *para*-methoxybenzyl (PMB) ethers to protect the alcohol (**100**) in 49% yield, and the TBS group was deprotected with HF in pyridine to afford the olefin **101** was generated in 74% yield. Compound **101** was then exposed to the Hoveyda-Grubbs second-generation catalyst to afford the (*E*)-organoboron compound **102** in 14% yield. Finally the Pd^0-mediated Suzuki conditions using radiolabeled [^{11}C]methyl iodide afforded the polyketide derivative **103** in 72% yield. In conclusion, Han and coworkers were able to identify a synthetic route to access a ^{11}C-

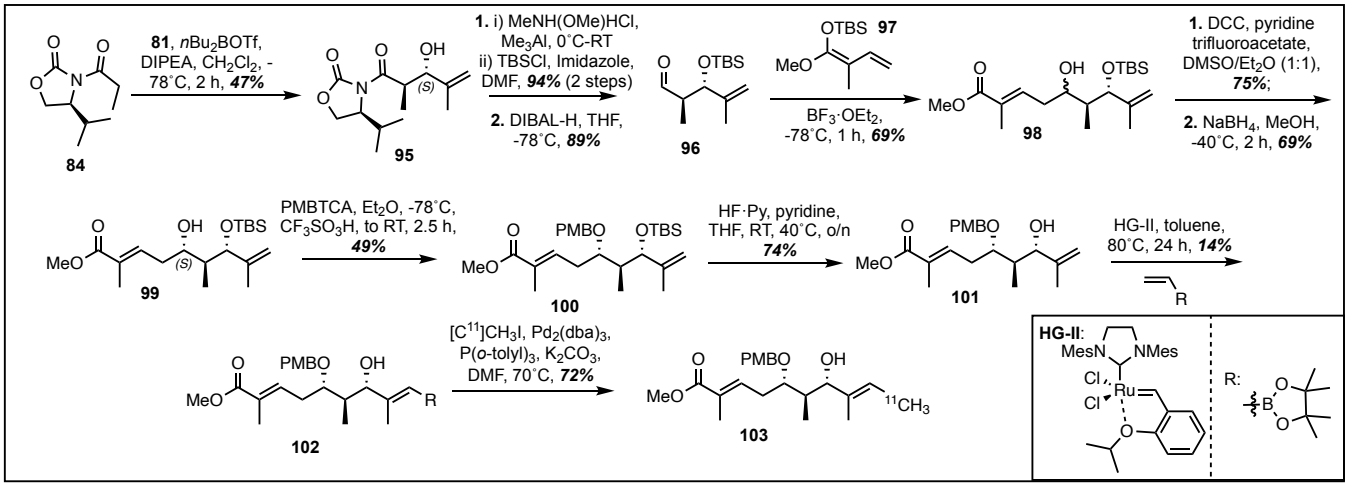

Scheme 9: Synthetic route to access the ^{11}C-PET tracer analog of **50**.

labeled polyketide fragment of **50**; however, future work will identify the utility of this strategy, as no biological data has been reported at this time.

2.8.1 SAR Investigations of Kulokekahilide-2

The work done by Nakao generated a library of compounds based on **50**, that were tested for cytotoxic activity shown in Table 5. This library examined the effects of the polypeptide of the NP (**104**), the effect of epimers about C2, C11, and C14, protecting groups on C23 alcohol, and

Table 5: SAR investigation of **50**.

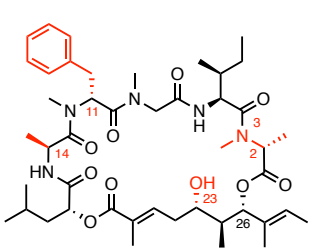

50. Kulokekahilide

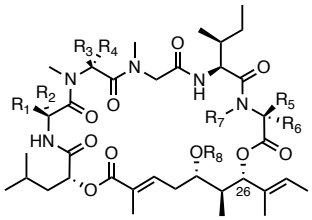

Kulokekahilide analogs (**108**-**122**)

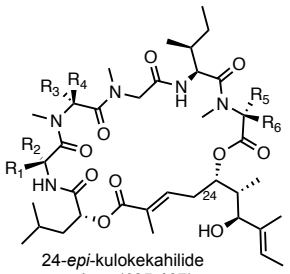

24-*epi*-kulokekahilide analogs (**105**-**107**)

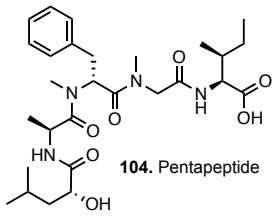

104. Pentapeptide

									Cell Lines Tested				
									P388	HeLa	A549	K562	MCF
	R_1	R_2	R_3	R_4	R_5	R_6	R_7	R_8	IC50 (ug/mL)		IC50 (nM)		
									0.004	-	-	-	-
50	Me	H	H	Bn	H	Me	H	H	0.016	0.0032	0.0021	0.0031	0.22
108	H	Me	Bn	H	Me	H	H	H	10	>10	-	-	-
109	H	Me	Bn	H	H	Me	H	H	>10	>10	-	-	-
110	Me	H	Bn	H	H	Me	H	H	0.4	0.039	-	-	-
111	Me	H	H	Bn	Me	H	H	H	0.016	0.0053	-	-	-
112	H	Me	H	Bn	H	Me	H	H	4.5	2	1045	584	1645
113	Me	H	H	Bn	Me	H	H	MTM	0.08	0.016	-	-	-
114	Me	H	H	Bn	H	Me	H	MTM	0.016	0.0072	0.00019	0.0063	6.3
115	Me	H	Bn	H	H	Me	H	MTM	0.4	0.039	-	-	-
116	Me	H	H	Bn	H	Me	Me	MTM	0.04	0.04	-	-	-
117	H	Me	H	Bn	H	Me	H	MTM	>10	>10	4336	1189	>10,000
118	Me	H	H	*p*ClBn	H	Me	H	H	0.0072	0.0014	0.00001	0.000011	0.003
119	Me	H	H	*p*ClBn	H	Me	H	MTM	0.016	0.0072	0.73	7.1	6.5
120	Me	H	H	Bn	H	Me	Me	H	0.0072	0.0072	-	-	-
121	Me	H	Bn	H	H	Bn	H	MTM	0.89	0.89	-	-	-
122	Me	H	H	Bn	H	Me	H	Bz	-	-	0.00058	1.8	2.9
105	Me	H	H	Bn	H	Me	-	-	-	-	0.0014	0.012	0.29
106	H	Me	H	Bn	H	Me	-	-	-	-	1077	1189	3692
107	Me	H	H	*p*ClBn	H	Me	-	-	-	-	0.000020	0.000216	0.025
104	-	-	-	-	-	-	-	-	-	-	>10,000	>10,000	>10,000

tested the 24-membered macrocyclic analogs (**105**, **106**, and **107**).[57,58] In summary, the 24-membered analog (**105**) retained cytotoxicity; however, inversion of stereochemistry about C14 (**108**, **109**, **112**, **117**, and **106**) showed significant decrease in activity (IC_{50} values shown in Table 4). Modest activity was retained from stereochemical changes about C11 (**110**, **115** and **121**). Neither the inversion of C2 (**111**, and **113**), nor protection of the C23 hydroxyl, via MTM or benzyl, had an effect on biological activity (**114**, **115**, **116**, and **122**). Interestingly, addition of a halogen on the 24-*D*-MePhe in the para position at C11 increased toxicity (**118**, **119**, and **107**). Finally, the pentapeptide (**104**) showed a complete loss in cytotoxicity.

2.8.2 Summary of Kulokekahilide-2 Polyketide Syntheses

In summary the polyketide portion of **50** was synthesized by Nakao and coworkers in 2004, and by Han and coworkers in 2014, both harnessing a similar route as used in the synthesis of **30**, shown in Figure 20. Key stereogenic steps include Evan's mediated aldol reactions followed by Mukaiyama aldol addition. The utility of the TMS-enol ether addition is an efficient method to access the carbon framework of the polyketide; however, this non-selective addition lead to a mixture of diastereomers and 1,3-*syn*-diol formation was used to correct the stereochemistry. Nakao and coworkers were able to generate a library of compounds which allowed for biological testing and SAR showing the importance of the stereochemistry in both the polyketide and peptide portion of **50**. Han and coworkers were able to introduce a radioactive ^{11}C-nuclei to be used as a PET tracer in future reports.

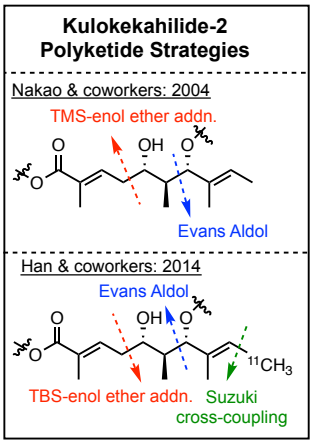

Figure 20: Summary of kulokekahilide-2 polyketide synthesis.

2.9 Synthesis of Odoamide Polyketide

Odoamide (**49**) was isolated from the marine cyanobacterium *Okeania sp.* in 2016 by Sueyoshi and coworkers.[59] To help determine the absolute stereochemistry of the NP, a synthetic route was devised to access the possible diastereomers about the C39 hydroxyl, and was inspired by the previous synthetic work by Mutou and coworkers, as shown in Scheme 10. Swern oxidation of **123** followed by Wittig olefination with ethyltriphenylphosphonium bromide (TEP) afforded **124** in 71% yield over 2 steps in a Z/E ratio of 7:1. Deprotection of the benzyl group over Pd with H_2 afforded the primary alcohol **125** with the reduced olefin. Again, the alcohol was oxidized via Swern conditions and subjected to Mukaiyama aldol conditions with the TMS-enol ether (**126**) to afford **127** in 85% yield over 2 steps. The methyl ester **127** was then oxidized to the ketone and the 1,3-*syn*-diol was generated using standard $NaBH_4$ conditions to afford **128** in 83% yield over 2 steps with a high degree of selectivity (dr > 97:3). Finally, the TBS deprotection with tetrabutylammonium fluoride (TBAF) afforded the methyl ester **129** in 81% yield. The diol was then converted to the acetonide for NMR characterization (not shown, 90% yield). Reduction with DIBAl-H followed by acetonide cleavage with HCl afforded the desired triol **130** to be compared

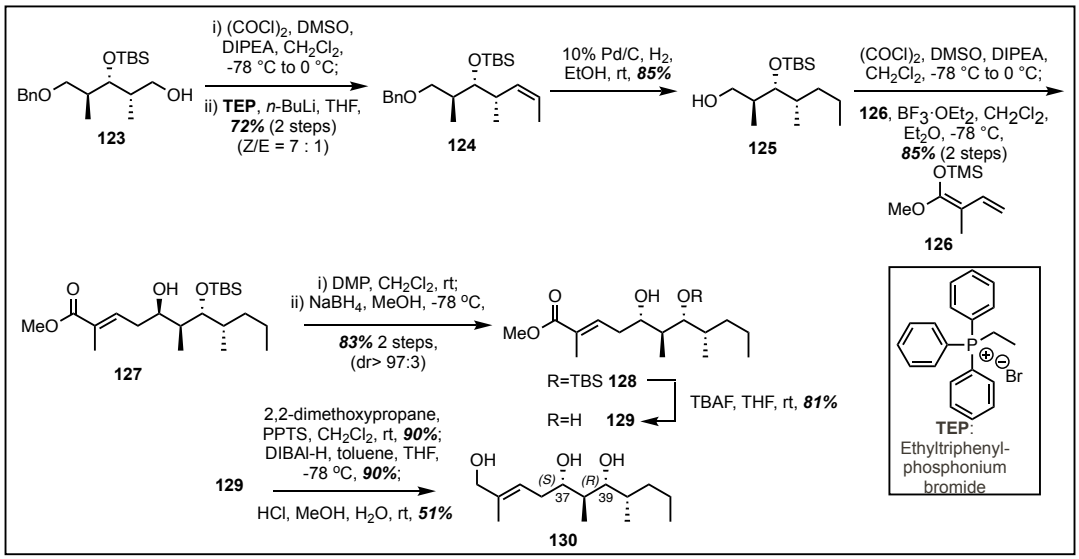

Scheme 10: Synthetic route to access the polyketide of odoamide.

with the polyketide derived from the NP. Comparison to the NP revealed a C37(*S*), C38(*S*), C39(*R*), and C40(*S*) stereochemical relationship, however there remained some ambiguity of the stereochemistry about C40 (exocyclic methyl).

In 2016 Sueyoshi and coworkers reported the total synthesis of odoamide (**49**).[60] To further validate their previous reports, a synthetic route was designed to access the diastereomers about C40, shown in Scheme 11. The route began with an aldol reaction between (*R*)-4-benzyl-3-propionyl-2-oxazolidinone (**131**) and the freshly generated aldehyde **132** affording **133** in 80% yield. The alcohol was protected via TBS (89% yield) and cleaved from the auxiliary using $LiBH_4$ (69% yield) to afford the primary alcohol **134**. Swern oxidation conditions followed by Wittig olefination with TEP provided the alkene (**135**) in 69% yield over 2 steps with a Z/E mixture of

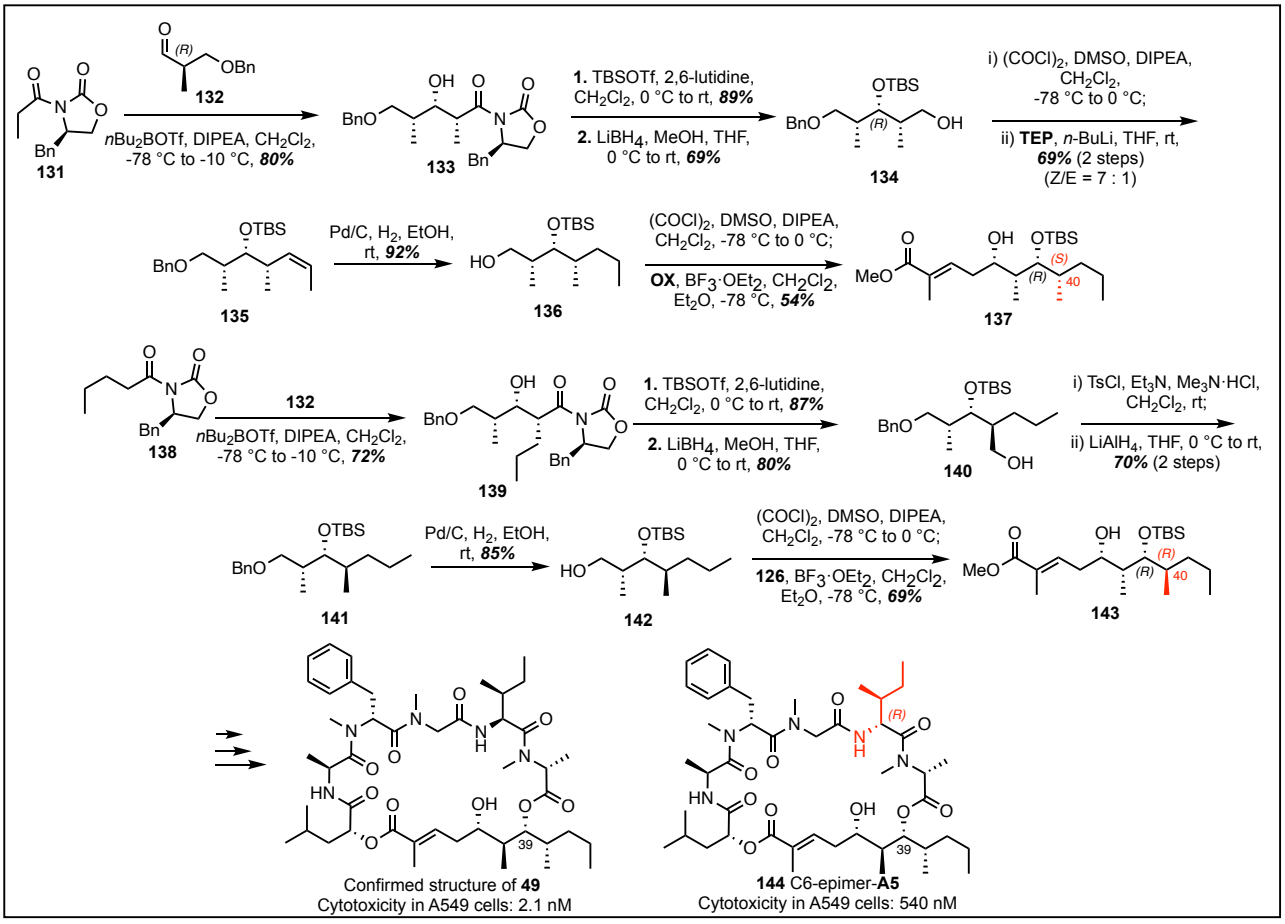

Scheme 11: Synthetic route to the total synthesis of odoamide.

7:1. Reduction of **135** with Pd/C and H_2 afforded the primary alcohol **136** in 92% yield. Oxidation to the aldehyde followed by Mukaiyama aldol conditions afforded the methyl ester **137** in 54% yield. Standard peptide chemistry was used to construct **49** which was validated by NMR and showed a cytotoxicity comparable to the NP (IC_{50} = 2.1 nM in A549 cells). In addition, the C6-epimer of the NP (**144**) was tested and showed a significant decrease in toxicity (IC_{50} = 540 nM). This work highlights the importance of the stereochemistry of the polyketide and stresses the need for a selective approach towards the polyketide of lagunamide C.

2.9.1 SAR of Odoamide

In 2018 the same lab reported the cytotoxicity of a set of odoamide analogs in A549 cell line, shown in Figure 21.[61] Inversions of single amino acid residues at C25 (**145,** IC_{50} = 1554 nM), C15 (**146** IC_{50} = 48 nM), or C6 (**147** IC_{50} = 645 nM) significantly decreased toxicity; however, inversion of the N-Me-*L*-Alanine at C2 position (**148** IC_{50} = 1.9 nM) increased the cytotoxicity. Interestingly, the researchers also noticed the NP slowly converts to the 24-membered analog (**149** IC_{50}= 1.9 nM) but retains toxicity. The addition of a methyl ether onto the C24 hydroxyl in both the 26 and 24-membered macrocyclic structure (**150** IC_{50} = 48 nM; **151** IC_{50} = 3383 nM**)** significantly decreased toxicity. Dehydration of the polyketide moiety (**152**) leads to a slight decrease in activity (IC_{50} = 28 nM). Finally, replacement of sarcosine with N-methyl-alanine (**153**), glycine (**154**), and *D*-Phe substitution (**155**) all slightly decreased toxicity (IC_{50} **153** = 74 nM; IC_{50} **154** = 31 nM; IC_{50} **155** = 5.4 nM). This work illustrates the chirality of the amino acids in the peptide portion play a critical role in the biological activity of the NP; further stressing the importance of a highly stereoselective approach in synthetic design towards the polyketide of lagunamide C.

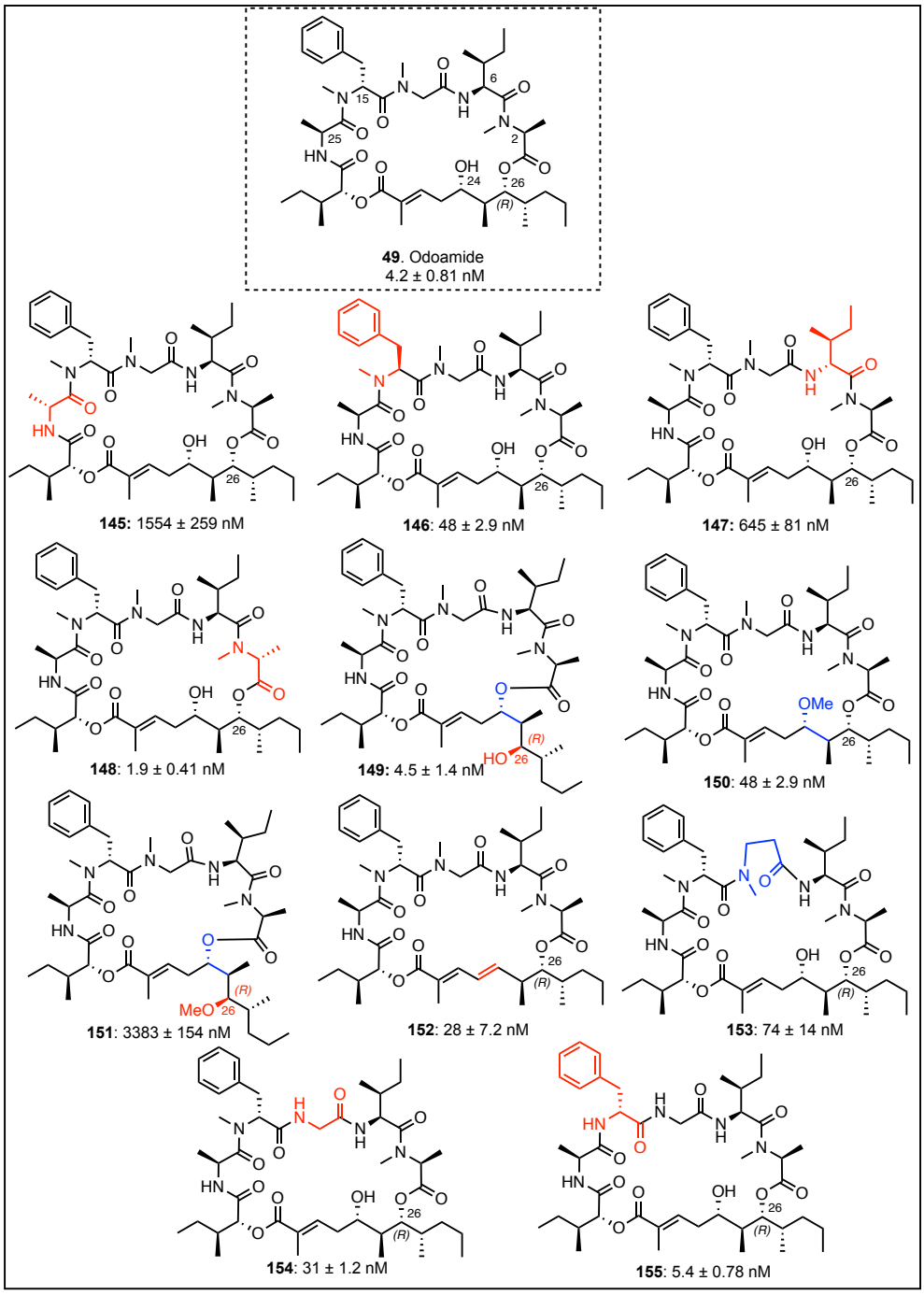

Figure 21: SAR of odoamide through analog synthesis and cytotoxic evaluation.

2.10 Synthetic Efforts Towards the Polyketide of Lagunamide A

Following the isolation of lagunamide A (**33,** in Figure 15) in 2010, Dai and coworkers set out to achieve the first total synthesis leading to the reconfiguration of several stereocenters.[34] Efforts towards the synthesis of the polyketide portion of **33** is shown in Scheme 12. The route began with an Evan's mediated aldol reaction between **131** and freshly generated *S*-2-methylbutanal, followed by auxiliary cleavage with $NaBH_4$. The resulting diol was protected with anisaldehyde in the presence of PPTS to provide the acetal **156** in an overall yield of 61% over 3 steps. Compound **156** was subjected to DIBAl-H reduction with subsequent oxidation with Dess-Martin Periodate (DMP) to afford an aldehyde (not shown) which was subjected to the diastereoselective allylation

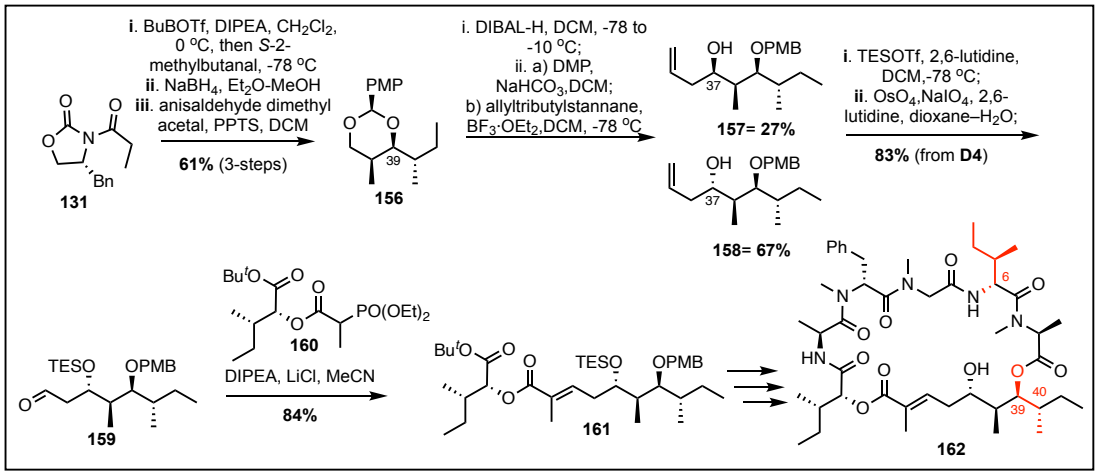

Scheme 12: Efforts by Dai and coworkers towards the total synthesis of lagunamide A.

using Keck's protocol[62] to afford the two diastereomers **157** and **158** in 27% and 67% yield, respectively. Protection with TES group on the newly formed hydroxyl followed by Johnson-Lemieux oxidation allowed access to aldehyde **159** in 83% yield. Compound **159** was subjected to HWE olefination conditions with the phosphonate **160** to afford the α,β-unsaturated ester **161** in 84% yield. Compound **161** was carried on producing compound **162**; however, neither H^1 nor C^{13} NMR matched the NP. At this point, researchers hypothesized that several stereocenters of the

proposed structure may have incorrect stereochemical assignment. Comparing the proposed structure to the aurilide class of NPs, the C39 alcohol, the C40 methyl, and the C6 *L-allo*-isoleucine of **162** (shown in red in Scheme 12) were identified as possible sources of the error in the assignment of the original structure. To identify the correct structure, the possible diastereomers of the proposed NP were synthesized, shown in Figure 22. This work identified three stereochemical corrections wherein the C6 *L-allo*-isoleucine was exchanged with *L*-isoleucine, in addition to the inversions of C39 alcohol to (*R*) and C40 methyl to (*S*).

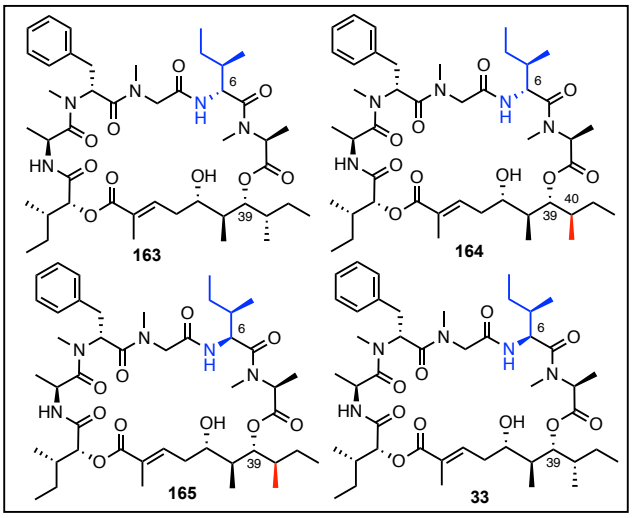

Figure 22: Isomers of lagunamide A synthesized to determine absolute stereochemistry.

Later in 2013 Huang and coworkers envisioned a new route involving a late stage cross-metathesis to afford **33**.[63] The commercially available *S*-2-methylbutanol (**166**, Scheme 13) was oxidized via Swern conditions to the aldehyde (**167**) followed by subjection to Paterson *anti*-aldol conditions.[64] Treatment of **168** with (*c*-hex)$_2$BCl in addition to Me$_2$NEt generated the trans enolate forming the aldol product **169** in 74% yield over 2 steps with high degree of diastereoselectivity (*dr*: 99:1). Protection of the C39 alcohol with TBS, followed by NaBH$_4$ reduction produced a

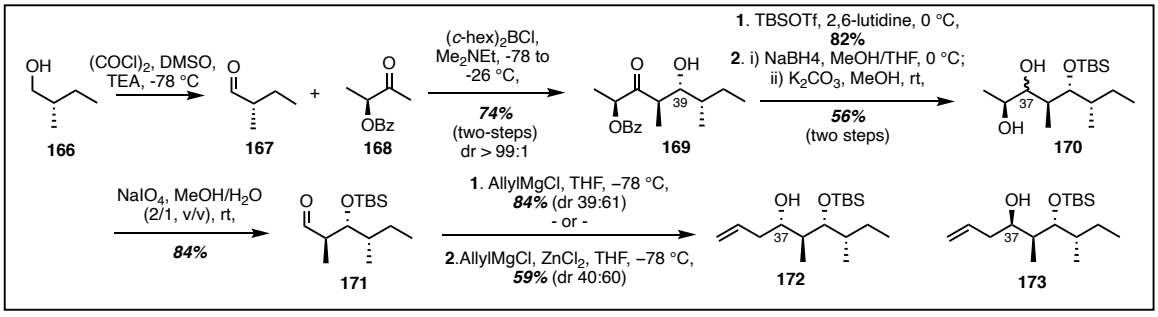

Scheme 13: Efforts towards lagunamide A polyketide by Huang and coworkers.

mixture of diastereomers of the diol **170** in 56% over 2 steps. Oxidative cleavage with $NaIO_4$ afforded the aldehyde **171** in 84% yield and was the synthetic handle needed for allylation. The addition of allyl magnesium bromide in THF at -78 °C gave an 84% yield with a dr of 39:61 in favor of the desired C37(*S*) configuration seen in compound **172**. Conversely, treatment of **171** in the presence of $ZnCl_2$ in THF at -78 °C gave 59% yield of the diastereomers with a 40:60 dr, in favor of the undesired diastereomer C37(*R*) shown as compound **173**. The lack of desired selectivity caused the authors to reinvestigate a new route to get more selective allylation. Visualization of the Cram's model, shown in Figure 23, identified the C3-OTBS group in the (*R*)-configuration (transition states A and B) has no steric bias and leads to a mixture of compounds. However, inversion of the C3-OTBS group to the (*S*)-configuration (shown as C and D) allows for slower nucleophilic attack on the *si*-face (shown as disfavored) enabling increased formation of the C39(*R*) isomer. It is critical to mention this selectivity is strongly dependent upon the 1,3-diol chelation that produces a 6-membered ring transition state. With this new vision in mind, the authors set out the synthesize the C39(*S*) isomer with the intentions of inverting the chirality later in the synthesis.

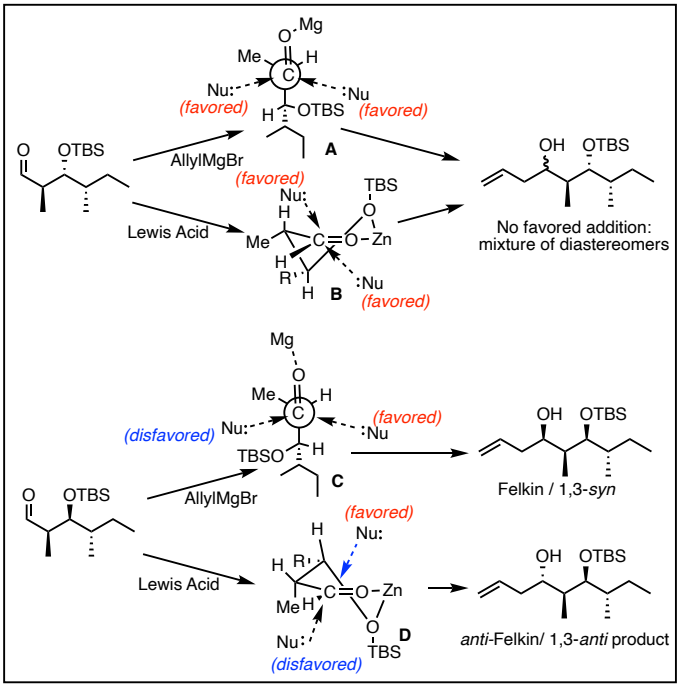

Figure 23: Transition state for selective allylation.

To this end a new route was developed that mimicked the previous reports towards **30**, shown in Scheme 14. To start, *N*-propyl oxazolidine (**131**) was subjected to aldol conditions with **167** to afford the C39(*S*) hydroxyl (**174**) in 93% yield reported as a single diastereomer. Alcohol protection with TBSCl (95% yield) followed by auxiliary cleavage and Swern oxidation provided compound **175** in an overall yield of 92% over 2 synthetic steps. With aldehyde **175** in hand, allylation conditions were explored leading to the desired C37(*S*) (**176**) hydroxyl in 90% yield with minor amounts of the undesired C37(*R*) (**177**: 10%). To invert the stereochemistry about C39, compound **176** was converted to **178** by removal of the TBS group on the C39 alcohol and selective TBS protection of the C37 alcohol. Compound **178** was then oxidized via DMP (92% yield) and reduced with lithium triethylborohydride (Et_3BHLi) (94% yield) to afford the 1,3-*syn*-diol, **179**.

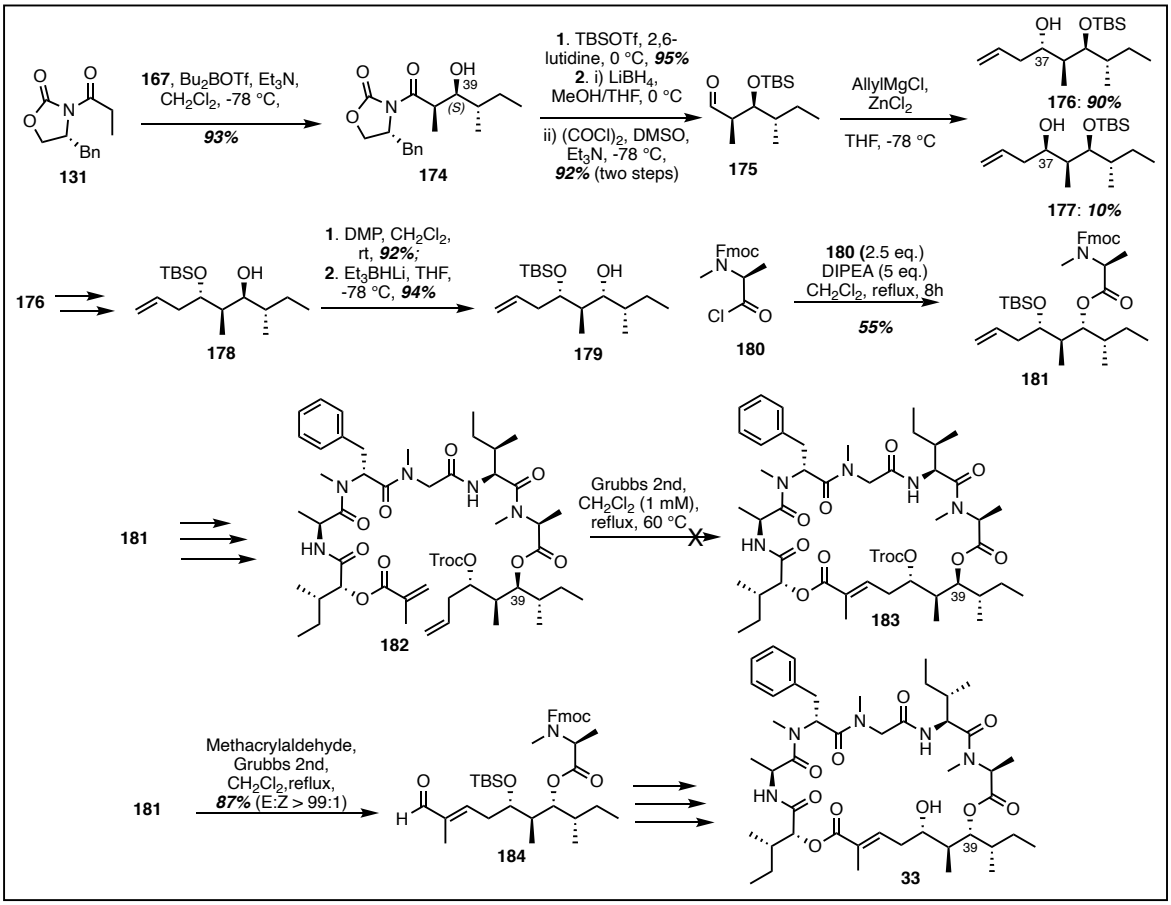

Scheme 14: Route to access lagunamide A via cross-metathesis.

The free hydroxyl at C39 was then coupled to the *N*-Me-Fmoc-*D*-Ala-OH (**180**) to afford the esterified product **181** in 55% yield. Compound **181** was advanced with standard peptide chemistry to afford compound **182** as the precursor for the ring-closing metathesis (RCM); however, all attempts to cyclize using Grubb's second-generation catalyst failed to form **33**. To overcome this limitation, compound **181** was exposed to Grubb's second-generation catalyst in the presence of methacrylaldehyde to form compound **184** in 87% yield with a E:Z ration of >99:1. Standard peptide chemistry was used to complete the total synthesis of **33** in addition to several analogs (shown in Figure 24) including; 39-*epi*-33 (**185**), 2-*epi*-33 (**186**), 7,37,39-*epi*-33 (**187**), and 7,39-*epi*-33 (**188**). A following report in 2016 described the biological activity of these analogs, also show in Figure 24.[63] Interestingly, all analogs of **33** showed significantly (>10x) decreased toxicity in all cell lines tested. Inversion of the C39 hydroxyl (**185**) inhibits all toxicity (IC_{50} range = 191-950 nM), while inversion about the methyl at C2 reduces toxicity (IC_{50}

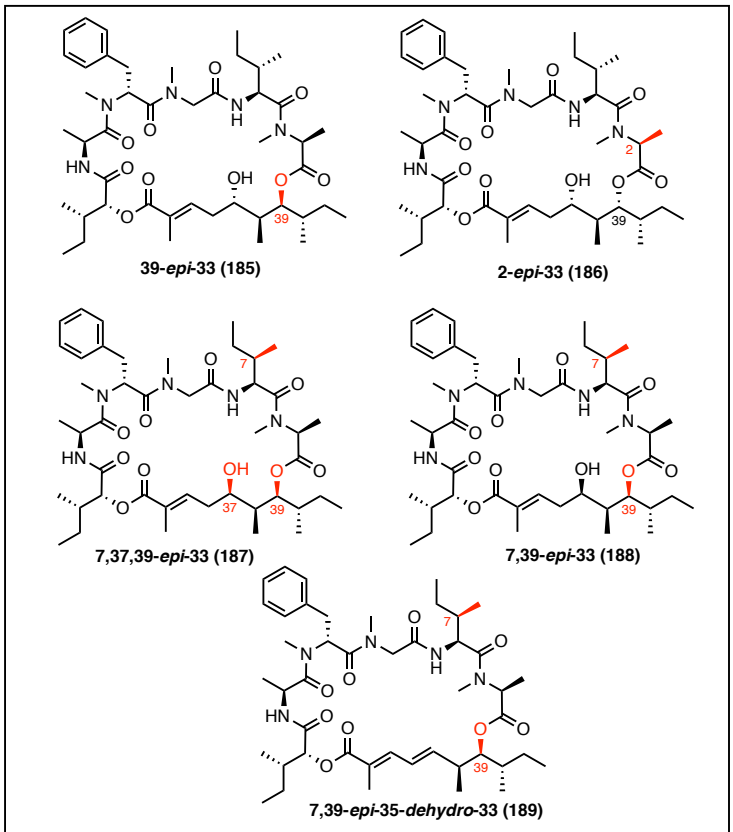

Cell Line	33	185	186	187	188	189
A549	8.7 ± 0.3	273.9 ± 38.3	62.3 ± 11.5	3400.3 ± 567.3	>10000	>10000
HeLa	17.0 ± 1.7	191.6 ± 63.7	67.3 ± 20.3	1377.7 ± 313.5	>10000	>10000
U2OS	8.6 ± 1.0	437.9 ± 58.0	59.3 ± 9.8	4036.7 ± 400.7	>10000	>10000
HepG2	11.4 ± 1.9	246.6 ± 9.7	67.4 ± 1.2	2537.3 ± 486.3	>10000	>10000
BEL-7404	11.0 ± 0.7	725.0 ± 153.5	59.9 ± 8.3	5859.3 ± 384.4	>10000	>10000
BGC-823	4.7 ± 0.4	231.7 ± 25.3	42.5 ± 1.8	3430.3 ± 577.1	>10000	>10000
HCT116	8.2 ± 1.2	200.0 ± 19.5	52.4 ± 5.1	3799.7 ± 332.7	>10000	>10000
MCF-7	18.7 ± 2.2	946.4 ± 206.8	145.8 ± 21.1	839.8 ± 407.8	>10000	>10000
HL-60	19.8 ± 0.9	713.9 ± 97.6	92.6 ± 1.9	8630.3 ± 515.1	>10000	>10000
A375	8.3 ± 1.8	212.6 ± 42.8	56.3 ± 6.6	970.2 ± 178.7	>10000	>10000

Cell viability was detected using MTS assay after 48 h of treatment with serial dilutions

Figure 24: SAR of lagunamide A analogs and cytotoxic evaluation.

186, range = 42-145 nM). Any inverted stereochemistry with respect to the NP; including 7,39-*epi*-35-*dehydro*-**33** analog (**189**), the C7, or C37 epimers render the molecule inactivity with IC_{50} > 10,000 nM. Additional biological testing revealed **33** disrupts the mitochondrial membrane potential and leads to overproduction of reactive oxygen species (ROS). Proteomic profiling identified that **33** altered the expression levels of the Bcl-2 family of proteins including up-regulation of Bcl-xL, Bcl-2, Mcl-1; in addition to down-regulation of Bax, Bad, and Bid all in a dose dependent manner. This family of proteins are known to be involved in regulation of the apoptotic cell death pathway.[65–67] In conclusion, this work illustrates the importance of stereochemical configuration of the NP and gives a rational for a diastereoselective synthesis of lagunamide C.

In 2014, a stereoselective approach towards the polyketide fragment of **33** was published by Lui and coworkers.[32] Freshly generated *S*-2-methylbutanal (**167**) was reacted with methanol in the presence of catalytic amounts of p-toluenesulfonic acid (*p*-TsOH) to form the dimethyl acetal compound **190** (Scheme 15). This compound was exposed to the enolate of the N-propyl thiazolidinethione (Crimmin's auxiliary) (**191**) to afford compound **192** in 62% yield, reported as a single diastereomer. Cleavage of the auxiliary with DIBAl-H followed by allylMgCl addition generated compounds **193** and **194** in 99% yield in a 2:3 mixture, respectively. Compound **194** was then TBS

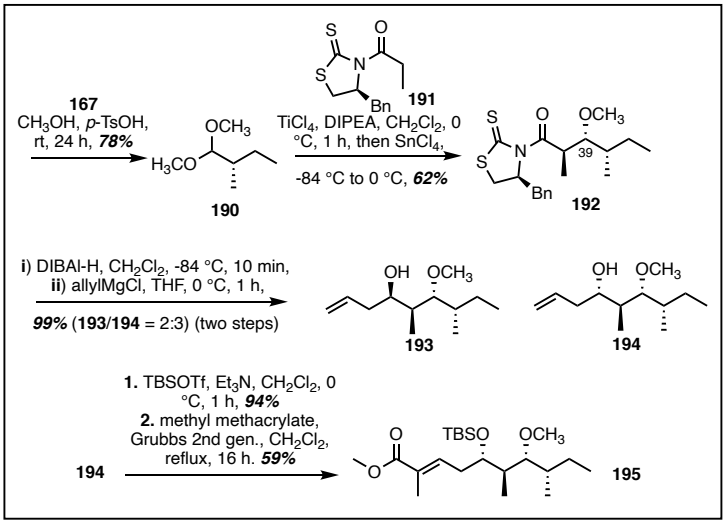

Scheme 15: Synthesis of the polyketide of lagunamide A by Lui and coworkers.

protected (94%) followed by CM using Grubb's second-generation catalyst to generate the polyketide **195** in 59% yield. At this point compound **195** was saponified and coupled to the first hydroxy acid; however, the total synthesis was not completed in this work due to limited material for cyclization attempts.

In 2016 Banasik and coworkers published a route that used iterative asymmetric vinylogous Mukaiyama aldol reactions (VMAR) to synthesize the polyketide portion of **33**, shown in Scheme 16.[36] The synthesis commenced with the chiral vinylketene silyl N,O-acetal (**196**) being

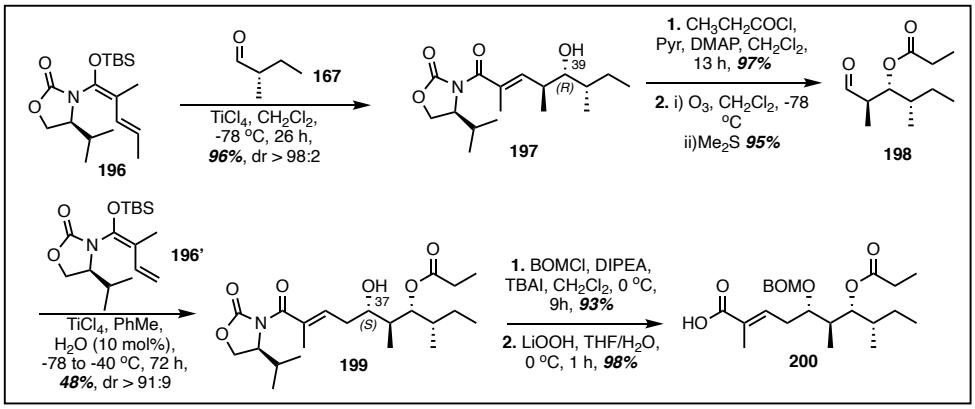

Scheme 16: Synthetic efforts towards the polyketide of L1 by Banasik and coworkers.

exposed to $TiCl_4$ at -78 °C in the presence of freshly generated S-(2)methyl butanal (**167**) to afford **197** in 96% yield with a dr > 98:2 in favor of the C39 (*R*) hydroxyl. The resulting hydroxyl was masked as a propionate (97% yield) and then exposed to ozonolysis to afford aldehyde **198** in 95% yield. The aldehyde was then subjected to the second VMAR with **196'** to produce **199** in 48% yield with a dr > 91:9 in favor of the C37 (*S*) hydroxyl. The authors suggest the selectivity of

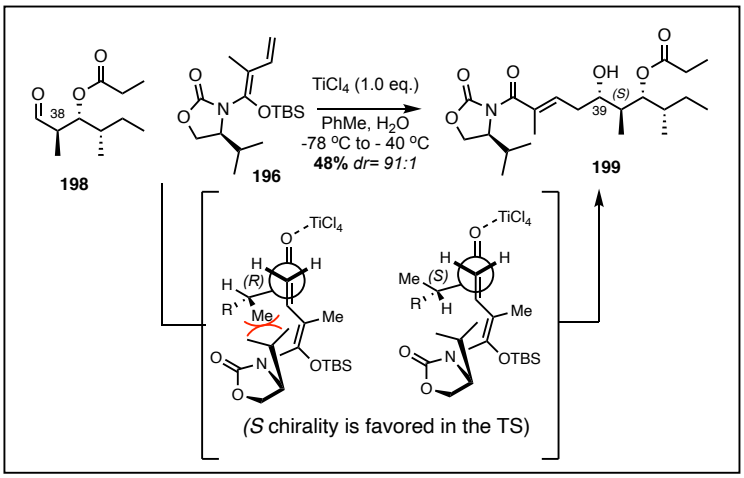

Figure 25: Predicted transition state of TBS enol ether addition.

the reaction can be rationalized by the Felkin-Ahn model shown in Figure 25. The authors postulate that the (*R*) stereochemistry of the alpha methyl at C38 leads to steric congestion with the chiral auxiliary and slows product formation. However, the reaction allows for selective formation of the desired C37 (*S*) hydroxyl. Protection of the alcohol to the BOM ether group followed by auxiliary cleavage with LiOOH provided the carboxylic acid **200** in 98% yield. However, these compounds were not carried on to the total synthesis but were coupled to the first hydroxy acid of the peptide fragment.

Developing highly selective methods to access the polyketide fragment have been explored extensively, and likely the most selective transformations was seen in the work by Gorges in 2018.[35] Employing a Matteson homologation strategy they were able to achieve the total synthesis of **33** through carbon chain elongation, as shown in Scheme 17. First, the methylboronic ester **201** was exposed to the ethyl Grignard reagent under homologation conditions to give the prolonged carbon chain shown in **202** in 99% yield as a single diastereomer. The next homologation took place with benzyl alcoholate as the nucleophile to provide compound **203** in 74% yield. To

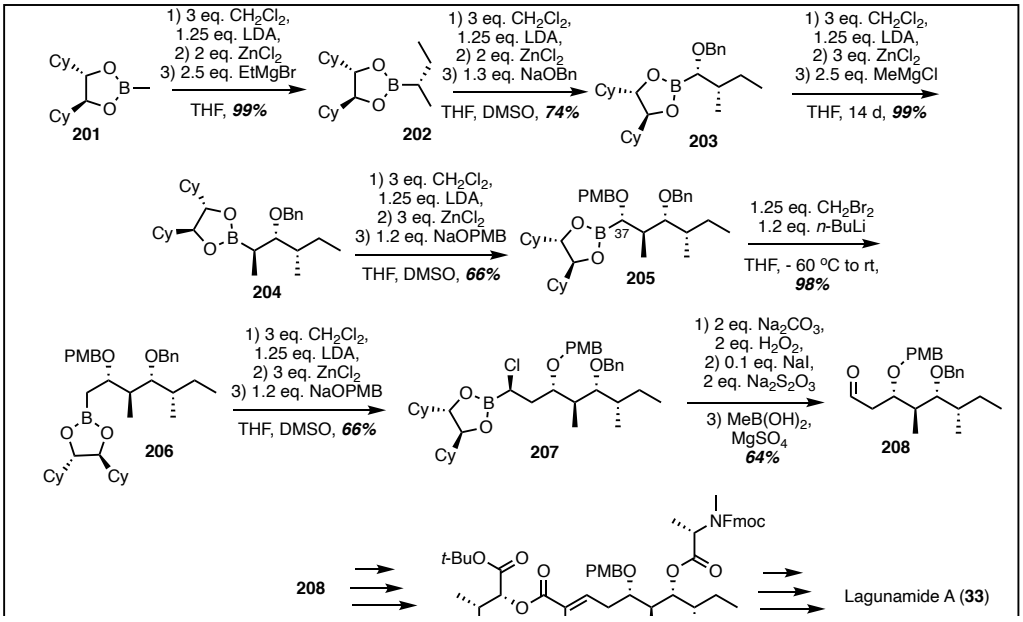

Scheme 17: Matteson homologation strategy to access lagunamide A.

elongate the chain further, methyl Grignard reagent produced compound **204** in 99% yield with a long reaction time of 14 days. The final C37 stereocenter was added by homologation with *p*-methoxybenzylate to give **205** in 66% yield. The homologation strategy to add CH_2 groups proved to be difficult upon initial attempts; however, *in situ* generation of bromomethyl lithium from dibromomethane and *n*-BuLi at -60 °C afforded the desired compound (**206**) in 98% yield. Compound **206** was elaborated onto the aldehyde **208** which, after several synthetic steps, was used in HWE olefination conditions to afford the polyketide containing compound **209**. Impressively, this route was used to complete the total synthesis of **33** as a single stereoisomer.

2.10.1 Synthetic Efforts Towards the Polyketide of Lagunamide B

Efforts towards **34** have been limited to the work published by Pal and coworkers in 2014.[68] Starting with an Evan's aldol reaction between compound **131** and tiglic aldehyde (**210**) in the presence of $TiCl_4$ provided the C39(*R*) alcohol (**211**) in 88% yield with a dr of 97:3 (Scheme 18).

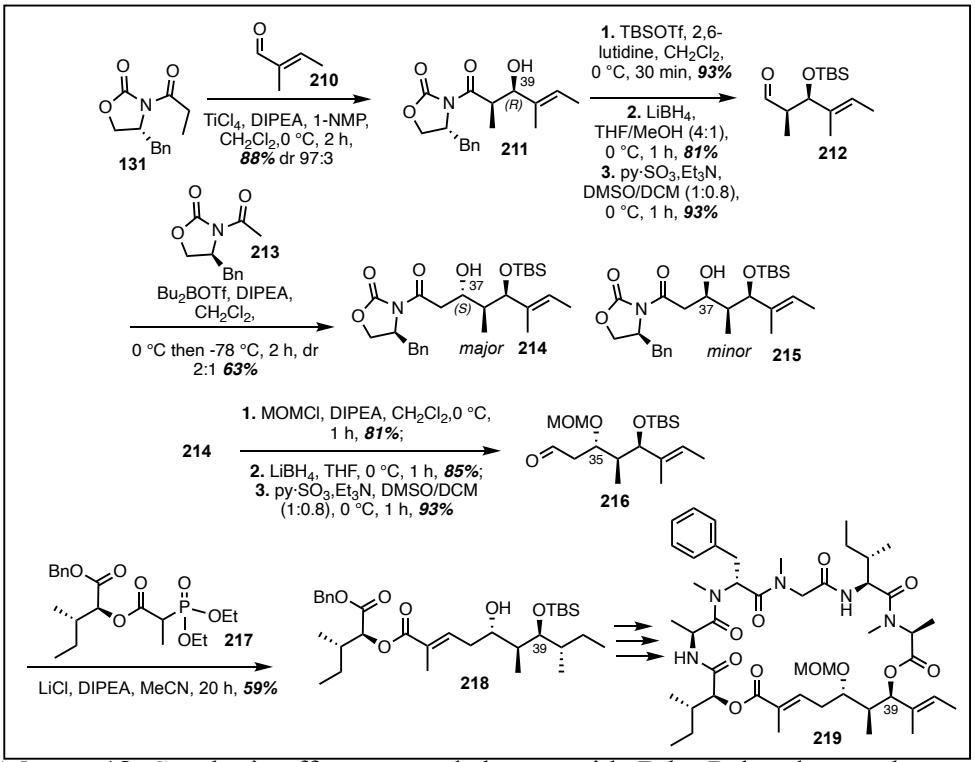

Scheme 18: Synthetic efforts towards lagunamide B by Pal and coworkers.

Alcohol protection via TBSOTf (93%) followed by auxiliary cleavage with $LiBH_4$ (81%) and subsequent oxidation using pyridine-sulfur trioxide complex with Et_3N provided the aldehyde **212** in 93% yield. The enolate of the chiral auxiliary (**213**) was generated in the presence of Bu_2BOTf and DIPEA leading to the formation of two diastereomers **214** and **215** in 63% yield with a dr of 2:1 favoring the C37(*S*) alcohol (**214**). The alcohol was protected as a MOM ether (81% yield), cleaved from the auxiliary with $LiBH_4$ (85% yield) and oxidized to generate aldehyde **216** in 93% yield. With the aldehyde in hand, fragment **217** was added in the presence of LiCl and DIPEA to facilitate HWE olefination to form the polyketide fragment (**218**) in 59% yield. However, inability to deprotect the MOM ether (**219**) hindered the completion of the total synthesis.

2.10.2 Summary of Lagunamide Polyketide Syntheses

The key synthetic transformations towards the polyketide fragments of the Lagunamide family are shown in Figure 26. In 2012, Dai and coworkers completed the first total synthesis of **33**, leading to the stereochemical revision about C6, C37 and C39. The key stereogenic transformations include an Evan's aldol, a diastereoselective allylation via Keck's protocol, and an HWE-olefination. In 2013, Huang and coworkers gained access to the polyketide by employing a Patterson/Evans aldol, a diastereoselective allylation, and an olefin cross-metathesis.[63] While the authors were unable to achieve the late stage macrocyclization from the diene, they were able to harness the CM condition to achieve the total

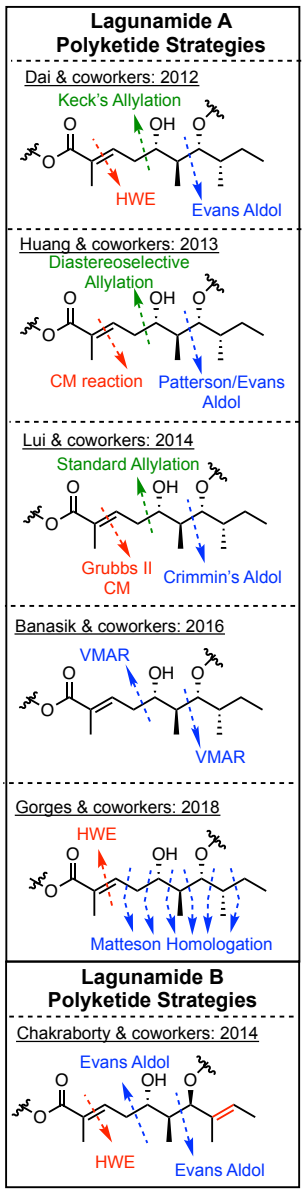

Figure 26: Summary of synthetic strategy to access the polyketide of lagunamides.

synthesis. In 2016, Banasik and coworkers reported their synthetic efforts using an iterative asymmetric VMAR to synthesize a polyketide intermediate towards **33**.[33] This route included consecutive use of 1,4 addition into TBS-enol ethers derived from Evan's chiral auxiliaries, and proved to be a highly efficient. This route is the shortest of the linear sequence but requires thermal control for enhanced stereoselectivity. In 2018, Gorges and coworkers employed Matteson homologation followed by HWE-olefination to synthesize the polyketide containing fragment of **33**. This route has high selectivity and was able to produce the polyketide as a single stereoisomer, but required long reaction times and costly reagents.

Compounds **33** differs from **34** by the saturation of the exocyclic carbon chain. While no total synthesis has been reported, Chakraborty and coworkers published their synthetic efforts in 2014.[68] The key transformations of this strategy include Evans-type aldol reactions followed by HWE-olefination; however, low yields upon macrolactonization failed to produce enough material to perform full characterization of the natural product.

In summary the synthetic approaches towards **33** and **34** are highly dependent on the 1,3-diol to control the stereoselectivity. Again, this renders the approaches unable to access the 1,4-diol of lagunamide C. Each of these routes were taken into consideration when developing a route towards lagunamide C.

2.10.3 SAR of Lagunamides

In 2016, Dang and coworkers employed MTS assay to determine toxicity of **33** and several synthetic derivatives, shown in Figure 27.[33] Compound **33** exhibited IC_{50} values less than 20 nM in all cell lines tested including; A549, HeLa, U2OS, HepG2, BEL-823, HCT116, MCF-7, HL-60 and A375. However, epimerization of a number of stereocenters including C2 (**220,** IC_{50} range = 42.5-145.8 nM), C39 (**221,** IC_{50} range = 191.6-725 nM), C7 (**222**, IC_{50} range = 839.8-8603.3 nM) led to a loss in cytotoxicity. Epimerization of the C37 hydroxyl (**223**, IC_{50} range = >10,000 nM), or dehydration (**224**, IC_{50} range = >10,000 nM) rendered the compounds inactive to all tested cell lines. Following toxicity profiling, the molecular mechanism of **33** was investigated using transmission electron microscopy (TEM) and flow cytometry. Exposing A549 cells to 10 nM of **33** caused pseudopodia retraction, shrinkage, chromatin condensation, and karyopyknosis. In addition to the flow cytometric analysis, these data indicate a mitochondrial-mediated apoptosis pathway were initiated by **33** treatment. In addition, Western blot analysis of cells treated with **33** showed an overproduction of reactive oxygen species (ROS) and altered the protein expression of the Bcl-2 family. Notably, treatment with **33** led to down-regulation of

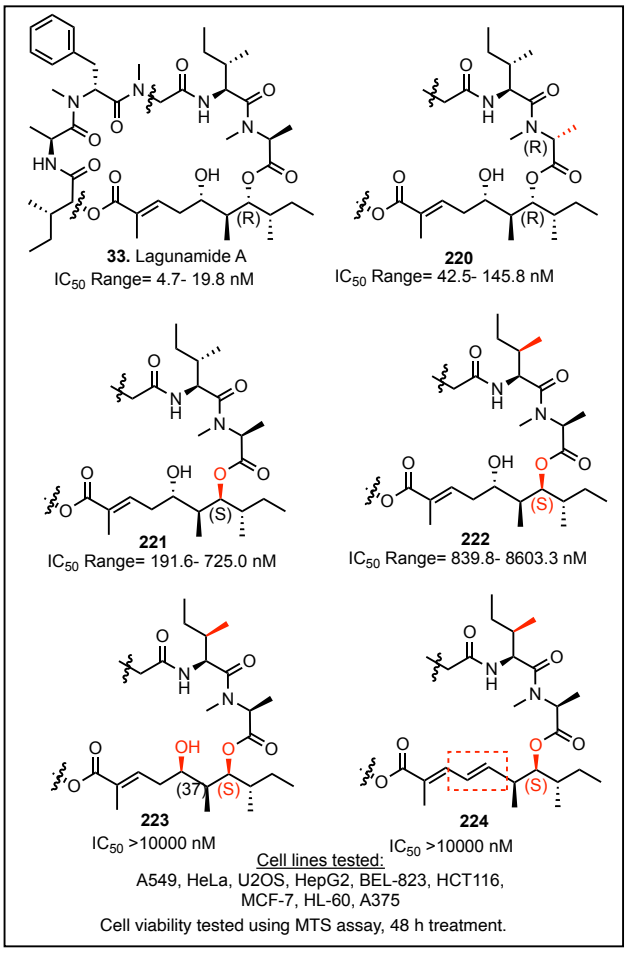

Figure 27: SAR evaluation of lagunamide analogs by Dang and coworkers.

antiapoptotic Bcl-2 family of proteins (Bcl-xL, Bcl-2, Mcl-1); but up-regulated the pro-apoptotic Bcl-2 family of proteins (Bax, Bad, Bid).

2.10.4 Isolation and Biological Evaluation of Lagunamide D

Luesch and coworkers published the structure elucidation of **36** in 2019.[31] Interestingly, HPLC purification of the NP led to two compounds **36** and **225**, a 24-membered analog, shown in Figure 28. Researchers hypothesized this compound was a result of the interconversion under HPLC conditions. Both compounds were tested for toxicity in A549 cells and identified **225** exhibited a nearly 10-fold decrease in toxicity (IC_{50} = 68.2 nM). There have been no further biological evaluation or synthetic efforts towards **36** to date.

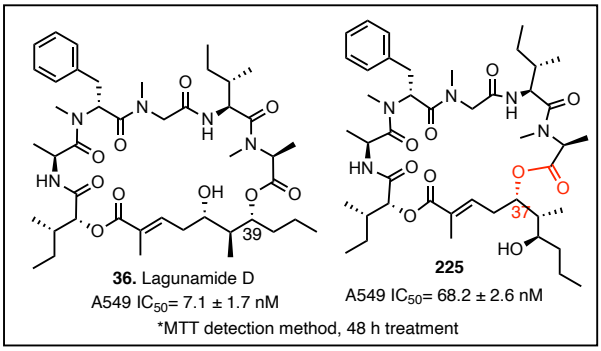

Figure 28: Lagunamide D and 24-epimer and cytotoxic evaluation.

2.11 Conclusion of Previous Work on Aurilide Family and Research Outlook

The synthetic efforts highlighted in this chapter have served as inspiration for the development of a route towards the polyketide lagunamide C. The limitations of the mentioned routes are due to the additional methylene (C39) which renders all strategies employing the *N*-propyl auxiliaries, either Evans or Crimmins, incapable of accessing the polyketide. In addition, most of the above routes set the C36 alcohol via predictable 1,3-*syn*-diol reactivity, as opposed to the 1,4-diol contained in lagunamide C. Overall many of the synthetic steps in the outlined work have served as the basis of our approach albeit with some alterations. The previous work outline in this report will discuss the process of developing a new route to access the polyketide in a

diastereoselective approach. In addition, our work towards the polyketide is the first step in providing evidence of our hypothesis that would change the understanding of the aurilide class of NPs. We believe that synthesis of lagunamide C in addition to the generation of amide analogs in place of the ester linkages will result is the inhibition of activity. We hypothesize the cytotoxic activity associated with the NP is dependent upon delivery of the polyketide into the cancer cell via the peptide fragment that facilitates cell membrane penetration. The peptide fragment is critical for cellular penetration and upon cleavage of the ester bonds allows release of the cytotoxic polyketide. The SAR investigations highlighted in this chapter present no evidence to counter this argument. The data in this chapter suggest that the peptide portion alone has no toxicity (as discussed in Table 5), and biological testing also indicates any alteration of the stereochemistry in the polyketide can have a significant impact on the activity. For this reason, we set out to develop a highly stereoselective approach towards the polyketide in order to perform further biological evaluations.

Chapter 3- Total Synthesis of Reniochalistatin E and Synthetic Efforts Towards Lagunamide C

3 Research Motivation and Chapter Outline

In order to further explore their cytotoxic activities a synthetic route was developed to access both reniochalistatin E and lagunamide C. Reniochalistatin E showed modest cytotoxic activities in myeloma cell lines, which is the most fatal of all blood-based cancers and has limited therapeutic options. To be discussed in this work is the total synthesis route developed to access reniochalistatin E and future work involves the development of a new prodrug delivery strategy. Lagunamide C was found to be highly toxic in several cancer cell lines including blood-based cancers. The work towards accessing lagunamide C involves the development of a novel approach to grant diastereoselective access to the polyketide subunit. Upon establishment of a synthetic route, SAR investigations will look to provide evidence of a prodrug moiety contained within the aurilide class of NPs. Previous work identifies the peptide portion of the NPs is devoid of cytotoxic activity, while stereochemical changes to the polyketide significantly attenuates the activity. For this reason, we believe the polyketide is the cytotoxic fragment and is released upon cellular uptake mediated by the peptide fragment. This chapter will discuss the synthetic efforts made towards each of these NPs and will highlight future experiments to validate the hypothesis.

3.1 Total Synthesis of Reniochalistatin E

Attention was drawn towards the synthesis of reniochalistatin E (**R1**) due to ability to penetrate cancer cells, specifically myeloma cells, as described in chapter 1. As mentioned, cyclic peptides, especially those that are proline-rich, have constrained geometries and leads to enhanced biological half-lives and enhanced cellular penetration. Reniochalistatin E was found to be

comprised of eight amino acids, which are: *L*-tryptophan, *L*-leucine, *L*-isoleucine, *L*-proline, and *L*-valine. There has been no total synthesis of reniochalistatin family to date. Therefore, a route was designed to access the structure for the first time with the intentions of using the molecular framework as a prodrug to delivery potent chemotherapeutics in future works.

3.1.1 Retrosynthetic Analysis of Reniochalistatin E

It was envisioned that reniochalistatin E (**23**) could be accessed via a macrocyclization from the linear percussors **226** or **227** (Scheme 19). Both linear precursors could arise from the coupling of the two tetrapeptides **228** and **229,** which could be synthesized via standard peptide coupling reagents discussed in chapter 2 from commercially available *L*-amino acids.

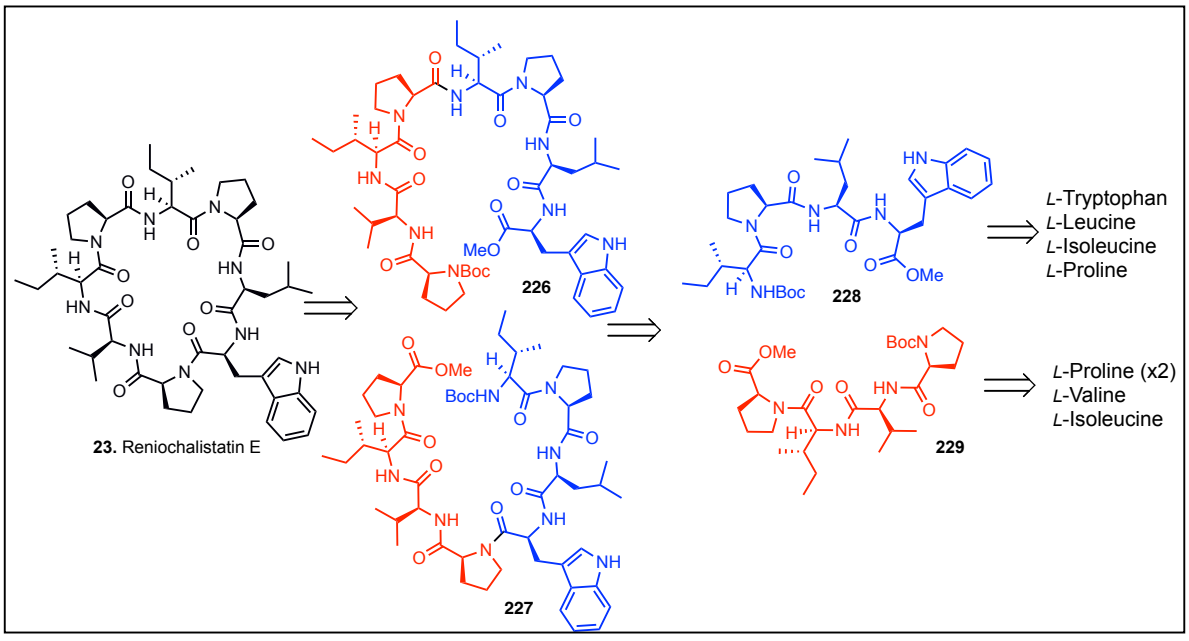

Scheme 19: Retrosynthetic analysis of reniochalistatin E (**23**).

*3.1.2 Construction of the Tetrapeptides **228** and **229***

The synthesis of **228** commenced with a (PyBOP)-mediated coupling of Boc-protected *L*-isoleucine (**230**) to methyl ester of *L*-proline (**231**), to afford the dipeptide (**232**) in 92% yield, as shown in Scheme 20. Analogously, Boc-*L*-leucine (**233**) was coupled to the methyl ester of *L*-

tryptophan (**234**) under the same conditions to access dipeptide **235** in 97% yield. Saponification of dipeptide **232** with lithium hydroxide in THF/H_2O furnished the free acid **236**, and Boc deprotection of **235** with HCl in dioxane afforded the amine hydrochloride salt **237**, both products were obtained in quantitative yields. The coupling of these two dipeptides was accomplished with PyBOP under standard conditions to give tetrapeptide **228** in 55% yield. However, when employing 1-ethyl-3-(3'-dimethylaminopropyl) carbodiimide hydrochloride (EDC·HCl) with HOBt rather than PyBOP the reaction was optimized to 86% yield.

With tetrapeptide **228** in hand, construction of tetrapeptide **229** was undertaken, shown in

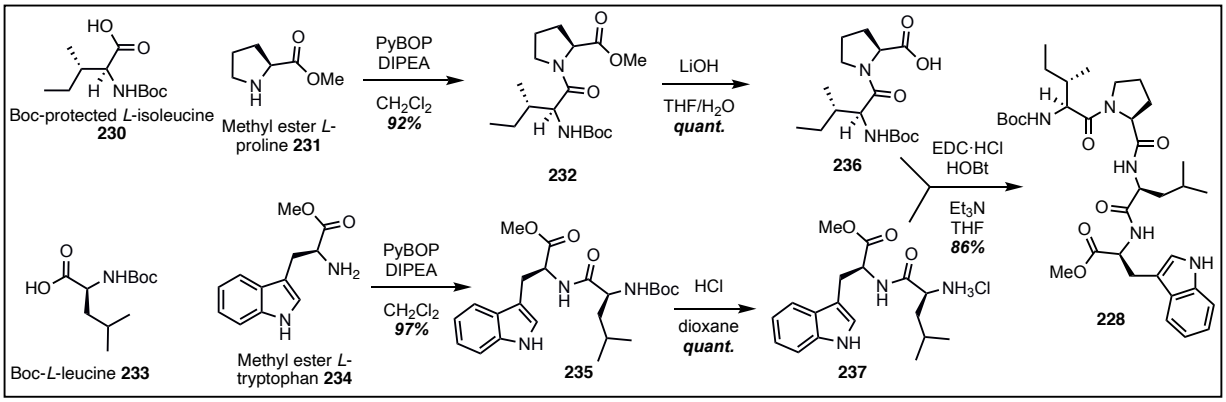

Scheme 20: Construction of tetrapeptide **228**.

Scheme 21. Coupling of Boc-*L*-proline (**238**) to methyl ester of *L*-leucine (**239**) was performed with PyBOP to furnish the dipeptide **240** in 97% yield. Treatment of **240** with lithium hydroxide in THF/H_2O gave access to the saponified free acid dipeptide (**241**) in quantitative yields. Boc

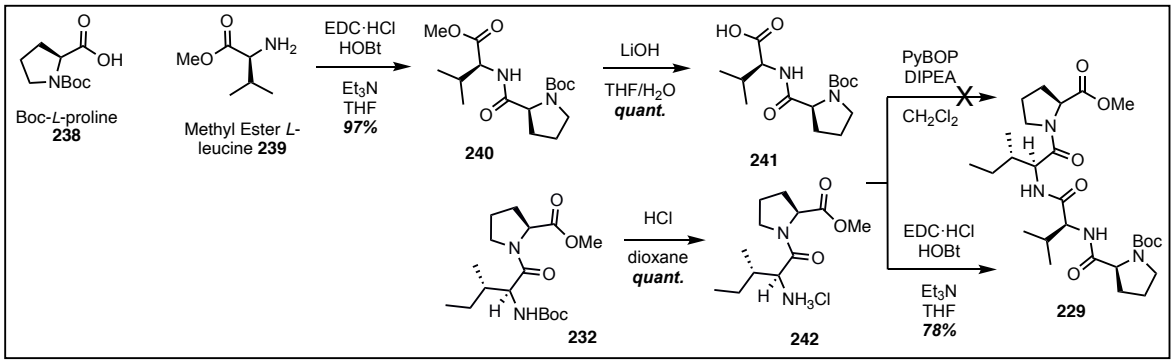

Scheme 21: Construction of tetrapeptide **229**

deprotection of **232** with HCl in dioxane gave access to the HCl amine salt (**242**) in quantitative yield. Coupling of **241** with **242** under the previously employed PyBOP conditions afforded the desired tetrapeptide **229**, but unfortunately the product was unable to be separated from the undesired urea by-products of the reaction, as described in chapter 2. Employing EDC·HCl and HOBt successfully accessed tetrapeptide **229** in 78% yield. The enhanced purity of the compound from these conditions was due to the aqueous soluble of the urea by-products of EDC·HCl coupling.

*3.1.3 Construction of the linear octapeptide **226** and **227** and macrocyclization attempts to **23***

As highlighted in Scheme 19, the linear octapeptide of **23** was envisioned to arise from the saponification and Boc deprotections of **228** and **229**. Coupling of the free acid of **228** to the free base of **229** with EDC·HCl condition furnished octapeptide **226** in 34% yield over three steps (Scheme 22). Compound **226** was subjected to saponification followed by Boc deprotection to

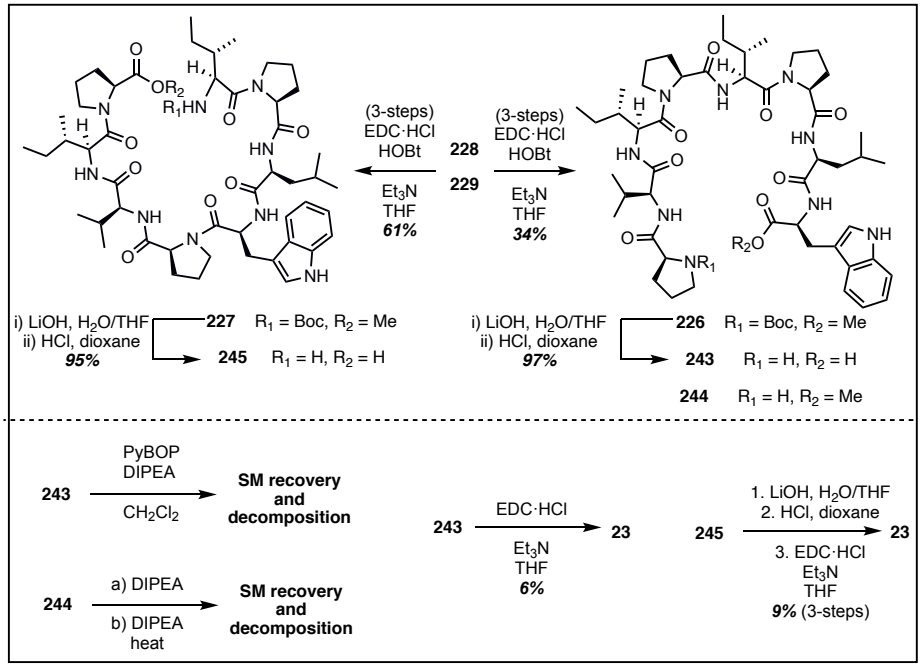

Scheme 22: Construction of the linear octapeptides **226** and **227** and initial attempts as macrocyclization to afford **23**.

afford its fully deprotected form **243** in 97% yield. Macrocyclization attempts with this material under PyBOP conditions only resulted in the return of starting material (55%) and decomposition. We hypothesized the secondary amines of the proline residue, and the BOP-activated ester of the tryptophan could provide enough steric congestion to slow the formation of **23**. To reduce the steric clash of the coupling, aminolysis was attempted for ring closure. To explore this, the Boc group on **226** was removed to afford **244**, with the methyl ester intact; however, all attempts at cyclization failed to provide **23** and resulted in the return of starting material (67%) and decomposition. Recognizing the difficulty of cyclizing via the two sterically encumbered proline and tryptophan residues of **226**, it was thought to couple these two groups first and perform macrocyclization elsewhere on the ring. To achieve this, **228** was Boc deprotected and **229** was saponified, both in quantitative yields. Introducing these to EDC·HCl coupling conditions gave the linear octapeptide **227** in 61% yield over three steps. Compound **227** was altered into its free acid and free amine counterpart in 95% yield and subjected to EDC·HCl coupling conditions to afford the desired natural product **23** in 9% yield. The ^{1}H and ^{13}C NMR spectra and the MS data of the synthesized **23** matched the literature data, shown in chapter 6.

Cyclization conditions to afford **23** with enhanced yields were explored, as shown in Table 6. Attempted PyBOP-mediated coupling of **245** (entry 8) provided only starting material (78%) and decomposition. Employing HOBt, a commonly used additive in peptide couplings, with EDC·HCl to cyclize **243** and **245** (entries 2 and 10) produced **23** albeit in low yields of 2% and 6%, respectively. Entry 10 reflects the

Table 6: Attempts to improve for the formation of **23**.

Trial	Compound	Coupling Agent	Additive	Result
1	**243**	EDC·HCl	N/A	6%
2		EDC·HCl	HOBt	8%
3		DEBPT	N/A	-
4		DEBPT	CsCl	-
5		HBTU	N/A	-
6		HBTU	DMAP	4%
7		TBTU	DMAP	trace
8	**245**	PyBOP		trace
9		EDC·HCl		9%
10		EDC·HCl		15%
11		DEBPT		-
12		DEBPT		5%
13		HBTU		-
14		HBTU		13%

highest yield of **23** via **245**. To expand our reagent scope, macrocyclization was attempted with 3-(diethoxyphosphoroyloxyl)-1,2,3-benzotriazine-4(3H)-one (DEPBT), a reagent that had been successful in the cyclization of similar amino acid based macrocycles.[69] Unfortunately, all attempts at cyclization with this reagent of **243** and **245** (entries 3 and 11, respectively) as well as using cesium chloride as an additive to promote carbonyl coordination (entries 4 and 12) failed to provide **23** in any increased yield. Uronium-based coupling reagents are well reported for their success in macrocyclizations, and as such, *N,N,N′,N′*-tetramethyl-O-(1H-benzotriazol-1-yl)uronium hexafluorophosphate (HBTU) and *N,N,N′,N′*-tetramethyl-O-(1H-benzotriazol-1-yl)uronium tetrafluoroborate (TBTU) were both attempted with **243** and **245** in the absence and presence of 4-(dimethylamino)pyridine (DMAP). In all attempted cyclization, these uronium-based reagents provided either none or low yields of **23**. Employing HBTU with DMAP to cyclize **245** provided a 13% yield of **23** (entry 14), but in our hands, EDC·HCl with HOBt gave the best, albeit low, 15% yield of the natural product.

3.1.4 Biological Evaluation of Reniochalistatin E and Synthetic Intermediates

Having accessed reniochalistatin E and the synthetic intermediates, including the di-, tetra-, and octapeptides in both fully protected and deprotected states, SAR investigations were

Table 7: Cytotoxicity comparison for natural and synthetic **23**, and *in vivo* toxicity of synthetic intermediates.

Cell Line	Cancer Type	Isolation IC_{50} (μM)	Synthesized IC_{50} (μM)	Compound **244** exp. IC_{50} (μM)	Compound **245** exp. IC_{50} (μM)
HeLa	Cervical	17.3	16.9 ± 1.3	>20	18.4 ± 1.7*
U937	Lymphoma	-	12.4 ± 2.4	9.5 ± 2.1*	>20
RPMI-8226	Myeloma	4.9	4.5 ± 1.8	>20	16.4 ± 3.5*
MM.1R	Lymphoblast	-	11.2 ± 1.0	>20	>20
MiaPaca	Pancreas	-	>20	19.1 ± 1.3	>20
A549	Lung	-	>20	>20	>20
MGC-803	Gastric	9.7	-	-	-

undertaken. All compounds in the route were screened for general cytotoxicity against six human cancer cell lines (A549, lung; HeLa, cervical; MiaPaca, pancreatic; U937, lymphoma, RPMI-8226, myeloma; and MM.1R, multiple myeloma). However, none of the di- or tetrapeptides in protected or partial deprotected states were found to have IC_{50} values lower than 30 μM against the cell lines tested. Our synthetic sample of reniochalistatin E possessed approximately the same IC_{50} value in HeLa and RPMI-8226 cell lines: IC_{50} of 16.9 μM (±1.9) relative to the reported 17.3 μM in HeLa and an IC_{50} of 4.5 (±2.2) relative to the reported 4.9 μM in RPMI-8226 (Table 7). Reniochalistatin E lacked cytotoxicity against all of the remaining tested cell lines showing values >10 μM. Neither **226** nor **227**, the protected octapeptides, showed cytotoxicity; however, the free acid/amine **243** showed moderate cytotoxicity toward U937 cell line with an IC_{50} of 9.5 ± 2.1 μM. In contrast to the free acid/amine **245** where no cytotoxicity was observed. At this time, no further investigation has been performed to draw a conclusion regarding SAR based upon these results. However, one can hypothesize the three prolines of **243** could impact the flexability of the structure to allow for cellular penetration and cytotoxicty, and would rationalize the low yeilds in cyclization attempts.

3.1.5 Reniochalistatin E as a Drug-Delivery Platform

With the synthetic route to reniochalistatin E in hand, and the knowledge of modest cytotoxicity associated with the natural compound, it was envisioned that this molecule be elaborated into a drug delivery vehicle. Although reniochalistatin E is not highly cytotoxic in comparison to known chemotherapeutics, its modest toxicity does indicate the compound is likely to penetrate various cells including multiple myeloma. Multiple myeloma is estimated to cause 12,830 deaths in the United States in 2020, with a 5-year survival rate of only 54%.[1,3,7]

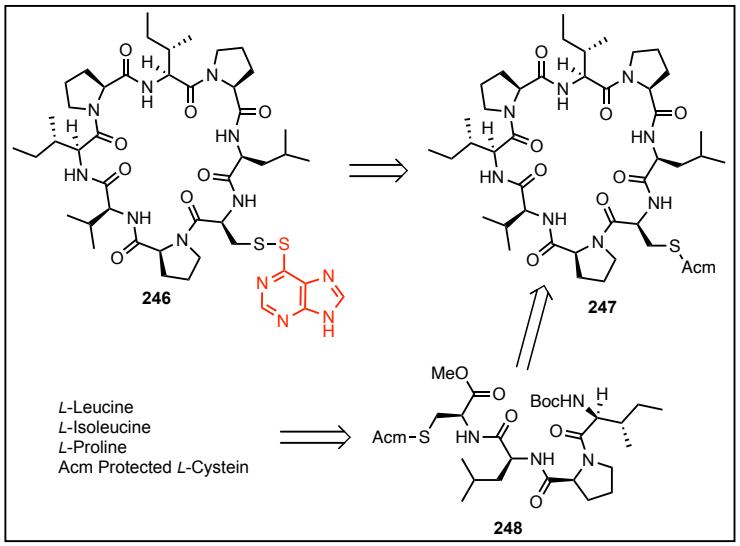

Scheme 22: Retrosynthetic scheme towards the reniochalistatin E disulfide drug delivery compound **246**.

With the *in vitro* ability of reniochalistatin E, an analog synthesis was designed to use this molecular framework as a way to delivery potent chemotherapeutic agents that would otherwise be inaccessible in myeloma treatments. However, first it is important to consider which amino acid would serve as the site for drug conjugation. The tryptophan was selected for its heterocyclic aromatic character which we could be easily substituted with many of the FDA approved anticancer drugs. Moreover, the Rafferty lab was exploring the biological properties of another blood cancer treatment option, 6-mercaptopurine (**1**), shown in Figure 2. This FDA approved drug is still being used for the treatment of acute lymphocytic leukemia (ALL), despite severe side-effects including kidney failure, white blood cell suppression, jaundice, severe vomiting, hepatotoxicity, and death.[70] With this in mind and the structural commonality between 6TP and

the indole moiety of tryptophan, efforts towards designing a linkage point that would allow for enhanced delivery of 6TP into myeloma cancer cells was undertaken. A prodrug moiety was envisioned which could arise from a disulfide linkage between a cysteine analog of reniochalistatin E (**247**) and the sulfur of 6TP to form compound **246** (shown in Scheme 22). The assembly of this reniochalistatin cysteine analog would arise from the same sequence of reactions with the single substitution from *L*-tryptophan for an acetomidly methyl (Acm) protected *L*-cysteine to afford the tetrapeptide **248**. However, before this could be completed, we considered the idea of the tryptophan importance for the cytotoxicity associated with reniochalistatin E. If the tryptophan is critical for the cytotoxic activity, then substitution in that position would render the molecule inactive. Therefore, a synthetic analog where *L*-tryptophan is replaced with *L*-phenylalanine was synthesized to determine the impact on the cytotoxicity.

To this end an analog with a *L*-phenylalanine in place of the tryptophan was designed, as shown in Scheme 23. This work was done in tandem with Ms. Giovana Baca and resulted in a trace amount of **249**. The newly syntheisized analog was tested for anticancer activity and showed a general retention of cytotoxcitiy in all cell lines, shown in Table 8. Interestingly, compound **249**

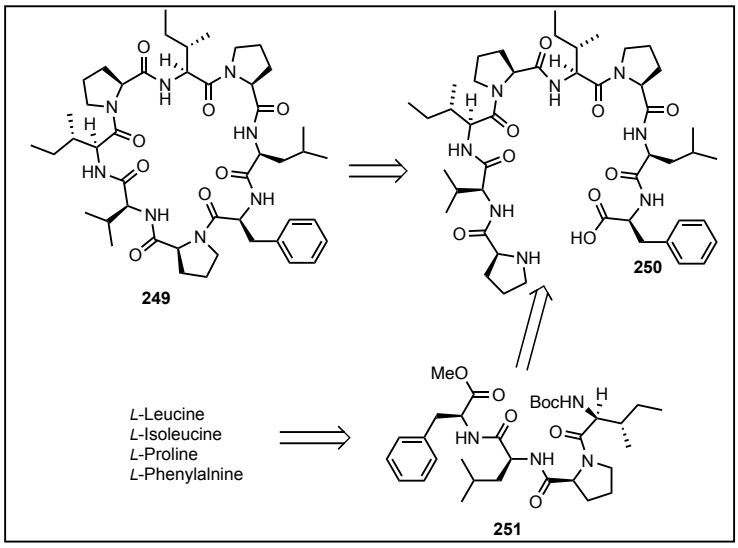

Scheme 23: Retrosynthetic analysis of L-phenylalanine analog of reniochalistatin E (**249**).

Table 8: Toxicity profiling of phenylalanine analogs (**249**)

	IC_{50} (μM)	
Cell Line	**23**	**249**
RPMI-8226	4.5±1.8	5.1 ±1.3
HeLa	16.9 ±1.9	15.2 ±2.1
U-937	12.4 ±2.4	13.8 ±1.6
MM.1R	11.2 ±1.0	11.0 ±2.3
A549	>20	>20

(384-well plates, 72 h, Alamar Blue Detection)

was not toxic towards A549 cell line, matching the observed toxicity of the synthesized NP. For this reason, we concluded the tyrptophan substitution has a limited impact on cytotoxicity. Future work will look to harness the route developed towards reniochalistatin E to introduce 6TP in place of the tyroptophan to be tested for cytotoxicity.

3.2 Synthetic Efforts Towards Lagunamide C

3.2.1 Retrosynthesis of Lagunamide C

3.2.1.1 Addressing the Stereochemical Ambiguity of Lagunamide C

The motivation to synthesize lagunamide C (**35**) drew from potent cytotoxicity in an array of cell lines and the interesting structural features of the aurilide family. The additional carbon unit within the polyketide (C39), renders the previously described synthetic routes incapable of accessing **35**, as described in chapter 2. In addition, total synthesis of **35** would allow for clarification about the absolute stereochemistry, in particular within the polyketide. In light of the stereochemical corrections defined by accessing lagunamide A, the C40 and C7 (shown in red in Scheme 12) stereocenters are likely to be analogously inverted in the corrected structure of lagunamide C. Therefore, a newly propose structure of lagunamide C is shown as compound **252** in Scheme 24. These stereochemical inversions will mimic the rest of the aurilide family and will match the stereochemical configurations as discussed by Dai and coworkers in their synthesis and structural elucidation of lagunamide A.

Retro-synthetically, accessing lagunamide C (Scheme 24) is envisioned to arise via macrolactonization by esterification of the polyketide **253** to the pentapeptide backbone (**254**) is envisioned. This work is focused on the diastereoselective construction of the proposed polyketide **253**. Originally this route was designed to set the C37 alcohol by a facially selective reduction using a Corey-Bakshi-Shibata reduction. Compound **253** would arise by performing a Mukaiyama Aldol between **255** and methyl-(E)-2-methylbut-2-enoate. In order to generate compound **255,** the key transformation of the proposed route wherein a facially selective Charette asymmetric cyclopropanation of **256** and subsequent ring opening would allow the terminal alkene assigning the stereochemistry of the C38 methyl. Assembly of **256** will be accomplished through Wittig olefination of aldehyde **257**, which can be constructed via an Aldol reaction by the chiral *N*-acetyl thiazolidinethione **258**. This reaction will require generation of (*S*)-2-methylbutanal similar to the reports by Huang et al discussed in chapter 2. This work focuses on developing a synthetic route to access the polyketide subunit of lagunamide C. Understanding the stereochemistry of C37, C38 and C40 were in question, a module based approach was designed a to access **253**, but could also generate any of the desired diastereomers, if the proposed structure was incorrect.

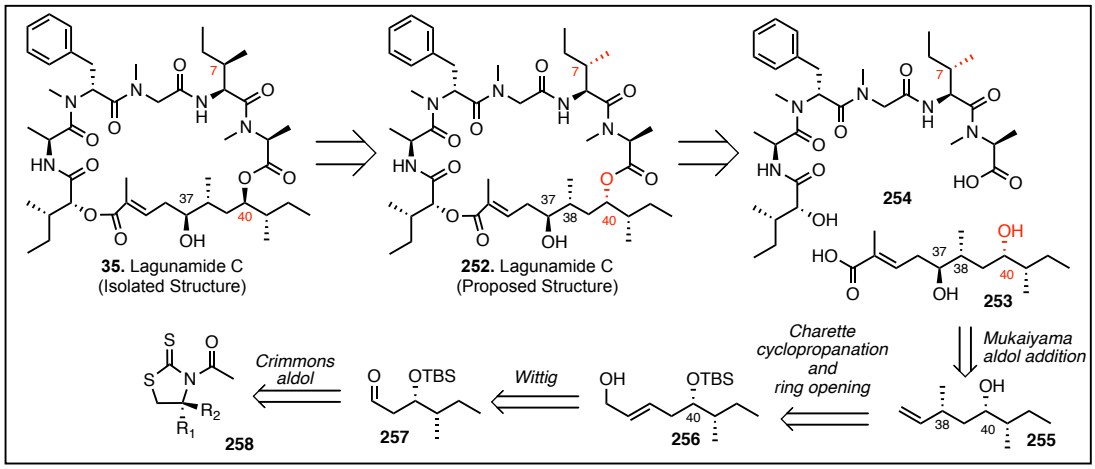

Scheme 24: Isolated structure of lagunamide C (**35**), newly proposed structure (**252**) with stereochemical inversions about C40 and C7 (shown in red), and retrosynthetic analysis of lagunamide C.

3.2.1.2 Module Based Approach Towards the Polyketide of Lagunamide C

The first module of the proposed synthesis of the polyketide of lagunamide C begins with a Crimmins titanium-mediated aldol reaction between the chiral thiazolidinethione auxiliary (**259**) and freshly generated (*S*)-2-methyl butanal (**167**), as shown in Scheme 25. Compound **260** can be silyl protected, and the auxiliary cleaved under reducing conditions to produce a primary alcohol (not shown) and subsequently oxidized to aldehyde **257**. This aldehyde can then undergo Wittig olefination and reduction to afford the allylic alcohol **256**. The second module involves an asymmetric Charrette cyclopropanation[71] to access the cyclopropanated compound **261**. The methyl source of the cyclopropanation ($IZnCH_2I$) can be controlled by boron chelation to set the stereochemistry of the C38 methylene. Halogen installation followed by ring-opening of **261** is envisioned to afford the stereoselective terminal alkene **255**. Oxidative cleavage under Johnson-Lemieux oxidation[72] will give access to aldehyde **262** which can then be subjected to a vinylogous Mukaiyama aldol[73] reaction with TMS-enol ether (**263**) to generate compound **264**. In the case that no selective addition can be achieved, oxidation to the ketone and chiral reduction would enable access to the diastereoselective synthesis of the polyketide portion of lagunamide C, shown

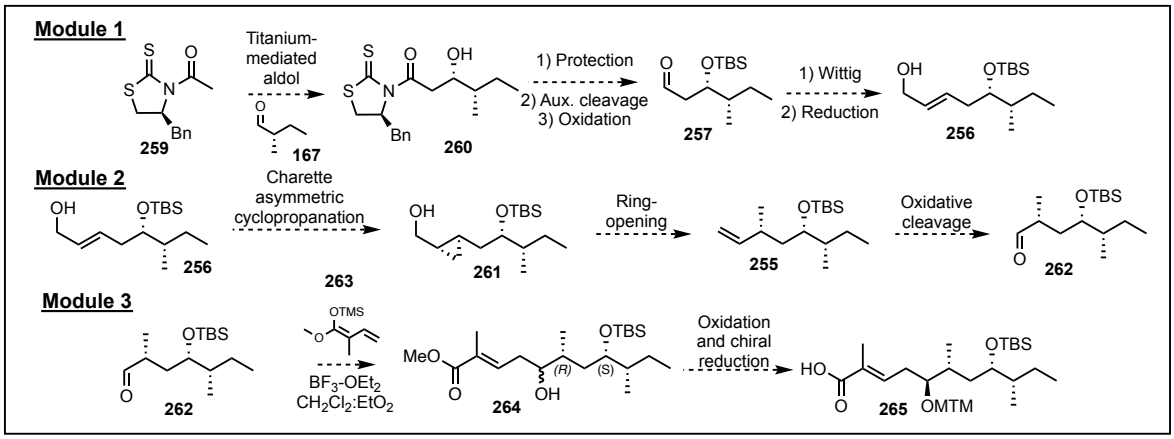

Scheme 25: Module based approach to access the diastereoselective polyketide of lagunamide C.

as **265**.

Given the proposed retrosynthesis route developed, the cyclopropanation and subsequent ring opening steps to set the C38 methyl were identified as the key step as well as the step with great uncertainty. As such, a model system was designed to identify the feasibility of these transformation wherein commercially available butanal (**266**) was used in place of (*S*)-2-methylbutanal (**167**) in the initial aldol reaction. Using compound **266** not only allows for easy access to the allylic alcohol (**267**) for exploration of cyclopropanation conditions, it also can be used to generate a new analog of the polyketide of lagunamide C (**268**) with the C41 methyl group removed (Figure 29).

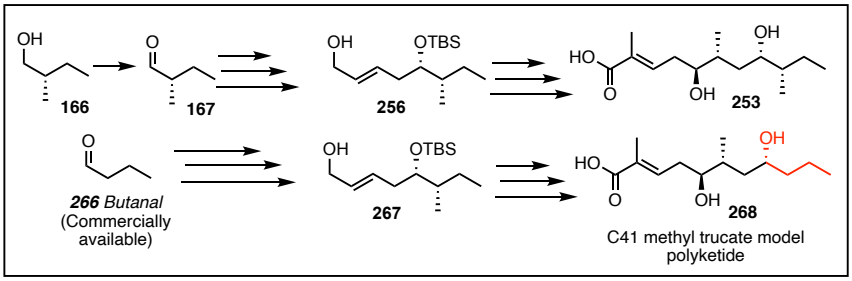

Figure 29: C41 methyl truncate model system.

3.2.2 Synthesis of the Polyketide Fragment of Lagunamide C

3.2.2.1 C41 Methyl Truncated Polyketide Model System

Synthesis of the C41 methyl truncated polyketide began with the construction of the acetylated thiazolidinethione (**271**), which was accessed from *L*-valine (**269,** Scheme 26). Reduction of **269** with $LiAlH_4$ in THF at reflux afforded *L*-valinol in 99% yield. Formation of the Crimmins auxiliary was performed under standard conditions[74,75] to access **270** in 95% yield over two-steps. Acetylation of the auxiliary with acetyl chloride and *n*-BuLi successfully furnished **271** in 98% yield with no column chromatography required.

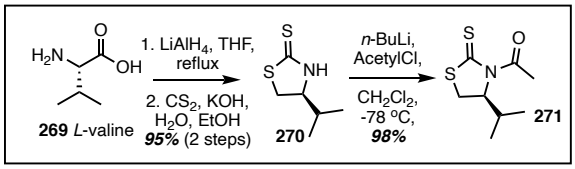

Scheme 26: Auxiliary generation for aldol reaction.

Initial aldol attempts between **271** and butanal employed the chiral base (-)-sparteine (0.5 eq) with titanium tetrachloride in CH_2Cl_2, which afforded the desired aldol product **273** in 27% and undesired aldol product **272** in <4% yield (Table 9, entry 1). The stereoisomers of **273** and **272** were also accessed by Zhou and co-workers[76] and were used to confirm product distribution through ^1H NMR and optical rotation comparisons. Zhou also employed the same Crimmins auxiliary, but under his condition of diisopropyl ethylamine (DIPEA) **272** was favored in a 2:1 ratio over **273**. Increasing the equivalents of the sparteine did provide an increased yield of **273**, but only by a marginal 3% with 0.75 equivalents and 8% with 1.2 equivalents (entries 2 and 3, respectively). Employing various amine bases in auxiliary based aldol reactions is well reported in the literature.[59,75] Given the poor yields with the chiral base (-)-sparteine, efforts were directed towards screening other amine bases. Exploring DIPEA (entries 4–6) as the base gave the opposite of the desired selectivity, favoring **272** over **273**, analogous to the reported observations from Zhou.[76] Varying the equivalences of the base failed to reverse the observed selectivity. The addition of NMP (N-methylpyrrolidone) in an equal molar ratio to the base returned the desired selectivity with yields of 30% of **273** and 13% of the undesired **272** (entry 7). Considering our previous works with the diamine base sparteine,

Table 9: Reaction optimization of aldol reaction to form **272/273.**

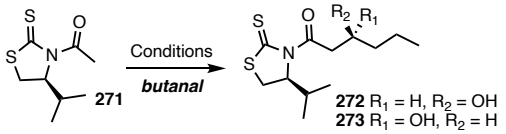

Entry	SM	Coordination	Base (eq)	NMP (eq)	% Yield *S-isomer*	% Yield *R-isomer*
1	A	$TiCl_4$	(-) sparteine (0.5)	-	<4	27
2			(-) sparteine (0.75)	-	<5	30
3			(-) sparteine (1.2)	-	<2	35
4			DIPEA (0.5)	-	36	13
5			DIPEA (1.1)	-	47	22
6			DIPEA (2.2)	-	47	25
7			DIPEA (1.05)	(1.05)	13	30
8			DIPEA (2.05)	(1.05)	23	38
9			TMEDA (1.05)	-	7	19
10			TMEDA (2.05)	-	8	21
11			TMEDA (2.05)	(1.2)	8	22
12			LDA (1.2)	-	11	53
13			**LDA (1.2)**	**(1.2)**	**4**	**79**
14			LDA (1.2)	(2.2)	<4	65
15			Et_3N	-	25	16
16	B	Bu_2BOTf				

we hypothesized bidentate ligand addition onto the titanium would facilitate aldol formation to return our desired stereoselectivity. Doubling the base equivalence increased the yield of **273** by 8%, but also increased **272** by 10% (entry 8). Employ the bidentate base TMEDA alone and with NMP failed to provide any yields greater than 22% of **273** (entries 9–11). With weak bases failing to provide the desired **273** in both high yields (over 50%) and in selectivity, strong bases were screened. Screening the reaction with LDA (entry 12) afforded **273** in 53%, and the undesired **272** in 11% yield. Utilizing an equal molar ratio of LDA to NMP afforded **273** in 79%, with only 4% of the undesired **272** (entry 13). Given the observed trends, increasing the NMP equivalence should correlate to increased yields. Unfortunately, this was not observed with LDA and resulted in a decreased yield (entry 14). Through these studies, we were able to access **273** in a 70% yield with a 20:1 dr.

With the optimized conditions in hand (Table 1, entry 13), TBS protection of the alcohol in **273** was performed with TBSCl, imidazole in THF in 45% yield (Scheme 27). Unfortunately, optimization of these conditions failed to result any increase in yield; however, employing 2,6-lutidine in DMF at room temperature afforded **274** in 65% yield. Increasing the temperature to 32 °C increased the yield to 86% of **274**. Increasing the temperature further led to decomposition of the starting material. Treatment of **274** to DIBAl-H in CH_2Cl_2 gave access to aldehyde **276** in 31% yield along with recovered starting material **274** in 29% yield. In this DIBAL-H reduction step 21% of the auxiliary **270** was obtained and subsequently acetylated to provide **271**. All attempts

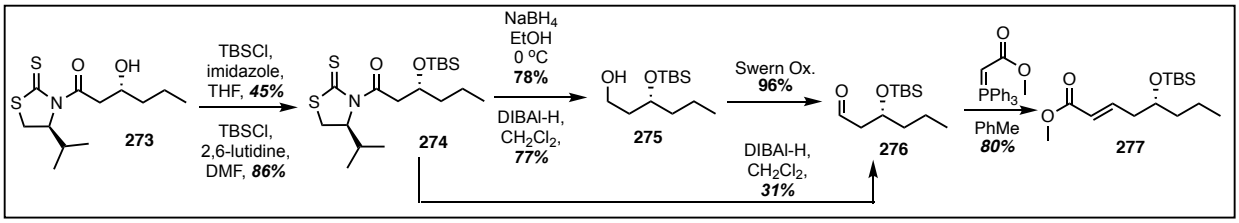

Scheme 27: First model towards the C41 methyl truncate polyketide (**268**).

to optimize these conditions to reduced **274** to the aldehyde **276** provide low overall yields. Employing 2.2 equivalents of DIBAl-H in CH_2Cl_2 afforded alcohol **275** in 77% which was then oxidized to **276** in 96% yield under Swern oxidation conditions. Subjecting **274** to $NaBH_4$ in ethanol furnished **275** in 91% yield, which was also oxidized to **276** in 96% yield. The $NaBH_4$ reduction also resulted in the recovery of 80% of auxiliary **270**, which was successfully recycled and elaborated onto **271**. Structural integrity of **271**, via recycled **270**, was confirmed by ^1H NMR spectral and optical rotation comparison to the originally synthesized **271**. Treating **276** with the activated ylide methyl-(triphenylphosphoranylidene) acetate in toluene afforded the allylic methyl ester **277** in 80% yield.

With the desired product from the first module in hand, efforts were directed towards exploring the cyclopropanation and ring-opening step. Reduction of **277** with $NaBH_4$ in ethanol afforded the allylic alcohol **267** in a 19% yield along with high amounts of decomposition. When $LiAlH_4$ was employed, it failed to provide a greater yield of **267** yielding 17%. The reaction was finally optimized by subjecting **277** to 2.5 equivalents of DIBAl-H in CH_2Cl_2 at -78 °C affording **267** in 92% yield (Scheme 28). With compound **267** in hand, efforts were turned towards identifying conditions for cyclopropanation and ring opening to prove that our proposed key-steps for the synthesis of lagunamide C was feasible. To explore this a non-facially selective cyclopropanation conditions was employed. Cyclopropanation with Et_2Zn, CH_2I_2, and $TiCl_4$ at 0 °C

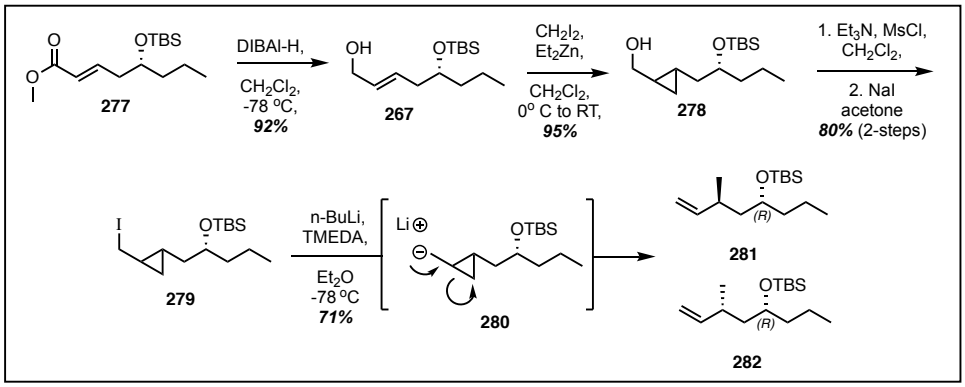

Scheme 28: Cyclopropanation and ring-opening on model system.

failed to generate the desired product, which led us to explore temperature effects. Increasing the temperature, nor cooling the reaction to 0 °C then lowering to -20 °C failed to provide any product. Finally, stirring the reaction at 0 °C and then allowing it to warm to room temperature, 45 min post reagent addition, led to a 3% yield of **278**. Excluding $TiCl_4$ resulted in an increase of yield to 48%, and running the reaction overnight resulted in a 95% conversion to the desired cyclopropanated material **278** as a mixture of diastereomers. Mesylate protection of the alcohol was accomplished via methane sulfonyl chloride with Et_3N in CH_2Cl_2 followed by iodine exchange with NaI in acetone to afford **279** in 80% yield over the 2 steps. The stability of **279** was found to be fleeting (1–2 h) and was immediately carried onto to the lithium-halogen exchange. Subjecting **279** to *n*-BuLi and TMEDA in diethyl ether at -78 °C afforded a mixture of the desired ring-open products

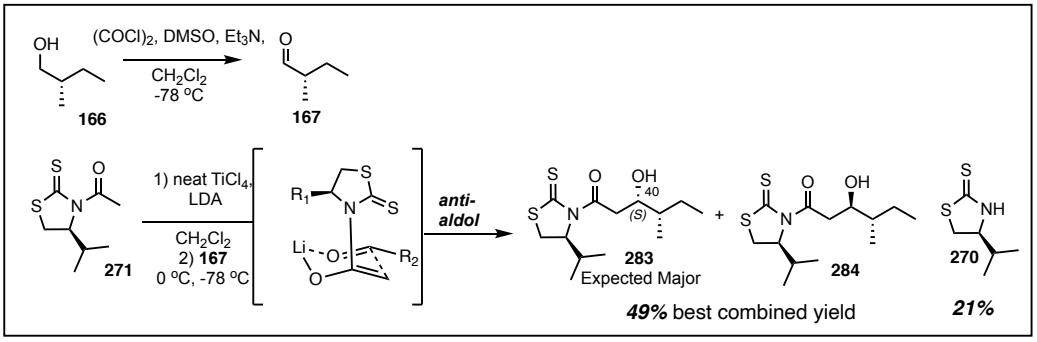

Scheme 29: Reaction conditions for aldol towards target polyketide.

281 and **282** in a combined yield of 71%. The reaction is hypothesized to retain stereochemistry set in the cyclopropanation conditions through intermediate **280**; however, starting with a racemic mixture lead to an inseparable mixture of diastereomers. Using less than 2.0 equivalents of tetramethylethylenediamine (TMEDA) resulted in a decrease in yields of **281**/**282** and led to an increase in decomposition of the starting material. Given the success of the model system, efforts were directed towards the synthesis of the target polyketide of lagunamide C.

3.2.3 Diastereoselective synthesis of the polyketide of lagunamide C

3.2.3.1 Aldol Reaction Optimization

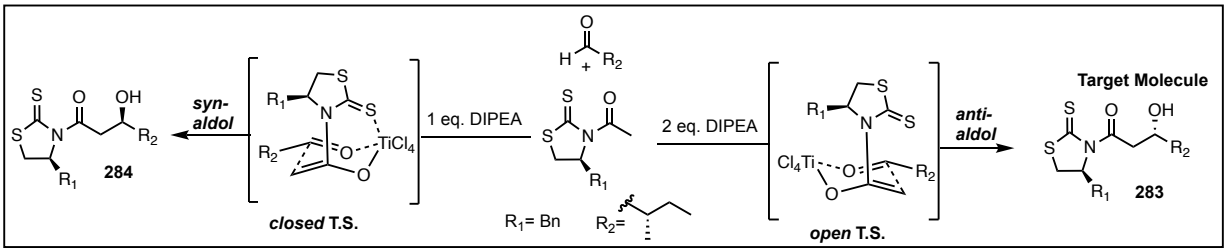

Scheme 30: Previously reported aldol transition states with one and two equivalents of base.

To begin the synthesis towards the target polyketide, the commercially available alcohol (*S*)-2-methylbutanol (**166**) was oxidized to its corresponding aldehyde via Swern Oxidation conditions. Unfortunately, attempts to isolate the aldehyde (**167**) proved challenging as the product is volatile and evaporates under reduced pressure. Therefore, efforts towards generating the aldehyde *in situ* followed by immediate addition to the enolate of the thiazolidine (**271**) as shown in Scheme 29 was attempted. To this end, the crude mixture from the Swern Oxidation was subjected to the optimized aldol conditions using LDA wherein the lithium promoted enolate is known to proceed through a 6-membered ring transition state to provide the *anti*-aldol product with the C40-(*S*) configuration, as shown in Scheme 29. Unfortunately, the highest reaction yield was 49% of the mixture of diastereomers **283**/**284** in a 3:2 dr. In addition, the thiazolidine (**270**) was obtained in yields up to 21% and is inseparable from the desired isomer **283**. There are limited reports of this deacetylation of the auxiliary.[77,78] Literature reports identified DIPEA as a more selective method of enolate generation. When DIPEA is added in two equivalents, aldol formation is known to proceed through an *open* 6-membered ring transition state and allow preferential addition of the aldehyde in an *anti*-fashion to produce compound **283** as the major isomer, as shown in Scheme 30. Addition of one equivalents of DIPEA should generate a *closed* transition state to promote formation of the *syn* aldol product (**284**). Reaction optimization attempts

identified that the starting material of the reaction was consumed with the two equivalent of base and therefore the major product of the reaction was believed to be the *anti*-aldol product (**283**).

In an attempt to further optimize reaction selectivity, the auxiliary was altered to include the more sterically encumbered benzyl thiozolidinones **285** and **286**, shown in Scheme 31 Interestingly, when neat $TiCl_4$ was substituted for a 1 M $TiCl_4$ in CH_2Cl_2 solution, the reaction yielded both diastereomers in 84% and 94%, respectively. However, the reaction continued to produce the unwanted deacetylated auxiliary. The deacetylation increased when the high room humidity (> 65%), and when the crude reaction mixture was allowed to warm to room temperature overnight. To understand why this was occurring an HPLC method was designed to quantify the undesired products of the reaction.

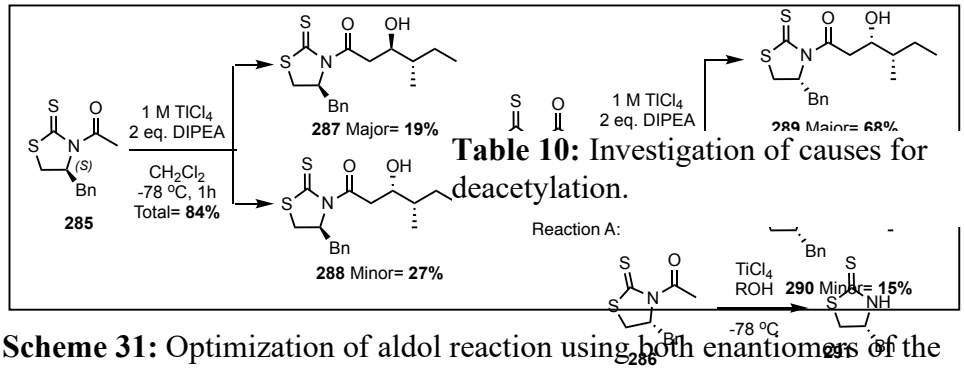

Scheme 31: Optimization of aldol reaction using both enantiomers of the benzyl thiozolidinones **285** and **286**.

When **286** was subjected to 1 equivalent of $TiCl_4$ in CH_2Cl_2 at -78 °C followed by dropwise addition of various solvents/compounds. Next, the reaction was quenched with NH_4Cl (sat) and the reaction was separated via HPLC and quantified based on the polarity. The addition of water lead to limited deacetylation (1%) in comparison to

Table 10: Investigation of causes for deacetylation.

Reaction B:

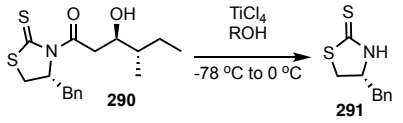

Additive	Reaction A Percent of decomposition (-78 °C quench)	Reaction B Percent of decomposition (-78 °C -to- 0 °C)
None	5%	17% to 11%
H_2O	1%	10% to 8%
EtOH	48%	30% to 76%
t-BuOH	2%	-
290 Aldol Product	3%	-
Isopropanol	3%	-
166 (S)-2-methyl butanol	-	9% to 55%
Benzyl Alcohol	-	33% to 58%

the control group (5%) where no solvent was added before reaction quench with NH_4Cl (sat) (shown in Table 10). However, when ethanol was added to **286**, 48% of **291** was recovered. The other solvents including *t*BuOH and isopropanol did. not increase in deacetylation showing 3% and 3%, respectively. Since none of the solvents tested are used or produced in the aldol reaction conditions, we expanded our test to include the aldol product of the reaction (**290**).

One distinct advantage of the Crimmins auxiliaries are the ease of cleavage after aldol product formation. Therefore, compound **290** was subjected to one equivalent of $TiCl_4$ and a variety of solvents/compounds to determine if this was the cause of the recovery of the deacetylated auxiliary (**291**). In addition, thermodynamic properties of this decomposition were explored by quenching half of the reaction at -78 ^oC and allowing the remainder of the reaction to warm to 0 ^oC before quench. Quantification of the by products via HPLC at -78 ^oC showed no significant increase in decomposition of water addition with 10% in comparison to the control group (17%). Increasing the temperature to 0 ^oC showed only 11% and 8% respectfully. When ethanol was added, 30% of **290** was recovered as **291**. Moreover, when the temperature was increased to 0 ^oC 76% of **290** had broken down into **291**. Interestingly, the addition of (*S*)-2-methylbutanol (**166**) at -78 ^oC led to a 9% recovery of the auxiliary, but more than half (55%) of the starting material had been broken down when warmed to 0 ^oC. The addition of benzyl alcohol also increased with temperature from 33% to 58%, respectively.

3.2.3.1.1 Decomposition of N-acetyl Auxiliary

This data shows evidence that primary alcohols enable decomposition of the *N*-acetylated Crimmins auxiliary (**286**) and the aldol product of the reaction (**290**). The instability of the N-acetylated Crimmins auxiliary is likely due to the lack of inductive effect by the alpha methyl of *N*-propyl auxiliaries, which are widely used and have no reports of decomposition. One can conceptualize the titanium coordination allows enough electron deficiency at the carbonyl carbon of **286** to allow for a primary alcohol to attack and cleave the auxiliary, as shown in Scheme 32. This attack produces a tetrahedral intermediate (**292**) that may collapse and cleave the thiazolidinone (**293**) containing and an ester (**294**). Proton transfer produces the thiazolidinone (**291**) which is readily isolated; however, isolation of the ester formed in this reaction has not been achieved. The inability to isolate the ester product is attributed to the low molecular weight of the compound; which are known to be volatile under reduced pressure. In conclusion, we believe that excessing room humidity (>65%) prevents full oxidation of (*S*)-2-methylbutanol allowing for

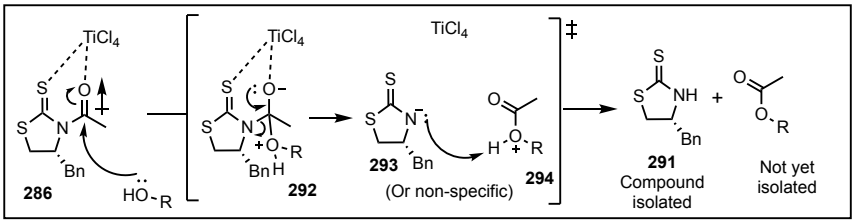

Scheme 32: Proposed mechanism for N-acylated auxiliary decomposition.

significant decomposition of both the *N*-acetylated thiazolidinone (**286**) and the aldol product (**289**/**290**) of the reaction. To combat this issue, we explored oxidation conditions for (*S*)-2-methylbutanol to decreased undesired decomposition.

To optimize the aldol reactivity and decrease undesired decomposition, we looked to explore oxidation conditions with minimal side-products and workup. Subjecting (*S*)-2-methylbutanol to TEMPO failed to oxidize to the aldehyde; however, PCC conditions allowed for full conversion of **166** to **167**. In addition, the PCC oxidation requires simple celite filtration before use in the aldol reaction. With these new optimized conditions, the aldol reaction proceeded smoothly producing **289** and **290** in a combined yield of 83% with a dr of 4.5:1. Gratifyingly, protection of the hydroxyl via TBS triflate provided compound **295** in quantitative yields and afforded crystals for X-ray diffraction analysis. The data indicated the absolute configuration of **289** at the C40 as *S*, shown in Scheme 33.

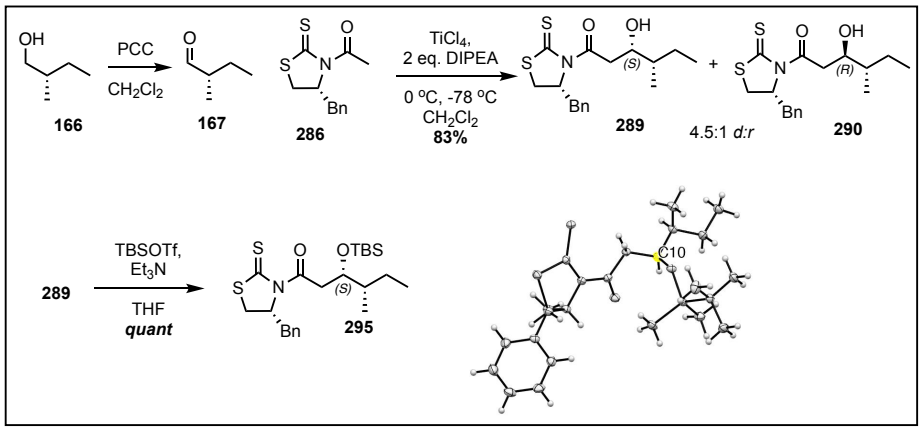

Scheme 33: Optimized aldol reaction and determination of stereochemistry via crystallographic data.

3.2.3.1.2 Inversion of Aldol Selectivity

The crystallographic data generated by this work challenges the proposed transition state discussed in the literature. As discussed, two equivalents of DIPEA is proposed to produce the *anti*-aldol formation as the major product. However, this study finds an inversion of selectivity

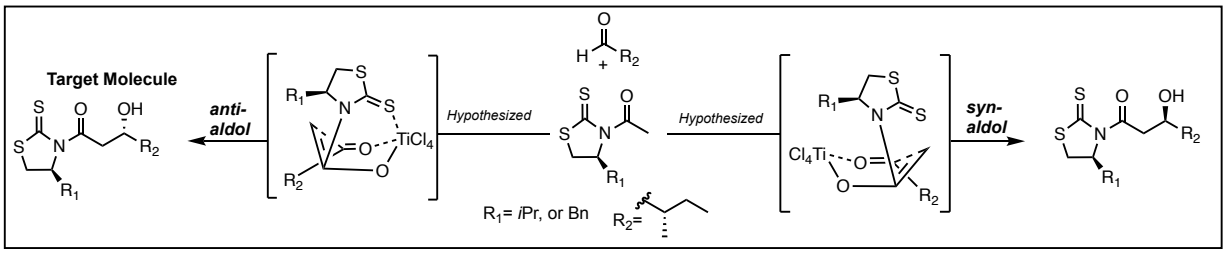

Scheme 34: Proposed boat transition state of N-acetyl Crimmins auxiliaries.

which can be attributed to the lack of steric influence associated with the *N*-acetyl variant of the auxiliary. The transition state previously described in Scheme 30 was originally derived from the work with the *N*-propyl auxiliary and contains a methyl in the alpha position of the enolate. This methyl induces selectivity by 1,3-diaxial interaction with the approaching aldehyde to enhance the selectivity. Contrary to this, the *N*-acetyl is devoid of this steric clash and can allow for conversion of the chair transition state to a boat-like transitions state, as shown in Scheme 34. The proposed boat transition state would produce the inverted selectivity, matching the observed selectivity in the afore mentioned aldol reactions.

3.2.3.2 Completion of Module 1 towards the Target Polyketide of Lagunamide C

With a new understanding of selective aldol formation, the synthesis of polyketide of lagunamide C was continued, Scheme 35. Compound **289** was subjected to TBS triflate conditions, as previously described, and was subjected to $NaBH_4$ to afford the primary alcohol **296** in 88% yield over 2 steps. Oxidation of **296** was performed by PCC and removal of the pyridinium by-

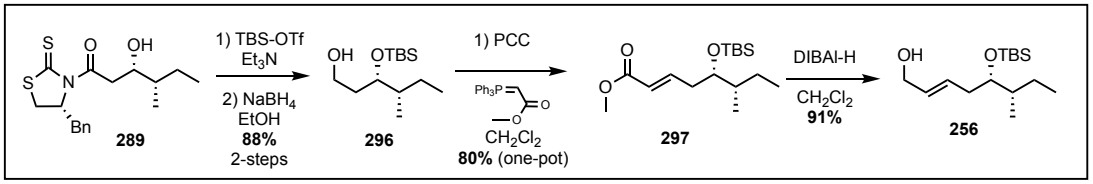

Scheme 35: Completion of module one towards target polyketide of lagunamide C.

product via celite filtration was subjected to Wittig olefination to afford compound **297** over 2 steps with an 80% yield. The allylic methyl ester (**297**) was then reduced to the allylic alcohol **256** via DIBAl-H reduction in 91% yield. Accessing the allylic alcohol completed the first module with high control and enabled the exploration of cyclopropanation conditions to control the chirality of the C38 stereocenter.

3.2.3.3 Optimization of Cyclopropanation Conditions and Module 2

The facially selective cyclopropanation upon the allylic alcohol **256** was performed with the addition of the chiral boric acid butylboronic acid *N,N,N,N*-tetramethyl-L-tartaric acid (**298**). Employing analogous conditions used in the C41 methyl truncate model system, with the addition of **298** furnished **261** in 76% yield. Elaboration of **261** to the desired iodinated compound **299** was accomplished in 84% yield over 2 steps. Interestingly, subjection **299** to the ring-opening conditions starting at –78 °C and warming to –30 °C afforded both **255** and **301** in 85% yield with a dr of 5:1. When the reaction was maintained at a temperature of -78 °C an enhanced selectivity of 10:1 dr and a 99% yield was observed, in favor of the desired isomer (**255**). The loss of selectivity in the ring-opening step is counterintuitive to the hypothesized transition state (shown as **300** in Scheme 36) and is unlikely to account for the racemization to the undesired diastereomer. Therefore, the selectivity of the reaction indicates the cyclopropanation step as a source of the undesired isomer leading to compound **301.** However, NMR characterization of the cyclopropanated compound **261** is unable to identify the dr of the reaction, and future work will look to determine this. Regardless, the route had allowed access to compound **255** as the major isomer validating module two of the proposed route.

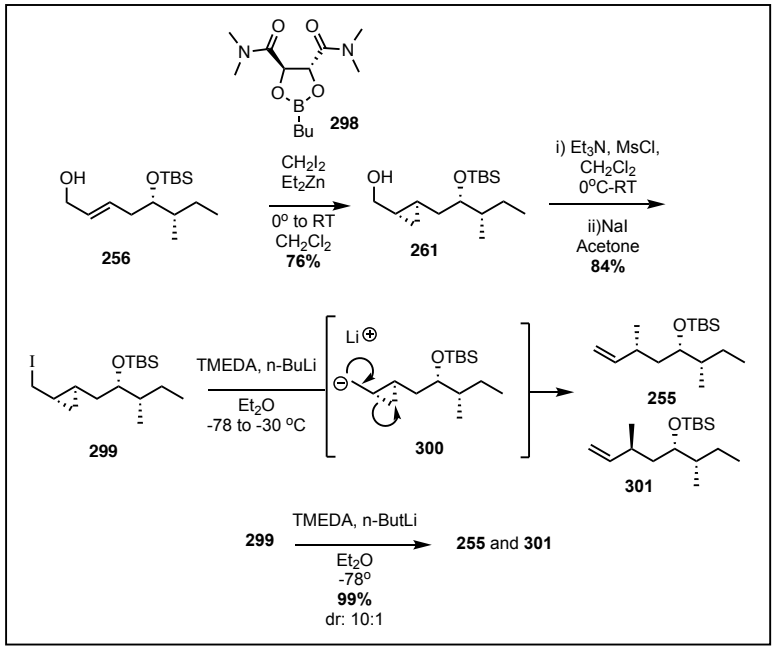

Scheme 36: Facially selective cyclopropanation and ring-opening.

3.2.3.4 Current Efforts on Module 3

3.2.3.4.1 VMAR Trial

To construct the polyketide of lagunamide C the final module looked to harness an enantioselective vinylogous Mukaiyama aldol reaction (VMAR) similar to the method employed by Bergdahl and coworkers.[36] Bergdahl and coworkers were able to access the polyketide of lagunamide A via a TBS enol based auxiliary approached (Figure 35 A). In their efforts, **199** was

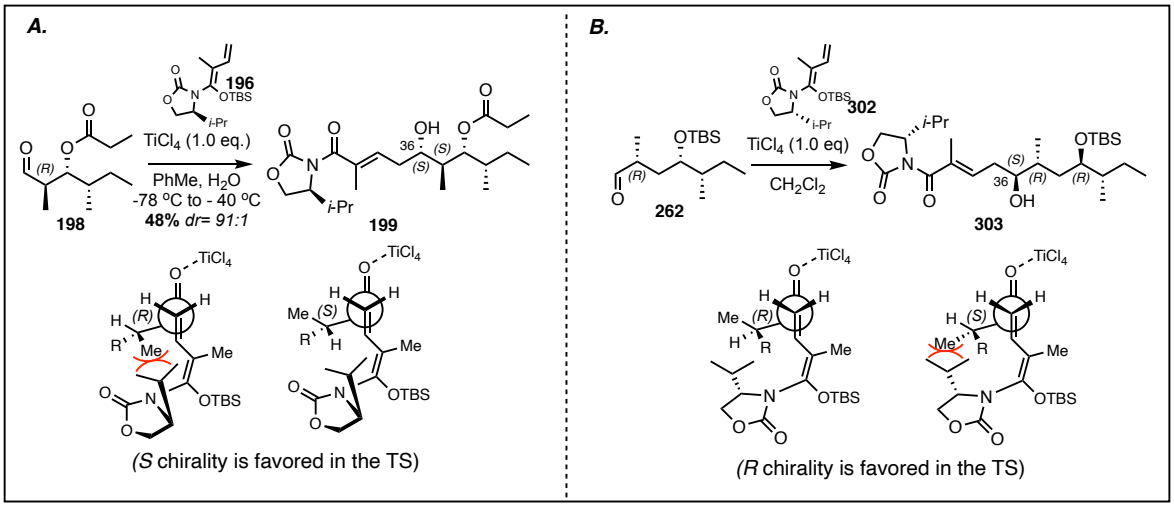

Scheme 37: A. Reported transition state of VMAR when using *R*-2-methyl aldehydes by Bergdahl; **B.** Corresponding transition state wherein the *R*-2-methyl aldehyde is favored.

generated in 48% yield with a dr of 91:1 in favor of the desired C37-*S* alcohol from the starting material aldehyde (**198**). The authors stated the *R*-2-methyl center of the aldehyde (**198**) was disfavored in the transition state due to chirality of the auxiliary and was responsible for the low yields. Based upon this data, and the fact that compound **262** possesses an *R*-2-methyl aldehyde, the enantiomer of the auxiliary was generated to explore the reaction further.

To investigate whether the *L* or *D* auxiliary would provide the desired stereoselectivity of the VMAR, a model system was undertaken. Two model aldehydes were chosen along with both the *D* and *L* valine-based auxiliaries. Oxidation of (S)-2-methylbutanol (**166**) to the aldehyde counterpart (**167**) was accomplished via PCC. In addition, both chiral oxazolidinones were constructed from their corresponding *L* and *D* valinol derivatives, respectively, and tiglic acid was amidated upon both auxiliaries followed by TBS enol ether formation to access both **196** and **302**. The TBS enol ethers were treated with both aldehydes, (S)-2-methylbutanal and benzaldehyde at -78 °C with LHMDS and $TiCl_4$ and allowed to run overnight (Table 11). Treatment of **196**, the *L* valinol derived auxiliary, with (S)-2-methylbutanal (**167**) afforded a 31% yield of the desired VMAR product with a dr of 1:0 (entry 1). Employing the *R*-auxiliary (**302**) under the same conditions afforded a 32% yield of the expected product with a dr of 2:1 (entry 2). Both entry 1 and 2 allowed the reaction to warm from -78 ºC to RT overnight; however, when the reaction was kept at -78 ºC for the duration of the reaction, a lower yield of 11% was obtained but with improved diastereoselectivity, a dr of 1:0 (entry 3). Interestingly, when benzaldehyde is exposed to similar conditions (entry 4) an improved yield of 65% is obtained along with the selectivity (1:0 dr). This suggests that the α-methyl center does slow the MVAR, but the desired diastereoselectivity can be achieved through construction of the correct auxiliary.

Table 11: Exploration of VMAR reactivity on model aldehydes (*S*)-2-methylbutanal and benzaldehyde using both enantiomers of the TBS enol ether.

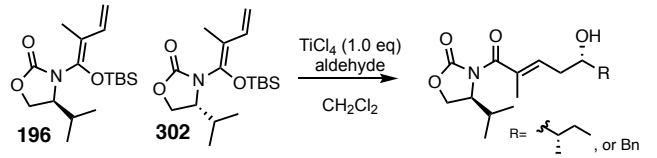

Entry	Auxiliary	Temp	Aldehyde	% Yield	*dr*
1	**196**:(*S*)	-78 ºC to RT	(*S*)-2-methylbutanal (**167**)	31%	1:0
2	**302**:(*R*)	-78 ºC to RT	(*S*)-2-methylbutanal (**167**)	32%	2:1
3	**302**:(*R*)	-78 ºC	(*S*)-2-methylbutanal (**167**)	11%	1:0
4	**302**:(*R*)	-78 ºC to 2 ºC	benzaldehyde	65%	1:0

Based upon the proven feasibility of the model system, efforts were directed towards accessing the required substrate to perform the MVAR to construct the carbon skeleton of the polyketide. Subjecting **255** to Lemieux-Johnson conditions, dihydroxylation with OsO_4 followed by oxidative cleavage with $NaIO_4$, furnished **262** in 68% yield (Scheme 38). Unfortunately, subjecting **262** to the same conditions outlined in Table 11 failed to provide any of the expected VMAR product (**304**). All of the attempted VMAR reactions performed on compound **262** returned the starting aldehyde and the auxiliary with the TBS group removed. Noting that the reactivity in this case is highly dependent on titanium coordination and addition into the aldehyde, it is hypothesized that the TBS protecting group at C40, may be the cause for the lack of reactivity. As previously discussed, relative reactivities of 1,4-diols are starkly different from 1,3-diols and can also be a cause of decreased reactivity. Given the inability to gain access to the polyketide via a VMAR, additional routes were explored.

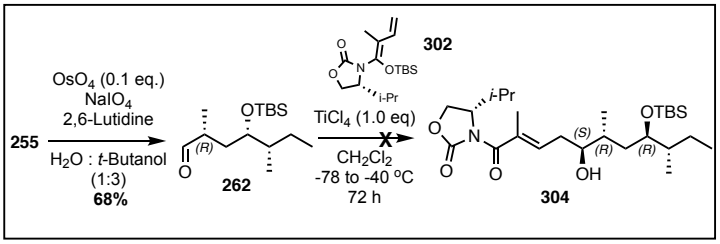

Scheme 38: Attempted VMAR to access the polyketide of lagunamide C.

3.2.3.4.2 Allylation and Cross-Metathesis Conditions

To access the carbon framework of the polyketide, an allylation strategy similar to the work by Lin and coworkers was envisioned.[63] To understand the reactivity of the cross metathesis (CM) conditions, a model system was devised, shown in Scheme 39. To start, benzaldehyde (**305**) was exposed to allylmagnesium bromide in diethyl ether to afford the alcohol product **306** in 91% yield as a mixture of enantiomers. The enantiomers were subjected to Grubb's second-generation catalyst in the presence of methyl methacrylate (**307**) under reflux condition; however, no product (**308**) was isolated. Oxidation of compound **306** to the ketone (**309**) also failed to provide the product desired product (**310**) when subjected to the CM conditions. The free electrons of the oxygen in these cases were identified as a possible cause of the poor reactivity, and therefore compound (**306**) was protected as a PMB ether to afforded compound **311** in 96% yield. Upon subjection of **311** to CM conditions the homodimer **312** was isolated in 49% yield. To probe if the formation of a sterically bulky trisubstituted olefin was slowing the reaction, we exposed the

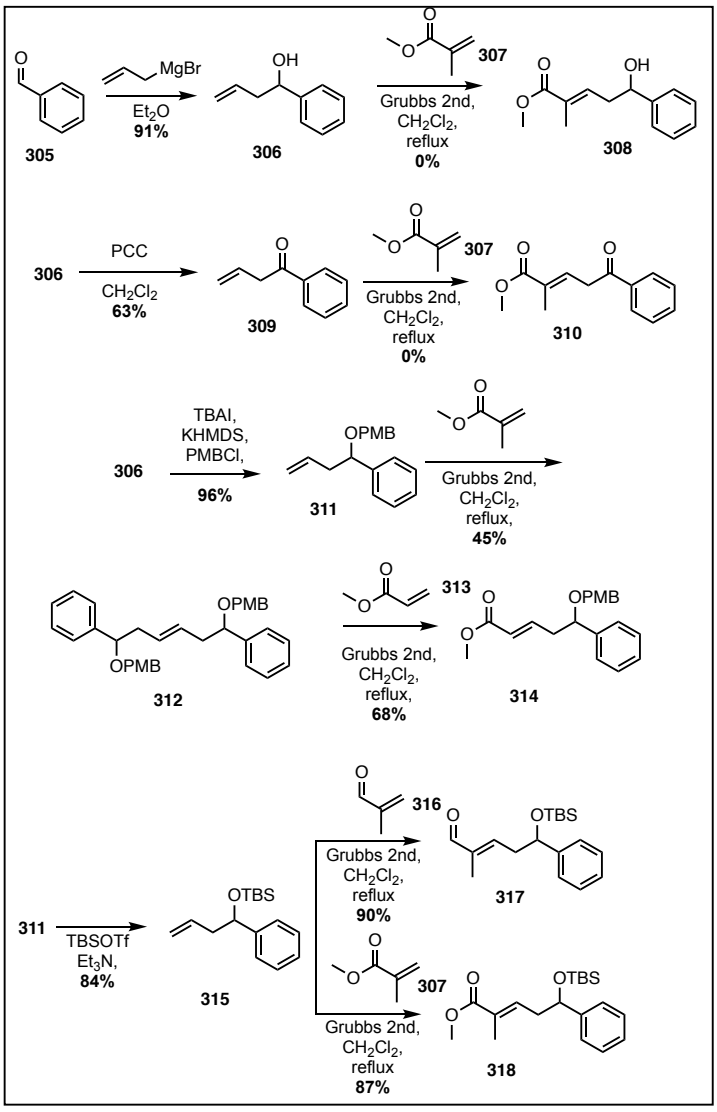

Scheme 39: Model system using benzaldehyde (**305**) to explore reactivity of cross-metathesis reaction.

homodimer (**312**) to methacrylate (**313**) to provide the desired di-substituted olefin (**314**) in 68% yield. To explore the effects of TBS protection, compound **311** was protected with TBS triflate to afford **315** in 84% yield. Compound **315** was subjected to CM conditions with the aldehyde (**316**) and afforded the disubstituted olefin product **317** in 90% yield. Gratifyingly, subjected **315** to CM conditions with methyl methacrylate (**307**) formed the trisubstituted olefin product **318** in 87% yield. The success of the model system encouraged attempts to perform the CM conditions towards accessing the polyketide of lagunamide C.

To access the terminal alkene needed for CM conditions, compound **262** was allylated with allylmagnesium bromide to produce **319** in 67% yield as a 1:1 mixture of diastereomers about the newly formed alcohol, shown in Scheme 40. Oxidation to the ketone via PCC afforded compound **320** in 75% yield resolving the mixture of diastereomers via NMR. Unsurprisingly, subjecting compound **320** to CM conditions with **307**, resulted in 59% recovery of the starting material. Compound **319** was protected as a PMB ether (**322**) in quantitative yields and subjected to CM conditions with **307** to afford compound **323** as a mixture of diastereomers in 36% yield. At this point a route had been developed to access the carbon framework of the polyketide, but a more diastereoselective approach was desired.

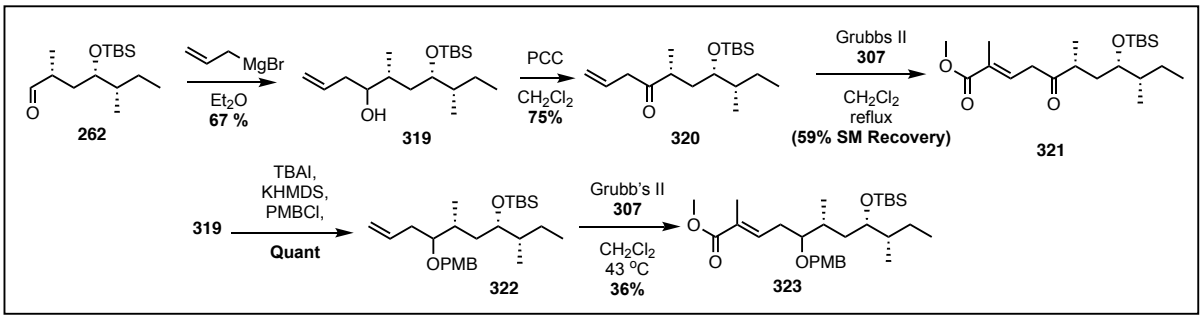

Scheme 40: Construction of the carbon framework of lagunamide C using allylation and CM conditions.

3.2.3.4.3 Diastereoselective Allylation and Access to the Polyketide of Lagunamide C

The reported literature of iridium catalyzed diastereoselective allylations prompted an investigation into the reactivity in this system.[79,80] To this end, a model system was envisioned to explore reactivity, shown in Scheme 41. The iridium catalyst (**324**) was generated based on the literature procedure and subjected to allylation conditions with compound **166** to afford the alcohol **325** in 43% yield with a dr of 2.5:1. Additionally, oxidative cleavage of the TBS protected compound **315** with OsO_4 followed by reduction with $NaBH_4$ generated compound **326** in 89% over 2 steps. Subjecting **326** to the iridium catalyst allylation conditions formed **327** in 27% yield with the TBS protected alcohol unaffected; however, the dr of the reaction was not determined. With the success of the model systems, compound **255** was subjected to oxidative cleavage conditions followed by reduction to generate **328** in 52% yield over 2 steps. Gratifyingly, allylation

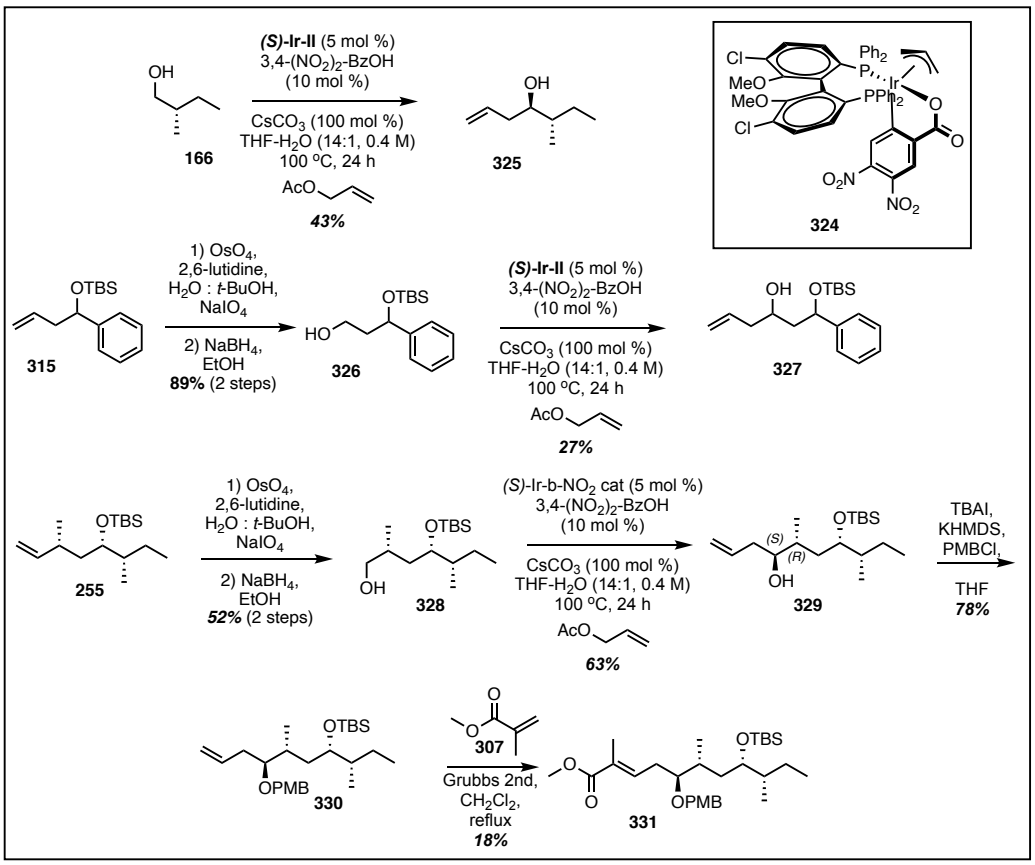

Scheme 41: Exploration of diastereoselective allylation conditions.

with the iridium catalyst afforded the desired compound **329** in 63% yield with a dr of 7:3. Protection of the alcohol via PMBCl afforded **330** in 78% yield and CM conditions with **307** afforded the methyl ester product **331** in 18% yield. This completes the third module of the proposed polyketide synthesis, and future work is aimed to complete the first total synthesis of lagunamide C using this route.

3.2.4 Biological Activity of Lagunamide C Intermediates for SAR

Several of the synthetic intermediates were tested in HeLa cell lines for cytotoxicity to identify SAR associated with the polyketide of lagunamide C, shown in Figure 30. Interestingly, the most potent compounds were enol containing compounds and had low μM toxicities including compounds **342**, **297**, and **344** which presented toxicity values of 3.12, 2.97 and 2.10 μM, respectively. These toxicity values are significantly different from the parent compound (low nM IC_{50} values), likely due to the lack of the peptide fragment which is critical for cellular penetration. Compounds without an enol functional group including **341**, **343, 256,** and **261** showed low toxicity values of 9.91, >10, >10, 8.01 μM. This data supports the Michael-acceptors hypothesis, which is contained within the polyketide of lagunamide C, and is likely responsible for the cytotoxic activity. Moreover, further SAR on the complete collection of synthetic intermediates will look to identify the enol as critical for toxicity in the aurilide family of NPs.

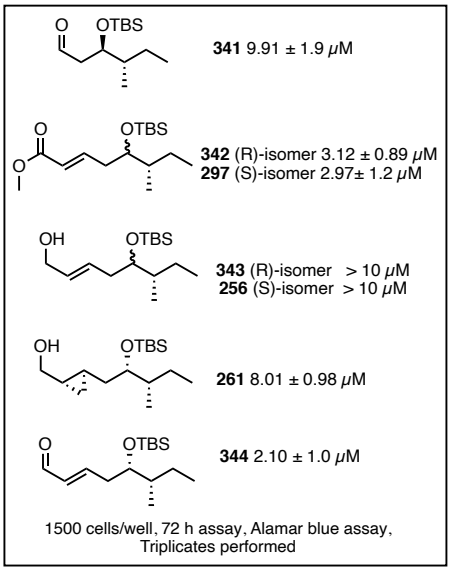

Figure 30: Biological evaluation of synthetic intermediates for SAR.

3.2.5 Chapter Conclusion

In conclusion, the first total synthesis of reniochalistatin E has been completed in 15 steps with an overall 5% yield. With this route established, a drug delivery system has been devised and current efforts towards developing a reniochalistatin E analog in which a disulfide bond is conjugated to 6TP is in progress. This newly generated analog is envisioned to enhance delivery of 6TP for treatment of the deadliest form of blood-based cancer, myeloma. In addition, a diastereoselective approach to access the polyketide of lagunamide C has been completed. The biological activity of several of the synthetic intermediates have identified the enol moiety as a critical for cytotoxic. This data supports our hypothesis regarding cellular penetration by the peptide backbone and delivery of the toxic polyketide subunit containing a Michael-acceptor as an enol. Future work will look prove the innate prodrug characteristic of lagunamide C and could illuminate the aurilide class as a rich source of inspiration for prodrug delivery systems.

Chapter 4: Conclusion and Future Work

With the total synthesis route to access reniochalistatin E achieved, future work will access analogs of the NP as a new drug delivery platform. As shown in Scheme 42, current efforts are towards accessing the cysteine analog of reniochalistatin E to conjugate the FDA approved chemotherapeutic 6TP. To identify if the tryptophan amino acid could be exchanged for other residues, a phenylalanine analog (**249**) was generated and showed retention of the cytotoxicity from the NP. The tryptophan amino acid was therefore identified as the first sight to attempt to install 6TP via disulfide conjugation. Current efforts are underway to synthesize the ACM protected cysteine analog which can be deprotected and 6TP can be incorporated via disulfide conjugation after macrocyclization. The newly generated disulfide analog (**246**) is envisioned to have enhanced cytotoxicity and future testing will determine the compounds potential as a chemotherapeutic option for the treatment of myeloma.

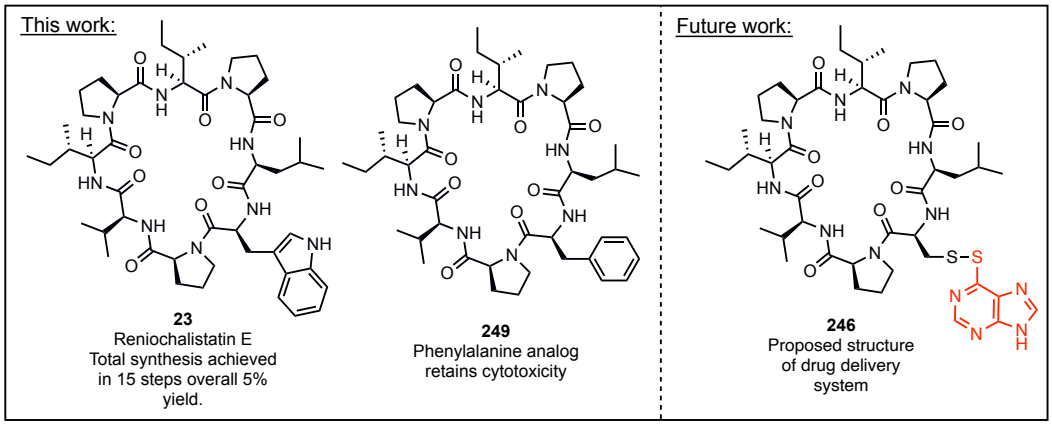

Scheme 42: Summary total synthesis of reniochalistatin E (**23**) structure of phenylalanine analog (**249**) which retained cytotoxicity and proposed drug delivery platform (**246**) through disulfide conjugation to 6TP (shown in red).

In addition, a diastereoselective route has been developed to access the polyketide of lagunamide C. While the total synthesis of the NP is pending, a module-based approach was designed to address the stereochemical ambiguity of the NP and allow for access to any of the diastereomers of the NP. The synthesis employs diastereoselective steps including a titanium mediated aldol reaction with a chiral auxiliary, an asymmetric cyclopropanation with tandem ring-opening, and finally an iridium catalyzed allylation. Future work will look to complete the first total synthesis of lagunamide C via incorporation of the peptide backbone and macrocyclization. Thus far, biological testing on a collection of the synthetic intermediates indicates the enol moiety of the polyketide may be responsible for the toxicity; however, the values are substantially lower (10-fold decrease) without the peptide fragment. Interestingly, previous works has shown the peptide fragment is devoid of toxicity and is likely to allow transport into cells wherein the polyketide is released acting as a prodrug. Future work will look to perform further biological testing on the intermediates in the route for SAR to prove this. Moreover, this route can also be used to access the amide analog (**345** in Scheme 43) to identify if lagunamide C acts as a prodrug. The amide analog will prevent cleavage of the ester bonds and will render the molecule inactive, if not less active.

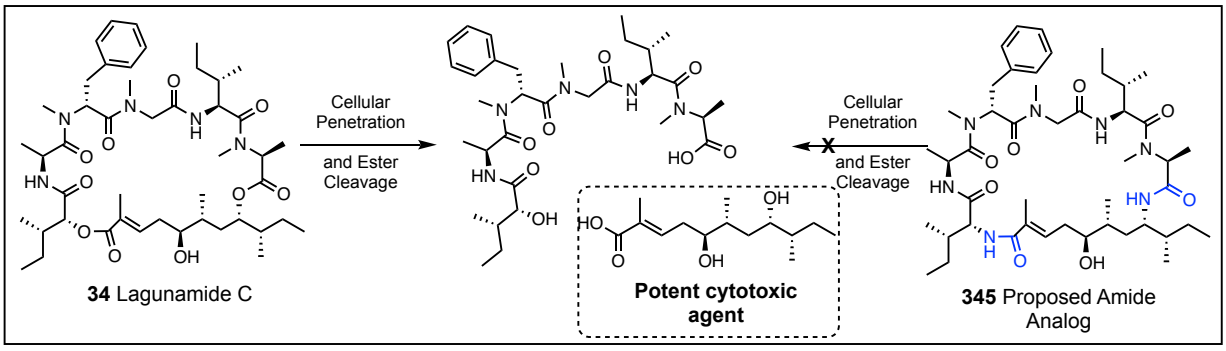

Scheme 43: Hypothesized mechanism of toxicity of lagunamide C (**34**) is via cellular penetration and ester clevage to release the polyketide, and proposed amide analog (**345**) to be generated for identifying the impact of ester bonds.

Chapter 5: References

1. Globocan. The Global Cancer Observatory - All cancers. *Int. Agent Res. Cancer - WHO* **419**, 199–200 (2020).
2. Greenstein, J. P. Some Biochemical Characteristics of Morphologically Separable Cancers. *Cancer Res.* **16**, 641–653 (1956).
3. Organization, W. H. *United States of America Fact Sheet 2020*. vol. 465 https://gco.iarc.fr/today/data/factsheets/cancers/39-All-cancers-fact-sheet.pdf (2020).
4. WCRF. Cancer Facts and Figures. *World Cancer Research Fund International* 1–4 (2021).
5. Spinney, L. Caught in time. *Nature* **442**, 736–738 (2006).
6. Siegel, R. L., Miller, K. D. & Jemal, A. Cancer statistics, 2020. *CA. Cancer J. Clin.* **70**, 7–30 (2020).
7. American Cancer Society. Cancer Treatment and Survivorship Facts and Figures 2019-2021. *Am. Cancer Soc.* 1–48 (2019).
8. DeVita, V. T. & Chu, E. A history of cancer chemotherapy. *Cancer Res.* **68**, 8643–8653 (2008).
9. DiMasi, J. A., Grabowski, H. G. & Hansen, R. W. Innovation in the pharmaceutical industry: New estimates of R&D costs. *J. Health Econ.* **47**, 20–33 (2016).
10. White Junod, S. FDA and Clinical Drug Trials: A Short History. *FDA U.S. Food Drug Adm.* 25–55 (2008).
11. Newman, D. J. & Cragg, G. M. Natural Products as Sources of New Drugs over the Nearly Four Decades from 01/1981 to 09/2019. *J. Nat. Prod.* **83**, 770–803 (2020).
12. Profiling, P. Chapter 5 Isolation , Purification & Characterization.

13. Nandi, A., Pan, S., Potumarthi, R., Danquah, M. K. & Sarethy, I. P. A proposal for six sigma integration for large-scale production of penicillin g and subsequent conversion to 6-APA. *J. Anal. Methods Chem.* **2014**, (2014).

14. Di, L. Strategic Approaches to Optimizing Peptide ADME Properties. *AAPS J.* **17**, 134–143 (2015).

15. Berditsch, M. *et al.* Antimicrobial peptide gramicidin S is accumulated in granules of producer cells for storage of bacterial phosphagens. *Sci. Rep.* **7**, 1–11 (2017).

16. Okamoto, S., Iwasaki, A., Ohno, O. & Suenaga, K. Isolation and Structure of Kurahyne B and Total Synthesis of the Kurahynes. *J. Nat. Prod.* **78**, 2719–2725 (2015).

17. Ruoli Bai, Susan J. Freidman, George R. Pettit, and E. H. Dolastatin15 A Potent Antimitotic Depsipeptide Derived from Dolabella Auricularia. *Biochem. Pharmacol.* **43**, 2637–2645 (1992).

18. Sun, L. Modern Chemistry & Applications Peptide-Based Drug Development. *Mod. Chem. Appl. Peer Rev.* **1**, 1–2 (2013).

19. Fang, W. Y., Dahiya, R., Qin, H. L., Mourya, R. & Maharaj, S. Natural proline-rich cyclopolypeptides from marine organisms: Chemistry, synthetic methodologies and biological status. *Mar. Drugs* **14**, (2016).

20. Zhong, J. & Chau, Y. Antitumor activity of a membrane lytic peptide cyclized with a linker sensitive to membrane type 1-matrix metalloproteinase. *Mol. Cancer Ther.* **7**, 2933–2940 (2008).

21. Roxin, Á. & Zheng, G. Flexible or fixed: A comparative review of linear and cyclic cancer-targeting peptides. *Future Med. Chem.* **4**, 1601–1618 (2012).

22. Zhan, K. X. *et al.* Reniochalistatins A-E, cyclic peptides from the marine sponge

Reniochalina stalagmitis. *J. Nat. Prod.* **77**, 2678–2684 (2014).

23. Suarez-Jimenez, G. M., Burgos-Hernandez, A. & Ezquerra-Brauer, J. M. Bioactive peptides and depsipeptides with anticancer potential: Sources from marine animals. *Mar. Drugs* **10**, 963–986 (2012).

24. Wang, X., Gong, X., Li, P., Lai, D. & Zhou, L. Structural diversity and biological activities of cyclic depsipeptides from fungi. *Molecules* **23**, (2018).

25. Weissman, K. J. & Leadlay, P. F. Combinatorial biosynthesis of reduced polyketides. *Nat. Rev. Microbiol.* **3**, 925–936 (2005).

26. Bowers, A. A. *et al.* Synthesis and conformation-activity relationships of the peptide isosteres of FK228 and largazole. *J. Am. Chem. Soc.* **131**, 2900–2905 (2009).

27. Kiyotake Suenaga, Tsuyoshi Mutou, Takunobu Shibata, Takashi Itoh, Hideo Kigoshi, and K. Y. Isolation and Stereostructure of Aurilide, a Novel Cyclodepsipeptide from the Japanese Sea Hare Dolabella auricularia. (1996).

28. Han, B., Gross, H., Goeger, D. E., Mooberry, S. L. & Gerwick, W. H. Aurilides B and C, cancer cell toxins from a Papua New Guinea collection of the marine cyanobacterium Lyngbya majuscula. *J. Nat. Prod.* (2006) doi:10.1021/np0503911.

29. Prinsep, M. R., Tan, L. T., Tripathi, A., Puddick, J. & Rottmann, M. Lagunamides A and B: Cytotoxic and Antimalarial Cyclodepsipeptides from the Marine Cyanobacterium Lyngbya majuscula . *J. Nat. Prod.* **73**, 1810–1814 (2010).

30. Tripathi, A. *et al.* Lagunamide C, a cytotoxic cyclodepsipeptide from the marine cyanobacterium Lyngbya majuscula. *Phytochemistry* **72**, 2369–2375 (2011).

31. Luo, D., Putra, M. Y., Ye, T., Paul, V. J. & Luesch, H. Isolation, structure elucidation and biological evaluation of lagunamide D: A new cytotoxic macrocyclic depsipeptide from

marine cyanobacteria. *Mar. Drugs* **17**, (2019).

32. Chang, C. Y., Liu, H. M., Chang, C. Y., Lai, Y. C. & Yang, M. D. An efficient synthesis of the C27-C45 fragment of lagunamide A, a cyclodepsipeptide with potent cytotoxic and antimalarial properties. *Tetrahedron Asymmetry* **25**, 187–192 (2014).
33. Huang, X. *et al.* Structure Determinants of Lagunamide A for Anticancer Activity and Its Molecular Mechanism of Mitochondrial Apoptosis. *Molecular Pharmaceutics* vol. 13 3756–3763 (2016).
34. Dai, L. *et al.* Total synthesis and stereochemical revision of lagunamide A. *Chem. Commun.* **48**, 8697–8699 (2012).
35. Gorges, J. & Kazmaier, U. Matteson Homologation-Based Total Synthesis of Lagunamide A. *Org. Lett.* **20**, 2033–2036 (2018).
36. Banasik, B. A., Wang, L., Kanner, A. & Mikael Bergdahl, B. Further insight into the asymmetric vinylogous Mukaiyama aldol reaction (VMAR); Application to the synthesis of the C27-C45 segment of lagunamide A. *Tetrahedron* **72**, 2481–2490 (2016).
37. Daliri, E. B. M., Oh, D. H. & Lee, B. H. Bioactive peptides. *Foods* **6**, 1–21 (2017).
38. Staunton, J. & Weissman, K. J. Polyketide biosynthesis: A millennium review. *Nat. Prod. Rep.* **18**, 380–416 (2001).
39. Al-Warhi, T. I., Al-Hazimi, H. M. A. & El-Faham, A. Recent development in peptide coupling reagents. *J. Saudi Chem. Soc.* **16**, 97–116 (2012).
40. Benoiton, N. L. *et al. Chemistry of Peptide Synthesis*. *Nanomedicine* vol. 2 (2014).
41. El-Faham, A. & Albericio, F. Peptide coupling reagents, more than a letter soup. *Chem. Rev.* **111**, 6557–6602 (2011).
42. Sheehan, J. C. & Hess, G. P. A new method of forming peptide bonds. *J. Am. Chem. Soc.*

77, 1067–1068 (1955).

43. Ho, G. J., Emerson, K. M., Mathre, D. J., Shuman, R. F. & Grabowski, E. J. J. Carbodiimide-Mediated Amide Formation in a Two-Phase System. A High-Yield and Low-Racemization Procedure for Peptide Synthesis. *J. Org. Chem.* **60**, 3569–3570 (1995).

44. Mutou, T. *et al.* Enantioselective Synthesis of Aurilide, a Cytotoxic 26-Membered Cyclodepsipeptide of Marine Origin. *Synlett* (1997) doi:10.1055/s-1997-753.

45. Suenaga, K. *et al.* Aurilide, a cytotoxic depsipeptide from the sea hare Dolabella auricularia: Isolation, structure determination, synthesis, and biological activity. *Tetrahedron* (2004) doi:10.1016/j.tet.2004.06.125.

46. Michon, S., Cavelier, F. & Salom-Roig, X. J. Synthesis and Biological Activities of Cyclodepsipeptides of Aurilide Family from Marine Origin. *Mar. Drugs* **19**, (2021).

47. Suenaga, K., Kajiwara, S., Kuribayashi, S., Handa, T. & Kigoshi, H. Synthesis and cytotoxicity of aurilide analogs. *Bioorganic Med. Chem. Lett.* **18**, 3902–3905 (2008).

48. Sato, S. I. *et al.* Marine natural product aurilide activates the opa1-mediated apoptosis by binding to prohibitin. *Chem. Biol.* **18**, 131–139 (2011).

49. Lee, H. & Yoon, Y. Mitochondrial membrane dynamics—functional positioning of OPA1. *Antioxidants* **7**, (2018).

50. Schuler, M. H. & Hughes, A. L. OPA1 and Angiogenesis: Beyond the Fusion Function. *Cell Metab.* **31**, 886–887 (2020).

51. Semenzato, M., Cogliati, S. & Scorrano, L. Prohibitin(g) cancer: Aurilide and killing by Opa1-dependent cristae remodeling. *Chem. Biol.* **18**, 8–9 (2011).

52. Takase, S. *et al.* A quantitative shRNA screen identifies ATP1A1 as a gene that regulates cytotoxicity by aurilide B. *Sci. Rep.* **7**, 1–9 (2017).

53. Nakao, Y. *et al.* Kulokekahilide-2, a cytotoxic depsipeptide from a cephalaspidean mollusk Philinopsis Speciosa. *J. Nat. Prod.* **67**, 1332–1340 (2004).

54. Takada, Y., Mori, E., Umehara, M., Nakao, Y. & Kimura, J. Reinvestigation of the stereochemistry of kulokekahilide-2. *Tetrahedron Lett.* **48**, 7653–7656 (2007).

55. Takada, Y., Umehara, M., Nakao, Y. & Kimura, J. Revised absolute stereochemistry of natural kulokekahilide-2. *Tetrahedron Lett.* **49**, 1163–1165 (2008).

56. Tracer, K.-P. E. T. *et al.* Acid Moiety for the Study on the Synthesis of. 269–277 (2014).

57. Umehara, M., Negishi, T., Maehara, Y., Nakao, Y. & Kimura, J. Stereochemical analysis and cytotoxicity of kulokekahilide-2 and its analogues. *Tetrahedron* **69**, 3045–3053 (2013).

58. Umehara, M., Negishi, T., Tashiro, T., Nakao, Y. & Kimura, J. Structure-related cytotoxic activity of derivatives from kulokekahilide-2, a cyclodepsipeptide in Hawaiian marine mollusk. *Bioorganic Med. Chem. Lett.* **22**, 7422–7425 (2012).

59. Sueyoshi, K. *et al.* Odoamide, a cytotoxic cyclodepsipeptide from the marine cyanobacterium Okeania sp. *Tetrahedron* **72**, 5472–5478 (2016).

60. Kaneda, M. *et al.* Total synthesis of odoamide, a novel cyclic depsipeptide, from an Okinawan marine cyanobacterium. *Org. Biomol. Chem.* **14**, 9093–9104 (2016).

61. Kaneda, M., Kawaguchi, S., Fujii, N., Ohno, H. & Oishi, S. Structure-Activity Relationship Study on Odoamide: Insights into the Bioactivities of Aurilide-Family Hybrid Peptide-Polyketides. *ACS Med. Chem. Lett.* **9**, 365–369 (2018).

62. Keck, G. & Abbott, D. Stereochemical Consequences for the lewis acid mediated addition of allul and crotyltri-n-butylstannane to chiral B-hydroxyaldehyde derivatives. *Tetrahedron Lett.* **25**, 1883–1886 (1984).

63. Huang, W., Ren, R. G., Dong, H. Q., Wei, B. G. & Lin, G. Q. Diverse synthesis of marine cyclic depsipeptide lagunamide A and its analogues. *J. Org. Chem.* **78**, 10747–10762 (2013).

64. Paterson, I. & Wallace, D. J. Anti aldol reactions of lactate-derived ketones: Application to the total synthesis of (-)-ACRL toxin IIIB. *Tetrahedron Lett.* **35**, 9477–9480 (1994).

65. Brown, R. The bcl-2 family of proteins. *Br. Med. Bull.* **53**, 466–477 (1996).

66. Van Delft, M. F. & Huang, D. C. S. How the Bcl-2 family of proteins interact to regulate apoptosis. *Cell Res.* **16**, 203–213 (2006).

67. Antonsson, B. Bax and other pro-apoptotic Bcl-2 family 'killer-proteins' and their victim, the mitochondrion. *Cell Tissue Res.* **306**, 347–361 (2001).

68. Pal, S. & Chakraborty, T. K. Toward the total synthesis of a lagunamide B analogue. *Tetrahedron Lett.* **55**, 3469–3472 (2014).

69. Fatino, A., Baca, G., Weeramange, C. & Rafferty, R. J. Total Synthesis of Reniochalistatin e. *J. Nat. Prod.* **80**, 3234–3240 (2017).

70. Cuffari, C., Théorêt, Y., Latour, S. & Seidman, G. 6-Mercaptopurine metabolism in Crohn's disease: Correlation with efficacy and toxicity. *Gut* **39**, 401–406 (1996).

71. Charette, A. B. & Juteau, H. Design of Amphoteric Bifunctional Ligands: Application to the Enantioselective Simmons-Smith Cyclopropanation of Allylic Alcohols. *J. Am. Chem. Soc.* **116**, 2651–2652 (1994).

72. Pappo, R., Allen, D. S., Lemieux, R. U. & Johnson, W. S. Osmium Tetroxide-Catalyzed Periodate Oxidation of Olefinic Bonds are also oxidized by lead tetraacetate in the presence Reductive Cleavage of Tosylates. *J. Org. Chem.* **21**, 478 (1956).

73. Teruaki Mukaiyama, Koschi Narasaka, and K. B. New ALDOL TYPE REACTION.

Chem. Lett. **21**, 1154–1157 (1973).

74. Crimmins, M. T., Shamszad, M. & Mattson, A. E. A highly convergent approach toward (-)-brevenal. *Org. Lett.* **12**, 2614–2617 (2010).

75. Crimmins, M. T., King, B. W., Tabet, E. A. & Chaudhary, K. Asymmetric aldol additions: Use of titanium tetrachloride and (-)-sparteine for the soft enolization of N-acyl oxazolidinones, oxazolidinethiones, and thiazolidinethiones. *J. Org. Chem.* **66**, 894–902 (2001).

76. Zhou, H. *et al.* A fungal ketoreductase domain that displays substrate-dependent stereospecificity. *Nat. Chem. Biol.* **8**, 331–333 (2012).

77. Su, H., Yang, J. H., Lu, C. F., Chen, Z. X. & Yang, G. C. A study of the alkylation and acylation of N-acylthiazolidinethione. *Indian J. Chem. - Sect. B Org. Med. Chem.* **52**, 769–775 (2013).

78. Wu, Y., Sun, Y. P., Yang, Y. Q., Hu, Q. & Zhang, Q. Removal of thiazolidinethione auxiliaries with benzyl alcohol mediated by DMAP. *J. Org. Chem.* **69**, 6141–6144 (2004).

79. Schmitt, D. C., Dechert-Schmitt, A. M. R. & Krische, M. J. Iridium-catalyzed allylation of chiral β-stereogenic alcohols: Bypassing discrete formation of epimerizable aldehydes. *Org. Lett.* **14**, 6302–6305 (2012).

80. Della-Felice, F., Sarotti, A. M., Krische, M. J. & Pilli, R. A. Total Synthesis and Structural Validation of Phosdiecin A via Asymmetric Alcohol-Mediated Carbonyl Reductive Coupling. *J. Am. Chem. Soc.* **141**, 13778–13782 (2019).

Chapter 6: Procedures and NMRs

General Methods

All commercially available reagents were used as received. Optical rotations were measured on an Atago Polax-2L polarimeter with a sodium lamp. IR spectra were recorded on a Cary 630 FT-IR spectrometer as thin films. Only the strongest and/or structurally important absorptions of IR spectra were reported in wavenumbers (cm^{-1}). ^{1}H (400, 600 MHz) and ^{13}C (101, 151) spectra were obtained on a Varian and Bruker-Ascend spectrometers. The chemical shifts are given in parts per million (ppm) relative to residual $CHCl_3$ δ 7.26 ppm for proton spectra and relative to $CDCl_3$ at δ 77.23 ppm for carbon spectra, unless otherwise noted. High-resolution mass spectra were obtained using a LCT Premier time of flight mass spectrometer. Flash column chromatography was performed with silica gel grade 60 (230-400 mesh). Dichloromethane (CH_2Cl_2), tetrahydrofuran (THF), toluene (PhMe), N,N-dimethylformamide (DMF), acetonitrile (CH_3CN), triethylamine (Et_3N), and methanol (MeOH) were all degassed with argon and passed through a solvent purification system containing alumina or molecular sieves.

Synthesis of *N*-Boc-(L)-Ile-(L)-Pro-OMe (232)

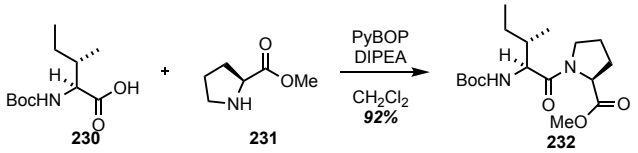

To a stirring solution of N-Boc-*L*- isoleucine (**230**; 1.0 g, 4.16 mmol, 1.0 equiv) in CH_2Cl_2 (42 mL) were added PyBOP (2.27 g, 4.37 mmol, 1.05 equiv) and *i*Pr_2EtN (1.09 mL, 6.24 mmol, 1.5 equiv). To a separate round-bottom flask (RBF) were added *L*-proline methyl ester (**231**; 1.03 g, 6.24 mmol, 1.5 equiv), *i*Pr_2EtN (2.17 mL, 12.48 mmol, 3.0 equiv), and CH_2Cl_2 (6.3 mL). Both reaction mixtures were left to stir for 1 h, at which time they were combined and left to stir overnight at room temperature (rt). The reaction was quenched with 1 M HCl (1 vol equiv), and the product was extracted with CH_2Cl_2 (×2), washed with $NaHCO_3$(satd), dried over sodium sulfate, and concentrated under reduced pressure. The crude material was purified via flash silica gel chromatography (1:2 EtOAc/hexane) to afford **232** (1.30 g, 92% yield).

^{1}H-NMR ($CDCl_3$, 400 MHz): δ 5.11 (d, *J* = 9.5 Hz, 1H), 4.52 – 4.44 (m, 1H), 4.24 (dd, *J* = 9.5, 7.2 Hz, 1H), 3.80 – 3.73 (m, 1H), 3.66 (s, 3H), 3.65 – 3.58 (m, 1H), 2.22 – 2.12 (m, 1H), 2.01 – 1.90 (m, 3H), 1.71 (ddq, *J* = 10.3, 6.5, 3.5 Hz, 1H), 1.53 (td, *J* = 7.2, 6.6, 3.2 Hz, 1H), 1.37 (s, 9H), 1.07 (ddd, *J* = 13.4, 6.7, 2.3 Hz, 1H), 0.96 (d, *J* = 6.8 Hz, 3H), 0.86 (t, *J* = 7.4 Hz, 3H).

^{13}C-NMR ($CDCl_3$, 101 MHz): δ 172.64, 171.65, 156.01, 79.70, 59.04, 56.46, 52.35, 47.42, 38.13, 29.29, 28.56, 25.17, 24.38, 15.47, 11.46.

IR (film) ν_{max}: 3436, 2973, 1746, 1642, 1436, 1217 cm^{-1}.

Optical Rotation: $[\alpha]_D^{25}$ = +40.3 (*c* 1.23, $CHCl_3$).

HRMS (ESI$^+$): *m/z* 343.2193 $[M+H]^+$ (calcd for $C_{17}H_{30}N_2O_5$ 343.2188).

Synthesis of *N*-Boc-(*L*)-Leu-(*L*)-Trp-OMe (235)

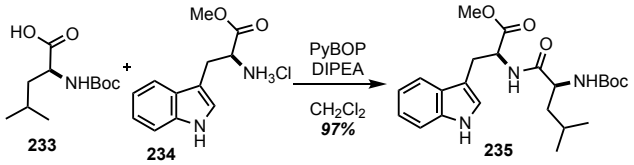

To a stirring solution of compound N-Boc-*L*-leucine (**233**; 1.0 g, 4.32 mmol, 1.0 equiv) in CH_2Cl_2 (43 mL) were added PyBOP (2.36 g, 4.54 mmol, 1.05 equiv) and *i*Pr2EtN (1.13 mL, 6.48 mmol, 1.5 equiv). To a separate RBF were added *L*-tryptophan methyl ester (**234**; 1.65 g, 6.48 mmol, 1.5 equiv), *i*Pr2EtN (2.26 mL, 12.96 mmol, 3.0 equiv), and CH_2Cl_2 (6.5 mL). Both reaction mixtures were left to stir for 1 h, at which time they were combined and left to stir overnight at rt. The reaction was quenched with 1 M HCl (1 vol equiv), and the product was extracted with CH_2Cl_2 (×2), washed with $NaHCO_3$(satd), dried over sodium sulfate, and concentrated under reduced pressure. The crude material was purified via flash silica gel chromatography (1:1 EtOAc/hexane) to afford **235** (1.81 g, 97% yield)

^{1}H NMR (400 MHz, DMSO-d_6): δ 10.85 (s, 1H), 8.06 (d, *J* = 7.4 Hz, 1H), 7.45 (d, *J* = 7.9 Hz, 1H), 7.31 (d, *J* = 8.1 Hz, 1H), 7.13 (d, *J* = 2.4 Hz, 1H), 7.07 – 7.02 (m, 1H), 6.96 (td, *J* = 7.5, 6.9, 1.1 Hz, 1H), 6.82 (d, *J* = 8.5 Hz, 1H), 4.51 (q, *J* = 7.1 Hz, 1H), 3.98 (td, *J* = 8.7, 6.0 Hz, 1H), 3.55 (s, 3H), 3.13 – 3.05 (m, 2H), 1.53 (dd, *J* = 13.6, 6.9 Hz, 2H), 1.35 (s, 9H), 1.26 (s, 1H), 0.84 (d, *J* = 6.6 Hz, 3H), 0.81 (d, *J* = 6.5 Hz, 3H).

^{13}C NMR (101 MHz, Chloroform-*d*): δ 172.99, 172.44, 155.95, 136.45, 127.76, 123.62, 122.15, 119.58, 118.63, 111.71, 109.49, 80.22, 53.46, 53.29, 52.54, 41.55, 28.52, 27.81, 24.92, 23.18, 22.04.

Optical Rotation: $[\alpha]_D^{25}$ = +26.93 (*c* 0.15, $CHCl_3$).

IR (film) ν_{max}: 3418, 3018, 2872, 1739, 1513, 1215 cm^{-1}.

HRMS (ESI$^+$): *m/z* 454.2308 $[M+Na]^+$ (calcd for $C_{23}H_{33}N_3O_5Na^+$ 454.2312).

Synthesis of *N*-Boc-(*L*)-Ile-(*L*)-Pro-OH (236)

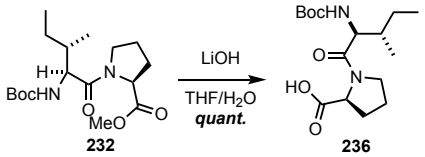

To a stirring solution of **232** (556 mg, 1.62mmol, 1.0 equiv) in 1:1 THF/H_2O (16 mL) was added LiOH (194 mg, 8.12 mmol, 5.0 equiv). The mixture was left to stir at rt for 5 h. The reaction was quenched with 1MHCl (1 vol equiv), and the product was extracted with CH_2Cl_2, washed with $NaHCO_3$(satd), dried over sodium sulfate, and concentrated under reduced pressure. The product **236** was obtained in quantitative yield as an oily residue, which was used without further purification.

IR (film) ν_{max}: 34356, 3304, 2977, 1704, 1314 cm^{-1}.

^{1}H NMR (400 MHz, Chloroform-*d*): δ 8.31 (s, 1H), 5.35 (d, *J* = 9.5 Hz, 1H), 4.57 (t, *J* = 6.4 Hz, 1H), 4.32 – 4.25 (m, 1H), 3.82 (dt, *J* = 9.6, 7.2 Hz, 1H), 3.64 (ddd, *J* = 9.7, 7.5, 5.4 Hz, 1H), 2.18 (dd, *J* = 10.0, 3.9 Hz, 2H), 2.07 – 1.99 (m, 2H), 1.76 (td, *J* = 7.0, 3.4 Hz, 1H), 1.64 – 1.48 (m, 2H), 1.41 (d, *J* = 7.7 Hz, 9H), 0.95 (d, *J* = 6.7 Hz, 3H), 0.87 (t, *J* = 7.2 Hz, 3H).

Synthesis of *N*-Boc-(*L*)-Leu-(*L*)-Trp-OH (237)

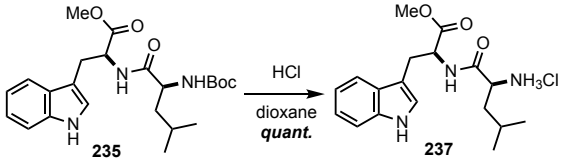

To a RBF was added 1 M HCl in dioxane (4.6 mL), which cooled to 0 °C, at which point 9 (500 mg, 1.16 mmol) was added. The reaction was allowed to stir for 1.5 h. The solvent was removed under reduced pressure to afford a crude white solid (11), which was used without further purification

IR (film) ν_{max}: 3416, 2879, 1651, 1176 cm^{-1}.

^{1}H NMR (400 MHz, DMSO-d_6): δ 9.04 (d, *J* = 7.2 Hz, 1H), 8.25 (s, 3H), 7.49 (d, *J* = 7.8 Hz, 1H), 7.35 (dt, *J* = 8.1, 1.0 Hz, 1H), 7.24 (d, *J* = 2.3 Hz, 1H), 7.07 (ddd, *J* = 8.1, 7.0, 1.3 Hz, 1H), 7.00 (ddd, *J* = 8.0, 7.0, 1.1 Hz, 1H), 4.63 – 4.54 (m, 1H), 3.81 (t, *J* = 7.2 Hz, 1H), 3.58 (s, 3H), 3.21 – 3.13 (m, 2H), 1.68 (dt, *J* = 13.3, 6.6 Hz, 2H), 1.57 (s, 2H), 0.90 (dd, *J* = 7.9, 6.4 Hz, 6H).

Synthesis of *N*-Boc-(*L*)-Ile-(*L*)-Pro-(*L*)-Leu-(*L*)-Trp-OMe (228)

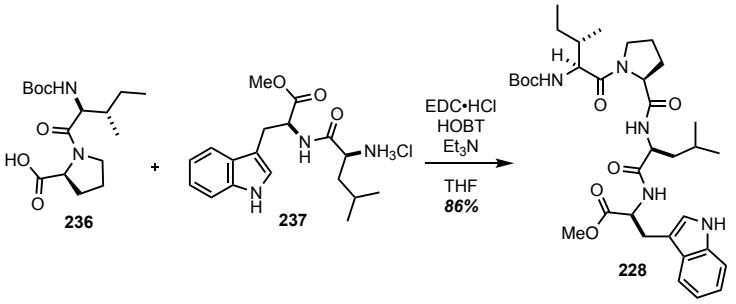

Compound **236** (1.32 g, 4.02 mmol, 1 equiv), compound **237** (1.08 g, 2.94 mmol, 1 equiv), and HOBt (473 mg, 3.09 mmol, 1.05 equiv) were dissolved in dry THF (40 mL) at rt under an argon atmosphere. The solution was cooled to 0 °C and stirred for 20 min, after which Et_3N (1.43 mL, 10.29 mmol, 3.5 equiv) was then added and stirred. Lastly, 20 min later EDC·HCl (592 mg, 3.09 mmol, 1.05 equiv) was added, and the reaction mixture was left to stir overnight. The reaction was quenched with H_2O (1 vol equiv), and the product was extracted with CH_2Cl_2, dried over sodium sulfate, and concentrated under reduced pressure. The crude material was purified via flash silica gel chromatography (3:1 EtOAc/hexane) to give afford **228** (2.22 g, 86% yield) as a clear liquid.

Optical Rotation: $[\alpha]_D^{25}$ = +48.08 (*c* 1.75, $CHCl_3$).

IR (film) ν_{max}: 3305, 3017, 2876, 1741, 1631, 1506, 1392, 1215 cm^{-1}.

^{1}H-NMR ($CDCl_3$, 400 MHz): δ 8.29 (s, 1H), 7.51 (d, *J* = 8.6 Hz, 1H), 7.33 (d, *J* = 8.0 Hz, 1H), 7.16 (td, *J* = 8.2, 7.6, 1.3 Hz, 1H), 7.13 – 7.05 (m, 1H), 7.03 (d, *J* = 2.4 Hz, 1H), 6.97 (d, *J* = 7.8 Hz, 1H), 6.70 (d, *J* = 7.9 Hz, 1H), 5.20 (d, *J* = 9.4 Hz, 1H), 4.90 (dt, *J* = 7.9, 5.5 Hz, 1H), 4.37 (d, *J* = 6.0 Hz, 1H), 4.27 (dd, *J* = 9.3, 7.0 Hz, 1H), 3.71 (d, *J* = 8.9 Hz, 1H), 3.66 (s, 3H), 3.60 – 3.51 (m, 1H), 3.30 (d, *J* = 5.5 Hz, 2H), 2.12 – 1.87 (m, 3H), 1.73 – 1.56 (m, 5H), 1.43 (s, 9H), 1.13 – 1.05 (m, 1H), 0.92 (d, *J* = 6.8 Hz, 3H), 0.90 – 0.80 (m, 11H).

^{13}C-NMR ($CDCl_3$, 101 MHz): δ 172.86, 172.49, 172.08, 171.74, 156.08, 136.32, 127.75, 123.57, 122.11, 119.61, 118.60, 111.55, 109.58, 79.89, 60.26, 56.61, 52.95, 52.56, 52.15, 47.99, 41.15, 37.95, 28.60, 25.58, 27.76, 25.31, 24.79, 24.42, 23.10, 23.05, 22.06, 15.65, 11.31.

HRMS (ESI^+): *m/z* 942.3817 $[M+H]^+$ (calcd for $C_{34}H_{52}N_5O_7$ 642.3822).

Synthesis of *N*-Boc-(*L*)-Pro-(*L*)-Val-OMe (240)

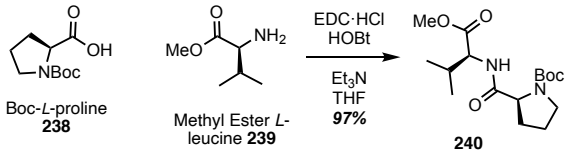

Compounds **238** (3.0 g, 13.94 mmol, 1equiv) and **239** (2.34 g, 13.94 mmol, 1 equiv) were added to a stirring solution of HOBt (2.24 g, 14.63 mmol, 1.05 equiv) in dry THF (139 mL) at rt under an argon atmosphere. The solution was then cooled to 0°C and stirred for 20 min, after which Et_3N (6.8 mL, 48.79 mmol, 3.5 equiv) was added. After an additional 20 min of stirring EDC·HCl (2.8 g, 14.63 mmol, 1.05 equiv) was added, and the reaction mixture was left to stir overnight. The reaction was quenched with H_2O (1 vol equiv), and the product was extracted with CH_2Cl_2, dried over sodium sulfate, and concentrated under reduced pressure. The crude material was purified via flash silica gel chromatography (1:1 EtOAc/hexane) to give **240** (4.45 g, 97% yield) as a clear liquid.

^{1}H-NMR ($CDCl_3$, 400 MHz): δ 4.50 (dd, *J* = 8.6, 5.1 Hz, 1H), 4.32 (s, 1H), 3.72 (s, 3H), 3.42 (s, 2H), 2.29 (s, 1H), 2.15 (pd, *J* = 6.9, 5.1 Hz, 2H), 1.95 – 1.84 (m, 3H), 1.48 (s, 9H), 0.92 (dd, *J* = 8.3, 6.8 Hz, 6H).

^{13}C-NMR (DMSO, 101 MHz): δ 172.71, 78.98, 59.71, 58.16, 52.30, 47.18, 31.67, 30.41, 28.80, 28.68, 23.61, 19.77, 18.99, 14.76.

Optical Rotation: $[\alpha]_D^{25}$ = +80.78 (*c* 2.05, $CHCl_3$).

IR (film) ν_{max}: 3680, 3323, 3415, 2973, 2879, 1740, 1681, 1216 cm^{-1}.

HRMS (ESI$^+$): *m/z* 329.2025 $[M+H]^+$ (calcd for $C_{16}H_{29}N_2O_5$ 329.2032).

Synthesis of *N*-Boc-(*L*)-Pro-(*L*)-Val-OH (241)

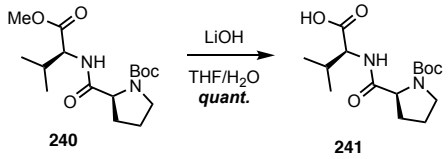

240 241

To a stirring solution of **240** (360 mg,1.1 mmol, 1 equiv) in 1:1 THF/H_2O (4.4 mL) was added LiOH (131 mg, 5.5 mmol, 5 equiv), and the mixture was left to stir at rt for 3 h. The reaction was quenched with 1M HCl (1 vol equiv), and the product was extracted with CH_2Cl_2, washed with $NaHCO_3$(satd), dried over sodium sulfate, and concentrated under reduced pressure. Crude **241** was obtained in quantitative yield as an oily residue and was used without further purification.

^{1}H-NMR ($CDCl_3$, 400 MHz): δ 10.37 (s, 1H), 7.51 (s, 1H), 4.50 (s, 1H), 4.40 – 4.19 (m, 1H), 3.50 – 3.28 (m, 2H), 2.31 – 2.09 (m, 3H), 1.94 – 1.79 (m, 2H), 1.43 (s, 9H), 0.91 (dd, *J* = 9.9, 6.9 Hz, 6H).

IR (film) ν_{max}: 3410 (b), 1676 cm^{-1}.

MS(ESI): *m/z* calc. for $C_{15}H_{26}N_2O_5$ $[M+H]^+$: 315.19, found: 315.19.

Synthesis of *H₂N*-(*L*)-Leu-(*L*)-Trp-OMe (242)

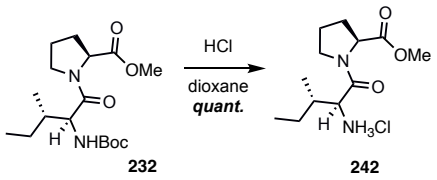

232 242

To a RBF containing **232** (857 mg, 2.5mmol) was added 1.0 M HCl in dioxane (10 mL), and the mixture was cooled to 0 °C. The reaction mixture was allowed to stir at the same temperature for 3 h. The solvent was removed under reduced pressure to afford crude **242** in quantitative yield as a white solid, which was used without further purification.

^{1}H-NMR ($CDCl_3$, 400 MHz): δ 8.34 – 8.27 (m, 3H), 4.61 (dd, *J* = 8.5, 5.3 Hz, 1H), 4.25 (s, 1H), 3.97 (s, 1H), 3.68 (s, 3H), 3.52 (d, *J* = 9.0 Hz, 1H), 2.28 (s, 1H), 2.05 – 1.91 (m, 4H), 1.68 (ddd, *J* = 13.5, 7.5, 3.3 Hz, 1H), 1.35 (ddd, *J* = 13.3, 10.0, 7.1 Hz, 1H), 1.12 (d, *J* = 6.8 Hz, 3H), 0.94 (t, *J* = 7.3 Hz, 3H).

IR (film) ν_{max}: 3416, 2879, 1651, 1454 cm^{-1}.

MS(ESI): *m/z* calc. for $C_{12}H_{23}N_2O_3$ $[M]^+$: 243.17, found: 243.16.

Synthesis of *N*-Boc-(*L*)-Pro-(*L*)-Val-(*L*)-Ile-(*L*)-Pro-OMe (229)

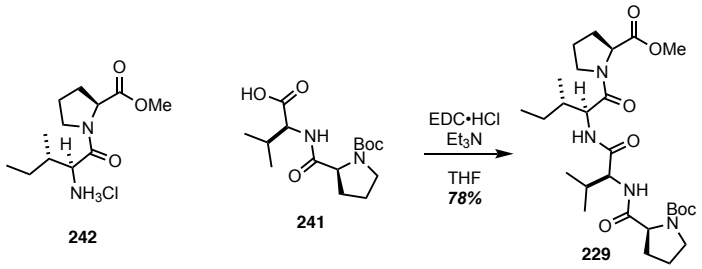

Compounds **242** (1.71 g, 7.06 mmol, 1 equiv) and **241** (2.24 g, 7.13 mmol, 1 equiv) were added to a stirring solution of HOBt (1.13 g, 7.41 mmol, 1.05 equiv) and dry THF (71 mL) at rt under an argon atmosphere. The solution was cooled to 0 °C and stirred for 20 min, after which Et_3N (3.46 mL, 24.71 mmol, 3.5 equiv) was added. After an additional 20 min of stirring, EDC·HCl (1.42 g, 7.41 mmol, 1.05 equiv) was added, and the mixture was stirred overnight. The reaction was quenched with H_2O (1 vol equiv), and the product was extracted with CH_2Cl_2, dried over sodium sulfate, and concentrated under reduced pressure. The crude material was purified via flash silica gel chromatography (7:1 EtOAc/hexane) to give **229** (1.52 g, 78% yield) as a clear liquid.

^{1}H-NMR ($CDCl_3$, 400 MHz): δ 7.48 (s, 1H), 6.65 (s, 1H), 6.42 (s, 1H), 4.58 (t, *J* = 8.2 Hz, 1H), 4.47 (dd, *J* = 8.6, 4.9 Hz, 1H), 4.31 (s, 1H), 4.26 (dd, *J* = 8.6, 5.6 Hz, 1H), 3.81 (dt, *J* = 9.8, 6.3 Hz, 1H), 3.68 (s, 3H), 3.64 – 3.59 (m, 1H), 3.46 – 3.28 (m, 2H), 2.33 (s, 1H), 2.19 (ddq, *J* = 12.9, 6.8, 3.7 Hz, 2H), 2.02 – 1.79 (m, 8H), 1.43 (s, 9H), 0.97 (d, *J* = 6.8 Hz, 3H), 0.89 – 0.80 (m, 9H).

Optical Rotation: $[\alpha]_D^{25}$ = +72.3 (*c* 3.21, $CHCl_3$).

IR (film) ν_{max}: 3673, 3412, 3306, 2879, 1743, 1632, 1368 cm^{-1}.

HRMS (ESI^+): *m/z* 561.3198 $[M+H]^+$ (calcd for $C_{27}H_{46}N_4O_7Na$ 561.3264).

Synthesis of *H₂N*-(*L*)-Ile-(*L*)-Pro-(*L*)-Leu-(*L*)-Trp-OMe (Free Amine of Tetrapeptide 228)

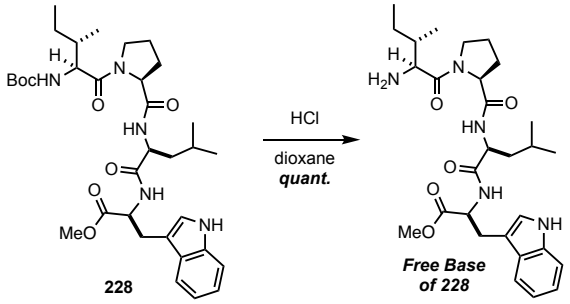

To a RBF containing **228** (1.03 g, 1.6 mmol) was added 1.0 M HCl in dioxane (6.4 mL), and the solution was cooled to 0 °C. The reaction mixture was allowed to stir at the same temperature for 3 h. The solvent was removed under reduced pressure to afford a crude white solid (free base of **228**), which was used without further purification.

IR (film) ν_{max}: 3323, 3018, 2879, 1633, 1449, 1216 cm^{-1}.

^{1}H-NMR ($CDCl_3$, 400 MHz): δ 8.17 (d, *J* = 44.9 Hz, 2H), 7.51 (d, *J* = 7.7 Hz, 1H), 7.32 (d, *J* = 8.0 Hz, 1H), 7.14 (t, *J* = 7.5 Hz, 1H), 7.10 – 7.05 (m, 2H), 6.83 (d, *J* = 8.3 Hz, 1H), 4.96 (d, *J* = 7.8 Hz, 1H), 4.83 – 4.63 (m, 4H), 4.42 (q, *J* = 7.8 Hz, 2H), 3.91 (d, *J* = 8.3 Hz, 1H), 3.79 – 3.70 (m, 2H), 3.65 (s, 5H), 3.30 (d, *J* = 6.0 Hz, 2H), 2.96 (ddt, *J* = 22.3, 10.3, 6.4 Hz, 2H), 1.95 – 1.81 (m, 7H), 1.29 – 1.22 (m, 3H), 0.89 – 0.76 (m, 22H).

Synthesis of *N*-Boc-(*L*)-Pro-(*L*)-Val-(*L*)-Ile-(*L*)-Pro-OH (Free Acid of Tetrapeptide 229)

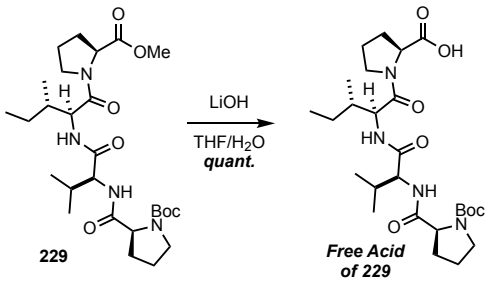

To a stirring solution of **229** (200 mg, 0.37 mmol, 1 equiv) in 1:1 THF/ H2O (1.5 mL) was added LiOH (45 mg, 1.86 mmol, 5 equiv), and the solution was left to stir at rt for 3 h. The reaction was quenched with 1M HCl (1 vol equiv), and the product was extracted with CH_2Cl_2, washed with $NaHCO_3$(satd), dried over sodium sulfate, and concentrated under reduced pressure. The crude material (free acid of **229**), obtained in quantitative yield as an oily residue, was used without further purification.

^{1}H-NMR ($CDCl_3$, 400 MHz): δ 7.50 (s, 0H), 4.63 (t, J = 8.9 Hz, 0H), 4.41 (d, J = 65.5 Hz, 4H), 3.88 (d, J = 10.7 Hz, 1H), 3.67 (s, 2H), 3.43 (s, 2H), 2.16 (s, 7H), 1.96 – 1.74 (m, 5H), 1.46 (s, 9H), 1.21 – 0.74 (m, 12H).

IR (film) ν_{max}: 3311, 3016, 2965, 1632, 1215 cm^{-1}.

Synthesis of Octapeptide *N-Boc*-Pro-Val-Ile-Pro-Ile-Pro-Leu-Trp-OMe (226)

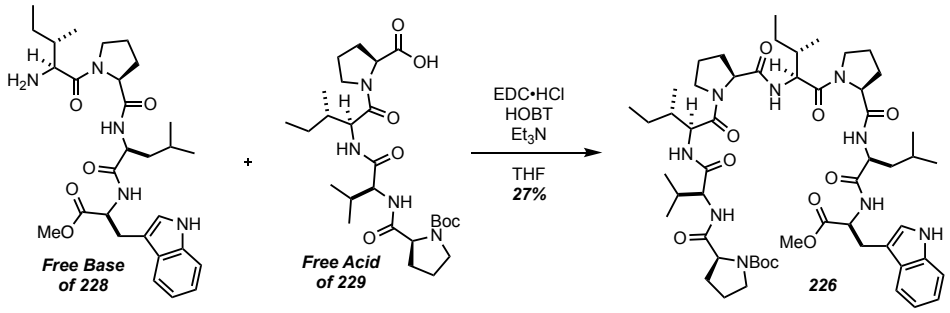

Free base of **228** (915 mg, 1.69 mmol, 1 equiv), free acid of **229** (784.5 mg, 1.5 mmol, 1 equiv), and HOBt (240 mg, 1.56 mmol, 1.05 equiv) were dissolved in dry THF (17 mL) at rt, under an argon atmosphere. The solution was then cooled to 0 °C and stirred for 20 min, after which Et_3N (0.731 mL, 5.25 mmol, 3.5 equiv) was added. After an additional 20 min of stirring, EDC·HCl (299 mg, 1.56 mmol, 1.05 equiv) was added, and the mixture was left to stir overnight. The reaction was quenched with H_2O (1 vol equiv), and the product was extracted with CH_2Cl_2, dried over sodium sulfate, and concentrated under reduced pressure. The crude material was purified via flash silica gel chromatography (1:9 EtOAc/MeOH) to afford **226** (605 mg, 27% (34% yield over 3 steps)) as an amber liquid.

^{1}H-NMR ($CDCl_3$, 400 MHz): δ 7.50 (d, J = 7.9 Hz, 1H), 7.31 (d, J = 8.0 Hz, 1H), 7.13 (t, J = 7.2 Hz, 1H), 7.10 – 7.03 (m, 2H), 6.82 (s, 1H), 4.97 (s, 1H), 4.65 (s, 2H), 4.42 (s, 2H), 4.25 (s, 1H), 3.88 (d, J = 9.4 Hz, 1H), 3.69 (s, 2H), 3.66 (s, 3H), 3.30 (d, J = 4.9 Hz, 2H), 2.07 (d, J = 145.9 Hz, 24H), 1.44 (s, 4H), 1.31 – 1.21 (m, 1H), 0.90 – 0.75 (m, 25H).

^{13}C-NMR ($CDCl_3$, 101 MHz): δ 17.38, 172.39, 151.82, 142.80, 140.68, 136.40, 127.78, 122.15, 119.63, 118.69, 111.44, 52.59, 48.15, 28.55, 24.87, 24.87, 23.06, 23.06, 19.62, 19.62, 15.33, 11.24.

Optical Rotation: $[\alpha]_D^{25}$ = -25.63 (*c* 0.21, MeOH).

HRMS (ESI$^+$): *m/z* 1070.6253 $[M+H]^+$ (calcd for $C_{55}H_{85}N_9O_{11}Na$ 1070.6267).

Synthesis of *H₂N*-(*L*)-Pro-(*L*)-Val-(*L*)-Ile-(*L*)-Pro-OMe (Free Amine of Tetrapeptide 229)

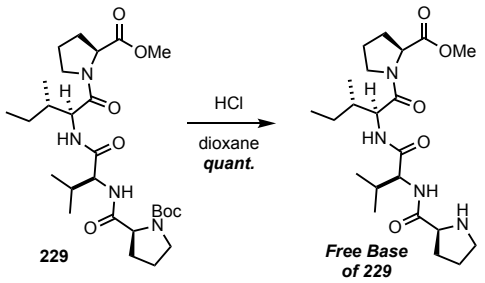

To an RBF containing **229** (151 mg, 0.28 mmol) was added 1.0 M HCl in dioxane (1.1 mL), and the solution was cooled to 0 °C. The reaction was allowed to stir at the same temperature for 3 h. The solvent was removed under reduced pressure, forming a crude white solid (free base **229**), which was used without further purification.

IR (film) ν_{max}: 3323, 2878, 1742, 1633, 1216 cm^{-1}.

^{1}H-NMR ($CDCl_3$, 400 MHz): δ 10.92 (s, 1H), 8.76 (s, 1H), 8.16 (s, 1H), 7.83 (d, J = 9.0 Hz, 1H), 4.92 (s, 1H), 4.76 – 4.68 (m, 1H), 4.52 – 4.35 (m, 2H), 3.87 (s, 2H), 3.69 (d, J = 2.2 Hz, 3H), 3.64 (dd, J = 8.5, 5.1 Hz, 1H), 3.44 (s, 3H), 2.63 (s, 1H), 2.46 – 2.17 (m, 5H), 2.00 (dd, J = 18.0, 6.0 Hz, 10H), 1.52 – 1.39 (m, 2H), 1.01 – 0.79 (m, 13H).

Synthesis of *N*-Boc-(*L*)-Ile-(*L*)-Pro-(*L*)-Leu-(*L*)-Trp-OH (Free Acid of Tetrapeptide 228)

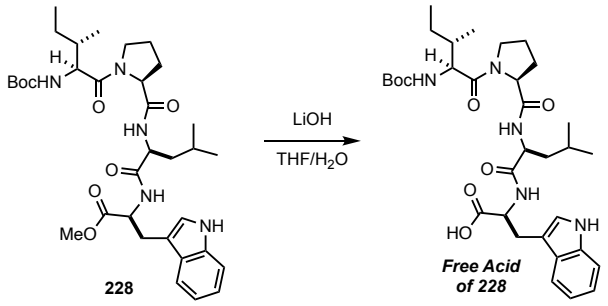

To a stirring solution of **228** (100 mg, 0.16 mmol, 1 equiv) in 1:1 THF/H2O (640 mL) was added LiOH (19 mg, 0.78 mmol, 5 equiv), and the solution was left to stir at rt for 3 h. The reaction was quenched with 1M HCl (1 vol equiv), and the product was extracted with CH_2Cl_2, washed with $NaHCO_3$(satd), dried over sodium sulfate, and concentrated under reduced pressure. Crude material was obtained in quantitative yield as an oily residue, which was used without further purification.

IR (film) ν_{max}: 3311 (bs), 2965, 1632, 1215 cm^{-1}.

^{1}H-NMR ($CDCl_3$, 400 MHz): δ 8.42 (s, 1H), 7.57 (d, J = 7.9 Hz, 1H), 7.31 (s, 1H), 7.12 (dq, J = 24.7, 9.6, 7.3 Hz, 3H), 5.22 (s, 1H), 4.83 (d, J = 7.5 Hz, 1H), 4.31 (d, J = 41.9 Hz, 2H), 3.73 (s, 2H), 3.54 (s, 1H), 3.30 (s, 2H), 2.08 – 1.72 (m, 0H), 1.43 (s, 9H), 1.10 – 0.57 (m, 12H).

Synthesis of Octapeptide *N-Boc*-Ile-Pro-Leu-Trp-Pro-Val-Ile-Pro-OMe (227)

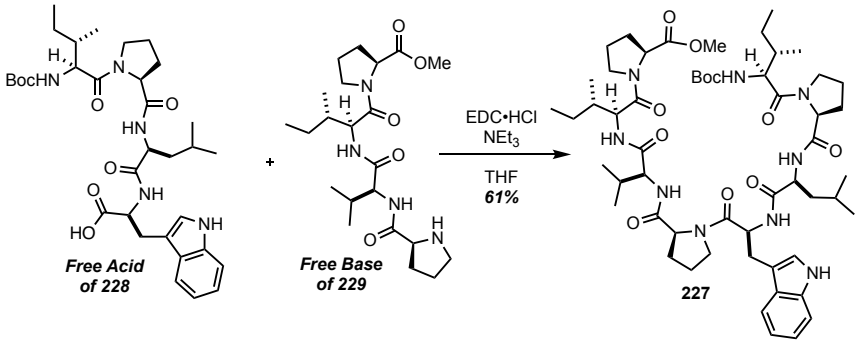

Free acid of **228** (137 mg, 0.31 mmol, 2.1 equiv) and free base of **229** (92 mg, 0.15 mmol, 1 equiv) were added to a stirring solution of HOBt (25 mg, 0.16 mmol, 1.05 equiv) in dry THF (3.1 mL) at rt under an argon atmosphere. The solution was cooled to 0 °C and stirred for 20 min, after which Et_3N (0.07 mL, 0.53 mmol, 3.5 equiv) was added and stirred. After an additional 20 min of stirring, EDC·HCl (31 mg, 0.16 mmol, 1.05 equiv) was added and the reaction mixture was left to stir overnight. The reaction was quenched with H_2O (1 vol equiv), and the product was extracted with CH_2Cl_2, dried over sodium sulfate, and concentrated under reduced pressure. The crude material was purified via flash silica gel chromatography (9:1 EtOAc/MeOH) to afford **227** (198 mg, 61% yield) as an amber liquid.

^{1}HNMR ($CDCl_3$, 400 MHz): δ 8.67 (s, 1H), 7.67 (d, J = 7.8 Hz, 1H), 7.62 – 7.27 (m, 4H), 7.20 – 6.85 (m, 6H), 5.21 (d, J = 9.3 Hz, 1H), 5.01 (q, J = 7.2 Hz, 1H), 4.75 – 4.00 (m, 10H), 3.80 (dt, J = 35.8, 5.2 Hz, 3H), 3.72 – 3.66 (m, 3H), 3.58 (s, 3H), 3.18 (d, J = 7.3 Hz, 1H), 2.36 – 1.85 (m, 16H), 1.42 (d, J = 4.6 Hz, 9H), 1.04 – 0.83 (m, 24H).

^{13}C-NMR ($CDCl_3$, 101 MHz): δ 172.76, 171.84, 171.74, 171.58, 170.90, 156.03, 136.30, 124.14, 123.58, 121.96, 119.58, 118.68, 111.55, 109.77, 79.70, 77.52, 77.04, 60.50, 60.27, 59.34, 59.11, 56.57, 55.13, 55.03, 52.31, 52.26, 52.10, 51.68, 48.01, 47.63, 47.55, 41.19, 37.93, 37.59, 37.53,

30.91, 30.26, 29.26, 28.58, 28.56, 28.11, 27.78, 25.36, 25.18, 24.80, 24.59, 24.53, 23.32, 23.01, 21.92, 19.59, 19.04, 18.36, 15.70, 15.60, 15.39, 11.33, 11.27.

Optical Rotation: $[\alpha]_D^{25}$ = -29.30 (*c* 0.78, MeOH).

IR (film) ν_{max}: 3423, 2925, 1741, 1687, 1612, 1452 cm^{-1}.

HRMS (ESI^+): *m/z* 1070.6253 $[M+H]^+$ (calcd for $C_{55}H_{85}N_9O_{11}Na$ 1070.6267).

Synthesis of Reniochalistatin E (23) via Octapeptide 227

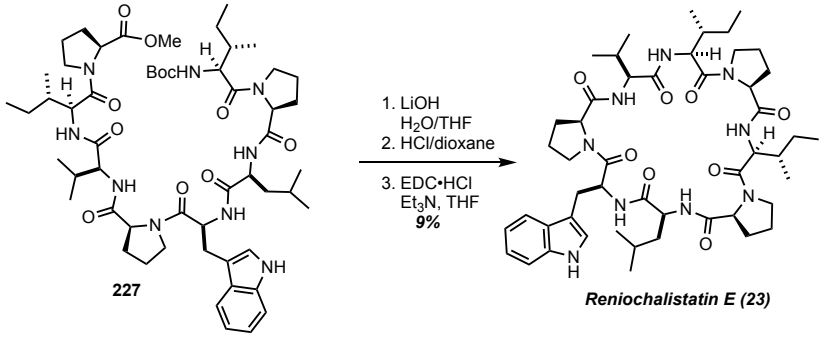

To a stirring solution of **227** (470 mg, 0.45 mmol, 1 equiv) in a 1:1 THF/H_2O (1.8 mL) was added LiOH (54 mg, 2.24 mmol, 5 equiv), and the solution was left to stir at rt for 3 h. The reaction was quenched with 1M HCl (1 vol equiv), and the product was extracted with CH_2Cl_2, dried with brine, dried over sodium sulfate, and concentrated under reduced pressure to afford the free acid of **227**, which was used without further purification. The free acid of **227** (365 mg, 0.72 mmol) was added to an RBF, and the flask was cooled to 0 °C, to which was added 1.0 M HCl in dioxane (2.9 mL). The reaction mixture was stirred for 3 h at rt. The solvent was removed under reduced pressure to afford the crude material (**245**), a white/orange solid that was used without further purification. The deprotected compound **245** (115 mg, 0.12 mmol, 1 equiv) was added to a stirring solution of HOBt (18 mg, 0.12 mmol, 1 equiv) in dry THF (12 mL) at rt under an argon atmosphere. The solution was cooled to 0 °C and stirred for 20 min, after which Et_3N (0.06 mL, 0.42 mmol, 3.5 equiv) was added. After an additional 20 min of stirring, EDC·HCl (25 mg, 0.13 mmol, 1.05 equiv) was added and the reaction mixture was left to stir overnight. The reaction was quenched with H_2O (2 vol equiv), and the product was extracted with CH_2Cl_2, dried over sodium sulfate, and concentrated under reduced pressure. The crude material was purified via flash silica gel chromatography (85:15 EtOAc/MeOH) to afford **23** (39 mg, 9% yield).

^{1}H-NMR ($CDCl_3$, 400 MHz): δ 10.96 – 10.84 (m, 1H), 8.11 – 7.78 (m, 1H), 7.52 (dd, J = 24.5, 7.9 Hz, 2H), 7.40 (d, J = 8.2 Hz, 1H), 7.32 (t, J = 8.7 Hz, 1H), 7.02 – 6.92 (m, 2H), 4.38 – 4.33 (m, 1H), 3.36 (s, 23H), 3.33 – 3.22 (m, 1H), 2.48 (s, 1H), 1.99 – 1.70 (m, 2H), 1.24 (s, 2H), 0.96 – 0.75 (m, 8H), 0.83 (s, 27H).

^{13}C-NMR (DMSO, 126 MHz): δ 172.37, 171.88, 171.81, 171.48, 171.31, 170.58, 170.22, 169.58, 136.59, 127.36, 124.18, 121.21, 118.60, 118.38, 111.71, 111.57, 61.20, 60.67, 59.59, 56.74, 55.85, 54.61, 54.39, 54.22, 47.81, 47.55, 47.41, 38.21, 37.49, 35.09, 33.21, 29.31, 25.22, 25.01, 24.95, 24.83, 24.10, 23.77, 22.71, 20.87, 19.21, 18.88, 15.69 ,15.10, 11.50, 9.81

Optical Rotation: $[\alpha]_D^{25}$ = -99.95 (*c* 0.16, MeOH).

IR (film) ν_{max}: 3290, 2960, 2927, 1670, 1615, 1501, 1445 cm^{-1}

HRMS (ESI^+): *m/z* 938.5475 $[M+H]^+$ (calcd for $C_{49}H_{73}N_9O_8Na$ 938.5473).

Comparison of Reniochalistatin E (Natural vs Synthetic) ^{13}C-NMR and *trans*-Proline Confirmation

Trans-Proline	Position	Natural (ppm) 500 MHz-DMSO	Synthetic (ppm) 500 MHz-DMSO
		172.3	172.37
		171.98	171.88
		171.84	171.81
		171.4	171.48
		171.4	171.31
		170.7	170.58
		170.3	170.22
		170	169.58
		136.5	136.59
		127.3	127.36
		124.1	124.18
		121.2	121.21
		118.6	118.60
		118.4	118.38
		111.7	111.71
		111.5	111.57
		61.3	61.20
		60.8	60.67
		59.7	59.59
		56.8	56.74
		55.9	55.85
		54.5	54.61
		54.5	54.39
		54.3	54.22
		47.9	47.81
		47.6	47.55
		47.4	47.41
		38.2	38.21
		37.5	37.49
		35.23	35.09
		33.2	33.21
$\Delta\delta_{C\beta\text{-}C\gamma}$ Pro Nat. Synth. 1 4.9 4.89 2 4.2 4.36 3 4.1 4.06	β of Pro1	30	30.01
	β of Pro 2	29.3	29.31
	β of Pro 3	29.3	29.28
	γ of Pro 3	25.2	25.22
	γ of Pro 1	25.1	25.12
	γ of Pro 2	25.1	24.95
		24.8	24.83
		24.2	24.10
		23.9	23.92
		23.7	23.77
		22.7	22.71
		20.9	20.87
		19.3	19.21
		18.8	18.88
		15.7	15.69
		15.1	15.10
		11.6	11.50
		9.8	9.81

Procedures towards the Lagunamide C C41 methyl truncate Model System:

Synthesis of (S)-4-isopropylthiazolidine-2-thione (270) via *L*-Valinol:

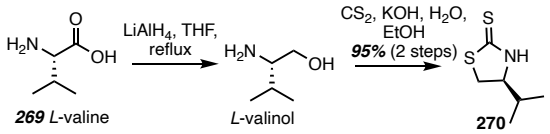

To a flame dried round bottom flask, $LiAlH_4$ (1.88 g, 51 mmol, 3 eq) and THF (0.24 M) were added, and cooled to 0 °C. L-valine (**269**) (2.00 g, 17 mmol, 1 eq) was added portion wise while stirring, after which the ice bath was removed and the mixture was warmed to room temperature. After 30 min, the reaction was refluxed overnight, then cooled to room temperature, and a saturated Rochelle salt solution was added and stirred overnight. The aqueous layer was extracted with CH_2Cl_2 (x3), and the resulting organic layers were combined, dried, and concentrated to afford an oily, crude product. The crude product was purified via short path vacuum distillation resulting in a clear oil (1.74 g, 99% yield) of L-valinol.

^{1}H-NMR ($CDCl_3$, 400 MHz): δ 3.63 (dd, J = 10.4, 4.0 Hz, 1H), 3.27 (dd, J = 10.4, 8.9 Hz, 1H), 2.54 (ddd, J = 8.9, 6.4, 4.0 Hz, 1H), 1.55 (dq, J = 13.5, 6.7 Hz, 1H), 0.91 (dd, J = 6.8, 6.1 Hz, 6H). Next, L-valinol (10.00 g, 96.7 mmol, 1 eq), CS_2 (15.2 mL, 251.8 mmol, 2.6 eq), and EtOH (29.3 mL, 3.3 M) were added to a round bottom flask and purged with argon. An addition funnel was added, flushed with argon, and charged with 2.25 M KOH (116.3 mL, 261.6 mmol, 2.25 M). The KOH was slowly added to the flask with vigorous stirring. After the KOH was added, the addition funnel was replaced with a condensing tube and flushed with argon. The solution was left to reflux at 80 °C for 72 h. Over the course of the reflux period, the solution changed from bright orange to light yellow. The flask was then cooled to room temperature and volatiles were removed under reduced pressure. The solution was acidified with 1 M HCl and extracted with CH_2Cl_2 (x3). The

combined organic layers were then dried and concentrated under reduced pressure, producing a crude light yellow solid (14.82 g, 95%) that was used without further purification.

^{1}H-NMR ($CDCl_3$, 400 MHz): δ 8.76 (s, 1H), 4.01 (td, J = 8.2, 6.0 Hz, 1H), 3.42 (dd, J = 11.2, 8.4 Hz, 1H), 3.20 (dd, J = 11.2, 7.9 Hz, 1H), 1.89 (hept, J = 6.7, 4.7 Hz, 1H), 0.90 (d, J = 6.7 Hz, 3H), 0.87 (d, J = 6.8 Hz, 3H);

^{13}C NMR ($CDCl_3$, 101 MHz): δ 201.10, 70.08, 35.96, 32.05, 18.85, 18.27; HRMS (ESI): calcd for $[C_6H_{11}NS_2 + H^+]$ 162.0406, found 162.0402.

Optical Rotation: $[\alpha]_D^{25}$ = +183.4 (*c* 1.9, $CHCl_3$).

IR (film) ν_{max}: 3185, 2652, 1492, 1380, 1375, 1306, 1270, 1231, 1164, 1144, 1111, 1056, 1033, 980 cm^{-1};

Synthesis of (S)-1-(4-isopropyl-2-thioxothiazolidin-3-yl)ethan-1-one (271):

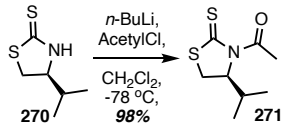

Crude **270** (1.00 g, 6.20 mmol, 1 eq) and anhydrous THF (4.13 mL, 1.5 M) were added to a flame dried round bottom flask under an argon atmosphere. The solution was cooled to -83 °C to which *n*-BuLi (4.48 mL, 6.82 mmol, 1.6 M in hexanes) was added dropwise, producing a color change from light yellow, to orange, to bright yellow. Approximately 25 min later, acetyl chloride (0.58 mL, 8.06 mmol, 1.3 eq) was added dropwise and allowed to stir for 20 min after which the solution was warmed to room temperature. The reaction was quenched with $NH_4Cl_{(sat'd)}$, extracted with CH_2Cl_2 (x3), dried, and concentrated under reduced pressure. The crude material was purified via flash silica chromatography (2:1 CH_2Cl_2: hexane) to afford **271** as a bright yellow oil (1.24 g, 98% yield).

Optical Rotation: $[\alpha]_D^{25}$ = +164.2 (*c* 0.54, $CHCl_3$).

^{1}H-NMR ($CDCl_3$, 400 MHz): δ 5.14 (dt, *J* = 7.7, 6.1, 1H), 3.50 (dd, *J* = 11.4, 8.0 Hz, 1H), 3.01 (dd, *J* = 11.5, 1.3 Hz, 1H), 2.76 (s, 3H), 2.36 (h, *J* = 6.8 Hz, 1H), 1.05 (d, *J* = 6.8 Hz, 3H), 1.05 (d, *J* = 6.7 Hz, 3H), 0.96 (d, *J* = 6.8 Hz, 3H);

^{13}C-NMR ($CDCl_3$, 101 MHz): δ 203.42, 170.9, 71.48, 30.99, 30.63, 27.14, 19.27, 17.97.

Synthesis of (R)-3-hydroxy-1-((S)-4-isopropyl-2-thioxothiazolidin-3-yl)hexan-1-one (272/273):

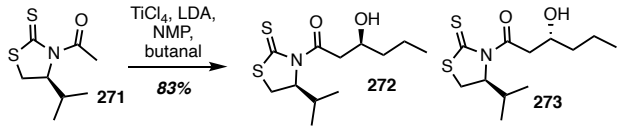

To a flame dried round bottom flask charged with argon was added (S)-1-(4-isopropyl-2-thioxothiazolidin-3-yl)ethan-1-one (**271,** 1.08 g, 5.31 mmol, 1 eq) and anhydrous CH_2Cl_2 (10.62 mL, 0.5 M) and cooled to 0 °C. $TiCl_4$ (0.62 mL, 5.58 mmol, 1.05 eq) was added dropwise, changing the solution from a bright yellow to a bright orange color. 20 min later, freshly prepared 0.64 M LDA (10.27 mL, 6.37 mmol, 1.2 eq) was added to the solution, changing the color from bright orange to deep burgundy and left to stir. While at temperature, NMP (0.61 mL, 6.37 mmol, 1.2 eq) was added, stirred for 5 min, and then cooled to -78 °C for 10 min, at which time butanal (0.65 mL, 8.00 mmol, 1.5 eq) in CH_2Cl_2 (1.5 mL, 5.4 M) was added and left to stir at temperature. The solution was warmed to 0 °C 30 min after the addition of butanal, quenched with $NH_4Cl_{(sat'd)}$, and extracted with CH_2Cl_2 (x4). The combined organic layers were washed with brine, dried, and concentrated under reduced pressure. The crude material was purified via flash silica chromatography (2:1 hexane/ EtOAc) and afforded **273** (1.05 g, 72% yield).

Optical Rotation: $[\alpha]_D^{25}$ = +231 (*c* 0.390, $CHCl_3$).

IR (film) ν_{max}: 3452, 2960, 2928, 2870, 1695, 1467 cm^{-1};

^{1}H NMR ($CDCl_3$, 400 MHz): δ 5.17 (ddd, *J* = 7.6, 6.4, 1.0, 1H), 4.03 (m, 1H), 3.55 – 3.40 (m, 2H), 3.31 (d, *J* = 17.2, 2.7 Hz, 1H), 3.18 (s, 1H), 3.03 (dd, *J* = 11.5 Hz, 1H), 2.35 (m, 1H), 1.60 – 1.34 (m, 4H), 1.06 (d, *J* = 6.8 Hz, 3H*),* 0.98 (d, *J* = 6.54 Hz, 3H), 0.93 (t, *J* = 7.0 Hz, 3H);

^{13}C NMR ($CDCl_3$, 101 MHz): δ 174.03, 71.57, 68.43, 45.37, 38.97, 30.99, 30.80, 19.31, 18.90, 18.04, 14.23;

HRMS (ESI): calcd for [$C_{12}H_{21}NS_2O_2 + Na^+$] 298.0906, found 298.0907.

Synthesis of (R)-3-((*tert*-butyldimethylsilyl)oxy)-1-((S)-4-isopropyl-2-thioxothiazolidin-3-yl)hexanone (274):

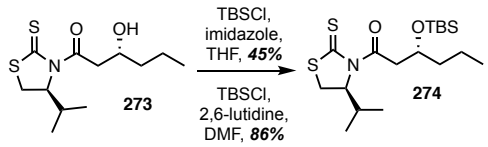

To a flame dried round bottom flask charged with argon was added (R)-3-hydroxy-1-((S)-4-isopropyl-2-thioxothiazolidin-3-yl)hexan-1-one, (**273**, 900 mg, 3.27 mmol), DMF (13.6 mL, 0.24 M), TBSCl (1.97 g, 13.08 mmol, 4 eq), and 2,6-lutidine (1.90 mL, 16.35 mmol, 5 eq). The solution was stirred at 32 °C under argon. After 24 h the reaction was cooled to room temperature, diluted with water and extracted with EtOAc (x3). The organic layers were combined, washed with brine, dried and concentrated under reduced pressure. The crude yellow compound was purified via flash silica chromatography (20:1 hexane/EtOAc) to produce **274** as a bright yellow viscous oil (1.10 g, 86% yield).

Optical Rotation: $[\alpha]_D^{25}$ = +207.3 (*c* 0.74, $CHCl_3$).

IR (film) ν_{max}: 2950, 1692, 1460 cm^{-1};

^{1}H NMR ($CDCl_3$, 400 MHz): δ 5.13 (ddd, *J* = 7.7, 5.9, 1.2 Hz, 1H), 4.26 (p, *J* = 5.8 Hz, 1H), 3.54 – 3.44 (m, 2H), 3.38 (dd, *J* = 16.8, 6.3 Hz, 1H), 3.01 (dd, *J* = 11.5, 1.2 Hz, 1H), 2.36 (dt, *J* = 13.5, 6.7 Hz, 1H), 1.47 – 1.32 (m, 4H), 1.05 (d, *J* = 6.8 Hz, 3H), 0.97 (d, *J* = 6.9 Hz, 3H), 0.90 (s, 3H), 0.87 (s, 9H), 0.07 (s, 3H), 0.05 (s, 3H);

^{13}C NMR ($CDCl_3$, 101 MHz): δ 174.03, 71.85, 68.99, 46.20, 40.11, 31.08, 30.38, 26.06, 25.92, 19.33, 18.49, 17.84, 14.45, -4.40; HRMS (ESI): calcd for [$C_{18}H_{35}NO_2S_2Si + Na^+$] 412.6772, found 412.6773.

Synthesis of (R)-3-((tert-butyldimethylsilyl)oxy)hexanal (276):

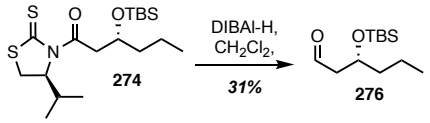

To a flame dried round bottom flask charged with argon was added **274** (225 mg, 0.58 mmol, 1.0 eq) and cooled to -78 °C, at which time, DIBAl-H (1 M in toluene, 0.59 mmol, 1.02 eq) was added. The reaction was allowed to stir until a second product spot was visible via TLC analysis, at which time Rochelle's $Salt_{(sat'd)}$ was added and allowed to stir overnight. The mixture was extracted with CH_2Cl_2 (x3); the organic layers were combined, washed with brine, dried, and concentrated under reduced pressure. The crude material was purified via distillation to afford **276** (41 mg, 31% yield), alcohol **275** (39 mg, 29% yield), and recovered auxiliary **270**.

IR (film) ν_{max}: 2958, 2931, 2858, 2720, 1722, 1255, 836, 776 cm^{-1};

^{1}H NMR ($CDCl_3$, 400 MHz): δ 9.81 (t, J = 2.5 Hz, 1H), 4.18 (p, J = 5.9 Hz, 1H), 2.51 (dd, J = 5.7, 2.5 Hz, 2H), 1.58 – 1.28 (m, 7H), 0.94 – 0.89 (m, 7H), 0.87 (s, 9H), 0.08 – 0.04 (m, 6H).

Synthesis of (R)-3-((tert-butyldimethylsilyl)oxy)hexanol (275):

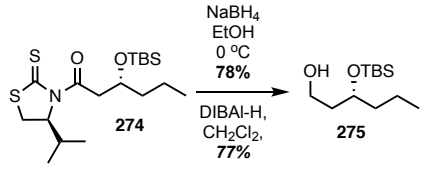

To a flame dried round bottom flask charged with argon was added **274** (1.76 g, 4.50 mmol), EtOH (26.47 mL, 0.17 M), followed by $NaBH_4$ (681 mg, 18 mmol, 4 eq). The solution was allowed to stir for approximately 4 h, over which time the bright yellow color of the starting material disappeared. The reaction was quenched with the slow addition of $NH_4Cl_{(sat'd)}$ and extracted with CH_2Cl_2 (x3). The organic layers were combined, washed with brine, dried, and concentrated under reduced pressure. The crude, clear oil was purified via flash silica chromatography (20% EtOAc/hexane) to afford **275** as a clear oil (951 mg, 91% yield) along with recovered auxiliary **270**.

Optical Rotation: $[\alpha]_D^{25}$ = -11.26 (*c* 4.51, $CHCl_3$).

IR (film) ν_{max}: 3358, 2952, 2930, 2858, 1744, 1461, 1250, 1109, 1072, 833, 774, 695 cm^{-1};

^{1}H NMR ($CDCl_3$, 400 MHz): δ 3.92 – 3.84 (m, 1H), 3.81 – 3.73 (m, 1H), 3.70 – 3.62 (m, 1H), 2.73 (s, 1H), 1.83 – 1.67 (m, 1H), 1.66 – 1.55 (m, 1H), 1.52 – 1.41 (m, 2H), 1.36 – 1.21 (m, 3H), 1.00 – 0.68 (m, 11H), 0.04 (d, *J* = 6.2 Hz, 6H);

^{13}C NMR ($CDCl_3$, 101 MHz): δ 71.99, 60.51, 39.29, 37.88, 26.05, 18.82, 18.19, 14.46, -4.22, -4.49;

HRMS (ESI): calcd for [$C_{19}H_{34}O_2Si + Na^+$] 345.2226, found 345.2213.

Synthesis of (R)-3-((tert-butyldimethylsilyl)oxy)hexanal (276 from 275):

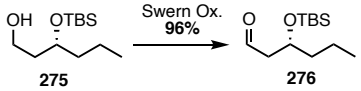

To a flame dried round bottom flask charged with argon was added oxalyl chloride (0.25 mL, 2.83 mmol, 1 eq) and CH_2Cl_2 (5.66 mL, 0.5 M). The solution was cooled to -78 °C and stirred for 10 min; then, DMSO (0.40 mL, 5.59 mmol, 2.2 eq) was slowly added to the solution. Approximately 15 min later, **275** (597.5 mg, 2.57 mmol, 1.0 eq) in CH_2Cl_2 (2.28 mL, 1.13 M) was added and left to stir at temperature. Approximately 1 h later triethylamine (1.78 mL, 12.85 mmol, 5 eq) was added. The reaction was stirred at -78 °C for 10 min, and then warmed to room temperature and stirred for 1 h, at which point, water was added, and the solution was extracted with CH_2Cl_2 (x3). The organic layers were combined, washed once with 2% HCl solution and once with 5% Na_2CO_3 solution, washed with brine, dried, and concentrated under reduced pressure to afford crude **276** (619 mg, 95% yield). The crude aldehyde was used immediately.

Synthesis of Methyl (R,E)-5-((tert-butyldimethylsilyl)oxy)oct-2-enoate (277):

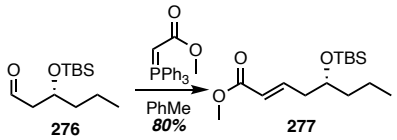

To a flame dried round bottom flask charged with argon was added the activated Witting reagent (1.28 g, 3.84 mmol, 1.5 eq) as well as anhydrous toluene (7.68 mL, 0.5 M) and stirred vigorously. Meanwhile, in a separate flame dried round bottom flask **276** (591 mg, 2.56 mmol, 1 eq) in anhydrous toluene (3.2 mL, 0.8 M) was added and allowed to stir. Approximately 20 min later, the second-round bottom flask containing the activated Wittig reagent was added to the original flask and allowed to stir under argon overnight at room temperature. The reaction was diluted with water and extracted with EtOAc (x3). The organic layers were combined, washed with brine, dried, and concentrated under reduced pressure. The crude oil was purified via flash silica chromatography (1:5, EtOAc/hexane) to afford **277** has a clear colorless oil (8.26 g, 80% yield).

Optical Rotation: $[\alpha]_D^{25}$ = +16.7 (*c* 0.63, $CHCl_3$).

IR (film) ν_{max}: 2957, 2929, 1725, 1645, 1251, 1173, 1038, 830, 773 cm^{-1};

^{1}H NMR ($CDCl_3$, 400 MHz): δ 7.02 – 6.93 (m, 1H), 5.84 (dd, 1H), 3.80 – 3.75 (m, 1H), 3.73 (s, 3H), 2.37 – 2.29 (m, 2H), 1.47 – 1.35 (m, 4H), 0.90 (d, *J* = 7.2 Hz, 3H), 0.89 – 0.87 (m, 9H), 0.04 (s, 6H);

^{13}C NMR ($CDCl_3$, 101 MHz): δ 191.67, 180.00, 146.60, 123.00, 71.28, 51.61, 40.46, 39.69, 26.05, 18.78, 14.39;

HRMS (ESI): calcd for [$C_{15}H_{30}O_3Si + Na^+$] 309. 1856, found 309.1860.

Synthesis of (R,E)-5-((tert-butyldimethylsilyl)oxy)oct-2-en-1-ol (267):

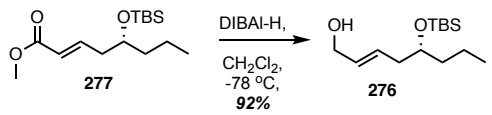

To a flame dried round bottom flask charged with argon was added **277** (375 mg, 1.31 mmol, 1 eq) and anhydrous CH_2Cl_2 (6.55 mL, 0.2 M) and was cooled to -78°C. After stirring for 15 min, DIBAL-H (1 M in toluene) (3.28 mL, 3.28 mmol, 2.5 eq) was added dropwise and was allowed to stir until TLC analysis showed no remaining starting material (approximately 10-15 minutes). Rochelle $Salt_{(sat'd)}$ was then added and left to stir overnight. The solution was extracted with CH_2Cl_2 (x3). The combined organic layers were washed with brine, dried, and concentrated under reduced pressure. The crude oil was purified via flash silica chromatography (1:5 EtOAc/hexane) to afford **276** as a clear pure oil (311 mg, 92% yield).

Optical Rotation: $[\alpha]_D^{25}$ = +17.5 (*c* 0.99, $CHCl_3$).

^{1}H NMR ($CDCl_3$, 400 MHz): δ 5.76 – 5.61 (m, 2H), 4.10 (d, *J* = 4.8 Hz, 2H), 3.71 – 3.67 (m, 1H), 2.24 – 2.14 (m, 2H), 1.43 – 1.27 (m, 7H), 0.90 – 0.86 (m, 12H), 0.04 (s, 6H);

^{13}C NMR ($CDCl_3$, 101 MHz): δ 131.33, 129.87, 72.04, 64.02, 40.47, 39.39, 26.10, 18.85, 18.37, 14.46, -4.16, -4.31;

HRMS (ESI): calcd for [$C_{14}H_{30}O_2Si + H^+$] 259.4845, found 259.4840.

Synthesis of (2-((R)-2-((tert-butyldimethylsilyl)oxy)pentyl)cyclopropyl)methanol (278):

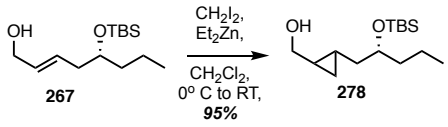

To a flame dried round bottom flask charged with argon was added **267** (257 mg, 0.99 mmol, 1 eq) and anhydrous CH_2Cl_2 (3.0 mL, 0.33 M); the mixture was cooled to 0 °C. In a separate flame dried round bottom flask charged with argon was added diiodomethane (0.24 mL, 3.95 mmol, 2.5 eq) and anhydrous CH_2Cl_2 (23 mL, 0.17 M); the mixture was cooled to 0°C. To each flask was added diethyl zinc (1 M in hexanes, 1.58 mL, 1.58 mmol, 1.5 eq) and stirred at temperature. The flasks were combined 45 min later, slowly allowed to warm and left to stir overnight. The reaction was quenched with the addition of $NH_4Cl_{(sat'd)}$ and was then extracted with CH_2Cl_2 (x3). The organic layers were combined, washed with brine, dried, and concentrated under reduced pressure. The crude material was purified via flash silica gel chromatography (4:1, hexane/EtOAc) to afford **278** as a clear oil (256 mg, 95% yield).

^{1}H NMR ($CDCl_3$, 400 MHz): δ 3.82 – 3.65 (m, 1H), 3.54 – 3.37 (m, 2H), 1.58 – 1.42 (m, 4H), 1.41 – 1.23 (m, 4H), 0.92 – 0.85 (m, 13H), 0.73 (s, 1H), 0.74 – 0.61 (m, 1H), 0.42 – 0.28 (m, 2H), 0.08 (s, 6H);

^{13}C NMR ($CDCl_3$, 101 MHz *d*): δ 72.73, 72.43, 67.43, 41.28, 41.05, 39.56, 39.35, 26.14, 21.55, 18.83, 14.54, 13.74, 13.49, 10.23, 10.00, -4.18;

Optical Rotation: $[\alpha]_D^{25}$ = +53.7 (*c* 1.1, $CHCl_3$).

HRMS (ESI): calcd for [$C_{15}H_{32}O_2Si + Na^+$] 295.4932, found 295.4934.

Reaction Note: Flask should ALWAYS be added to flask A. Drawing out the activated methylating and Et_2Zn and reacts with air violently.

Synthesis of Tert-butyl(((2R)-1-(2-(iodomethyl)cyclopropyl)pentan-2-yl)oxy)dimethylsilane (279)

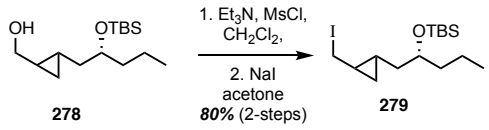

278 279

To a dry round bottom flask was added **278** (260 mg, 2.27 mmol, 1 eq), CH_2Cl_2 (15 mL, 0.15 M) , triethylamine (0.94 mL, 6.81 mmol, 3 eq), and methylsulfonyl chloride (0.30 mL, 3.86 mmol, 1.7 eq) which was cooled to 0°C. The solution was stirred for 10 min before warming to room temperature and stirring for an additional 25 min. The solvent was then removed under reduced pressure, resulting in a yellow solid. To the solid was added dry acetone (15 mL, 0.15 M) and NaI (3.06 g, 20.43 mmol, 9 eq). The solution was stirred for 1 h at room temperature under argon. The reaction was quenched with sodium bicarbonate$_{(sat'd)}$ and sodium thiosulfate$_{(sat'd)}$ and washed with ether (x3). The combined organic layers were washed with brine, dried, and concentrated under reduced pressure. The crude product was purified via flash silica chromatography (4:1 hexane/EtOAc) to afford **279** as a clear oil, composed of two diastereomers, (694 mg, 80% yield).

^{1}H NMR ($CDCl_3$, 400 MHz): δ 3.71 (p, *J* = 5.8 Hz, 1H), 3.30 – 3.02 (m, 2H), 1.52 – 1.25 (m, 6H), 1.11 – 1.01 (m, 1H), 0.92 – 0.86 (m, 12H), 0.79 – 0.72 (m, 1H), 0.67 – 0.57 (m, 1H), 0.50 – 0.42 (m, 1H), 0.04 (d, *J* = 3.3 Hz, 6H);

^{13}C NMR ($CDCl_3$, 101 MHz): δ 72.73, 67.43, 41.28, 41.05, 39.56, 39.35, 26.14, 21.55, 18.83, 14.54, 13.74, 10.23, -4.18.

Synthesis of Tert-butyldimethyl(((4R)-6-methyloct-7-en-4-yl)oxy)silane (281/282):

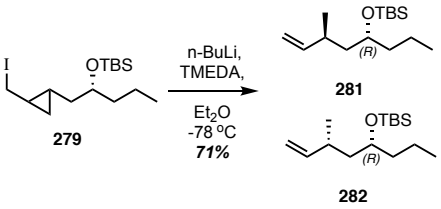

To a flamed dry round bottom flask charged with argon was added **279** (830 mg, 2.17 mmol, 1.0 eq), cooled to -78 °C, then TMEDA (0.66 mL, 4.34 mmol, 2.0 eq.) followed by *n*-BuLi (1.6 M in hexanes, 2.72 mL, 4.34 mmol, 2.0 eq.) was added. The reaction was warmed to -30 °C for 45 mins. The reaction was warmed to 0 °C 3 h later, at which the reaction was quenched with water and extracted with diethyl ether (x3). The organic layers were combined, washed with 10% HCl, 5% $NaHCO_3$ and brine, then dried and concentrated under reduced pressure. The crude material was purified via flash silica gel chromatography (4:1 hexane/EtOAc) to afford **281** and **282** in (395 mg) 43% and 28% yields, respectively.

^{1}H NMR ($CDCl_3$, 400 MHz): δ 5.89 – 5.62 (m, 1H), 5.06 – 4.84 (m, 2H), 3.78 – 3.57 (m, 1H), 2.31 – 1.93 (m, 2H), 1.52 – 1.25 (m, 7H), 1.00 – 0.90 (m, 4H), 0.90 – 0.87 (m, 9H), 0.04 (s, 6H);

^{13}C NMR ($CDCl_3$, 101 MHz): δ139.23, 114.50, 112.46, 72.20, 70.23, 44.47, 39.61, 36.77, 34.47, 26.15, 24.80, 20.52, 18.47, 14.55, -4.06;

HRMS (ESI): calcd for [$C_{15}H_{32}OSi + Na^+$] 279.4942, found 279.4939.

Procedures Towards the Target Polyketide of Lagunamide C:

Synthesis of (*S*)-2-methylbutanal (167) via Swern Oxidation.

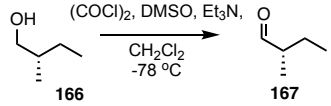

To a flame dried round bottom flask charged with argon was added oxalyl chloride (1.05 mL, 11.8 mmol, 1.2 eq) and CH_2Cl_2 (23.6 mL, 0.5 M). The solution was cooled to -78 °C and stirred for 10 min; then, DMSO (1.54 mL, 21.64 mmol, 2.2 eq) was slowly added to the solution. Approximately 15 min later, **166** (1.07 mL, 9.84 mmol, 1.0 eq) was added dropwise and left to stir at temperature. Approximately 1 h later triethylamine (6.86 mL, 49.18 mmol, 5 eq) was added. The reaction was stirred at -78 °C for 10 min, and then warmed to room temperature and stirred for 1 h, at which point, $NH_4Cl$was added, and the solution was extracted with CH_2Cl_2 (x3). The organic layers were combined, washed once with 1 M HCl solution and once with brine, dried, and concentrated under reduced pressure at room temperature to afford crude **167** (619 mg, 95% yield). The crude aldehyde was used immediately.

Reaction Reference: AF2-310

NMR FILE: AF2-370-400

Synthesis of (*S*)-2-methylbutanal (167) via PCC Oxidation:

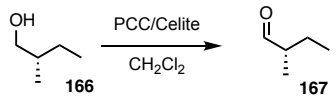

To a FDRBF, PCC and celite were added in a 1:1 mass ratio (1,610 mg, 7.47 mmol, 1.5 eq. of PCC and 1,610 mg of celite) and charged with anhydrous CH_2Cl_2 (0.5 M, 10 mL). Next, (*S*)-2-methylbutanol (**166**) (0.54 mL, 4.98 mmol, 1 eq.) was added dropwise and allowed to stir for 1 h. After that time diethyl ether was added to the reaction mixture and allowed to stir for another 5 mins. The reaction mixture was then filtered through celite and directly added to the next reaction.

Reaction Reference: AF5-275

Synthesis of (*R*)-4-benzylthiazolidine-2-thione:

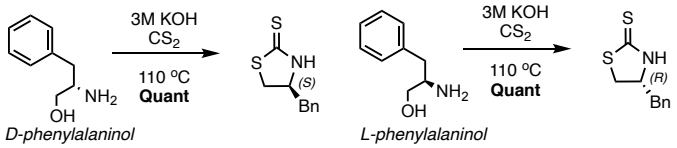

Freshly prepared 3M KOH (66.2 mL, 198.6 mmol, 6.0 eq.) was added to a RBF and allowed to cool to room temperature (rt). *L*-Phenylalinol (5 g, 33.1 mmol, 1 eq.) was then added in one portion, followed by CS_2 (10 mL, 165.5 mmol, 5 eq.). The mixture was then warmed to 110 ºC and reflux overnight. The reaction was then cooled to rt and was diluted with DCM. Then the reaction mixture was quenched with saturated NH_4Cl and allowed to stir. After a few mins the reaction was quenched with 1 M HCl slowly to avoid boiling over. The resulting mixture was then extracted with DCM (3x), dried with Na_2SO_4, and concentrated under reduced pressure to produce crude product without further purification to produce the product in quant. yields and used without further purification. The same reaction was fun with *D*-phenylalaninol to provide 285 in quant yields.

(*S*) isomer:

^{1}H NMR (400 MHz, Chloroform-*d*) δ 7.4 – 7.3 (m, 5H), 7.3 – 7.2 (m, 1H), 4.5 – 4.4 (m, 1H), 3.6 (dd, *J* = 11.2, 7.7 Hz, 1H), 3.4 (dd, *J* = 11.2, 6.9 Hz, 1H), 3.0 (dd, *J* = 7.3, 3.0 Hz, 2H).

Reaction Reference and File Name: AF4-426-400

(*R*) Isomer:

^{1}H NMR (400 MHz, Chloroform-*d*) δ 7.4 – 7.3 (m, 5H), 7.3 – 7.2 (m, 1H), 4.5 – 4.4 (m, 1H), 3.7 (dd, *J* = 11.2, 7.6 Hz, 1H), 3.4 (dd, *J* = 11.2, 7.0 Hz, 1H), 3.0 (d, *J* = 7.3 Hz, 2H).

Reaction Reference and File Name: AF4-100-400

General Procedure for Acetylation of (*S/R*)-4-benzylthiazolidine-2-thione to form 285 and 286:

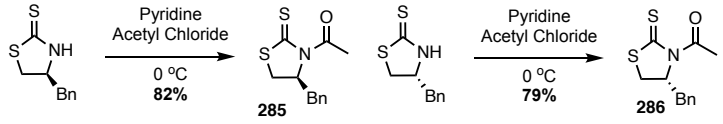

To a FDRBF was charged with (*S/R*)-4-benzylthiazolidine-2-thione (1 eq.) and Dry DCM (1M). The mixture was cooled to 0 ºC and then pyridine (1.2 eq.) was added and stirred for 15 mins. Then acetyl chloride (1.5 eq.) was added and allowed to stir for 1h. The reaction was warmed to rt and then quenched with water and saturated NH_4Cl. The compound was then extracted with DCM (3x) and dried with Na_2SO_4 and concentrated under reduced pressure. The compound was then purified using flash chromatography (1:1 EtOAc/hexane) mixture to produce yellow crystalline compound (82% of **285** and 79% of **286**).

NMR File Names: 285 =AF3-121-A-400, **286** = AF5-187-600

285: ^{1}H NMR (400 MHz, Chloroform-*d*) δ 7.40 – 7.35 (m, 2H), 7.31 (dd, *J* = 7.4, 1.3 Hz, 3H), 5.44 – 5.37 (m, 1H), 3.41 (ddd, *J* = 11.6, 7.3, 1.2 Hz, 1H), 3.25 (dd, *J* = 13.1, 3.8 Hz, 1H), 3.06 (dd, *J* = 13.2, 10.6 Hz, 1H), 2.91 (dd, *J* = 11.5, 0.7 Hz, 1H), 2.82 (s, 3H).

A8: **^{1}H NMR (400 MHz, Chloroform-*d*)** δ 7.40 – 7.35 (m, 2H), 7.31 (dd, *J* = 7.4, 1.3 Hz, 3H), 5.44 – 5.37 (m, 1H), 3.41 (ddd, *J* = 11.6, 7.3, 1.2 Hz, 1H), 3.25 (dd, *J* = 13.1, 3.8 Hz, 1H), 3.06 (dd, *J* = 13.2, 10.6 Hz, 1H), 2.91 (dd, *J* = 11.5, 0.7 Hz, 1H), 2.82 (s, 3H).

^{13}C NMR (101 MHz, $CDCl_3$) δ 201.61, 170.77, 136.53, 129.48, 128.94, 127.25, 68.25, 36.70, 31.83, 27.11.

General Procedure for Aldol reaction to form (4*S/R*)-1-((*S/R*)-4-benzyl-2-thioxothiazolidin-3-yl)-3-hydroxy-4-methylhexan-1-one (287, 288, 289, and 290).

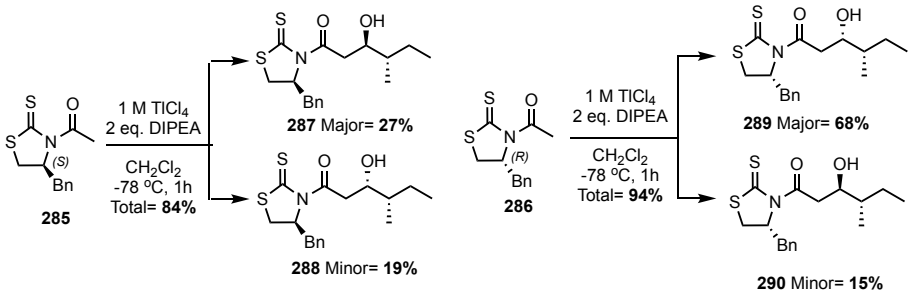

To a FDRBF was charged with DCM (0.17 M) and (*S/R*)-1-(4-benzyl-2-thioxothiazolidin-3-yl)ethan-1-one (**285/286**) (1 eq.) and molecular sieves were cooled to 0 ºC. A solution of 1 M $TiCl_4$ in DCM (1 eq.) was added dropwise to the mixture and allowed to stir for 5 mins. DIPEA (2 eq.) was added dropwise and allowed to stir for 20 mins. The reaction was cooled to -78 ºC and (*S*)-2-methylbutanal (crude transfer calculated for 3 eq.) in the DCM/ether mixture after celite purification was added dropwise and allowed to stir for 2 h. The resulting mixture was immediately quenched with saturated NH_4Cl and then warmed to rt. The product was extracted with DCM (3x), dried with Na_2SO_4, and concentrated under reduced pressure. The resulting mixture of diastereomers was a yellow oil was then purified using column chromatography (1:3 EtOAc/hexane). Each diastereomer was then collected as a yellow oil (**290**= 15% and **289**= 68%) yields, and a mixed yield of 11%. Total yield for this reaction, by weight, produces an 94% yield. The same reaction procedure with changes to amounts added was done to produce **287** (19%) and **288** (27%) with a mixture of isomers (38%).

Notebook entry: AF4-361, AF4-090

NMR File Name: 289= AF5-182-C-2-600, **290=** AF5-182-A-2-600, **288=** AF4-096-A-400, **287**= AF4-096-C-400

287: **^{1}H NMR (400 MHz, Chloroform-*d*)** δ 7.4 – 7.3 (m, 5H), 5.4 (ddd, *J* = 10.8, 7.1, 4.0 Hz, 1H), 4.1 – 4.0 (m, 1H), 3.6 (dd, *J* = 17.9, 2.0 Hz, 1H), 3.4 (ddd, *J* = 11.6, 7.2, 1.0 Hz, 1H), 3.3 (dd, *J* = 13.2, 4.0 Hz, 1H), 3.2 (dd, *J* = 17.8, 10.2 Hz, 1H), 3.1 (dd, *J* = 13.2, 10.5 Hz, 1H), 2.9 (d, *J* = 11.6 Hz, 1H), 1.7 – 1.6 (m, 3H), 1.3 – 1.2 (m, 2H), 1.0 (dd, *J* = 8.2, 6.9 Hz, 3H).

288: **^{1}H NMR (400 MHz, Chloroform-*d*)** δ 7.4 – 7.3 (m, 5H), 5.4 (ddd, *J* = 10.7, 7.1, 4.0 Hz, 1H), 4.0 (dtd, *J* = 10.3, 4.2, 2.2 Hz, 1H), 3.6 (dd, *J* = 17.3, 10.1 Hz, 1H), 3.4 (dd, *J* = 11.6, 7.2, 1.1 Hz, 1H), 3.3 – 3.2 (m, 2H), 3.1 (dd, *J* = 13.2, 10.3 Hz, 1H), 3.0 (d, *J* = 4.2 Hz, 1H), 2.9 (d, *J* = 11.5 Hz, 1H), 1.3 – 1.2 (m, 2H), 1.0 – 0.9 (m, 6H).

289: **^{1}H NMR (600 MHz, Chloroform-*d*)** δ 7.40 – 7.35 (m, 2H), 7.34 – 7.29 (m, 3H), 5.43 (ddd, *J* = 10.8, 7.1, 4.0 Hz, 1H), 4.16 – 4.09 (m, 1H), 3.59 (dd, *J* = 17.7, 2.0 Hz, 1H), 3.43 (ddd, *J* = 11.5, 7.2, 1.1 Hz, 1H), 3.28 – 3.20 (m, 2H), 3.08 (dd, *J* = 13.2, 10.5 Hz, 1H), 2.93 (d, *J* = 11.5 Hz, 1H), 2.53 (d, *J* = 3.9 Hz, 1H), 1.56 – 1.50 (m, 2H), 1.31 – 1.19 (m, 1H), 0.96 (t, *J* = 6.9 Hz, 6H).

^{13}C NMR (151 MHz, $CDCl_3$) δ 201.49, 173.75, 136.45, 129.48, 128.97, 127.32, 77.25, 77.04, 76.83, 70.67, 68.43, 43.51, 39.76, 36.85, 32.07, 25.56, 14.15, 11.83.

290: ^{1}H NMR (600 MHz, Chloroform-*d*) δ 7.37 – 7.33 (m, 2H), 7.31 – 7.27 (m, 3H), 5.42 (ddd, *J* = 10.8, 7.2, 3.9 Hz, 1H), 3.94 (dt, *J* = 8.0, 4.0 Hz, 1H), 3.49 (dd, *J* = 17.4, 10.2 Hz, 1H), 3.41 (dd, *J* = 11.5, 7.2 Hz, 1H), 3.30 (dd, *J* = 17.4, 2.0 Hz, 1H), 3.23 (dd, *J* = 13.3, 4.0 Hz, 1H), 3.14 (d, *J* = 4.2 Hz, 1H), 3.05 (dd, *J* = 13.2, 10.4 Hz, 1H), 2.91 (d, *J* = 11.5 Hz, 1H), 1.59 (d, *J* = 6.3 Hz, 1H), 1.55 – 1.50 (m, 1H), 1.23 – 1.15 (m, 1H), 0.95 – 0.90 (m, 6H).

^{13}C NMR (151 MHz, $CDCl_3$) δ 201.78, 174.59, 136.52, 129.59, 129.10, 127.44, 72.20, 68.49, 42.21, 40.13, 36.90, 32.12, 29.85, 25.19, 14.71, 11.76.

General Procedure for TBS protection of Aldol Product: (3*S*,4*S*)-1-((*R*)-4-benzyl-2-thioxothiazolidin-3-yl)-3-hydroxy-4-methylhexan-1-one (295).

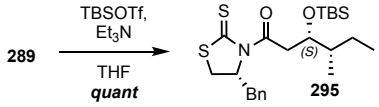

A FDRBF was charged with **A8** (341 mg, 1.01 mmol, 1 eq.) and dry DCM (0.1 M, 10.1 mL) and was cooled to 0 ºC. Et_3N (0.56 mL, 4.04 mmol, 4 eq.) was added in one portion and allowed to react for 10 mins. Then tert-Butyldimethylsilyl trifluoromethanesulfonate (TBSOTf) (0.46 mL, 2.02 mmol, 2 eq.) was added and allowed to stir overnight warming to rt. The resulting mixture was then quenched with saturated NH_4Cl, extracted with DCM (3x), dried with Na_2SO_4, and concentrated under reduced pressure. The resulting yellow oil was then separated via column chromatography (1:12 EtOAc/hexane) to produce a yellow oil in 495 mg quantitive yield.

^{1}H NMR (600 MHz, Chloroform-*d*) δ 7.38 (t, *J* = 7.5 Hz, 2H), 7.35 – 7.29 (m, 3H), 5.29 (ddd, *J* = 10.7, 7.0, 3.7 Hz, 1H), 4.34 (dt, *J* = 8.7, 3.1 Hz, 1H), 3.58 (dd, *J* = 17.0, 8.7 Hz, 1H), 3.36 (ddd, *J* = 11.5, 7.1, 1.1 Hz, 1H), 3.28 (dd, *J* = 13.2, 3.7 Hz, 1H), 3.11 – 3.00 (m, 2H), 2.91 (d, *J* = 11.4 Hz, 1H), 1.64 (ddd, *J* = 13.2, 7.5, 4.4 Hz, 1H), 1.50 (td, *J* = 6.3, 3.4 Hz, 1H), 1.10 – 1.03 (m, 1H), 0.97 – 0.91 (m, 6H), 0.91 – 0.89 (m, 4H), 0.89
(s, 3H), 0.87 (s, 9H), 0.04 (d, *J* = 8.3 Hz, 6H).

NMR File: AF5-183-600

Crystallographic data:

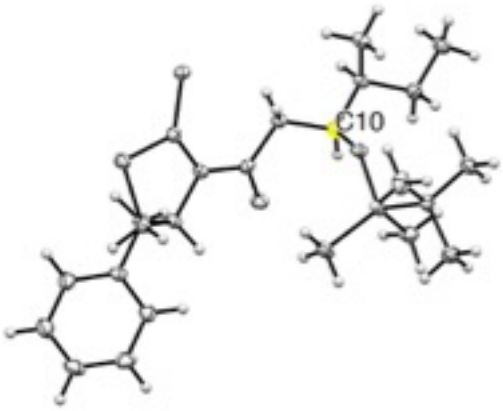

General Procedure for Auxiliary cleavage to form (3*R/S*,4*S*)-3-((*tert*-butyldimethylsilyl)oxy)-4-methylhexan-1-ol.

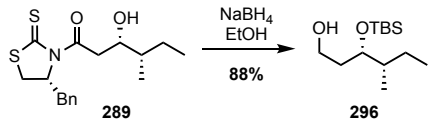

289 296

An RBF was charged with (3*S/3R*,4*S*)-1-((*S*)-4-benzyl-2-thioxothiazolidin-3-yl)-3-((*tert*-butyldimethylsilyl)oxy)-4-methylhexan-1-one (1 eq.) and dissolved in EtOH (0.17 M) and cooled to 0 ºC. In one addition, $NaBH_4$ (4 eq.) was added and allowed to stir overnight warming to rt. The resulting mixture was then cooled to 0 ºC and quenched with (½ saturated) NH_4Cl, extracted with DCM (3x), dried with Na_2SO_4, and concentrated under reduced pressure. The crude material was then separated with flash silica gel chromatography (1:6 EtOAc/hexane) to produce (78%) a clear/yellowish oil.

^{1}H NMR (600 MHz, Chloroform-*d*) δ 3.81 – 3.69 (m, 3H), 2.09 (t, *J* = 5.1 Hz, 1H), 1.70 (td, *J* = 7.2, 5.6 Hz, 2H), 1.65 – 1.60 (m, 1H), 1.52 (td, *J* = 6.7, 3.5 Hz, 1H), 1.09 – 1.01 (m, 1H), 0.92 (s, 12H), 0.87 (d, *J* = 6.8 Hz, 3H), 0.10 (d, *J* = 14.5 Hz, 6H).

^{13}C NMR (151 MHz, $CDCl_3$) δ 75.38, 60.97, 40.34, 34.28, 25.89, 23.87, 18.06, 15.07, 12.20, -4.32, -4.55.

NMR File Name: AF5-185-B-600

296': AF5-189-600

^{1}H NMR (600 MHz, Chloroform-*d*) δ 3.82 (ddd, *J* = 8.4, 4.9, 3.4 Hz, 1H), 3.79 – 3.75 (m, 2H), 2.24 – 2.20 (m, 1H), 1.73 – 1.65 (m, 1H), 1.64 – 1.54 (m, 2H), 1.38 (ddd, *J* = 13.0, 7.5, 5.2 Hz, 1H), 1.15 – 1.05 (m, 1H), 0.92 (s, 12H), 0.89 (d, *J* = 6.8 Hz, 3H), 0.11 (d, *J* = 14.0 Hz, 6H).

^{13}C NMR (151 MHz, $CDCl_3$) δ 74.94, 61.09, 40.52, 33.07, 26.03, 25.88, 18.04, 13.36, 12.18, -4.31, -4.62.

General Procedure for Wittig Olefination: Methyl (5*S/R*,6*S*,*E*)-5-((*tert*-butyldimethylsilyl)oxy)-6-methyloct-2-enoate.

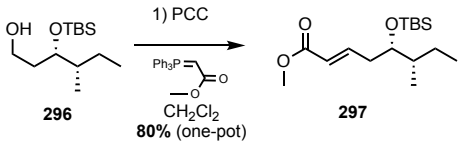

A FDRBF was charged with PCC and Celite (2.5 eq.) and dry DCM (0.08 M) and then (3*R/S*,4*S*)-3-((*tert*-butyldimethylsilyl)oxy)-4-methylhexan-1-ol (1eq.) was dissolved in minimal volume of DCM and added dropwise and allowed to stir for 1 h at rt. The resulting mixture was then quenched with ether and allowed to stir. After 10 mins, the mixture is filtered through celite and, then the yilide was added and left to stir o/n. The reaction was quenched with water and NH_4Cl, extracted with DCM (3x), dried with Na_2SO_4, and concentrated under reduced pressure. The resulting extract was then purified via flash column chromatography (1:12 EtOAc/hexane) to produce a colorless oil (80%).

297:

NMR File Name: AF5-016-400

^{1}H NMR (400 MHz, Chloroform-*d*) δ 6.94 (dt, *J* = 15.4, 7.5 Hz, 1H), 5.84 (dt, *J* = 15.7, 1.5 Hz, 1H), 3.73 (s, 3H), 3.69 – 3.64 (m, 1H), 2.37 – 2.27 (m, 2H), 1.53 – 1.45 (m, 1H), 1.42 – 1.36 (m, 1H), 1.08 (s, 1H), 0.88 (s, 12H), 0.84 (d, *J* = 6.7 Hz, 3H), 0.03 (s, 6H).

^{13}C NMR (151 MHz, $CDCl_3$) δ 166.95, 147.06, 122.51, 74.69, 51.45, 40.05, 37.16, 25.86, 25.23, 18.12, 13.80, 12.11, -4.30, -4.56.

297':

NMR File Name: AF5-190-3-600

^{1}H NMR (600 MHz, Chloroform-*d*) δ 7.01 (dt, *J* = 15.4, 7.5 Hz, 1H), 5.86 (dt, *J* = 15.6, 1.4 Hz, 1H), 3.75 (s, 3H), 3.67 (s, 1H), 2.34 – 2.27 (m, 2H), 1.50 (s, 1H), 1.44 – 1.40 (m, 1H), 1.16 – 1.04 (m, 1H), 0.90 (s, 12H), 0.89 – 0.83 (m, 3H), 0.05 (d, *J* = 3.2 Hz, 6H).

^{13}C NMR (151 MHz, $CDCl_3$) δ 166.94, 147.51, 122.50, 74.87, 51.42, 40.51, 35.86, 29.73, 25.85, 25.20, 18.10, 14.05, 11.99, -4.43, -4.56.

General Procedure for reduction to allylic alcohol: (5*S/R*,6*S*,*E*)-5-((*tert*-butyldimethylsilyl)oxy)-6-methyloct-2-en-1-ol.

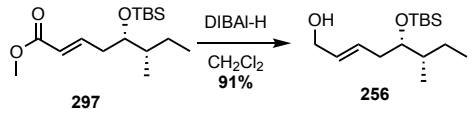

297 256

A FDRBF was charged with Methyl (5*S/R*,6*S*,*E*)-5-((*tert*-butyldimethylsilyl)oxy)-6-methyloct-2-enoate (1 eq.) and dry THF (0.2 M) and cooled to -78 ºC. Freshly diluted DIBAl-H in THF in a 1M solution (2.5 eq.), was then added and allowed to stir o/n warming to rt. The reaction was then cooled to 0 ºC and quenched slowly with Rochelle's salts, and allowed to stir o/n. The resulting solution was then quenched again with 1 M HCl, extracted with EtOAc (3x), dried with Na_2SO_4, and concentrated under reduced pressure. The resulting material was then purified via flash chorography (1:6 EtOAc/hexane) to produce a colorless oil (98.8 mg, 91%).

NMR File Name: AF5-191-A-400

^{1}H NMR (400 MHz, Chloroform-*d*) δ 5.76 – 5.59 (m, 2H), 4.22 – 3.97 (m, 2H), 3.60 (td, *J* = 6.2, 3.5 Hz, 1H), 2.30 – 2.07 (m, 2H), 1.55 – 1.35 (m, 2H), 1.29 – 1.21 (m, 1H), 1.17 – 1.02 (m, 1H), 0.90 (s, 12H), 0.86 (t, *J* = 6.7 Hz, 3H), 0.05 (s, 6H).

^{13}C NMR (151 MHz, $CDCl_3$) δ 130.78, 130.33, 75.33, 63.88, 39.50, 37.13, 25.91, 25.47, 18.17, 13.65, 12.15, -4.11, -4.54.

General Procedure for facially selective cycloropanation: ((1*S*,2*R*)-2-((2*S*,3*S/R*)-2-((*tert*-butyldimethylsilyl)oxy)-3-methylpentyl)cyclopropyl)methanol.

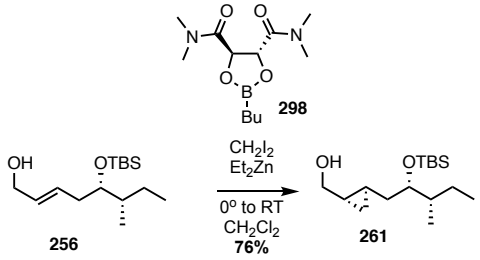

A FDRBF (A) was charged with dry DCM (0.1 M), with MS, and cooled to 0 ºC. A 1M solution in Et_2Zn in THF, (10 eq.) was added and stirred for 15 mins, followed by the addition of CH_2I_2 (20 eq.) in a dropwise manner. To a second FDRBF (B) (5*S/R*,6*S*,*E*)-5-((*tert*-butyldimethylsilyl)oxy)-6-methyloct-2-en-1-ol (1 eq.) was added with dry DCM (0.1M) and MS. A dropwise addition of **298** (4*R*,5*R*)-2-butyl-N^4,N^4,N^5,N^5-tetramethyl-1,3,2-dioxaborolane-4,5-dicarboxamide (1.2 eq.) was added and both RBF were allowed to stir for 15 mins. The contents of flask B were then added to flask A via cannula and allowed to stir o/n. The resulting mixture was quenched with saturated NH_4Cl (until the emulsion broke), extracted with DCM (3x), dried with Na_2SO_4, and concentrated under reduced pressure. The resulting extract was then purified via flash column chromatography (1:6 EtOAc/hexane) to produce a colorless oil (76%).

NMR File Name: AF5-206-B-400

^{1}H NMR (400 MHz, Chloroform-*d*) δ 3.68 – 3.62 (m, 1H), 3.55 (dd, *J* = 11.1, 6.8 Hz, 1H), 3.39 (dd, *J* = 11.1, 7.3 Hz, 1H), 1.59 – 1.50 (m, 2H), 1.45 – 1.40 (m, 1H), 1.40 – 1.32 (m, 1H), 1.32 – 1.26 (m, 2H), 1.15 – 1.03 (m, 1H), 0.91 (d, *J* = 2.2 Hz, 12H), 0.83 (d, *J* = 6.7 Hz, 3H), 0.68 – 0.59 (m, 1H), 0.42 (dt, *J* = 8.7, 4.7 Hz, 1H), 0.36 (dt, *J* = 8.2, 5.0 Hz, 1H), 0.05 (s, 6H).

^{13}C NMR (151 MHz, $CDCl_3$) δ 75.92, 67.19, 39.44, 37.61, 25.93, 25.40, 21.34, 13.99, 13.84, 12.31, 9.93, -4.21, -4.46.

General Procedure for Iodination: *tert*-butyl(((2*S*,3*S/R*)-1-((1*R*,2*S*)-2-(iodomethyl)cyclopropyl)-3-methylpentan-2-yl)oxy)dimethylsilane.

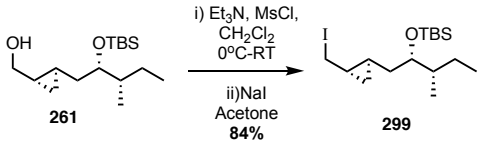

A FDRBF was charged with ((1*S*,2*R*)-2-((2*S*,3*S/R*)-2-((*tert*-butyldimethylsilyl)oxy)-3-methylpentyl)cyclopropyl)methanol (1 eq.) with dry DCM (0.15 M) and 4 A MS. Upon cooling the solution to 0 ºC Et_3N (3 eq.) was added followed by MsCl (1.5 eq.). The resulting solution was stirred for 15 mins, then warmed to rt. The solution was then concentrated under reduced pressure. The yellowish solid was then dissolved in acetone (0.15M) with 4A MS followed by the addition of NaI (9 eq.) in one portion. The solution was stirred for 1 h and then quenched with a 50:50 mixture of saturated $NaCO_3H$ and saturated $Na_2S_2O_3$. The compound was then extracted with Et_2O (3x), dried with Na_2SO_4, and concentrated under reduced pressure. The resulting extract was then purified via flash column chromatography (1:30 EtOAc/hexane) to produce a colorless oil (84%).

299:

NMR File Name: AF5-330-600

^{1}H NMR (600 MHz, Chloroform-*d*) δ 3.70 – 3.58 (m, 1H), 3.27 (dd, 1H), 3.08 (dd, *J* = 9.8, 8.3 Hz, 1H), 1.56 – 1.48 (m, 1H), 1.40 – 1.31 (m, 1H), 1.16 – 1.04 (m, 2H), 0.90 (d, *J* = 3.4 Hz, 14H), 0.82 (d, *J* = 8.4, 6.7 Hz, 3H), 0.76 – 0.74 (m, 1H), 0.65 (dt, *J* = 8.3, 5.2 Hz, 1H), 0.48 (dt, *J* = 9.0, 4.7 Hz, 1H), 0.06 (s, 6H).

^{13}C NMR (151 MHz, $CDCl_3$) δ 75.70, 75.21, 39.60, 37.88, 25.94, 25.24, 23.38, 22.67, 18.13, 17.81, 13.93, 13.80, 12.33, -4.09, -4.44.

299':

NMR File Name: AF3-317-A-400

^{1}H NMR (600 MHz, Chloroform-*d*) δ 3.65 (td, *J* = 6.2, 2.9 Hz, 1H), 3.27 (dd, *J* = 9.7, 7.2 Hz, 1H), 3.09 (dd, *J* = 9.7, 8.4 Hz, 1H), 1.55 – 1.48 (m, 2H), 1.36 – 1.31 (m, 2H), 1.11 – 1.04 (m, 2H), 0.92 – 0.88 (m, 13H), 0.83 (d, *J* = 6.8 Hz, 3H), 0.75 (dq, *J* = 12.1, 6.1 Hz, 1H), 0.65 (dt, *J* = 8.3, 5.2 Hz, 1H), 0.48 (dt, *J* = 9.1, 4.7 Hz, 1H), 0.06 (d, *J* = 0.7 Hz, 6H).

^{13}C NMR (151 MHz, $CDCl_3$) δ 77.25, 77.04, 76.83, 75.70, 39.60, 37.88, 29.73, 25.94, 25.24, 23.38, 22.67, 18.13, 17.82, 13.93, 13.80, 12.33, -4.09, -4.43.

General Procedure for Ring-openeing Reaction: tert-butyl(((3S,4S,6R)-3,6-dimethyloct-7-en-4-yl)oxy)dimethylsilane (Q3/Q4):

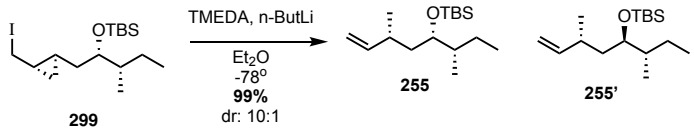

299 **255** **255'**

A FDRBF was charged with (**299**) and cooled to -78 °C with MS. Dropwise addition of TMEDA (2 eq.) followed by dropwise addition to *n*-BuLi (1.2 eq of 1.6 M solution). The reaction was maintained at -78 °C for 1 h and quenched with H_2O. Upon warming to rt, the compound was diluted with NH_4Cl (sat.), extracted with ether (3x), dried over Na_2SO_4 and the solvents were evaporated under ambient temperature. The resulting extract was then purified via flash column chromatography (1:3 heptane/hexane) to produce a colorless oil (99%).

255:

NMR File Name: AF5-257-400

^{1}H NMR (400 MHz, Chloroform-*d*) δ 5.77 – 5.62 (m, 1H), 5.02 – 4.90 (m, 2H), 3.68 – 3.61 (m, 1H), 2.31 – 2.16 (m, 1H), 1.59 – 1.54 (m, 1H), 1.47 – 1.37 (m, 1H), 1.37 – 1.26 (m, 2H), 1.16 – 1.03 (m, 1H), 1.00 (dd, *J* = 6.7, 5.2 Hz, 3H), 0.92 – 0.88 (m, 12H), 0.82 (dd, *J* = 6.8, 3.8 Hz, 3H), 0.06 (d, *J* = 1.6 Hz, 6H).

^{13}C NMR (101 MHz, $CDCl_3$) δ 112.69, 77.34, 77.02, 76.71, 73.75, 40.28, 39.98, 34.31, 25.99, 25.94, 24.42, 21.19, 18.18, 14.12, 12.40, -4.21.

255':

NMR File Name: AF4-184-400

(*R*,*E*)-4-isopropyl-3-(2-methylbut-2-enoyl)oxazolidin-2-one.

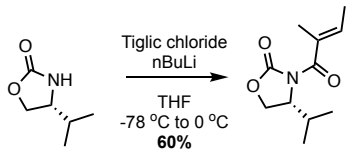

A FDRBF was charged with (*R*)-4-isopropyloxazolidin-2-one (543.8 mg, 4.21 mmol, 1.0 eq.) and dry THF (8.4 mL, 0.5 M) and cooled to -78 ºC. A 1.37 M solution of nBuLi (3.69 mL, 5.05 mmol, 1.2 eq.) was added dropwise and allowed to stir for 20 mins. Freshly distilled tiglic acid (498.6 mg, 4.21 mmol, 1 eq.) was dissolved in dry THF (4.21 mL, 1 M) was cooled to -78 ºC and then was added to the mixture in a dropwise fashion. The solution was allowed to stir for 30 mins then warmed to 0 ºC. The reaction was then quenched with saturated NH_4Cl, extracted with DCM (3x), washed with sat Na_aCO_3H, dried with Na_2SO_4, and concentrated under reduced pressure. The resulting extract was then purified via flash column chromatography (1:3 EtOAc/hexane) to produce the final compound (533.1 mg, 60%).

^{1}H NMR (400 MHz, Chloroform-*d*) δ 6.21 (t, *J* = 7.0, 1.5 Hz, 1H), 4.55 – 4.48 (m, 1H), 4.31 (t, *J* = 8.9 Hz, 1H), 4.17 (dd, *J* = 9.0, 5.5 Hz, 1H), 2.41 – 2.31 (m, 1H), 1.93 – 1.88 (m, 3H), 1.80 (dq, *J* = 6.9, 1.2 Hz, 3H), 0.91 (t, *J* = 6.8 Hz, 6H).

^{1}H NMR (400 MHz, Chloroform-*d*) δ 6.25 – 6.15 (m, 1H), 4.55 – 4.48 (m, 1H), 4.30 (t, *J* = 8.9 Hz, 1H), 4.16 (dd, *J* = 9.0, 5.5 Hz, 1H), 1.90 – 1.87 (m, 3H), 1.79 (dq, *J* = 7.0, 1.1 Hz, 3H), 0.90 (t, *J* = 6.9 Hz, 6H).

General Procedure for TBS-enol ether formation: (*R*,*Z*)-3-(1-((*tert*-butyldimethylsilyl)oxy)-2-methylbuta-1,3-dien-1-yl)-4-isopropyloxazolidin-2-one.

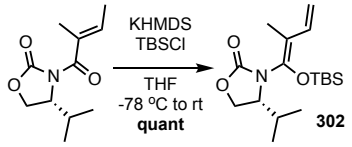

To a FDRBF was added the starting material (1 eq), with dry THF (0.1 M) and the solution was cooled to -78 °C. Following this KHMDS (1.5 eq.) was added dropwise and stirred for 10 mins. After this time, TBSOTf (1.5 eq.) was added and left to stir for 20 mins. At this point the reaction was quenched with NH_4Cl (sat.), extracted with DCM (3x), dried over Na_2SO_4, and and concentrated under reduced pressure. The crude material was used in the next reaction without further purification.

302: AF3-391-400

^{1}H NMR (400 MHz, Chloroform-*d*) δ 6.59 – 6.48 (m, 1H), 5.14 (d, *J* = 17.3 Hz, 1H), 5.03 (dd, *J* = 10.8, 1.4 Hz, 1H), 4.32 (t, *J* = 8.8 Hz, 1H), 4.11 (t, *J* = 7.8 Hz, 1H), 4.01 (s, 1H), 1.96 – 1.90 (m, 1H), 1.60 (s, 1H), 1.27 – 1.24 (m, 3H), 0.98 (s, 9H), 0.94 – 0.89 (m, 5H), 0.20 (s, 6H).

196: AF3-373-400

^{1}H NMR (400 MHz, Chloroform-*d*) δ 6.60 – 6.51 (m, 1H), 5.14 (dd, *J* = 16.8 Hz, 1H), 5.03 (dd, *J* = 10.8, 1.3 Hz, 1H), 4.32 (t, *J* = 8.7 Hz, 1H), 4.11 (t, *J* = 8.5 Hz, 1H), 4.06 – 3.98 (m, 1H), 1.98 – 1.91 (m, 1H), 1.57 (s, 1H), 0.99 (s, 12H), 0.94 – 0.90 (m, 5H), 0.20 (s, 6H).

Synthesis of (2*R*,4*S*,5*S*)-4-((*tert*-butyldimethylsilyl)oxy)-2,5-dimethylheptanal (262):

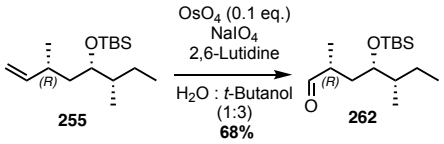

To a RBF was added **255** in a 3:1 mixture of Dioxane:H_2O (0.13 M total).To this was added 2,6-lutidine (1.3 eq.) then OsO_4 (2.5g/100 mL in *t*BuOH, 0.15 eq.) and stirred for 30 mins. At this time, $NaIO_4$ (2.3 eq.) and stirred o/n. The reaction is quenched with $Na_2S_2O_3$ and allowed to stir. The mixture was then extracted with ether, dried over Na_2SO_4 and the solvents were evaporated under ambient temperature. The resulting extract was then purified via flash column chromatography (1:30 EtOAc/hexane) to produce a colorless oil (68%).

262:

NMR File Name: AF5-043-B-400

^{1}H NMR (400 MHz, Chloroform-*d*) δ 9.66 – 9.58 (m, 1H), 3.70 – 3.63 (m, 1H), 2.53 – 2.44 (m, 1H), 1.91 – 1.82 (m, 1H), 1.46 (dddd, *J* = 14.1, 8.6, 7.4, 3.0 Hz, 2H), 1.15 – 1.02 (m, 4H), 0.93 (d, *J* = 1.9 Hz, 1H), 0.91 – 0.89 (m, 12H), 0.88 – 0.82 (m, 3H), 0.08 – 0.04 (m, 6H).

^{13}C NMR (101 MHz, $CDCl_3$) δ 204.93, 77.34, 77.03, 76.71, 73.63, 42.99, 39.94, 34.09, 25.92, 24.22, 14.37, 12.24, -4.32.

Synthesis of (2*R*,4*S*,5*S*)-4-((*tert*-butyldimethylsilyl)oxy)-2,5-dimethylheptan-1-ol (328):

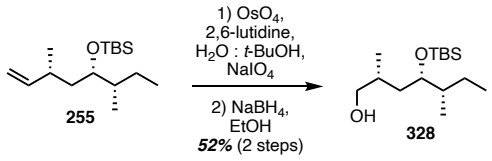

To an RBF was added **255** (1 eq., 91.8 mg, 0.34 mmol) with a 3:1 mixture of dioxane in water (1.5 mL diox: 0.5 mL H_2O, overall 0.13 M soln.) was added 2,6-lutidine (1.3 eq., 0.05 mL, 0.15 mmol) and OsO_4 (as a 2.5 g/100 mL solution) (0.15 eq., 0.51 mL, 0.05 mmol) and the reaction was stirred for 30 mins. At that point $NaIO_4$ (2.3 eq., 166.8 mg, 0.78 mmol) was added and the reaction was left to stir overnight. The reaction is quenched with $Na_2S_2O_3$ and allowed to stir. The mixture was then extracted with ether, dried over Na_2SO_4 and the solvents were evaporated under ambient temperature. The crude material was then cooled to 0 °C and dissolved into EtOH (0.17 M, 2 mL) to which $NaBH_4$ (2.5 eq., 31.8 mg, 0.85 mmol) was added and allowed to stir overnight warming to rt. The reaction was cooled to 0 °C quenched with NH_4Cl (sat.) extracted with CH_2Cl_2 (3x), dried over Na_2SO_4 and the solvents were evaporated under ambient temperature. The resulting extract was then purified via flash column chromatography (1:30 EtOAc/hexane) to produce a colorless oil (52% yield over 2 steps, 48.2 mg)**.**

NMR File Name: AF5-244-B-2

^{1}H NMR (400 MHz, Chloroform-*d*) δ 3.7 – 3.6 (m, 1H), 3.5 – 3.4 (m, 2H), 1.9 – 1.7 (m, 1H), 1.7 – 1.5 (m, 1H), 1.5 – 1.4 (m, 3H), 1.3 – 1.2 (m, 2H), 1.1 (ddt, *J* = 22.1, 9.0, 7.1 Hz, 1H), 1.0 – 0.9 (m, 12H), 0.9 – 0.8 (m, 4H), 0.1 – 0.0 (m, 6H).

^{13}C NMR (101 MHz, $CDCl_3$) δ 77.35, 77.03, 76.71, 74.41, 68.54, 38.85, 38.62, 32.11, 25.96, 25.91, 25.27, 23.89, 18.13, 17.93, 14.38, 11.78, -4.11, -4.52.

(5*R*,7*S*,8*S*)-7-((*tert*-butyldimethylsilyl)oxy)-5,8-dimethyldec-1-en-4-ol (319).

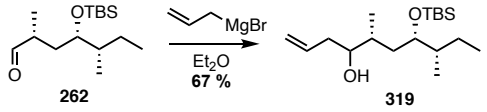

The starting material (**262**, 1 eq.) was added to a FDRBF with ether and cooled to 0 °C. AllylMgBr (2 eq.) was added and the reaction was stirred for 30 mins warming to rt. Upon consumption of the SM, the reaction was quenched with NH_4Cl (sat), extracted with DCM (3x), dried over Na_2SO_4, and the solvents were evaporated. The resulting extract was then purified via flash column chromatography (1:7 EtOAc/hexane) to produce a colorless oil (67%) as a mixture of diastereomers.

262:

NMR File Name: AF5-160-600

^{1}H NMR (600 MHz, Chloroform-*d*) δ 5.94 – 5.81 (m, 1H), 5.20 – 5.10 (m, 2H), 3.74 – 3.62 (m, 1H), 3.58 – 3.43 (m, 1H), 2.24 – 2.10 (m, 1H), 1.72 – 1.60 (m, 2H), 1.52 – 1.39 (m, 2H), 1.35 – 1.23 (m, 2H), 1.20 – 1.10 (m, 1H), 0.94 (dd, *J* = 6.8, 2.2 Hz, 3H), 0.92 – 0.89 (m, 13H), 0.86 – 0.82 (m, 3H), 0.09 – 0.05 (m, 6H).

Synthesis of 1-phenylbut-3-en-1-ol (306)

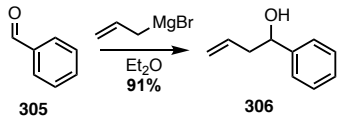

To a FDRBF was added diethyl ether (2 mL, 1 M), magnesium metal (48.6 mg, 2 eq., 2 mmol), then allyl bromide (0.13 mL, 1.5 eq., 1.5 mmol) in diethyl ether (1.5 mL, 1 M) and allowed to stir at rt. After 30 mins benzaldehyde (**305**) (0.10 mL, 1 eq., 1 mmol) was added and the reaction was allowed to stir overnight. The reaction was cooled to 0 ºC and quenched with NH_4Cl (sat), and allowed to warm to rt for 2 h. The product was extracted with diethyl ether (3x), dried over Na_2SO_4, and the solvents were evaporated. The resulting extract was then purified via flash column chromatography (1:9 EtOAc/hexane) to produce a colorless oil (127.6 mg, 91%) as a mixture of enantiomers.

^{1}H NMR (400 MHz, Chloroform-*d*) δ 7.44 – 7.29 (m, 5H), 5.91 – 5.77 (m, 1H), 5.24 – 5.14 (m, 2H), 4.82 – 4.73 (m, 1H), 2.60 – 2.48 (m, 2H), 2.08 (d, *J* = 3.3 Hz, 1H).

Notebook Entry: AF4-405-B

Synthesis of methyl (*E*)-5-((*tert*-butyldimethylsilyl)oxy)-2-methyl-5-phenylpent-2-enoate (318)

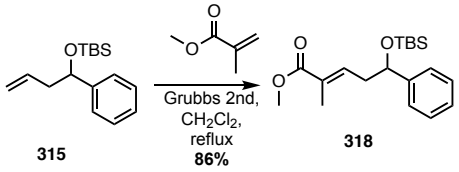

To a FDRBF was added **315** (100 mg, 0.38 mmol, 1 eq.) and dry CH_2Cl_2 (0.04 M, 9.5 mL) with molecular sieves. Methyl methacrylate (**307**) (0.41 mL, 3.8 mmol, 10 eq.) then Grubbs II was added (4 mg, 0.0004 mmol, 0.01 eq.). The reaction was warmed to 43 ^oC in an oil bath and left to stir overnight. The reaction was then allowed to cool to rt and the solvents were evaporated under reduced pressure. The resulting crude material was purified via flash chromatography (1:9 EtOAc/hexane) to produce a colorless oil (109.7 mg, 86%) as a mixture of enantiomers.

^{1}H NMR (400 MHz, Chloroform-*d*) δ 7.3 (d, *J* = 3.9 Hz, 4H), 7.3 – 7.2 (m, 1H), 6.9 (tq, *J* = 7.6, 1.5 Hz, 1H), 4.8 (dd, *J* = 7.6, 4.9 Hz, 1H), 3.7 (s, 3H), 2.6 – 2.5 (m, 2H), 1.8 (d, *J* = 1.3 Hz, 3H), 0.9 (s, 9H), 0.0 (s, 3H), -0.1 (s, 3H).

Reaction Reference/NMR File: AF5-027

Synthesis of 1-phenylbut-3-en-1-one (309)

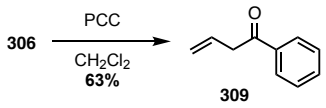

To a vial containing **306** (201.4 mg, 1.36 mmol, 1 eq.) was added dry CH_2Cl_2 (2.7 mL, 0.5 M) then PCC (586.3 mg, 2.72 mmol, 2 eq.) and allowed to stir for 2 h. At that time the reaction was diluted with diethyl ether and allowed to stir. The crude reaction was filtered through celite and the solvents were reduced. The resulting mixture was then purified via flash chromatography (1:9 EtOAc/hexane) to produce a colorless oil (125.9 mg, 63%) as a single enantiomers.

Reaction Reference/NMR: AF5-042

Synthesis of *tert*-butyldimethyl((1-phenylbut-3-en-1-yl)oxy)silane (315)

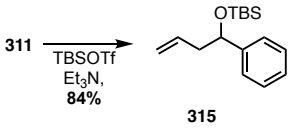

To a FDRF was added **311** (411.6 mg, 2.8 mmol, 1 eq.) in CH_2Cl_2 (0.1 M, 28 mL) and the reaction was cooled to 0 °C. At that time, Et_3N (1.56 mL, 11.2 mmol, 4 eq.) was added, followed by TBSoTf (1.29 mL, 5.6 mmol, 2 eq.) and allowed to stir overnight. The reaction was quenched with NH_4Cl (sat), extracted with CH_2Cl_2 (3x), dried over Na_2SO_4, and the solvents were evaporated. The resulting extract was then purified via flash column chromatography (1:9 EtOAc/hexane) to produce a colorless oil (620.4 mg, 84%) as a mixture of enantiomer.

^{1}H NMR (400 MHz, Chloroform-*d*) δ 7.37 – 7.28 (m, 5H), 7.27 – 7.22 (m, 1H), 5.87 – 5.74 (m, 1H), 5.07 – 5.00 (m, 2H), 4.70 (dd, *J* = 7.3, 5.2 Hz, 1H), 2.52 – 2.34 (m, 2H), 1.14 – 1.03 (m, 1H), 0.90 (d, *J* = 5.4 Hz, 13H).

Reaction Reference/NMR: AF5-296-400

Synthesis of 1-methoxy-4-(((1-phenylbut-3-en-1-yl)oxy)methyl)benzene (311)

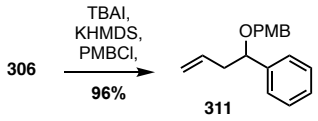

To a FDRBF was added **306** (127.6 mg, 0.86 mmol, 1 eq.) with dry THF (4.3 mL, 0.2 M) and cooled to 0 ºC. To the solution was added TBAI (15.9 mg, 0.043 mmol, 0.05 eq.) then KHMDS (0.5 M soln. in toluene, 3.44 mL, 1.72 mmol, 2.0 eq.) and allowed to stir for 30 mins. Next PMBCl (0.19 mL, 1.38 mmol, 1.6 eq.) and allowed to stir overnight warming to rt. The reaction was quenched with NH_4Cl (sat), extracted with EtOAc (3x), dried over Na_2SO_4, and the solvents were evaporated. The resulting extract was then purified via flash column chromatography (1:9 EtOAc/hexane) to produce a colorless oil (127.6 mg, 91%) as a mixture of enantiomers.

^{1}H NMR (400 MHz, Chloroform-*d*) δ 7.43 – 7.32 (m, 5H), 7.28 – 7.22 (m, 2H), 6.93 – 6.87 (m, 2H), 5.86 – 5.74 (m, 1H), 5.09 – 5.00 (m, 2H), 4.43 (d, *J* = 11.5 Hz, 1H), 4.37 (dd, *J* = 7.7, 5.9 Hz, 1H), 4.23 (d, *J* = 11.5 Hz, 1H), 3.84 (d, *J* = 3.3 Hz, 3H), 2.68 – 2.60 (m, 1H), 2.49 – 2.40 (m, 1H).

Notebook Entry/NMR: AF4-411-A-400

Synthesis of (*E*)-1,6-bis((4-methoxybenzyl)oxy)-1,6-diphenylhex-3-ene (312)

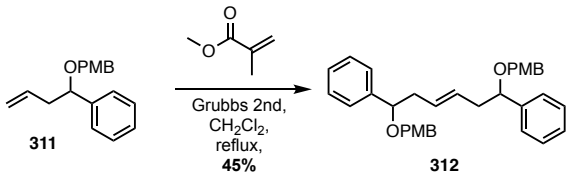

To a FDRBF was added **311** (221.3 mg, 0.82 mmol, 1 eq.) with dry CH_2Cl_2 (20.5 mL, 0.04 M) followed by Grubbs II (6.8 mg, 0.0082 mmol, 0.01 eq.) then methyl methacrylate (**307**) (0.9 mL, 8.25 mmol, 10 eq.) and the reaction was heated to 45 ºC in an oil bath and left to stir overnight. The reaction was then cooled to rt and the solvents were removed under reduced pressure. The resulting mixture was purified via flash column chromatography (1:9 EtOAc/hexane) to produce a colorless oil (125.9 mg, 45%).

^{1}H NMR (400 MHz, Chloroform-*d*) δ 7.4 – 7.2 (m, 10H), 6.9 – 6.8 (m, 2H), 5.4 – 5.3 (m, 1H), 4.5 – 4.3 (m, 2H), 4.3 – 4.1 (m, 2H), 2.6 – 2.5 (m, 1H), 2.4 – 2.3 (m, 1H).

Reaction Reference/NMR: AF5-013

Reaction Note: Addition of Grubbs II before MMA leads to homodimer formation.

Synthesis of methyl (*E*)-5-((4-methoxybenzyl)oxy)-5-phenylpent-2-enoate (314)

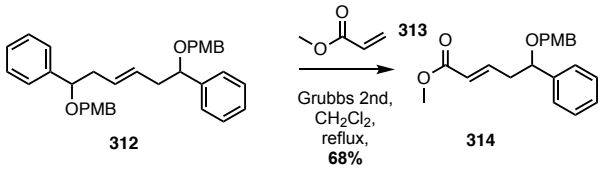

Cross-metathesis conditons as previous described produced **314** as a colorless oil in 55.1 mg 68% yield.

^{1}H NMR (400 MHz, Chloroform-*d*) δ 7.4 – 7.3 (m, 6H), 7.3 – 7.2 (m, 2H), 7.0 (dt, *J* = 15.7, 7.2 Hz, 1H), 6.9 – 6.9 (m, 2H), 5.8 (dt, *J* = 15.7, 1.5 Hz, 1H), 4.5 – 4.4 (m, 2H), 4.3 – 4.2 (m, 1H), 3.8 (s, 3H), 3.7 (d, *J* = 2.5 Hz, 3H), 2.8 – 2.7 (m, 1H), 2.6 (dddd, *J* = 14.6, 7.0, 5.3, 1.5 Hz, 1H).

Reaction Reference/NMR: AF5-018

Synthesis of (*E*)-5-((*tert*-butyldimethylsilyl)oxy)-2-methyl-5-phenylpent-2-enal (317)

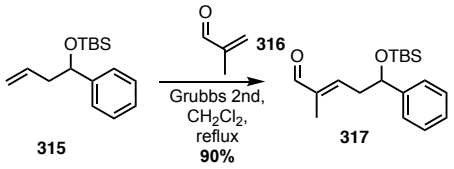

Analogous CM conditions were used to produce 317 as a colorless oil in 90% yield 122.9 mg.

^{1}H NMR (400 MHz, Chloroform-*d*) δ 9.4 (s, 1H), 7.4 – 7.3 (m, 4H), 7.3 – 7.3 (m, 1H), 6.6 (tq, *J* = 7.4, 1.4 Hz, 1H), 4.9 (dd, *J* = 7.1, 4.9 Hz, 1H), 2.8 – 2.7 (m, 2H), 1.7 (q, *J* = 1.0 Hz, 3H), 1.3 (s, 1H), 0.9 (s, 9H), 0.1 (s, 3H), -0.1 (s, 3H).

Reaction Reference/NMR: AF5-059

(5*R*,7*S*,8*S*)-7-((*tert*-butyldimethylsilyl)oxy)-5,8-dimethyldec-1-en-4-one (320):

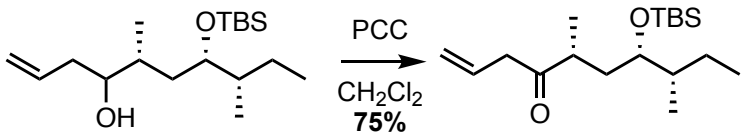

319 **320**

Standard PCC oxidation conditions as described above resulted in a colorless oil which was resulted in crude material in 75% yield.

^{1}H NMR (600 MHz, Chloroform-*d*) δ 5.99 – 5.90 (m, 1H), 5.23 – 5.11 (m, 2H), 3.61 – 3.53 (m, 1H), 3.31 – 3.18 (m, 2H), 2.74 – 2.59 (m, 1H), 1.91 – 1.71 (m, 1H), 1.58 – 1.52 (m, 1H), 1.46 – 1.38 (m, 1H), 1.32 – 1.25 (m, 1H), 1.10 (d, 3H), 0.93 – 0.88 (m, 13H), 0.86 (dd, *J* = 11.9, 5.1 Hz, 3H), 0.10 – 0.01 (m, 6H).

NMR File Name/NMR: AF4-430-600

***tert*-butyl(((3*S*,4*S*,6*R*)-7-((4-methoxybenzyl)oxy)-3,6-dimethyldec-9-en-4-yl)oxy)dimethylsilane (322):**

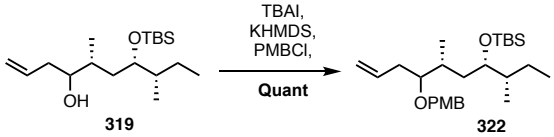

To a FDRB was added **319** (1 eq.) and charged with dry THF (0.2 M). TBAI (0.05 eq.) was added followed by dropwise addition of KHMDS (2.0 eq.), and PMBCl (1.6 eq.) and left to stir o/n. After this time, the reaction was quenched with *n*-Butyamine, extracted with ether (3x), dried over Na_2SO_4, and the solvents were evaporated. The resulting extract was then purified via flash column chromatography (1:9 EtOAc/hexane) to produce a colorless oil (in quantitative yields) as a mixture of diastereomers.

NMR File Name/NMR: AF5-162-B-600

^{1}H NMR (600 MHz, Chloroform-*d*) δ 7.17 – 7.05 (m, 1H), 6.92 – 6.81 (m, 3H), 5.99 – 5.76 (m, 1H), 5.18 – 5.01 (m, 2H), 4.55 – 4.40 (m, 2H), 3.86 – 3.80 (m, 3H), 3.40 – 3.18 (m, 1H), 2.40 – 2.22 (m, 2H), 1.76 – 1.62 (m, 1H), 1.48 – 1.41 (m, 1H), 1.38 – 1.34 (m, 1H), 1.28 (s, 3H), 1.20 – 1.14 (m, 1H), 0.93 (t, 3H), 0.92 – 0.89 (m, 12H), 0.81 (d, J = 6.9 Hz, 3H), 0.07 – 0.03 (m, 6H).

Synthesis of Methyl (6*R*,8*S*,9*S*,*E*)-8-((*tert*-butyldimethylsilyl)oxy)-5-((4-methoxybenzyl)oxy)-2,6,9-trimethylundec-2-enoate (323):

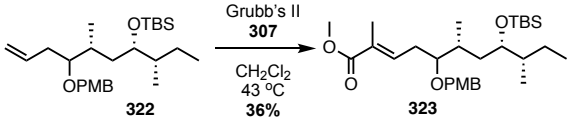

The starting material (**322**, 1 eq.) was added to a FDRBF with dry DCM (0.04 M). Compound **307** (10 eq.) was added then the Grubbs second generation catalyst (0.1 eq.). The mixture was heated to 43 ºC and allowed to reflux o/n. After this time, the reaction solvents were reduced under low pressure and he resulting extract was then purified via flash column chromatography (1:10 EtOAc/hexane) to produce a colorless oil (36%) as a mixture of diastereomers.

NMR File Name/NMR: AF5-120-B-2-400

^{1}H NMR (600 MHz, Chloroform-*d*) δ 7.17 – 7.05 (m, 1H), 6.92 – 6.81 (m, 3H), 5.99 – 5.76 (m, 1H), 5.18 – 5.01 (m, 2H), 4.55 – 4.40 (m, 2H), 3.86 – 3.80 (m, 3H), 3.40 – 3.18 (m, 1H), 2.40 – 2.22 (m, 2H), 1.76 – 1.62 (m, 1H), 1.48 – 1.41 (m, 1H), 1.38 – 1.34 (m, 1H), 1.28 (s, 3H), 1.20 – 1.14 (m, 1H), 0.93 (t, 3H), 0.92 – 0.89 (m, 12H), 0.81 (d, *J* = 6.9 Hz, 3H), 0.07 – 0.03 (m, 6H).

General Procedure for diastereoselective allylation: methyl (5*S*,6*R*,8*S*,9*S*,*E*)-8-((*tert*-butyldimethylsilyl)oxy)-5-((4-methoxybenzyl)oxy)-2,6,9-trimethylundec-2-enoate (329):

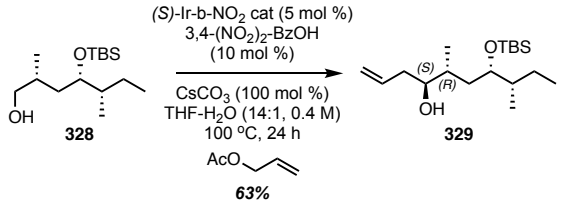

To a flame dried pressure tube was added the SM (1 eq.) in dry THF (0.4 M), 3,4-$(NO_2)_2$-BzOH (0.1 eq.), $CsCO_3$ (1 eq.), allyl acetate (2 eq.), and water (10 eq.). The reaction tube was sealed and heated to 100 °C and left to stir o/n. The solvents of the crude reaction were then reduced and then purified via flash column chromatography (1:9 EtOAc/hexane) to produce a colorless oil (63%).

NMR File Name/NMR: AF5-285-2-400

^{1}H NMR (400 MHz, Chloroform-*d*) δ 5.97 – 5.79 (m, 1H), 5.25 – 5.10 (m, 2H), 3.71 (td, 1H), 3.47 (q, 1H), 2.40 – 2.23 (m, 1H), 2.19 – 2.07 (m, 2H), 1.73 – 1.61 (m, 2H), 1.51 – 1.44 (m, 1H), 1.36 – 1.21 (m, 3H), 1.15 (ddd, *J* = 11.9, 7.3, 3.6 Hz, 1H), 0.96 – 0.87 (m, 15H), 0.87 – 0.78 (m, 3H), 0.07 (d, *J* = 6.3 Hz, 6H).

^{13}C NMR (101 MHz, $CDCl_3$) δ 135.0, 118.0, 74.71, 73.63, 38.56, 36.90, 35.13, 25.94, 16.31, 13.34, 11.5, -0.45, -0.47.

Synthesis of *tert*-butyl(((3*S*,4*S*,6*R*,7*S*)-7-((4-methoxybenzyl)oxy)-3,6-dimethyldec-9-en-4-yl)oxy)dimethylsilane (330):

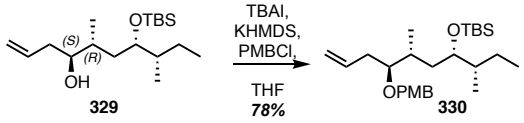

Standard PMB protection conditions were used to afford a colorless oil in 78% yield.

NMR File Name/NMR: AF5-288-A-400

^{1}H NMR (400 MHz, Chloroform-*d*) δ 7.33 – 7.20 (m, 2H), 6.89 (d, *J* = 8.6 Hz, 2H), 5.98 – 5.78 (m, 1H), 5.16 – 5.01 (m, 2H), 4.56 – 4.41 (m, 2H), 3.83 (s, 3H), 3.71 (ddd, *J* = 8.0, 5.4, 2.2 Hz, 1H), 3.25 (dt, *J* = 6.6, 5.1 Hz, 1H), 2.28 (ddd, *J* = 8.1, 6.1, 2.0 Hz, 2H), 1.78 – 1.71 (m, 1H), 1.69 – 1.62 (m, 1H), 1.49 – 1.42 (m, 1H), 1.35 (dd, *J* = 10.0, 4.4 Hz, 1H), 1.23 – 1.13 (m, 2H), 0.94 – 0.86 (m, 15H), 0.81 (t, *J* = 6.8, 5.0 Hz, 3H), 0.05 (d, 6H).

NMR File Name/NMR: AF5-288-A-MeOD-600

^{1}H NMR (600 MHz, Methanol-d_4) δ 7.33 – 7.21 (m, 2H), 6.90 (d, *J* = 8.6 Hz, 2H), 5.93 – 5.82 (m, 1H), 5.15 – 5.00 (m, 2H), 4.57 – 4.39 (m, 2H), 3.80 (s, 3H), 3.78 – 3.68 (m, 1H), 3.28 (dt, *J* = 6.6, 4.9 Hz, 1H), 2.35 – 2.24 (m, 2H), 1.75 – 1.66 (m, 2H), 1.52 – 1.43 (m, 1H), 1.37 (q, *J* = 7.2 Hz, 1H), 1.22 – 1.14 (m, 2H), 0.94 – 0.89 (m, 15H), 0.82 (d, 3H), 0.07 (d, 6H).

^{13}C NMR (151 MHz, MeOD) δ 159.35, 135.45, 130.71, 129.29, 129.18, 115.63, 113.23, 82.99, 73.32, 71.16, 54.24, 38.43, 36.75, 34.52, 32.58, 25.86, 25.05, 17.62, 15.00, 11.93, 11.25.

Synthesis of Methyl (5*S*,6*R*,8*S*,9*S*,*E*)-8-((*tert*-butyldimethylsilyl)oxy)-5-((4-methoxybenzyl)oxy)-2,6,9-trimethylundec-2-enoate (331):

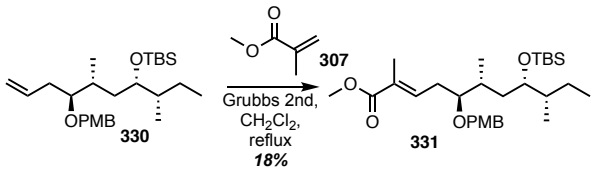

The previously described CM conditions were used to provide colorless oil in 18% yield.

NMR File Name/NMR: AF5-294-600

^{1}H NMR (400 MHz, Chloroform-*d*) δ 7.33 – 7.20 (m, 2H), 6.89 (d, *J* = 8.6 Hz, 2H), 5.98 – 5.78 (m, 1H), 5.16 – 5.01 (m, 2H), 4.56 – 4.41 (m, 2H), 3.83 (s, 3H), 3.71 (ddd, *J* = 8.0, 5.4, 2.2 Hz, 1H), 3.25 (dt, *J* = 6.6, 5.1 Hz, 1H), 2.28 (ddd, *J* = 8.1, 6.1, 2.0 Hz, 2H), 1.78 – 1.71 (m, 1H), 1.69 – 1.62 (m, 1H), 1.49 – 1.42 (m, 1H), 1.35 (dd, *J* = 10.0, 4.4 Hz, 1H), 1.23 – 1.13 (m, 2H), 0.94 – 0.86 (m, 15H), 0.81 (t, *J* = 6.8, 5.0 Hz, 3H), 0.05 (d, 6H).

^{13}C NMR (151 MHz, $CDCl_3$) δ 129.33, 113.72, 71.39, 55.30, 38.58, 32.84, 25.94, 15.52, 12.33.

EXTRA REACTIONS NOT SHOWN IN TEXT:

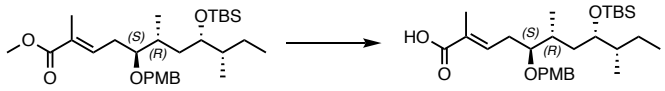

NMR File Name/NMR: AF5-155-crude-600

^{1}H NMR (600 MHz, Chloroform-*d*) δ 7.3 – 7.2 (m, 2H), 7.0 – 7.0 (m, 1H), 6.9 – 6.9 (m, 2H), 4.5 – 4.4 (m, 2H), 3.8 (d, *J* = 3.9 Hz, 3H), 3.8 – 3.7 (m, 1H), 3.4 – 3.3 (m, 1H), 2.4 – 2.3 (m, 2H), 1.9 – 1.8 (m, 3H), 1.8 – 1.7 (m, 2H), 1.5 – 1.4 (m, 2H), 1.4 – 1.3 (m, 1H), 1.2 – 1.2 (m, 2H), 1.0 – 0.9 (m, 3H), 0.9 – 0.9 (m, 12H), 0.8 – 0.8 (m, 3H), 0.1 (d, *J* = 2.4 Hz, 6H).

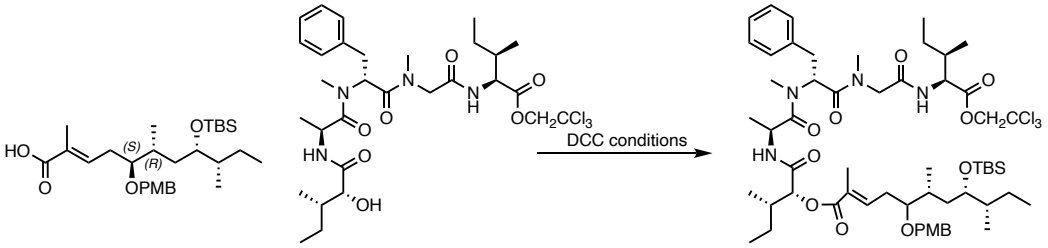

^{1}H NMR (600 MHz, Chloroform-*d*) δ 7.3 – 7.1 (m, 9H), 7.1 – 6.9 (m, 1H), 6.9 – 6.8 (m, 2H), 6.5 (d, *J* = 8.7 Hz, 1H), 5.6 (t, *J* = 7.6 Hz, 1H), 5.3 – 5.2 (m, 1H), 4.9 (d, *J* = 12.0 Hz, 1H), 4.8 (p, *J* = 6.9, 5.8 Hz, 1H), 4.7 (dd, *J* = 8.8, 4.6 Hz, 1H), 4.6 (d, *J* = 11.9 Hz, 1H), 4.5 (pd, *J* = 10.9, 6.5 Hz, 2H), 4.3 (dd, *J* = 15.3, 3.6 Hz, 1H), 3.8 (d, *J* = 4.4 Hz, 3H), 3.7 (dt, *J* = 10.7, 4.0 Hz, 2H), 3.4 – 3.4 (m, 1H), 3.3 – 3.2 (m, 1H), 3.1 (s, 3H), 2.9 – 2.9 (m, 3H), 2.4 (q, *J* = 9.7, 8.6 Hz, 1H), 2.1 – 2.1 (m, 2H), 2.0 (ddq, *J* = 9.6, 4.9, 2.5 Hz, 2H), 1.9 (d, *J* = 6.3 Hz, 3H), 1.8 – 1.7 (m, 2H), 1.7 – 1.6 (m, 3H), 1.5 (dq, *J* = 16.5, 7.2, 6.0 Hz, 2H), 1.4 – 1.3 (m, 3H), 1.3 (s, 6H), 1.2 – 1.2 (m, 2H), 1.0 – 0.9 (m, 12H), 0.9 (t, *J* = 3.5 Hz, 9H), 0.8 (dd, *J* = 16.1, 6.7 Hz, 3H), 0.1 (d, *J* = 8.0 Hz, 6H)

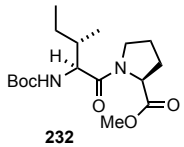

232

^{1}H-NMR

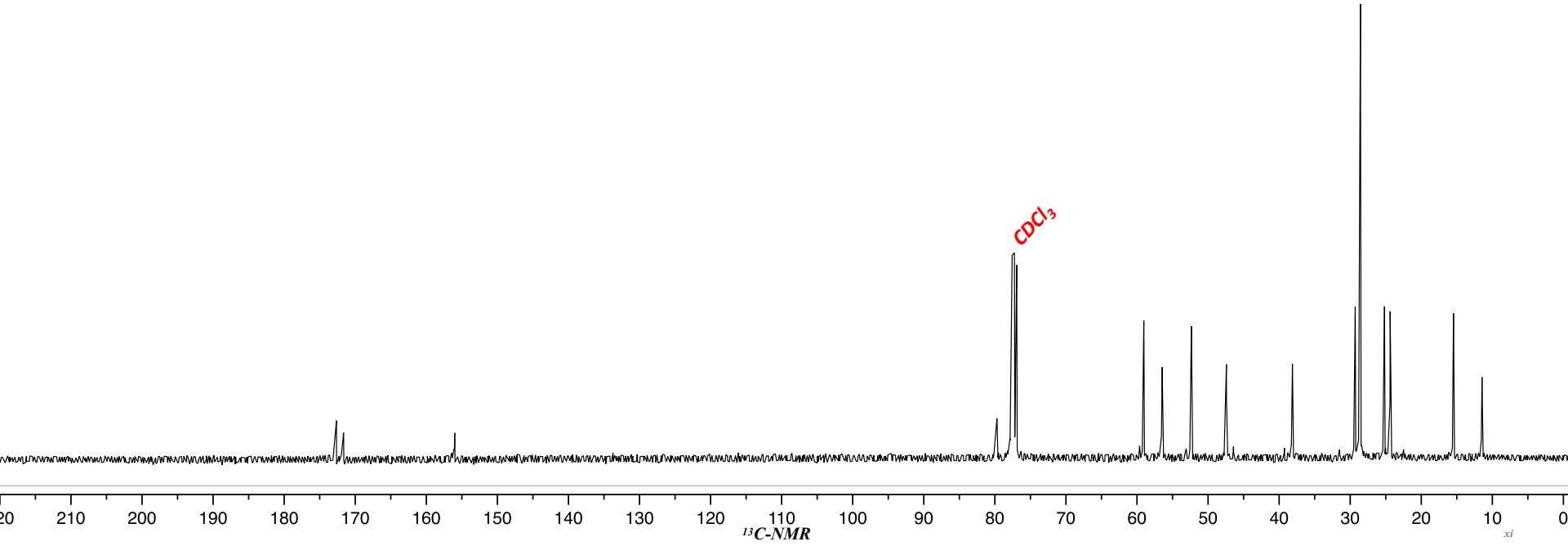

^{13}C-NMR

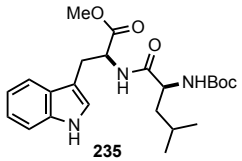

235

^{1}H-NMR

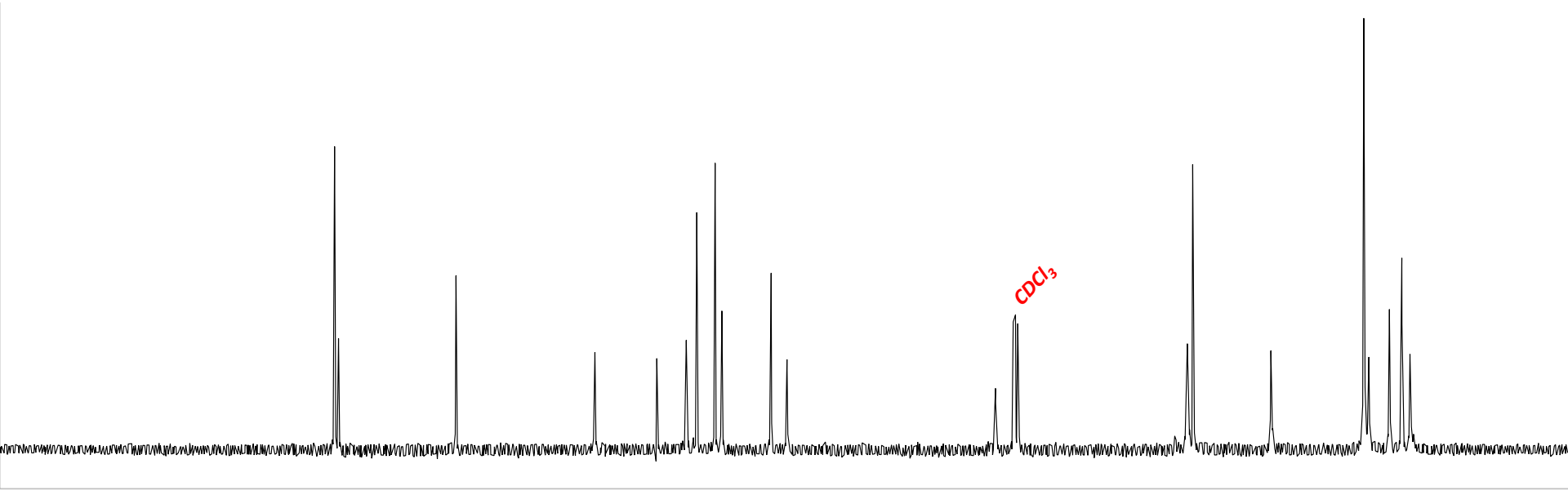

^{13}C-NMR

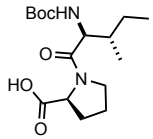

236

CRUDE NMR

^{1}H-NMR

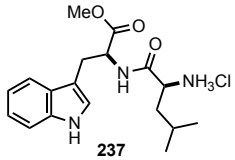

237

CRUDE NMR

^{1}H-NMR

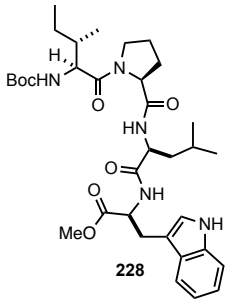
BocHN
H
N
O
O
HN
O
NH
O
MeO
NH

228

CDCl3
0.92
1.00
1.04
1.25
1.19
1.06
1.05
1.03
1.01
1.09
1.19
1.32
1.06
2.94
1.17
2.08
3.93
6.02
9.16
1.26
3.18
9.06
0.0
9.5
9.0
8.5
8.0
7.5
7.0
6.5
6.0
5.5
5.0
4.5
4.0
3.5
3.0
2.5
2.0
1.5
1.0
0.5
0.0
1H-NMR

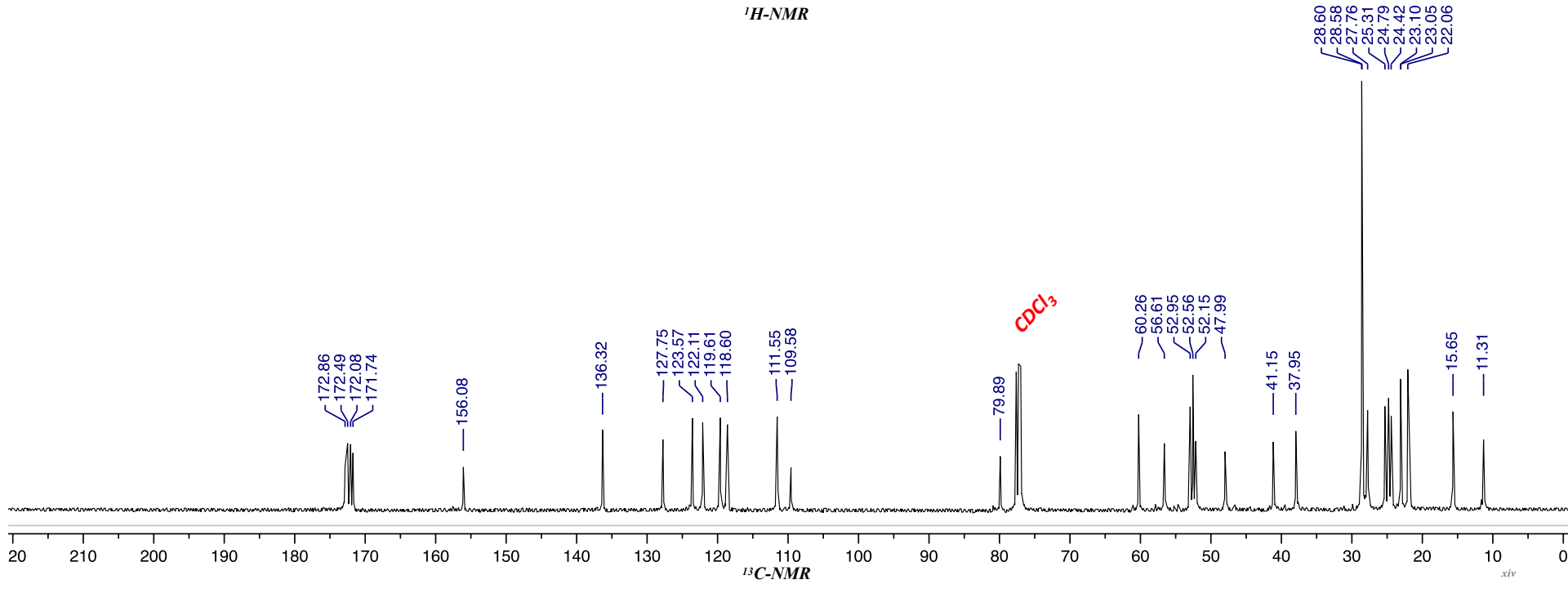
28.60
28.58
27.76
25.31
24.79
24.42
23.10
23.05
22.06
172.86
172.49
172.08
171.74
156.08
136.32
127.75
123.57
122.11
119.61
118.60
111.55
109.58
79.89
CDCl3
60.26
56.61
52.95
52.56
52.15
47.99
41.15
37.95
15.65
11.31
20
210
200
190
180
170
160
150
140
130
120
110
100
90
80
70
60
50
40
30
20
10
0
13C-NMR

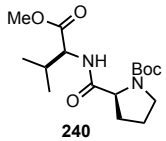

240

^{1}H-NMR

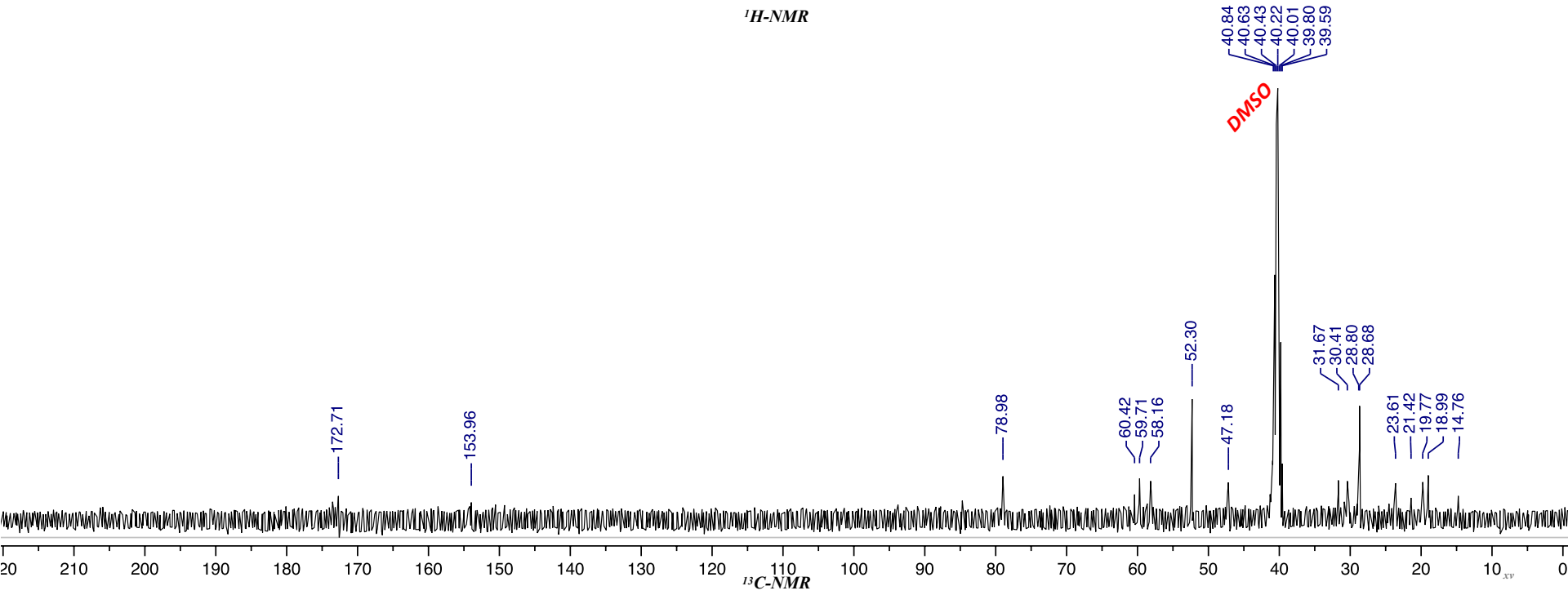

^{13}C-NMR

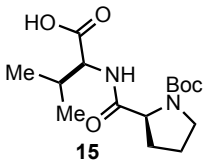

15

CRUDE NMR

$CDCl_3$

0.98 0.46 0.38 1.09 1.10 2.16 2.98 2.08 9.15 6.00

^{1}H-NMR

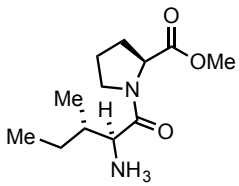

16

CRUDE NMR

$CDCl_3$

3.00 1.27 1.03 1.20 3.00 1.26 1.30 4.03 1.25 1.30 3.00 3.13

^{1}H-NMR

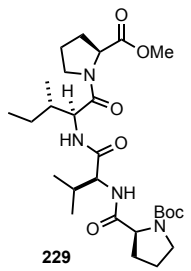
O
OMe
N
H
O
HN
O
NH
Boc
O
N

229

CDCl3
0.68
1.07
0.63
1.00
0.87
0.77
1.17
1.12
2.71
1.13
2.17
0.85
2.22
8.09
8.97
2.86
8.81
9.5
9.0
8.5
8.0
7.5
7.0
6.5
6.0
5.5
5.0
4.5
4.0
3.5
3.0
2.5
2.0
1.5
1.0
0.5

^{1}H-NMR

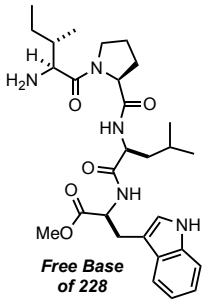

Free Base of 228

CRUDE NMR

$CDCl_3$

2.33 0.99 1.00 1.08 1.75 0.82 0.78 3.74 2.01 0.97 2.29 5.44 1.86 2.40 7.22 2.69 21.67

0.0 9.5 9.0 8.5 8.0 7.5 7.0 6.5 6.0 5.5 5.0 4.5 4.0 3.5 3.0 2.5 2.0 1.5 1.0 0.5 0.0

^{1}H-NMR

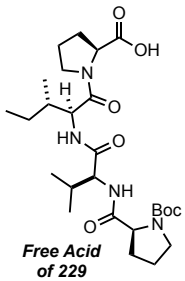

Free Acid of 229

CRUDE NMR

$CDCl_3$

1.51 1.33 3.61 1.46 2.14 2.38 6.61 4.64 9.00 12.29

0.0 9.5 9.0 8.5 8.0 7.5 7.0 6.5 6.0 5.5 5.0 4.5 4.0 3.5 3.0 2.5 2.0 1.5 1.0 0.5 0.0

^{1}H-NMR

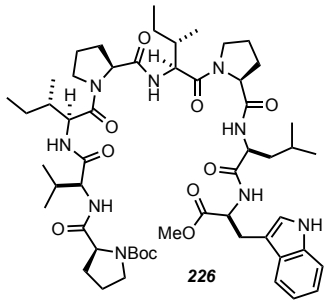

^{1}H-NMR

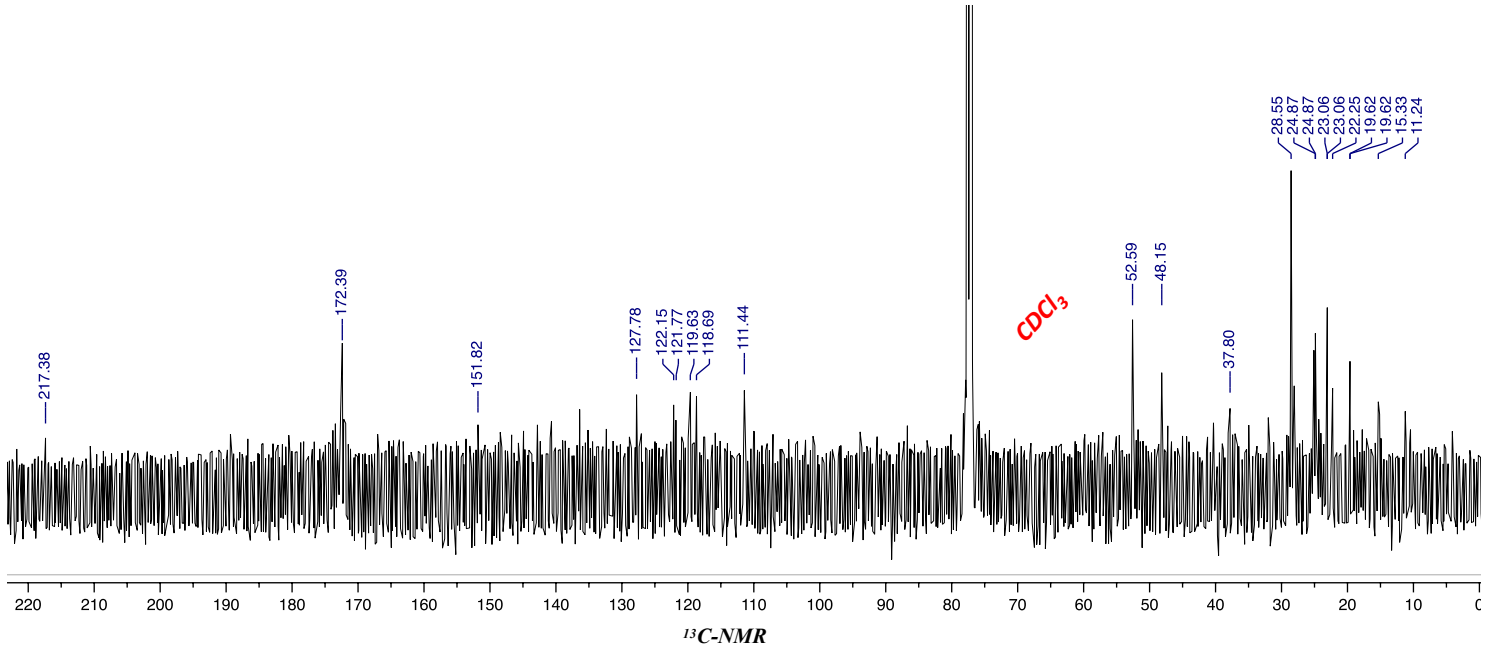

^{13}C-NMR

ixx

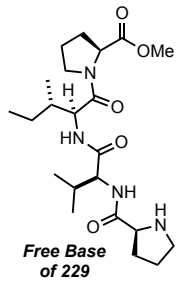

Free Base of 229

CRUDE NMR

$CDCl_3$

1.01 0.99 1.06 1.00 1.22 1.00 2.21 2.03 3.29 1.49 2.70 1.34 4.56 9.50 1.46 1.59 13.06

^{1}H-NMR

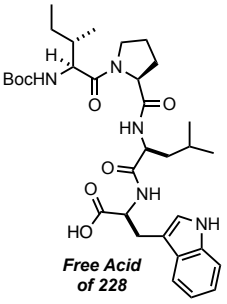

Free Acid of 228

CRUDE NMR

$CDCl_3$

1.04 0.90 1.00 3.36 0.81 0.80 2.44 1.72 0.98 1.76 3.64 8.89 12.07

^{1}H-NMR

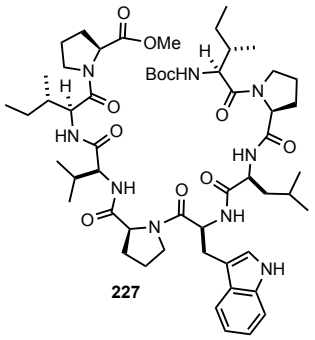
OMe
BocHN
HN
NH
NH
HN
NH
NH

227

CDCl3
1.00
1.07
4.42
6.49
1.05
0.82
10.02
2.93
2.86
3.11
1.22
15.50
9.67
8.86
24.41
0.0
9.5
9.0
8.5
8.0
7.5
7.0
6.5
6.0
5.5
5.0
4.5
4.0
3.5
3.0
2.5
2.0
1.5
1.0
0.5
0.
1H-NMR

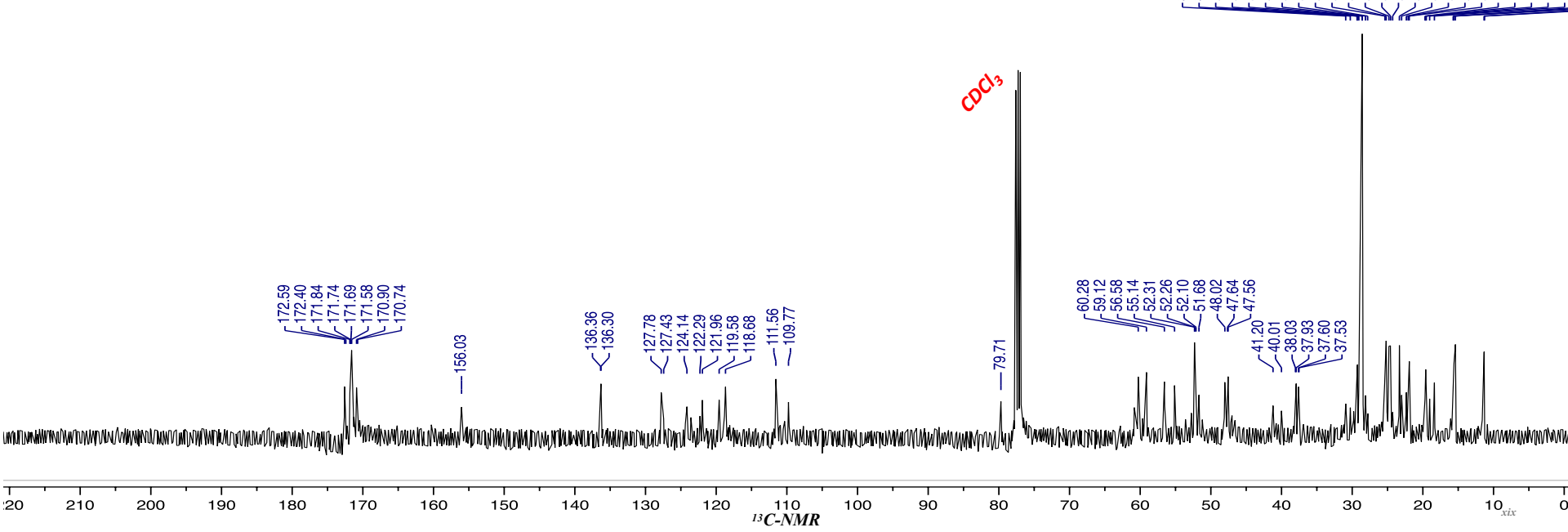
30.92
30.27
29.31
29.26
29.06
28.58
28.57
28.12
27.81
25.36
25.19
24.80
24.56
24.28
23.32
23.01
22.34
22.08
21.93
19.70
19.60
19.52
19.04
18.37
CDCl3
172.59
172.40
171.84
171.74
171.69
171.58
170.90
170.74
156.03
136.36
136.30
127.78
127.43
124.14
122.29
121.96
119.58
118.68
111.56
109.77
79.71
60.28
59.12
56.58
55.14
52.31
52.26
52.10
51.68
48.02
47.64
47.56
41.20
40.01
38.03
37.93
37.60
37.53
220
210
200
190
180
170
160
150
140
130
120
110
100
90
80
70
60
50
40
30
20
10
0
13C-NMR

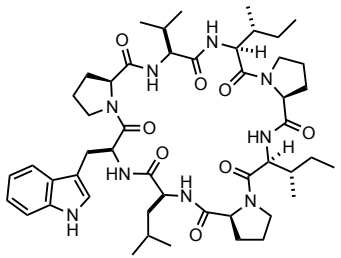

Reniochalistatin E (23)

^{1}H-NMR

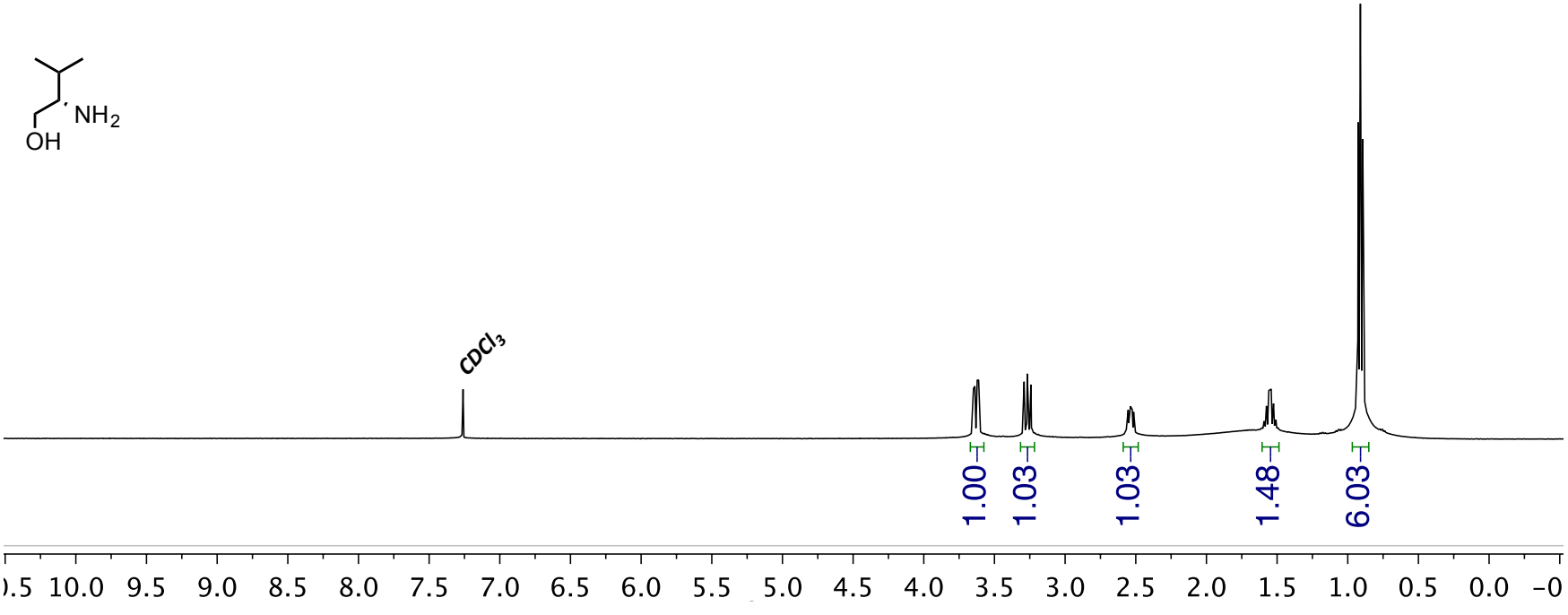
NH2
OH
CDCl3
1.00
1.03
1.03
1.48
6.03
10.0 9.5 9.0 8.5 8.0 7.5 7.0 6.5 6.0 5.5 5.0 4.5 4.0 3.5 3.0 2.5 2.0 1.5 1.0 0.5 0.0

^{1}H-NMR

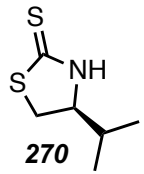

270

^{1}H-NMR

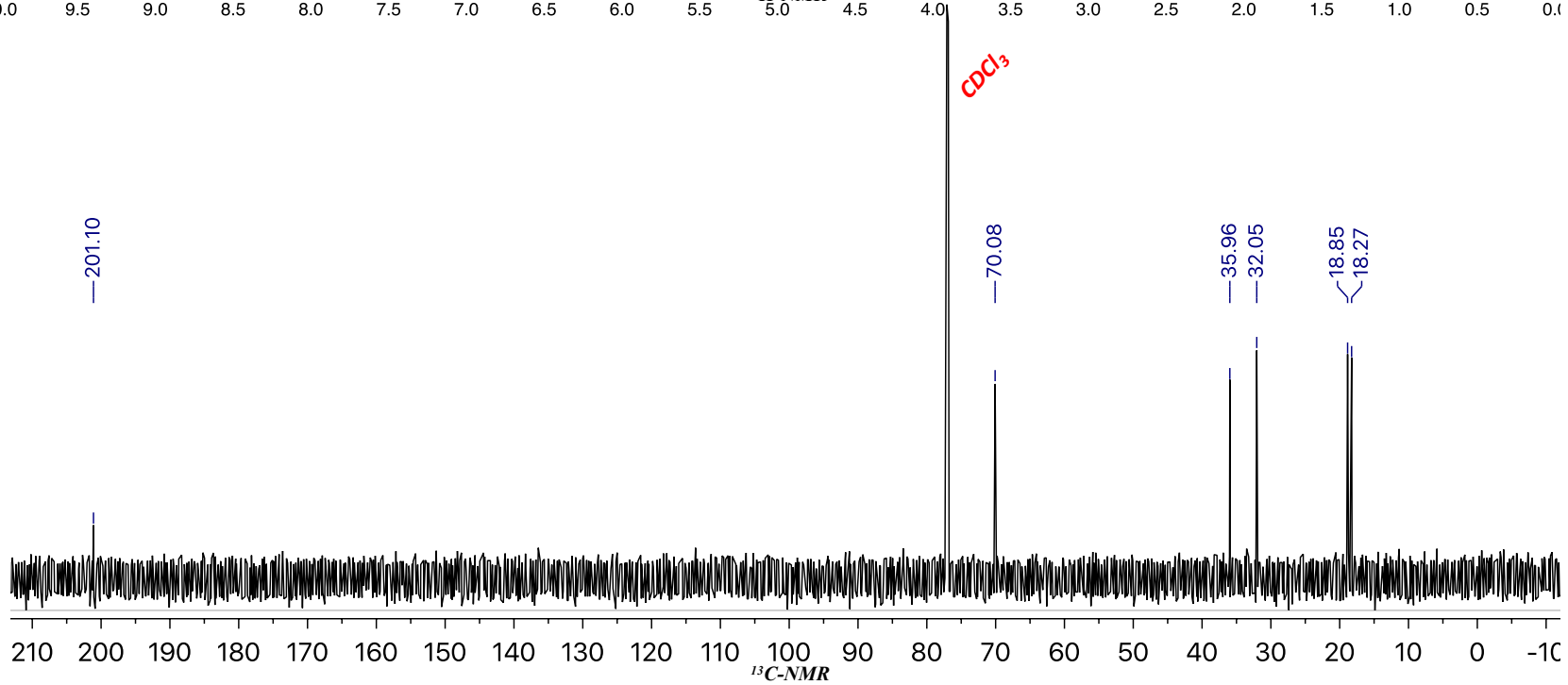

^{13}C-NMR

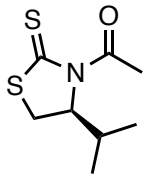

271

^{1}H-NMR

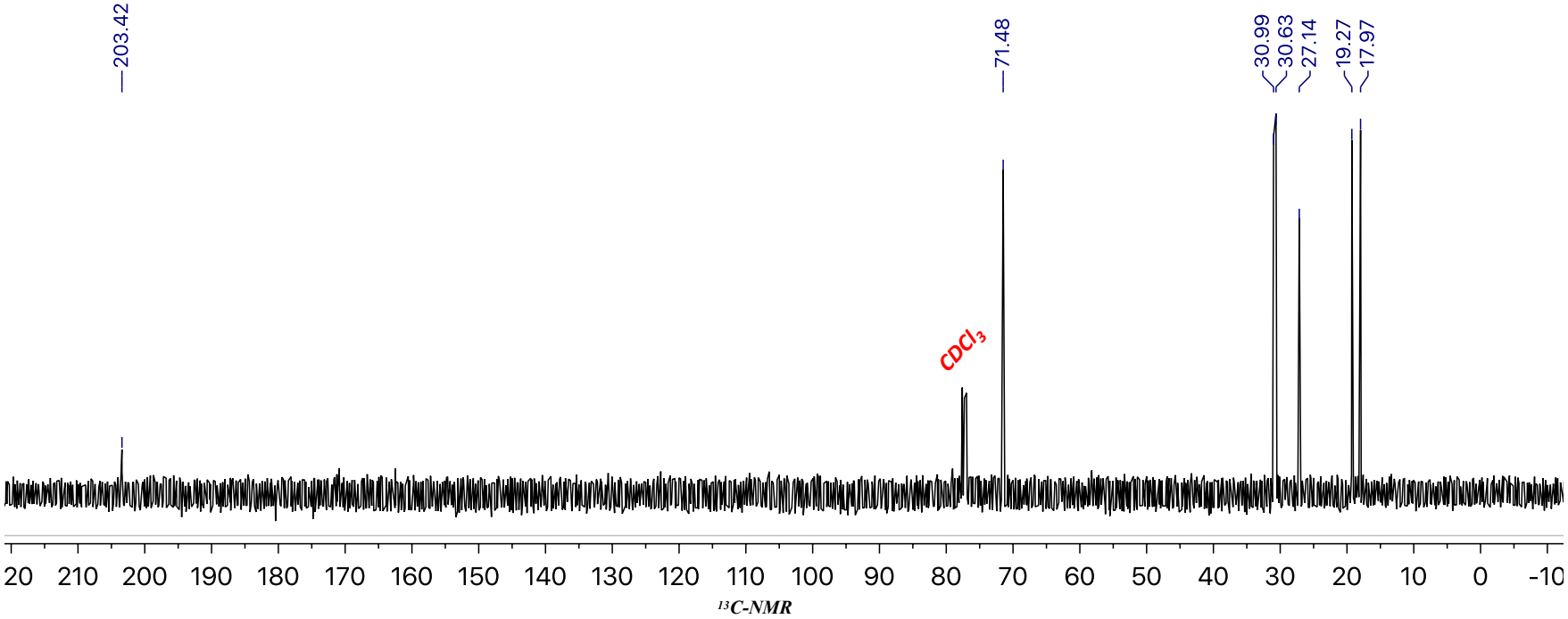

^{13}C-NMR

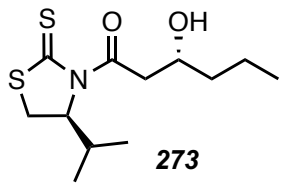
S
O
OH
S
N

273

CDCl3
0.84
1.00
2.11
0.61
0.99
0.89
4.01
2.80
2.98
2.57
0.0
9.5
9.0
8.5
8.0
7.5
7.0
6.5
6.0
5.5
5.0
4.5
4.0
3.5
3.0
2.5
2.0
1.5
1.0
0.5
0.0
1H-NMR

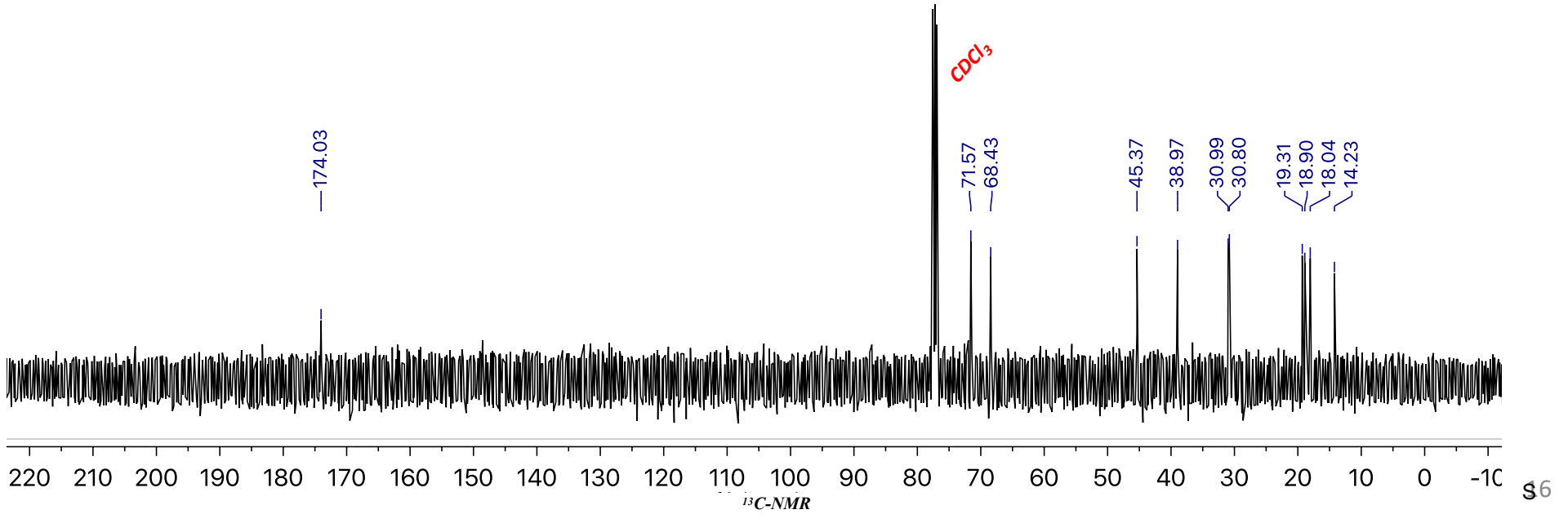
CDCl3
174.03
71.57
68.43
45.37
38.97
30.99
30.80
19.31
18.90
18.04
14.23
220
210
200
190
180
170
160
150
140
130
120
110
100
90
80
70
60
50
40
30
20
10
0
-10
13C-NMR

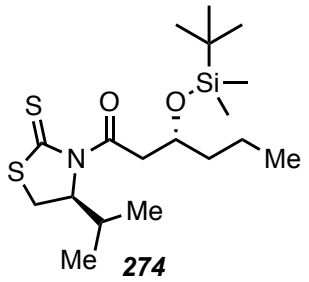

274

^{1}H-NMR

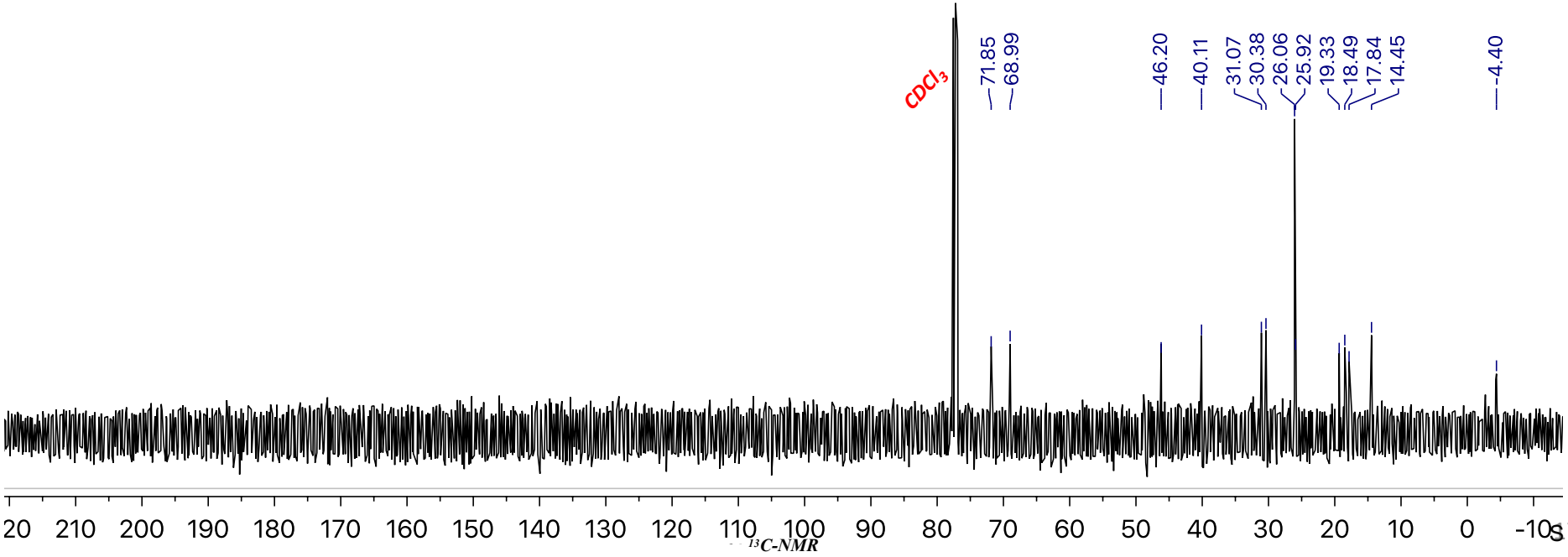

^{13}C-NMR

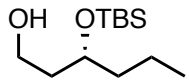
OH
OTBS

275

CDCl3
1.02
1.24
1.21
1.00
1.03
1.21
2.55
3.00
11.08
6.21
10.0 9.5 9.0 8.5 8.0 7.5 7.0 6.5 6.0 5.5 5.0 4.5 4.0 3.5 3.0 2.5 2.0 1.5 1.0 0.5 0.0 -0
1H-NMR

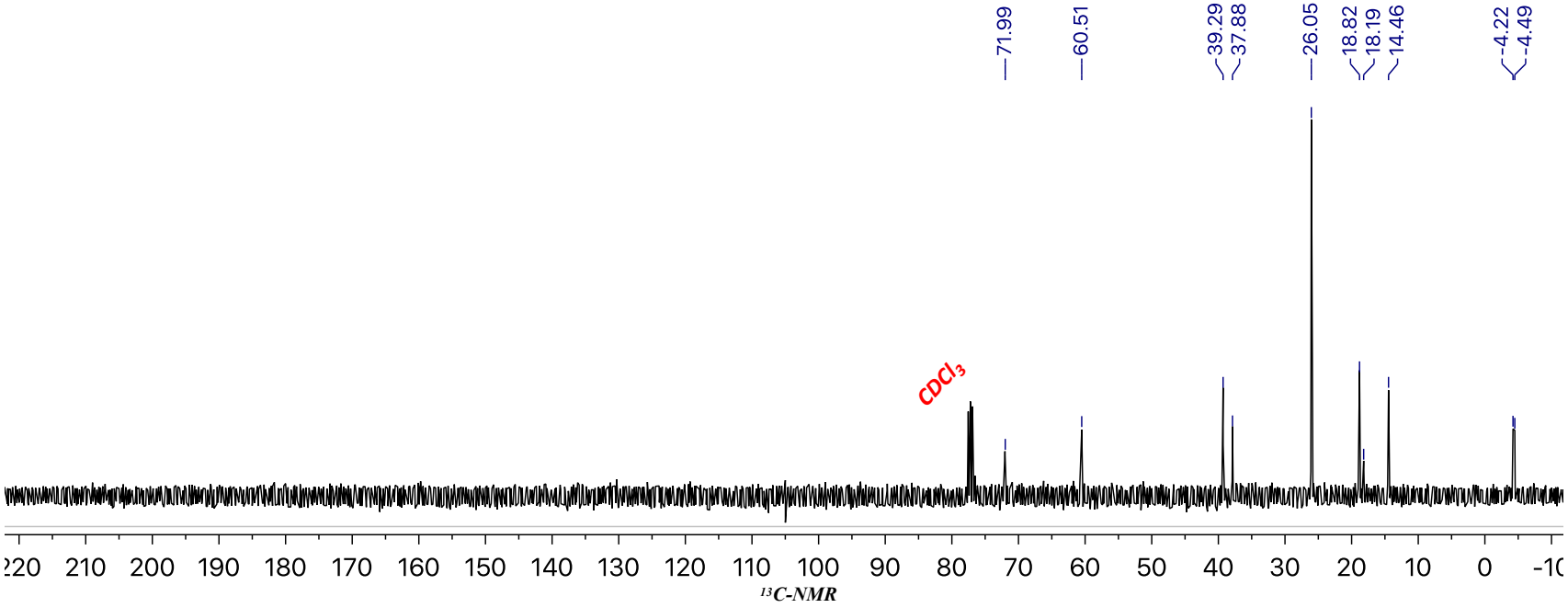
71.99
60.51
39.29
37.88
26.05
18.82
18.19
14.46
-4.22
-4.49
CDCl3
220 210 200 190 180 170 160 150 140 130 120 110 100 90 80 70 60 50 40 30 20 10 0 -10
13C-NMR

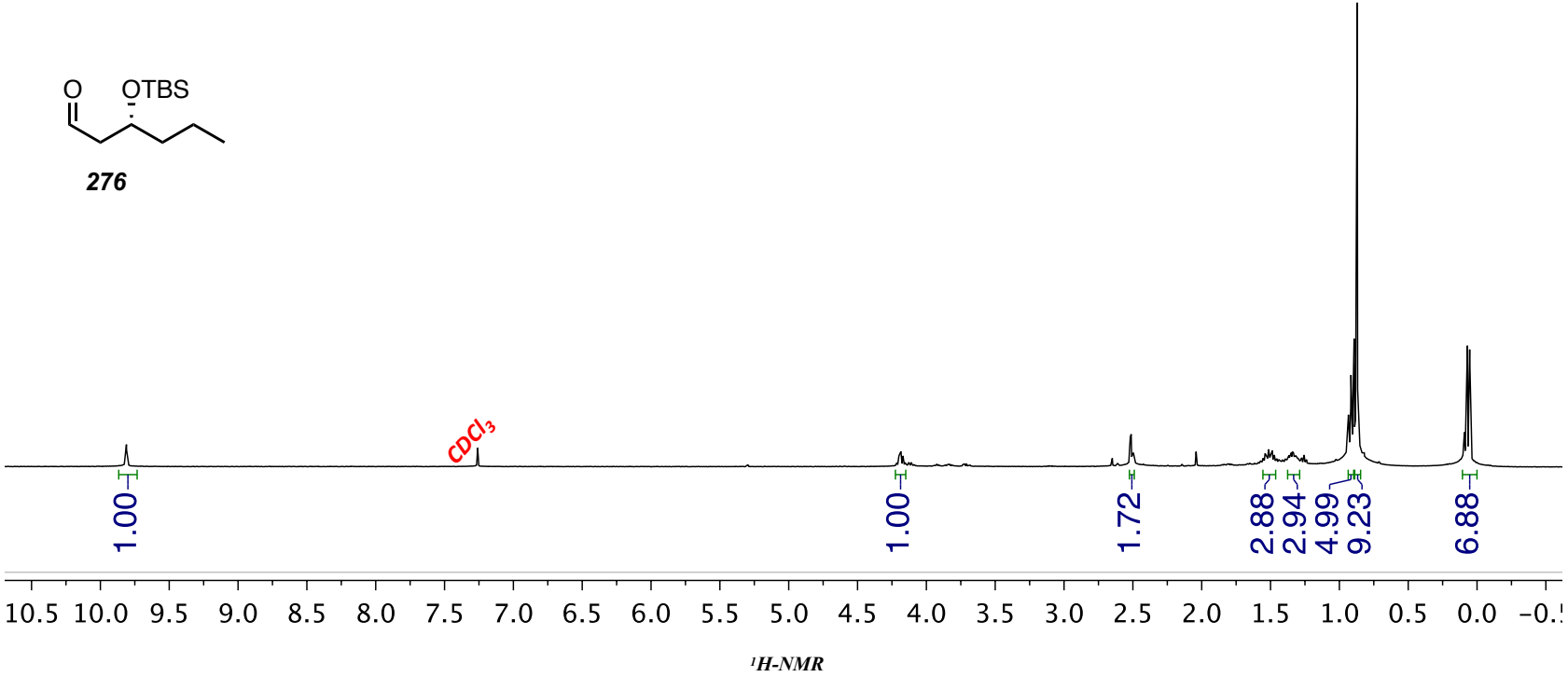
O
OTBS
276
CDCl3
1.00
1.00
1.72
2.88
2.94
4.99
9.23
6.88
10.5 10.0 9.5 9.0 8.5 8.0 7.5 7.0 6.5 6.0 5.5 5.0 4.5 4.0 3.5 3.0 2.5 2.0 1.5 1.0 0.5 0.0 -0.5

^{1}H-NMR

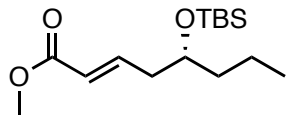
O
OTBS
O

277

CDCl3
1.18
1.00
1.59
3.23
2.95
4.57
3.73
9.03
6.84
10.0 9.5 9.0 8.5 8.0 7.5 7.0 6.5 6.0 5.5 5.0 4.5 4.0 3.5 3.0 2.5 2.0 1.5 1.0 0.5 0.0
1H-NMR

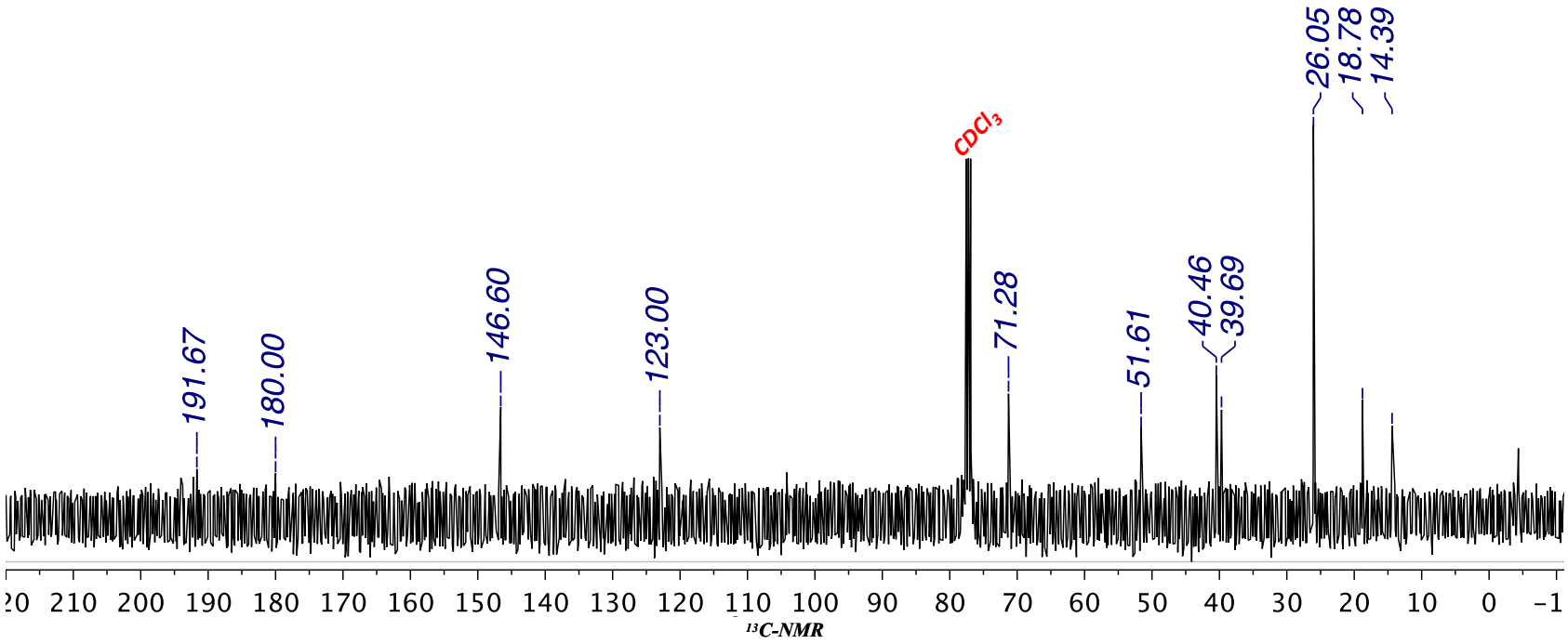
191.67
180.00
146.60
123.00
CDCl3
71.28
51.61
40.46
39.69
26.05
18.78
14.39
210 200 190 180 170 160 150 140 130 120 110 100 90 80 70 60 50 40 30 20 10 0
13C-NMR

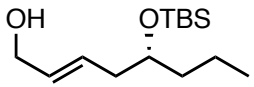

276

^{1}H-NMR

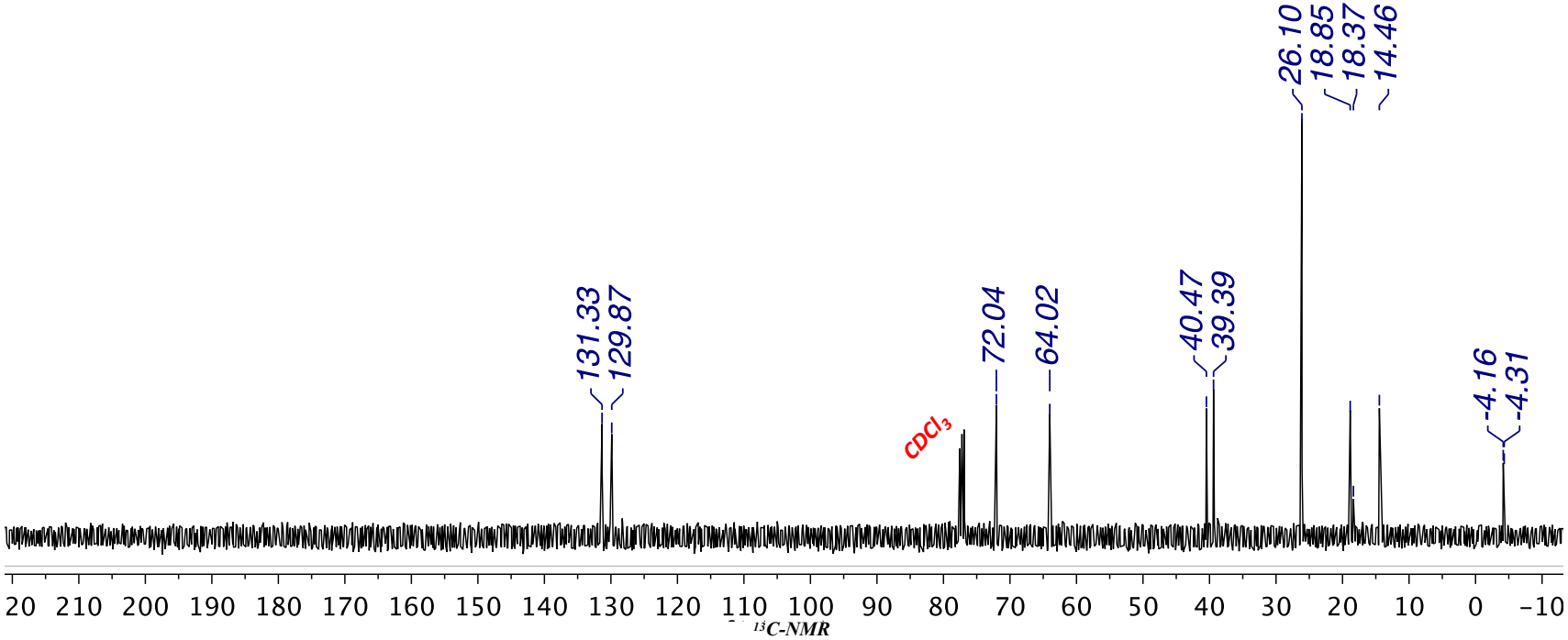

^{13}C-NMR

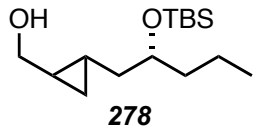
OH
OTBS

278

CDCl3
1.00
2.18
4.79
4.18
12.37
1.44
2.43
6.05
0.5 10.0 9.5 9.0 8.5 8.0 7.5 7.0 6.5 6.0 5.5 5.0 4.5 4.0 3.5 3.0 2.5 2.0 1.5 1.0 0.5 0.0 -0
1H-NMR

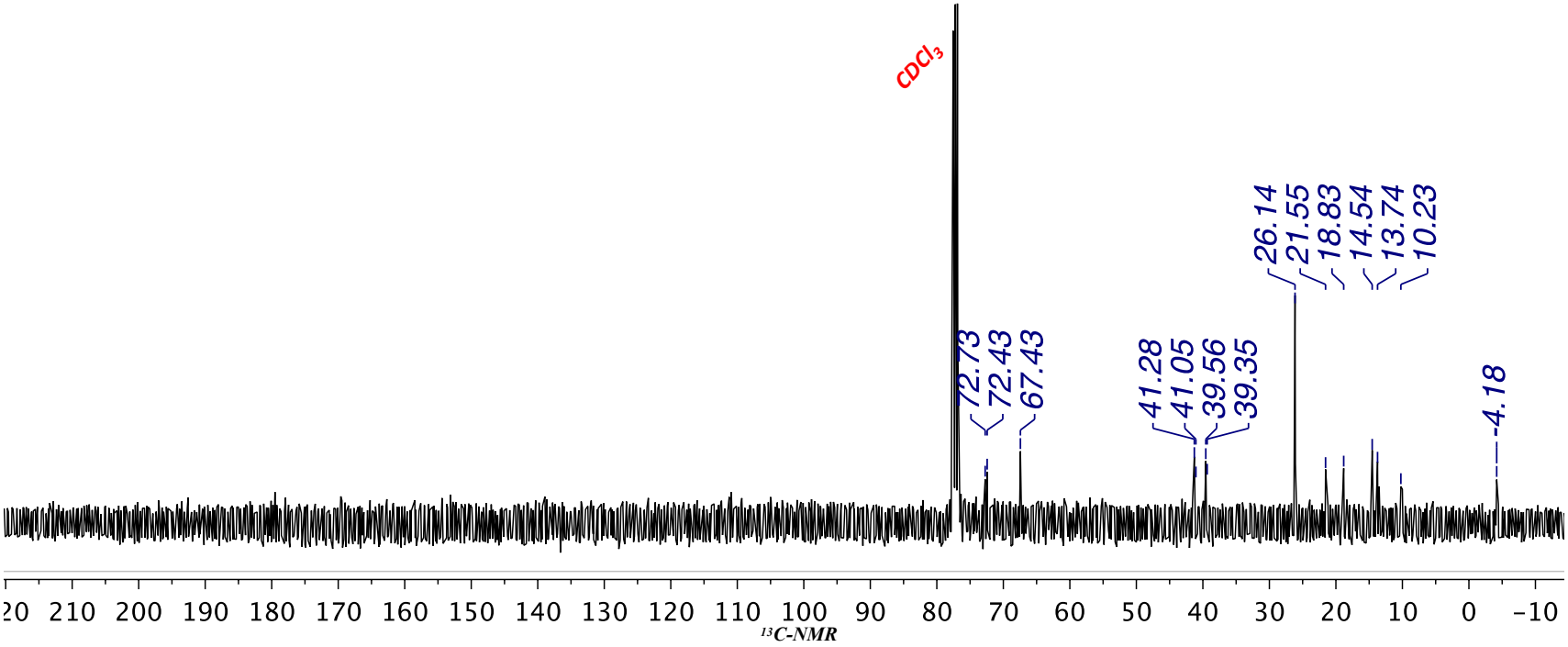
CDCl3
72.73
72.43
67.43
41.28
41.05
39.56
39.35
26.14
21.55
18.83
14.54
13.74
10.23
-4.18
20 210 200 190 180 170 160 150 140 130 120 110 100 90 80 70 60 50 40 30 20 10 0 -10
13C-NMR

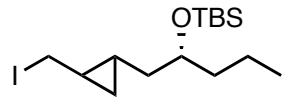
OTBS
I

279

CDCl3
1.00
2.52
7.91
1.52
12.28
1.74
1.72
1.41
6.25
5 10.0 9.5 9.0 8.5 8.0 7.5 7.0 6.5 6.0 5.5 5.0 4.5 4.0 3.5 3.0 2.5 2.0 1.5 1.0 0.5 0.0 -0.5
1H-NMR

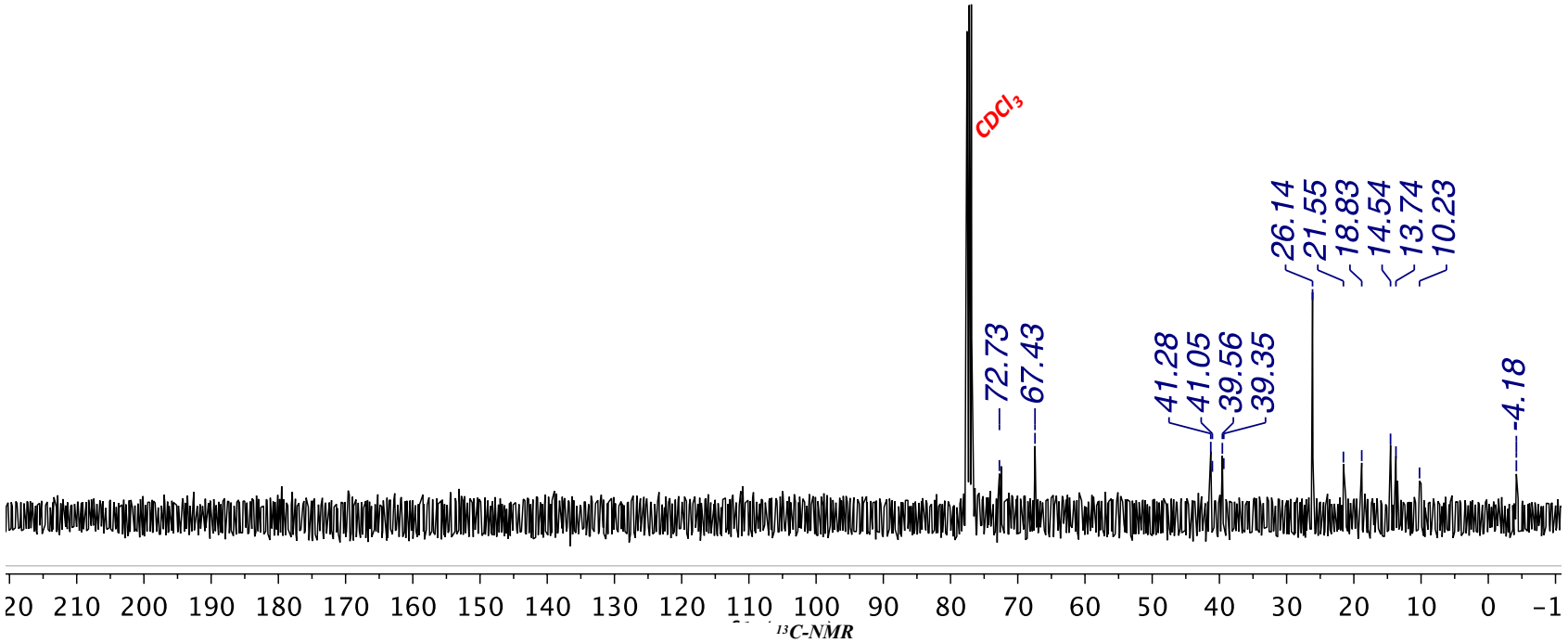
CDCl3
72.73
67.43
41.28
41.05
39.56
39.35
26.14
21.55
18.83
14.54
13.74
10.23
-4.18
20 210 200 190 180 170 160 150 140 130 120 110 100 90 80 70 60 50 40 30 20 10 0 -1
13C-NMR

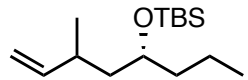
OTBS

281/282

CDCl3
0.99
2.01
1.00
1.48
8.97
4.55
9.15
6.31
10.0 9.5 9.0 8.5 8.0 7.5 7.0 6.5 6.0 5.5 5.0 4.5 4.0 3.5 3.0 2.5 2.0 1.5 1.0 0.5 0.0
¹H-NMR

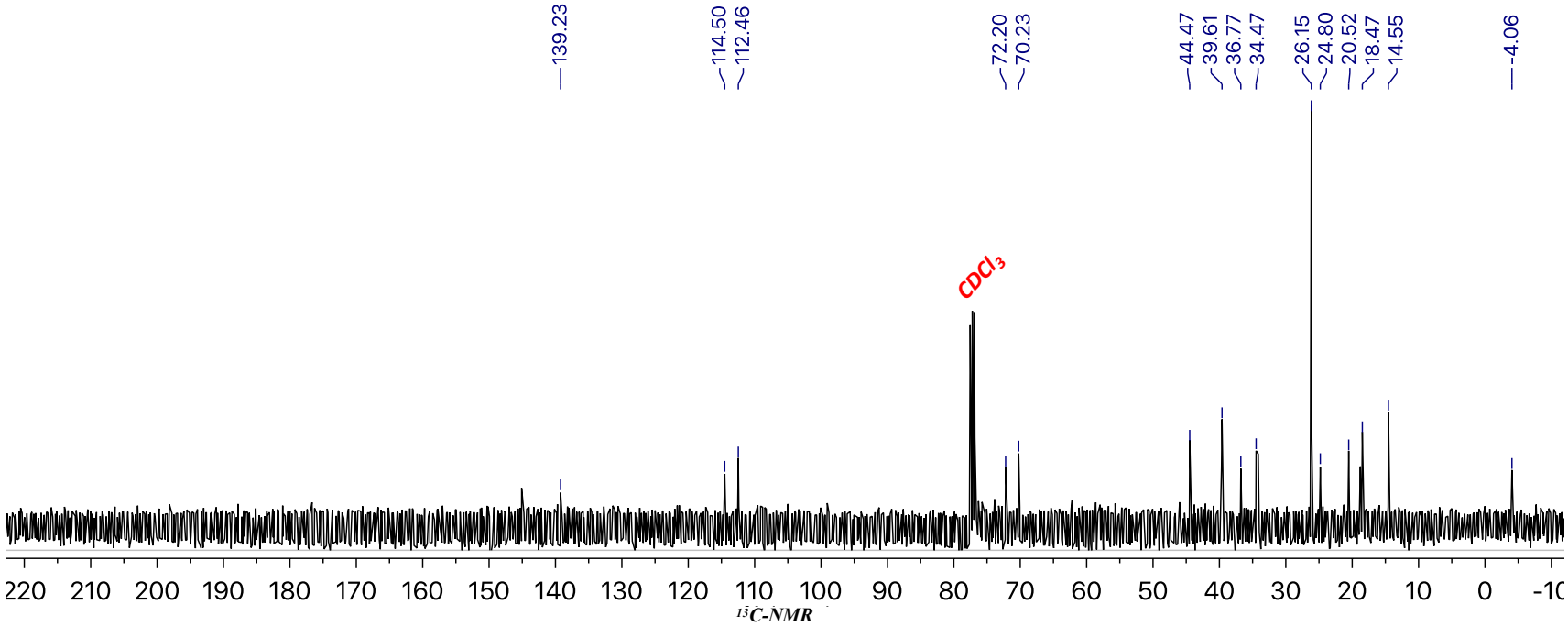
139.23
114.50
112.46
72.20
70.23
44.47
39.61
36.77
34.47
26.15
24.80
20.52
18.47
14.55
-4.06
CDCl3
220 210 200 190 180 170 160 150 140 130 120 110 100 90 80 70 60 50 40 30 20 10 0
¹³C-NMR

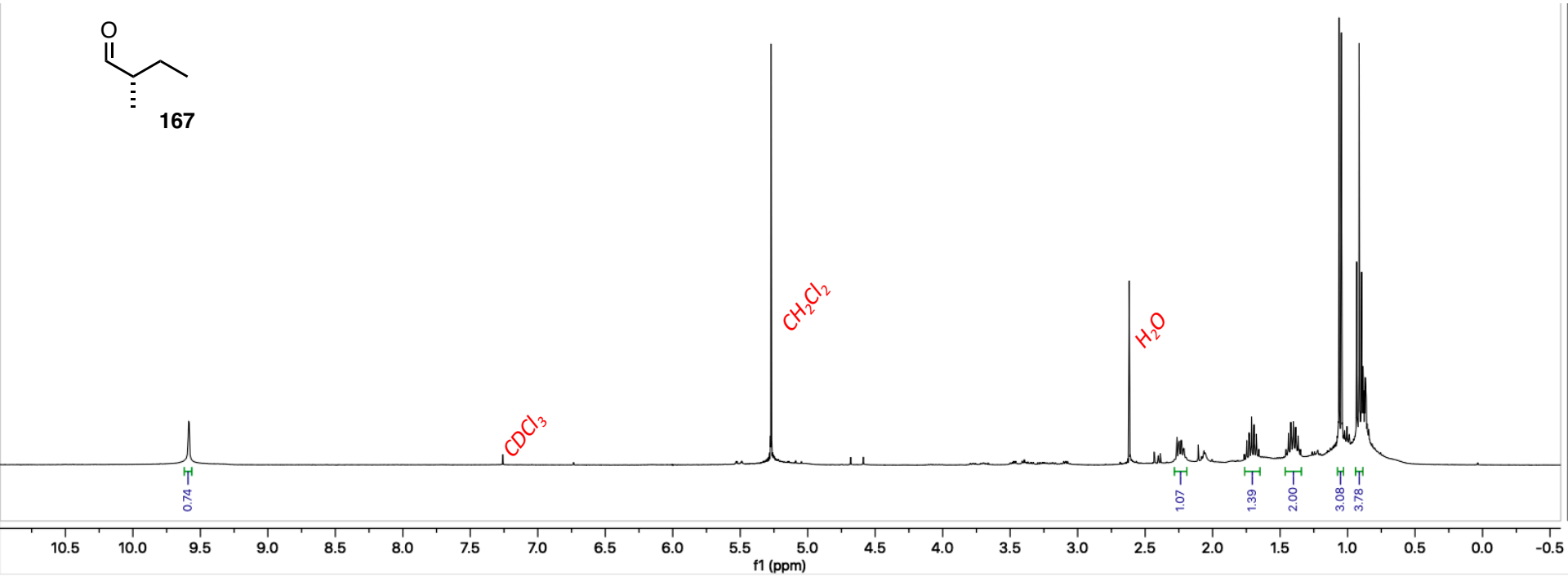
O
167
CDCl3
CH2Cl2
H2O
0.74
1.07
1.39
2.00
3.08
3.78
10.5
10.0
9.5
9.0
8.5
8.0
7.5
7.0
6.5
6.0
5.5
5.0
4.5
4.0
3.5
3.0
2.5
2.0
1.5
1.0
0.5
0.0
-0.5
f1 (ppm)

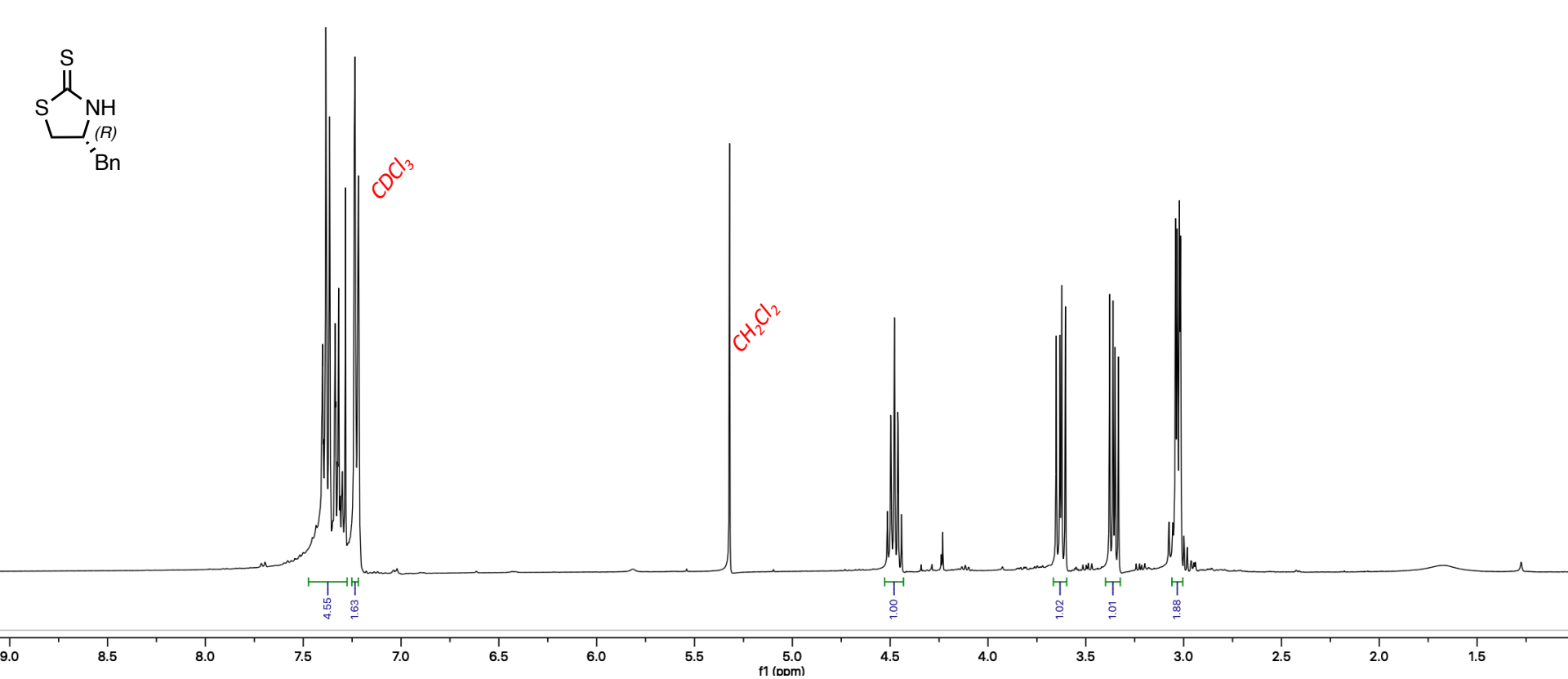
S
S
NH
(R)
Bn
CDCl3
CH2Cl2
4.55
1.63
1.00
1.02
1.01
1.88
9.0
8.5
8.0
7.5
7.0
6.5
6.0
5.5
5.0
4.5
4.0
3.5
3.0
2.5
2.0
1.5
f1 (ppm)

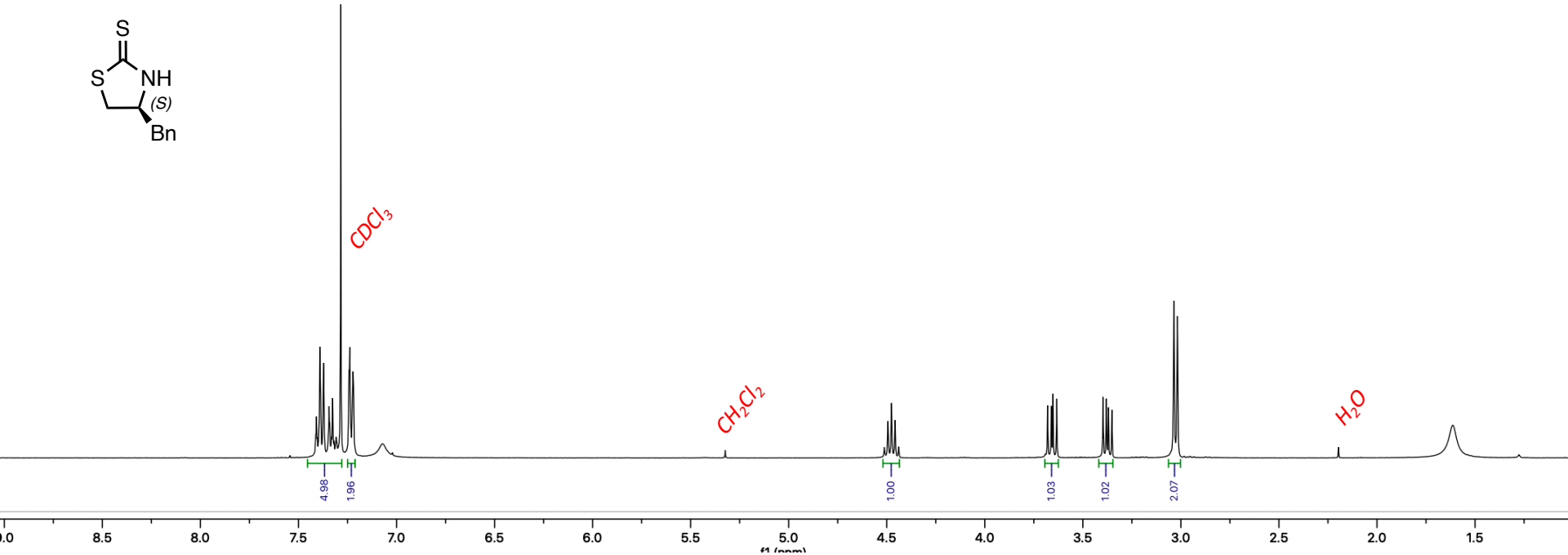
S
S
NH
(S)
Bn
CDCl3
CH2Cl2
H2O
4.98
1.96
1.00
1.03
1.02
2.07
8.5
8.0
7.5
7.0
6.5
6.0
5.5
5.0
4.5
4.0
3.5
3.0
2.5
2.0
1.5

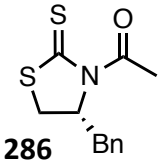
S
O
S
N
Bn

286

CDCl3
H2O
2.01
2.96
1.00
1.04
1.03
1.04
1.02
3.01
f1 (ppm)

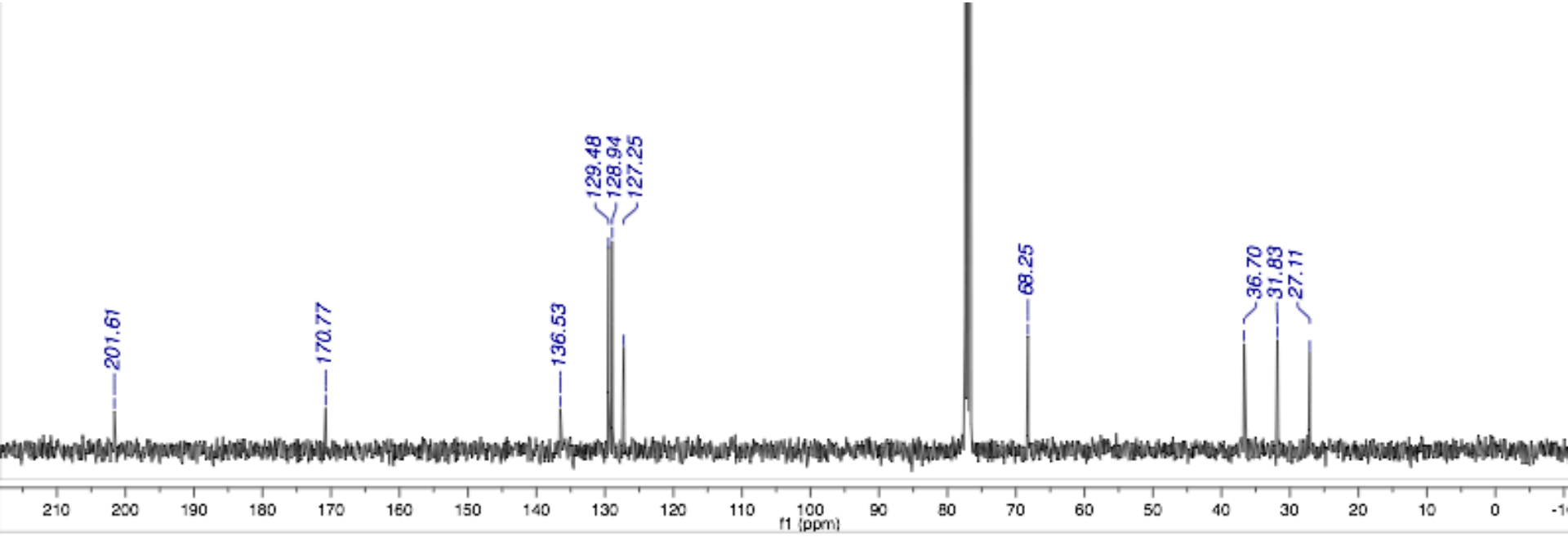
201.61
170.77
136.53
129.48
128.94
127.25
68.25
36.70
31.83
27.11
f1 (ppm)

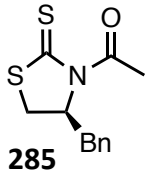
S
O
S
N
Bn

285

CDCl3
5.28
1.00
1.27
1.32
1.50
1.58
3.04
9.5
9.0
8.5
8.0
7.5
7.0
6.5
6.0
5.5
5.0
4.5
4.0
3.5
3.0
2.5
2.0
1.5
1.0
0.5
f1 (ppm)

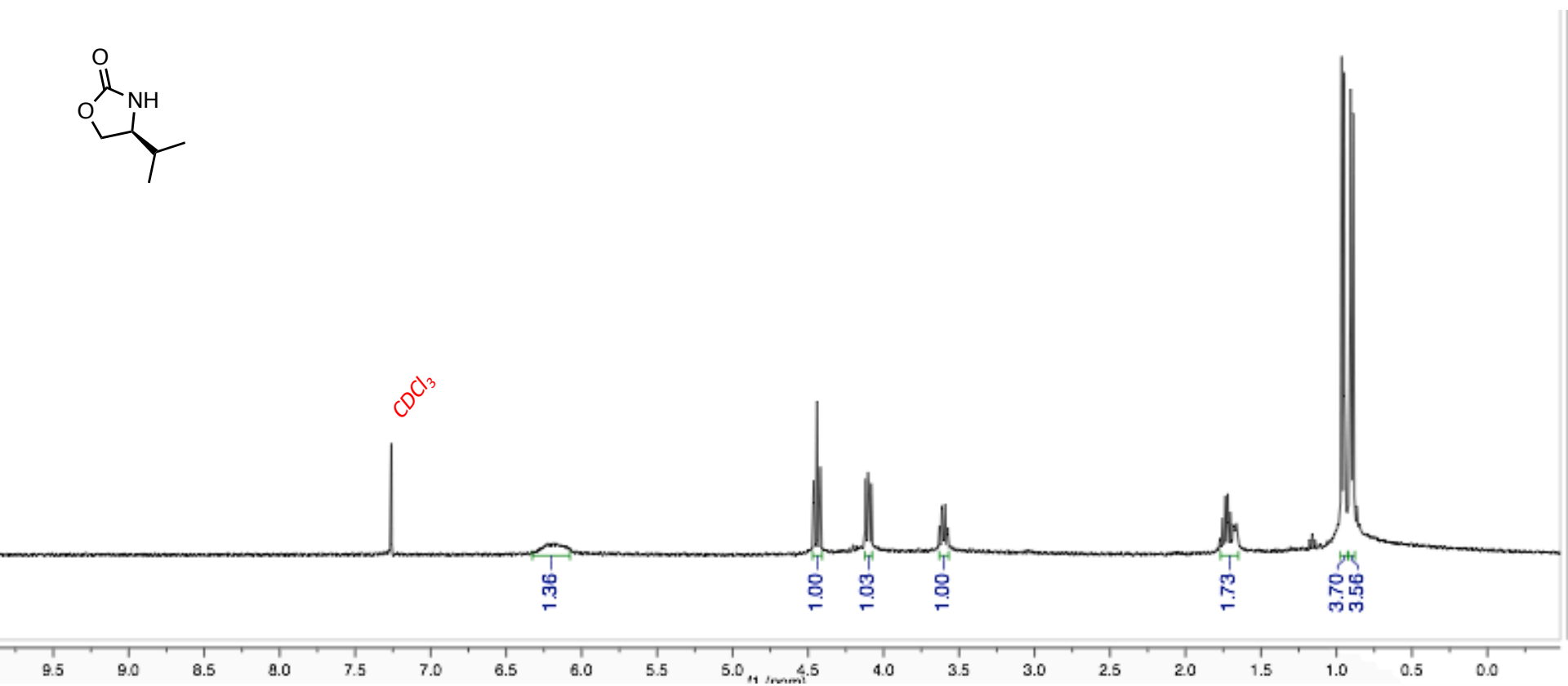
O
NH
O
CDCl3
1.36
1.00
1.03
1.00
1.73
3.70
3.56
9.5
9.0
8.5
8.0
7.5
7.0
6.5
6.0
5.5
5.0
4.5
4.0
3.5
3.0
2.5
2.0
1.5
1.0
0.5
0.0

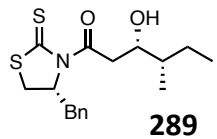
S
O
OH
S
N
Bn

289

CDCl3
H2O
2.01
3.16
1.00
0.91
0.93
1.02
2.02
1.08
1.04
0.86
1.80
1.36
6.28
f1 (ppm)
201.493
173.75
136.45
129.48
128.97
127.32
70.67
68.43
43.51
39.76
36.85
32.07
25.56
14.15
11.83
f1 (ppm)

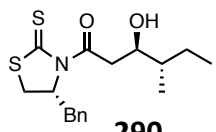
S
O
OH
S
N
Bn

290

CDCl3
5.30
CH2Cl2
1.56
H2O
1.25
Grease?
2.07
3.21
1.01
0.93
0.96
1.04
0.99
1.13
0.88
1.12
1.07
1.15
1.03
1.28
6.41
f1 (ppm)

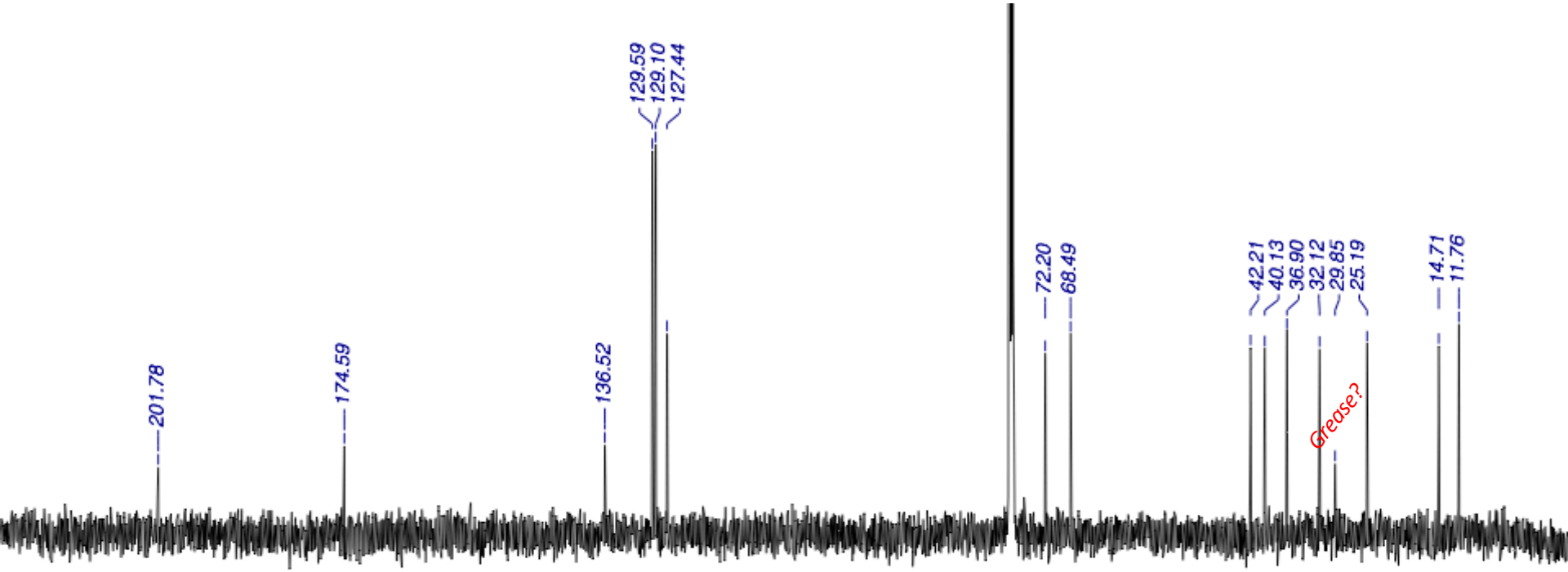
129.59
129.10
127.44
201.78
174.59
136.52
72.20
68.49
42.21
40.13
36.90
32.12
29.85
25.19
Grease?
14.71
11.76

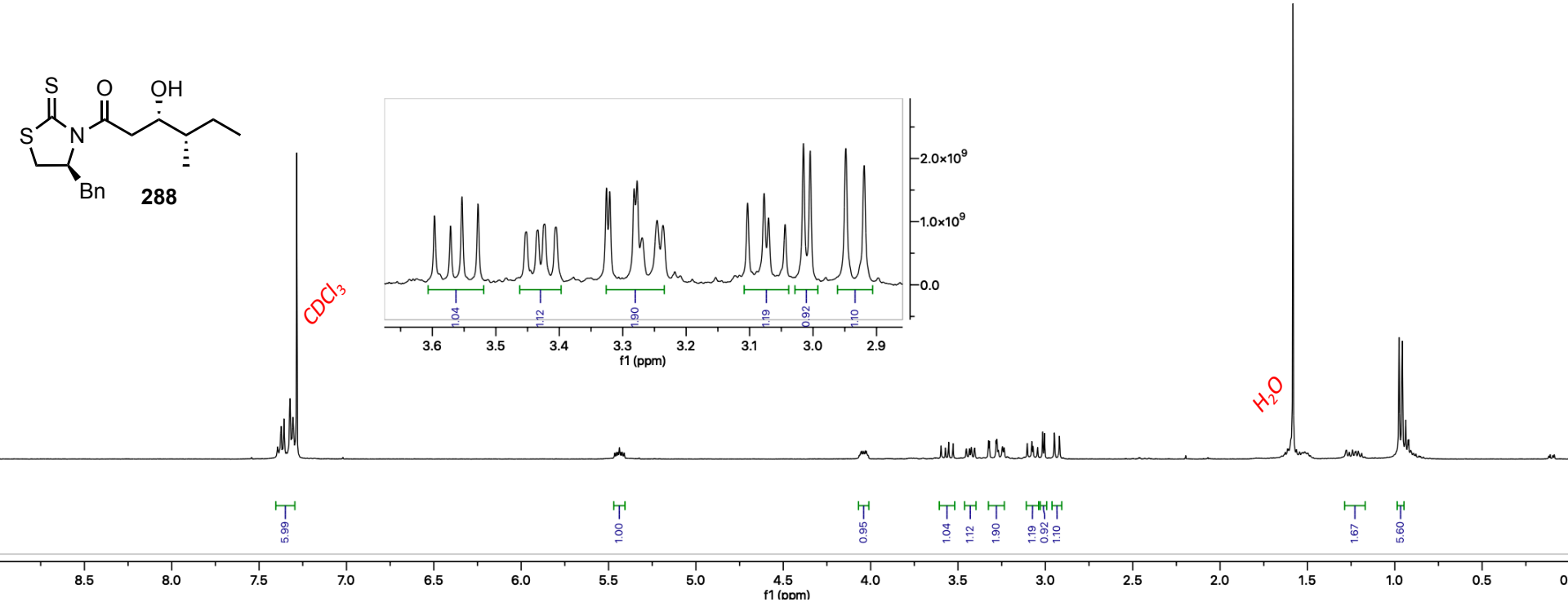
S
O
OH
S
N
Bn
288
CDCl3
H2O
2.0×10^9
1.0×10^9
0.0
1.04
1.12
1.90
1.19
0.92
1.10
3.6
3.5
3.4
3.3
3.2
3.1
3.0
2.9
f1 (ppm)
5.99
1.00
0.95
1.04
1.12
1.90
1.19
0.92
1.10
1.67
5.60
8.5
8.0
7.5
7.0
6.5
6.0
5.5
5.0
4.5
4.0
3.5
3.0
2.5
2.0
1.5
1.0
0.5
0
f1 (ppm)

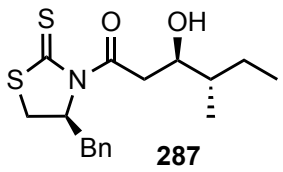

287

(Contains **270**)

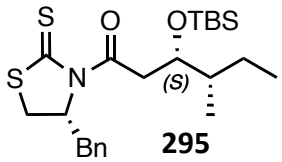
S
O
OTBS
S
N
(S)
Bn

295

CDCl3
CH2Cl2
H2O
2.04
3.42
1.00
0.95
1.05
1.12
1.07
2.18
1.10
1.14
1.19
1.79
6.42
4.14
3.43
8.82
2.93
6.16
f1 (ppm)

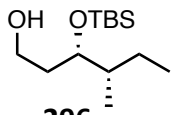
OH
OTBS

296

CDCl3
H2O
3.54
1.00
2.29
1.04
1.09
1.31
12.48
3.63
6.88
f1 (ppm)

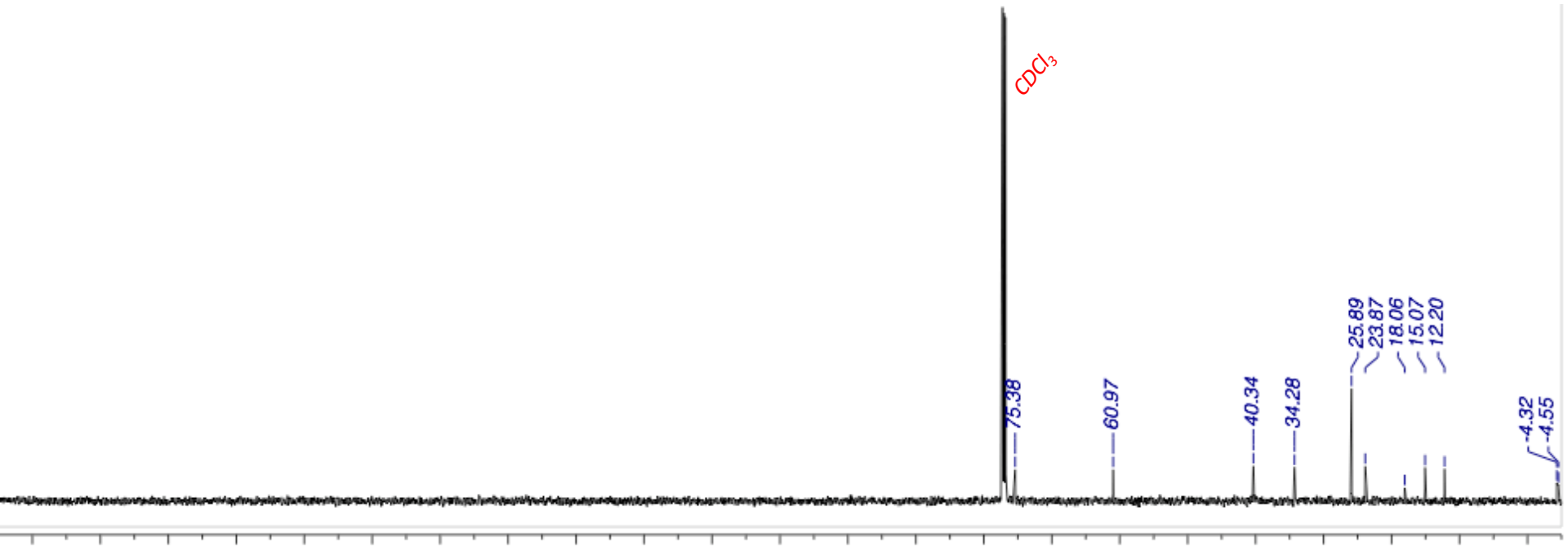
CDCl3
75.38
60.97
40.34
34.28
25.89
23.87
18.06
15.07
12.20
-4.32
-4.55

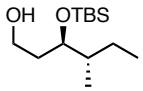
OH
OTBS

296'

CDCl3
H2O
1.00
2.10
0.90
1.68
2.17
1.04
1.09
12.11
3.61
6.57
f1 (ppm)

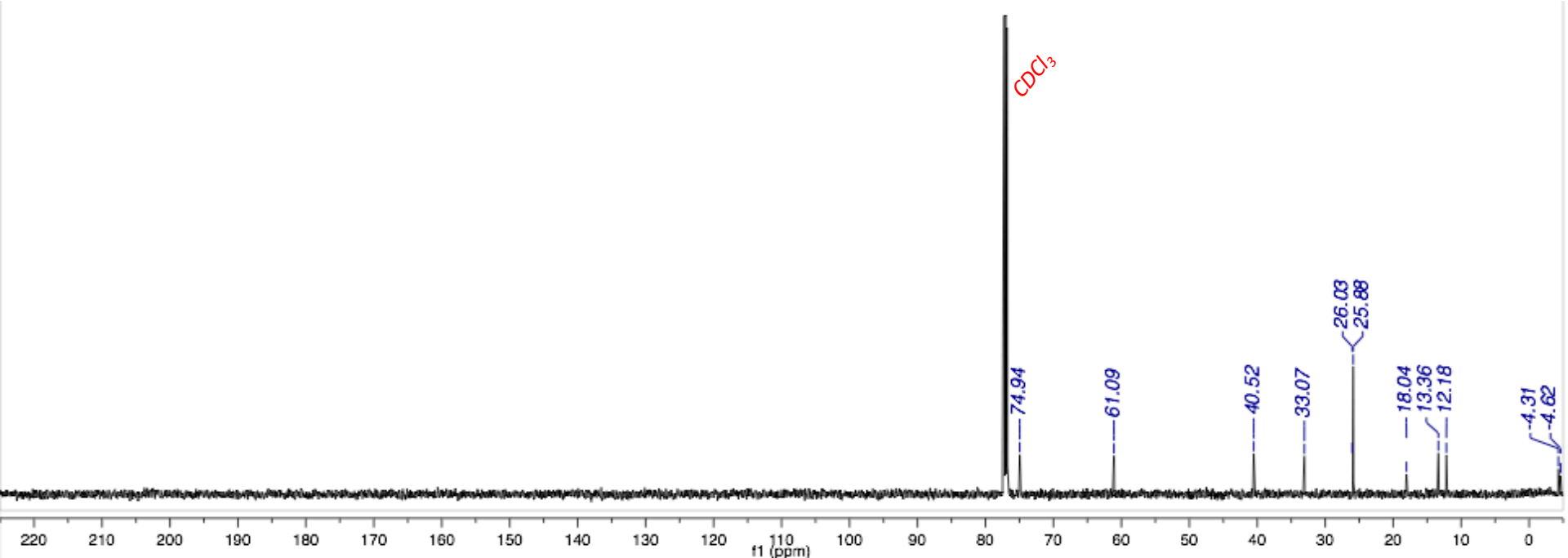
CDCl3
74.94
61.09
40.52
33.07
26.03
25.88
18.04
13.36
12.18
-4.31
-4.62
f1 (ppm)

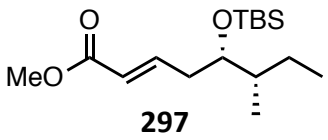
O
OTBS
MeO

297

CDCl3
CH2Cl2
H2O
1.00
1.05
3.05
1.05
2.01
1.08
1.14
1.25
12.76
3.30
6.21
f1 (ppm)
166.95
147.06
122.51
74.69
51.45
40.05
37.16
25.86
25.23
18.12
13.80
12.11
4.30
-4.56
f1 (ppm)

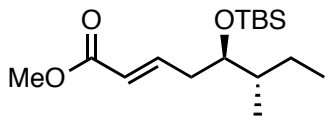
O
OTBS
MeO

CDCl3
1.00
1.17
3.22
1.05
2.02
1.22
1.13
1.13
12.23
3.93
6.88
f1 (ppm)

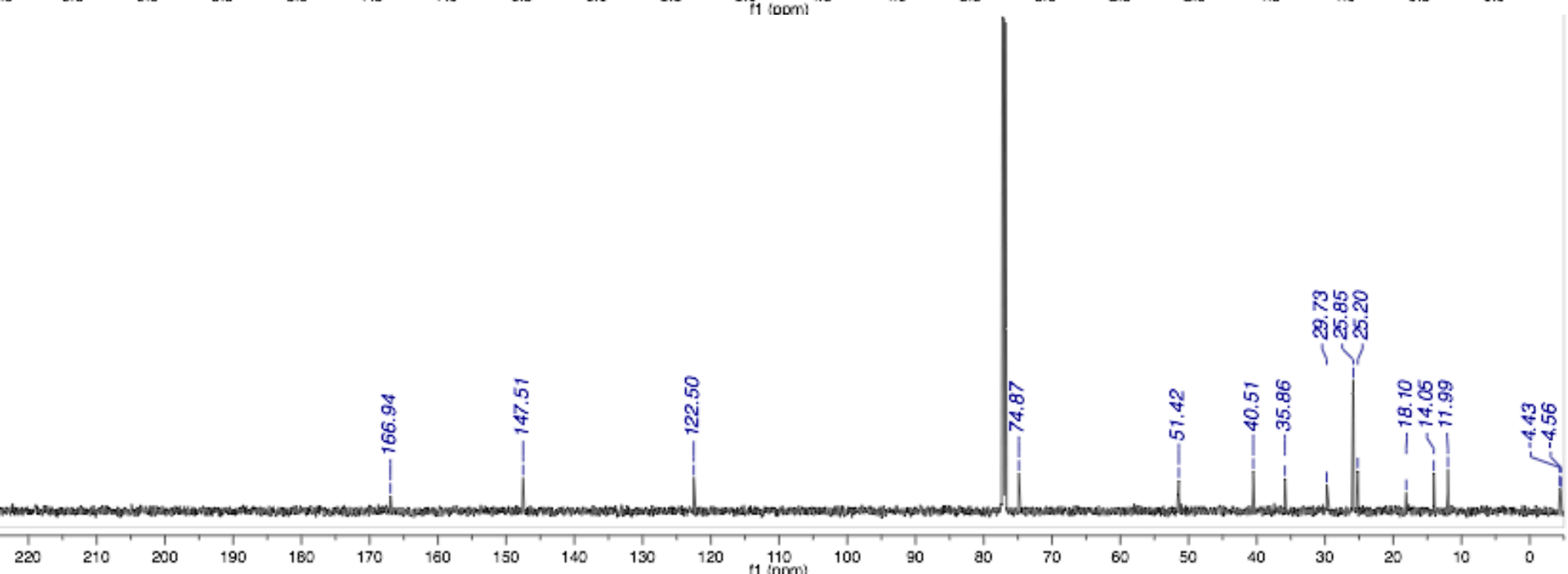
166.94
147.51
122.50
74.87
51.42
40.51
35.86
29.73
25.85
25.20
18.10
14.05
11.99
-4.43
-4.56
f1 (ppm)

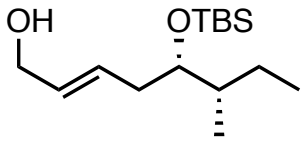
OH
OTBS

256

CDCl3
1.91
1.97
1.00
2.05
2.26
1.35
1.24
12.02
3.09
6.52
9.5
9.0
8.5
8.0
7.5
7.0
6.5
6.0
5.5
5.0
4.5
4.0
3.5
3.0
2.5
2.0
1.5
1.0
0.5
0.0
130.78
130.33
77.33
63.88
39.50
37.13
25.91
25.47
18.17
13.65
12.15
-4.11
-4.54
250
240
230
220
210
200
190
180
170
160
150
140
130
120
110
100
90
80
70
60
50
40
30
20
10
0
-1

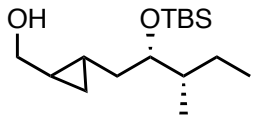
OH
OTBS

278

CDCl3
H2O
1.00
1.00
0.99
0.69
1.40
0.96
1.77
1.35
0.54
1.07
0.59
9.84
2.10
3.18
1.22
2.08
6.00
f1 (ppm)

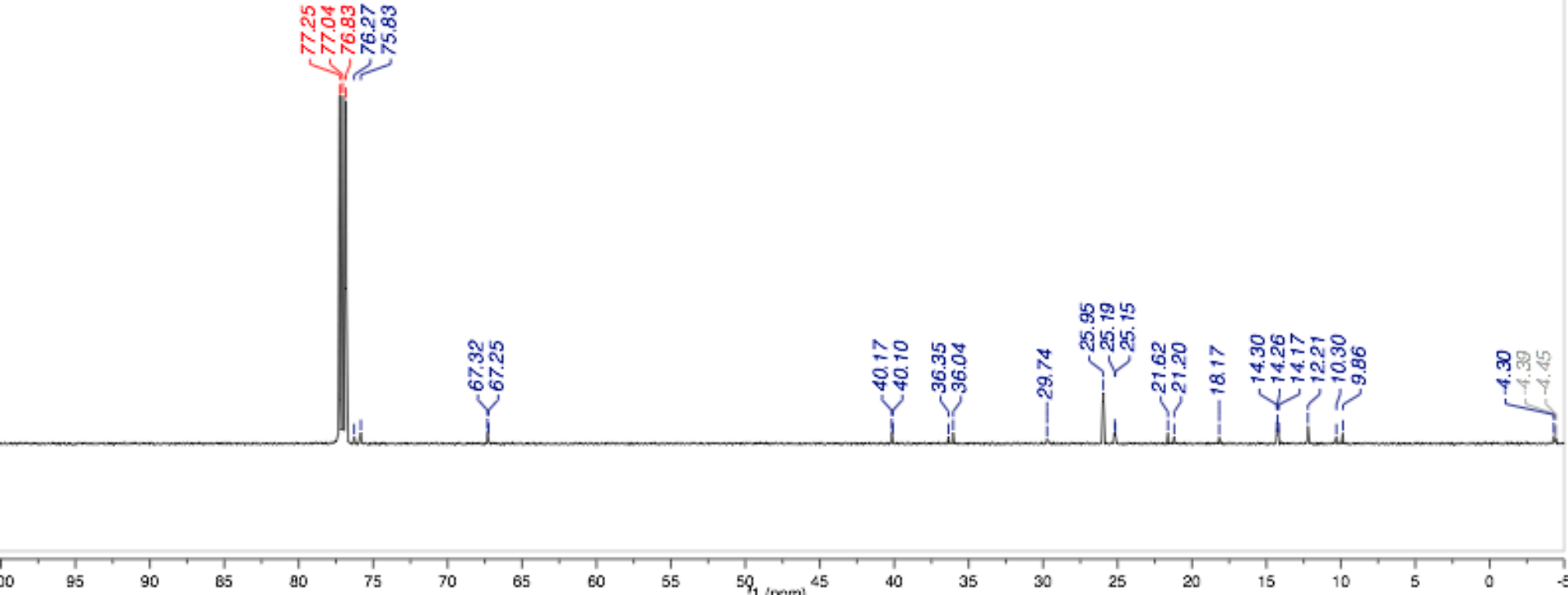
77.25
77.04
76.83
76.27
75.83
67.32
67.25
40.17
40.10
36.35
36.04
29.74
25.95
25.19
25.15
21.62
21.20
18.17
14.30
14.26
14.17
12.21
10.30
9.86
-4.30
-4.39
-4.45
f1 (ppm)

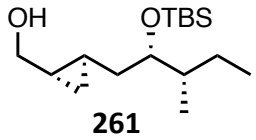
OH
OTBS

261

CDCl3
1.78
0.98
1.00
2.30
2.12
3.20
3.41
1.21
13.35
3.34
0.96
0.92
1.00
6.11
f1 (ppm)

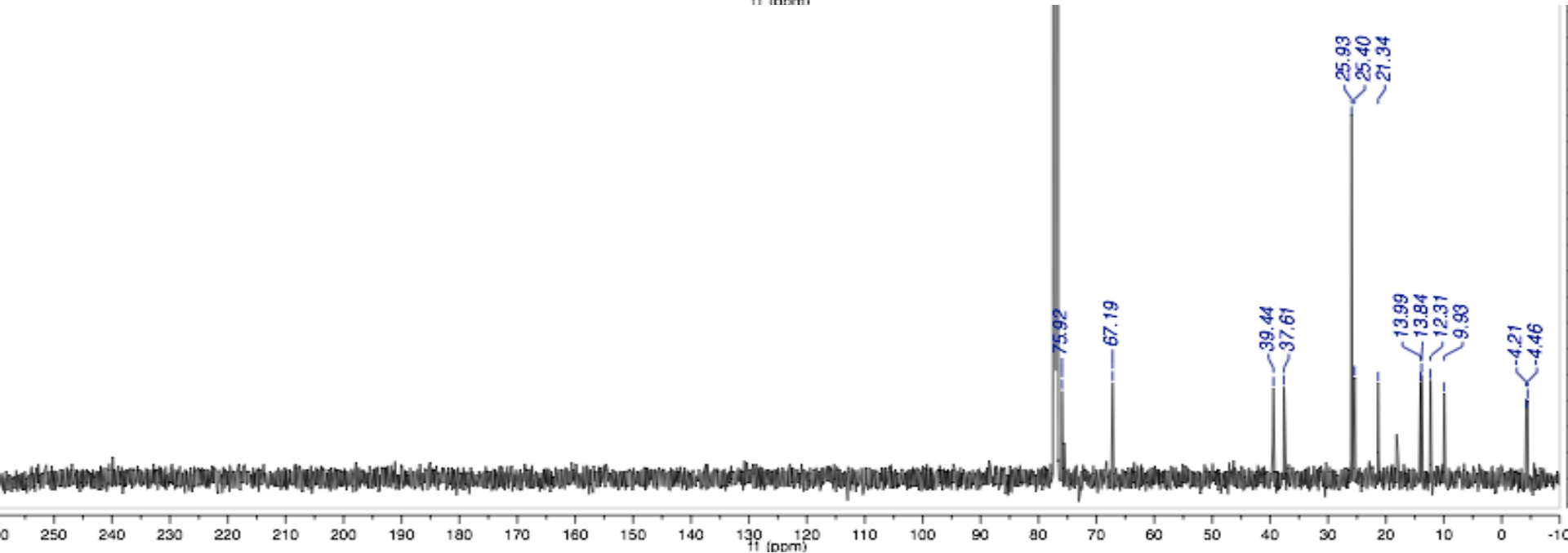
25.93
25.40
21.34
75.92
67.19
39.44
37.61
13.99
13.84
12.31
9.93
-4.21
-4.46
f1 (ppm)

Cosy of **261**

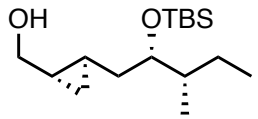
OH
OTBS

7.5
7.0
6.5
6.0
5.5
5.0
4.5
4.0
3.5
3.0
2.5
2.0
1.5
1.0
0.5
0.0
-0.5
f2 (ppm)
-0.5
0.0
0.5
1.0
1.5
2.0
2.5
3.0
3.5
4.0
4.5
5.0
5.5
6.0
6.5
7.0
7.5

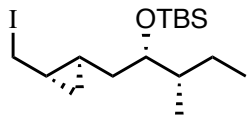
I
OTBS

299

CDCl3
H2O
1.35
1.00
0.58
1.02
2.39
2.07
2.73
16.59
3.95
1.05
1.11
1.17
6.75
f1 (ppm)

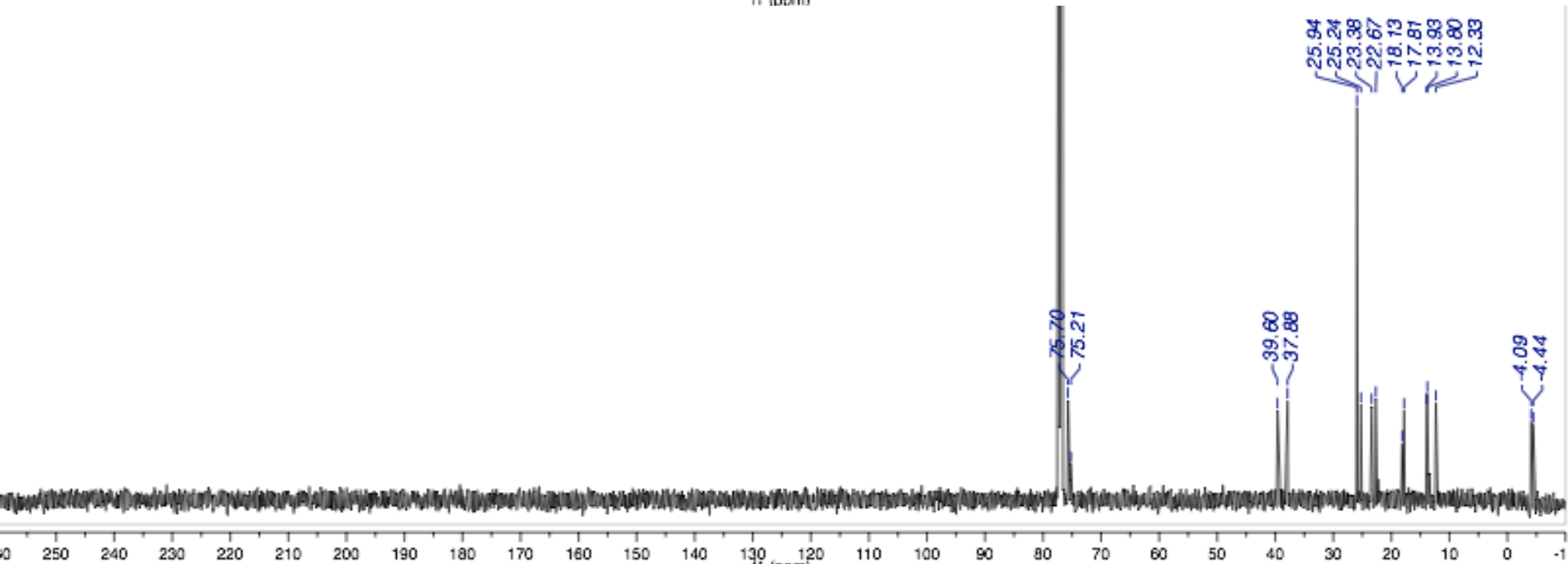
25.94
25.24
23.38
22.67
18.13
17.81
13.93
13.80
12.33
75.70
75.21
39.60
37.88
-4.09
-4.44

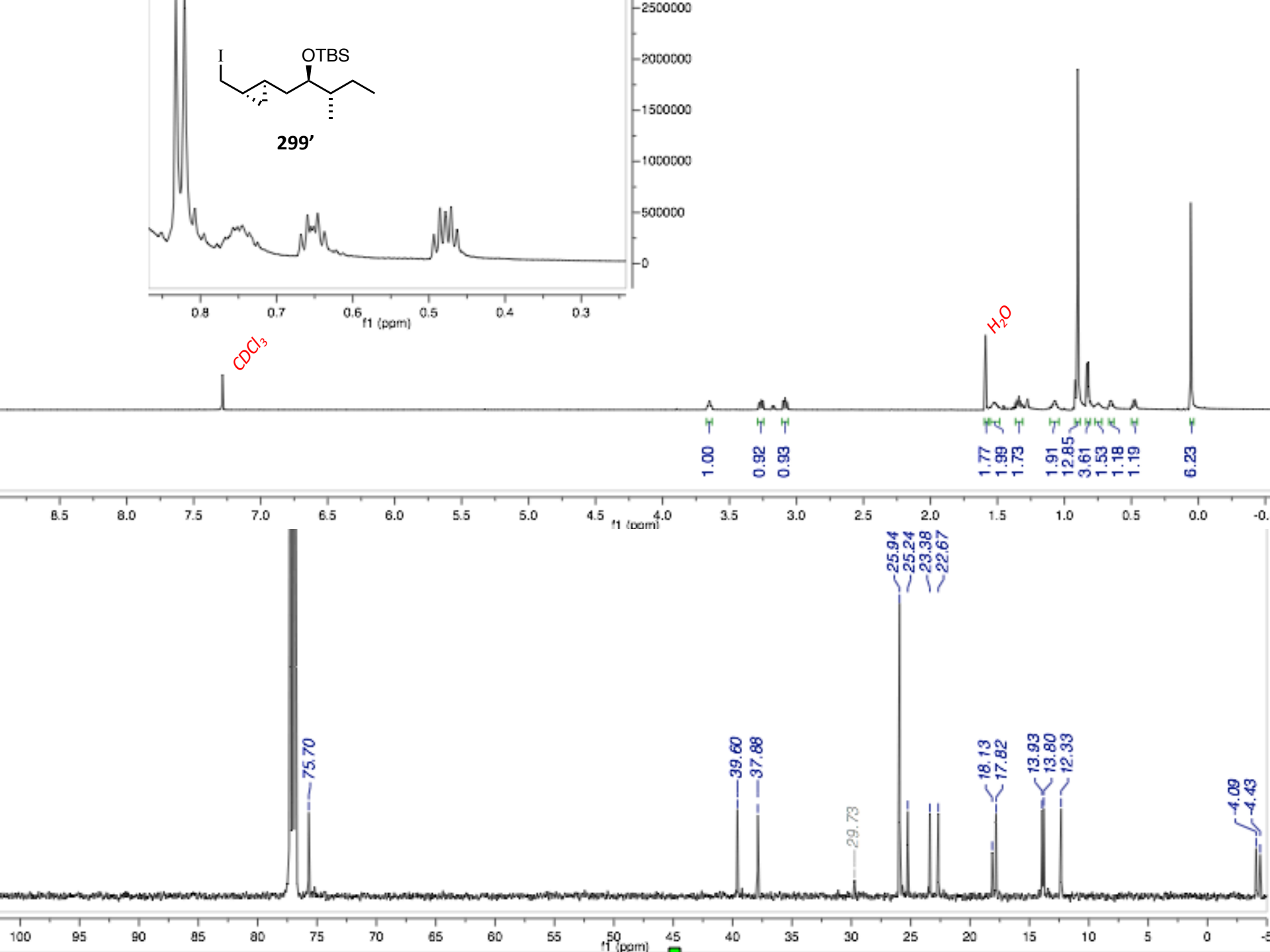
I
OTBS
299'
2500000
2000000
1500000
1000000
500000
0
0.8
0.7
0.6
0.5
0.4
0.3
f1 (ppm)
CDCl3
H2O
1.00
0.92
0.93
1.77
1.99
1.73
1.91
12.85
3.61
1.53
1.18
1.19
6.23
f1 (ppm)
75.70
39.60
37.88
29.73
25.94
25.24
23.38
22.67
18.13
17.82
13.93
13.80
12.33
4.09
4.43
f1 (ppm)

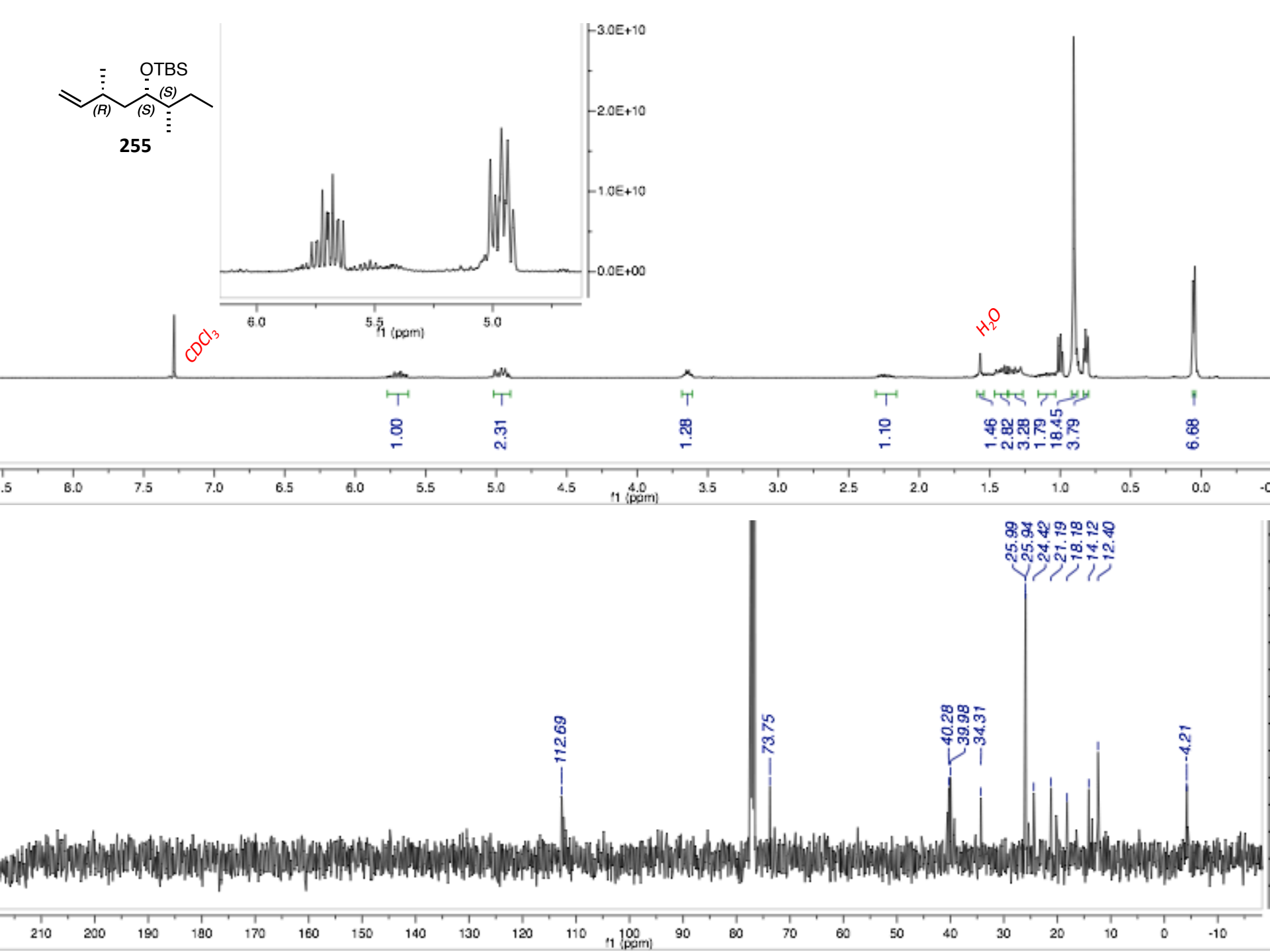
OTBS
(S)
(R)
(S)
255
3.0E+10
2.0E+10
1.0E+10
0.0E+00
6.0
5.5
5.0
f1 (ppm)
CDCl3
H2O
1.00
2.31
1.28
1.10
1.46
2.82
3.28
1.79
18.45
3.79
6.68
f1 (ppm)
25.99
25.94
24.42
21.19
18.18
14.12
12.40
112.69
73.75
40.28
39.98
34.31
-4.21
f1 (ppm)

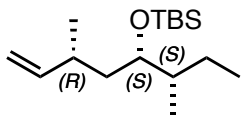

Cosy of **255**

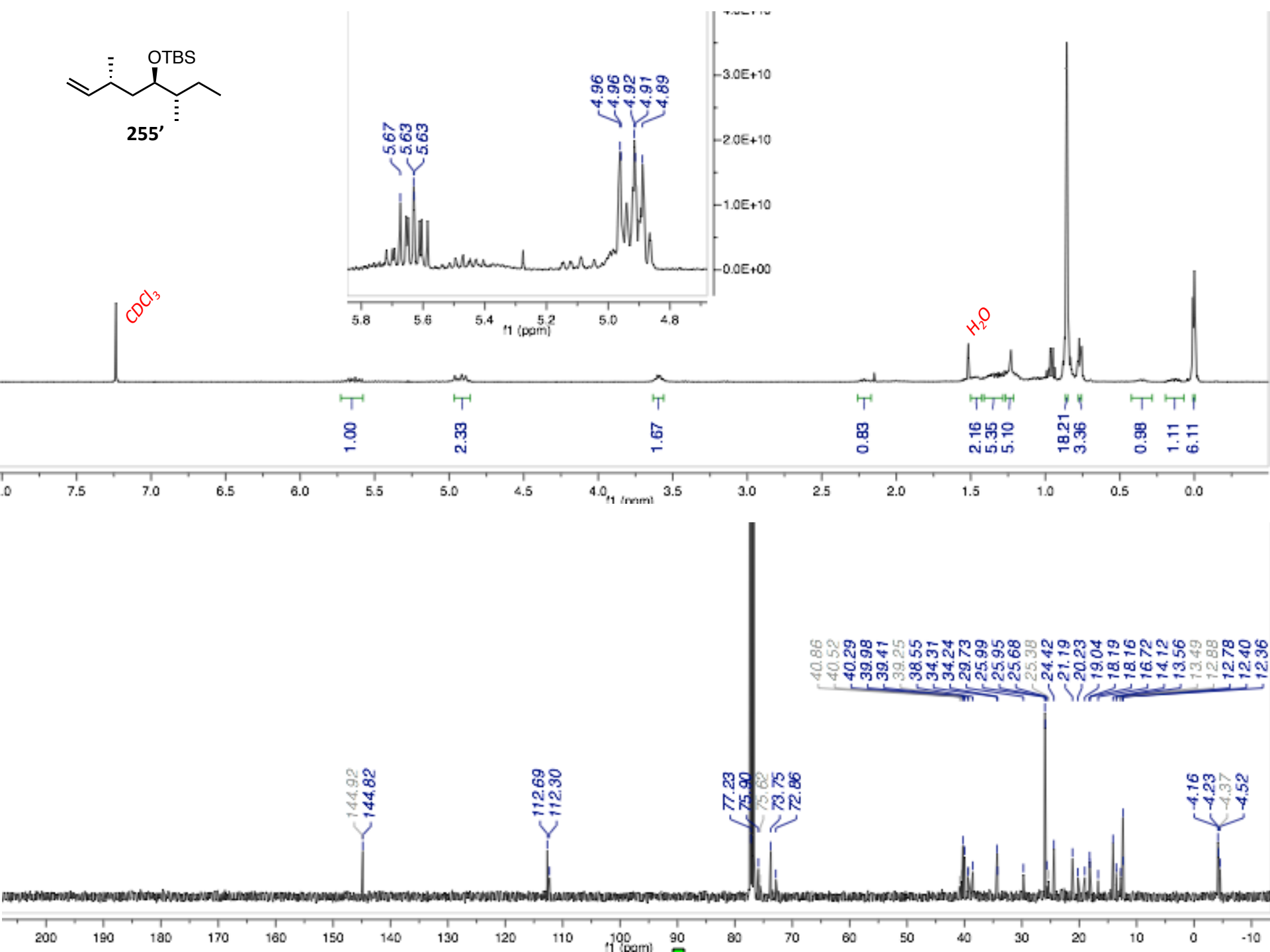
OTBS
255'
CDCl3
H2O
5.67
5.63
5.63
4.96
4.96
4.92
4.91
4.89
3.0E+10
2.0E+10
1.0E+10
0.0E+00
f1 (ppm)
1.00
2.33
1.67
0.83
2.16
5.35
5.10
18.21
3.36
0.98
1.11
6.11
144.92
144.82
112.69
112.30
77.23
75.90
75.62
73.75
72.86
40.86
40.52
40.29
39.98
39.41
39.25
38.55
34.31
34.24
29.73
25.99
25.95
25.68
25.38
24.42
21.19
20.23
19.04
18.19
18.16
16.72
14.12
13.56
13.49
12.88
12.78
12.40
12.36
-4.16
-4.23
-4.37
-4.52

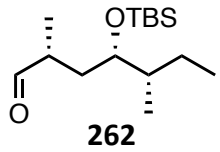
OTBS
O

262

$CDCl_3$
H_2O
0.96
1.00
0.93
0.87
2.18
2.27
4.16
1.54
12.18
3.26
6.52
f1 (ppm)

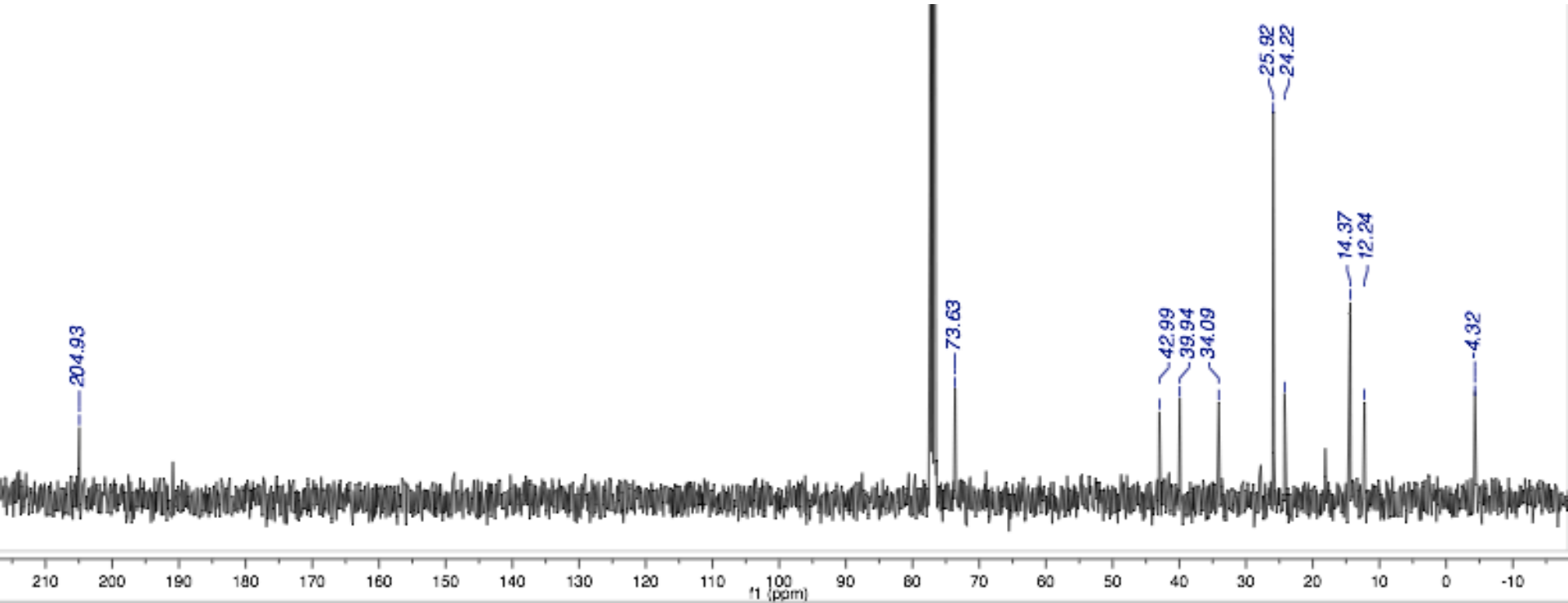
204.93
73.63
42.99
39.94
34.09
25.92
24.22
14.37
12.24
-4.32
f1 (ppm)

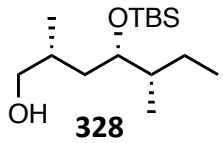
OTBS
OH

328

CDCl3
1.00
1.39
0.68
1.08
2.11
1.04
12.73
4.08
6.30
f1 (ppm)

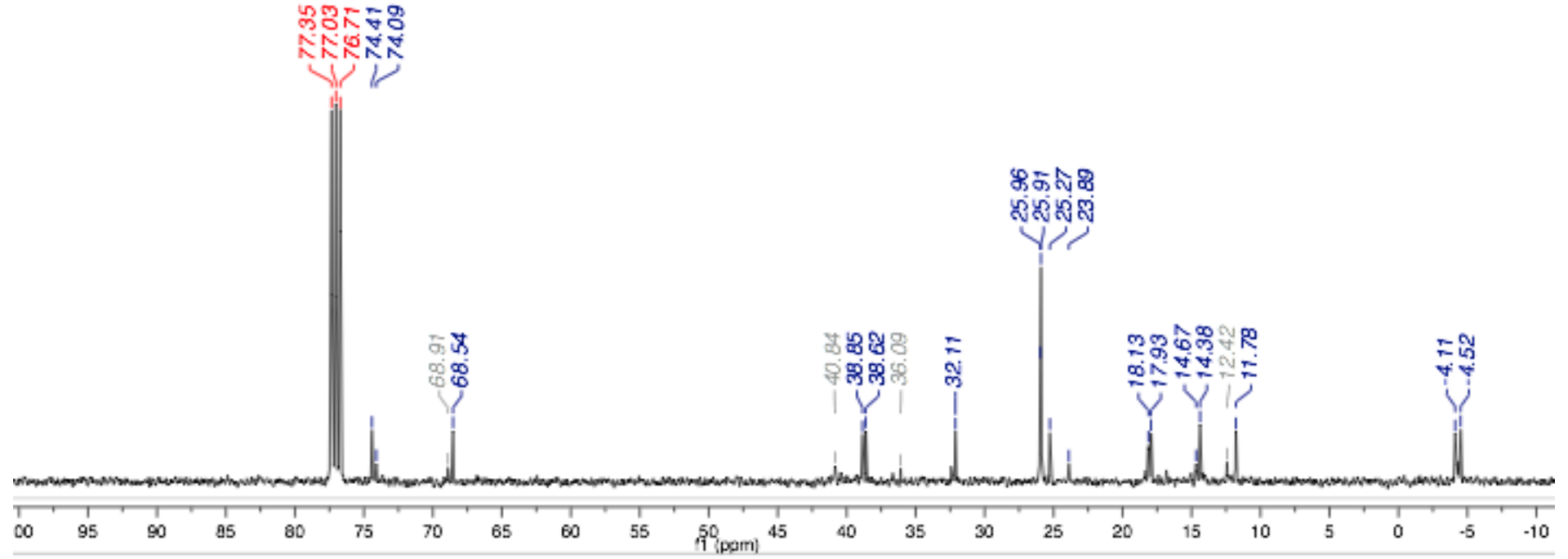
77.35
77.03
76.71
74.41
74.09
68.91
68.54
40.84
38.85
38.62
36.09
32.11
25.96
25.91
25.27
23.89
18.13
17.93
14.67
14.38
12.42
11.78
-4.11
-4.52
f1 (ppm)

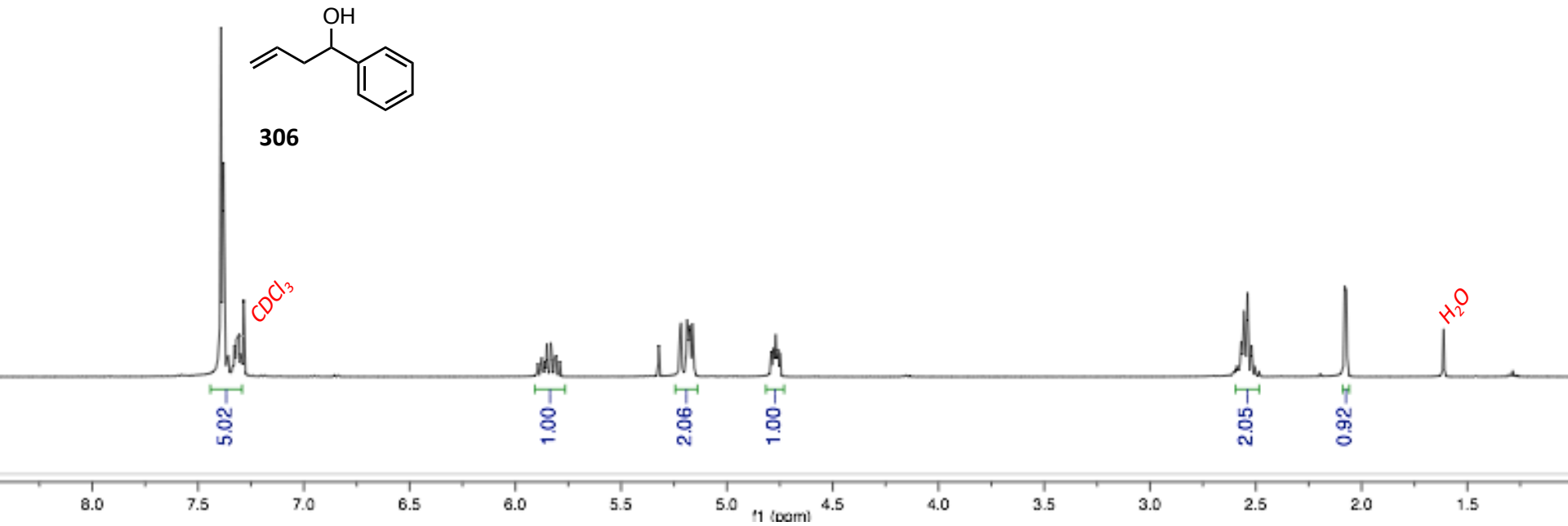
OH
306
CDCl3
H2O
5.02
1.00
2.06
1.00
2.05
0.92
8.0
7.5
7.0
6.5
6.0
5.5
5.0
4.5
4.0
3.5
3.0
2.5
2.0
1.5
f1 (ppm)

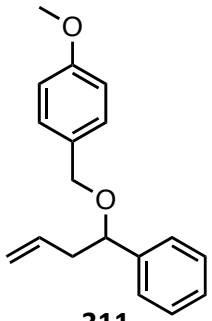

311

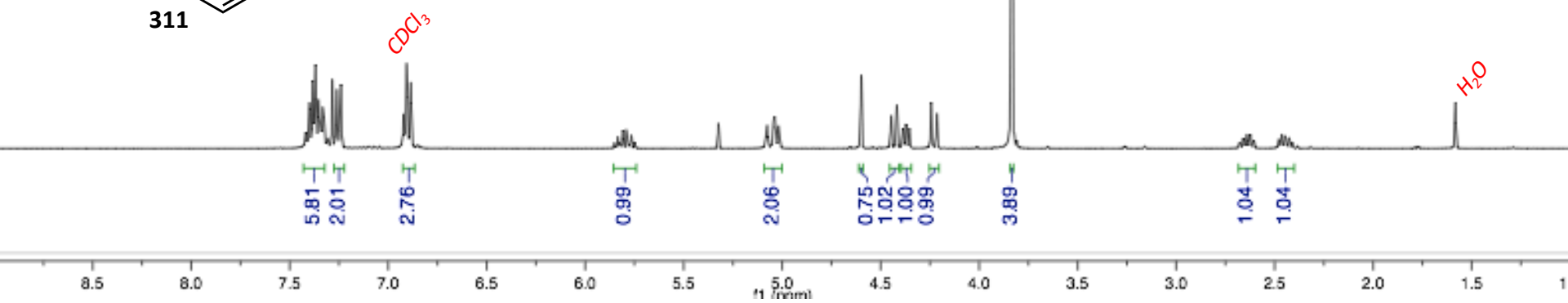
CDCl3
H2O
5.81
2.01
2.76
0.99
2.06
0.75
1.02
1.00
0.99
3.89
1.04
1.04
8.5
8.0
7.5
7.0
6.5
6.0
5.5
5.0
4.5
4.0
3.5
3.0
2.5
2.0
1.5

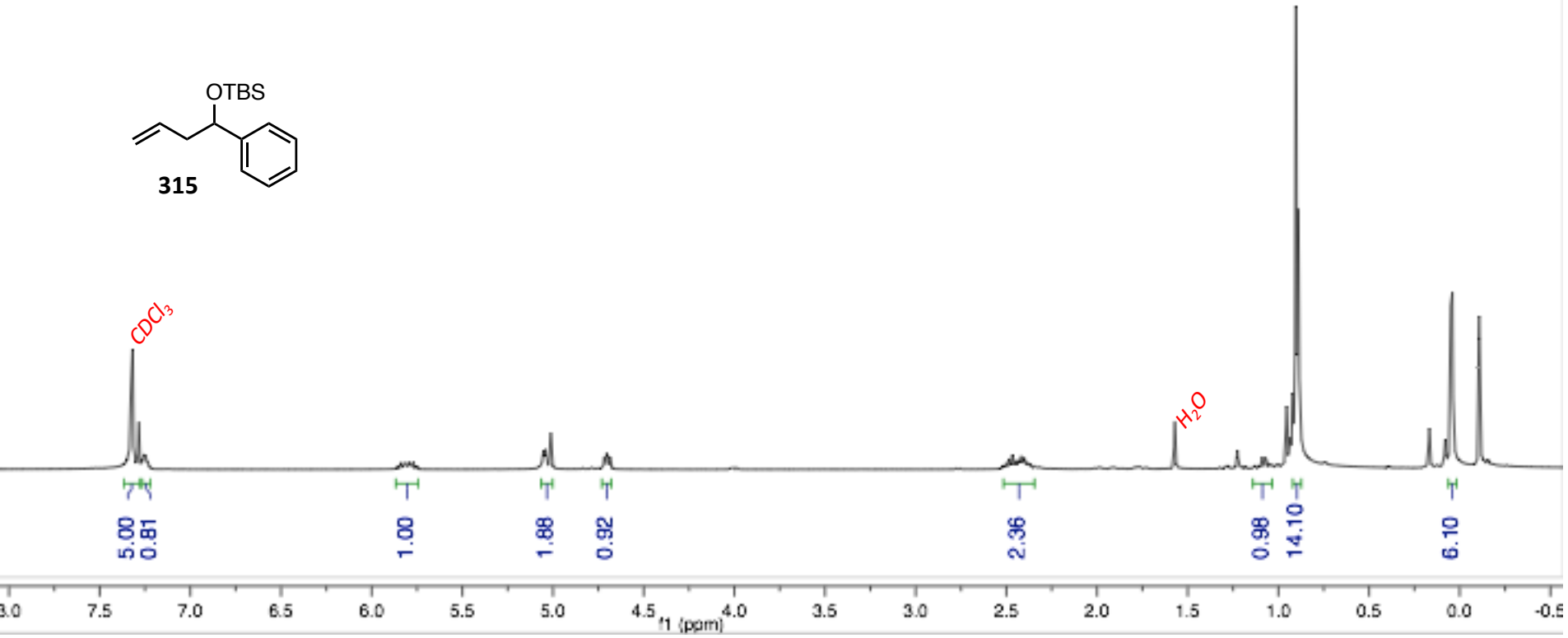
OTBS
315
CDCl3
H2O
5.00
0.81
1.00
1.88
0.92
2.36
0.98
14.10
6.10
f1 (ppm)

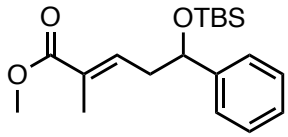
O
OTBS
O

318

CDCl3
4.45
0.91
1.00
1.09
3.22
2.29
2.77
9.70
3.13
3.14
8.0
7.5
7.0
6.5
6.0
5.5
5.0
4.5
4.0
3.5
3.0
2.5
2.0
1.5
1.0
0.5
0.0
f1 (ppm)

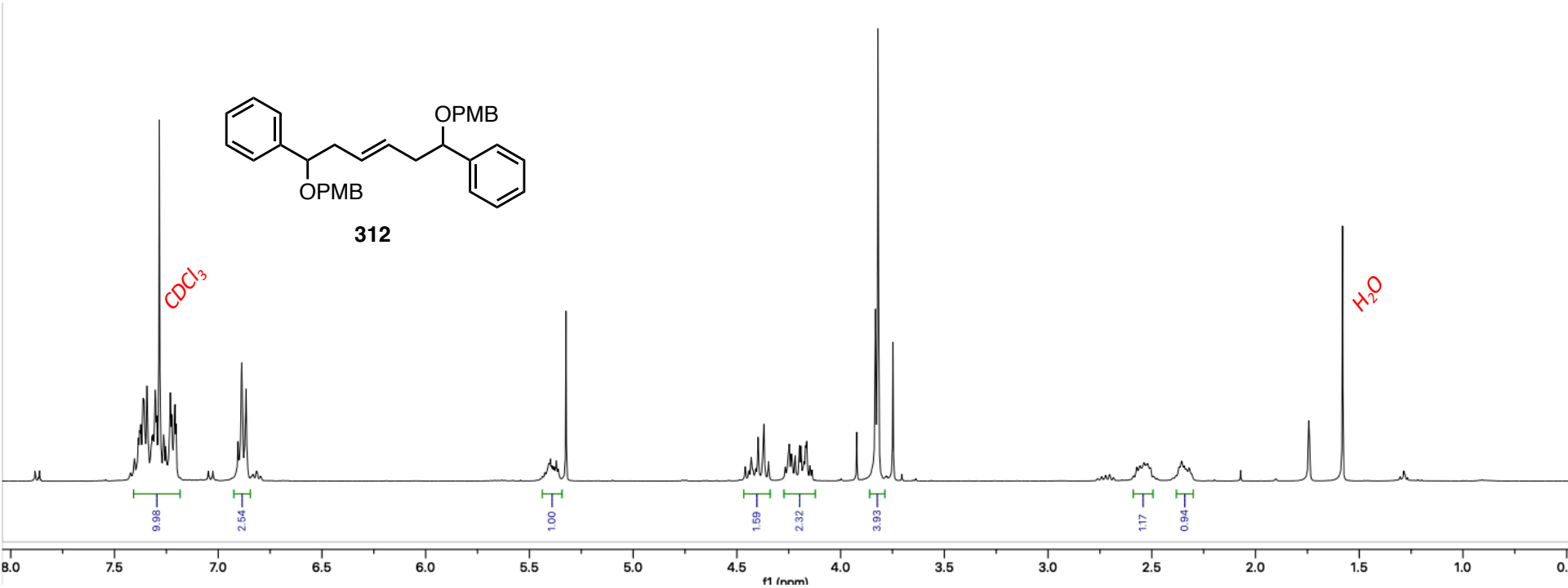
OPMB
OPMB
312
CDCl3
H2O
9.98
2.54
1.00
1.59
2.32
3.93
1.17
0.94
8.0
7.5
7.0
6.5
6.0
5.5
5.0
4.5
4.0
3.5
3.0
2.5
2.0
1.5
1.0
f1 (ppm)

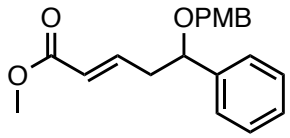
O
OPMB
O

314

CDCl3
H2O
5.33
1.92
1.09
1.96
0.83
1.98
1.07
3.31
2.75
1.00
1.00
7.5
7.0
6.5
6.0
5.5
5.0
4.5
4.0
3.5
3.0
2.5
2.0
1.5
f1 (ppm)

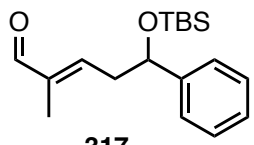
O
OTBS

317

CDCl3
H2O
0.96
3.87
1.43
1.00
0.97
1.94
2.99
0.77
9.54
2.94
2.98
9.5
9.0
8.5
8.0
7.5
7.0
6.5
6.0
5.5
5.0
4.5
4.0
3.5
3.0
2.5
2.0
1.5
1.0
0.5
0.0
f1 (ppm)

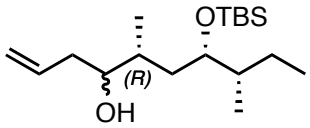
OTBS
(R)
OH

322

CDCl3
H2O
1.00
2.03
1.09
1.01
1.11
1.36
2.22
2.31
2.44
1.08
2.87
12.68
2.77
5.69
7.5
7.0
6.5
6.0
5.5
5.0
4.5
4.0
3.5
3.0
2.5
2.0
1.5
1.0
0.5
0.0
-0.5
f1 (ppm)

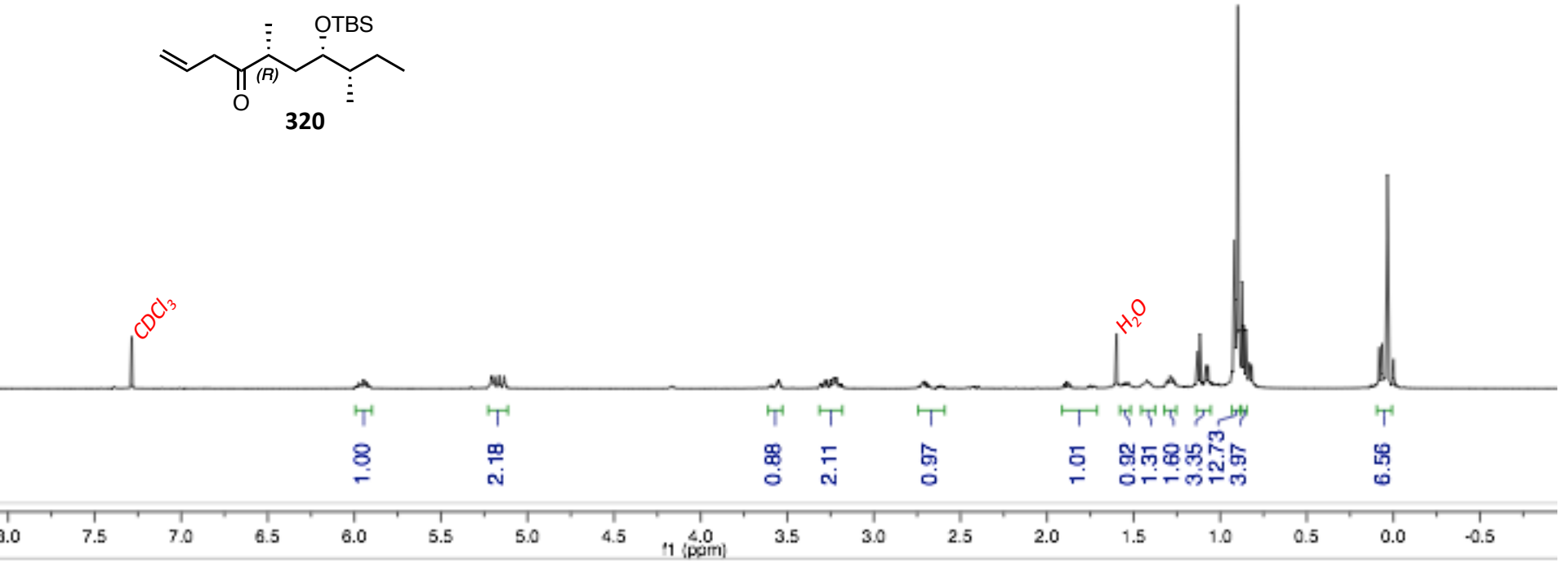
OTBS
(R)
O
320
CDCl3
H2O
1.00
2.18
0.88
2.11
0.97
1.01
0.92
1.31
1.60
3.35
12.73
3.97
6.56
f1 (ppm)

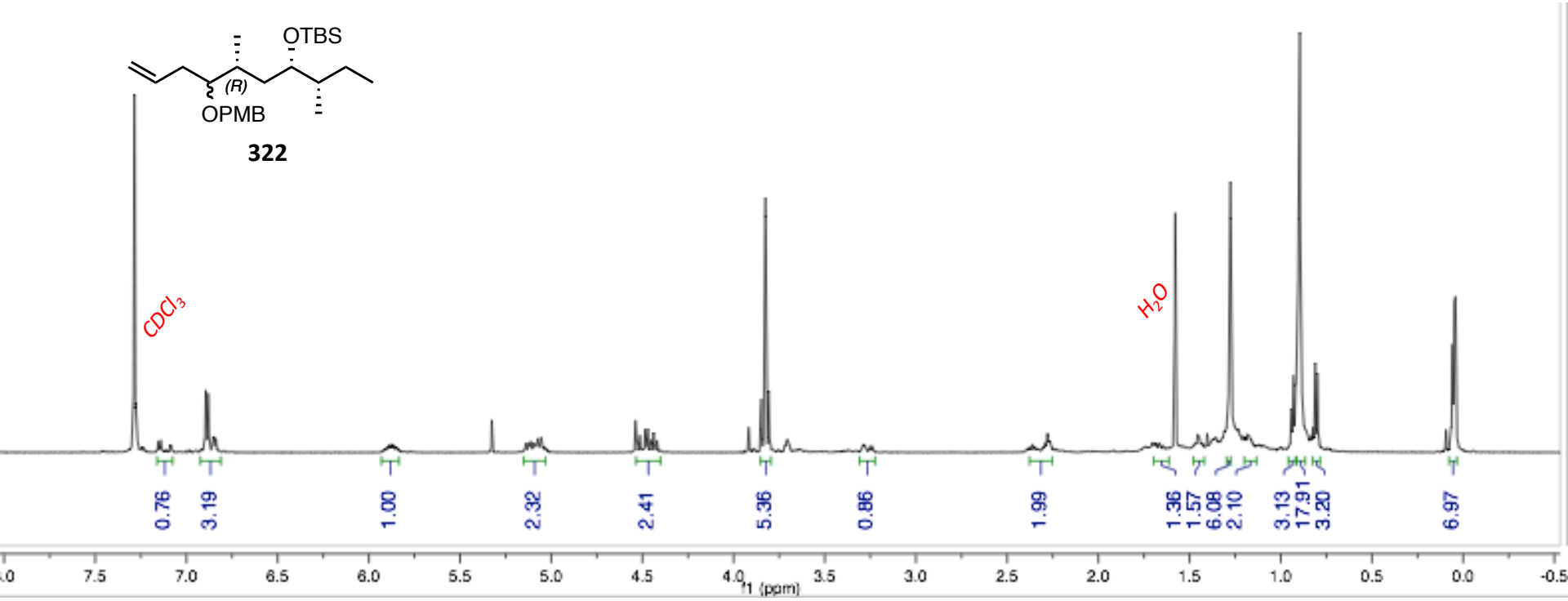
OTBS
(R)
OPMB
322
CDCl3
H2O
0.76
3.19
1.00
2.32
2.41
5.36
0.86
1.99
1.36
1.57
6.08
2.10
3.13
17.91
3.20
6.97
7.5
7.0
6.5
6.0
5.5
5.0
4.5
4.0
3.5
3.0
2.5
2.0
1.5
1.0
0.5
0.0
-0.5
f1 (ppm)

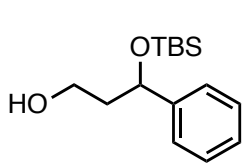
OTBS
HO

CDCl3
5.94
1.00
2.51
1.08
2.43
9.82
3.43
3.61
8.5
8.0
7.5
7.0
6.5
6.0
5.5
5.0
4.5
4.0
3.5
3.0
2.5
2.0
1.5
1.0
0.5
0.0
-0.5
f1 (ppm)

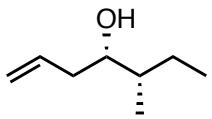
OH

CDCl3
1.00
1.90
1.72
1.02
1.11
2.86
1.80
7.19
8.5
8.0
7.5
7.0
6.5
6.0
5.5
5.0
4.5
4.0
3.5
3.0
2.5
2.0
1.5
1.0
0.5
f1 (ppm)

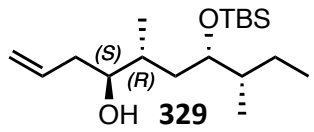
OTBS
(S)
(R)
OH

329

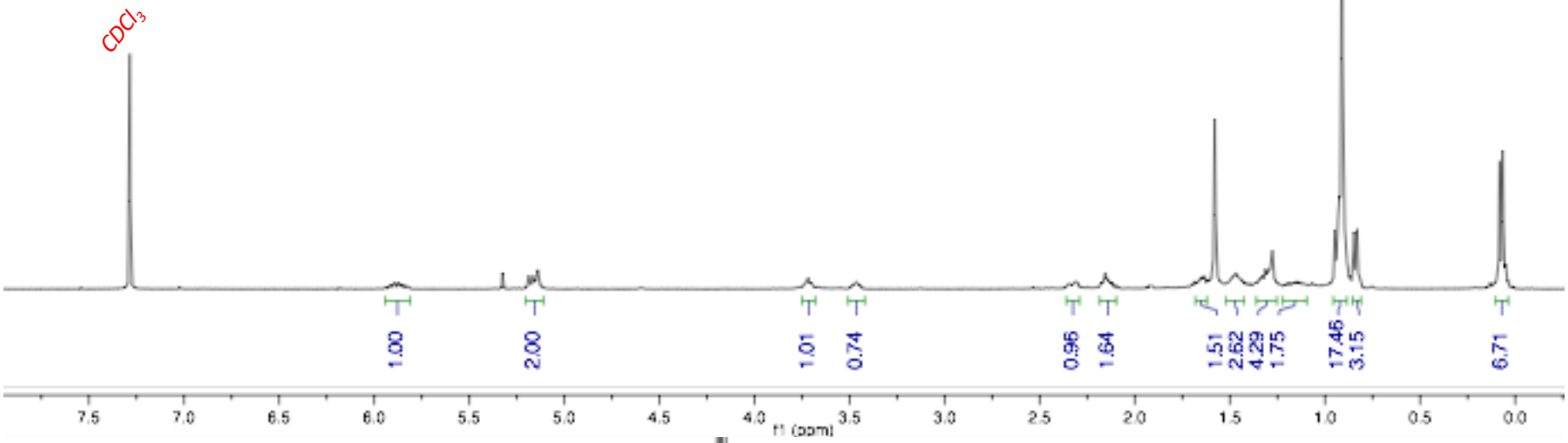
CDCl3
1.00
2.00
1.01
0.74
0.96
1.64
1.51
2.62
4.29
1.75
17.46
3.15
6.71
f1 (ppm)

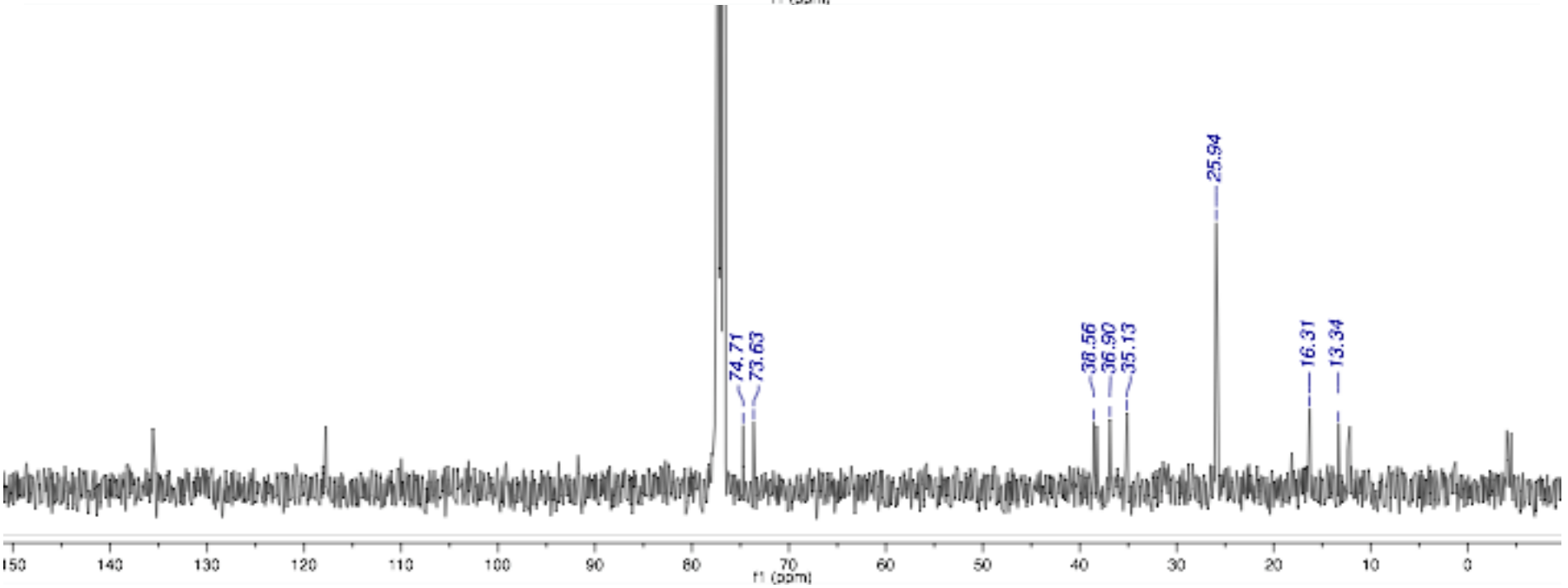
74.71
73.63
36.56
36.50
35.13
25.94
16.31
13.34
f1 (ppm)

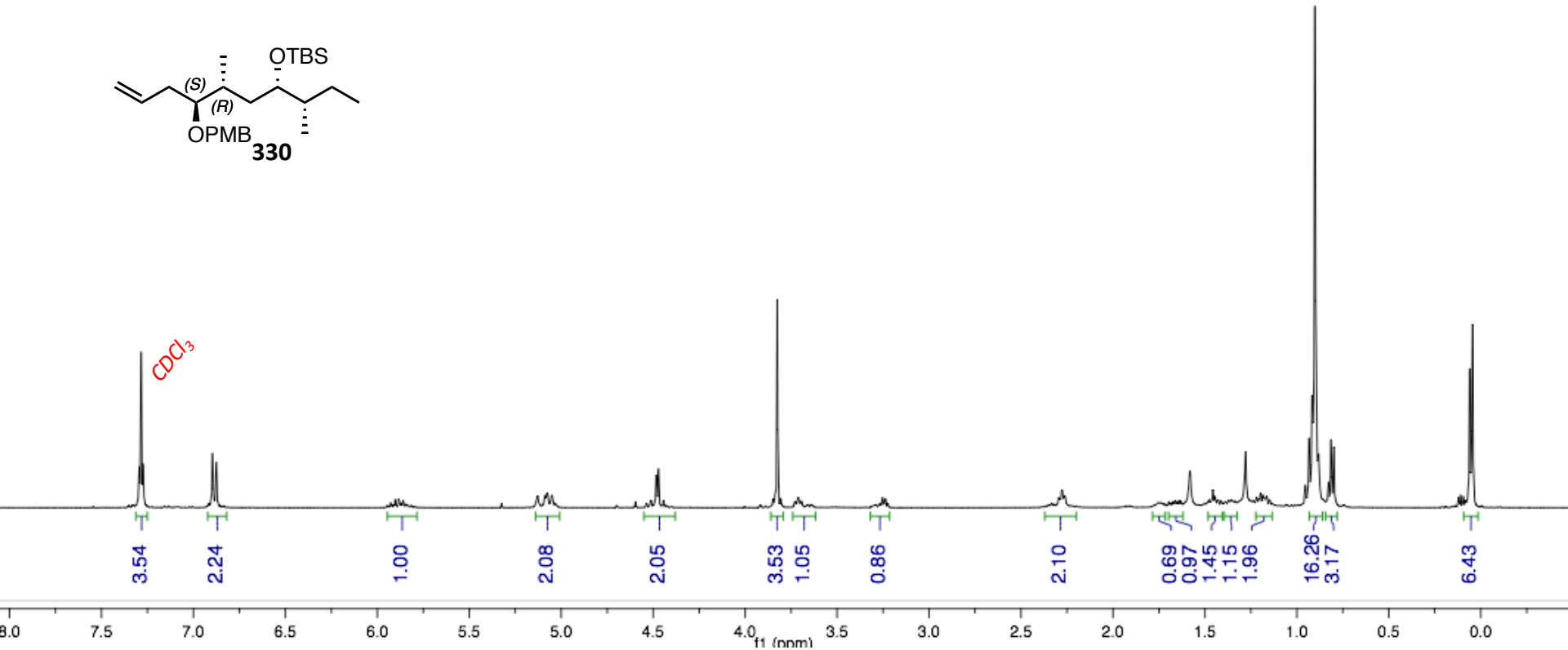
OTBS
(S)
(R)
OPMB
330
CDCl3
3.54
2.24
1.00
2.08
2.05
3.53
1.05
0.86
2.10
0.69
0.97
1.45
1.15
1.96
16.26
3.17
6.43
8.0
7.5
7.0
6.5
6.0
5.5
5.0
4.5
4.0
3.5
3.0
2.5
2.0
1.5
1.0
0.5
0.0
f1 (ppm)

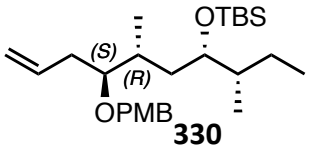
OTBS
(S)
(R)
OPMB

330

CH2Cl2
MeOD
1.96
2.07
1.00
2.24
2.18
3.19
1.34
0.76
2.18
2.05
1.35
1.27
1.90
15.47
2.95
6.18
f1 (ppm)

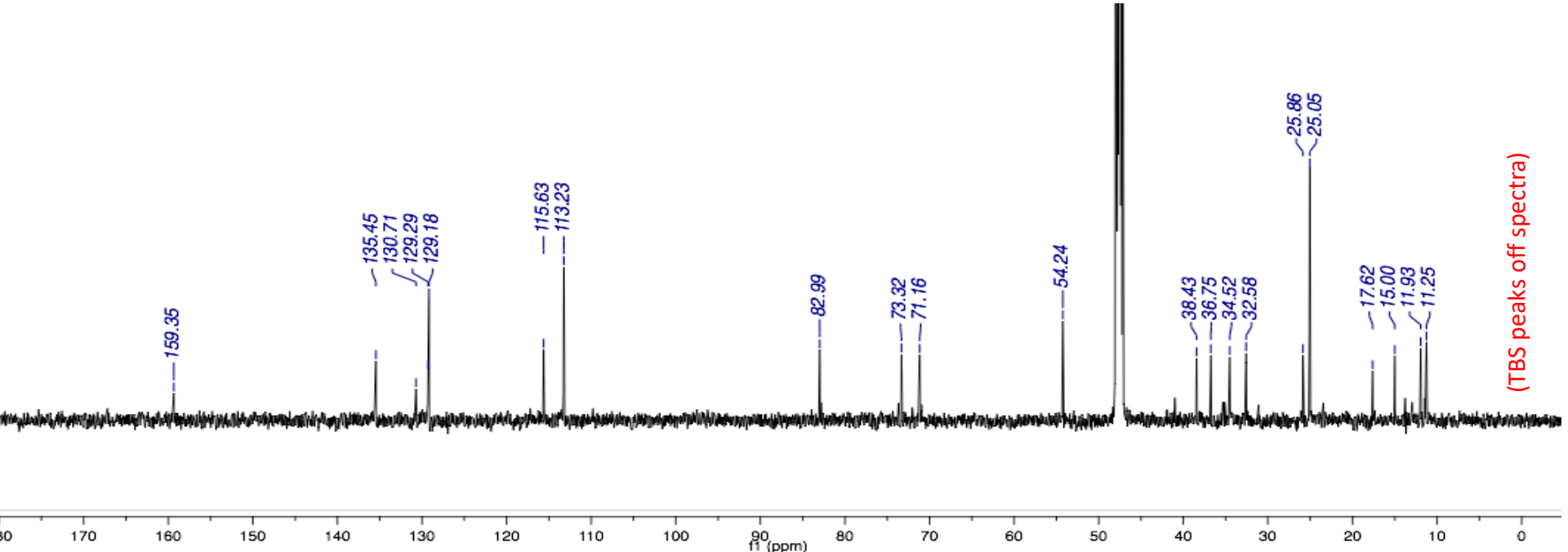
159.35
135.45
130.71
129.29
129.18
115.63
113.23
82.99
73.32
71.16
54.24
38.43
36.75
34.52
32.58
25.86
25.05
17.62
15.00
11.93
11.25
(TBS peaks off spectra)
f1 (ppm)

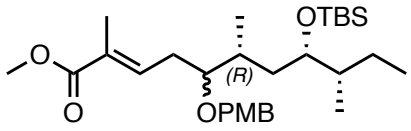
OTBS
O
(R)
O
OPMB

323

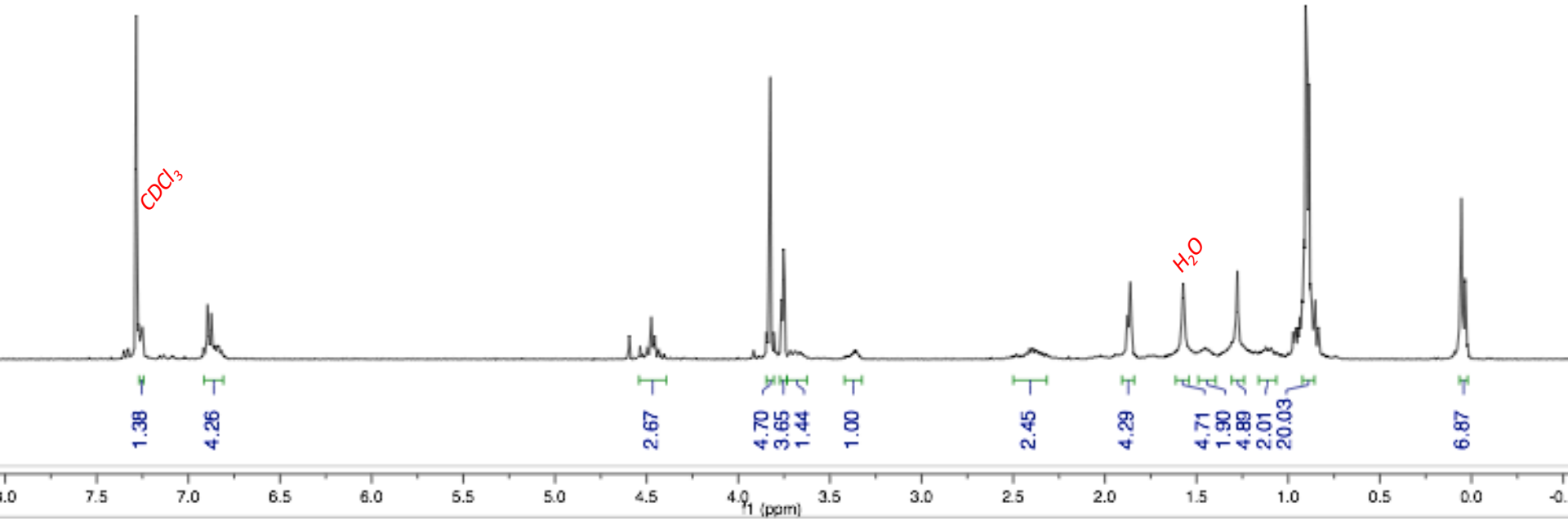
CDCl3
H2O
1.38
4.26
2.67
4.70
3.65
1.44
1.00
2.45
4.29
4.71
1.90
4.89
2.01
20.03
6.87
7.5
7.0
6.5
6.0
5.5
5.0
4.5
4.0
3.5
3.0
2.5
2.0
1.5
1.0
0.5
0.0
f1 (ppm)

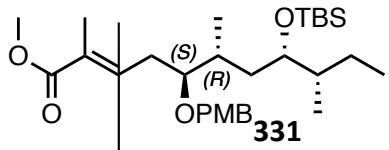
OTBS
O
(S)
(R)
O
OPMB

331

CDCl3
H2O
2.26
2.87
2.13
3.07
3.05
1.32
1.00
2.06
3.03
1.48
1.69
1.85
1.88
2.47
8.93
3.89
3.46
6.28
f1 (ppm)

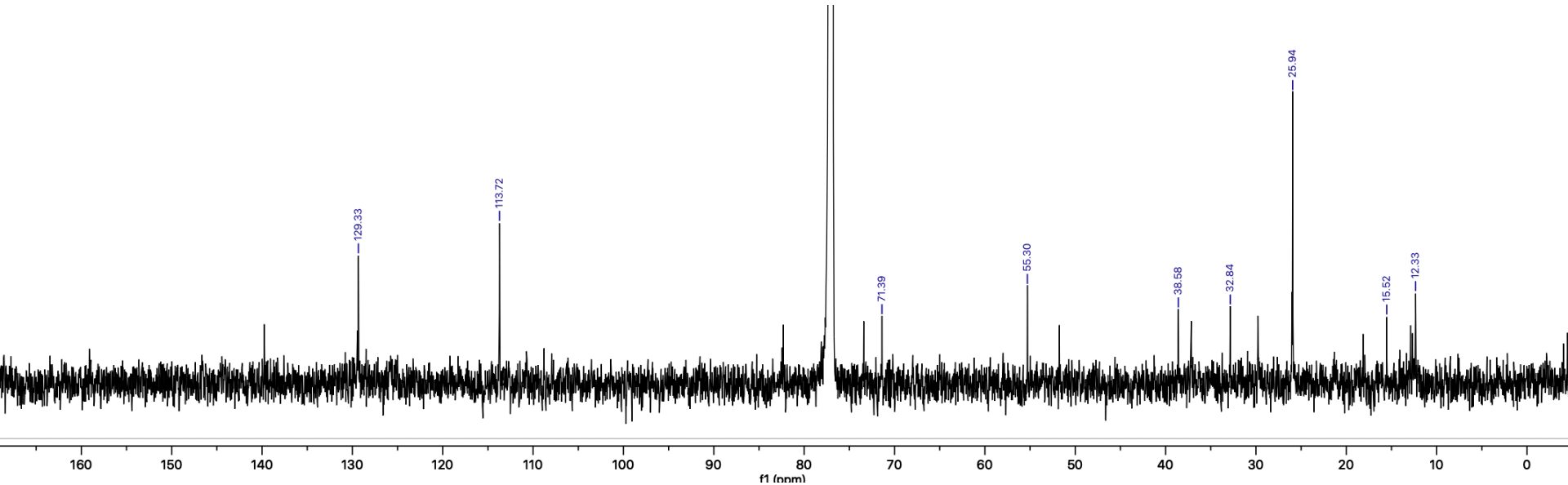
129.33
113.72
71.39
55.30
38.58
32.84
25.94
15.52
12.33
f1 (ppm)

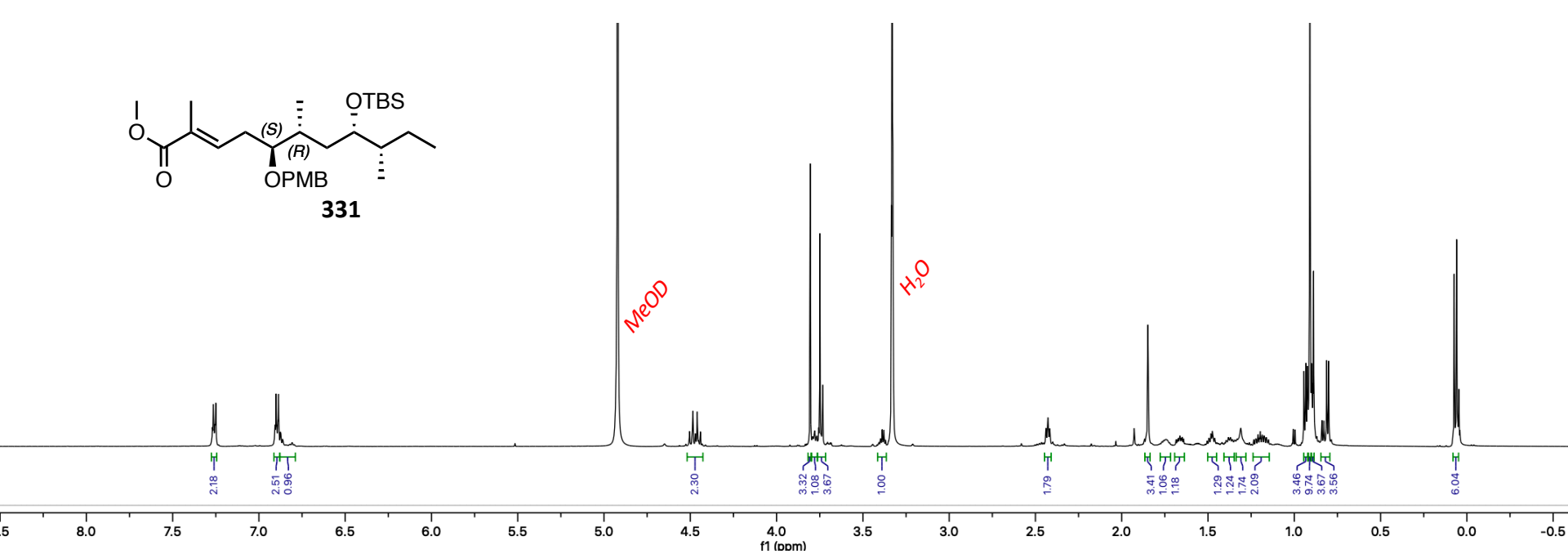
OTBS
O
(S)
(R)
O
OPMB
331
MeOD
H2O
2.18
2.51
0.96
2.30
3.32
1.08
3.67
1.00
1.79
3.41
1.06
1.18
1.29
1.24
1.74
2.09
3.46
9.74
3.67
3.56
6.04
8.0
7.5
7.0
6.5
6.0
5.5
5.0
4.5
4.0
3.5
3.0
2.5
2.0
1.5
1.0
0.5
0.0
-0.5
f1 (ppm)

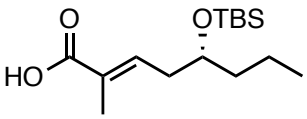
O
OTBS
HO

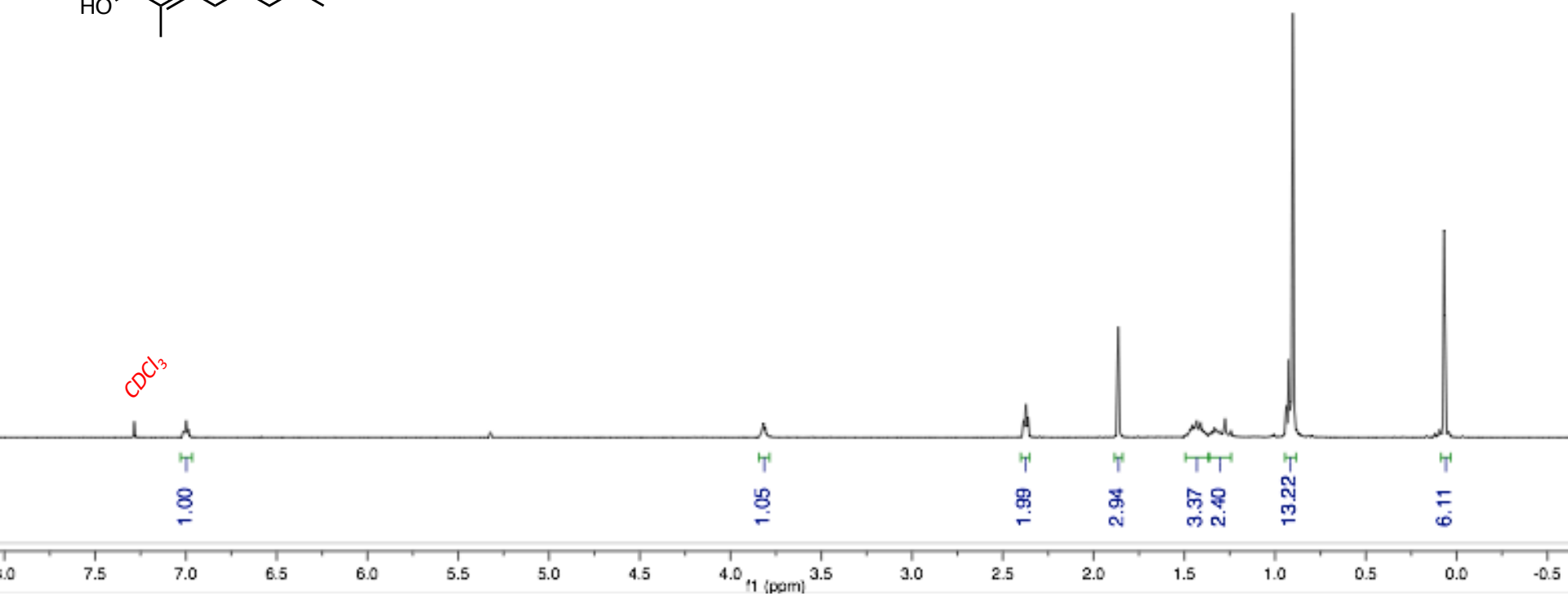
CDCl3
1.00
1.05
1.99
2.94
3.37
2.40
13.22
6.11
7.5
7.0
6.5
6.0
5.5
5.0
4.5
4.0
3.5
3.0
2.5
2.0
1.5
1.0
0.5
0.0
-0.5
f1 (ppm)

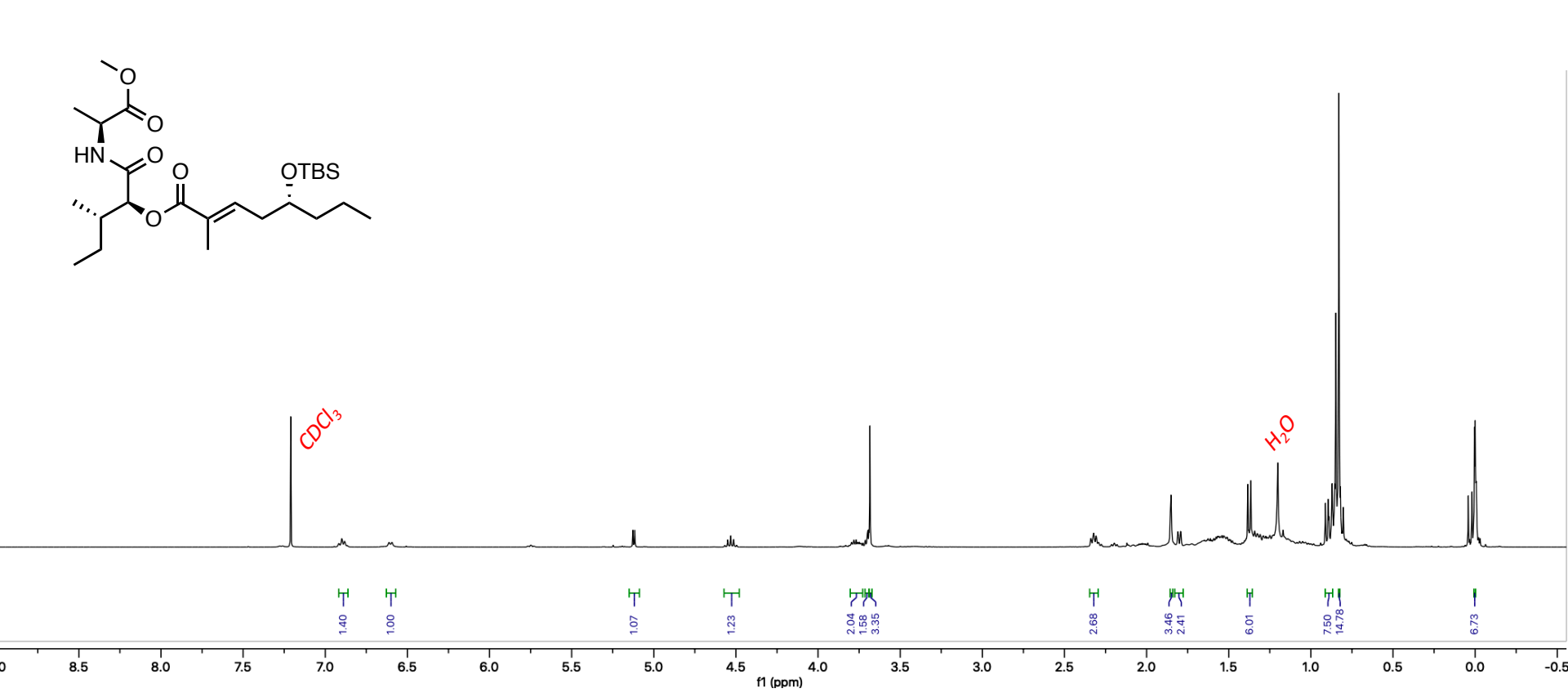
O
O
HN
O
O
O
OTBS
CDCl3
H2O
1.40
1.00
1.07
1.23
2.04
1.58
3.35
2.68
3.46
2.41
6.01
7.50
14.78
6.73
8.5
8.0
7.5
7.0
6.5
6.0
5.5
5.0
4.5
4.0
3.5
3.0
2.5
2.0
1.5
1.0
0.5
0.0
-0.5
f1 (ppm)

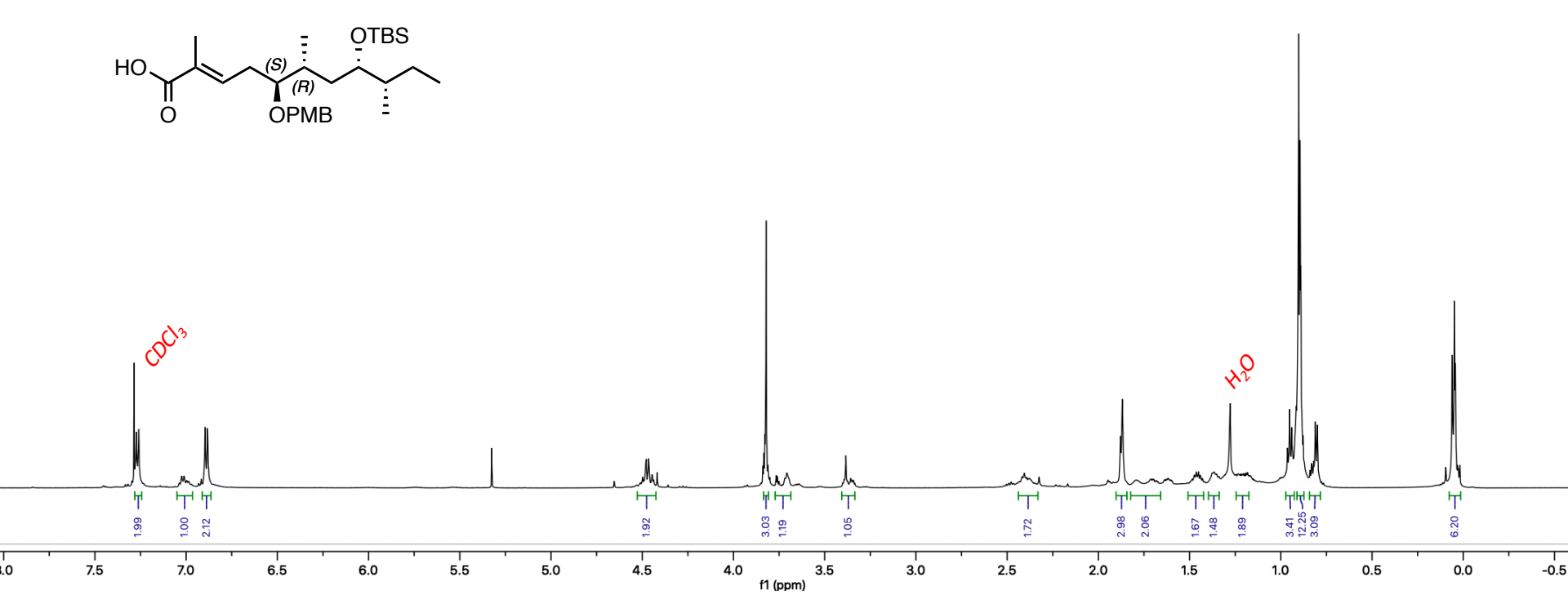
HO
O
(S)
(R)
OPMB
OTBS
CDCl3
H2O
1.99
1.00
2.12
1.92
3.03
1.19
1.05
1.72
2.98
2.06
1.67
1.48
1.89
3.41
12.25
3.09
6.20
7.5
7.0
6.5
6.0
5.5
5.0
4.5
4.0
3.5
3.0
2.5
2.0
1.5
1.0
0.5
0.0
-0.5
f1 (ppm)

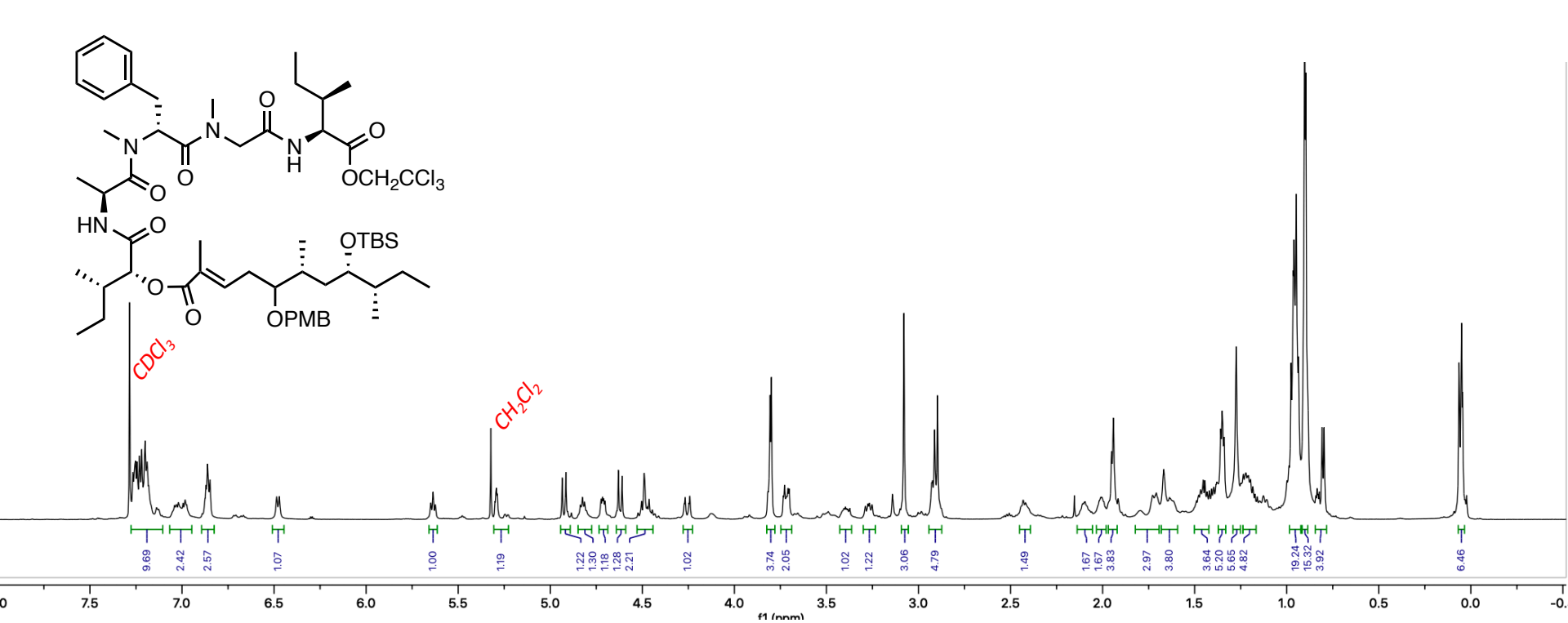
OCH2CCl3
OTBS
OPMB
HN
CDCl3
CH2Cl2
9.69
2.42
2.57
1.07
1.00
1.19
1.22
1.30
1.18
1.28
2.21
1.02
3.74
2.05
1.02
1.22
3.06
4.79
1.49
1.67
1.67
3.83
2.97
3.80
3.64
5.20
5.65
4.82
19.24
15.32
3.92
6.46
7.5
7.0
6.5
6.0
5.5
5.0
4.5
4.0
3.5
3.0
2.5
2.0
1.5
1.0
0.5
0.0
f1 (ppm)

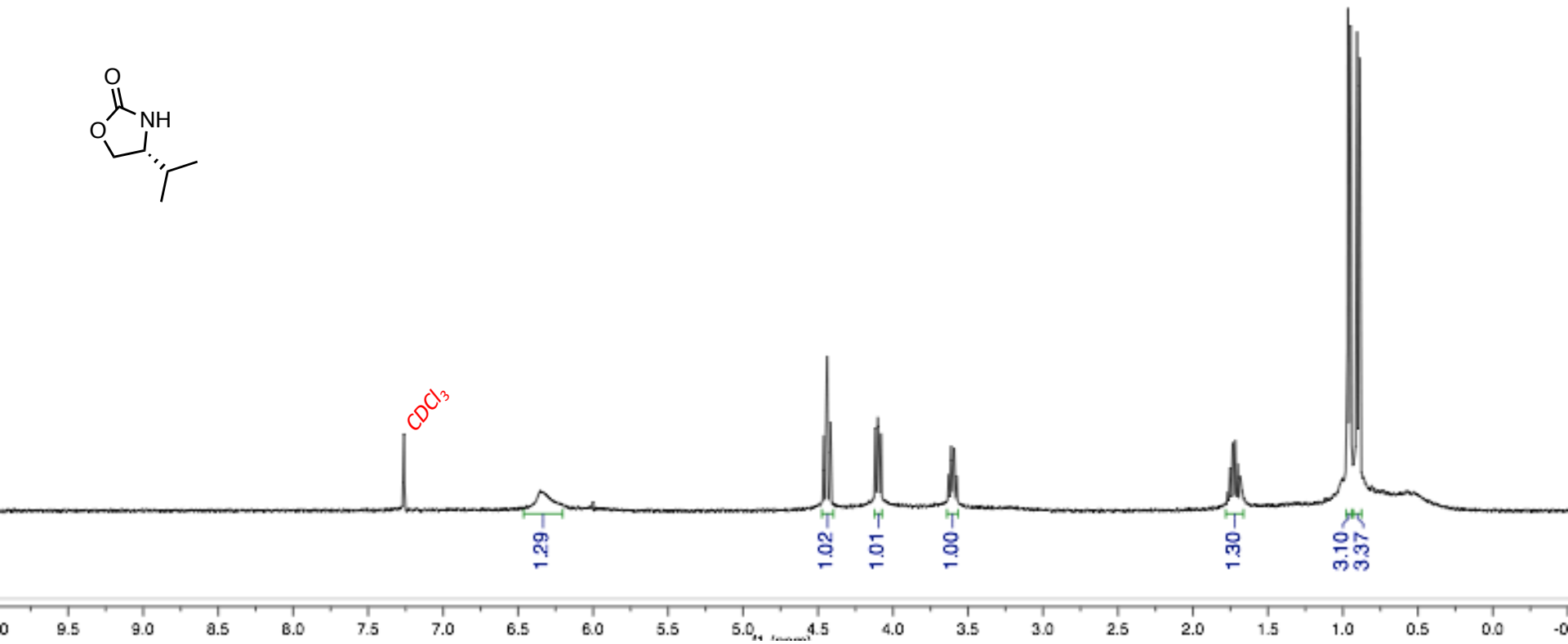
O
NH
O
CDCl3
1.29
1.02
1.01
1.00
1.30
3.10
3.37
9.5
9.0
8.5
8.0
7.5
7.0
6.5
6.0
5.5
5.0
4.5
4.0
3.5
3.0
2.5
2.0
1.5
1.0
0.5
0.0

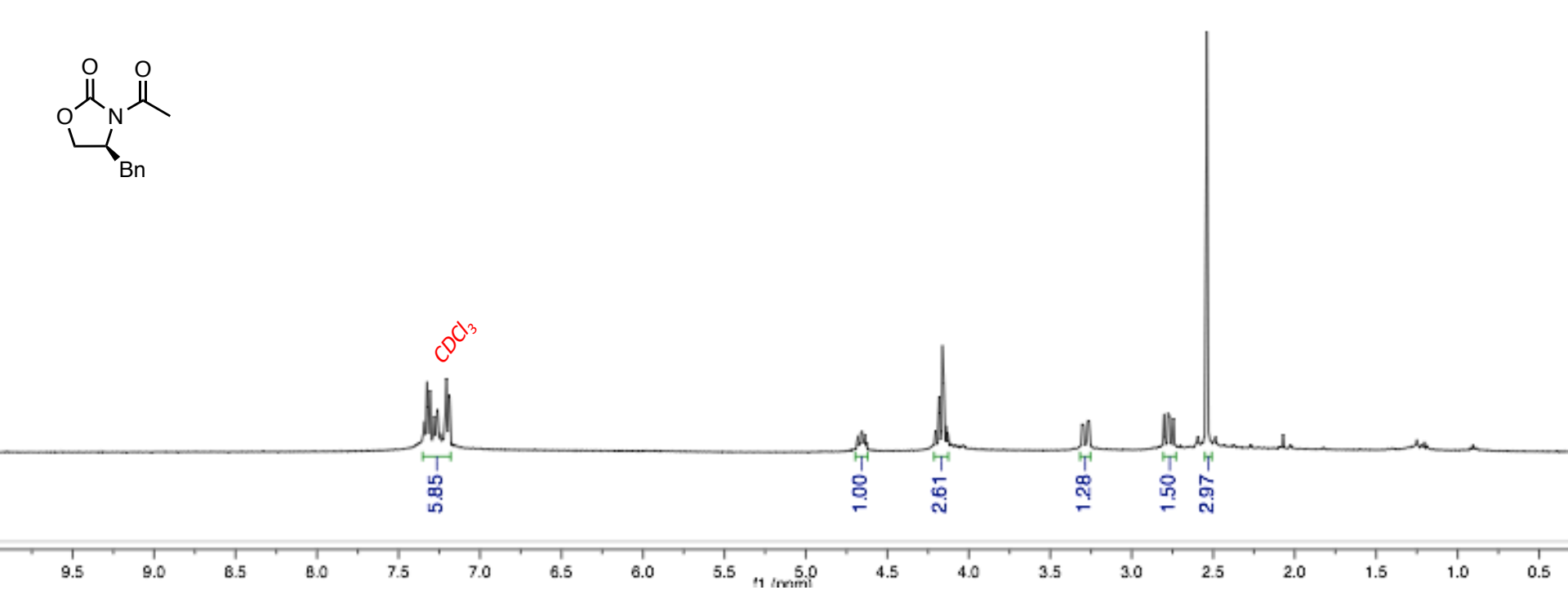
O
O
O
N
Bn
CDCl3
5.85
1.00
2.61
1.28
1.50
2.97
9.5
9.0
8.5
8.0
7.5
7.0
6.5
6.0
5.5
5.0
4.5
4.0
3.5
3.0
2.5
2.0
1.5
1.0
0.5
f1 (ppm)

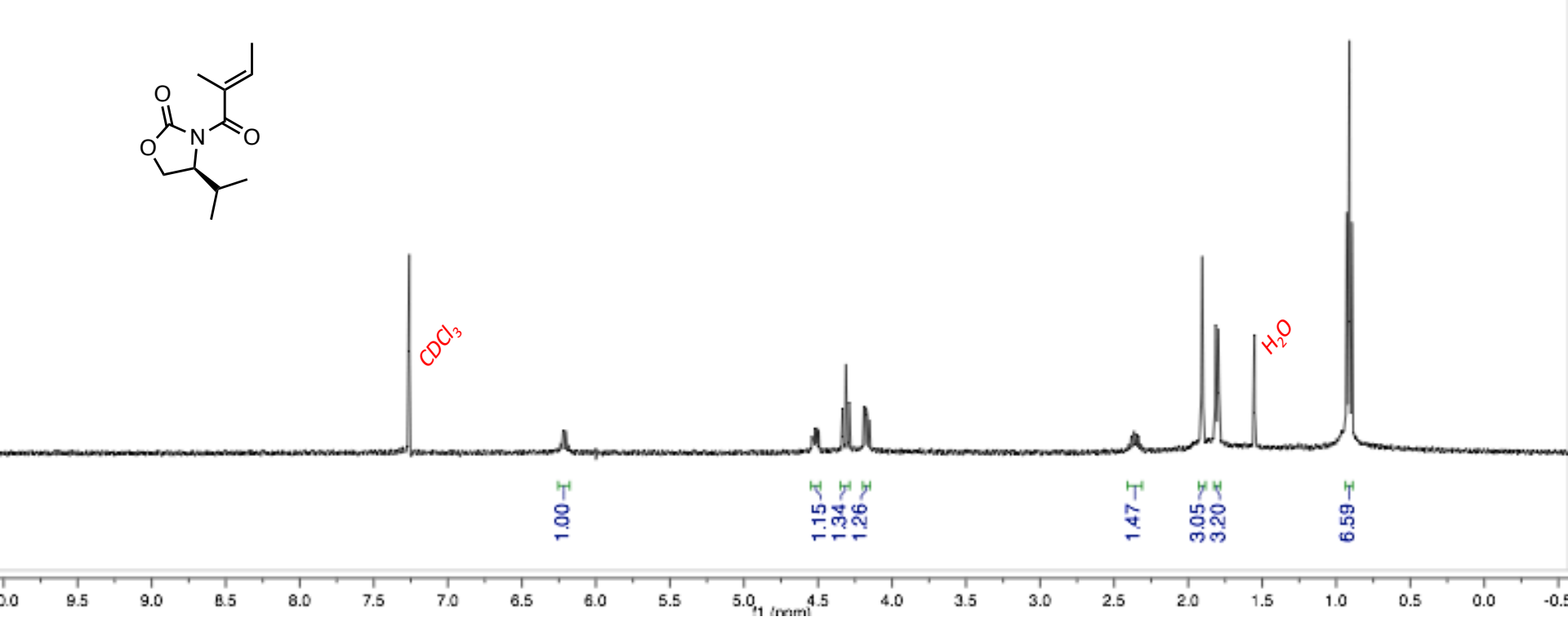
O
N
O
O
CDCl3
H2O
1.00
1.15
1.34
1.26
1.47
3.05
3.20
6.59
f1 (ppm)

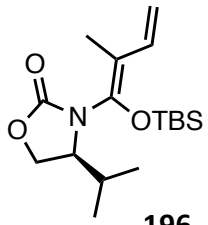
O
N
O
OTBS

196

CDCl3
H2O
1.00
1.82
1.58
1.65
2.52
1.70
1.09
1.12
2.67
9.08
14.43
5.88
9.5
9.0
8.5
8.0
7.5
7.0
6.5
6.0
5.5
5.0
4.5
4.0
3.5
3.0
2.5
2.0
1.5
1.0
0.5
0.0
-0.5

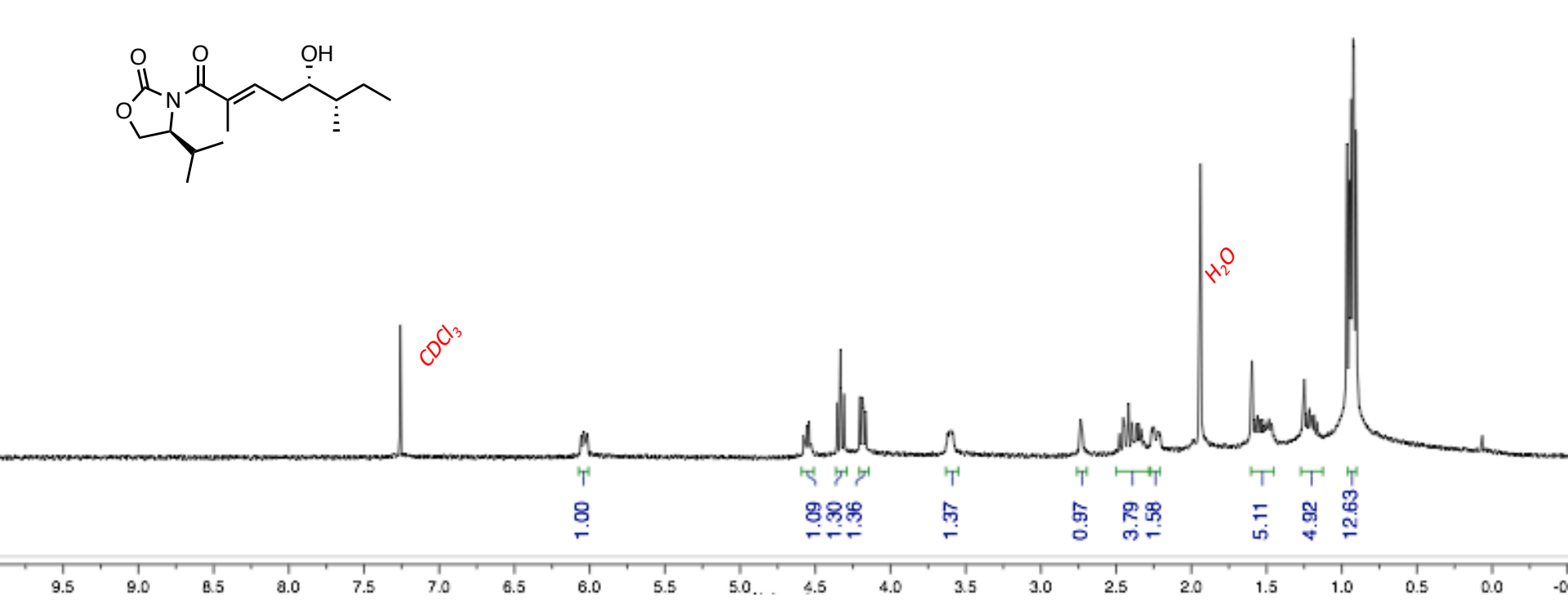
O
O
OH
N
O
CDCl3
H2O
1.00
1.09
1.30
1.36
1.37
0.97
3.79
1.58
5.11
4.92
12.63
9.5
9.0
8.5
8.0
7.5
7.0
6.5
6.0
5.5
5.0
4.5
4.0
3.5
3.0
2.5
2.0
1.5
1.0
0.5
0.0

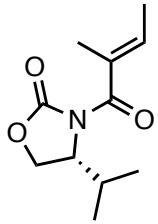
O
O
N
O
O

CDCl3
1.00
1.24
1.42
1.34
1.34
3.28
3.75
6.56
9.5
9.0
8.5
8.0
7.5
7.0
6.5
6.0
5.5
5.0
4.5
4.0
3.5
3.0
2.5
2.0
1.5
1.0
0.5
0.0

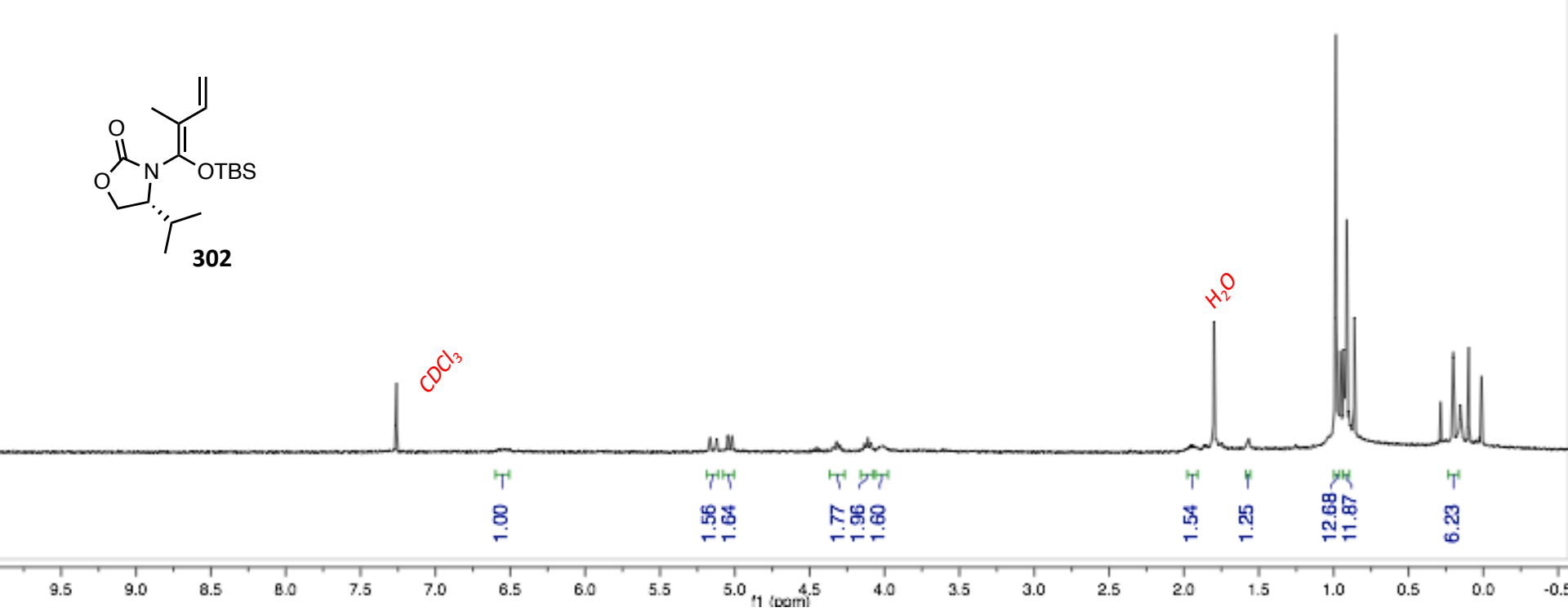
O
N
O
OTBS
302
CDCl3
H2O
1.00
1.56
1.64
1.77
1.96
1.60
1.54
1.25
12.68
11.87
6.23
9.5
9.0
8.5
8.0
7.5
7.0
6.5
6.0
5.5
5.0
4.5
4.0
3.5
3.0
2.5
2.0
1.5
1.0
0.5
0.0
-0.5
f1 (ppm)

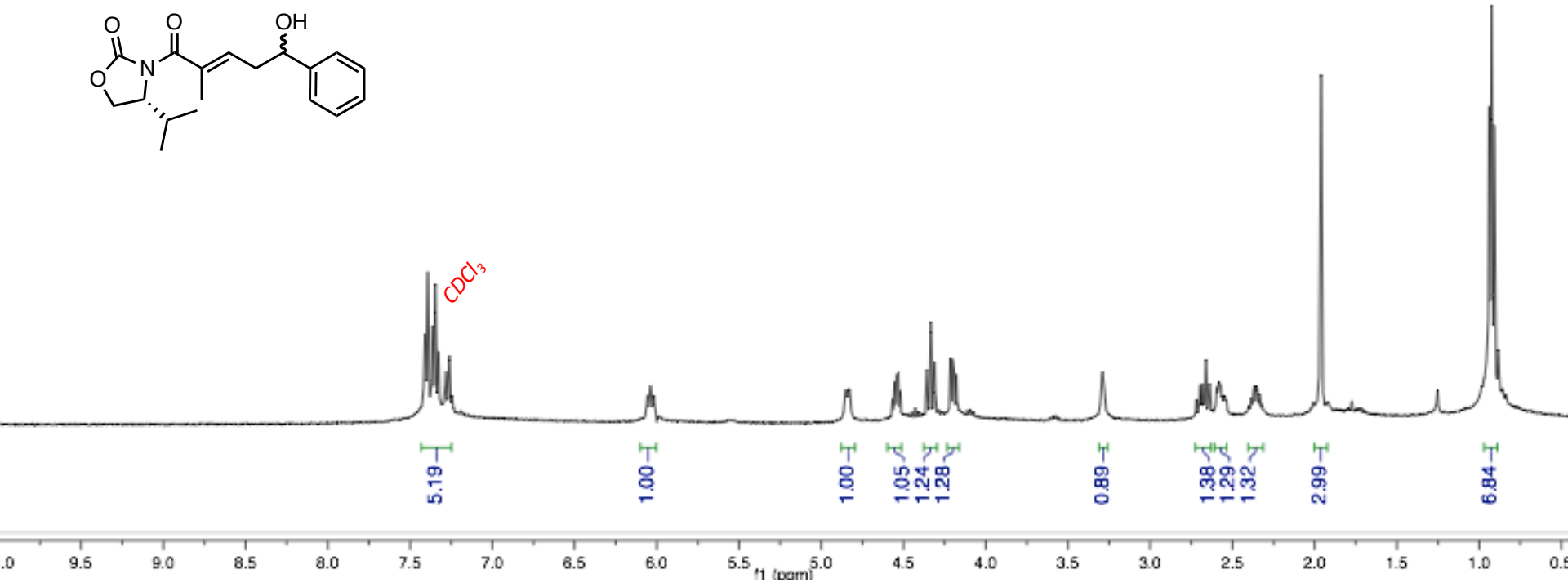
O
O
OH
N
O
CDCl3
5.19
1.00
1.00
1.05
1.24
1.28
0.89
1.38
1.29
1.32
2.99
6.84
f1 (ppm)

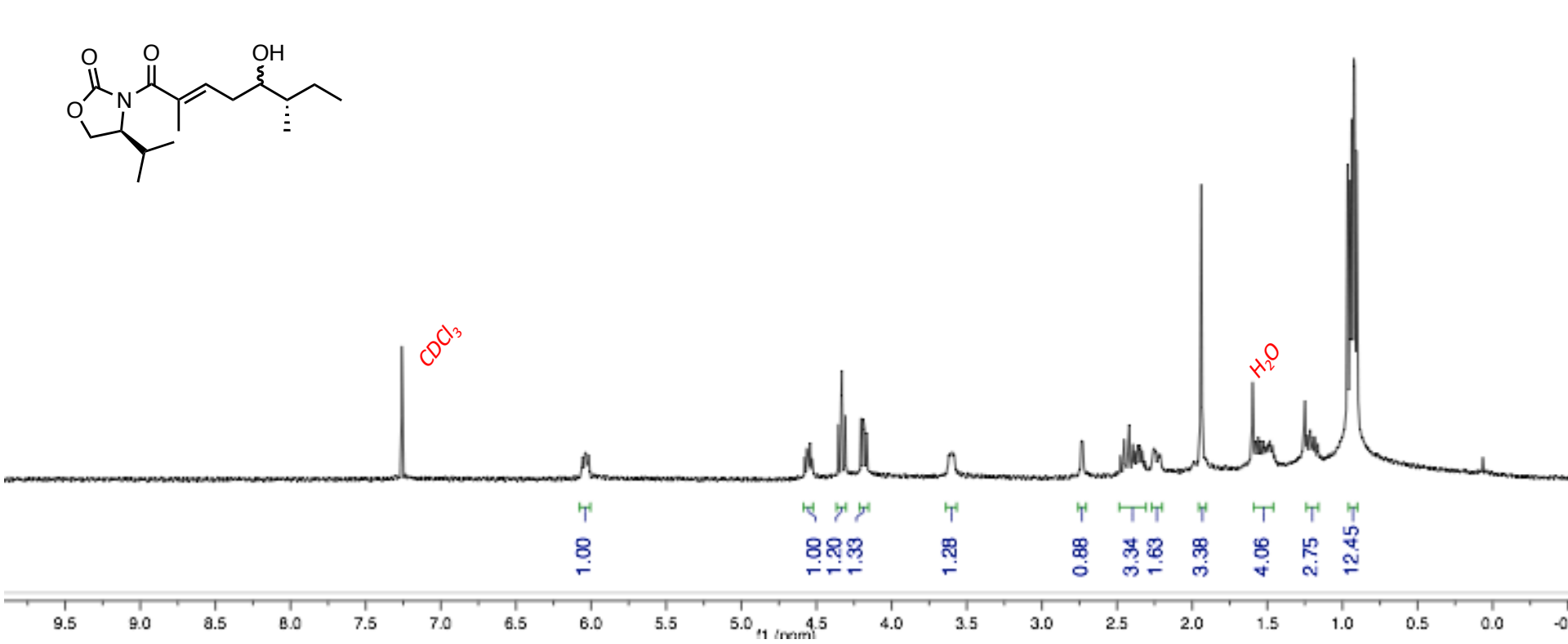
O
O
OH
N
O
CDCl3
H2O
1.00
1.00
1.20
1.33
1.28
0.88
3.34
1.63
3.38
4.06
2.75
12.45
9.5
9.0
8.5
8.0
7.5
7.0
6.5
6.0
5.5
5.0
4.5
4.0
3.5
3.0
2.5
2.0
1.5
1.0
0.5
0.0
f1 (ppm)

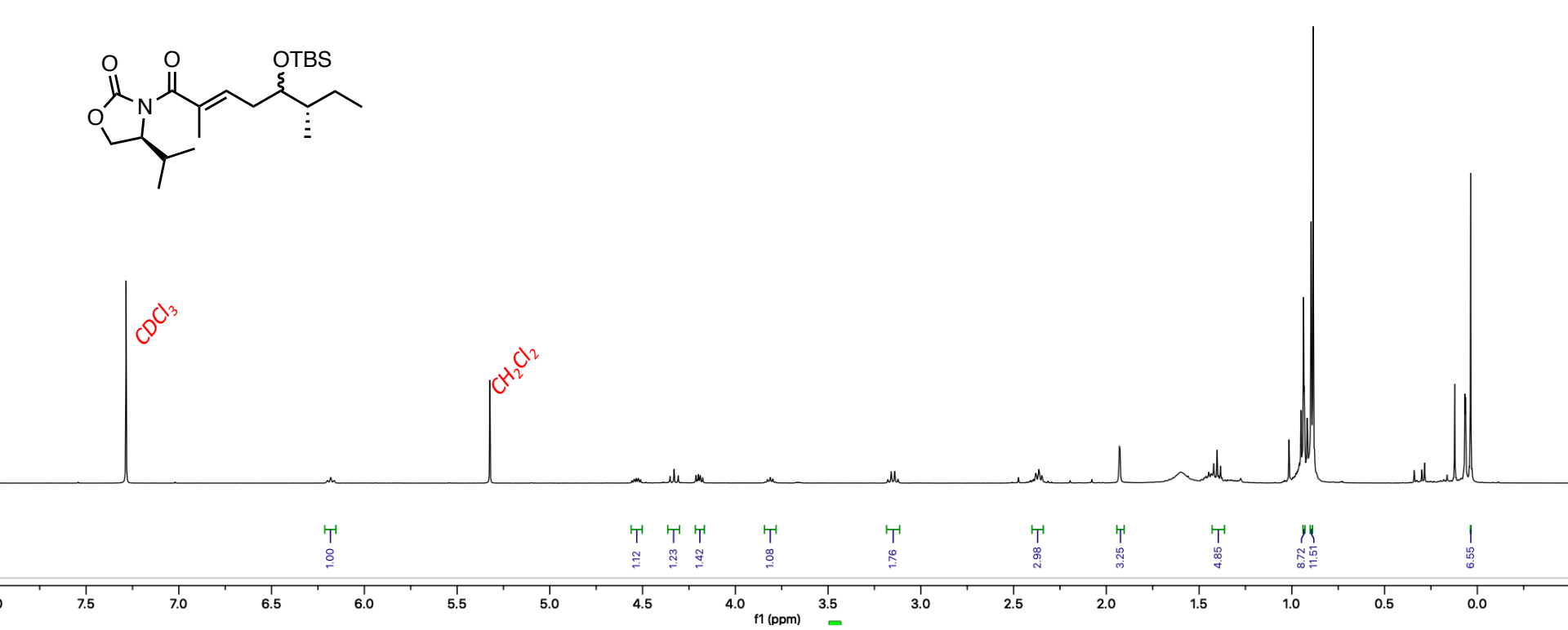
O
O
OTBS
N
O
CDCl3
CH2Cl2
1.00
1.12
1.23
1.42
1.08
1.76
2.98
3.25
4.85
8.72
11.51
6.55
7.5
7.0
6.5
6.0
5.5
5.0
4.5
4.0
3.5
3.0
2.5
2.0
1.5
1.0
0.5
0.0
f1 (ppm)

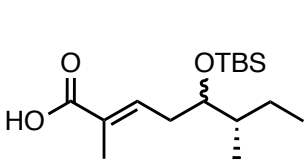
O
OTBS
HO

CDCl3
1.00
1.03
1.99
2.88
3.08
1.64
3.96
9.38
6.14
7.5
7.0
6.5
6.0
5.5
5.0
4.5
4.0
3.5
3.0
2.5
2.0
1.5
1.0
0.5
0.0
f1 (ppm)

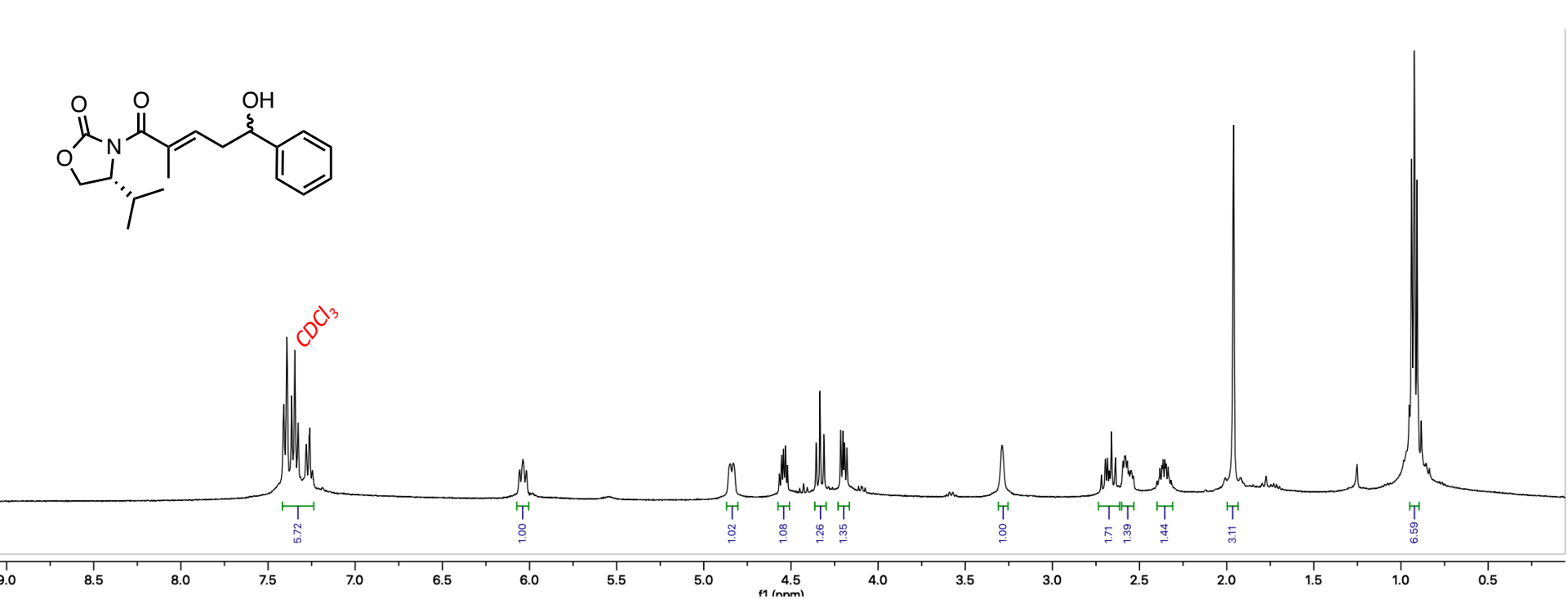
O
O
OH
N
O
CDCl3
5.72
1.00
1.02
1.08
1.26
1.35
1.00
1.71
1.39
1.44
3.11
6.59
9.0
8.5
8.0
7.5
7.0
6.5
6.0
5.5
5.0
4.5
4.0
3.5
3.0
2.5
2.0
1.5
1.0
0.5
f1 (ppm)

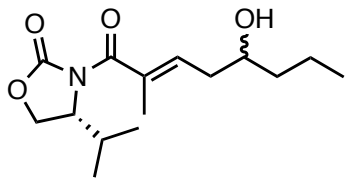
O
O
OH
N
O

CDCl3
1.00
0.96
1.03
1.03
1.03
0.89
2.13
1.02
3.02
0.73
1.17
1.93
1.00
9.00
9.5
9.0
8.5
8.0
7.5
7.0
6.5
6.0
5.5
5.0
4.5
4.0
3.5
3.0
2.5
2.0
1.5
1.0
0.5
f1 (ppm)

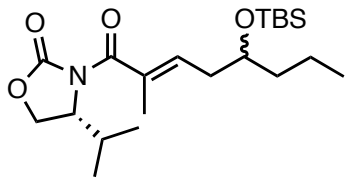
O
O
N
O
OTBS

CDCl3
1.00
0.99
1.03
1.04
1.03
0.87
3.19
3.06
1.74
2.60
1.12
20.01
6.38
f1 (ppm)

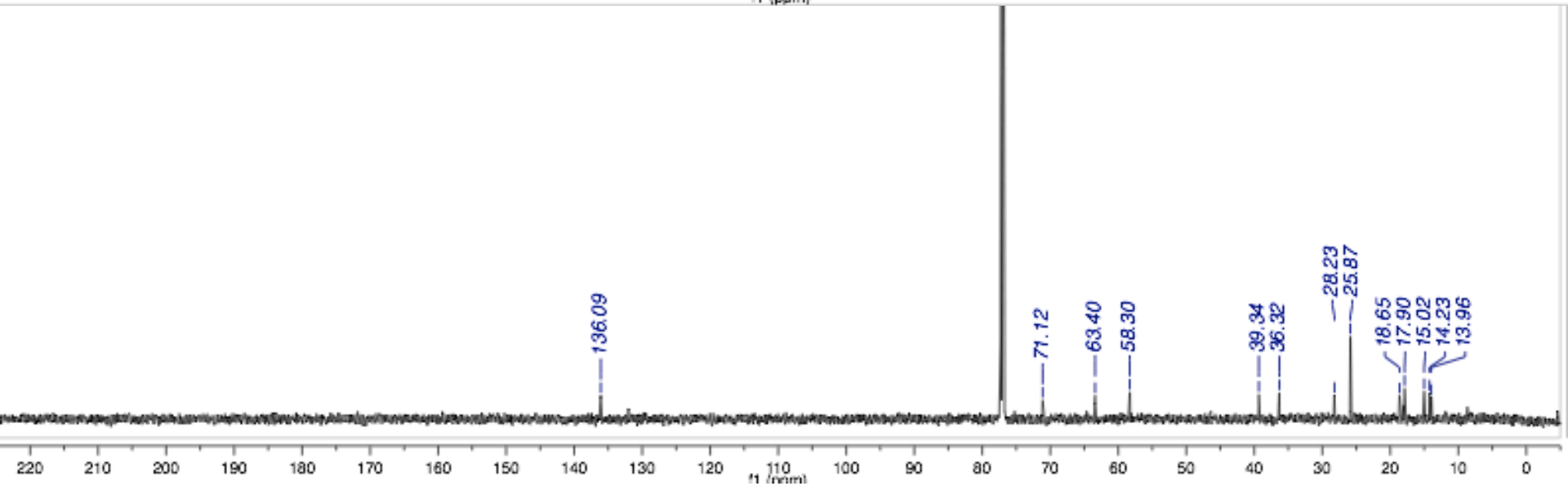
136.09
71.12
63.40
58.30
39.34
36.32
28.23
25.87
18.65
17.90
15.02
14.23
13.96
f1 (ppm)

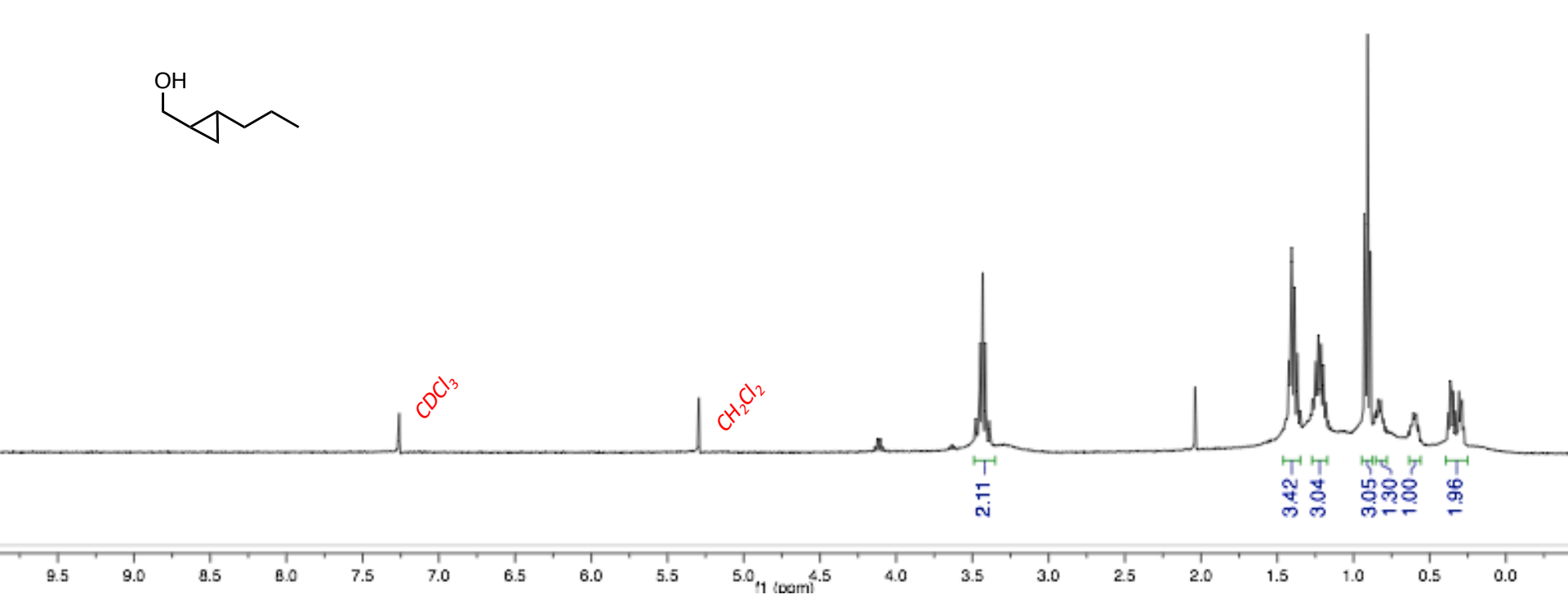
OH
CDCl3
CH2Cl2
2.11
3.42
3.04
3.05
1.30
1.00
1.96
9.5
9.0
8.5
8.0
7.5
7.0
6.5
6.0
5.5
5.0
4.5
4.0
3.5
3.0
2.5
2.0
1.5
1.0
0.5
0.0
f1 (ppm)

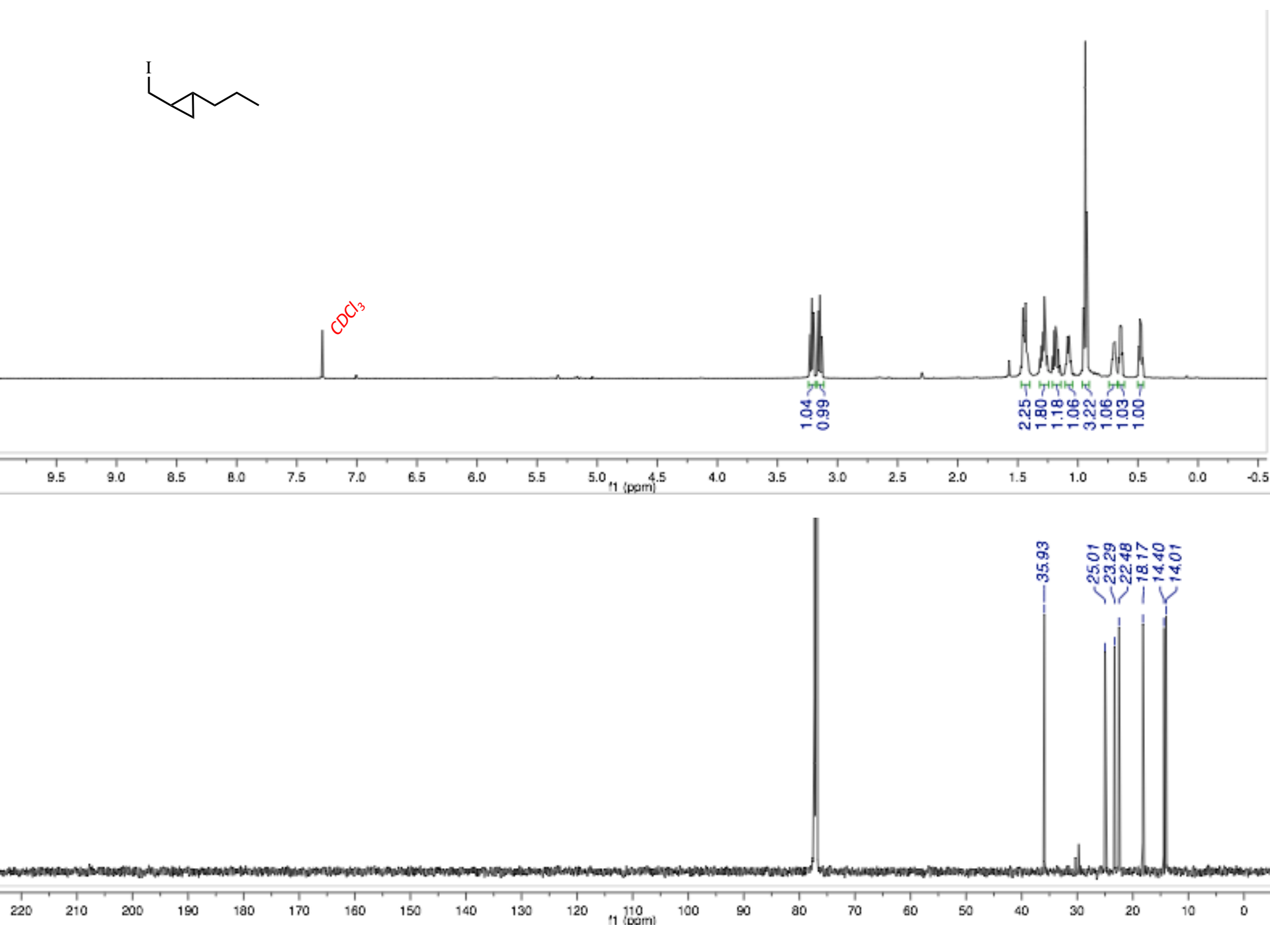
I
CDCl3
1.04
0.99
2.25
1.80
1.18
1.06
3.22
1.06
1.03
1.00
f1 (ppm)
35.93
25.01
23.29
22.48
18.17
14.40
14.01
f1 (ppm)

Anthony Fatino

Department of Chemistry | Kansas State University
| anthonyfatino11@gmail.com | Phone: (816)277-9025

EDUCATION AND TRAINING

Postdoctoral Fellow, University of Texas Southwestern, (Pending 2021)

Advisors: Prof. Jef De Brabander and Prof. Deepak Nijhawan

Research focus: Synthesis and target identification of medicinal compounds employing photo-affinity labeling.

Ph. D. Organic/Biological Chemistry, Kansas State University, 2016-2021

Advisor: Prof. Ryan J. Rafferty

Research focus: Natural product total synthesis and biological evaluation.

B.S. Biochemistry, University of Central Missouri, 2011- 2015

Advisor: Prof. Chen Zhou

Research focus: Gold nanopartical synthesis and characterization of Cu^{2+} ion sensing in biological media.

SCIENTIFIC CONTRIBUTION

Graduate Publications

Fatino, A.; Rafferty, R. J. "Mechanism of N-acetyl thiazolidine decomposition" (In preparation)

Torres, A. X.; Weeranmange C.; Desman P.; **Fatino, A.**; Haney, O.; Rafferty, R. J. "Efforts in Redesigning the Antileukemic Drug 6-Thiopurine: Decreasing Toxic Side Effects while Maintaining Efficacy" *Med. Chem. Comm.* **2018,** *10*, 169-179.

Fatino, A.; Weese, C.; Valdez, S.; Jimenez-Somarribas, A.; Rafferty, R. J. "Synthetic studies towards lagunamide C: Polyketide assembly investigations" *J. Org. Chem.* **2018**, *59*, 624-627.

Fatino, A.; Baca, G.; Weeramange, C.; Rafferty, R. J. "Total Synthesis of Reniochalistatin E" J. Nat. Prod. **2017**, 80, 3234-3240.

Undergraduate Publications

Fatino, A.; Steinkruger, J. D.; Hao, J.; Yang S.; Zhou, C. "Luminescent Gold Nanoparticles as dual-modality sensors for selective Copper (II) ion detection" *Mater. Lett.,* **2018**, 232, 70-73.

Graduate Presentations

Fatino, A.; Perera, S.; Funk, B.; Dallman, J.; Weese, C.; Rafferty, R. J. "Synthetic Efforts Towards Lagunamide C and Biological Evaluation" Poster session; Natural Products and Bioactive Compounds, Gordon Research Conference, Andover NH, July **2019**

Fatino, A.; Weese, C.; Baca, G.; Dallman, J.; Rafferty, R. J. "Synthetic endeavors towards Lagunamide C, and the total synthesis of Reniochalistatin E and applications as a drug delivery platform" Short oral introduction, and poster session; Natural Products and Bioactive Compounds, Gordon Research Conference, Andover NH, July **2018**.

Fatino, A.; Weese, C.; Baca, G.; Rafferty, R. J. "Synthesis of Complex Molecules: Total Synthesis and Biological Evaluation of Reniochalistatin E and Analogs and Synthetic Work Towards Lagunamide C" Oral presentation; 253rd National ACS meeting, San Francisco CA, April **2017**.

Fatino, A.; Baca, G.; Rafferty, R. J. "Synthetic efforts towards the proline rich and cytotoxic cyclic octapeptide Reniochalistatin E" Poster presentation; Midwest region ACS meeting, Manhattan KS, October **2016**.

Undergraduate Presentations

Fatino, A.; Zhou, C. "Luminescent Gold Nanoparticles-based Fluorescence and Dynamic Light Scattering Dual-Modality Sensor for Copper (II) detection" Poster presentation; 249th annual ACS meeting, Denver, CO, March **2015**.

Fatino, A.; Zhou, C. "Luminescent Gold Nanoparticles-based Fluorescence and Dynamic Light Scattering Dual-Modality Sensor for Copper (II) detection" Poster presentation; Midwestern Regional ACS Meeting, Kansas City MO, October **2015**.

Fatino, A.; Zhou, C. "Luminescent Gold Nanoparticles for Cu (II) Ion Sensing in Physiological Environment" Oral presentation; UCM Scholars Symposium, April **2014** & April **2015**.

AWARDS AND RECOGNITION

- Elected Co-chair of the 2022 Gordon Research Seminar on Natural Products
- Jerry and Judy Reed Fellowship in Chemistry: 2021
- Dane Hansen Award: 2017
- UCM Undergraduate Research Grant: 2014, 2015, 2016
- The Donald R. Kelsey Undergraduate Research Award: 2014, 2015
- Nance Family Scholarship: 2015-2016

TEACHING EXPERIENCE

Advanced Organic Chemistry Laboratory Teaching Assistant (CHM 551): Fall 2017- Spring 2021;

Organic 2 Teaching Assistant (CHM 550): Spring 2019

Organic 1 Teaching Assistant (CHM 531): Spring 2018, Fall 2018, Spring 2020;

Undergraduate Organic Chemistry Laboratory Teaching Assistant (CHM 532): Spring 2017; Spring 2021

Chemistry 1 Laboratory Teaching Assistant (CHM 210): Fall 2016;

RELEVANT EXPERIENCE

Rafferty laboratory safety officer: 2017- 2021

Head of solvent system maintenance: 2017- 2021

Interim NMR technician: Spring 2017- Summer of 2017

COMMUNITY INVOLVMENT

Phi Lambda Epsilon (Alpha Epsilon):

Chapter Secretary 2017-2018;

Chapter President 2017-2020

- Initiated career development seminars for graduate students by hosting discussion panel from academic and industrial backgrounds. Promoted diversity in STEM by providing funding for the Midwest Retreat for Diversity in Chemistry (MWRDC)

Investigating the Pleiotropic Effect of Flavonoids: Photoaffinity Library Construction

Research Proposition Oral Examination

Anthony Fatino

Department of Chemistry- Kansas State University
Principle Investigator: Dr. Ryan J. Rafferty

Table of Contents:

Specific Aims:

Understanding neurological diseases such as Parkinson's disease, Alzheimer's disease and chronic traumatic encephalopathy continue to challenge clinicians and researchers due to the complexity of disease development and limited access to the brain. To begin developing treatments for such diseases it is critical to determine what factors effect disease pathophysiology. This report will look to explore new pathways of investigating disease development, specifically regarding neuroinflammation. Through the construction of small molecular probes, this proposal will look to find new targets within microglia cells of the brain for targeted drug therapy.

Specific Aim 1: Development of a synthetic route based on the flavonoid natural products to create a library of small molecule probes. Incorporation of both a diazirine photo-crosslinker and an alkyne tag will provide a covalent adduct and a protein purification handle.

Specific Aim 2: Incubation of photoaffinity probes in microglia cells to determine the pathway of anti-inflammation within the brain. Treatment of cells with an inflammation inducer, such as lipopolysaciride, will allow for *in-vitro* quantification of neuroinflammation. Upon treatment of microglia cells with flavonoid and UV irradiation the active proteins will be determined via standard proteomic measures.

Section 1.1: *Introduction and Specific Aims*

Neuroinflammation can be produced through a variety of ways including; cytokines, chemokines, reactive oxygen species, or secondary messengers,[1] however, is generally defined as any type of inflammatory response within the brain or spinal cord.[2] Microglia cells are the resident immune cells within the brain and are known to regulate neuroinflammation. Intercellular conditions cause microglia cells to become activated into various states by sensing their environment. There are many diseases that are caused by, or enhanced by, prolonged neuroinflammation including, but not limited to: Parkinson's disease, Alzheimer's disease, chronic traumatic encephalopathy (CTE), multiple sclerosis (MS), and amyotrophic lateral sclerosis (ALS).[3] To combat such diseases, researchers have been interested in developing neuroprotective and anti-inflammatory drugs to help reduce the onset, or impact, of inflammation. One such class of molecules includes the naturally occurring polyphenols, flavonoids. Regular dosage of certain flavonoids have been investigated for treatment and prevention of neurological diseases, but mode-of-action studies for flavonoids suggests these molecules interact with several biological pathways.[4–6]

The specific aims of this proposal are to enhance our understanding of neuroinflammation through determining new pathways of drug interaction, and to possibly identify novel therapeutic targets for treatment. To begin, a library of photoaffinity probes (PAPs) based on the class of polyphenol natural products, flavonoids, will be synthesized. To understand how these small molecules are interacting with the immune system of the brain, these PAPs will be incubated in microglial cells *in-vitro*, and UV irradiated to covalently bind the probe to the interacting proteins. Standard proteomic strategies will be used to identify the active enzymes involved in anti-inflammation. Upon completion, this work will look to both heighten our understanding of neuroinflammation and potentially provide new targets for treating neurodegenerative diseases.

Section 1.2*: Background and Significance*

There is recent evidence suggesting that malfunction of the cerebral immune system may have a significant impact on many diseases involving cognitive decline.[7–9] Resident immune cells,

called microglia, function as maintenance for cellular debris and waste within the brain.[10–13] Various exogenous factors lead to chronic inflammation, while simultaneously leading to the release of toxic molecules and biomarkers into the intercellular space. This chronic up-regulation of the microglial activity leads to severe toxicity and neurodegradation.

Flavonoids are a class of natural products which are known to reduce neuroinflammation through various different pathways. These compounds are known as pleotropic natural products, meaning they elicit therapeutic action through multiple distinct pathways allowing for enhanced phenotypic change. These naturally occurring compounds derived from plants, including flowers, fruits and vegetables, are known to possess antioxidant and anti-inflammatory activity.[14–16] An example of these low molecular weight phenolic compounds is shown in Figure 1A. The molecular scaffold of flavonoids contains a tricyclic structure and is considered a down-stream biosynthetic intermediate of the bicyclic chalcones.

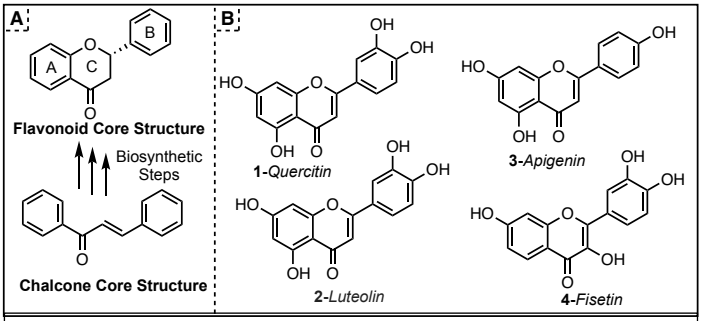

Figure 1: A) Core structure of both Flavonoid core and biosynthetic upstream intermediate chalcones. B) Select flavonoids known to interact within CNS

The biological activity of these molecules is known to have an array of interactions throughout the body, and these scaffolds are known to penetrate the blood-brain barrier (B-BB) and allow for interaction within the central nervous system (CNS).[17–22] Figure 1B displays a collection of CNS active flavonoids. Quercetin (**1**) is known to inhibit acetylcholinesterase, a known therapeutic pathway for the treatment of AD.[23] Luteolin (**2**) has neuroprotective properties via different mechanisms to have antioxidative and cytoprotective properties through interaction within the NRF2 pathway.[24,25] Apigenin (**3**) was discovered to affect the production of multiple enzymes, such as cyclooxygenase-2 (COX-2) within cultured microglial cells.[27] COX-2 enzymes are known to produce prostaglandin E_2, which is a proinflammatory signaling molecule in the brain.[28] Studies show that BV2 cells, cultured with lipopolysaccharide (LPS) have a reduced nitric oxide (NO) production when treated with apigenin. Based on these findings, a dose dependent decrease of COX-2 enzyme production was observed using an immunochemistry assay. In addition, evidence supports that mitogen-activated protein kinase, an up-stream

signaling enzyme, is also affected. Lastly, fisetin (**4**) acts on multiple pathways to reduce the impact of aging involved in neurotropic signaling.[26] From these data it is clear that the pleotropic reactivity of structurally similar molecules have a variety of interactions in the brain. These mode-of-action investigations highlight the downstream effects of these molecules, but the specific molecular interaction has not been identified. Since these molecules may be interacting weakly with various proteins, it is important to determine all the proteins responsible for the reduced inflammatory response. This proposal will seek to confirm previous flavonoid mode-of-action studies and determine new weak binding proteins that may be involved in reducing neuroinflammation.

Identifying drug-protein interaction is one of many important aspects for early development of pharmaceuticals to determine specific mode of action and identify possible side effects. Early detection of undesired side effects can prevent the high cost of drug development and clinical failures.[29] Current techniques for identifying drug-protein interactions include genome-wide genetic assays,[29] chemical proteomics,[30] expression profiling, and bioinformatics.[30] In addition, cellular thermal shift,[32] drug affinity responsive targets (DARTS),[33] and chromatography assays can also be used to identify drug targets.[33] However, recently the use of PAPs has become more popular for determining novel drug targets and to identify off targets side effects.

The use of PAPs has become a powerful tool for chemical biologists interested in understanding molecular interactions of drugs. This technique has been developed for identifying specific protein-drug interactions,[35] mapping binding sites,[36] identifying ligand targets,[37] investigating protein-protein interactions,[38] and imaging live cells.[39] An illustration of the two functional groups required for protein identification are shown in Figure 2. Figure 2-A shows a diazirine which is a photo-crosslinker that generates a reactive intermediate when excited with UV light. Diazirines and other groups, such as azides and benzophenones become covalently bound to the protein through direct insertion into the active-site of the nearby protein.[35]

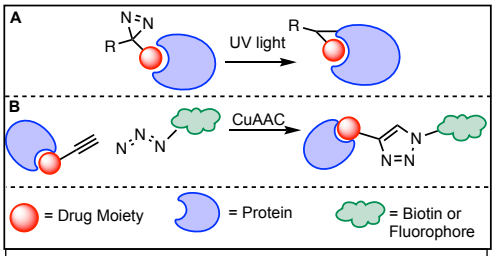

Figure 2: Illustration of the two major components of PAP synthesis. **A)** Photo-cross linker for covalent additions. **B)** Terminal alkyne for Huisgen "click-chemistry."

Additionally, incorporation of terminal alkyne moiety allows for a copper mediated [2+3] cycloaddition, known as click-chemistry, to a florescent tag or a biotin moiety (Figure 2-B). This reaction allows for the addition of either a fluorophore or a biotin to the covalently bound drug-protein complex; allowing visualization, or purification of cell lysate to identify the bound protein. This proposal will focus on the synthesis of diazirine containing probes to generate a carbene within the active-site of a protein to produce a drug-protein complex, and will be discussed later. Click-chemistry to the terminal alkyne moiety with a biotin containing azide will allow for purification of the cell lysate with streptavidin affinity beads. After the select proteins have been extracted from the lysate, gel electrophoresis purification methods are used to separate the protein targets. Following the purification, standard proteomic strategies will be used to identify the unknown bound proteins. With the use of bioinformatics the protein of interest can be identified and then verified by other molecular biology tools. This proposal will look to identify multiple individual proteins to highlight the pleotropic effect produced by the flavonoid molecules.

Section 1.3*: Innovation*

The incorporation of PAPs has been the focus of many research publications and is known to work well on many different substrates.[37,40,41] In this proposal, diazirines will be incorporated into flavonoid molecules to determine active proteins within microglia cells. Contrary to the azide and benzophenone functional groups which produce either a nitrene or a diradiacal; diazirine containing probes produce a carbene, a species with extremely short lifetimes and high reactivity (Figure 3).[37] The reactive carbene can insert into nearby C–H or O–H bonds, or with various residues within the active site. In addition to the fast kinetics of the carbene generation, other benefits of using diazirine probes include the non-hazardous irradiation at 340-

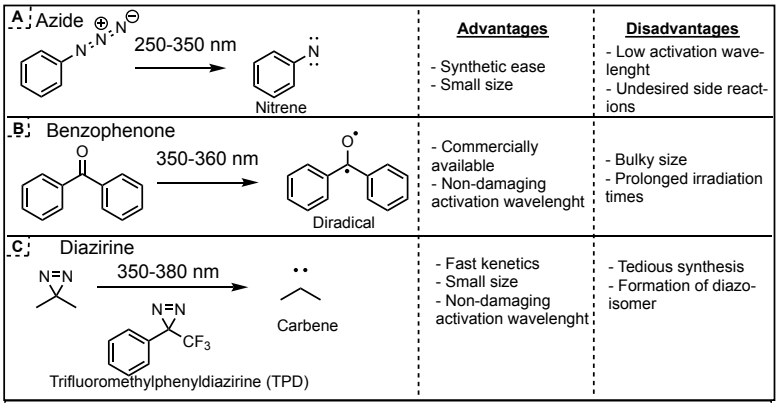

Figure 3: Most common types of PAP moieties with respective advantages and disadvantages of each.

380 nm to allow for live cell imaging, and the small size to avoid the effects of steric bulk within the enzyme active-site.[41] To increase the stability of the diazirine compound, it was determined that the addition of trifluoromethyl group in the alpha position increases stability and reduces the formation of undesired side reactions.[36] Without this electron withdrawing character of the trifluoromethyl, a prolonged reactive diazoisomer can be produced. This prolonged decay will eventually regress to a carbene resulting in off-target conjugation. With addition of these groups, the trifluoromethyl phenyl diazirine (TPD) have been found to be stable in both biological settings and through many synthetic manipulations.[39] In brief, TPDs have been found to tolerate a range of reaction conditions including reduction,[42,43] oxidation,[44–46] acid,[42,47] base,[48,49] hydrolysis,[50,51] nucleophiles,[52] electrophiles,[37] thermal heat,[53] metal catalysis,[42] and ambient light.[39]

The incorporation of diazirines has been categorized into 3 different subclasses; appended, replaced, and nested,[39] as shown in Figure 4 (adapted from reference 39). These classes can be ranked corresponding to the degreed of alteration of the photoprobe from the parent compounds. Of the three, nested is considered to have the lowest amount of structural perturbation, meaning there is less alteration in the structures physiochemical properties (PCPs), and shortest proximity to the pharmacophore.[54] Minimal PCP alteration is important for retention of cellular mode-of-action and penetration of parent compounds to allow for similar interaction with active proteins. Moreover, appended and replaced diazirines onto the compounds leads to an increased likelihood of limiting interactions within cells, leading to false negatives, and low labeling efficiency.[54] However, due to challenging synthesis, the nested strategy has had limited application with current reports indicating only 20% of diazirine in literature are nested. The other two strategies have had more attention with 52% appended, and 28% replaced.[54] This proposal will detail a synthetic strategy towards nested TPDs to limit the amount of perturbation from the parent pharmacophore in hopes to identify the weak interactions within microglia that are key for determining pleotropic effects.

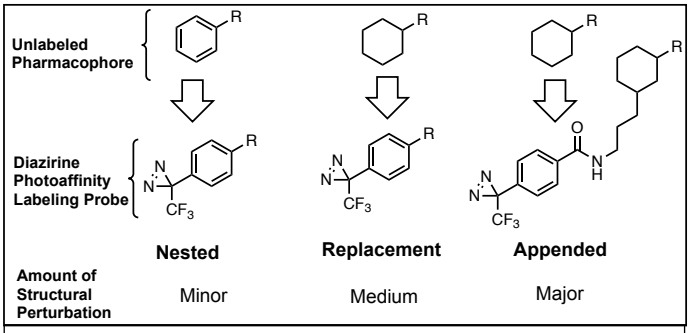

Figure 4: Types of diazirine replacement strategies onto unlabeled pharmacophore, and the ranking efficacy.

The main focuses of this route are to harness known chemistry to selectively install trifluoroacetyl groups without using ketone protecting groups, and to install the diazirine late in the synthesis to prevent any functional group intolerance or minor light mediated decomposition. Starting from a bromo-aryl compound, the reported literature use standard lithium halogen exchange, or Grignard formation to add trifluoroacetyl. However, due to both a ketone and enone system within the target molecules and intermediates, a new strategy is needed to eliminate ketone protecting groups. To overcome this obstacle, this proposal will harness the Weinreb amide chemistry to install trifluoroacetyl group for the use of PAPs.

The synthetic route to install the TPD is shown in Scheme 1. Using a reaction developed by Buchwald and co-workers a Pd-catalyzed aminocarbonylation at atmospheric pressure can be performed to afford the Weinreb amide (**6**) from the aryl bromide (**5**).[55] In addition, this reaction has shown to be selective to the installation at the bromine carbon and has no effect on adjacent ketones on the starting material.[56] The Weinreb amide can then be converted into the compound **7** by the use of a Ruppert–Prakash reagent (TMS–CF_3) under mild conditions.[57] With the installation of the trifluoroacetyl there is many literature precedence that describe the installation of the diazirine through various conditions.[58–60] It is envisioned that the electron deficiency of the trifluoroacetyl will be more reactive than the adjacent ketone functionality in the formation of the diaziridine (**10**). Various conditions can be used to form the diazirine compound (**11**).

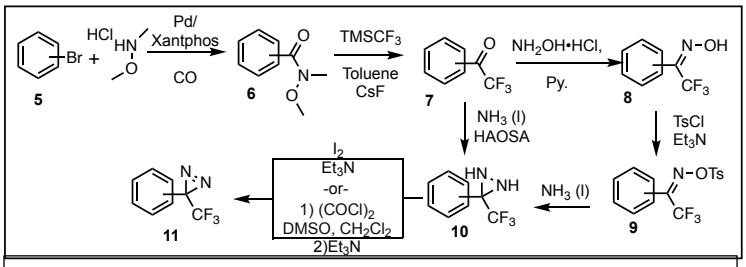

Scheme 1: Synthetic protocols to install TPD onto a general aromatic substrates.

Section 1.4*: Approach and Methods*

The construction of a diverse library of PAPs will allow for the identification of multiple enzymes involved in the flavonoids mediated reduction of neuroinflammation. As a proof of concept several molecules deriving from the fisetin (**4**) will be reported here. To ensure that none of the weakly bound proteins are missed in the target validation; a range of molecules are envisioned from the same starting material. Figure 5 highlights some of the target molecules and shows the potential effects that positioning of the PAP functional groups may have on cellular interaction. For example, **12** and **13** differ by the positioning of the diazirine moiety which may be important for interactions in the protein. Molecules **14** and **15** differ in the saturation of their core ring structure which also may affect the molecules ability to bind into the active sites.

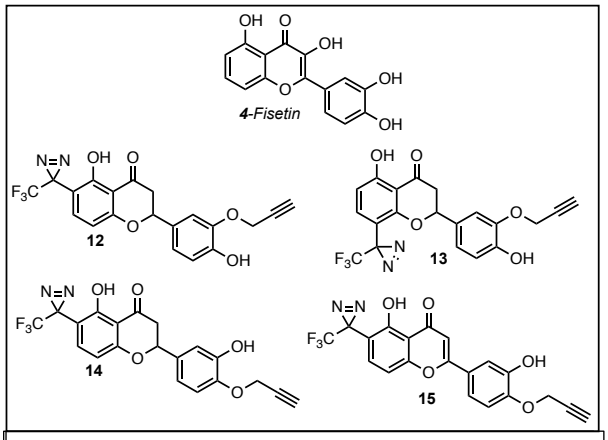

Figure 5: Examples of diazirine containing fiestin analogs considered for this route.

In order to develop a more complex library, this proposal will use inspiration from the biosynthetic pathway to first access the chalcone in route to the flavonoid compound. This will allow for testing of both types of compounds and allow for a more diverse library to be created.[61] Fortuitously, the chalcone intermediates within the synthesis can also be synthesized into PAPs and tested for activity. In addition a route that allows for late stage manipulations will create a complex library of flavonoid analogs quickly. As shown in the proposed retrosynthetic analysis in Figure 6, to reduce undesired side reactions it will be important to install the diazirine and the terminal alkyne functional groups in the final steps of the synthesis shown as structure **16**. Orthogonal phenolic protecting groups will be used for selective deprotection and manipulations of core structure (**19** and **20**). One major step in the synthesis will be the

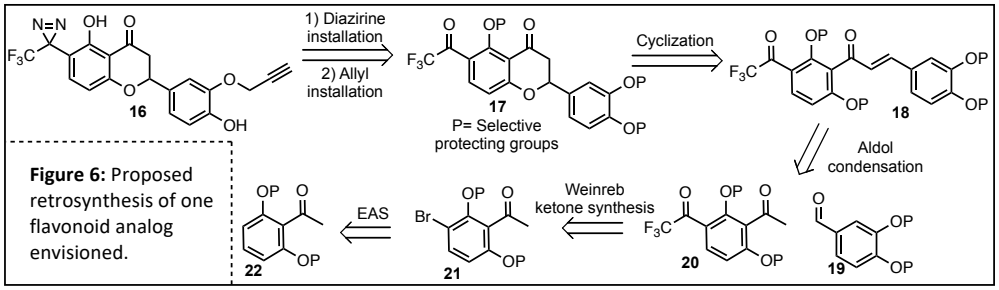

Figure 6: Proposed retrosynthesis of one flavonoid analog envisioned.

installation of the trifluoroacetyl group onto the protected benzophenone compound **21** to **22**. The use of Weinreb amide over Grinard formation or lithium-halogen exchange will reduce the need to protect the starting material ketone. This route in Figure 6 can also be applied to various different mono and di-phenolic compounds which will allow for the synthesis of structural analogs.

Diversification of the flavonoid library can be expanded by the use of synthetic manipulations to create various different core ring structures. The chalcone based substrates can be cyclized under various conditions to produce different ring sizes, oxidation states, and degree of unsaturation around the central C ring, as shown in Scheme 2. While these cyclization reactions are well precedented in the literature, the functional group compatibility with advanced material will need to be investigated.

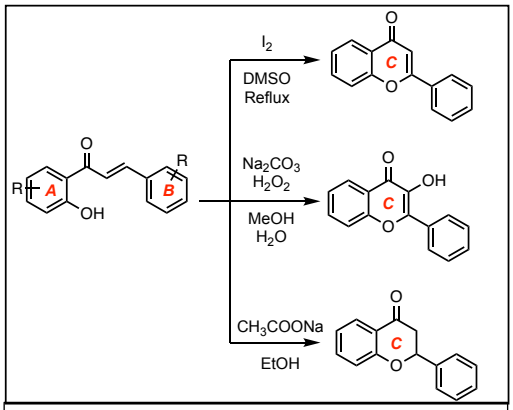

Scheme 2: Cyclization conditions from chalcone intermediate to flavonoid compounds.

Upon construction of the library, initial efforts will be to determine which of the analogs gives the strongest phenotypic change for anti-inflammation. There are several assays that allow for the detection and quantification of inflammation for BV-2 cells *in vitro*.[62] Detection of selected biomarkers can indicate neuroinflammation including: NO production via Griess reaction,[63] ELISA based cytokines production including IL-6 and TNF-α,[64] total protein level via Lowry Assay,[65] and cell viability via MTT assay.[66] Compounds that show the best overall anti-inflammatory activity will be selected as lead compounds to move onto the protein identification process. Ideally, lead compounds will have high degree of activity in multiple enzymatic pathways, as this will allow for identification of many protein-drug interactions within the microglial cells.

Parent natural products can be purchased from commercially available sources to allow for testing of the original phenotypic response. Achievement of probe synthesis will also allow for competitive binding assays between parent compound and PAP analogs and will provide a range of ligand binding values to the various enzymatic partners. This data will serve as a

structure activity relationship (SAR) and help determine the important components of each structure for specific enzyme interaction.

Quantification of unknown binding partners can be done through the combination of biochemical and analytical techniques, such as gel purification and LC-MS/MS analysis.[67] To allow for identification of active proteins, a terminal alkyne incorporation onto the drug will allow for copper catalyzed click-chemistry, with an azide containing biotin, to allow for the pull-down of conjugated enzymes.[68] The cell lysate can then be purified with either gel electrophoresis,[69] or streptavidin pull-down assays,[70] respectively. This allows for the isolation of enzymes based on florescent and affinity properties of the conjugate. Upon isolation of the protein, LC-MS/MS is performed to fragment the peptide and determine the sequence. To confirm these findings, several additional methods for validation can be performed, in addition to individual gene knockout therapies to selectively eliminate potential targets.

The protein bands of interest can be extracted and digested into peptide fragments before LC-MS/MS analysis is used to determine common sequences. From the data the overall protein size and the sequences of the fragmented peptide can be used in tandem with bioinformatics to identify possible partners.[71] Such computer software as MaxQuant, Peaks, and OpenMS are used to predict possible proteins based on these common sequences and overall protein size. However, due to a high degree of homologs, the computer software's may produce many possible matches. Validation of target protein can be time consuming, but the additional methods, mentioned above, can be done to repeat findings of initial bioinformatic results.

Section 1.5 *Synthetic Route and Application*

Creation of polyphenol natural products requires orthogonal protecting groups for selective synthesis of core ring structure. To achieve this, a linear sequence of deprotection will need to be considered, in addition to the stability of the alkyne tag. Shown in Figure 7, is the linear sequence of the selective deprotections

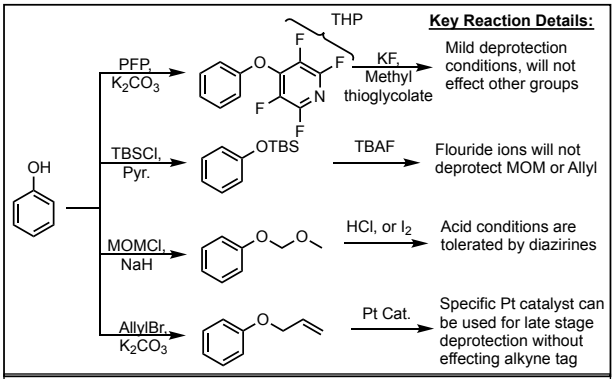

Figure 7: Types of O-protections and deprotection conditions that can be used in phenolic positions. Specific Pt catalyst is referenced in text.

that will allow for synthesis of PAP containing TPDs. The mildest of these protecting groups is the triflouropyridine (TFP) group which is easily cleaved under mild conditions with KF and methyl thioglycolate.[72] These conditions will allow for selective deprotected without effecting the other groups. Following this the use of standard silyl protecting groups can be deprotected using fluoride ions. The strategy will require for the silyl deprotection to occur before the third deprotection which is the methoxymethyl acetals (MOM) group which requires acidic conditions. Literature precedence shows that late stage deprotection under both TFA and aqueous HCl are possible without diazirine decomposition.[73,74] Finally, allyl protection of the phenolic position can allow for deprotection and is stable under all of the above conditions. While the standard deprotection conditions of H_2 and Pt are not ideal considering the target molecule contains a terminal alkyne tag, there have been reported literature that involves a bulky Pt catalyst that allow for allyl deprotection without reduction of the alkyne.[75] This sequence of deprotection conditions will allow for selectivity of the synthetic route.

Synthetic manipulations to prepare the diphenolic acetophenone compound **23** for aldol conditions is shown in scheme 3. Employing 1 equivalent of THP will afford compound **24** followed by MOM installation of the other phenolic group to afford compound **25,** allowing for orthogonal protecting groups. As shown compound **25** will allow for a mixture of otho- and para- bromonations to occur (**26** and **27**), however both compounds can be utilized in the library construction. It is suggested that the compound **26** will be favored in this addition due to electronics of the acetyl group acting as an EWG. From here, **26** and **27** can be carried on to aldol conditions, or the trifluoroacetyl group can be installed via reactions previously mentioned using the Weinreb amide protocol to afford **28** or **29**.

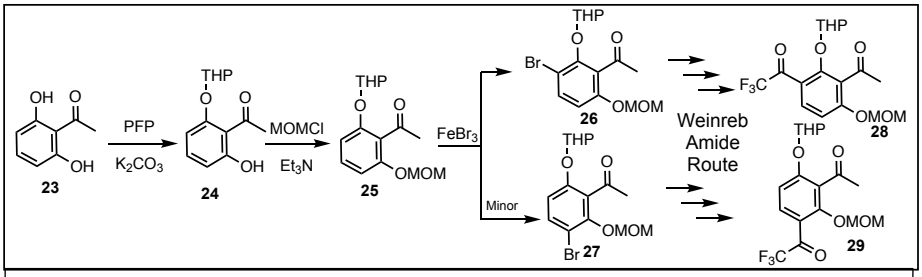

Scheme 3: Preparation of acetophenone starting material before aldol conditions.

Concurrently, the aldehyde unit (**30**) will also be prepared for aldol condensation conditions, as shown in Scheme 4. The propargyl cross-linker can be installed first with propargyl bromide and potassium carbonate to afford compound **31** or **32**. Again, a mixture of compounds will be produced, but this allows for diversification of library synthesis. Following this installation, the remaining phenolic OH can be protected with TBSCl and pyridine to give compounds **33** and **34**. The terminal alkyne contains acidic protons that will be liable in the strongly basic aldol conditions, so selective silylation in the terminal position can install a trimethylsilane using $ZnBr_2$ to afford compounds **35** and **36**.[76] Fortuitously, both protecting groups on this molecule will be liable under TBAF conditions which should be considered as one of the final steps in the synthesis. If this terminal silyl protecting group fails to void decomposition in the following steps, then dual TBS protections will be considered as an alternative route (**37**), and will require late stage propargyl installation.

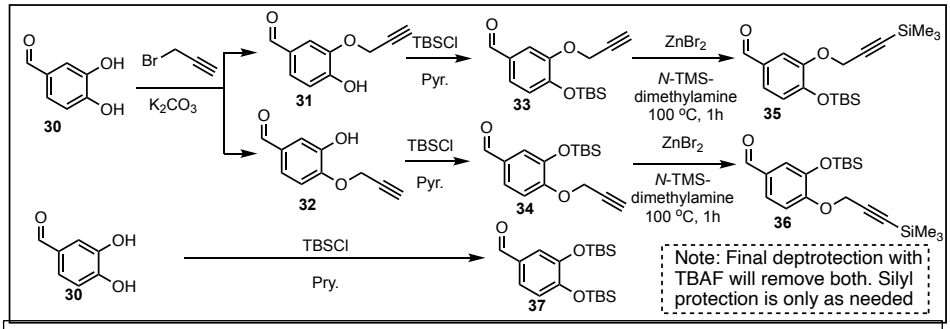

Scheme 4: Preparation of aldehyde starting material before aldol conditions.

With **28** and **35** in hand, aldol condensation conditions with KOH in EtOH will afford the chalcone intermediate (**38**), as shown in Scheme 5. From here, phenolic deprotection of compound **38** and addition of PAP functional groups will allow for testing of the chalcone intermediate. Parallel to this, selective deprotection of the THP group using mild KF conditions, will afford compound **39** to be prepared for cyclization conditions. The conditions discussed earlier will be used to synthesize the various core

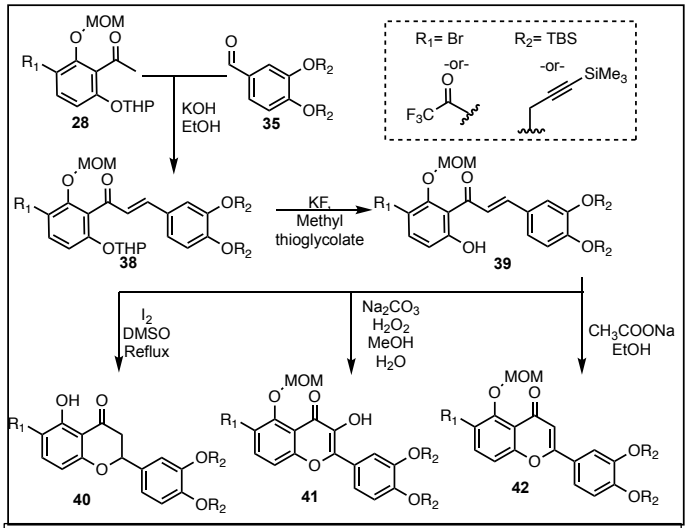

Scheme 5: Aldol reactions to create chalcone and cyclization to flavonoid core structure.

flavonoid ring structures (**40**-**42**). Again, these steps will need to be examined for stability of functional groups to ensure phenolic oxygens remain protected. If the ketone functionality of the flavonoid core becomes problematic later in the synthesis, then during cyclization the enolate intermediate can be trapped as a TMS ether for protection and can be released in final steps. The iodine cyclization step towards compound **40,** will also deprotect the phenolic MOM groups, which could strategically shorten the synthetic route. Although early installation of the diazirine would be ideal for diversification it may be necessary to optimize protecting groups through experimental testing.

Upon cyclization of the various intermediates, the final steps will be to install the PAP functional groups, and to deprotect the phenolic protecting groups. As shown in Scheme 6, following the installation of the trifluoroacetyl group to compound **41**, the addition of hydroxyamine will install the N-oxide (**43**). Tosylation of **43** and treatment with liquid ammonia will afford the diazirine containing compound (**44**). Final deprotection of the TBS groups upon treatment with TBAF will afford compound **45** with either the free phenolic OH on the B-ring, or will complete they deprotection of the terminal alkyne in tandem to afford the final product (**46**).

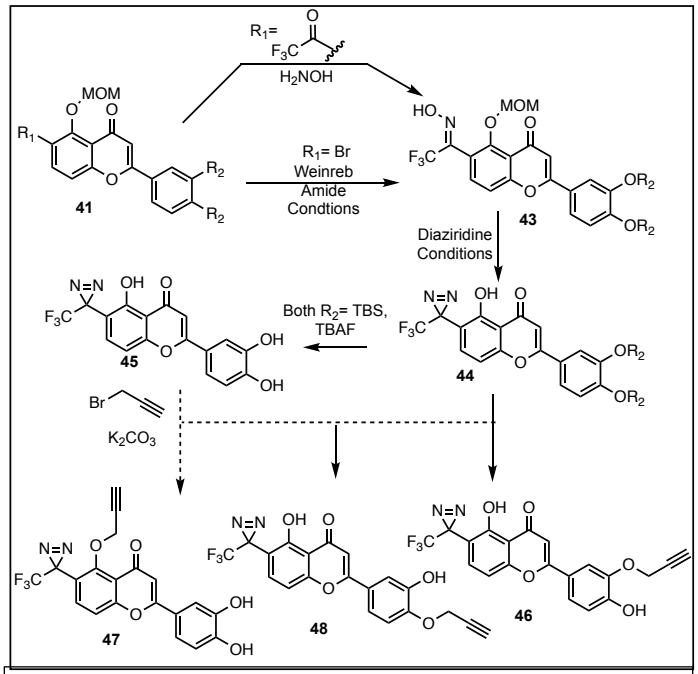

Scheme 6: Synthesis of final flavonoid analog compounds.

If dual TBS installation was required for synthetic stability, then following the deprotection, a non-selective alkylation will be performed to create compounds **46**, **47** or **48**. This late stage installation will afford several analogs that can be tested for various binding values within proteins.

In summary, while this synthesis may require extensive use of selective phenolic protecting groups throughout, this pathway will afford several compounds for testing from each

of the products formed. In addition the generality of the synthesis will allow for reapplication of the route to the different starting materials and will allow for a large collection of compounds to be gathered quickly. As mentioned before, it is pivotal to synthesize a variety of analogs that will have various structural difference to be able to detect the weak binding partners that may have a significant impact within microglial proteomes.

There are many steps in the protein purification and separation that will need to be optimized during this work. The process of identification will be done with the help of collaborations with researchers in the proteomic field. Potential works with known researchers in this field include Deepak Nijhawan and Jef De Brabander at UTSW, and John Pezacki at the UOttowa have both communicated interest in collaboration/training. Each respective group have produced several publications in the synthesis and use of PAPs.

Section 1.6*: Conclusion and Broader Impacts*

Recently the use of diazirine based PAPs has begun to attract more attention for their innate characteristics to bind near the active site without effecting the original drugs properties. This proposal seeks to synthesize a library of flavonoid analogs with diazirines to monitor the weak interactions that dictate the pleotropic effect of these molecules. It is envisioned that these molecules will be able to interact with the immune system of the brain to reduce the amount of neuroinflammation in various disease states. Upon collection of this molecular probe library, detection of microglial proteomic activity on a basal level vs. inflammatory conditions will provide an SAR investigation for important pharmacophore properties. By doing this it may be possible to determine the underlying mechanisms of inflammatory diseases and could illuminate undiscovered avenues of treatment.

If this proposal were to fall short on providing a drugable target within microglial cells, the library of PAPs could have lasting implications for more discoveries in chemical biology. The aim of this proposal was based on modulation of microglia activity in the brain; however, flavonoids are also known to interact within other biological systems of the body. Using these PAPs on various cancer cell lines *in-vitro* could also indicate new paths of treatment in cancer cells. Another possible application would be identification of the mechanism responsible for B-

BB penetration. A B-BB model system can be made of a CaCo-2 monolayer of cells, and the PAPs can be used to find new mechanisms of small molecule penetration to the brain.

If these PAPs lack all reactivity in cells, the route proposed here can be applied to more complex natural products including flavon-chalcone hybrids that could have altered activity within cells. Moreover, another avenue of reapplication could be to move the active cross-linker further way from the active portion of the molecule. A carbon chain tether will covalently bind adjacent proteins acting as secondary proteins. Overtime a library of complex molecules can be collected and tested on a variety of biological systems, and with more advanced biological and genetic tools being developed, our understanding of challenging diseases will continue to improve.

Section 1.7: *Timeline*

The synthesis of the PAP library could be accessed over an extended period with increasing diversity. However compounds can be accessed quickly and be tested immediately. This will allow for testing of individual polyphenols to be examined within the first year of research onset. Any of these probes could provide several hits for the identification of interacting proteins. With advancements in automation and proteomic assays, identification of a target could be done within 3 years. Finding this new target could lead to several synthetic efforts in medicinal chemistry for drug design and synthesis.

Section 1.8: *Bibliography*

1. Microglial_priming_in_neurodeg.pdf.
2. Sundt, T. M. Commentary: The devil is in the details. *J. Thorac. Cardiovasc. Surg.* **157**, 2214–2215 (2019).
3. Chen, W. W., Zhang, X. & Huang, W. J. Role of neuroinflammation in neurodegenerative diseases (Review). *Mol. Med. Rep.* **13**, 3391–3396 (2016).
4. Solanki, I., Parihar, P., Mansuri, M. L. & Parihar, M. S. Flavonoid-Based Therapies in the Early. *Am. Soc. Nutr. Adv. Nutr.* **6**, 64–72 (2015).
5. Ginwala, R., Bhavsar, R., Chigbu, D. G. I., Jain, P. & Khan, Z. K. Potential role of flavonoids in treating chronic inflammatory diseases with a special focus on the anti-inflammatory activity of apigenin. *Antioxidants* **8**, 1–28 (2019).
6. Leyva-López, N., Gutierrez-Grijalva, E. P., Ambriz-Perez, D. L. & Basilio Heredia, J. Flavonoids as cytokine modulators: A possible therapy for inflammation-related diseases. *Int. J. Mol. Sci.* **17**, (2016).
7. Smith, J. A., Das, A., Ray, S. K. & Banik, N. L. Role of pro-inflammatory cytokines released from microglia in neurodegenerative diseases. *Brain Res. Bull.* **87**, 10–20 (2012).
8. Tang, Y. & Le, W. Differential Roles of M1 and M2 Microglia in Neurodegenerative Diseases. *Mol. Neurobiol.* **53**, 1181–1194 (2016).
9. Song, G. J. & Suk, K. Pharmacological modulation of functional phenotypes of microglia in neurodegenerative diseases. *Front. Aging Neurosci.* **9**, (2017).
10. Hernandez-Ontiveros, D. G. *et al.* Microglia activation as a biomarker for traumatic brain injury. *Front. Neurol.* **4 MAR**, 1–9 (2013).
11. McCarty, M. F. Down-regulation of microglial activation may represent a practical strategy for combating neurodegenerative disorders. *Med. Hypotheses* **67**, 251–269 (2006).
12. Bachiller, S. *et al.* Microglia in neurological diseases: A road map to brain-disease dependent-inflammatory response. *Front. Cell. Neurosci.* **12**, 1–17 (2018).
13. Marcin, W., Beata, S., Tomasz, S. & Pawel, L. P. Microglial cells in neurodegenerative disorders. *Folia Neuropathol.* **43**, 311–321 (2005).
14. Pan, M. H., Lai, C. S. & Ho, C. T. Anti-inflammatory activity of natural dietary flavonoids. *Food Funct.* **1**, 15–31 (2010).
15. García-Lafuente, A., Guillamón, E., Villares, A., Rostagno, M. A. & Martínez, J. A. Flavonoids as anti-inflammatory agents: Implications in cancer and cardiovascular disease. *Inflamm. Res.* **58**, 537–552 (2009).
16. Yuan, G., Wahlqvist, M. L., He, G., Yang, M. & Li, D. Natural products and anti-inflammatory activity. *Asia Pac. J. Clin. Nutr.* **15**, 143–152 (2006).
17. Jäger, A. K. & Saaby, L. Flavonoids and the CNS. *Molecules* **16**, 1471–1485 (2011).
18. Matias, I., Buosi, A. S. & Gomes, F. C. A. Functions of flavonoids in the central nervous system: Astrocytes as targets for natural compounds. *Neurochem. Int.* **95**, 85–91 (2016).
19. De Andrade Teles, R. B. *et al.* Flavonoids as therapeutic agents in Alzheimer's and Parkinson's diseases: A systematic review of preclinical evidences. *Oxid. Med. Cell. Longev.* **2018**, (2018).
20. Romano, B. *et al.* Novel insights into the pharmacology of flavonoids. *Phyther. Res.* **27**, 1588–1596 (2013).
21. Faria, A., Mateus, N. & Calhau, C. Flavonoid transport across blood-brain barrier: Implication for their direct neuroprotective actions. *Nutr. Aging* **1**, 89–97 (2012).
22. Youdim, K. A. *et al.* Interaction between flavonoids and the blood-brain barrier: In vitro studies. *J. Neurochem.* **85**, 180–192 (2003).
23. Khan, M. T. H. *et al.* Cholinesterase inhibitory activities of some flavonoid derivatives and chosen xanthone and their molecular docking studies. *Chem. Biol. Interact.* **181**, 383–389 (2009).
24. Zuo, Q. *et al.* The dietary flavone luteolin epigenetically activates the Nrf2 pathway and blocks cell transformation in human colorectal cancer HCT116 cells. *J. Cell. Biochem.* **119**, 9573–9582 (2018).
25. ur Rashid, H., Xu, Y., Ahmad, N., Muhammad, Y. & Wang, L. Promising anti-inflammatory effects of chalcones via inhibition of cyclooxygenase, prostaglandin E 2 , inducible NO synthase and nuclear factor κb activities. *Bioorg. Chem.* **87**, 335–365 (2019).
26. Maher, P. Modulation of multiple pathways involved in the maintenance of neuronal function by fisetin. *Micronutr. Brain Heal.* 189–

206 (2009). doi:10.1007/s12263-009-0142-5

27. Ha, S. K. *et al.* Apigenin inhibits the production of NO and PGE2 in microglia and inhibits neuronal cell death in a middle cerebral artery occlusion-induced focal ischemia mice model. *Neurochem. Int.* **52**, 878–886 (2008).
28. Ricciotti, E., A, G. & Fitzgerald. [Eicosanoid neuroinflammation] Prostaglandins and Inflammation. *Arter. Thromb Vasc Biol.* **31**, 986–1000 (2011).
29. Terstappen, G. C., Schlüpen, C., Raggiaschi, R. & Gaviraghi, G. Target deconvolution strategies in drug discovery. *Nat. Rev. Drug Discov.* **6**, 891–903 (2007).
30. Sleno, L. & Emili, A. Proteomic methods for drug target discovery. *Curr. Opin. Chem. Biol.* **12**, 46–54 (2008).
31. Chan, J. N. Y., Nislow, C. & Emili, A. Recent advances and method development for drug target identification. *Trends Pharmacol. Sci.* **31**, 82–88 (2010).
32. Molina, D. M., Jafari, R., Ignatushchenko, M. & Seki, T. D (4). **341**, 84–88 (2013).
33. Lomenick, B. *et al.* Target identification using drug affinity responsive target stability (DARTS). *Proc. Natl. Acad. Sci. U. S. A.* **106**, 21984–21989 (2009).
34. Yamamoto, K., Yamazaki, A., Takeuchi, M. & Tanaka, A. A versatile method of identifying specific binding proteins on affinity resins. *Anal. Biochem.* **352**, 15–23 (2006).
35. Murale, D. P., Hong, S. C., Haque, M. M. & Lee, J. S. Photo-affinity labeling (PAL) in chemical proteomics: A handy tool to investigate protein-protein interactions (PPIs). *Proteome Sci.* **15**, 1–34 (2017).
36. Manzi, L. *et al.* Carbene footprinting accurately maps binding sites in protein-ligand and protein-protein interactions. *Nat. Commun.* **7**, 1–9 (2016).
37. Ge, S. S. *et al.* Current advances of carbene-mediated photoaffinity labeling in medicinal chemistry. *RSC Adv.* **8**, 29428–29454 (2018).
38. Sumranjit, J. & Chung, S. J. Recent advances in target characterization and identification by photoaffinity probes. *Molecules* **18**, 10425–10451 (2013).
39. Hill, J. R. & Robertson, A. A. B. Fishing for Drug Targets: A Focus on Diazirine Photoaffinity Probe Synthesis. *J. Med. Chem.* **61**, 6945–6963 (2018).
40. Brunner, J., Senn, H. & Richards, F. M. 3-Trifluoromethyl-3-phenyldiazirine. A new carbene generating group for photolabeling reagents. *J. Biol. Chem.* **255**, 3313–3318 (1980).
41. Halloran, M. W. & Lumb, J. P. Recent Applications of Diazirines in Chemical Proteomics. *Chem. - A Eur. J.* **25**, 4885–4898 (2019).
42. Nakashima, H., Hashimoto, M., Sadakane, Y., Tomohiro, T. & Hatanaka, Y. Simple and versatile method for tagging phenyldiazirine photophores. *J. Am. Chem. Soc.* **128**, 15092–15093 (2006).
43. Song, Z. & Zhang, Q. Fluorous aryldiazirine photoaffinity labeling reagents. *Org. Lett.* **11**, 4882–4885 (2009).
44. Lim, E., Ricci, J. & Jung, M. Synthesis of a dual-labeled probe of dimethyl lithospermate B with photochemical and fluorescent properties. *Molecules* **16**, 9886–9899 (2011).
45. Ambroise, Y., Pillon, F., Mioskowski, C., Valleix, A. & Rousseau, B. Synthesis and tritium labeling of new aromatic diazirine building blocks for photoaffinity labeling and cross-linking. *European J. Org. Chem.* 3961–3964 (2001). doi:10.1002/1099-0690(200110)2001:20<3961::AID-EJOC3961>3.0.CO;2-R
46. Kato, K. *et al.* Molecular characterization of flubendiamide sensitivity in the lepidopterous ryanodine receptor Ca2+ release channel. *Biochemistry* **48**, 10342–10352 (2009).
47. Cheng, W. W. L. *et al.* Mapping two neurosteroid-modulatory sites in the prototypic pentameric ligand-gated ion channel GLIC. *J. Biol. Chem.* **293**, 3013–3027 (2018).
48. Husain, S. S. *et al.* P-trifluoromethyldiazirinyl-etomidate: A potent photoreactive general anesthetic derivative of etomidate that is selective for ligand-gated cationic ion channels. *J. Med. Chem.* **53**, 6432–6444 (2010).
49. Biasotti, B. *et al.* Synthesis of photoactivable inhibitors of osteoclast vacuolar ATPase. *Bioorganic Med. Chem.* **11**, 2247–2254 (2003).
50. Dien et al., 2013. A traceless Staudinger reagent to deliver diazirines. *Bone* **23**, 1–7 (2008).
51. Yang, T., Liu, Z. & Li, X. D. Developing diazirine-based chemical probes to identify histone modification 'readers' and 'erasers'. *Chem.*

Sci. **6**, 1011–1017 (2015).

52. Ge, S. S. *et al.* Current advances of carbene-mediated photoaffinity labeling in medicinal chemistry. *RSC Adv.* **8**, 29428–29454 (2018).
53. Jennings, B. M. & Liu, M. T. H. Mechanism of Thermal Decomposition of Diazirine. Evidence for Diazomethane Intermediate. *J. Am. Chem. Soc.* **98**, 6416–6417 (1976).
54. Ichiishi, N., Moore, K. P., Wassermann, A. M., Wolkenberg, S. E. & Krska, S. W. Reducing Limitation in Probe Design: The Development of a Diazirine-Compatible Suzuki-Miyaura Cross Coupling Reaction. *ACS Med. Chem. Lett.* **10**, 56–61 (2019).
55. Martinelli, J. R., Freckmann, D. M. M. & Buchwald, S. L. Convenient method for the preparation of weinreb amides via PD-catalyzed aminocarbonylation of aryl bromides at atmospheric pressure. *Org. Lett.* **8**, 4843–4846 (2006).
56. Grosjean, R. *et al.* High pressures pathway toward boron-based nanostructured solids. *Dalt. Trans.* **47**, 7634–7639 (2017).
57. Rudzinski, D. M., Kelly, C. B. & Leadbeater, N. E. A Weinreb amide approach to the synthesis of trifluoromethylketones. *Chem. Commun.* **48**, 9610–9612 (2012).
58. Dubinsky, L., Krom, B. P. & Meijler, M. M. Diazirine based photoaffinity labeling. *Bioorganic Med. Chem.* **20**, 554–570 (2012).
59. Kumar, N. S. & Young, R. N. Design and synthesis of an all-in-one 3-(1,1-difluoroprop-2-ynyl)-3H-diazirin-3-yl functional group for photo-affinity labeling. *Bioorganic Med. Chem.* **17**, 5388–5395 (2009).
60. Al-Omari, M., Banert, K. & Hagedorn, M. Bi-3H-diazirin-3-yls as precursors of highly strained cycloalkynes. *Angew. Chemie - Int. Ed.* **45**, 309–311 (2005).
61. Kant, R. *et al.* Synthesis of newer 1,2,3-triazole linked chalcone and flavone hybrid compounds and evaluation of their antimicrobial and cytotoxic activities. *Eur. J. Med. Chem.* **113**, 34–49 (2016).
62. Gresa-Arribas, N. *et al.* Modelling Neuroinflammation In Vitro: A Tool to Test the Potential Neuroprotective Effect of Anti-Inflammatory Agents. *PLoS One* **7**, (2012).
63. Tsikas, D. Analysis of nitrite and nitrate in biological fluids by assays based on the Griess reaction: Appraisal of the Griess reaction in the l-arginine/nitric oxide area of research. *J. Chromatogr. B Anal. Technol. Biomed. Life Sci.* **851**, 51–70 (2007).
64. Tanaka, T. *et al.* General anesthetics inhibit LPS-induced IL-1β expression in glial cells. *PLoS One* **8**, 1–13 (2013).
65. Kashyap, M. L., Hynd, B. A. & Robinson, K. A rapid and simple method for measurement of total protein in very low density lipoproteins by the Lowry assay. *J. Lipid Res.* **21**, 491–495 (1980).
66. Woo, K. W., Moon, E., Park, S. Y., Kim, S. Y. & Lee, K. R. Flavonoid glycosides from the leaves of Allium victorialis var. platyphyllum and their anti-neuroinflammatory effects. *Bioorganic Med. Chem. Lett.* **22**, 7465–7470 (2012).
67. Shevchenko, A., Tomas, H., Havliš, J., Olsen, J. V. & Mann, M. In-gel digestion for mass spectrometric characterization of proteins and proteomes. *Nat. Protoc.* **1**, 2856–2860 (2007).
68. McKay, C. S. & Finn, M. G. Click chemistry in complex mixtures: Bioorthogonal bioconjugation. *Chem. Biol.* **21**, 1075–1101 (2014).
69. Duncan, R. & Hershey, J. W. Identification and quantitation of levels of protein synthesis initiation factors in crude HeLa cell lysates by two-dimensional polyacrylamide gel electrophoresis. *J. Biol. Chem.* **258**, 7228–7235 (1983).
70. Castaño, A. & Maurer, M. S. Biotin Elution Protocol. **20**, 163–178 (2015).
71. Wang, P. & Wilson, S. R. Mass spectrometry-based protein identification by integrating de novo sequencing with database searching. *BMC Bioinformatics* **14 Suppl 2**, (2013).
72. Brittain, W. D. G. & Cobb, S. L. Tetrafluoropyridyl (TFP): a general phenol protecting group readily cleaved under mild conditions. *Org. Biomol. Chem.* **17**, 2110–2115 (2019).
73. Masuda, Y. *et al.* Design, synthesis, and biological evaluation of beauveriolide analogues bearing photoreactive amino acids. *Chem. Pharm. Bull.* **64**, 754–765 (2016).
74. MacKinnon, A. L., Garrison, J. L., Hegde, R. S. & Taunton, J. Photo-leucine incorporation reveals the target of a cyclodepsipeptide inhibitor of cotranslational translocation. *J. Am. Chem. Soc.* **129**, 14560–14561 (2007).
75. Murakami, H., Minami, T. & Ozawa, F. Facile and selective deallylation of allyl ethers using diphosphinidenecyclobutene-coordinated palladium catalysts. *J. Org. Chem.* **69**, 4482–4486 (2004).
76. Andreev, A. A. *et al.* Direct Electrophilic Silylation of Terminal Alkynes. *Org. Lett.* **6**, 421–424 (2004).

Tetrahedron Letters 59 (2018) 624–627

Contents lists available at ScienceDirect

Tetrahedron Letters

journal homepage: www.elsevier.com/locate/tetlet

Synthetic studies towards lagunamide C: Polyketide assembly investigations

Anthony Fatino [a], Chelsea Weese [a], Salvador Valdez [b], Alberto Jiménez-Somarribas [c], Ryan J. Rafferty [a,*]

[a] Department of Chemistry, Kansas State University, 1212 Mid-Campus Drive North, 203 CBC, Manhattan, KS 66506, USA
[b] Department of Chemistry, Kansas State University, 1711 Clafin Road, KS 66506, USA
[c] Emory Institute for Drug Discovery, Emory University, 201 Dowman Drive, Atlanta, GA 30322, USA

ARTICLE INFO

Article history:
Received 20 November 2017
Revised 26 December 2017
Accepted 29 December 2017
Available online 4 January 2018

Keywords:
Lagunamide C
Natural Products
Cyclopropanation
Crimmin's Auxiliary
Aldol Addition

ABSTRACT

Lagunamide C is a depsipeptide natural product with low nM cytotoxicity towards numerous cancer cell lines. Synthetically, it is disconnected to a pentapeptide backbone and polyketide unit that possesses four stereogenic centers, of which two of centers are in question (C38 & 40). Our model system highlights a high-selective aldol addition via a Crimmin's auxiliary setting the C40 ester linkage, and a non-facially selective cyclopropanation with subsequent ring opening for the installation of the C38 methyl center.

Introduction

The *Lyngbya* genus of marine cyanobacteria continues to be a plentiful source for the discovery of new natural products.[1,2] The secondary metabolites isolated from this genus have been found to possess diverse biological activity across multiple health related diseases. Specifically, they show antimicrobial, antimalarial, as well as cytotoxic and neurotoxic properties.[3–8] In addition to their shared biological activities, the natural products from this genus also share common structural characteristics (amino acid based backbone and polyketide unit). In the quest to discover new bioactive secondary metabolites, Tan and co-workers successfully identified a persistent strain of filamentous marine cyanobacterium, *Lyngbya majuscula*.[9] Investigations into this strain led to the discovery of the lagunamide family of cyclodepsipeptide natural products in 2010 shown in Fig. 1; lagunamide A (**1**) and B (**2**)[10] followed by C (**3**) in 2011.[11]

The family has low nM cytotoxicity against lymphoma (P388), and **3** possesses additional cytotoxicity towards lung cancer (A549), prostate cancer (PC), ileocecal colorectal adenocarcinoma (HCT8), and ovarian cancer (SK-OV) with IC_{50} values of 2.4, 2.6, 2.1, and 4.5 nM, respectively. All three molecules also possess antimalarial activity towards *Plasmodium falciparum* with IC_{50}'s of 0.19, 0.91, and 0.29 μM, respectively.[10,11] Anti-swarming activity against the gram-negative bacterial strain *Pseudomonas aeruginosa* (PA01) has also been reported for **1** (62%), **2** (56%), and **3** (49%) relative to controls. The potent cytotoxicity exhibited by the lagunamide family has drawn the interest by multiple groups[12] and resulted in two total syntheses of **1**.[13,14] In addition to the common potent cytotoxicity, the lagunamide family shares a highly conserved amino acid based backbone and a polyketide unit, wherein the presence and stereochemistry of a C37-hydroxyl (R-configuration) and C38-methyl (R-configuration) are conserved. The key structural difference between **1&2** and **3** is the presence of an additional methylene carbon within **3** upon C39. The same C39 position within **1** and **2** is the ester linkage position connecting the amino acid based backbone. It was the common biological activity exhibited by this family, along with the presence of an extra methylene within **3** drew our attention. While the stereochemistry about these two carbon centers are conserved, the extra methylene unit does impact the confirmation of **3** relative to **1** & **2**. This structural difference, methyl insertion, could translate into variable binding upon the cellular target(s) for cytotoxicity. Recalling the similarities in cytotoxicity's between the family members, it could be assumed that the compound-target interactions should be the same. As such, we propose that the amino acid based backbone directs penetration, and possibly general selectivity. Upon cellular uptake, the backbone is cleaved off, in full or in-part, exposing the cytotoxic arm of this family that could allow and justify the

* Corresponding author.
E-mail address: rjraff@ksu.edu (R.J. Rafferty).

https://doi.org/10.1016/j.tetlet.2017.12.083
0040-4039/

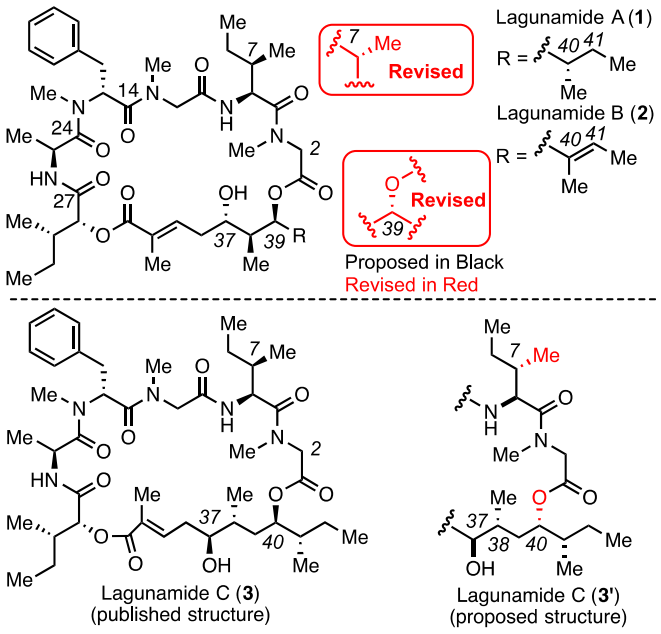

Fig. 1. Lagunamide family of natural products. Including their proposed and revised structures for A&B and published and proposed for C.

common cytotoxicity profiles. Given the interesting methylene addition within the polyketide, potent cytotoxicity, ambiguity of the C38 stereocenter (*vida infra*), and our proposed mechanism of action, our laboratory has undertaken synthetic efforts towards lagunamide C.

Lagunamide A was first synthesized by Dai et al. in 2012,[13] and a second total synthesis was accomplished by Huang et al. in 2013.[14] In the route established by Dai et al., assembly of the polyketide commenced with the enolization of the Evans (*R*)-oxazolidinone (**4**) with dibutylboron ditriflate followed by (*S*)-2-methylbutanal (**5**) to give access to the aldol product (Scheme 1). The corresponding alcohol was converted into the anisylidine acetal (**6**), which was further elaborated onto the PMB protected alcohol homoallylic alcohol **7**. Through three synthetic steps (dihydroxylation, oxidative cleavage, and Horner-Wadsworth-Emmons reaction), **7** was successfully elaborated onto the desired polyketide (**8**) present within lagunamide A. Construction of the pentapeptide backbone was accomplished with successive coupling of commercially available amino acids. Esterification about the C39 carbon to the backbone followed by macrolactamization gave access to the reported structure of lagunamide A. Comparison of the natural and synthetic material access revealed that the proposed stereochemistry about the C7 and C39 were incorrect (Fig. 1). The route was adjusted to allow for the two epimers about these carbons to be installed and cyclized in the same fashion. This furnished the macrocycle, which allowed for the elucidation of the final, and correct, structure of lagunamide A (Fig. 1). The route developed by Huang et al. accessed **1** in an analogous fashion to Dai et al., via polyketide unit (**8**). Huang's approach towards **8** was based upon a crotylation strategy upon (*S*)-2-methylbutanol (**9**) that furnished olefin **10** over multiple steps. The polyketide **8** was accessed by the cross-metathesis of 2-methyl-acrolein (**11**) and **10**. Their total synthesis also confirmed the structural assignment of lagunamide A. To date, no total synthesis of lagunamide B has been reported, but an analog, C28 epimer, has been constructed by Pal and Chakraborty[15] employing the route developed by Dai and co-workers. In an analogous route to that employed by Huang et al., they constructed the polyketide via a HWE-olefination reaction from the aldehyde surrogate of **7**.

Unfortunately, employing the methods developed by Dai and Huang will not give access to polyketide **12** for the construction of lagunamide C. These routes fail to provide synthetic means for the installation of the extra methylene carbon at C39 within **12** (highlighted by the dash box insert within Scheme 1). Furthermore, there is ambiguity about the stereochemical assignment of the C38 methyl (proposed R-configuration) within lagunamide C.[11] Therefore, any route designed and employed to gain access to polyketide **12** must allow for synthetic versatility about the C38 center for structural elucidation studies, and be robust for structural-activity relationship studies for biological evaluation and mode of action of studies.

Our envisioned route to access lagunamide C (Scheme 2) relies upon esterification and macrolactonization of the polyketide **12** to the pentapeptide backbone similar to previous routes.[13–15] Our proposed route differs in the construction of the functionalized polyketide unit **13**. Installation of the C37 alcohol within **12**, will be accomplished through a Corey-Bakshi-Shibata reduction upon ketone **13**.[16] Performing a Mukaiyama Aldol between **14** and methyl-(*E*)-2-methylbut-2-enoate will give access to ketone **13**. The key step in our proposed route invokes a facially selective Charette cyclopropanation upon **15** with subsequent ring opening, accessing **14**. This critical step will allow access to both the R and S versions of the polyketide unit about the C38 carbon for final structural elucidation. Assembly of **15** will be accomplished through a Wittig olefination upon the aldehyde of **16**, and the construction

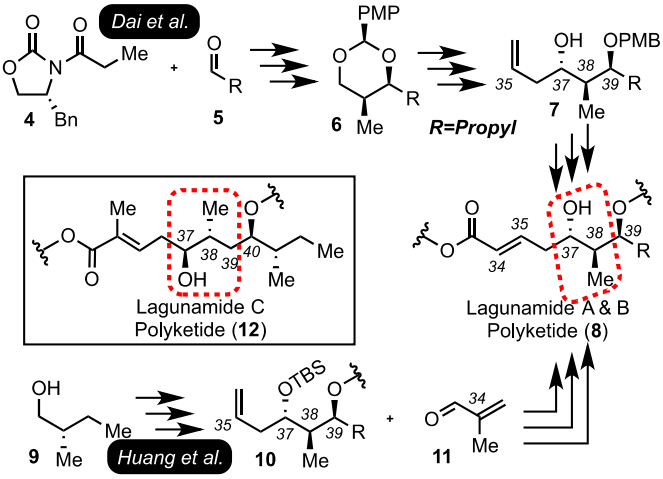

Scheme 1. Construction of polyketides within lagunamide A & B.

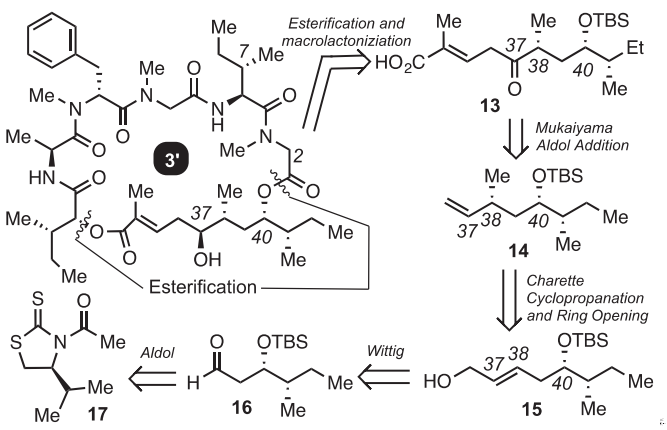

Scheme 2. Retrosynthetic analysis of lagunamide C.

of **16** from an Aldol reaction of an acetylate thiazolidinethione, **17**, and (*S*)-2-methylbutanal in an analogous fashion to Huang et al.[14] Rather than employing the Evans auxiliary, we chose to utilize the Crimmins auxiliary for potential enhanced facial selectivity through the use a bidentate amine to favor coordination of the titanium to the amines rather than the thiocarbonyl sulfur, thus, favoring the desired *cis* aldol product. The key step in our proposed synthesis route of polyketide (**13**) lies within the cyclopropanation and subsequent ring opening steps. Said steps are known for their substrate sensitivity, and difficulty in optimization. Noting the need to investigate if cyclopropane ring opening is achievable in our system, gaining access to the C40 methyl center, cyclopropanation was performed under non-facially selective conditions in this explorative work. To expedite accessing these key, and critical steps, we chose to employ butanal, lacking the desired C41 methyl group, as our starting aldehyde.

Results and discussion

Assembly of the C41 methyl truncated version of **12** commenced with the construction of the acetylated thiazolidinethione, accessed from L-valine (**18**) outlined in Scheme 3. The reduction of **18** was accomplished with $LiAlH_4$ in THF at reflux to afford L-valinol in 99% yield. Formation of the Crimmins auxiliary was performed under standard conditions[17–20] to access **19** in 96% yield over two-steps. Acetylation of the auxiliary with acetyl chloride and *n*-BuLi successfully furnished **17** in 98% yield with no column chromatography required.

The chiral base (−)-sparteine (0.5 eq) was used for the aldol reaction between **17** and butanal with titanium tetrachloride in CH_2Cl_2, which afforded the desired aldol product **20a** in 27% and undesired aldol product in <4% yield (Table 1, entry 1). The stereochemistry of the **20a/b** was confirmed through ^1H NMR and optical rotation comparisons to the same compound accessed by Zhou and co-workers[21] in a different synthetic fashion (data shown in the Supplemental). Zhou also employed the same Crimmins auxiliary, but under his condition of diisopropyl ethylamine **20b** was favored in a 2:1 ratio over **20a**. Increasing the equivalents of the sparteine did provide an increase in **20a**, but only by a marginal 3% with 0.75 equivalents and 8% with 1.2 equivalents (entries 2 and 3, respectively). Employing various amine bases in auxiliary based aldol reactions is well reported in the literature.[19,22] Given the poor yields with the chiral base (−)-sparteine, efforts were directed towards screening other amine bases. Exploring diisopropyl ethylamine (entries 4–6) as the base rather than sparteine, a diamine base, gave the opposite of the desired selectivity, favoring **20b** over **20a**, analogous to the reported observations from Zhou.[21] Varying the equivalences of the base failed to reverse the observed selectivity. The addition of NMP (N-methylpyrrolidone) in an equal molar ratio to the base returned the desired selectivity with yields of 30% of **20a** and 13% of the undesired **20b** (entry 7). Recalling the selectivity observed with sparteine, a diamine base, the return to the desired selectivity is assumed to be through a similar bidentate ligand addition onto the titanium. Doubling the base equivalence increased the yield of **20a** by 8%, but also increased **20b** by 10% (entry 8). Employ the bidentate base TMEDA alone and with NMP failed to provide any yields greater than 22% of **20a** (entries 9–11). With weak bases failing to provide the desired **20a** in both high yields (over 50%) and in high selectivity, strong bases were screened. Screening the reaction with LDA (entry 12) afforded **20a** in 53%, and the undesired **20b** in 11% yield. Optimization of this condition was undertaken, but failed to provide any increase in yield or selectivity. Utilizing an equal molar ratio of LDA to NMP afforded **20a** in 79%, with only 4% of the undesired **20b** (entry 13). Given the observed trends, increasing the NMP equivalence should correlate to increased yields. Unfortunately, this was not observed with LDA and resulted in a decreased yield (entry 14). Through these studies, accessing **20a** in a 70% yield with a 20:1 dr was obtained, a stark difference from the 1:2 dr observed by Zhou.[21]

Table 1
Optimization of Aldol Reaction Conditions.

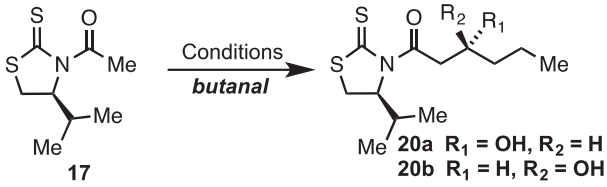

Entry	Reaction conditions[a]	Yield (%)	
		20a	**20b**
1	$TiCl_4$, sparteine (0.5 eq)	27	<4
2	$TiCl_4$, sparteine (0.75 eq)	30	<4
3	$TiCl_4$, sparteine (1.2 eq)	35	<2
4	$TiCl_4$, DIPEA (0.5 eq)	13	36
5	$TiCl_4$, DIPEA (1.1 eq)	22	47
6	$TiCl_4$, DIPEA (2.2 eq)	25	47
7	$TiCl_4$, DIPEA (1.05 eq), NMP (1.05 eq)	30	13
8	$TiCl_4$, DIPEA (2.05 eq), NMP (1.05 eq)	38	23
9	$TiCl_4$, TMEDA (1.05 eq)	19	7
10	$TiCl_4$, TMEDA (2.05 eq)	21	8
11	$TiCl_4$, TMEDA (2.05 eq), NMP (1.2 eq)	22	8
12	$TiCl_4$, LDA (1.2 eq)	53	11
13	$TiCl_4$, LDA (1.2 eq), NMP (1.2 eq)	79	4
14	$TiCl_4$, LDA (1.2 eq), NMP (2.2 eq)	65	<4

[a] Reactions run with 1.05 eq. of $TiCl_4$ in CH_2Cl_2 at [0.5 M] relative to **17**.

With the optimized conditions in hand (Table 1, entry 13), protection of the alcohol within **20a** was performed. Treating **20a** under standard TBSCl protection conditions, imidazole in THF, afforded the TBS protected alcohol **21** in 45% (Scheme 4). Optimization of these conditions failed to afford any increase in yield. Employing 2,6-lutidine in DMF at RT afforded **21** in 65% yield. Increasing the temperature to 32 °C increased the yield to 86% of **21**. Any further increasing in temperature failed to result in yield increase, but rather lead to decomposition of the material. Treat-

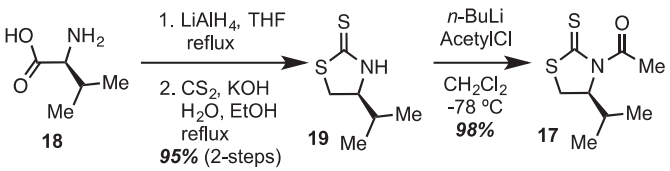

Scheme 3. Formation of the acetylated Crimmin's auxiliary.

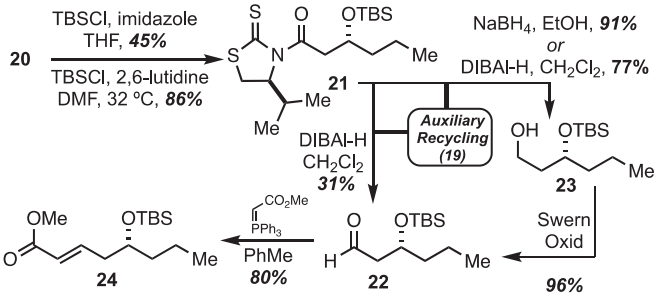

Scheme 4. Chain elongation and olefin installation-via Wittig olefination.

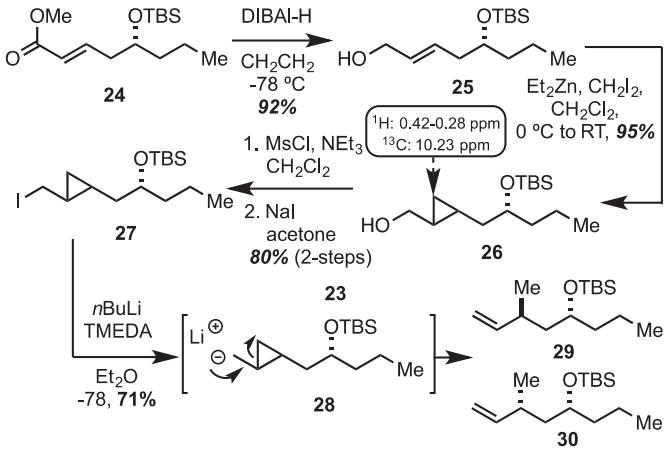

Scheme 5. Cyclopropanation & ring opening accessing the C38 center material.

ment of **21** to DIBAl-H in CH_2Cl_2 gave access to aldehyde **22** in addition to alcohol **23** in 31% and 29% yields, respectively. In this DIBAL-H reduction step 21% of the auxiliary **19** was obtained and acetylated, thus providing **17**. All attempts at the optimization of the DIBAl-H reduction of **21** to give **22** failed to provide any increase in yields. Alcohol **23**, obtained in the DIBAL-H reduction, was oxidized to **22** in 96% yield under Swern oxidation conditions. Employing 2.2 equivalents of DIBAl-H gave access to alcohol **23** in 77% yield, but subjecting **21** to $NaBH_4$ in ethanol furnished **23** in 91% yield, which was subsequently oxidized to **22** in 96% yield. The $NaBH_4$ reduction also resulted in the recovery of 80% of auxiliary **19**, which was successfully recycled and elaborated onto **17**. Structural integrity of **19**, via recycled **17**, was confirmed by ^{1}H NMR spectral and optical rotation comparison to the originally synthesized **19**. Treating **22** with the activated ylide methyl-(triphenylphosphoranylidene)acetate in toluene afforded the allylic methyl ester **24** in 80% yield.

With **24** in hand, the reduction of the ester to its corresponding allylic alcohol **25** was then undertaken. The reduction of **24** with $NaBH_4$ in ethanol afforded allylic alcohol **25** in a 19% yield along with high levels of decomposition. Employing $LiAlH_4$ failed to provide a greater yield of **25** (17% yield). All optimization conditions with these reductants failed to afford **25** in yields greater than 19%. Subjecting **24** to 2.5 equivalents of DIBAl-H in CH_2Cl_2 at −78 °C afforded **25** in 92% yield (Scheme 5). With **25** in hand, efforts towards cyclopropanation and ring opening could be performed. Non-facially selective cyclopropanation conditions were attempted first in the efforts to prove that our proposed key-steps for the synthesis of lagunamide C was feasible. The initial attempts of cyclopropanation with Et_2Zn, CH_2I_2, and $TiCl_4$ at 0 °C failed to provide any of the desired material, which led us to explore temperature optimization. Starting the reaction at 0 °C and then lowering to −20 °C failed to provide any product, as did the increase of temperatures. To our surprise, setting up the reaction at 0 °C and then warming to room temperature, 45 min post reagent addition, led to a 3% yield of **26**. Exclusion of $TiCl_4$ under the same conditions resulted in an increase in yield to 48%, and upon running the reaction overnight resulted in a 95% conversion to the desired cyclopropanated material **26** as a mixture of diastereomers. Mesylate protection of the alcohol was accomplished with methanesulfonyl chloride, NEt_3 in CH_2Cl_2. The material was subsequently converted to the iodine counterpart (**27**) with NaI in acetone with an 80% yield over the 2-steps. The stability of **27** was found to be fleeting (1–2 h) and was therefore pushed onto the lithium-halogen exchange step immediately. Subjecting **27** to *n*BuLi and TMEDA in diethyl ether at −78 °C afforded a mixture of the desired terminal alkenes **29** and **30** in 71% combined yield, via intermediate **28**. Using less than 2.0 equivalents of TMEDA resulted in a rapid decrease in yields of **29/30** and led to an increase in decomposition of material.

Conclusion

We have developed a route that will allow for the assembly of the polyketide required to access lagunamide C, as well as possible analogs for the elucidation of the stereochemical assignment about C38. This strategy highlights the employed valinol based Crimmins auxiliary, used in the setting of the C40 stereocenter, via an optimized LDA/NMP aldol reaction with a 20:1 selectivity. This highly selective aldol, in comparison to the literature on like systems, presents a new method on accessing these type of β-hydroxyl-carbonyl. Elaboration of this material onto the allylic alcohol successively allowed for the proof-of-concept in our route; cyclopropanation with subsequent ring opening. Through this developed route, the proposed polyketide is currently being assembled and will be used for the first total synthesis of lagunamide C. Through these efforts, key mode of action studies will be explored to elucidate the means at which this family elicits their cytotoxic properties.

Acknowledgements

We would like to thank Kansas State Universities Office of Research and Department of Chemistry for funding this work through providing startup capital. We are especially grateful to the Johnson Cancer Center at KSU for providing a summer graduate research fellowship for CW and funding this and related work through an innovative research award. We would like to thank Olivia Haney for her technical assistance in the assembly of this manuscript. This paper is warmly dedicated to Emeritus Professor Marcus Meilahn in recognition and appreciation of his teaching and mentorship.

A. Supplementary data

Supplementary data associated with this article can be found, in the online version, at https://doi.org/10.1016/j.tetlet.2017.12.083.

References

1. Ehrenreich IM, Waterbury JB, Webb EA. *Appl Environ Microbiol*. 2005;71:7401.
2. Jones AC, Monroe EA, Podell S, et al. *Proc Natl Acad Sci*. 2011;108:8815.
3. Costa M, Costa-Rodrigues J, Fernandes MH, Barros P, Vasconcelos V, Martins R. *Mar Drugs*. 2012;10:2181.
4. Tan LT. *Phytochemistry*. 2007;68:954.
5. Nunnery JK, Mevers E, Gerwick WH. *Curr Opin Biotechnol*. 2010;21:787.
6. Gerwick WH, Tong Tan L, Sitachitta N. *Alkaloids: Chem Biol*. 2001;57:75.
7. Singh RK, Tiwari SP, Rai AK, Mohapatra TM. *J Antibiot*. 2011;64:401.
8. Linington RG, Clark BR, Trimble EE, et al. *J Nat Prod*. 2009;72:14.
9. Tripathi A, Puddick J, Prinsep MR, Lee PPF, Tan LT. *Phytochemistry*. 2010;71:307.
10. Tripathi A, Puddick J, Prinsep MR, Rottmann M, Tan LT. *J Nat Prod*. 2010;73:1810.
11. Tripathi A, Puddick J, Prinsep MR, et al. *Phytochemistry*. 2011;72:2369.
12. Tripathi A, Fang W, Leong DT, Tan LT. *Mar Drugs*. 2012;10:1126.
13. Dai L, Chen B, Lei H, et al. *Chem Commun*. 2012;48:8697.
14. Huang W, Ren R-G, Dong H-Q, Wei B-G, Lin G-Q. *J Org Chem*. 2013;78:10747.
15. Pal S, Chakraborty TK. *Tetrahedron Lett*. 2014;55:3469.
16. Corey EJ, Bakshi RK, Shibata S. *J Am Chem Soc*. 1987;109:5551.
17. Ko K-S, Alexander MD, Fontaine SD, Biggs-Houck JE, La Clair JJ, Burkart MD. *Org Biomol Chem*. 2010;8:5159.
18. Crimmins MT, Chaudhary K. *Org Lett*. 2000;2:775.
19. Crimmins MT, King BW, Tabet EA, Chaudhary K. *J Org Chem*. 2001;66:894.
20. Crimmins MT, Shamszad M, Mattson AE. *Org Lett*. 2010;12:2614.
21. Zhou H, Gao Z, Qiao K, Wang J, Vederas JC, Tang Y. *Nat Chem Biol*. 2012;8:331.
22. Kaneda M, Sueyoshi K, Teruya T, Ohno H, Fujii N, Oishi S. *Org Biomol Chem*. 2016;14:9093.

JOURNAL OF NATURAL PRODUCTS

Article

Cite This: J. Nat. Prod. 2017, 80, 3234−3240

pubs.acs.org/jnp

Total Synthesis of Reniochalistatin E

Anthony Fatino, Giovanna Baca, Chamitha Weeramange, and Ryan J. Rafferty*

Department of Chemistry, Kansas State University, Manhattan, Kansas 66506, United States

Supporting Information

ABSTRACT: Reniochalistatin E (**1**) is one of the five related cyclic peptides isolated from the marine sponge *Reniochalina stalagmitis*. The discovery of these compounds resulted from a screening program directed toward the identification of proline-rich bioactive compounds. Reniochalistatin E is the only member of the family to possess a tryptophan amino acid residue. Given the cytotoxicity observed for **1**, efforts were directed toward developing a synthetic route to **1**. The first total synthesis of **1** has been accomplished in a 15-step route in an overall 5.0% yield. The synthetic sample of reniochalistatin E was shown to have similar activity toward HeLa and RPMI-8226 cell lines compared to the natural sample, with IC_{50} values of 16.9 vs 17.3 μM and 4.5 vs 4.9 μM, respectively. Interestingly, both of the fully deprotected octapeptides constructed toward the synthesis of reniochalistatin E were shown to have cytotoxicity. The route provides a means to probe the structure−activity relationship of **1** and further biological investigations.

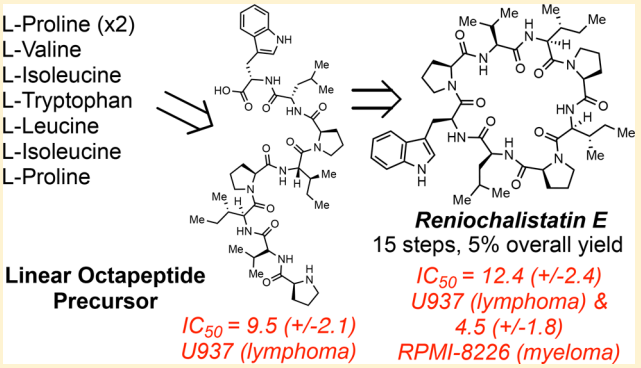

The reniochalistatin family of cyclic peptides was isolated from the marine sponge *Reniochalina stalagmitis* near Yongxing Island in the South China Sea in 2014 by Lin and co-workers.[1] The family was discovered as part of a screening program designed to find new bioactive cyclic peptides from marine sponges in the South China Sea.[2−5] Cyclic peptides that are proline-rich have been shown to have a variety and wide scope of biological activity, such as antiviral, antitumor, antimicrobial, and general cytotoxic properties.[6−8] The members of the reniochalstatin family were found to be proline-rich and composed of apolar and aromatic amino acid residues. Leucine and isoleucine are present in all five members, along with multiple proline units (two within reniochalistatins A, B, and C and three within D and E). The aromatic amino acid residue varies among the members of the family; B, C, and D contain phenylalanine, whereas E is the only one with a tryptophan residue.[8] Reniochalistatins A through D are cyclic heptaptides, whereas E is the only cyclic octapeptide that was isolated. Only reniochalistatin E showed biological activity, with cytotoxicity toward myeloma (RPMI-8226, IC_{50} of 4.9 μM) and gastric (MGC-803, IC_{50} of 9.7 μM) cancer cell lines. It was the activity toward myeloma that drew the attention of our laboratory and resulted in a total synthesis campaign to be undertaken.

We envisioned that **1** could be synthesized via successive amino acid couplings in tandem with selective deprotection steps. The cyclic compound could be obtained from the coupling and macrocyclization of the two desired tetrapeptides (**2** and **3**). Each of these tetrapeptides could be constructed from their corresponding commercially available L-amino acids, with selective protection about either the free carboxylic acid or amine (Scheme 1).

According to the retrosynthetic plan outlined in Scheme 1, efforts were directed toward the construction of tetrapeptide **2** (Scheme 2). Starting from the Boc-protected L-isoleucine (**4**) an amidation was performed though a benzotriazole-L-yl-oxy-tris-pyrrolidino-phosphonium hexafluorophosphate (PyBOP)-mediated coupling with the methyl ester of L-proline (**5**), affording the dipeptide **6** in 92% yield. Analogously, Boc-L-leucine (**7**) was coupled to the methyl ester of L-tryptophan (**8**) under the same conditions to access dipeptide **9** in 97% yield. Saponification of dipeptide **6** furnished the free acid **10**, and Boc deprotection of **9** accessed the amine hydrochloride salt **11**. Both reactions provided quantitative yields. The coupling of these two dipeptides was accomplished with PyBOP under standard conditions to give tetrapeptide **2** in 55% yield. Employing 1-ethyl-3-(3'-dimethylaminopropyl)carbodiimide hydrochloride (EDC·HCl) with HOBt as the coupling conditions, yields were optimized at 86%.

With tetrapeptide **2** in hand, efforts were directed toward the construction of tetrapeptide **3** (Scheme 3), which will allow for access to **1**. The coupling of Boc-L-proline (**12**) to the methyl ester of L-leucine (**13**) was performed with PyBOP to furnish the dipeptide **14** in 97% yield. Saponification of **14** gave access to the free acid dipeptide **15** in quantitative yields. The second half of the tetrapeptide was accessed from the Boc deprotection of dipeptide **6** in quantitative yield. The coupling of **15** to **16** under the previously employed PyBOP conditions afforded the desired tetrapeptide **3**, but unfortunately as an impure mixture based upon the ^{1}H NMR spectrum obtained. All attempts at

Received: July 29, 2017
Published: December 8, 2017

DOI: 10.1021/acs.jnatprod.7b00656
J. Nat. Prod. 2017, 80, 3234−3240

Scheme 1. Retrosynthetic Approach to Reniochalistatin E

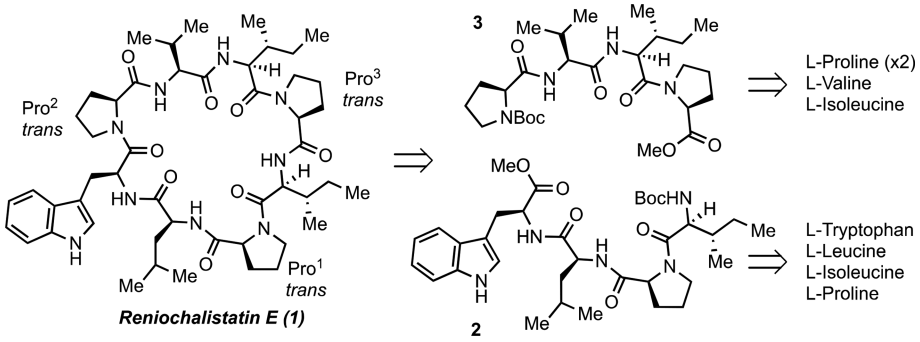

Scheme 2. Assembly of Tetrapeptide 2 with Successive PyBOP Coupling and Deprotection Steps

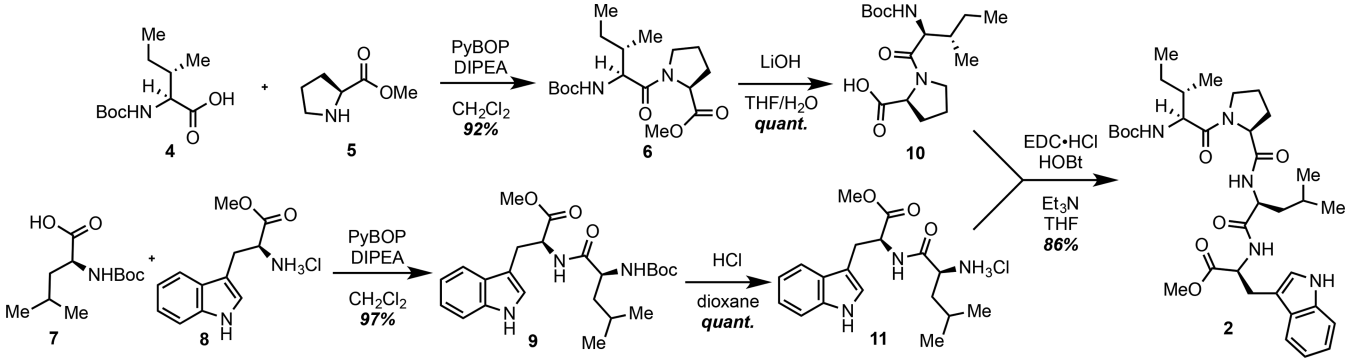

Scheme 3. Construction of Tetrapeptide 3 through Successive Amide Forming Coupling Reactions along with Deprotection Steps

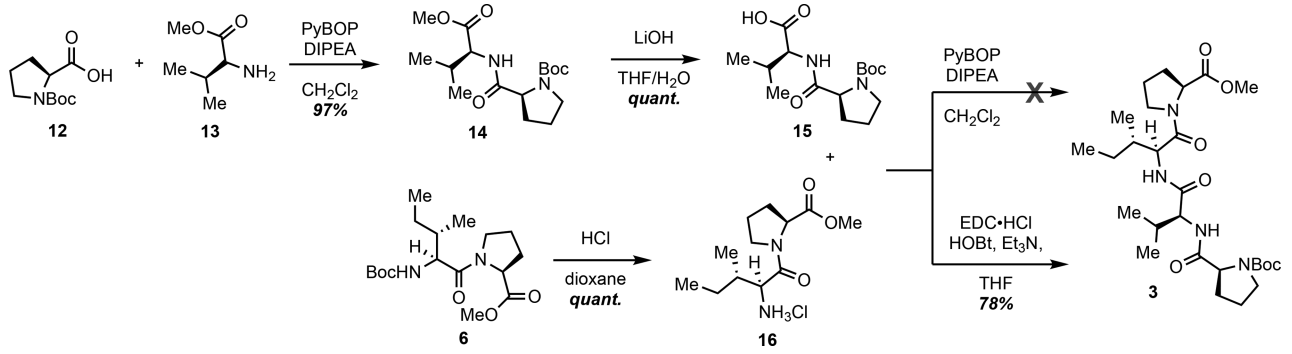

Scheme 4. Tetrapeptide Couplings and Cyclization Strategies Accessing Reniochalistatin E (1)

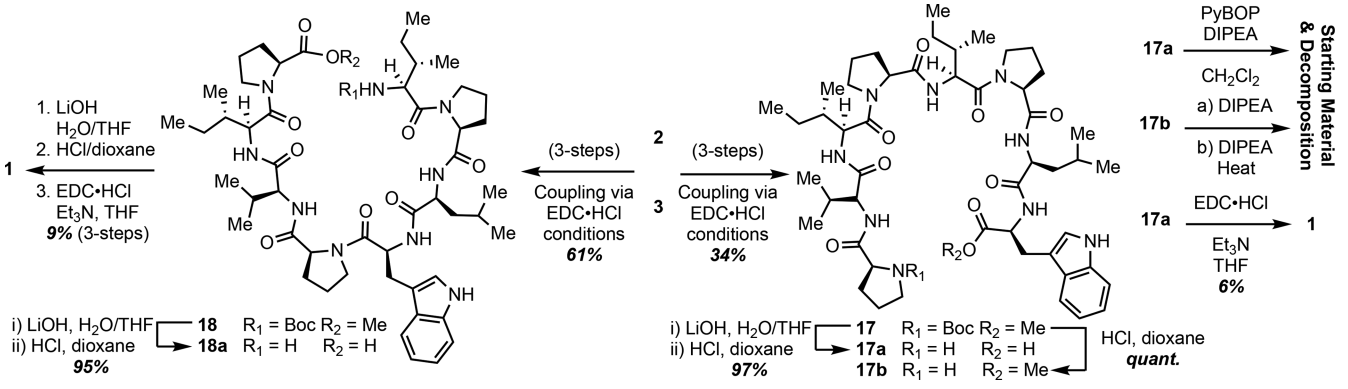

purification (workup procedures, chromatographic eluents, and silica) of this material continued to provide the same contaminant peaks within the acquired ^{1}H NMR spectrum. When this material was carried forward, either through saponification or Boc deprotection, none of the desired material was collected. Pure tetrapeptide **3** was successfully accessed through the use of EDC·HCl and HOBt in 78% yield.

DOI: 10.1021/acs.jnatprod.7b00656
J. Nat. Prod. 2017, 80, 3234−3240

Having accessed both of the desired tetrapeptides **2** and **3**, the coupling and macrocyclization were performed. The initial approach to the linear octapeptide of **1** was through the saponification of **2** and the Boc deprotection of **3**. Coupling of the free acid of **2** to the free base of **3** with EDC·HCl furnished octapeptide **17** in 34% yield over three steps (Scheme 4). Compound **17** was subjected to saponification followed by Boc deprotection to afford its fully deprotected form **17a** in 97% yield. The attempted macrocyclization of this material under PyBOP conditions failed to provide any of the desired product, but rather resulted in the return of starting material (55%) and decomposition. It is hypothesized that the bulk of both the secondary amine within the proline residue and the BOP-activated ester of the tryptophan residue could provide sufficient steric congestion, thereby preventing cyclization from occurring. To reduce the steric hindrance about these centers, aminolysis was then attempted for ring closure. For this, the Boc group on **17** was removed to afford **17b**, with the methyl ester intact. Unfortunately, all attempts at cyclization in this fashion failed to provide **1** and resulted in the return of starting material (67%) and decomposition. Recognizing the difficulty in macrocyclization of these two sterically encumbered proline and tryptophan residues of **17a**, it was envisioned that coupling of these two centers to access the linear octapeptide would be more attainable followed then by macrocyclization. As such, **2** was saponified to its free acid and Boc deprotection of **3** afforded the free amine, both accomplished in quantitative yields. The EDC·HCl coupling of these two units furnished the linear octapeptide **18** in 61% yield over three steps. Compound **18** was transformed into its free acid and free amine counterpart in 95% yield and then subjected to EDC·HCl coupling conditions to afford the desired natural product **1** in 9% yield. The ^{1}H and ^{13}C NMR spectra as well as the MS data of the synthesized **1** match with the literature data (see the Supporting Information). Confirmation of the *trans* prolines within **1** was confirmed based on the comparison of the reported $\Delta\delta_{C\beta\text{-}C\gamma}$ values of proline residues (4.9, 4.2, and 4.1 ppm for Pro,[1] Pro,[2] and Pro,[3] respectively). The successful macrocyclization of the free acid/amine of **18** with EDC·HCl on the first attempt led us to attempt the same conditions for cyclization upon the unsuccessful closure of the free acid/amine of **17**. To our surprise, treating **17a** with EDC·HCl afforded reniochalistatin E in 6% yield. All spectroscopic (NMR and IR) and MS data matched both the literature and the previously synthesized material.

Screening various coupling reagents and conditions was then performed to increase the yield of **1** (Table 1). Entries 1 and 9 highlight the coupling affording **1** outlined in Scheme 4 from **17a** and **18a**, respectively. The attempted PyBOP-mediated coupling of **18a** (entry 8) provided only recovered starting material (78%) and decomposition. Employing HOBt, a commonly used additive in peptide couplings, with EDC·HCl to cyclize **17a** and **18a** (entries 2 and 10) resulted in low yields of **1** of 2% and 6%, respectively. Entry 10 reflects the highest yield of **1** in our synthetic approach via **18a**. Next, macrocyclization was attempted employing 3-(diethoxyphosphoroyloxyl)-1,2,3-benzotriazine-4(3*H*)-one (DEPBT), a reagent that has been successful in the cyclization of similar amino acid based macrocycles.[9] Unfortunately, all attempts at cyclization with this reagent of **17a** and **18a** (entries 3 and 11) as well as using cesium chloride as an additive to promote carbonyl coordination (entries 4 and 12) failed to provide **1** in any increased yield. Uronium-based coupling reagents are well reported for their success in macrocyclizations, and as such, *N,N,N′,N′*-tetramethyl-*O*-(1*H*-benzotriazol-1-yl)uronium hexafluorophosphate (HBTU)[10−13] and *N,N,N′,N′*-tetramethyl-*O*-(1*H*-benzotriazol-1-yl)uronium tetrafluoroborate (TBTU)[13−16] were both attempted with **17a** and **18a** in the absence and presence of 4-(dimethylamino)pyridine (DMAP).[17,18] In all attempted cyclizations, these uronium-based reagents provided either none or low yields of **1**. Employing HBTU with DMAP to cyclize **18a** provided a 13% yield of **1** (entry 14), but in our hands, EDC·HCl with HOBt gave the best, albeit low, 15% yield of the natural product.

Table 1. Screening of Coupling Conditions of Fully Deprotected 17a and 18a

entry	cmpd	coupling agent	additive	result
1	**17a**	EDC·HCl	N/A	6%
2		EDC·HCl	HOBt	8%
3		DEBPT	N/A	
4		DEBPT	CsCl	
5		HBTU	N/A	
6		HBTU	DMAP	4%
7		TBTU	DMAP	trace
8	**18a**	PyBOP	N/A	trace
9		EDC·HCl	N/A	9%
10		EDC·HCl	HOBt	15%
11		DEBPT	N/A	
12		DEBPT	CsCl	5%
13		HBTU	N/A	
14		HBTU	DMAP	13%

With reniochalistatin E and numerous di-, tetra-, and octapeptides in both fully protected and deprotected states in hand, all compounds were screened for general cytotoxicity against six human cancer cell lines (A549, lung; HeLa, cervical; MiaPaca, pancreatic; U937, lymphoma, RPMI-8226, myeloma; and MM.1R, multiple myeloma). None of the di- or tetrapeptides in protected and partial deprotected states were found to have IC_{50} values lower than 30 μM against these cell lines. Our synthetic sample of reniochalistatin E possessed approximately the same IC_{50} value toward the HeLa and RPMI-8226 cell lines: IC_{50} of 16.9 μM ($\pm$1.9) relative to the reported 17.3 μM in HeLa and an IC_{50} of 4.5 ($\pm$2.2) relative to the reported 4.9 μM in RPMI-8226 (Table 1). Reniochalistatin E lacked cytotoxicity against all of the tested cell lines (cytotoxicity = IC_{50} < 10 μM). Both **17** and **18**, diprotected octapeptides, were shown to have no cytotoxicity. Interestingly, the free acid/amine **17a** was shown to have borderline cytotoxicity toward the U937 cell line with an IC_{50} of 9.5 $\pm$ 2.1 μM. In comparison to the free acid/amine **18a**, no cytotoxicity was observed. No further investigational studies at this time have been performed that could draw conclusions regarding structure−activity relationships based upon the results obtained.

In conclusion, we have accomplished the first total synthesis of reniochalistatin E in 15 steps with an overall 5.0% yield from commercially available materials. Cytotoxicity studies with reniochalistatin E and all intermediates accessed within the route revealed a general lack of cytotoxicity. However, the synthetic and isolated reniochalistatin E are shown to possess nearly the same activity toward the HeLa cervical cancer cell line, further supporting the total synthesis outlined herein. In addition, an interesting and unexpected cytotoxicity was observed for the free acid/amine of **17a** (linear octapeptide precursors to the natural product) toward the U937 cell line. With a route established to this cyclic octapeptide, efforts are

DOI: 10.1021/acs.jnatprod.7b00656
J. Nat. Prod. 2017, 80, 3234−3240

Table 2. Evaluation of Reniochalistatin E and Linear Octapeptides for Cytotoxicity

	observed IC_{50} (μM)[a]					
cmpd	A549	HeLa	MiaPaca	U937	RPMI-8226	MM.1R
1	>20	16.9 ± 1.9	>20 μM	12.4 ± 2.4	4.5 ± 1.8	>11.2 ± 1.0
17	>20	>20	19.1 ± 1.3	>20	>20	>20
17a	>20	>20	>20	9.5 ± 2.1	>20	>20
18	>20	>20	>20	>20	>20	>20
18a	>20	18.4 ± 1.7	>20	>20	16.4 ± 3.5	>20

[a]Cytotoxicity evaluated in 384-well plates, 1500 (2000 U937) cells/well, 72 h incubation period, and evaluated via Alamar Blue.

currently being pursued toward probing the effects of single amino acid variations as well as the transposition of phenylalanine for tryptophan. The resulting analogues of **1** will be evaluated for cytotoxicity.

EXPERIMENTAL SECTION

General Experimental Procedures. Optical rotations were measured on an Atago Polax-2L polarimeter with a sodium lamp. IR spectra were recorded on a Cary 630 FT-IR spectrometer as thin films. Only the strongest and/or structurally important absorptions of IR spectra were reported in wavenumbers (cm^{-1}). ^1H (400, 500 MHz) and ^{13}C (100, 151 MHz) spectra were obtained on Varian and Bruker-Ascend spectrometers. The chemical shifts are given in parts per million (ppm) relative to residual $CHCl_3$ at δ 7.26 ppm for proton spectra and relative to $CDCl_3$ at δ 77.23 ppm for carbon spectra, unless otherwise noted. High-resolution mass spectra were obtained using an LCT Premier time-of-flight mass spectrometer. Flash column chromatography was performed with silica gel grade 60 (230−400 mesh). Dichloromethane (CH_2Cl_2), tetrahydrofuran (THF), toluene (PhMe), *N*,*N*-dimethylformamide (DMF), CH_3CN, triethylamine (Et_3N), and MeOH were all degassed with argon and passed through a solvent purification system containing alumina or molecular sieves. All commercially available reagents were used as received.

***N*-Boc-L-Ile-L-Pro-OMe (6).** To a stirring solution of *N*-Boc-L-isoleucine (**4**; 1.0 g, 4.16 mmol, 1.0 equiv) in CH_2Cl_2 (42 mL) were added PyBOP (2.27 g, 4.37 mmol, 1.05 equiv) and iPr$_2$EtN (1.09 mL, 6.24 mmol, 1.5 equiv). To a separate round-bottom flask (RBF) were added L-proline methyl ester (**5**; 1.03 g, 6.24 mmol, 1.5 equiv), iPr$_2$EtN (2.17 mL, 12.48 mmol, 3.0 equiv), and CH_2Cl_2 (6.3 mL). Both reaction mixtures were left to stir for 1 h, at which time they were combined and left to stir overnight at room temperature (rt). The reaction was quenched with 1 M HCl (1 vol equiv), and the product was extracted with CH_2Cl_2 (×2), washed with $NaHCO_{3(satd)}$, dried over sodium sulfate, and concentrated under reduced pressure. The crude material was purified via flash silica gel chromatography (1:2 EtOAc/hexane) to afford **6** (1.30 g, 92% yield): $[\alpha]_D^{25}$ +40.3 (*c* 1.23, $CHCl_3$); IR (film) ν_{max} 3436, 2973, 1746, 1642, 1436, 1217 cm^{-1}; ^1H NMR ($CDCl_3$, 400 MHz) δ 5.11 (d, *J* = 9.5 Hz, 1H), 4.52−4.44 (m, 1H), 4.24 (dd, *J* = 9.5, 7.2 Hz, 1H), 3.80−3.73 (m, 1H), 3.66 (s, 3H), 3.65−3.58 (m, 1H), 2.22−2.12 (m, 1H), 2.01−1.90 (m, 3H), 1.71 (ddq, *J* = 10.3, 6.5, 3.5 Hz, 1H), 1.53 (td, *J* = 7.2, 6.6, 3.2 Hz, 1H), 1.37 (s, 9H), 1.07 (ddd, *J* = 13.4, 6.7, 2.3 Hz, 1H), 0.96 (d, *J* = 6.8 Hz, 3H), 0.86 (t, *J* = 7.4 Hz, 3H); ^{13}C NMR ($CDCl_3$, 101 MHz) δ 172.64, 171.65, 156.01, 79.70, 59.04, 56.46, 52.35, 47.42, 38.13, 29.29, 28.56, 25.17, 24.38, 15.47, 11.46; HRESIMS *m*/*z* 343.2193 $[M + H]^+$ (calcd for $C_{17}H_{30}N_2O_5$, 343.2188).

***N*-Boc-L-Leu-L-Trp-OMe (9).** To a stirring solution of compound *N*-Boc-L-leucine (**7**; 1.0 g, 4.32 mmol, 1.0 equiv) in CH_2Cl_2 (43 mL) were added PyBOP (2.36 g, 4.54 mmol, 1.05 equiv) and iPr$_2$EtN (1.13 mL, 6.48 mmol, 1.5 equiv). To a separate RBF were added L-tryptophan methyl ester (**8**; 1.65 g, 6.48 mmol, 1.5 equiv), iPr$_2$EtN (2.26 mL, 12.96 mmol, 3.0 equiv), and CH_2Cl_2 (6.5 mL). Both reaction mixtures were left to stir for 1 h, at which time they were combined and left to stir overnight at rt. The reaction was quenched with 1 M HCl (1 vol equiv), and the product was extracted with CH_2Cl_2 (×2), washed with $NaHCO_{3(satd)}$, dried over sodium sulfate, and concentrated under reduced pressure. The crude material was purified via flash silica gel chromatography (1:1 EtOAc/hexane) to afford **9** (1.81 g, 97% yield): $[\alpha]_D^{25}$ +27 (*c* 0.15, $CHCl_3$); IR (film) ν_{max} 3418, 3018, 2872, 1739, 1513, 1215 cm^{-1}; ^1H NMR (400 MHz, DMSO-d_6) δ 10.85 (s, 1H), 8.06 (d, *J* = 7.4 Hz, 1H), 7.45 (d, *J* = 7.9 Hz, 1H), 7.31 (d, *J* = 8.1 Hz, 1H), 7.13 (d, *J* = 2.4 Hz, 1H), 7.07−7.02 (m, 1H), 6.96 (td, *J* = 7.5, 6.9, 1.1 Hz, 1H), 6.82 (d, *J* = 8.5 Hz, 1H), 4.51 (q, *J* = 7.1 Hz, 1H), 3.98 (td, *J* = 8.7, 6.0 Hz, 1H), 3.55 (s, 3H), 3.13−3.05 (m, 2H), 1.53 (dd, *J* = 13.6, 6.9 Hz, 2H), 1.35 (s, 9H), 1.26 (s, 1H), 0.84 (d, *J* = 6.6 Hz, 3H), 0.81 (d, *J* = 6.5 Hz, 3H); ^{13}C NMR (101 MHz, $CDCl_3$) δ 172.99, 172.44, 155.95, 136.45, 127.76, 123.62, 122.15, 119.58, 118.63, 111.71, 109.49, 80.22, 53.46, 53.29, 52.54, 41.55, 28.52, 27.81, 24.92, 23.18, 22.04; HRESIMS *m*/*z* 454.2308 $[M + Na]^+$ (calcd for $C_{23}H_{33}N_3O_5Na^+$, 454.2312).

***N*-Boc-L-Ile-L-Pro-OH (10).** To a stirring solution of **6** (556 mg, 1.62 mmol, 1.0 equiv) in 1:1 THF/H_2O (16 mL) was added LiOH (194 mg, 8.12 mmol, 5.0 equiv). The mixture was left to stir at rt for 5 h. The reaction was quenched with 1 M HCl (1 vol equiv), and the product was extracted with CH_2Cl_2, washed with $NaHCO_{3(satd)}$, dried over sodium sulfate, and concentrated under reduced pressure. The product **10** was obtained in quantitative yield as an oily residue, which was used without further purification. IR (film) ν_{max} 3456, 3304, 2977, 1704, 1314 cm^{-1}; ^1H NMR (400 MHz, $CDCl_3$) δ 8.31 (s, 1H), 5.35 (d, *J* = 9.5 Hz, 1H), 4.57 (t, *J* = 6.4 Hz, 1H), 4.32−4.25 (m, 1H), 3.82 (dt, *J* = 9.6, 7.2 Hz, 1H), 3.64 (ddd, *J* = 9.7, 7.5, 5.4 Hz, 1H), 2.18 (dd, *J* = 10.0, 3.9 Hz, 2H), 2.07−1.99 (m, 2H), 1.76 (td, *J* = 7.0, 3.4 Hz, 1H), 1.64−1.48 (m, 2H), 1.41 (d, *J* = 7.7 Hz, 9H), 0.95 (d, *J* = 6.7 Hz, 3H), 0.87 (t, *J* = 7.2 Hz, 3H).

***N*-Boc-L-Leu-L-Trp-OH (11).** To a RBF was added 1 M HCl in dioxane (4.6 mL), which cooled to 0 °C, at which point **9** (500 mg, 1.16 mmol) was added. The reaction was allowed to stir for 1.5 h. The solvent was removed under reduced pressure to afford a crude white solid (**11**), which was used without further purification. IR (film) ν_{max} 3416, 2879, 1651, 1176 cm^{-1}; ^1H NMR (400 MHz, DMSO-d_6) δ 9.04 (d, *J* = 7.2 Hz, 1H), 8.25 (s, 3H), 7.49 (d, *J* = 7.8 Hz, 1H), 7.35 (dt, *J* = 8.1, 1.0 Hz, 1H), 7.24 (d, *J* = 2.3 Hz, 1H), 7.07 (ddd, *J* = 8.1, 7.0, 1.3 Hz, 1H), 7.00 (ddd, *J* = 8.0, 7.0, 1.1 Hz, 1H), 4.63−4.54 (m, 1H), 3.81 (t, *J* = 7.2 Hz, 1H), 3.58 (s, 3H), 3.21−3.13 (m, 2H), 1.68 (dt, *J* = 13.3, 6.6 Hz, 2H), 1.57 (s, 2H), 0.90 (dd, *J* = 7.9, 6.4 Hz, 6H).

***N*-Boc-L-Ile-L-Pro-L-Leu-L-Trp-OMe (2).** Compound **10** (1.32 g, 4.02 mmol, 1 equiv), compound **11** (1.08 g, 2.94 mmol, 1 equiv), and HOBt (473 mg, 3.09 mmol, 1.05 equiv) were dissolved in dry THF (40 mL) at rt under an argon atmosphere. The solution was cooled to 0 °C and stirred for 20 min, after which Et_3N (1.43 mL, 10.29 mmol, 3.5 equiv) was then added and stirred. Lastly, 20 min later EDC·HCl (592 mg, 3.09 mmol, 1.05 equiv) was added, and the reaction mixture was left to stir overnight. The reaction was quenched with H_2O (1 vol equiv), and the product was extracted with CH_2Cl_2, dried over sodium sulfate, and concentrated under reduced pressure. The crude material was purified via flash silica gel chromatography (3:1 EtOAc/hexane) to give afford **2** (2.22 g, 86% yield) as a clear liquid: $[\alpha]_D^{25}$ +48.1 (*c* 1.75, $CHCl_3$); IR (film) ν_{max} 3305, 3017, 2876, 1741, 1631, 1506, 1392, 1215 cm^{-1}; ^1H NMR ($CDCl_3$, 400 MHz) δ 8.29 (s, 1H), 7.51 (d, *J* = 8.6 Hz, 1H), 7.33 (d, *J* = 8.0 Hz, 1H), 7.16 (td, *J* = 8.2, 7.6, 1.3 Hz, 1H), 7.13−7.05 (m, 1H), 7.03 (d, *J* = 2.4 Hz, 1H), 6.97 (d, *J* = 7.8 Hz, 1H), 6.70 (d, *J* = 7.9 Hz, 1H), 5.20 (d, *J* = 9.4 Hz, 1H), 4.90 (dt, *J* = 7.9, 5.5 Hz, 1H), 4.37 (d, *J* = 6.0 Hz, 1H), 4.27 (dd, *J* = 9.3, 7.0 Hz, 1H), 3.71 (d, *J* = 8.9 Hz, 1H), 3.66 (s, 3H), 3.60−3.51 (m, 1H), 3.30 (d, *J* = 5.5 Hz, 2H), 2.12−1.87 (m, 3H), 1.73−1.56 (m, 5H), 1.43 (s, 9H), 1.13−1.05 (m, 1H), 0.92 (d, *J* = 6.8 Hz, 3H), 0.90−0.80 (m, 11H); ^{13}C NMR ($CDCl_3$, 101 MHz) δ 172.86, 172.49, 172.08, 171.74, 156.08, 136.32, 127.75, 123.57, 122.11,

DOI: 10.1021/acs.jnatprod.7b00656
J. Nat. Prod. 2017, 80, 3234−3240

119.61, 118.60, 111.55, 109.58, 79.89, 60.26, 56.61, 52.95, 52.56, 52.15, 47.99, 41.15, 37.95, 28.60, 25.58, 27.76, 25.31, 24.79, 24.42, 23.10, 23.05, 22.06, 15.65, 11.31; HRESIMS m/z 642.3817 $[M + H]^+$ (calcd for $C_{34}H_{52}N_5O_7$, 642.3822).

***N*-Boc-L-Pro-L-Val-OMe (14).** Compounds **12** (3.0 g, 13.94 mmol, 1 equiv) and **13** (2.34 g, 13.94 mmol, 1 equiv) were added to a stirring solution of HOBt (2.24 g, 14.63 mmol, 1.05 equiv) in dry THF (139 mL) at rt under an argon atmosphere. The solution was then cooled to 0 °C and stirred for 20 min, after which Et_3N (6.8 mL, 48.79 mmol, 3.5 equiv) was added. After an additional 20 min of stirring EDC·HCl (2.8 g, 14.63 mmol, 1.05 equiv) was added, and the reaction mixture was left to stir overnight. The reaction was quenched with H_2O (1 vol equiv), and the product was extracted with CH_2Cl_2, dried over sodium sulfate, and concentrated under reduced pressure. The crude material was purified via flash silica gel chromatography (1:1 EtOAc/hexane) to give **14** (4.45 g, 97% yield) as a clear liquid: $[\alpha]_D^{25}$ = +80.8 (*c* 2.05, $CHCl_3$); IR (film) ν_{max} 3680, 3323, 3415, 2973, 2879, 1740, 1681, 1216 cm^{-1}; ^1H NMR ($CDCl_3$, 400 MHz) δ 4.50 (dd, *J* = 8.6, 5.1 Hz, 1H), 4.32 (s, 1H), 3.72 (s, 3H), 3.42 (s, 2H), 2.29 (s, 1H), 2.15 (pd, *J* = 6.9, 5.1 Hz, 2H), 1.95−1.84 (m, 3H), 1.48 (s, 9H), 0.92 (dd, *J* = 8.3, 6.8 Hz, 6H); ^{13}C NMR (DMSO-d_6, 101 MHz) δ 172.71, 78.98, 59.71, 58.16, 52.30, 47.18, 31.67, 30.41, 28.80, 28.68, 23.61, 19.77, 18.99, 14.76; HRESIMS m/z 329.2025 $[M + H]^+$ (calcd for $C_{16}H_{29}N_2O_5$, 329.2032).

***N*-Boc-L-Pro-L-Val-OH (15).** To a stirring solution of **14** (360 mg, 1.1 mmol, 1 equiv) in 1:1 THF/H_2O (4.4 mL) was added LiOH (131 mg, 5.5 mmol, 5 equiv), and the mixture was left to stir at rt for 3 h. The reaction was quenched with 1 M HCl (1 vol equiv), and the product was extracted with CH_2Cl_2, washed with $NaHCO_{3(satd)}$, dried over sodium sulfate, and concentrated under reduced pressure. Crude **15** was obtained in quantitative yield as an oily residue and was used without further purification: IR (film) ν_{max} 3410 (b), 1676 cm^{-1}; ^1H NMR ($CDCl_3$, 400 MHz) δ 10.37 (s, 1H), 7.51 (s, 1H), 4.50 (s, 1H), 4.40−4.19 (m, 1H), 3.50−3.28 (m, 2H), 2.31−2.09 (m, 3H), 1.94−1.79 (m, 2H), 1.43 (s, 9H), 0.91 (dd, *J* = 9.9, 6.9 Hz, 6H).

***H*$_2$*N*-L-Leu-L-Trp-OMe (16).** To a RBF containing **6** (857 mg, 2.5 mmol) was added 1.0 M HCl in dioxane (10 mL), and the mixture was cooled to 0 °C. The reaction mixture was allowed to stir at the same temperature for 3 h. The solvent was removed under reduced pressure to afford crude **16** in quantitative yield as a white solid, which was used without further purification. IR (film) ν_{max} 3416, 2879, 1651, 1454 cm^{-1}; ^1H NMR ($CDCl_3$, 400 MHz) δ 8.34−8.27 (m, 3H), 4.61 (dd, *J* = 8.5, 5.3 Hz, 1H), 4.25 (s, 1H), 3.97 (s, 1H), 3.68 (s, 3H), 3.52 (d, *J* = 9.0 Hz, 1H), 2.28 (s, 1H), 2.05−1.91 (m, 4H), 1.68 (ddd, *J* = 13.5, 7.5, 3.3 Hz, 1H), 1.35 (ddd, *J* = 13.3, 10.0, 7.1 Hz, 1H), 1.12 (d, *J* = 6.8 Hz, 3H), 0.94 (t, *J* = 7.3 Hz, 3H); HSESIMS m/z 243.1658 $[M + H]^+$ (calcd for $C_{12}H_{23}N_2O_3$, 243.1664).

***N*-Boc-L-Pro-L-Val-L-Ile-L-Pro-OMe (3).** Compounds **16** (1.71 g, 7.06 mmol, 1 equiv) and **15** (2.24 g, 7.13 mmol, 1 equiv) were added to a stirring solution of HOBt (1.13 g, 7.41 mmol, 1.05 equiv) and dry THF (71 mL) at rt under an argon atmosphere. The solution was cooled to 0 °C and stirred for 20 min, after which Et_3N (3.46 mL, 24.71 mmol, 3.5 equiv) was added. After an additional 20 min of stirring, EDC·HCl (1.42 g, 7.41 mmol, 1.05 equiv) was added, and the mixture was stirred overnight. The reaction was quenched with H_2O (1 vol equiv), and the product was extracted with CH_2Cl_2, dried over sodium sulfate, and concentrated under reduced pressure. The crude material was purified via flash silica gel chromatography (7:1 EtOAc/hexane) to give **3** (1.52 g, 78% yield) as a clear liquid: $[\alpha]_D^{25}$ +72.3 (*c* 3.21, $CHCl_3$); IR (film) ν_{max} 3673, 3412, 3306, 2879, 1743, 1632, 1368 cm^{-1}; ^1H NMR ($CDCl_3$, 400 MHz) δ 7.48 (s, 1H), 6.65 (s, 1H), 6.42 (s, 1H), 4.58 (t, *J* = 8.2 Hz, 1H), 4.47 (dd, *J* = 8.6, 4.9 Hz, 1H), 4.31 (s, 1H), 4.26 (dd, *J* = 8.6, 5.6 Hz, 1H), 3.81 (dt, *J* = 9.8, 6.3 Hz, 1H), 3.68 (s, 3H), 3.64−3.59 (m, 1H), 3.46−3.28 (m, 2H), 2.33 (s, 1H), 2.19 (ddq, *J* = 12.9, 6.8, 3.7 Hz, 2H), 2.02−1.79 (m, 8H), 1.43 (s, 9H), 0.97 (d, *J* = 6.8 Hz, 3H), 0.89−0.80 (m, 9H); ^{13}C NMR ($CDCl_3$, 101 MHz) δ 172.63, 172.40, 171.29, 171.25, 170.63, 80.70, 61.37, 59.96, 59.00, 58.70, 55.04, 52.35, 47.51, 47.25, 37.65, 31.41, 30.58, 29.29, 28.55, 25.17, 24.52, 19.50, 17.45, 15.41, 11.30; HSESIMS m/z 561.3198 $[M + H]^+$ (calcd for $C_{27}H_{46}N_4O_7Na$, 561.3264).

***H*$_2$*N*-L-Ile-L-Pro-L-Leu-L-Trp-OMe (Free Amine of Tetrapeptide 2).** To a RBF containing **2** (1.03 g, 1.6 mmol) was added 1.0 M HCl in dioxane (6.4 mL), and the solution was cooled to 0 °C. The reaction mixture was allowed to stir at the same temperature for 3 h. The solvent was removed under reduced pressure to afford a crude white solid (free base of **2**), which was used without further purification. IR (film) ν_{max} 3323, 3018, 2879, 1633, 1449, 1216 cm^{-1}; ^1H NMR ($CDCl_3$, 400 MHz) δ 8.17 (d, *J* = 44.9 Hz, 2H), 7.51 (d, *J* = 7.7 Hz, 1H), 7.32 (d, *J* = 8.0 Hz, 1H), 7.14 (t, *J* = 7.5 Hz, 1H), 7.10−7.05 (m, 2H), 6.83 (d, *J* = 8.3 Hz, 1H), 4.96 (d, *J* = 7.8 Hz, 1H), 4.83−4.63 (m, 4H), 4.42 (q, *J* = 7.8 Hz, 2H), 3.91 (d, *J* = 8.3 Hz, 1H), 3.79−3.70 (m, 2H), 3.65 (s, 5H), 3.30 (d, *J* = 6.0 Hz, 2H), 2.96 (ddt, *J* = 22.3, 10.3, 6.4 Hz, 2H), 1.95−1.81 (m, 7H), 1.29−1.22 (m, 3H), 0.89−0.76 (m, 22H).

***N*-Boc-L-Pro-L-Val-L-Ile-L-Pro-OH (Free Acid of Tetrapeptide 3).** To a stirring solution of **3** (200 mg, 0.37 mmol, 1 equiv) in 1:1 THF/H_2O (1.5 mL) was added LiOH (45 mg, 1.86 mmol, 5 equiv), and the solution was left to stir at rt for 3 h. The reaction was quenched with 1 M HCl (1 vol equiv), and the product was extracted with CH_2Cl_2, washed with $NaHCO_{3(satd)}$, dried over sodium sulfate, and concentrated under reduced pressure. The crude material (free acid of **3**), obtained in quantitative yield as an oily residue, was used without further purification. IR (film) ν_{max} 3311, 3016, 2965, 1632, 1215 cm^{-1}; ^1H NMR ($CDCl_3$, 400 MHz) δ 7.50 (s, 0H), 4.63 (t, *J* = 8.9 Hz, 0H), 4.41 (d, *J* = 65.5 Hz, 4H), 3.88 (d, *J* = 10.7 Hz, 1H), 3.67 (s, 2H), 3.43 (s, 2H), 2.16 (s, 7H), 1.96−1.74 (m, 5H), 1.46 (s, 9H), 1.21−0.74 (m, 12H).

Octapeptide *N*-Boc-L-Pro-L-Val-L-Ile-L-Pro-L-Ile-L-Pro-L-Leu-L-Trp-OMe (17). Free base of **2** (915 mg, 1.69 mmol, 1 equiv), free acid of **3** (784.5 mg, 1.5 mmol, 1 equiv), and HOBt (240 mg, 1.56 mmol, 1.05 equiv) were dissolved in dry THF (17 mL) at rt, under an argon atmosphere. The solution was then cooled to 0 °C and stirred for 20 min, after which Et_3N (0.731 mL, 5.25 mmol, 3.5 equiv) was added. After an additional 20 min of stirring, EDC·HCl (299 mg, 1.56 mmol, 1.05 equiv) was added, and the mixture was left to stir overnight. The reaction was quenched with H_2O (1 vol equiv), and the product was extracted with CH_2Cl_2, dried over sodium sulfate, and concentrated under reduced pressure. The crude material was purified via flash silica gel chromatography (1:9 EtOAc/MeOH) to afford **17** (605 mg, 34% yield) as an amber liquid: $[\alpha]_D^{25}$ −26 (*c* 0.21, MeOH); ^1H NMR ($CDCl_3$, 400 MHz) δ 7.50 (d, *J* = 7.9 Hz, 1H), 7.31 (d, *J* = 8.0 Hz, 1H), 7.13 (t, *J* = 7.2 Hz, 1H), 7.10−7.03 (m, 2H), 6.82 (s, 1H), 4.97 (s, 1H), 4.65 (s, 2H), 4.42 (s, 2H), 4.25 (s, 1H), 3.88 (d, *J* = 9.4 Hz, 1H), 3.69 (s, 2H), 3.66 (s, 3H), 3.30 (d, *J* = 4.9 Hz, 2H), 2.07 (d, *J* = 145.9 Hz, 24H), 1.44 (s, 4H), 1.31−1.21 (m, 1H), 0.90−0.75 (m, 25H); ^{13}C NMR ($CDCl_3$, 101 MHz) δ 17.38, 172.39, 151.82, 142.80, 140.68, 136.40, 127.78, 122.15, 119.63, 118.69, 111.44, 52.59, 48.15, 28.55, 24.87, 24.87, 23.06, 23.06, 19.62, 19.62, 15.33, 11.24; HRESIMS m/z 1070.6253 $[M + H]^+$ (calcd for $C_{55}H_{85}N_9O_{11}Na$, 1070.6267).

***H*$_2$*N*-L-Pro-L-Val-L-Ile-L-Pro-OMe (Free Amine of Tetrapeptide 3).** To an RBF containing **3** (151 mg, 0.28 mmol) was added 1.0 M HCl in dioxane (1.1 mL), and the solution was cooled to 0 °C. The reaction was allowed to stir at the same temperature for 3 h. The solvent was removed under reduced pressure, forming a crude white solid (free base **3**), which was used without further purification. IR (film) ν_{max} 3323, 2878, 1742, 1633, 1216 cm^{-1}; ^1H NMR ($CDCl_3$, 400 MHz) δ 10.92 (s, 1H), 8.76 (s, 1H), 8.16 (s, 1H), 7.83 (d, *J* = 9.0 Hz, 1H), 4.92 (s, 1H), 4.76−4.68 (m, 1H), 4.52−4.35 (m, 2H), 3.87 (s, 2H), 3.69 (d, *J* = 2.2 Hz, 3H), 3.64 (dd, *J* = 8.5, 5.1 Hz, 1H), 3.44 (s, 3H), 2.63 (s, 1H), 2.46−2.17 (m, 5H), 2.00 (dd, *J* = 18.0, 6.0 Hz, 10H), 1.52−1.39 (m, 2H), 1.01−0.79 (m, 13H).

***N*-Boc-L-Ile-L-Pro-L-Leu-L-Trp-OH (Free Acid of Tetrapeptide 2).** To a stirring solution of **14** (100 mg, 0.16 mmol, 1 equiv) in 1:1 THF/H_2O (640 mL) was added LiOH (19 mg, 0.78 mmol, 5 equiv), and the solution was left to stir at rt for 3 h. The reaction was quenched with 1 M HCl (1 vol equiv), and the product was extracted with CH_2Cl_2, washed with $NaHCO_{3(satd)}$, dried over sodium sulfate, and concentrated under reduced pressure. Crude **15** was obtained in quantitative yield as an oily residue, which was used without further purification. IR (film) ν_{max} 3311 (bs), 2965, 1632, 1215 cm^{-1}; ^1H NMR ($CDCl_3$, 400 MHz) δ 8.42 (s, 1H), 7.57 (d, *J* = 7.9 Hz, 1H), 7.31 (s, 1H), 7.12 (dq, *J* = 24.7, 9.6, 7.3 Hz, 3H), 5.22 (s, 1H), 4.83 (d, *J* = 7.5 Hz, 1H), 4.31 (d, *J* = 41.9 Hz, 2H), 3.73 (s, 2H), 3.54 (s, 1H), 3.30 (s, 2H), 2.08−1.72 (m, 0H), 1.43 (s, 9H), 1.10−0.57 (m, 12H).

DOI: 10.1021/acs.jnatprod.7b00656
J. Nat. Prod. 2017, 80, 3234−3240

Octapeptide *N*-Boc-L-Ile-L-Pro-L-Leu-L-Trp-L-Pro-L-Val-L-Ile-L-Pro-OMe (18). Free acid of **2** (137 mg, 0.31 mmol, 2.1 equiv) and free base of **3** (92 mg, 0.15 mmol, 1 equiv) were added to a stirring solution of HOBt (25 mg, 0.16 mmol, 1.05 equiv) in dry THF (3.1 mL) at rt under an argon atmosphere. The solution was cooled to 0 °C and stirred for 20 min, after which Et_3N (0.07 mL, 0.53 mmol, 3.5 equiv) was added and stirred. After an additional 20 min of stirring, EDC·HCl (31 mg, 0.16 mmol, 1.05 equiv) was added and the reaction mixture was left to stir overnight. The reaction was quenched with H_2O (1 vol equiv), and the product was extracted with CH_2Cl_2, dried over sodium sulfate, and concentrated under reduced pressure. The crude material was purified via flash silica gel chromatography (9:1 EtOAc/MeOH) to afford **18** (198 mg, 61% yield) as an amber liquid: $[\alpha]_D^{25}$ −29 (*c* 0.78, MeOH); IR (film) ν_{max} 3423, 2925, 1741, 1687, 1612, 1452 cm^{-1}; ^1H NMR ($CDCl_3$, 400 MHz) δ 8.67 (s, 1H), 7.67 (d, *J* = 7.8 Hz, 1H), 7.62−7.27 (m, 4H), 7.20−6.85 (m, 6H), 5.21 (d, *J* = 9.3 Hz, 1H), 5.01 (q, *J* = 7.2 Hz, 1H), 4.75−4.00 (m, 10H), 3.80 (dt, *J* = 35.8, 5.2 Hz, 3H), 3.72−3.66 (m, 3H), 3.58 (s, 3H), 3.18 (d, *J* = 7.3 Hz, 1H), 2.36−1.85 (m, 16H), 1.42 (d, *J* = 4.6 Hz, 9H), 1.04−0.83 (m, 24H); ^{13}C NMR ($CDCl_3$, 101 MHz) δ 172.76, 171.84, 171.74, 171.58, 170.90, 156.03, 136.30, 124.14, 123.58, 121.96, 119.58, 118.68, 111.55, 109.77, 79.70, 77.52, 77.04, 60.50, 60.27, 59.34, 59.11, 56.57, 55.13, 55.03, 52.31, 52.26, 52.10, 51.68, 48.01, 47.63, 47.55, 41.19, 37.93, 37.59, 37.53, 30.91, 30.26, 29.26, 28.58, 28.56, 28.11, 27.78, 25.36, 25.18, 24.80, 24.59, 24.53, 23.32, 23.01, 21.92, 19.59, 19.04, 18.36, 15.70, 15.60, 15.39, 11.33, 11.27; HSESIMS *m*/*z* 1070.6253 $[M + H]^+$ (calcd for $C_{55}H_{85}N_9O_{11}Na$, 1070.6267).

Reniochalistatin E (1) via 18. To a stirring solution of **18** (470 mg, 0.45 mmol, 1 equiv) in a 1:1 THF/H_2O (1.8 mL) was added LiOH (54 mg, 2.24 mmol, 5 equiv), and the solution was left to stir at rt for 3 h. The reaction was quenched with 1 M HCl (1 vol equiv), and the product was extracted with CH_2Cl_2, dried with brine, dried over sodium sulfate, and concentrated under reduced pressure to afford the free acid of **18**, which was used without further purification. The free acid of **18** (365 mg, 0.72 mmol) was added to an RBF, and the flask was cooled to 0 °C, to which was added 1.0 M HCl in dioxane (2.9 mL). The reaction mixture was stirred for 3 h at rt. The solvent was removed under reduced pressure to afford the crude material **18a**, a white/orange solid that was used without further purification. Compound **18a** (115 mg, 0.12 mmol, 1 equiv) was added to a stirring solution of HOBt (18 mg, 0.12 mmol, 1 equiv) in dry THF (12 mL) at rt under an argon atmosphere. The solution was cooled to 0 °C and stirred for 20 min, after which Et_3N (0.06 mL, 0.42 mmol, 3.5 equiv) was added. After an additional 20 min of stirring, EDC·HCl (25 mg, 0.13 mmol, 1.05 equiv) was added and the reaction mixture was left to stir overnight. The reaction was quenched with H_2O (2 vol equiv), and the product was extracted with CH_2Cl_2, dried over sodium sulfate, and concentrated under reduced pressure. The crude material was purified via flash silica gel chromatography (85:15 EtOAc/MeOH) to afford **1** (39 mg, 9% yield): $[\alpha]_D^{25}$ −100 (*c* 0.16, MeOH); IR (film) ν_{max} 3290, 2960, 2927, 1670, 1615, 1501, 1445 cm^{-1}; ^1H NMR ($CDCl_3$, 500 MHz) δ 10.96−10.84 (m, 1H), 8.11−7.78 (m, 1H), 7.52 (dd, *J* = 24.5, 7.9 Hz, 2H), 7.40 (d, *J* = 8.2 Hz, 1H), 7.32 (t, *J* = 8.7 Hz, 1H), 7.02−6.92 (m, 2H), 4.38−4.33 (m, 1H), 3.36 (s, 23H), 3.33−3.22 (m, 1H), 2.48 (s, 1H), 1.99−1.70 (m, 2H), 1.24 (s, 2H), 0.96−0.75 (m, 8H), 0.83 (s, 27H); ^{13}C NMR (DMSO-d_6, 126 MHz) δ 172.37, 171.88, 171.81, 171.48, 171.31, 170.58, 170.22, 169.58, 136.59, 127.36, 124.18, 121.21, 118.60, 118.38, 111.71, 111.57, 61.20, 60.67, 59.59, 56.74, 55.85, 54.61, 54.39, 54.22, 47.81, 47.55, 47.41, 38.21, 37.49, 35.09, 33.21, 30.01, 23.92, 29.31, 29.28, 25.22, 25.12, 24.95, 24.83, 24.10, 23.77, 22.71, 20.87, 19.21, 18.88, 15.69, 15.10, 11.50, 9.81; HRESIMS *m*/*z* 938.5475 $[M + H]^+$ (calcd for $C_{49}H_{73}N_9O_8Na$, 938.5473).

Reniochalistatin E via 17. To a stirring solution of **17** (249 mg, 0.24 mmol, 1 equiv) in 1:1 THF/H_2O (1 mL) was added LiOH (29 mg, 1.2 mmol, 5 equiv), and the mixture was left to stir at rt for 3 h. The reaction was quenched with 1 M HCl (1 vol equiv), and the product was extracted with CH_2Cl_2, washed with brine, dried over sodium sulfate, and concentrated under reduced pressure. The crude material (free acid of **17**) was obtained in 68% yield as a white powder, which was used without further purification. The free acid of **17** (167 mg, 0.16 mmol) was added to an RBF, and the flask was cooled to 0 °C, to which 1.0 M HCl in dioxane (0.64 mL) and 1 mL of dioxane were added. The reaction mixture was stirred for 3 h at the same temperature, then allowed to warm to rt overnight. The solvent was removed under reduced pressure to afford the crude material **17a**, a white/orange solid that was used without further purification. Compound **17a** (152 mg, 0.16 mmol, 1 equiv) was added to the stirring solution of HOBt (25 mg, 0.16 mmol, 1 equiv) in dry THF (16 mL) at rt under an argon atmosphere. The solution was cooled to 0 °C and stirred for 20 min, after which Et_3N (0.08 mL, 0.56 mmol, 3.5 equiv) was added. After an additional 20 min of stirring, EDC·HCl (32 mg, 0.17 mmol, 1.05 equiv) was added, and the reaction mixture was left to stir overnight. The reaction was quenched with H_2O (1.5 vol equiv), and the product was extracted with CH_2Cl_2, washed with brine, dried over sodium sulfate, and concentrated under reduced pressure. The crude material was purified via flash silica gel chromatography with a gradient solvent system (9:1 EtOAc/MeOH; 7:3 EtOAc/MeOH) to afford **1** (8.6 mg, 6% yield). All NMR and MS data matched those of **1** accessed via **18**.

Biological Assays. *Cell Culture Information.* Cells were grown in media supplemented with fetal bovine serum (FBS) and antibiotics (100 μg/mL penicillin and 100 U/mL streptomycin). Specifically, experiments were performed using the following cell lines and media compositions: HeLa, A549, RPMI-8226, MM.1R, and U-937 (RPMI-1640 + 10% FBS) and Mia PaCa-2 (DMEM + 10% FBS). Cells were incubated at 37 °C in a 5% CO_2, 95% humidity atmosphere for all experiments.

IC_{50} Value Determination for Adherent Cells Using Alamar Blue. Adherent cells were added to a 384-well plate (1500 cells/well) in 10 μL of media and were allowed to adhere for 2−3 h. Compounds were solubilized in DMSO (10 μM stock solutions) and added to a 96-well plate over a range of concentrations (31.6 nM to 200 μM) with media, and 40 μL was added to the 384-well plate in triplicate for each concentration of compound. After 69 h of continuous exposure, 5 μL of Alamar Blue was added to each well, and the cells were allowed to incubate for an additional 3 h. The plates were then read for fluorescence intensity with an excitation of 560 nm and emission of 590 nm on a BioTek Synergy H1 plate reader. Doxorubin and etoposide were both used as positive death controls, and wells with no compounds added as negative death controls. IC_{50} values were determined from three or more independent experiments using GraphPad Prism 7.0. (LaJolla, CA, USA)

IC_{50} Value Determination for Nonadherent Cells Using Alamar Blue. The same procedure for adherent cells was used, with the following modifications. Cells (2000 cell/well) in media (10 μL) were added after 40 μL of compound in media was added to the 384-well plate. No time was given to allow cells to adhere.

■ ASSOCIATED CONTENT

Supporting Information

The Supporting Information is available free of charge on the ACS Publications website at DOI: 10.1021/acs.jnatprod.7b00656.

^1H NMR and ^{13}C NMR spectra for all new compounds (PDF)

■ AUTHOR INFORMATION

Corresponding Author

*E-mail (R. J. Rafferty): rjraff@ksu.edu. Phone: 785-532-6624.

ORCID

Ryan J. Rafferty: 0000-0002-4835-6343

Notes

The authors declare no competing financial interest.

■ ACKNOWLEDGMENTS

This work could not have been undertaken without the gracious financial support from the Johnson Cancer Center of Kansas State University and Startup Capital from Kansas State University. This paper is warmly dedicated to Professor Richard

DOI: 10.1021/acs.jnatprod.7b00656
J. Nat. Prod. 2017, 80, 3234−3240

M. Hyslop in recognition of his mentorship, guidance, and friendship.

REFERENCES

(1) Zhan, K.-X.; Jiao, W.-H.; Yang, F.; Li, J.; Wang, S.-P.; Li, Y.-S.; Han, B.-N.; Lin, H.-W. *J. Nat. Prod.* **2014**, *77*, 2678−2684.
(2) Tabudravu, J.; Morris, L.; Kettenes-van den Bosch, J. J.; Jaspars, M. *Tetrahedron Lett.* **2001**, *42*, 9273−9276.
(3) Song, J.; Jeon, J.-e.; Won, T.; Sim, C.; Oh, D.-C.; Oh, K.-B.; Shin, J. *Mar. Drugs* **2014**, *12*, 2760.
(4) Napolitano, A.; Bruno, I.; Rovero, P.; Lucas, R.; Peris, M. P.; Gomez-Paloma, L.; Riccio, R. *Tetrahedron* **2001**, *57*, 6249−6255.
(5) Vera, B.; Vicente, J.; Rodríguez, A. D. *J. Nat. Prod.* **2009**, *72*, 1555−1562.
(6) Fang, W.-Y.; Dahiya, R.; Qin, H.-L.; Mourya, R.; Maharaj, S. *Mar. Drugs* **2016**, *14*, 194.
(7) Ibrahim, S. R. M.; Min, C. C.; Teuscher, F.; Ebel, R.; Kakoschke, C.; Lin, W.; Wray, V.; Edrada-Ebel, R.; Proksch, P. *Bioorg. Med. Chem.* **2010**, *18*, 4947−4956.
(8) Blunt, J. W.; Copp, B. R.; Keyzers, R. A.; Munro, M. H. G.; Prinsep, M. R. *Nat. Prod. Rep.* **2012**, *29*, 144−222.
(9) Liu, M.; Tang, Y. C.; Fan, K. Q.; Jiang, X.; Lai, L. H.; Ye, Y. H. *J. Pept. Res.* **2005**, *65*, 55−64.
(10) Schmidt, R.; Neubert, K. *Chem. Biol. Drug Design* **1991**, *37*, 502−507.
(11) Tang, Y.-C.; Gao, X.-M.; Tian, G.-L.; Ye, Y.-H. *Chem. Lett.* **2000**, *29*, 826−827.
(12) Ye, Y.-h.; Gao, X.-m.; Liu, M.; Tang, Y.-c.; Tian, G.-l. *Lett. Pept. Sci.* **2003**, *10*, 571−579.
(13) Abdelmoty, I.; Albericio, F.; Carpino, L. A.; Foxman, B. M.; Kates, S. A. *Lett. Pept. Sci.* **1994**, *1*, 57−67.
(14) Grabowska, K.; Puszko, A. K.; Lipiński, P. F.; Laskowska, A. K.; Wileńska, B.; Witkowska, E.; Perret, G. Y.; Misicka, A. *Bioorg. Med. Chem.* **2017**, *25*, 597−602.
(15) Gholap, S. S.; Ugale, S. R. *Chem. Sel.* **2017**, *2*, 7445−7449.
(16) Jou, G.; González, I.; Albericio, F.; Lloyd-Williams, P.; Giralt, E. *J. Org. Chem.* **1997**, *62*, 354−366.
(17) Bastiaans, H. M. M.; van der Baan, J. L.; Ottenheijm, H. C. J. *J. Org. Chem.* **1997**, *62*, 3880−3889.
(18) Tang, Y. c.; Xie, H. b.; Tian, G. l.; Ye, Y. H. *J. Pept. Res.* **2002**, *60*, 95−103.

DOI: 10.1021/acs.jnatprod.7b00656
J. Nat. Prod. 2017, 80, 3234−3240

MedChemComm

Accepted Manuscript

This article can be cited before page numbers have been issued, to do this please use: A. X. Torres Hernandez, C. Weeramange, P. Desman, A. Fatino, O. Haney and R. J. Rafferty, *Med. Chem. Commun.*, 2018, DOI: 10.1039/C8MD00463C.

ROYAL SOCIETY OF CHEMISTRY

rsc.li/medchemcomm

View Article Online
DOI: 10.1039/C8MD00463C

Efforts in Redesigning the Antileukemic Drug 6-Thiopurine: Decreasing Toxic Side Effects while Maintaining Efficacy

Arnaldo X. Torres Hernandez,[‡ab] Chamitha J. Weeramange,[‡b] Prathibha Desman,[b] Anthony Fatino,[b] Olivia Haney,[b] and Ryan J. Rafferty*[b]

[a]Department of Chemistry, Pontifical Catholic University of Puerto Rico, 2250 Boulevard Luis A. Ferré Aguayo, Suite 626 Ponce, PR 00717-0777

[b]Department of Chemistry, Kansas State University, 1212 Mid-Campus Drive North, Manhattan, KS 66506

‡These authors contributed equally to the work.

View Article Online
DOI: 10.1039/C8MD00463C

ABSTRACT

6-Thiopurine (6TP) is a currently prescribed drug in the treatment of diseases ranging from Crohn's disease to acute lymphocytic leukemia. While its potent mode of action is through incorporation into DNA as a thiol mimic of deoxyguanosine, severe toxicities are associated with its administration which hinder the potential therapeutic application. We have previously reported *in vitro* that the oxidative metabolites of 6TP, specifically 6-thiouric acid (6TU, K_i 7 μM), are potent inhibitors of UDP-glucose dehydrogenase (UDPGDH), an enzyme that is responsible for the formation of UDP-glucuronic acid (UDPGA), an essential substrate that is used in detoxification processes in the liver. An i*n vivo* investigation was undertaken to probe if 6TU inhibits UDPGDH in rat hepatocytes, and it was observed that 6TU does greatly suppress the conjugation of bilirubin with UDPGA. The failed excretion of bilirubin is linked to a majority of the reported toxicities associated with 6TP administration. Efforts were undertaken for the construction of 6TP analogs, substituted at the C8 position, to reduce inhibition of UDPGDH while retaining therapeutic efficacy. Three new 6TP analogs bearing a halogen (Br, Cl, and F) at the C8 position have been achieved over five-synthetic steps in overall yields of 16 to 32%. Each of these analogs were shown to have reduced inhibition towards UDPGDH, with K_i values of 192, 163, 215 μM, respectively. In addition, the bromine, chlorine, and fluorine analogs were shown to possess cytotoxicity towards the REH cell line (acute lymphocytic leukemia) having IC_{50} values of 9.54 μM (±0.97), 3.95 μM (±1.94), and 4.71 μM (±1.40), respectively. These three new 6TP analogs represent the first steps in the redesign of this potent anticancer agent into a better drug that possesses reduced toxic side effects while retaining therapeutic potency.

View Article Online
DOI: 10.1039/C8MD00463C

1. Introduction

6-Thiopurine (6TP, **1**) has been a continuously prescribed therapeutic since its FDA approval in 1952, shortly after its discovery in 1950 by Gertrude Elion and George Hitchings at Burroughs Wellcome.[1] This potent therapeutic serves as a treatment option for numerous diseases, such as, but not limited to: acute lymphocytic leukemia (ALL),[2, 3] non-Hodgkin's leukemia,[4, 5] Crohn's disease,[6-8] and inflammatory bowel disease.[9, 10] 6TP has no therapeutic properties itself, however, it is metabolized into a therapeutic form, a deoxyguanosine nucleotide mimic, commencing with the phosphoribosylation by hypoxanthine-guanine phosphoribosyltransferase (HGPRT) forming the nucleotide mimic 6-thioinosinic acid monophosphate (TIMP, **2**). HGPRT is an enzyme that usually catalyzes phosphoribosylation of hypoxanthine (C6 hydroxyl) to inosinic acid (IMP).[11] Oxidation of the C2 position of 6TP is accomplished by inosine-5'-monophosphate dehydrogenase (IMPD), an enzyme that is overexpressed in the presence of 6TP, followed by C2 amine installation by guanine monophosphate synthase (GMPS) giving rise to either thioguanosine mono phosphate (TGMP or dTGMP, **3**).[11-13] Multiple kinase transformations then afford dTGTP (**4**), which gets incorporated into DNA in place of dGTP. However, incorporation of dTGTP does not immediately result in apoptosis, via base pair mismatching, but requires multiple passages through the S-phase allowing for sufficient dTGTP incorporation into DNA.[14] It has also been shown that 6-thioguanine (6TG, **5**) can be used in conjunction with 6TP and is acted upon by HGPRT accessing the monophosophate nucleotide formed via 6TP metabolism.

Checkpoint activation is required for recognition of the mismatched base pairing within DNA post **4** incorporation; a process commonly suppressed within cancer cells.[15-17] Mutually 6TP and 6TG can be methylated to form the corresponding thiol ethers by thiopurine methyltransferase (TPMT), neither possessing any cytotoxic properties, but do induce checkpoint activation.[18]

View Article Online
DOI: 10.1039/C8MD00463C

Additionally, TIMP (**2**) can be transformed into its corresponding methyl thiol ether, but rather than activating checkpoints this species has been proven to inhibit *de novo* purine biosynthesis.[19] This inhibition allows for the cellular uptake of purines to increase, including 6TP, which corresponds to a higher probability of dTGTP incorporation into DNA that can then lead to apoptosis, via base pair mismatching.

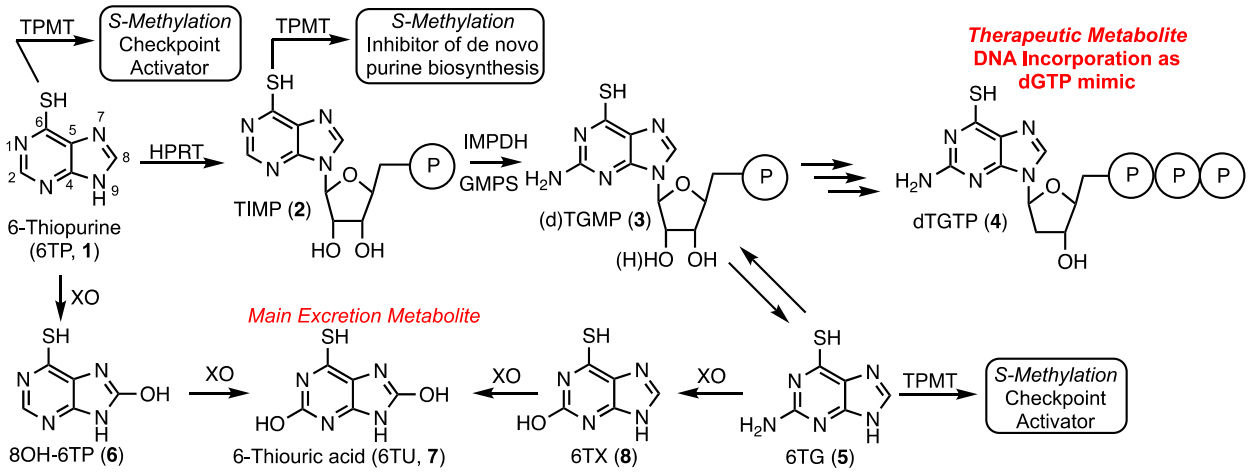

Fig. 1 Metabolism of 6-Thiopurine: 1) Therapeutic pathway forming dTGTP, a dGTP mimic, which incorporates into DNA resulting in apoptosis, and 2) the excretion pathway allowing for the removal of 6-thiopurine and its biosynthetic metabolites.

In parallel to 6TP's therapeutic metabolism, efficient oxidative pathways remove 6TP from the body, thereby decreasing its therapeutic potential. Xanthine oxidase (XO) can directly oxidize the C8 position of 6TP forming 8-OH-6TP (**6**), a species that is not a substrate for HGPRT, thus, eliminating any therapeutic potential.[20] Moreover, **6** can be further oxidized at the C2 position forming 6-thiouric acid (6TU, **7**), which is the terminal excretion metabolite. This highly efficient oxidation by XO limits the bioavailability of 6TP. In route to dTGTP (**4**), dTGMP (**3**) can be formed into 6TG, which is rapidly oxidized to 6-thioxanthine (6TX, **8**), a species that is further

View Article Online
DOI: 10.1039/C8MD00463C

oxidized by XO to 6TU. Once 6TU is formed, it is well retained by the body beyond 24-hours post-6TP administration.[20]

As with nearly all therapeutic drugs, the benefits come with side effects that limit effectiveness and general applications. 6TP is not immune to this trend, with multiple toxicities associated with its use including, but not limited to: pulmonary lesions, myocarditis, reticulocytopenia, depletion of cellularity in bone marrow, intestinal ulcerations, jaundice, hepatotoxicity, and even death.[13, 15] Of these, the most predominate toxic side effects are jaundice and hepatotoxicity, corresponding to the reported increase in bilirubin levels within patients taking 6TP. In addition to the toxicities listed above, increased bilirubin levels within the body can cause hyperbilirubinemia, kernicterus, Crigler-Najjar syndrome, Gilbert's syndrome, liver failure, and death.[21-23] While 6TP is a currently prescribed anticancer agent, its toxic side effects are so potent and prevalent that the administration of 6TP is given in an on/off strategy, allowing time for the toxic species to be cleared by the body. Unfortunately, this greatly reduces its therapeutic efficacy, restricts the quality of life of the patients taking the drug, and has ultimately limited its use as an anticancer therapy. Our laboratory is interested in repurposing dismissed or under-utilized anticancer therapies, such as 6TP. Noting the common connection between the predominate toxic side effects possibly originating in the bilirubin pathway, this prompted us to begin a systematic study to explore the effects of 6TP and its oxidative metabolites.

The bilirubin pathway refers to the excretion of bilirubin from the body through detoxification in the liver.[24-26] Heme groups are released when red blood cells undergo senescence, which in the presence of oxygen and NADPH, reduces the heme to bilirubin (**11**, also referred to as unconjugated bilirubin, UCB).[24] Bilirubin is a relatively large non-polar compound that is not easily excreted by the body (Figure 2A).[27] The excretion of bilirubin is achieved through

View Article Online
DOI: 10.1039/C8MD00463C

conjugation by UDP-glucuronyl transferase (UGT-1A) with two UDP-glucuronic acids (UDPGA, **10**) forming bilirubin diglucuronide (BDG, **12**), a water-soluble and excretable compound.[28, 29] Physiologically, UDPGA (**10**) is formed from the oxidation of UDP-glucose (UDPG, **9**) via UDP-glucose dehydrogenase (UDPGDH).[30] We have reported that 6TP and its excretion/oxidative metabolites inhibit UDPGDH, but not UGT-1A (Figure 2B).[31] Furthermore, *in vitro* investigations revealed that 6TP and its excretion metabolites resulted in an increase in bilirubin and a decrease in conjugated bilirubin levels, relative to controls. While 6TP was shown to have low inhibition towards UDPGDH, its main excretion metabolite 6TU has a 41-fold increase in inhibition. Noting that the formation of 6TU via XO is rapid, we were led to investigate the other oxidative metabolites. Investigations of 6-thioxanthine (**8**, C2 hydroxyl) revealed a five-fold increase in inhibition towards UDPGDH and 8-OH-6TP a 20-fold increase in inhibition, relative to 6TP. From this, it is suggested that the C8 position is critical in the inhibition properties towards UDPGDH.[31] As such, we propose that analogs that block the C8 position of 6TP, thereby preventing oxidation by XO to the C8-OH, will limit, if not eliminate, inhibition of UDPGDH. We speculate that the reduced inhibition of UDPGDH will result in a higher concentration of the UDPGA liable pool to allow for conjugation of bilirubin and its excretion, thereby reducing one of the predominate toxic side-effects of 6TP administration.

View Article Online
DOI: 10.1039/C8MD00463C

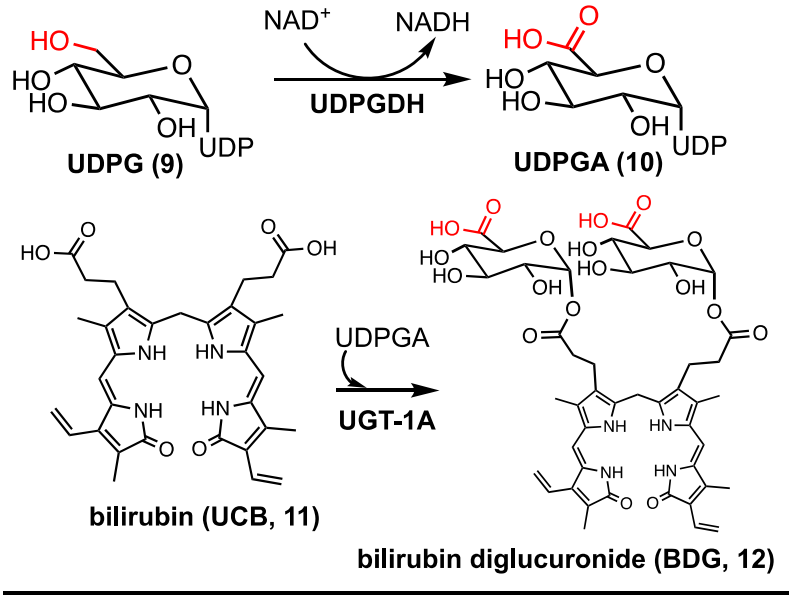

		UDPGDH	UGT-1A
R_1	R_2	K_i (μM)	K_i (μM)
H	H	288	>100
H	OH	14	>100
OH	H	54	>100
OH	OH	7	>100

Fig. 2 (Upper) Biosynthesis of UDPGA from the oxidation of UDPG by UDPGDH and conjugation of bilirubin with UDPGA by UGT-1A forming the excretable bilirubin diglucuronide. (Lower) Inhibition profiles of 6TP and excretion metabolites towards UDPGDH and UGT-1A.

Fig. 2 (Upper) Biosynthesis of UDPGA from the oxidation of UDPG by UDPGDH and conjugation of bilirubin with UDPGA by UGT-1A forming the excretable bilirubin diglucuronide. (Lower) Inhibition profiles of 6TP and its excretion metabolites towards UDPGDH and UGT-1A.

2. Results and discussion

2.1 Hepatotoxicity Evaluation of 6-Thiopurine and 6-Thiouric acid

Previously, our lab has shown that the excretion metabolites of 6TP, specifically those hydroxylated at both, or either, C2/8, possess inhibition towards UDPGDH but not UGT-1A, when both enzymes were screened independently *in vitro* .[31] To further corroborate these findings and to give a potential correlation to *in vivo* effects, we set forth to investigate our initial claim that 6TP and 6TU inhibit UDPGDH in a bio-mimic *in vivo* assay, via isolated perfused livers of rat

View Article Online
DOI: 10.1039/C8MD00463C

hepatocytes. While it is difficult to correlate the exact enzyme being inhibited by a small molecule in a whole cell experiment, we decided to explore UDPGDH inhibition with regards to these two steps through quantification of the glucuronidated bilirubin species. Full glucuronidation of UCB leads to the formation of BDG (**12**, Figure 2), however monoglucuronidation results in two different monoglucuronidated bilirubin species (BMG1 and 2); in this work, both BMG1 and 2 were quantified together (herein refered to as BMG). Rat liver hepatocytes were used for the assessment of formation of BMG and BDG in the presence of 6TP and 6TU at high and low concentrations. Table 1 shows the quantification of UCB, BMG, and BDG in hepatocytes. Quantification of the bilirubin species throughout this study is normalized to the BMG levels of the control set.

Table 1 Hepatocyte studies with 25 and 50 μM of 6TP and 5 and 10 μM of 6TU. Each group is an average of three independent runs with standard error bars shown.

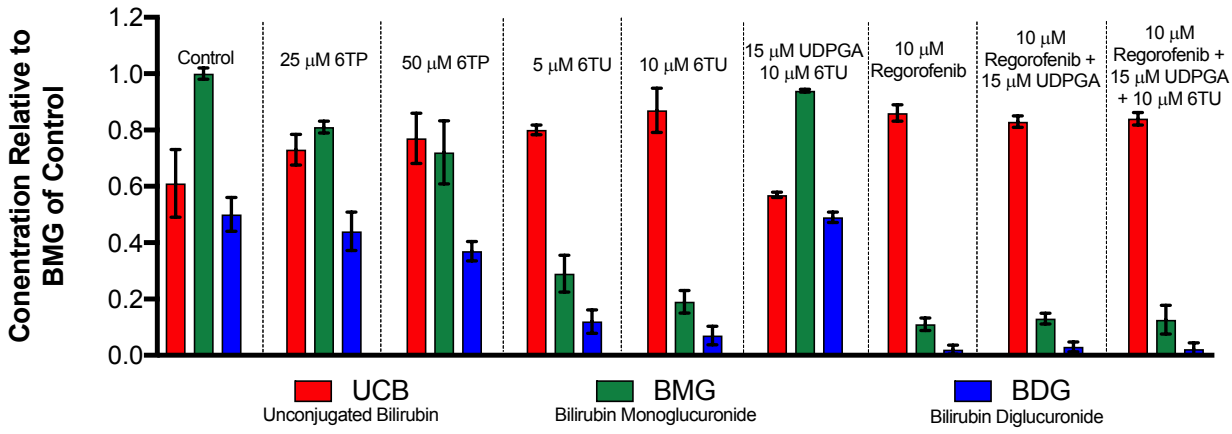

Subjecting the harvested hepatocytes to 25 μM 6TP showed an overall decrease in the conjugation of UCB and formation of BDG; relative to the control set, UCB levels increased by 19%, and both BMG and BDG levels were decreased by 19% and 12%, respectively. Based upon our previous conducted *in vitro* assays, this finding was not unexpected and further supports that

View Article Online
DOI: 10.1039/C8MD00463C

inhibition of UDPGDH is responsible for the decrease in bilirubin conjugation and subsequent toxicity. Increasing the dosage of 6TP to 50 μM revealed greater decrease in BMG and BDG levels, 28% and 26%, respectively, relative to controls. The observed decrease in BMG and BDG levels is assumed to arise from the increased conversion of 6TP to 6TU via XO, thereby inhibiting UDPGDH. Treatment with 5 and 10 μM of 6TU revealed potent inhibition of BMG and BDG formation, far greater than when 6TP was administered. When 5 μM of 6TU was employed an increase of 31% in UCB levels was observed, relative to the controls. Furthermore, BMG and BDG levels decreased by 71% and 76, respectively. The levels of BMG formation decreased by 81% and BDG levels by 86% when 10 μM of 6TU was used, with an increase in UCB levels by 42%, all relative to the controls. If the reduced BDG formation does originate from the decrease in the liable pool of UDPGA, addition of UDPGA to the system should allow recovery of the system similar to the controls. The addition of 15 μM of UDPGA along with 10 μM of 6TU resulted in the production of BDG levels similar to that of the control group, suggesting that 6TU does suppresses the formation of UDPGA via inhibition of UDPGDH *in vivo* but does not inhibit UGT-1A, but does require further investigations into UGT-1A itself is required to substantiate this claim.

Treatment with 10 μM regorafenib, a known inhibitor of UGT-1A and proven non-inhibitor of UDPGDH by our group (see Supplementary Information), resulted in strong inhibition in the formation of both BMG (89% decrease) and BDG (96% decrease) is observed, both greater than 6TU. When treated with 10 μM regorafenib and 15 μM of UDPGA a similar pattern of reduced BMG and BDG formation is observed. Furthermore, treatment with 10 μM of regorafenib, 10 μM 6TU, and 15 μM of UDPGA also showed the same profile of BMG and BDG levels. Thus, the

View Article Online
DOI: 10.1039/C8MD00463C

decrease in BMG and BDG levels from regorafenib are from UGT-1A inhibition, which can be translated into confirming that the effects of 6TP and 6TU are upon UDPGDH and not UGT-1A.

With the confirmation of *in vivo* inhibition of UDPGDH by 6TP and 6TU, the latter being more potent with regards to suppressing BDG formation, the construction of 6TP analogs was considered the next logical step. From previously conducted *in vitro* investigations, it was observed that hydroxylation upon the C2 and C8 positions does translate into inhibition of UDPGDH.[31] The C2 position of 6TP cannot be modified as amine installation post phosphoribosylation is required to form its therapeutically active form; therefore, modification of the C8 position is considered the only viable strategy for analog construction.

2.2 Chemistry

Construction of C8-substituted purine systems is reported in the literature,[32, 33] however the inclusion of the C6 thiol with C8 substitution, restricted to alkyl and phenyl analogs, is limited. In the efforts to construct analogs that block the C8 position from oxidation by XO, we set forth to construct analogs that bear halogens about the C8 position in hopes of retaining the therapeutic character of 6TP. Halogens were chosen for the C8 substitution, rather than alkyl or aryl substituents, to decrease the probability of failed DNA incorporation due to sterics about the C8 position. Starting from the commercially available 6-chloropurine (**13**), protection of the N9 nitrogen was successfully accomplished with potassium carbonate and *para*-methoxybenzyl chloride (PMBCl) to access **14** in 58% yield (Scheme 1), matching reported characterization found in the literature.[34-36] In addition to obtaining pure **14**, these conditions also allow access to the N7 PMB protected compound (**15**) in 34% yield. Further synthetic elaborations were conducted upon **14** but not **15**. While **15** can be employed in the efforts of accessing C8 halogen 6TP analogs in the same route as **14**, there is a decrease in yields using this material and will be discussed below.

View Article Online
DOI: 10.1039/C8MD00463C

With **14** in hand, efforts towards the installation of halogens (bromine,[37, 38] chlorine,[34] and fluorine[39]) at the C8 position were undertaken through modifications of reported procedures. Deprotonation of the C8 hydrogen of **14** was accomplished with freshly prepared LDA; the lithiated species was then treated with 1,2-dibromotetrachloroethane to access the C8-bromo compound (**16a**) in 75% yield. The substitution of the 6-chloro group upon purines has precedent in the literature,[40, 41] following these reported procedures, thiol installation with thiourea and ethanol reflux, afforded **17a** in 92% yield over two-steps. Deprotection of the PMB protecting group was performed by refluxing sulfuric acid, thus, gaining access to the 8-bromo-6TP (**18a**) in 81% yield, with an overall 32% yield over five synthetic transformations from **13**. Additional 8-Br-6TP (**18a**) was accessed from **15** by subjecting it to the same conditions with comparable yields, except about the thiol installation step. From the N7-PMB variant of **16a**, subjection to thiol installation provided a 58% yield. It is thought that the additional steric congestion brought from the N7 PMB is the cause for the decrease in yields, as nearly 34% of starting material is recovered.

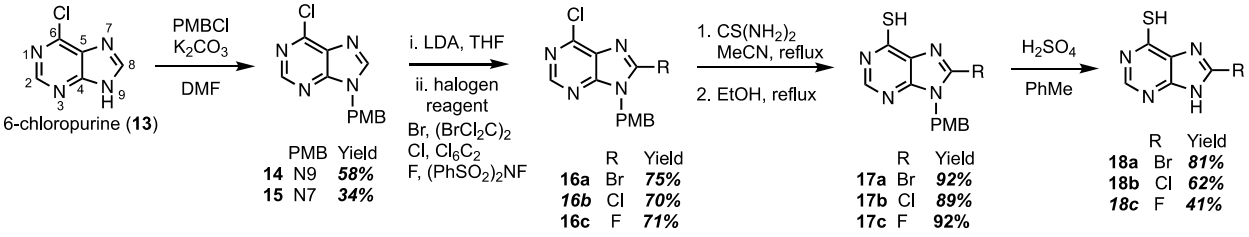

Scheme 1 Synthetic route accessing the bromo-, chloro-, and fluoro-C8-substituted 6TP analogs from 6-chloropurine.

Following the same approach described in Scheme 1, accessing the C8 chloride and fluoride analogs were undertaken. Deprotonation of the C8 hydrogen of **14** was accomplished with LDA and subsequent treatment with hexachloroethane afforded 6,8-dichloro-*N*-

View Article Online
DOI: 10.1039/C8MD00463C

paramethoxbenzylpurine (**16b**) in 70% yield. In an analogous fashion, treatment with N-fluorobenzenesulfonimide (NFSI) afforded **16c** in 71% yield, with 19% of starting material recovered. Thiol installation was performed upon **16b** and **16c** accessing **17b** and **17c** in 89% and 92% yields, respectively. When the same transformation was attempted upon the N7 variants, a suppression in yields were obtained similar to the bromine analog described previously. Removal of the PMB group was performed under refluxing sulfuric acid to give access to **18b** and **18c** in 62% and 41% yields. The chloro- and fluoro-analogs were constructed over five-steps in overall yields of 22% and 16%, respectively.

2.3 Biological evaluation of 6TP analogs

Inhibition assessment of the synthesized C8-halogenated 6TP analogs was performed independently against the two enzymatic steps of the bilirubin pathway, UPDGDH and UGT-1A. A cytotoxicity assessment was performed against the acute lymphocytic leukemia cell line REH as well.

2.3.1 Inhibition Evaluation Towards UDPGDH

To investigate the inhibition properties of the analogs towards UDPGDH, a previously disclosed and employed UV/Vis method was used.[31] Recalling the potent inhibitory properties of the C2 and/or C8 hydroxylated 6TP excretion metabolites towards UDPGDH, we were surprised to find that each of the analogs possess minimal inhibition (Table 2-D). The C8 bromine analog was observed to inhibit UDPGDH with a K_i of 192 μM, the C8 chlorine analog was shown to have the strongest inhibition of the C8 halogenated 6TP analogs with a K_i of 163 μM, and the C8 fluorine analog the weakest inhibition with an observed K_i of 215 μM (Table 2 A-C). Previously, we reported a K_i of 288 μM for 6TP towards UDPGDH, and relative to the analogs synthesized a similar weak inhibition profiles were observed. While the minimal inhibition possessed by the

View Article Online
DOI: 10.1039/C8MD00463C

three newly constructed analogs towards UDPGDH represent a positive step in eliminating the toxicity associated with 6TP, further evaluation towards UGT-1A is required, as is assessment on whether these analogs retain a similar cytotoxicity comparable to 6TP.

Table 2 Inhibitor assessment towards UDP-glucose dehydrogenase *in vitro* by C8-halogenated 6TP analogs through Lineweaver-Burk plot analysis under UDPG varying NAD^+ saturating conditions. A) Concentration of 8-Br-6TP, varying UDPG, screened were 0, 50, 75, 100 μM with the calculated slopes of each line equaling 0.098, 0.121, 0.132, 0.153, respectively. Plotting slopes versus concentration gave a regression line of y=0.0005x+0.096. B) Concentration of 8-Cl-6TP, varying UDPG, screened were 0, 50, 75, 100 μM with the calculated slopes of each line equaling 0.097, 0.129, 0.137, 0.156, respectively. Plotting slopes versus concentration gave a regression line of y=0.0006x+0.098. C) Concentration of 8-F-6TP, varying UDPG, screened were 0, 50, 75, 100 μM with the calculated slopes of each line equaling 0.106, 0.132, 0.145, 0.152, respectively. Plotting slopes versus concentration gave a regression line of y=0.0005x+0.108. D) Summary of previously determined K_i values towards UDPGDH for 6TP and its excretion metabolites; summary of the found K_i of synthesized analogs. Each group is an average of three independent runs with standard error bars shown.

View Article Online
DOI: 10.1039/C8MD00463C

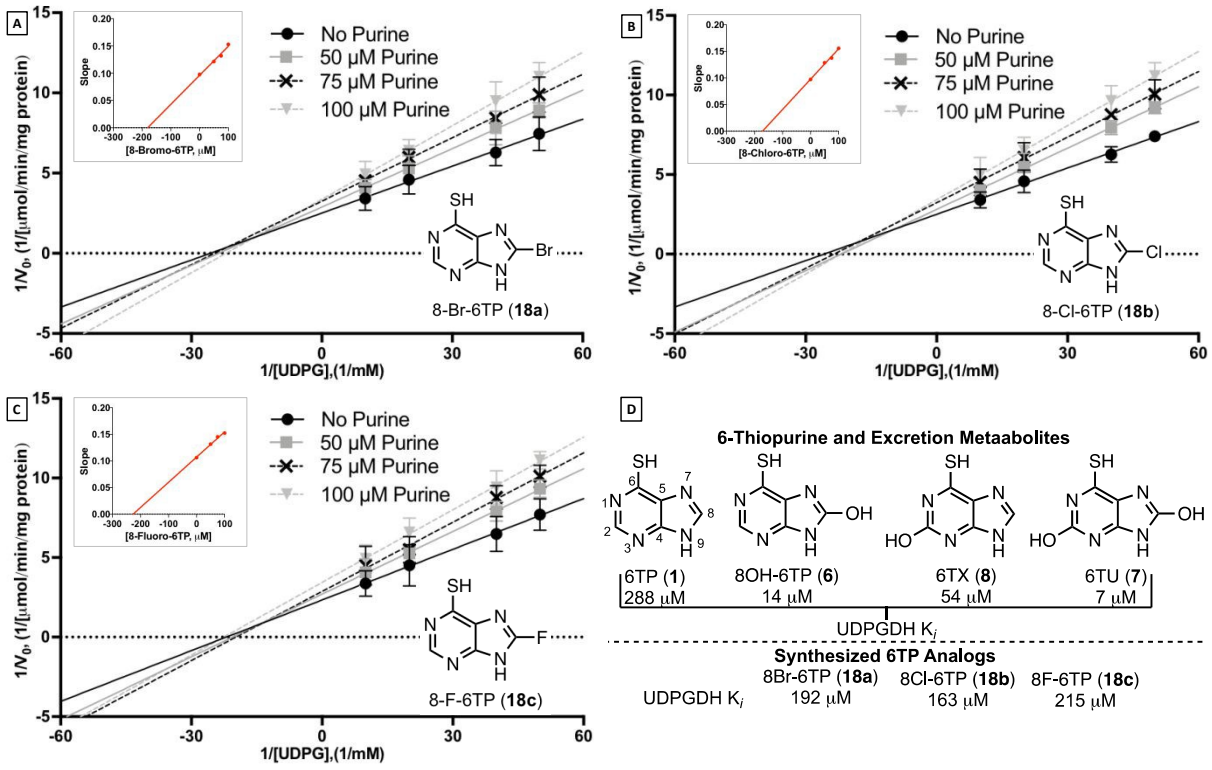

2.3.2 Inhibition Evaluation Towards UGT-1A

While neither 6TP or any of its oxidative metabolites were shown to have inhibition properties toward UGT-1A, the same cannot be assumed for the constructed analogs and, as such, assessment is required. To accomplish this, we employed our previously reported *in vitro* HPLC method for the assessment of UGT-1A inhibition.[31] In this method, the levels of BDG formation is lower than physiological levels given the incubation time (45-minutes). The control showed expected production of BMG exceeding that of BDG. The evaluation of conjugation in the presence of 75 μM 6TP and 75 μM 6TU, independently, showed similar patterns of UCB, BMG, BDG levels with respect to the control group, thus, indicating no inhibition by either purine towards UGT-1A, similar to what was previously reported and observed (Table 3). Similar to the control group and both 6TP and 6TU, each of the analogs were observed to have the same pattern of bilirubin levels. As such, no inhibition towards UGT-1A was observed with any of the 6TP analogs constructed in

View Article Online
DOI: 10.1039/C8MD00463C

this study. Validation of UGT-1A activity was accomplished with the use of regorafenib, previously mentioned as a selective inhibitor of UGT-1A, which showed nearly full inhibition of UGT-1A.

Table 3 Inhibition studies of UGT-1A by 6TP, 6TU, regorafenib, and the three C8-halogenated 6TP analogs. Quantification of unconjugated bilirubin (UCB), monoglucuronide bilirubin (BMG, sum of BMG1 and 2), and diglucuronide bilirubin (BDG) accomplished via the bilirubin standard curve (see supplemental information). Each group is an average of three independent runs with standard error bars shown.

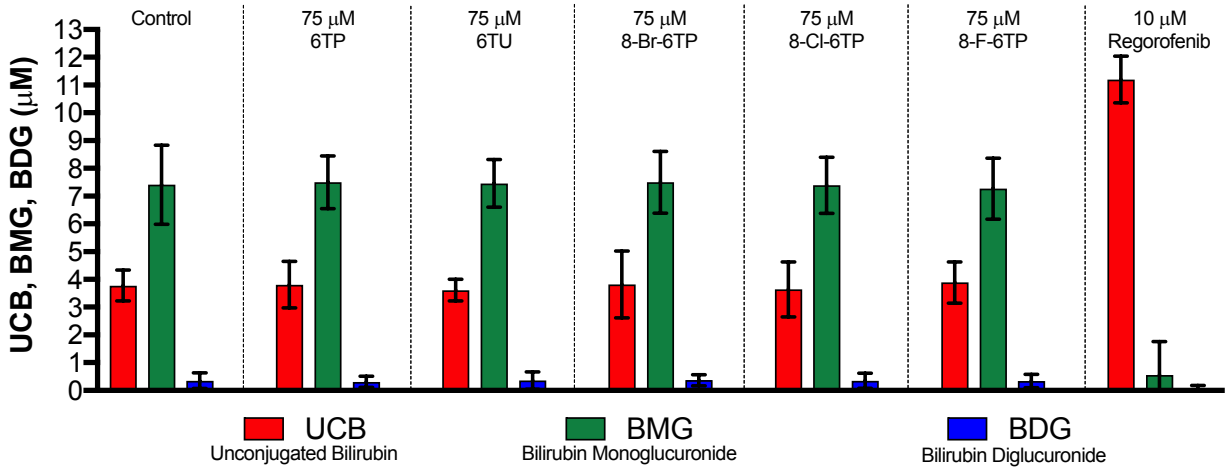

2.3.4 Cytotoxicity Evaluation against REH

While the C8-halogenated analogs were shown to possess weak inhibition towards UDPGDH and no inhibition towards UGT-1A, investigations into the possible retention of cytotoxicity was undertaken. To explore the analogs cytotoxic properties, each analog, 6TP, 6TX, 8-OH-6TP, 6TU, and doxorubicin (control) was evaluated towards the acute lymphocytic leukemia cell line, REH, over a 48-hour period. Cytotoxicity was assessed via cellular viability, Alamar blue quantification, over 48 h and data was analyzed via Prism 7.0 by GraphPad Pro. 6TP was shown to have an IC_{50}

View Article Online
DOI: 10.1039/C8MD00463C

of 2.94 μM (±0.48) and doxorubicin of 0.285 (±0.008) as shown in Table 4. Neither 6TU nor 6TX, both C2 hydroxylated purines, were observed to have cytotoxicity below 10 μM in the REH cancerous cell line. It is thought that the lack of cytotoxicity by these two oxidative metabolites arises from the hydroxyl at the C2 position, thus preventing phosphoribosylation by HGPRT and ultimate formation of dTGTP (**4**). While the C2 position of TIMP does undergo C2 hydroxylation followed by amine installation, these steps are performed upon the nucleotide variant of 6TP and not the free 6TP nitrogenous base form. Furthermore, the affinity of 6TU and 6TX towards UDPGDH could be stronger than that of HGPRT, thus preventing formation of **4**. In comparison, the C8 hydroxyl of 8-OH-6TP was observed to be cytotoxic, possessing an IC_{50} value of 9.91 μM (±2.36). This suggests that substitution about the C8 position is tolerable, and, most importantly, could translate into retention of cytotoxicity. Each of the analogs were shown to possess cytotoxicity, with IC_{50} values of: **18a** (C8 Br) 9.54 μM (±0.97), **18b** (C8 Cl) 3.95 μM (±1.94), and **18c** (C8 F) 4.71 μM (±1.40).

It is assumed that the cytotoxicity of these analogs arise from their incorporation into DNA, in a similar pathway and sequence to that of 6TP, but this has not been proven in this study. Assuming the same mode of action as 6TP, the observed lower potency of the bromine compared to the chlorine and fluorine analogs is thought to arise from its size. The size of bromine upon the C8 position of the purine within the deoxyguanosine mimic could hinder DNA incorporation. Similarly, the increase bulk of the bromine upon the C8 position could prevent enzymatic recognition by the HGPRT, as well as, the other enzymatic steps leading to the formation of **4**. The increased cytotoxicity observed by both the chlorine and fluorine analogs lend further support to the possible role of size in the observed trend of cytotoxicity. However, the greater cytotoxicity exhibited by the chlorine analog versus the fluorine analog contradicts the argument of size as a

View Article Online
DOI: 10.1039/C8MD00463C

function of activity, but could also lead to an electronic argument for activity. Further investigations are required to fully understand the observed trend. Most importantly, through these analogs it was shown that substitution of the C8 position is not only tolerated, but does give access to 6TP analogs that retain cytotoxicity.

Table 4 Evaluation of 6TP, excretion metabolites, and synthesized 8-substituted analogs towards inhibition of UDPGDH and UGT-1A and cytotoxicity towards REH (acute lymphocytic leukemia) cancerous cell lines. All experiments were carried out in triplicate and standard error is reported.

Compound	IC_{50} (μM) REH
6TP	2.94 (±0.48)
6TU	>10
6TX	>10
8-OH-6TP	9.91 (±2.36)
18a (Br)	9.54 (±0.97)
18b (Cl)	3.95 (±1.94)
18c (F)	4.71 (±1.40)
Doxorubicin	0.285 (±0.08)

3. Conclusions

Through this study, further investigations into the mode of toxicity associated with the therapeutic application of 6-thiopurine has been accomplished. It has been found that inhibition of UDPGDH, one of two critical steps in the bilirubin pathway, is highly inhibited by 6TU, the primary excretion metabolite of 6TP. Based upon previous structure-activity relationships of the excretion metabolites of 6TP, it was postulated that substitution about the C8 position could decrease inhibition towards UDPGDH while retaining its cytotoxic character. The synthesis of the C8 substituted bromine, chlorine, and fluorine analogs were successfully accomplished from 6-chloropurine in 32%, 22%, and 16% yields, respectively, all over five synthetic steps. Each of the

View Article Online
DOI: 10.1039/C8MD00463C

analogs were shown to have low inhibition (192, 163, 215 μM, respectively) towards UDPGDH, similar to 6TP (288 μM) and no inhibition towards UGT-1A. The C8-bromo analog had limited cytotoxicity towards the acute lymphocytic leukemia cell line REH, IC_{50} of 9.54 μM, however the chloro- and fluoro-6TP analogs were shown to retain cytotoxicity with IC_{50} values of 3.95 and 4.71 μM, respectively. These results have effectively shown that structural modifications of 6-thiopurine will not only retain cytotoxicity, but also decrease inhibition towards UDPGDH, a critical step found to be responsible for the most predominate toxic side effects of 6TP administration. It is anticipated that with a decrease in toxicity of new 6TP analogs, an increase in dosage can be administered, resulting in further increase of therapeutic properties of 6TP treatment. As such, newly constructed analogs of 6TP will lead to a more potent anti-leukemic drug that can help maintain the quality of life for patients through decreased associated toxicities.

4. Experimental Section

4.1 Chemistry

All reagents were commercially available and used without purification unless otherwise stated. NMR spectra were recorded with a Varian 400 MHz instrument. The chemical shifts are given in parts per million (ppm) relative to residual $CHCl_3$ at δ 7.26 ppm or DMSO δ 2.50 ppm for proton spectra and relative to $CDCl_3$ at δ 77.23 ppm or DMSO δ 39.52 ppm for carbon spectra, unless otherwise noted. Low-resolution mass spectra were obtained using a Waters Xevo-TQD via direct injection; samples were dissolved in methanol, filtered, and the supernatant injected. Flash column chromatography was performed with silica gel grade 60 (230-400 mesh). Dichloromethane (CH_2Cl_2), tetrahydrofuran (THF), toluene (PhMe), *N,N*-dimethylformamide (DMF), and

View Article Online
DOI: 10.1039/C8MD00463C

acetonitrile (CH_3CN) were all degassed with argon and passed through a solvent purification system containing alumina or molecular sieves. All commercially available reagents were used as received. All procedures including anhydrous solvents were performed with rigorously dried glassware under inert atmosphere.

4.1.1. Synthesis of 6-chloro-9-(4-methoxybenzyl)-9*H*-purine (14). To a stirring solution of 6-chloropurine (**13**; 1.5 g, 9.6 mmol, 1.0 eq.) in DMF (30 mL) was added K_2CO_3 (2.7 g, 19.2 mmol, 2.0 eq.) and *para*-methoxybenzyl chloride (1.44 g, 10.6 mmol, 1.1 eq.) and left to stir for 20 h. The reaction was quenched with the addition of water (1 vol. eq.) and the product was extracted with EtOAc (x3). The organic layers were combined, wash with brine, dried over sodium sulfate, and concentrated under reduced pressure. The crude material was purified via flash silica gel chromatography (gradient elution EtOAc:hexane of 1:2 to 9:1) to afford **14** (1.55 g, 58% yield) and **15** (0.9 g, 34% yield). ^{1}H NMR (DMSO, 400 MHz) δ (ppm): 8.81 (s, 1H), 8.78 (s, 1H), 7.33 (d, J = 8.0 Hz, 2H), 6.89 (d, J = 8.1 Hz, 2H), 5.43 (s, 2H), 3.70 (s, 3H). ^{13}C NMR (DMSO, 101 MHz) δ (ppm): 159.8, 152.3, 149.8, 148.0, 145.3, 131.5, 130.1, 128.6, 114.8, 55.8, 47.3. LRMS (ESI): *m/z* calcd for $C_{13}H_{11}ClN_4NaO$: $[M+ Na]^+$ 297.05, found 297.12.

4.1.2. General procedure for the synthesis of 8-substituted 6-chloro-9-(4-methoxybenzyl)-9*H*-purine analogs (16a-c). To a mixture of anhydrous diisopropyl amine (1.3 eq.) in THF (0.3 M) at -78 °C, under an argon atmosphere, was slowly added *n*-BuLi (1.6 M, 1.3 eq.) over 5 min. After 45 min of stirring at -78 °C purine **14** (1 eq.) in THF (0.1 M) was added slowly, followed by 2.5 eq. of a prepared 1 M anhydrous solution of halogenating reagent in THF over 15 min. The mixture was allowed to room temperature slowly, and was then quenched with saturated ammonium chloride, and the product was extracted with CH_2Cl_2 (x3). The organic layers were

View Article Online
DOI: 10.1039/C8MD00463C

combined, dried over sodium sulfate, and concentrated under reduced pressure. Product purification is described below.

4.1.2.1. 8-Bromo-6-chloro-9-(4-methoxybenzyl)-9H-purine (**16a**): The crude material was purified via flash silica gel chromatography (Et_2O:hexane 1:1) to afford **16a** in 75% as a yellowish amorphous solid (mp: 115-117). ^{1}H NMR (DMSO, 400 MHz) δ (ppm): 8.81 (s, 1H), 7.23 (d, J=8.4 Hz, 2H), 6.88 (d, J=8.4 Hz, 2H), 5.41 (s, 2H), 3.70 (s, 3H). ^{13}C NMR (DMSO, 101 MHz) δ (ppm): 159.7, 153.6, 152.7, 148.3, 136.2, 131.8, 129.6, 127.6, 114.9, 55.8, 47.9. LRMS (ESI): *m/z* calcd for $C_{13}H_{10}ClBrN_4NaO^+$: [M+Na^+] 374.96, found 375.08.

4.1.2.2. 6,8-Dichloro-9-(4-methoxybenzyl)-9H-purine (**16b**): The crude material was purified via flash silica gel chromatography (Et_2O:hexane 3:1) to afford **16b** in 70% yield as a white amorphous solid (mp: 111-113 °C). ^{1}H NMR (DMSO, 400 MHz) δ (ppm): 8.84 (s, 1H), 7.26 (d, J = 8.5 Hz, 2H), 6.88 (d, J = 8.5 Hz, 2H), 5.42 (s, 2H), 3.70 (s, 3H). ^{13}C NMR (DMSO, 101 MHz) δ (ppm): 159.5, 152.2, 152.1, 149.6, 147.8, 131.3, 129.9, 128.4, 114.6, 55.6, 47.1. LRMS (ESI): *m/z* calcd for $C_{13}H_{10}Cl_2N_4NaO^+$: [M+Na^+] 331.01, found 331.04.

4.1.2.3. 8-Fluoro-6-chloro-9-(4-methoxybenzyl)-9H-purine (**16c**): The crude material was triturated in diethyl ether and filtered (x2) to afford **16c** in 71% yield as a white apmorphous solid (mp: 110-112). ^{1}H NMR (DMSO, 400 MHz) δ (ppm): 8.99 (s, 1H), 7.23 (d, J = 8.5 Hz, 2H), 6.72 (d, J = 8.5 Hz, 2H), 6.06 (s, 2H), 3.63 (s, 3H). ^{13}C NMR (DMSO, 101 MHz) δ (ppm):159.7, 152.7, 146.5, 139.2 & 136.26 (C8), 131.8, 127.6, 114.9, 105.0, 55.8, 47.9. LRMS (ESI): *m/z* calcd for $C_{13}H_{10}ClFN_4NaO^+$: [M+Na^+] 315.04, found 315.03.

4.1.3. General procedure for thiol installation (17a-c). To a stirring solution of **16** (1 eq.) in MeCN (0.15 M) under an argon atmosphere was added thiourea (2 eq.) and brought to reflux for 2 h. The solvent was removed under reduced pressure to afford the thiourea purine, to which was

View Article Online
DOI: 10.1039/C8MD00463C

added ethanol (1.5 volume equivalents) and refluxed. After 2 h, the reaction mixture was allowed to cool to room temperature, and purification for each compound is described below.

4.1.3.1. 8-Bromo-9-(4-methoxybenzyl)-9H-purine-6-thiol (**17a**): Once at room temperature, the resulting yellow crystals were filtered via vacuum filtration, washed with diethyl ether, and left to dry over night to afford **17a** (181 mg 92% yield) as a white amorphous solid. ^{1}H NMR (DMSO, 400 MHz) δ (ppm): 13.52 (bs, 1H), 8.23 (s, 1H), 7.31 (d, J = 8.4 Hz, 2H), 6.85 (d, J = 8.5 Hz, 2H), 5.26 (s, 2H), 3.70 (s, 3H). ^{13}C NMR (DMSO, 101 MHz) δ (ppm): 169.5, 164.5, 159.4, 147.1, 144.0, 130.1, 128.5, 125.9, 114.5, 55.8, 45.6. LRMS (ESI): *m/z* calcd for $C_{13}H_{11}BrN_4NaOS^+$: [M+ Na^+] 372.97, found 372.95.

4.1.3.2. 8-Chloro-9-(4-methoxybenzyl)-9H-purine-6-thiol (**17b**): Once at room temperature, the resulting yellow crystals were filtered via vacuum filtration, washed with diethyl ether, and left to dry over night to afford **17b** (177 mg 89% yield) as a white amorphous solid. ^{1}H NMR (DMSO, 400 MHz) δ (ppm): 13.51 (s, 1H), 8.23 (s, 1H), 7.31 (d, J = 8.5 Hz, 2H), 6.85 (d, J = 8.5 Hz, 2H), 5.26 (s, 2H), 3.69 (s, 3H). ^{13}C NMR (DMSO, 101 MHz) δ (ppm): 169.3, 164.2, 159.2, 147.0, 143.8, 129.8, 128.3, 125.6, 114.3, 55.5, 45.4. LRMS (ESI): *m/z* calcd for $C_{13}H_{11}ClN_4NaOS^+$: [M+ Na^+] 329.02, found 328.99.

4.1.3.3. 8-Fluoro-9-(4-methoxybenzyl)-9H-purine-6-thiol (**17c**): Once at room temperature, the resulting yellow crystals were filtered via vacuum filtration, washed with methanol, and left to dry over night to afford **17c** (181 mg 92% yield) as a white amorphous solid. ^{1}H NMR (DMSO, 400 MHz) δ (ppm): 13.51 (s, 1H), 8.27 (s, 1H), 7.25 (d, J = 8.4 Hz, 2H), 6.82 (d, J = 8.4 Hz, 2H), 5.26 (s, 2H), 3.61 (s, 3H). ^{13}C NMR (DMSO, 101 MHz) δ (ppm): 176.5, 159.1, 149.9, 145.9, 140.5 & 134.9 (C8), 130.1, 128.9, 114.1, 110.0, 55.4, 47.2. LRMS (ESI): *m/z* calcd for $C_{13}H_{11}FN_4NaOS^+$: [M+ Na^+] 313.05, found 313.05.

View Article Online
DOI: 10.1039/C8MD00463C

4.1.4. General procedure for PMB deprotection. Under the protection of an argon atmosphere, concentrated sulfuric acid (2 eq.) was added drop wise to a stirring solution of **17** (1 eq.) in PhMe (0.085 M) and allowed to stir. After 2.5 h, the reactions were purified via the procedures described below.

4.1.4.1. 8-Bromo-9H-purine-6-thiol **(18a)**: The PhMe was decanted off, and the residue was triturated with Et_2O and filtered via vacuum filtration to obtain red/orange crude crystals. The water-soluble impurities were removed by partially dissolving the material in water, gently heating the mixture, and then allowed to cool to room temperature. The resulting yellow crystals that formed were collected by vacuum filtration and washing with Et_2O to obtain **18a** in 81% yield. ^{1}H NMR (DMSO, 400 MHz) δ (ppm): 13.70 (bs, 1H), 8.50 (s, 1H). ^{13}C NMR (DMSO, 101 MHz) δ (ppm): 176.2, 165.0, 148.7, 137.4, 133.1. LRMS (ESI): *m/z* calcd for $C_5H_3BrN_4NaS^+$: $[M+ Na]^+$ 252.92, found 252.92.

4.1.4.2. 8-Chloro-9H-purine-6-thiol **(18b)**: The PhMe was decanted off, and the residue was triturated with Et_2O and filtered via vacuum filtration to obtain the crude crystals. The water-soluble impurities were removed by partially dissolving the material in water, gently heating the mixture, and then allowed to cool to room temperature. The resulting white crystals that formed were collected by vacuum filtration and washing with Et_2O to obtain **18b** in 62% yield. ^{1}H NMR (DMSO, 400 MHz) δ (ppm): 13.71 (bs, 1H), 13.51 (bs, 1H), 8.52 (s, 1H). ^{13}C NMR (DMSO, 101 MHz) δ (ppm): 177.5, 165.3, 148.5, 135.1, 131.9. LCMS (ESI): *m/z* calcd for $C_5H_3ClN_4NaS^+$: $[M+ Na]^+$ 208.97, found 208.91.

4.1.4.3. 8-Fluoro-9H-purine-6-thiol **(18c)**: The PhMe was decanted off, and the residue was triturated with Et_2O and filtered via vacuum filtration to obtain the crude crystals. The resulting solid was then dissolved in a minimum amount of warm ethanol, followed by a slow addition of

View Article Online
DOI: 10.1039/C8MD00463C

$NaHCO_{3\ (aq)}$ forming a pale-yellow cloudy solution. Dropwise addition of 1 M $HCl_{(aq)}$ to a pH of 2.5 gave a transparent solution that upon cooling to 0 °C afforded yellow/orange crystals, which were filtered and rinsed with cold ethanol (x3) and left to dry to obtain **18c** in 41% yield. ^{1}H NMR ($DMSO_3$, 400 MHz) δ (ppm): 13.68 (bs, 1H), 12.42 (bs, 1H), 8.28 (s, 1H). ^{13}C NMR (DMSO, 101 MHz) δ (ppm): 177.1, 168.9, 159.2, 153.1 & 149.9 (C8), 133.7. LCMS (ESI): *m/z* calcd for $C_5H_3FN_4NaS^+$: $[M+ Na]^+$ 193.00, found 192.97.

4.2. Biological

4.2.1. UDP-Glucose Dehydrogenase Inhibition Assay

Inhibitor Assessment – General Procedure: Spectrometric analysis was performed on a Hewlett-Packard 8452 Diode Array UV/Vis spectrometer equipped with a Lauda Brinkman Ecocline RE 106 E100 circulating water bath. The water bath was maintained at 25 °C and the diode array was set at 340 nm, both were allowed to warm up 10-minutes prior to analysis. To a 1 mL cuvette, 300 mL of 0.5 M Gly-Gly (0.15 M final concentration), nanopure water, varying NAD^+ and UDPG concentration in varying inhibitor concentrations were added and placed in the diode array for a 2 min thermal equilibration. Once 1.5 minutes elapsed, the instrument was zeroed to obtain an initial rate change in absorbance versus time. The reaction was initiated by addition of 20 μL of the UDPGDH solution. Thorough mixing by inversion of the cuvette was performed as quickly as possible and then placed in the holder for analysis. The reaction was monitored from 20 to 120 seconds after enzyme addition, and the slope was calculated from 20 to 40 seconds using the diode array software.

4.2.1.1 Inhibitor Assessment – Saturating NAD^+ varying UDPG concentration: For each analysis, the cuvette was prepared in the same fashion as outlined above. The final concentration

View Article Online
DOI: 10.1039/C8MD00463C

of the components of the mixture were 150 mM Gly-Gly, 0.1 unit/mL UDPGDH, 3 mM NAD^+ and varied concentrations of 0.1, 0.05, 0.025 and 0.02 mM of UDPG, obtained from stock solution addition. Nanopure water was used as a variable component to ensure that a final volume of 1 mL was obtained. Inhibitor analysis of the four purines was performed at two concentrations: 50 and 100 μM for 6TP, 20 and 50 μM for 6TX and 8OH-6TP, and 5 and 10 μM for 6TU, obtained from their corresponding stock solutions. Each assessment was performed in triplicate. The average of the three were plotted and the slopes were used to determined inhibition values.

4.2.2. UDP-glucuronosyltransferase activity assay

4.2.2.1. Quantification of Bilirubin, and Mono/Di-glucuronide Levels: Bilirubin was quantified directly from the generated standard curve (see Supplementary Information). A total of ten peaks for the glucuronide species, including their isomers were detected in the incubation samples. Peak assignment and identification of UCB, BMG1, BMG2, BDG and their isomers were based on their lipophilicity and polarity, as well as the elution pattern, chromatographic peak position and relative retention time from previous reports.[21-23, 42] The calibration curves for bilirubin were used to determine the concentration of the mono- and di-glucuronide species employing the gradient HPLC bilirubin method described above. Quantification of UDPGA levels was determined through the use of the constructed standard curve within the isocratic HPLC method developed for UDGPA.

Bilirubin Glucuronide Formation: Bilirubin glucuronidation was performed at 37 °C in a shaking water bath. All steps taken were performed in the lowest light conditions possible; the glucuronide formed was found to be unstable to ambient lighting. The following was added to an Eppendorf tube to achieve the final concentrations indicated, final volume 200 μL: potassium phosphate buffer (50 mM, pH 7.4), bilirubin (10 μM), $MgCl_2 \cdot 6H_2O$ (0.88 mM), rat liver

View Article Online
DOI: 10.1039/C8MD00463C

microsomes (RLM, 100 μg of protein/mL), alamethicin (22 μg/mL), and allowed to pre-incubated for 2 min. Addition of UDPGA (3.5 mM), referred to as the zero-time point, initiated the reaction. The mixture was allowed to shake at 37 °C for each of the time course experiments. To each reaction 600 μL of ice-cold methanol containing 200 mM ascorbic acid was added to terminate the enzymatic reaction, vortexed for 2 min, and then centrifuged at 12,000 rpm for 10 min. The supernatant was then analyzed by the developed gradient HPLC protocol for separation and quantification of UCB, BMG1, BMG2, and BDGs.

Validation of Bilirubin Glucuronide Formation: Quantification of UCB, BMG1&2 and BDGs were performed post the quenching of UGT1A1, which was performed by immersing the Eppendorf tube with the reaction mixture in a cold-water bath for two min. No ascorbic acid was used, as the residual material would quench the glucuronidase enzyme to be added. To this sample 0.1 mg/mL glucuronidase enzyme was added, inverted (x3), and then analyzed by the HPLC protocol developed to quantify the levels of bilirubin and BMG1&2 and BDGs for formation confirmation.

4.2.2.2. Inhibitor Assessment of Bilirubin Glucuronide Formation: Employing the same protocol delineated above for the formation of the bilirubin glucuronide species, inhibitor assessment was performed. To the Eppendorf tube, the purine (50 and 75 μM final concentrations) was added alongside a control (no purine added) and allowed to pre-incubate for 2 min. Addition of UDPGA initiated the reaction for each of the time course experiments. The gradient HPLC method was employed for the 45-min time course experiments for the quantification of the glucuronide species.

4.2.3. IC_{50} Value Determination in REH using Alamar Blue Quantification

View Article Online
DOI: 10.1039/C8MD00463C

The acute lymphocytic leukemia cell line REH was grown in media supplemented with fetal bovine serum (FBS) and antibiotics (100 μg/mL penicillin and 100 U/mL streptomycin). Cells were incubated at 37 °C in a 5% CO_2, 95% humidity atmosphere. Cellular viability was determined by quantification via Alamar blue.

General Procedure: Compounds were solubilized in DMSO (10 μM stock solutions) and added to a 96-well plate over a range of concentrations (31.6 nM to 200 μM) with media, and 40 μL was added to the 384-well plate in triplicate for each concentration of compound. Cells were then added to the plate (2,000 cells/well) in 10 μL of media. After 69 h of continuous exposure, 5 μL of Alamar Blue was added to each well, and the cells were allowed to incubate for an additional 3 h. The plates were then read for fluorescence intensity with an excitation of 560 nm and emission of 590 nm on a BioTek Synergy H1 plate reader. Doxorubin and etoposide were both used as positive death controls, and wells with no compounds added as negative death controls. IC_{50} values were determined from three or more independent experiments using GraphPad Prism 7.0. (LaJolla, CA, USA)

4.2.4 Investigations into UDPGDH Inhibition by 6TP and 6TU in Hepatocytes

A male Sprague-Dawley rat was housed in an animal care room, kept at 25 °C with a 12 h light/dark cycle, and had free access to food and water. The rat was anesthetized by IP injection of ketamine/xylazine mixture (ketamine 100 mg/kg and xylazine at 15 mg/kg). Rat hepatocytes were isolated through the procedure outlined by Ogimura[43] and Ito.[44] Through the portal vein and inferior vena cava was inserted an IV cannula. The liver was washed with a perfusion solution (Ca^{2+} free, EDTA-containing perfusion buffer) for 10 min, followed by a perfusion with a collagenase containing buffer. Hepatocytes were isolated, filtered through a sterile nylon mesh, and purified via a Percoll solution, and washed with WME media (comprised of 10% FBS, 5%

View Article Online
DOI: 10.1039/C8MD00463C

penicillin and streptomycin, and 22 μg/mL alamethicin). Hepatocyte viability was assessed by Trypan blue exclusion, and cells with viabilities of >90% were used for the study. Cells were seeded onto a collagen-coated tissue culture plate, density of 500,000 cells/well, in 1 mL of WME media in a 12-well plate and incubated at 37 °C in a 5% CO_2, 95% humidity atmosphere. Following the procedure established by Ito,[44] cell media was exchanged and the hepatocytes were left to grow for 5 days.

Assessment: Hepatocytes were transferred to a 24-well plate (20,000 cells/well) in 500 of HWE media and allowed to adhere for 24 h. The media was removed and replaced with 1 mL of a buffer solution comprised of: HWE, bilirubin (10 μM), $MgCl_2 \cdot 6H_2O$ (0.88 mM), alamethicin (22 μg/mL), and 15 μM UDPG and left to incubate. To this buffered solution was added the purines of interest, as well 15 μM UDPGA and 10 μM of regorafenib. The addition of the buffered solution was considered the 0-min time point. After 24 h, the liquid mixture was transferred to labelled Eppendorf tubes and 2 mL of trypsin was added to well and left to incubate for 20 min at which 4 mL of WME media was added. The 6 mL of the cell mixture was then centrifuged (10,000 g, 2 min), the supernatant removed, washed three times with PBS buffer via gentle resuspension and centrifugation. The pellet was treated with 0.7 mL of a lysis solution (ETA, SDS, Tris HCl at pH 8.00) and 600 μL of ice-cold methanol containing 200 mM ascorbic acid was added to terminate the enzymatic reaction, vortexed for 2 min, centrifuge at 20,0000 x g for 15 min (pellet large cellular debris), the supernatant was added to the original liquid and assessed for UCB, BMG, and BDG levels via the HPLC previously described.

Ethics statement

View Article Online
DOI: 10.1039/C8MD00463C

All animal experiments were conducted under the supervision of Kansas State University Institutional Animal Care and Use Committee (IACUC) and were conducted according to approved protocols in accordance with all applicable federal, state, local and institutional laws or guidelines governing animal research.

Conflicts of interest

The authors declare no conflict of interest.

Acknowledgements

This work could not have been undertaken without the gracious financial support from the Johnson Cancer Research Center of Kansas State University and Startup Capital from Kansas State University. Funding for this research was provided by the NSF REU program under grant number *CHE-1460898*. A.X.T.H. was supported by the NSF-REU program.

References

1. G. H. Hitchings and G. B. Elion, *Pharmacological Reviews*, 1963, **15**, 365-405.
2. J. M. Torpy, C. Lynm and R. M. Glass, *JAMA*, 2009, **301**, 452-452.
3. T. Moriyama, R. Nishii, T.-N. Lin, K. Kihira, H. Toyoda, N. Jacob, M. Kato, K. Koh, H. Inaba and A. Manabe, *Pharmacogenetics and genomics*, 2017, **27**, 236-239.
4. O. Eden, *Journal of clinical pathology*, 2000, **53**, 55-59.
5. C. Vendrik, J. Bergers, W. De Jong and P. Steerenberg, *Cancer chemotherapy and pharmacology*, 1992, **29**, 413-429.
6. C. Cuffari, E. Seidman, S. Latour and Y. Theoret, *Can. J. Physiol. Pharmacol.*, 1996, **74**, 580-585.
7. D. S. Rampton, *BMJ: British Medical Journal*, 1999, **319**, 1480.
8. M. L. Seinen, D. P. van Asseldonk, N. K. de Boer, N. Losekoot, K. Smid, C. J. Mulder, G. Bouma, G. J. Peters and A. A. van Bodegraven, *Optimalisation of conventional therapies in inflammatory bowel disease*, 2016, **7**, 812-819.
9. X. Roblin, L. P. Biroulet, J. M. Phelip, S. Nancey and B. Flourie, *The American journal of gastroenterology*, 2008, **103**, 3115.

View Article Online
DOI: 10.1039/C8MD00463C

10. R. B. Gearry and M. L. Barclay, *Journal of gastroenterology and hepatology*, 2005, **20**, 1149-1157.
11. J. A. Nelson, J. W. Carpenter, L. M. Rose and D. J. Adamson, *Cancer Research*, 1975, **35**, 2872-2878.
12. S. Haglund, J. Taipalensuu, C. Peterson and S. Almer, *British Journal of Clinical Pharmacology*, 2008, **65**, 69-77.
13. K. Rowland, L. Lennard and J. S. Lilleyman, *Xenobiotica*, 1999, **29**, 615-628.
14. D. M. Tidd and A. R. P. Paterson, *Cancer Research*, 1974, **34**, 738-746.
15. P. Karran and N. Attard, *Nat Rev Cancer*, 2008, **8**, 24-36.
16. P. Karran, *British Medical Bulletin*, 2006, **79-80**, 153-170.
17. L. Chouchana, A. A. Fernández-Ramos, F. Dumont, C. Marchetti, I. Ceballos-Picot, P. Beaune, D. Gurwitz and M.-A. Loriot, *Genome Medicine*, 2015, **7**, 37.
18. T. Dervieux, J. G. Blanco, E. Y. Krynetski, E. F. Vanin, M. F. Roussel and M. V. Relling, *Cancer Research*, 2001, **61**, 5810-5816.
19. T. Dervieux, T. L. Brenner, Y. Y. Hon, Y. Zhou, M. L. Hancock, J. T. Sandlund, G. K. Rivera, R. C. Ribeiro, J. M. Boyett, C.-H. Pui, M. V. Relling and W. E. Evans, *Blood*, 2002, **100**, 1240-1247.
20. J. M. Carethers, M. T. Hawn, D. P. Chauhan, M. C. Luce, G. Marra, M. Koi and C. R. Boland, *Journal of Clinical Investigation*, 1996, **98**, 199-206.
21. G. Ma, J. Lin, W. Cai, B. Tan, X. Xiang, Y. Zhang and P. Zhang, *J. Pharm. Biomed. Anal.*, 2014, **92**, 149-159.
22. D. Zhang, T. J. Chando, D. W. Everett, C. J. Patten, S. S. Dehal and W. G. Humphreys, *Drug Metabolism and Disposition*, 2005, **33**, 1729-1739.
23. J. Zhou, T. S. Tracy and R. P. Remmel, *Drug Metabolism and Disposition*, 2011, **39**, 322-329.
24. R. Troxler and S. Brown, in *Bilirubin*, CRC Press, 2018, pp. 1-38.
25. L. Weaver, A.-R. A. Hamoud, D. E. Stec and T. D. Hinds, *American Journal of Physiology-Gastrointestinal and Liver Physiology*, 2018.
26. B. H. Billing, in *Bilirubin*, CRC Press, 2018, pp. 85-102.
27. M. Vögelin, L. Biedermann, P. Frei, S. R. Vavricka, S. Scharl, J. Zeitz, M. C. Sulz, M. Fried, G. Rogler and M. Scharl, *PLoS ONE*, 2016, **11**, e0155218.
28. E. A. Hullah, P. A. Blaker, A. M. Marinaki, M. P. Escudier and J. D. Sanderson, *Journal of Oral Pathology & Medicine*, 2015, **44**, 761-768.
29. P. P. Siva, K. M. Murali, A. Deepak, S. Murali, S. Michael and M. Sandhya, *Drug Metabolism Letters*, 2016, **10**, 264-269.
30. N. R. Beattie, N. D. Keul, A. M. Sidlo and Z. A. Wood, *Biochemistry*, 2017, **56**, 202-211.
31. C. J. Weeramange, C. M. Binns, C. Chen and R. J. Rafferty, *J. Pharm. Biomed. Anal.*, 2018, **151**, 106-115.
32. G. B. Elion, E. Burgi and G. H. Hitchings, *JACS*, 1952, **74**, 411-414.
33. R. Sariri and G. Khalili, *Russ. J. Org. Chem.*, 2002, **38**, 1053-1055.
34. Z. Luo, Z. Jiang, W. Jiang and D. Lin, *The Journal of Organic Chemistry*, 2018, **83**, 3710-3718.
35. M. Brændvang and L.-L. Gundersen, *Biorg. Med. Chem.*, 2007, **15**, 7144-7165.
36. L.-L. Gundersen, J. Nissen-Meyer and B. Spilsberg, *J. Med. Chem.*, 2002, **45**, 1383-1386.
37. S. H. Jung, G.-S. Hwang, S. I. Lee and D. H. Ryu, *The Journal of organic chemistry*, 2012, **77**, 2513-2518.

View Article Online
DOI: 10.1039/C8MD00463C

38. J. Bergman and L. Venemalm, *The Journal of Organic Chemistry*, 1992, **57**, 2495-2497.
39. A. K. Ghosh, P. Lagisetty and B. Zajc, *The Journal of Organic Chemistry*, 2007, **72**, 8222-8226.
40. S. Prekupec, D. Svedružić, T. Gazivoda, D. Mrvoš-Sermek, A. Nagl, M. Grdiša, K. Pavelić, J. Balzarini, E. De Clercq, G. Folkers, L. Scapozza, M. Mintas and S. Raić-Malić, *J. Med. Chem.*, 2003, **46**, 5763-5772.
41. S. Ciro, C. Rubio, K. Estieu-Gionnet, L. Latxague, G. Déléris, R. Bareille, J. Amédée and C. Baquey, *ChemBioChem*, 2002, **3**, 341-347.
42. M. G. Bartlett and G. R. Gourley, *Seminars in Perinatology*, 2011, **35**, 127-133.
43. E. Ogimura, S. Sekine and T. Horie, *Biochem. Biophys. Res. Commun.*, 2011, **416**, 313-317.
44. C. Liu, S. Sekine and K. Ito, *Toxicol. Appl. Pharmacol.*, 2016, **302**, 23-30.